ODESSA ASTRONOMICAL PUBLICATIONS

Volume 12 (1999)

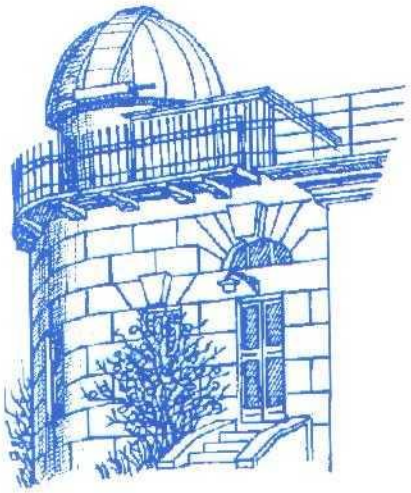

Odessa State University

ODESSA ASTRONOMICAL PUBLICATIONS

Volume 12 (1999)

(Известия Одесской Астрономической Обсерватории)

Special issue devoted to the 95^{th} anniversary of the birthday of G. A. Gamow

Address:
Astronomical Observatory, Odessa State University
T.G.Shevchenko Park, Odessa 270014 UKRAINE
Tel., Fax: + 038 + 0482 + 22 84 42

E-mail: astro@paco.odessa.ua
http://www.astro.od.ua (AO)
http://oap12.webjump.com (OAP)

Печатается по решению Ученого Совета Астрономической Обсерватории
Одесского государственного университета им. И.И.Мечникова
от 20 декабря 1999 г., протокол N 10

Printed in the UKRAINE
ASTROPRINT PUBLISHING COMPANY

FOREWORD

The present 12 volume of the "Odessa Astronomical Publications" (News of the Astronomical observatory of the Odessa State University) is the collection of papers based on the contributions presented at the Gamow Memorial International Conference (GMIC'99): " The Universe of Gamow: Original Ideas in Astrophysics and Cosmology ", devoted to Georgij Antonovich Gamow (1904-1968), one of the most prominent scientistst in physics, astrophysics and cosmology of the finishing XX century.

The present conference has become a second (first was organized in 1994) and traditional one, being organized once per five years by the Astronomical Observatory and Department of Astronomy of the I.I.Mechnikov Odessa State University, together with the Odessa Astronomical Society with a support by the Euro-Asian Astronomical Society (Moscow) and the Ukrainian Astronomical Association (Kiev). The conference was financially supported by the INTAS.

The conference was held on August 16-22, 1999 in the Odessa city, in which G.A.Gamow has grown, has entered the Russian society of the amateurs of "knowledge of the world" (ROLM), has become the student of a high school, worked as the calculator of the Astronomical observatory and began his way in science. Just in Odessa had formed his scientific interests, the understanding of necessity of reception of maximum fundamental education in the field most close to his interests.

At the conference "GMIC'99", the memorial session was carried out, with the talks by the son and nephew of G.A.Gamow - the professor I.R.Gamow (USA) and I.L.Gamow (Moldova), the report of the pupil of G.A.Gamow - professor R.A.Alpher (USA) and a number of contributions by the scientists from various countries. Except for memorial session, also worked 5 problem sections, and also a special section, where the reports on the projects granted by the INTAS have been presented. The extensive cultural program w as proposed to the participants of the conference.

Totaly at the conference were presented 122 oral contributions, among which 31 plenary, and 63 posters. All plenary reports submitted by their authors, are published in the present volume. Here are published also 33 other contributions which have caused the greatest interest. All submitted contributions are available in the electronic version of the proceedings (http://oap12.webjump.com). Some of the works, presented at the conference, are already published in other journals.

V.G. Karetnikov

CONTENTS

Quasars and active nuclei of galaxies

Galactic objects and Interstellar Medium

Stars

Sun and Solar System

MEMORIES OF MY FATHER, GEORGE GAMOW

R. Igor Gamow

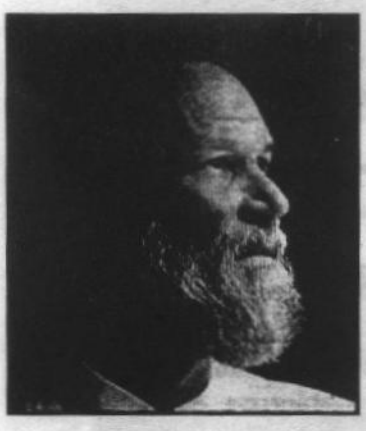

Dear friends and colleagues:

To say that I am happy to be here today is such an understatement that I shiver in embarrasment. But, say it I must. For the first time in my life I am not only in the country and city of my Father's birth, but also for the first time in my life I am in a country where everyone is speaking Russian. And to top it all off, it is as if I drank a magic potion, because I can understand the language! It was the language of my childhood. Not only the language I understood but also the spirit and magic of the Russian language. I remember Father's love for Pushkin and how as a boy he went with his Father to the opera to see Pushkin's Russlan and Ludmilla fairy tale and how excited Father was to see and to hear how the hero, Russlan, searched for Chernomor and then finally killed the black magician. Today, I feel the same excitement my Father felt seeing this opera. In my Russian bones, I feel the excitement that Russlan must have felt when he found his stolen bride, Ludmilla. I have found Odessa. I not only found Odessa, or Odessa me, but with my great cousin, Igor L. Gamow, we found the birthplace of my Father and we, of course, drank vodka at this place in his memory.

There are a hundred stories (perhaps in the spirit of the Russian language I should say 40 stories!) about Father, but I have chosen two. The first story I have chosen happened in 1949, when I was fourteen, and we were vacationing in California and staying in a beach front motel. While swimming in the surf, I found a sea gull (I can still hear Father say Chauka) which, because of a nearby oil rig, was covered with oil. I swam to shore with my prized sea gull and took her (I assumed she was a princess that I rescued) to the motel for cleaning. The only cleaning fluid available was cigarette lighter fluid for my Father's ever present Zippo lighter. You can imagine what a mess everything was: a wet oily bird, towel after towel covered with heavy crude oil and sand, my beautiful Russian Mother, Rho, complaining about the disorder, and my smiling Father in his wild colorful Hawaiian shirt looking on. In the midst of all this commotion appeared two somber men dressed in black suits who introduced themselves as G-men (government men in charge of American security). Father, because of his past Soviet experiences, was of course concerned, but they reassured Father that they simply needed to know whether he had ever served in the armed forces of any country. Father smiled and said that as a matter of fact he had and was pleased to tell them he was once a colonel in the Red Army in the Artillery School of the Red October! You can imagine the G-men's excitement when they learned that one of America's top atomic scientists was once a colonel in the Red Army and they had never asked him! A few days later, the excitement disappeared when it was revealed that Father's position was given to him through the University of Leningrad's academic program and he was therefore of little security concern. But for a while it was quite exciting. The sea gull, by the way, survived and may still be flying over the beaches in California. Sea gulls live a long time, and in one's imagination, forever!

My second story concerns my Father and Mother's attempted escape in a small "Faltboat" from Crimea to Turkey. I, of course, heard many stories of this voyage. I heard about the storms, the porpoises that they played with, their small boat, Father's kidney stone attack in the midst of all this, and finally their forced beaching-not in Turkey, alas, but on the ever present Soviet soil. How my heart raced when Misha Ryabov and his his colleagues took me sailing on the Black Sea in a small boat not filled with Brandy and hard chocolate as my parents boat had been but with vodka and sausages. I felt I was following the wake of a little mystical boat that held my two parents so many, many years ago.

So, my friends, here are my two stories, but I hope in the years to come to tell you many more stories. My Father loved *Alice in Wonderland* and I can hear his voice quoting the Walrus: "The time has come to speak of many things..."

Figure 1. George Gamow (3 years old) at the village near Odessa.

George Gamow and his father Anton Gamow

Copyright - The Gamow Family

Figure 2. George Gamow and his parents.

George Gamow and his mother Alexandra Lebedenez Gamow

Copyright - The Gamow Family

George Gamow

Copyright - The Gamow Family

Figure 3, 4. G.A. Gamow and his wife L.N.Vokhmintseva.

Figure 5. G. Gamow and W. Pauli

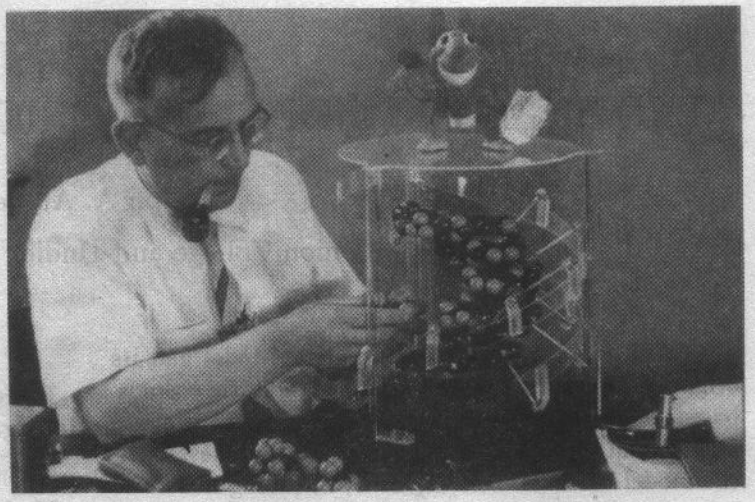

Figure 6. G.A. Gamow and DNA

Figure 8.
G.A. Gamow.

Figure 7. Awarded Kalinga Prize by UNESCO for popularization of science.

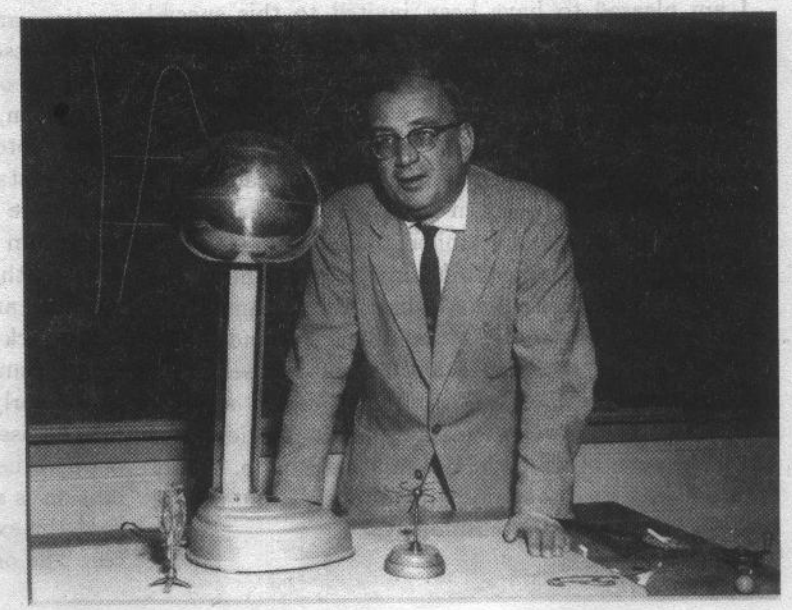

Figure 9. G.A. Gamow – visiting Professor of the University of California, Berkeley (1954).

THE BIG BANG MODEL: ITS ORIGIN AND DEVELOPMENT

Ralph A. Alpher

Union College and Dudley Observatory

ABSTRACT. The current Big Bang Model had its origin in Einstein's attempt to model a static cosmos, based on his general theory of relativity. Friedmann and Lemaître, as well as de Sitter, further developed the model to cover other options, including nonstatic behavior. Lemaître in the 1930s and, particularly, Gamow in 1946 first put physics into the nonstatic model. By 1946 there had been significant developments in the mathematics of the model due to Robertson, Walker, Tolman and many others. The Hubble law had given an essential observational basis for the Big Bang, as did the attribution of cosmic significance to element abundances by Goldschmidt. Following early suggestions by George Gamow, the first attempt to explain nucleosynthesis in a hot, dense, early universe was done by Alpher, Bethe and Gamow in 1948, a paper whose principal importance was that it suggested that the early universe was in fact hot and dense, and that hydrogen and helium and perhaps other light elements were primeval. In that same year Alpher and Herman first predicted a cosmic background radiation at 5 kelvin as an essential feature of the model. The Hubble expansion rate, the primordial and stellar abundances of the elements, and the cosmic microwave background are major pillars today for the Big Bang model.

Key words: History of Astronomy: general relativity: Big Bang.

I am pleased to have been invited to this special George Gamow memorial session. Its been a long time association for me. I first met Gamow in early 1942, 57 years ago.

I wish I could have been here, but I am sure Prof. Chernin will do an admirable job at reading my communication. It has been more than 50 years since the alpha-beta-gamma (Alpher, Bethe and Gamow) paper on prestellar nonequilibrium nucleosynthesis was published, and since the late Robert Herman and I predicted a consequent present cosmic background radiation at about 50°K. Herman and I worked closely with Gamow from the late 1940s until his death, and we much say that he was at least a spiritual guide even in the research in which he did not participate. A day does not go by without my remembering Gamow, and his love for physics and cosmology.

Introduction of physics into cosmological modeling.

Modern mathematical modeling of the universe began with Einstein. In 1917 he developed the first general relativistic model of the cosmos with assumptions that the universe was homogeneous and isotropic, and that the smearing out of all structure, averaged over the universe, led to a single cosmic density of matter. This material was taken to be a dilute ideal gas with an appropriate equation of state. This, together with an equation for the conservation of energy in a comoving volume, as well as Einstein's basic field equations which relate the curvature of space-time to the cosmic content of energy and momentum, provided the description of the model.

The then-current wisdom was that the universe was static, and that the peculiar velocities of objects in the heavens were certainly nonrelativistic. The model was inherently unstable, which led Einstein to add a term containing a "cosmological constant" to force stability. Covariance was preserved. Einstein's concluding statement in his paper was "That term is necessary only for the purpose of making possible a quasi-static distribution of matter, as required by the fact of the small velocities of the stars".

While this added feature did not damage the mathematics particularly, Einstein apparently felt somewhat embarrassed later when the Hubble law, which synthesized observational evidence for a general cosmic expansion, was published in the late 1920s. He is widely quoted as having said that the introduction of this constant, Λ, was his "greatest blunder". Einstein may have sold himself short. A nonzero Λ has been used from time to time to reconcile the age of the universe with the age of contained structures. Gamow, Herman and I did this when the Big Bang was under attack for giving too short an age. Alternatively, some cosmologists studying the possibility of inflation in the early universe introduce Λ. There is recent evidence based on Type 1a supernovae that the universe is open, i.e., that the mean density of matter and radiation is significantly less than a critical density and that the expansion shows acceleration at large distances. The origin of this acceleration may be Λ acting as

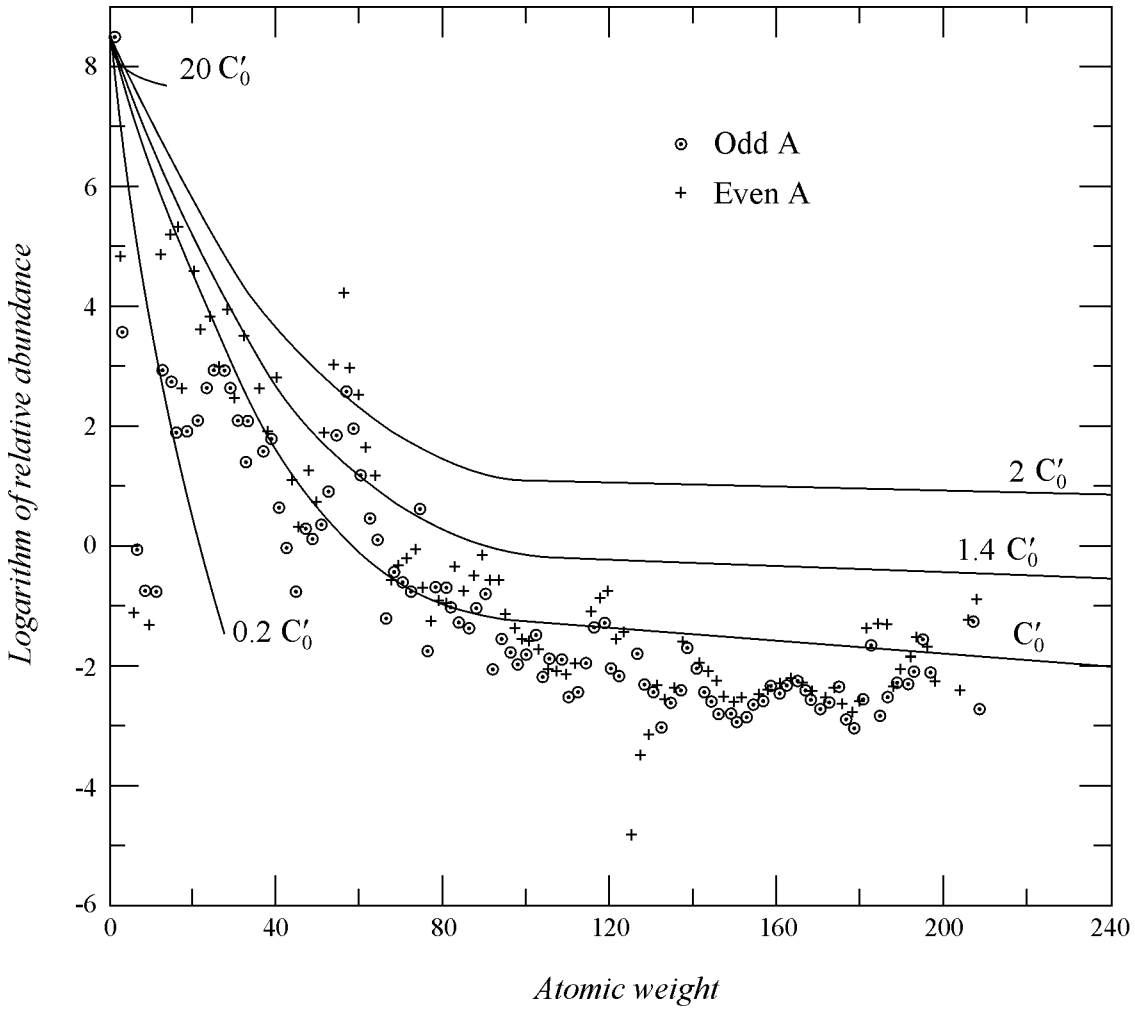

Figure 1: Comparison of observed relaive abundances with results of simple prestellar neutron-capture sequence calculation. Starting conditions are $T = 0.11$ MeV and time=140 seconds (published in 1950), with $C_0^{'}$ being the starting baryon concentration (about $10^{17} cm^{-3}$).

a repulsive driving force, or, as has been suggested recently, in a phenomenon called "quintessence", which is a fluctuating dynamic driving force.

Relative Abundance of the Elements.

In the early years of this century physical chemists, working with limited knowledge of the relative abundance of the chemical elements, concluded that these abundances must reflect nuclear rather than chemical properties. Over the next several decades determinations of the relative abundances in various cosmic locales improved, culminating in the late 1930s with the work of a geochemist, V.M. Goldschmidt, who constructed a relative abundance table which became accepted as being cosmic. This was a profound step forward, in the sense that the elements must have been formed in locales of rather extreme physical conditions, such as the interior of stars, or, as first suggested by Gamow, in some early configuration of the universe, a locale suitable for thermonuclear reactions.

Study of the composition of the universe is much more than a cottage industry among astronomers and geochemists, since improvements in the data give further clues both to phenomenology in the early universe, and in interstellar space, as well as to the formation and evolution of stars. In particular increasing attention is being paid to the abundances of the lightest elements, since it is now almost certain that these elements were formed by thermonuclear processes in the early stages of a hot, dense expanding universe which has evolved into what we see now, while all the other elements in the periodic table are formed later primarily in stellar interiors. They are then released either in the violent outburst accompanying the death of stars as stars exhaust their source of fusion energy, or from thermonuclear explosions in the atmospheres of white dwarfs as they accumulate critical masses of material from a neighboring star in binary systems.

A graph exhibiting cosmic relative abundances according to data in the 1950s is given in Figure 1, which shows also the best fit Herman and I could obtain with neutron-capture reaction sequences. The free parameter is related to the density of matter at the onset of nucleosynthesis.

Expansion of the Universe

Studies of the rate of expansion of the universe as well as the mean density of matter, particularly as these relate to the reality of measurements of acceleration at large redshifts, is an active area of cosmological research.

In the early days of our work on the standard Big Bang model, the calculated age of the Big Bang was less than the much-better-known age of the Earth. This was a major deterrent to any wide-spread acceptance of the Big Bang model at the time, and led to a period in which the steady state model was ascendant. It was possible to resolve the age discrepancy by invoking a nonzero value of Λ, but that was generally thought not to be appropriate at the time. Criticism of the Big Bang model by the steady state school was in our view unduly harsh, given the inherent difficulties in determining the requisite parameters. Moreover we felt that the steady state model had more deficiencies than the Big Bang. Refinement of values of the Hubble parameter and the mean density, as well as improved ages for galactic clusters, are leading to acceptable ages for the universe and its contents.

Development of mathematical nonstatic models

Some years after the Einstein model was described, Alexander Friedmann, in the Soviet Union, with whom Gamow studied relativity theory, studied nonstatic models with an arbitrary cosmological constant (1922 and 1924). Such nonstatic solutions were explored, apparently independently, by Georges Lemaître, a Belgian cleric, in 1929-1930.

Some of us now to refer to the Friedmann-Lemaître-Robertson-Walker equation as the basic equation of the Big Bang, giving the latter two men recognition for the explication of a line element for the model.

By 1929 cosmic expansion had come to be widely accepted, and Lemaître became the first to discuss some physics involved in a nonstatic model. He tried to reconcile the model with Hubble's observed expansion rate and mean density of matter in the universe. The bottom line in Lemaître's work at the time was his particular interest in explaining the origin of cosmic rays. His idea was that the cosmos began as a all-encompassing gigantic nucleus which broke up into nuclear-sized pieces. Some of these nuclear pieces came away from the breakup with very high energy, he suggested, and might have survived to be identifiable as cosmic rays. Current views are that cosmic rays originate in supernova explosions as well as from the conversion of photons from gamma-ray bursters. Many years later (1948) Maria Göppert-Mayer and Edward Teller again proposed a single cosmic nucleus whose breakup served as the origin of all matter and energy in the universe. It appears that Lemaître should be c redited as being the first to try to introduce some physics into modeling. It also appears that the next scientist to try to do this was George Gamow.

George Gamow's Early Foray into Cosmology

In 1935, Gamow noted the discovery of the neutron and the consequent study of neutron-capture reactions by Enrico Fermi in Italy. This led him to suggest that such reactions established the abundance distribution of nuclear species, and that neutrons undoubtedly played a role in reactions producing energy in stars (a precursor of the s-process in stellar nucleosynthesis). In 1942 he again suggested that the elements were formed somehow by nuclear reactions in a system not in thermodynamic equilibrium. In 1946 he published a more specific set of ideas on nuclei being formed in the early universe. He was motivated toward this end by the failure of global equilibrium theories of element synthesis.

In 1946 it was still Gamow's hope to find a single locale for explaining the entire abundance distribution. Given the difficulties with single locale equilibrium theories he posited that the early expanding universe would have physical conditions suitable for nuclear reactions to occur in a nonequilibrium manner over a short period of time and then be quenched by dilution in the expansion and by the exhaustion of starting material. He went on to propose that nuclei could be built up from an initial neutron gas by some means of agglomeration, with the final states being arrived at by intervening beta decay of neutron-rich fragments into more stable nuclei. In 1945 I had completed a master's dissertation on sources of energy in stars and was accepted by Gamow to work on a Ph.D. dissertation. After I was scooped by E. Lifshitz in the Soviet Union on my first dissertation topic on the growth of instabilities in a relativistic expanding medium, we picked a second dissertation topic, namely, developing the rather primitive 1946 ideas of Gamow on element building.

I arrived at The Applied Physics Laboratory of the Johns Hopkins University (APL/JHU) in 1944, and shortly thereafter met Herman who had been there for

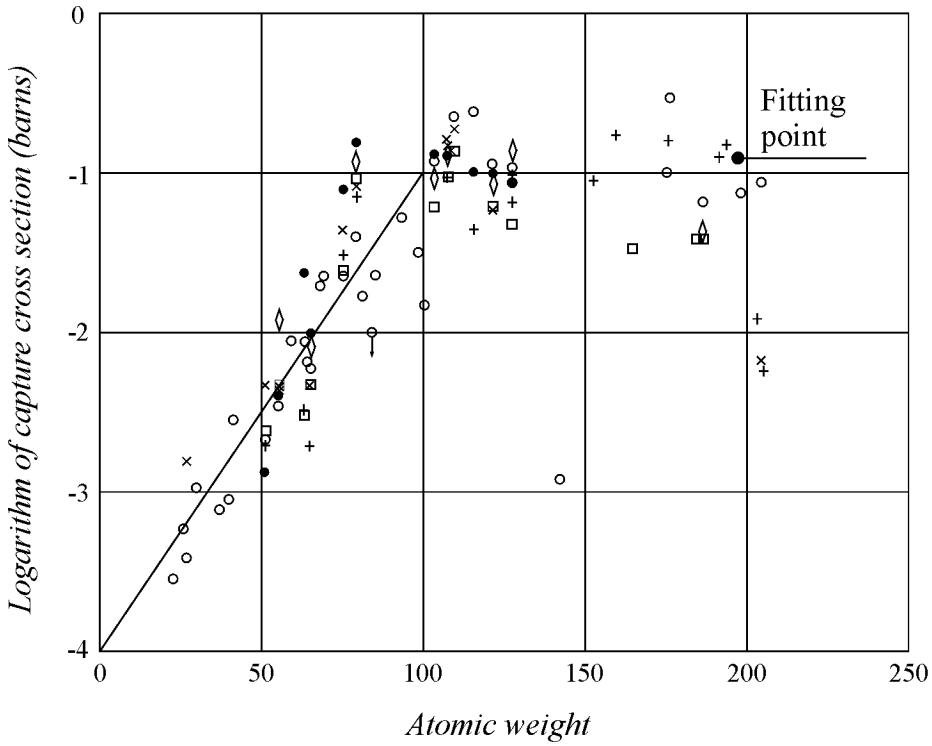

Figure 2: Probability of (n, γ) reactions as published by Donald Hughes (Argonne), measured with 1 MeV neutrons. Other avaliable data are also shown (1950 plot).

several years. When the war ended, we both joined a newly formed Research Center, We had a commonality of interest in astrophysics and cosmology, and almost daily discussions ensued with Herman, and of course with Gamow, who became an APL/JHU consultant after the war. Our official tasks at APL/JHU were on very different matters.

The Alpher-Bethe-Gamow Paper

The alpha-beta-gamma theory was the result of my second foray into cosmology. We proposed to see if we might understand the synthesis of the chemical elements in a hot, dense early phase of the expanding universe. The success of such a program would be judged by how well the calculations matched the presently observed cosmic abundances of the elements. We hoped that one theory would explain it all.

The mathematical model for consideration of the early universe was based on the Friedmann-Lemaître-Robertson-Walker line element. Given the anticipated high ambient temperatures, it was expected that the total density and the consequent dynamics of the universe was dominated by radiation (R.C. Tolman in 1934 discussed a model consisting of blackbody radiation). It was not clear how much of the total density at early times to ascribe to the matter then present, except we expected it would make a very small contribution, and its numerical value would be determined by the conditions for synthesizing the elements. The main stumbling-block initially was our lack of detailed knowledge of the cross sections for the various kinds of nuclear reactions among the species likely to be present.

We had just emerged from World War II, and data for such reactions, under conditions of high temperature and density, were still classified or were just beginning to be declassified. As luck would have it, we got a boost from the work of Donald J. Hughes, then at Argonne, and later at Brookhaven. Hughes surveyed any and all materials which might be of interest in reactor construction using neutrons at energies of about 1 MeV (about 10^{10} °K, which, incidentally, would have been the cosmic temperature at about a second into the expansion), and measured the cross sections for (n,g) reactions. The exciting result of his work is shown in Figures 2, 3. The top diagram shows the variation with atomic weight of the neutron-capture cross-sections, where one should note the exponential rise of the probability to an atomic weight of about one hundred, and essential constancy for heavier nuclei, a mirror image of the run of abundance data. The second diagram is a correlation of the probability of neutron-capture reactions with abundances. This was all quite suggestive.

On this basis we undertook to calculate in a very approximate way the growth of abundances by neutron-capture reactions. We assumed that the initial material

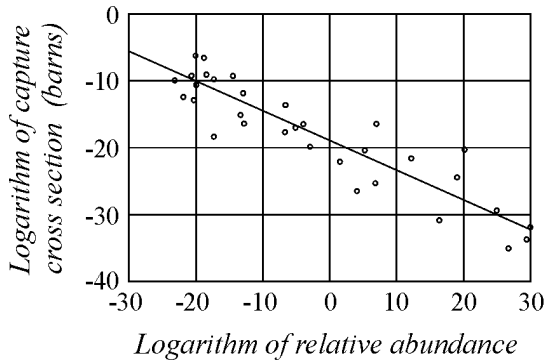

Figure 3: Correlation of reaction cross sections with observed relative abundances.

was a neutron gas, with a density being chosen to give the best subsequent representation of observed abundances. Hughes' neutron-capture reaction cross sections were corrected to 0.1 Mev by 1/E (to be well below photodissociation energies), and followed the general run of the probabilities shown in Figures 2 and 3, with the successive reactions beginning with the capture of a primordial neutron by a newly formed proton resulting from neutron beta-decay (half-life of about 800 seconds). The nucleus thus formed would have been a deuteron; next the deuteron would have absorbed a neutron to form a triton, the nucleus of tritium, the heaviest isotope of hydrogen. And so on. Clearly at this point we had to gloss over any details in cross sections. When nuclei so formed had an overabundance of neutrons and were therefor unstable, be ta-decay would have adjusted the relative number of neutrons and protons toward the valley of stability. Then successively heavier nuclei which formed would in turn adjust by beta-decay so as not to be overly neutron-rich and would then be stable on a time scale of the order of the duration of the period of formation of nuclei. For purposes of a calculation one could carry out at a time when digital computers were scarce, it was assumed that the reaction rates would be fast compared to the rate of expansion of the universe, and therefore the calculations dealt basically with a static model.

This very simplified calculation led to what then seemed a very exciting representation of the overall cosmic abundances of nuclei, as illustrated in Figure 1. Moreover the calculation rationalized the high relative abundance of helium (an aspect of relative abundance data which had long been puzzling). I should mention that Bethe was not associated with the alpha-beta-gamma paper, but did not object to his name being added on the grounds that the result might even be right.

Standard Big Bang Models studied by Alpher and Herman

After the alpha-beta-gamma manuscript had been sent in, Herman and I proceeded immediately to reconsider the entire calculation in a series of papers, with the intent of removing some of the assumptions which had been made. There was one particular problem, recognized early on, that nature had not provided us with sufficiently stable nuclei at atomic weights 5 and 8, so that the notion of a sequential build-up of nuclei by neutron capture could not be correct in detail for the light elements.

The one free parameter whose value we chose in model calculations was the density of matter at a particular epoch in the expansion, and it was satisfying that the value we found later with improved calculations was close to that chosen in the alpha-beta-gamma paper.

In late 1949 I gave a colloquium with Enrico Fermi in the audience. Fermi was intrigued with our lack of nuclear reaction data for the light elements; when he returned to Chicago he enlisted his colleague, Anthony Turkevich, a nuclear chemist, and between them they developed a list of some 28 reactions among the light elements, using observations of reaction rates where they were available, and using nuclear theory, as well as educated intuition, to estimate other rates. Their results were most interesting, and we show them in Figure 4. For brevity I have chosen not to show some of the intermediate solutions Herman and I produced. Fermi and Turkevich used ambient conditions similar to those in the alpha-beta-gamma paper and sent their results to us to be included in an extensive review paper Herman and I wrote in 1950 on the general problem of the origin of the elements. They too were stymied by the gap due to the lack of nuclei at atomic weights 5 and 8, as was Eugene Wigner in a separate encounter.

Starting Conditions for Nucleosynthesis.

Our starting conditions for primordial nucleosynthesis had been primitive. A major improvement was due to Chushiro Hayashi of Japan in 1950. The universe was surely hotter and denser before nucleosynthesis began; in all of our earlier calculations, including those of Fermi and Turkevich, the ratio of neutrons to protons at the start of element-building was taken to be what resulted from the free decay of primordial neutrons prior to a specific starting time at about 0.1 Mev. (See Figure 5 for a listing of relationships inherent in the Big Bang model. In particular, note the power law relation involving the densities of matter and radiation). Hayashi proposed that the ratio of neutrons and protons be whatever resulted from spontaneous and induced beta-decay processes in the early stages of the expansion, in the presence of electrons, positrons, neutrinos and antineutrinos. Element building would then proceed with the consequent neutrons

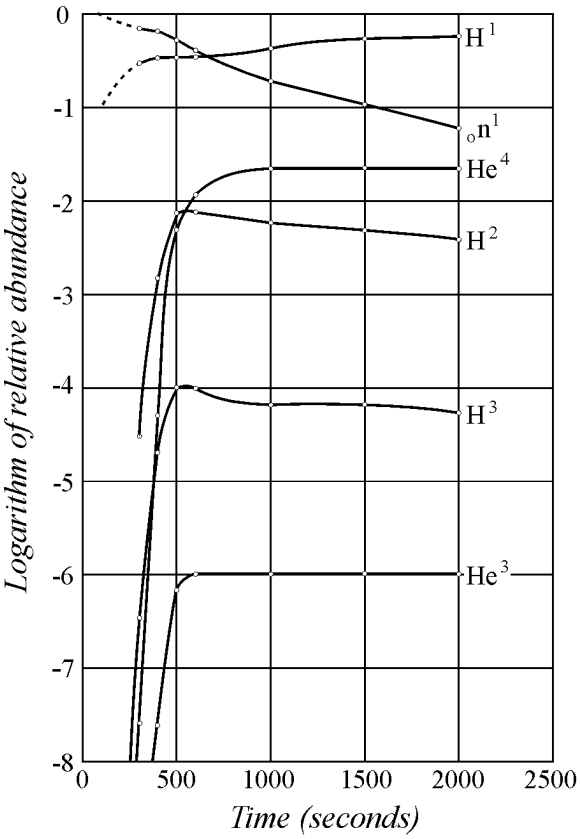

Figure 4: Calculation of light element relative abundances by Enrico Fermi and Anthony Turkevich, using ambient conditions as described in the Alpher-Bethe-Gamow paper in 1948. Fermi and Turkevich asked that their work be published in a 1950 review of the origin of the elements by Alpher and Herman. They surveyed 28 nuclear reactions with reaction probabilities either as measured or as they estimated them to be. They also were unable to bridge the gap at atomic weights 5 and 8, but confirmed the high abundance of helium, as had our earlier work.

and protons present as the temperature dropped low enough to rule out any photodissociation reactions.

Hayashi's calculation gave values of the neutron-proton ratio which precluded a successful generation of the relative abundance distribution by our simple neutron-capture picture. There were some difficulties with his calculation, and Herman and I were joined by James W. Follin, Jr., in 1953 in an improved approach, which has become a more-or-less standard starting point for modern nucleosynthesis calculations.

In our 1953 paper we did not go so far as predicting the resulting relative abundance distribution of the elements. We did such calculations later but they were given only in some short presentations at meetings of the American Physical Society prior to 1965. Herman and Gamow and I went on to other positions in 1965, while Follin stayed at Johns Hopkins, a situation which made it difficult to put together a detailed paper (no electronic mail then). Others did such calculations later, using detailed reaction probabilities which were becoming available. We did determine that improved initial conditions still did not obviate the difficulties with the atomic weight gaps at 5 and 8. It was also clear that the initial conditions, and subsequent nucleosynthesis, would depend significantly on the neutrino types introduced into the calculation. One interesting consequence of these calculations was the realization that prior to the onset of nucleosynthesis all of the reactions between neutrons, protons, radiation, and the other elementary particles present went on so rapidly compared to the rate of universal expansion that the mixture was basically in thermodynamic equilibrium. If one accepts the premises of thermodynamics, then it must be so that the equilibrium state conceals any prior history of the system, which has give us pause from time to time about inflationary models.

Nevertheless, it seems sensible to consider some phenomena associated with the earliest times in the expansion which survived the equilibrium period, such as the present nonexistence of magnetic monopoles, the present preponderance of matter over antimatter, the existence of very small fluctuations which somehow survived to become the anisotropies observed in the cosmic microwave background radiation by the COBE satellite and in other recent observations, and the question of how the early universe came to be at such a uniform temperature.

There are other interesting consequences of the detailed examination of the state of the universe just prior to nucleosynthesis. When, in the expansion, temperatures were greater than the rest mass energy of baryons these would be created and destroyed freely. When the temperature dropped below this value, the then extant abundances of neutrons and protons would be frozen in, until reactions ensued, except for radioactive decay of the neutron. Later, when the temperature had dropped to a value of less than the rest mass of a pair of leptons, the abundance of electrons and positrons relative to one another would have frozen in. In a similar vein, one can show that neutrinos and their antiparticles would have frozen in, at a temperature whose precise value depends on whether the neutrinos oscillate, have a nonzero mass, and on the number of colors. Because the interaction of neutrinos with other matter and radiation is extremely small, the neutrinos should then have participated in the expansion and cooling of the universe as though they were a radiative component, and there should now be a background of neutrinos which has cooled down to a temperature of the order of 2 kelvin. Their number density should be comparable to the number density of 2.8 kelvin photons, but there seems to be no observational procedure waiting in the wings for detecting these low energy background neutrinos.

I would make two further comments about our early

$R(t)$ = expansion scale factor.
Redshift $z = \frac{\Delta\lambda}{\lambda}$.
Consrevation of baryoms throughout expansion
$\rho_m R^3 = constant$ or $\rho_m = \rho_{m,0}(1+z)^3$.
Adiabatic expansion of radiation throughout expansion
$\rho_r R^4 = constant$ or $\rho_r = \rho_{r,0}(1+z)^4 = \frac{\alpha T^4}{c^2}$.
Hence $\rho_r \rho_m^{-4/3} = constant$ throughout expansion and
Temperature $T = T_0(1+z)$.
At early times $T = \frac{1.52 \cdot 10^{10}\ ^\circ K}{\sqrt{t}} = \frac{1.31 MeV/k}{\sqrt{t}}$,
where t is in seconds. (Numerator=universal constants).
At early times, $\rho_m << \rho_r$ and $\rho_m \propto t^{-3/2}$

Figure 5: Basic relationships in the Big Bang

work on nucleosynthesis. The very simplified model we used predicted abundances of lithium, beryllium and boron which were high compared to observation. In 1948, Gamow, Herman, and I reported a calculation wherein we showed that once the neutron-capture sequence was essentially done, the temperature was still high enough so that the remaining nuclei could interact with the abundant protons present, which would reduce the abundances of these light elements by appropriate amounts. Recent work on primordial deuterium abundance seems to contradict this. A second comment has to do why one does not observe equal numbers of nucleons and antinucleons in the universe. In our work Herman and I showed that the present asymmetry could not be the result of a statistical fluctuation in the early universe. At the time of our study we argued that the abundance of antinucleons relative to nucleons must be less than one part in 10^7, since anything greater than this would be able to account for all the energy generation in our galaxy or in the cosmos as a whole. Much more recent work on this question suggests that there was a basic symmetry-breaking in reactions at high temperatures in which nucleons go into antinucleons, and vice versa, with a consequent favoring of a final abundance ratio of far less than a part in 10^7.

Further Development of Nucleosynthesis Calculations

In 1957 a seminal paper was published by Burbidge, Burbidge, Fowler and Hoyle, who did a fine job of explaining the relative abundances of most of the heavier elements as having been generated in stellar interiors, with modification and distribution in space of the synthesized elements when the stars ran out of nuclear fuel and went into a collapse and explosion mode.

The synthesis of light elements was still problematical in the scheme of things among steady state theorists until Hoyle and Tayler, in 1964, used the Alpher-Follin-Herman methodology to conclude that helium must have been generated by light element reactions in the early universe. This was a major step forward (or backward, depending on your predilections for cosmological models) for these authors, since they were strong advocates of a steady-state model of the universe, with no hot dense early universe to make light elements. They also noted that the calculations were somewhat sensitive to the assumed types of neutrinos for the prenucleosynthesis era, as we had found in 1953. A light element calculation using our methodology was done by Peebles in 1966, with useful results for the abundances. The first full-scale light element calculations were carried out in 1967 by Robert Wagoner, Willie Fowler and Fred Hoyle, in the context of the standard Big Bang model as well as in massive stars, ca. 10^8 solar masses, then thought to be possible alternative sites. The latter long since vanished as a viable option.

In 1973 Wagoner carried out an improved calculation of light element abundances, and the computer code he developed, with modern updates, is still in use by those examining such abundances. As we have mentioned several times earlier, the one free parameter in Big Bang nucleosynthesis calculations is the extant density of matter when such reactions became important. Wagoner's work strongly indicated that if observed deuterium abundances were primordial, then the required matter density was well below what would be needed in present observations to close the universe. This seems still to be the case. Its value is the subject of much of observational cosmology. Recent observations appear to favor a value of the ratio of total density of baryons to the density for closure, $\Omega < l$,. It now seems clear that the value of Ω may in fact be more than can be inferred from the requirements of nucleosynthesis, so that there may still be a need for dark matter. But W may not be as large as 1 , as researchers on the inflationary model of the universe would insist it has to be, although the deficiency may actually reflect a vacuum energy density causing acceleration of the universe.

Since the Wagoner paper of 1973, there has been a considerable effort in improving the abundance calculation for light elements. We have reproduced in Figure 6 a state-of-the-art calculation of light element abundances compared with observation in the standard Big Bang model, from a paper by Schramm and Turner in 1998. The use of the present matter density as a variable follows from the simple power law already mentioned, namely, $\rho_r \rho_m^{-4/3} = constant$ throughout the expansion.

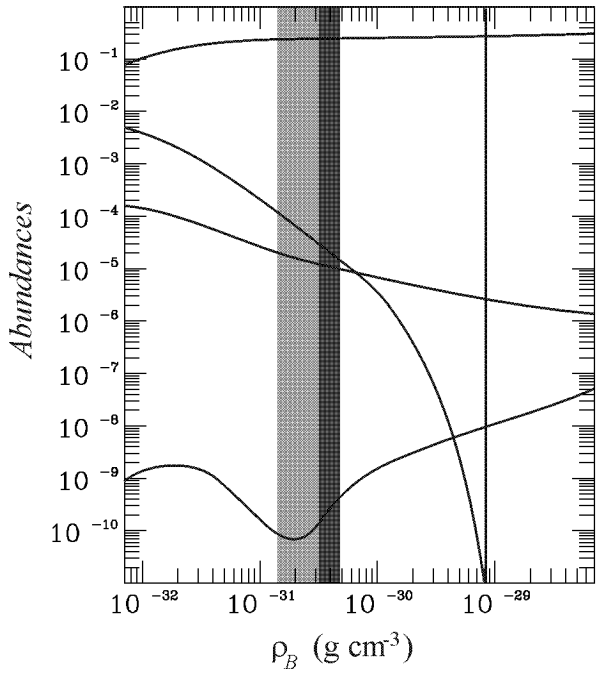

Figure 6: The most recent publishrd calculations of prestellar rewlative abundances, as published by Schramm and Turner in Reviews of Modern Physics, 1998.

Neutrinos in the Early Universe

We have characterized the simple Big Bang picture of nucleosynthesis as depending on one free parameter, namely, the density of matter during nucleosynthesis. However, as was found in the Alpher-Follin-Herman study, and in subsequent developments of nucleosynthesis calculations, the initial conditions for this period involve the choice of the number of neutrino families. This choice affects the density history prior to and during nucleosynthesis; most modern calculations indicate that the best choice is three families of neutrinos and their antiparticles. Some researchers conclude that the calculations suggest an upper limit of four families, so the matter may not be completely settled. Nevertheless, it appears currently that three is a good number, and subsequent to the statements supporting this, it was shown by experiments at CERN that there were indeed three. With the prediction of the background radiation, and the prediction that there should be three families of neutrinos, we have two cases in which cosmological prediction really preceded terrestrial observations.

If neutrinos indeed have nonzero mass, they would contribute significantly to the mean density of matter in the universe, although calculations suggest that while they are numerous, with number densities like those of photons, they are probably not massive enough to influence the formation processes in stars and galaxies, and would not yield a high enough density of all matter to make the universe closed.

The Initial Singularity in the Big Bang

The basic equations describing the Big Bang model, show a "singularity" at zero time. To put it differently, without introducing some new physical ideas, we would conclude that regardless of where one is in the universe, one would find an infinite density and an infinite temperature at the origin of time $t = 0$. Is there a simple way of avoiding this dilemma? Perhaps not, for Steven Hawking and Roger Penrose some years ago showed that a singularity was an inevitable concomitant of relativistic models of the universe, and of black holes. There are several ways which may possibly get around this dilemma. One which we have already mentioned is to consider that early in the standard model, prior to nucleosynthesis, there was a state of equilibrium which effectively screens us from knowing what went before such a state. Some would say that this is statement is "technobabble", and is not different from ascribing "creation" to a "Prime Mover" or other extramundane entity. A second is to invoke an "inflationary model" of the early universe, in which just after $t = 0$ the universe underwent one or more of a variety of changes from an initial vacuum state, time, matter and radiation coming into being. Models involving "quantum gravity" and inflation are outside the scope of this paper.

The Formation of Structure in the Universe

There is virtually no end of problems one may list which remain for cosmological modeling. One which has seen much activity during our lifetimes is the origin of structure in the cosmos. It is worth a comment that for the period of time when the microwave background radiation was thought to be remarkably isotropic, cosmologists were concerned about the formation of structure in a medium with no "seeds" for nucleation present. The observation of the 10^{-5} level departures from isotropy after several years of COBE data taking removes this concern, even though the transition to observed structure is not yet understood.

A major problem in all these matters is the now agreed-upon fact that the luminous matter by which we study objects in the heavens may only be a fraction of the matter present in these objects. There is "missing mass", whose nature is still not known. It is almost surely not all baryonic, for baryons in the required densities would have participated in early nucleosynthesis in the expanding universe and would have destroyed any agreement between theory and current observa-

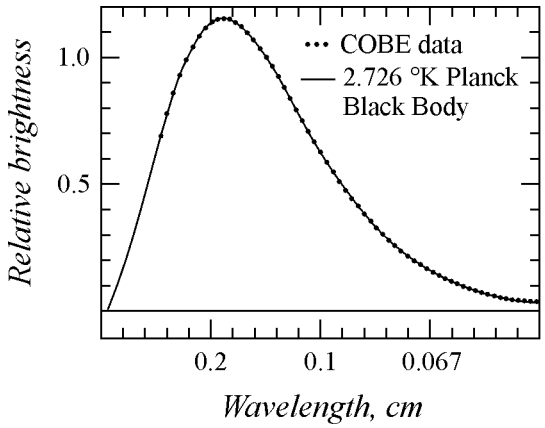

Figure 7: Measurement of the cosmic microwave background radiation carried out by the COBE satellite (John C. Mather, principal investigator at NASA-Goddard). The plot involves literally millions of data points, accumulated over four years, and is without doubt the most precise black body spectrum ever measured, with T = 2.726 kelvin as an extraordinarily accurate cosmological parameter. Error bars on the measurements lie within the width of the fitted line.

tion. The matter could not be very hot, because the chance of being captured by gravity in galaxies and clusters of galaxies would have been quite small. It might be some form of cold matter; or it might be condensations of matter into nonstellar objects. But again such objects would be baryonic, and the requirements of nucleosynthesis provide an upper limit on the number and mass of such objects. Nevertheless astronomers are seeking such objects, and new techniques are being employed, as for example, gravitational lensing or microlensing. The reality of such lensing, predicted by general relativity, has been amply demonstrated

The Cosmic Microwave Background (CMBR)

I have saved for last a discussion of the cosmic microwave background radiation (CMBR), work in which Herman and I have taken a lot of pride, but which also has caused us many problems. Let me return to the beginning of our CMBR foray. In the summer of 1948 Gamow was resident at Los Alamos, and sent us a draft of a short paper he was sending to *Nature*. There were some typically Gamowian problems with his paper, which dealt with a simplified view of light element nucleosynthesis, and consequences for galaxy formation, with essentially the same initial conditions which were developed in the alpha-beta-gamma paper. What these errors were is now of no interest, but suffice it to say that we pointed out the errors to him, and he encouraged us to submit a companion paper to *Nature*. I might mention that in his paper Gamow tried to calculate the size of a typical galaxy based on the conditions for primordial nucleosynthesis and using the Jeans criterion for condensations. In preparing our paper, Herman and I found that we could integrate the Friedmann-Lemaître-Robertson-Walker equations without approximation, and obtained a relationship connecting the densities of matter and radiation at any selected times in the cosmic expansion. (We quickly realized that it was far simpler to use the power law in Figure 5). In this 1948 note in *Nature* Herman and I said "... and the temperature in the universe at the present time is found to be about 5°K".

We published the procedure we used, as well as the results, in a number of papers in the next few years, and carried on a friendly argument with Gamow for several years on two major points. For one, he doubted that our calculation had any particular meaning, and for another, if there was a background radiation its observation in the vicinity of the earth would be confused with other radiation (Teller used the same argument), such as integrated starlight, providing comparable energy densities. We did point out the difference in the resulting spectrum. Gamow basically capitulated when in a 1950 paper he stated that the background temperature is 3°K, without any indication of where he got the number. It turns our that calculating the background radiation temperature in the Big Bang is absurdly simple. We noted that early in the expansion the universe is dominated and controlled by blackbody radiation. Assuming conservation of matter, and adiabatic expansion of radiation, then the power law in Figure 5 follows. Consider the situation at about one second into the expansion. We obtain the density of matter from the initial conditions for primordial nucleosynthesis. The density of radiation at that time depends only on universal constants, and is therefore unequivocally known. If now we have an observation at the present time of the mean density of matter, then the constancy of the above expression enables a calculation of the density of radiation, and thence the equivalent background radiation temperature. Using the present matter density suggested by Hubble in the late 1940s, we got about 5°K. Using more contemporary values of the matter density gives a background temperature compatible with the COBE results. It is unfortunately so that aside from the several publications in which Herman and described our results, Gamow went on to describe an approach in which he erroneously extrapolated approximations for early matter and radiation densities to the present time. Prior to 1965 there were eight publications on background radiation by Herman and me, and by Gamow, so that there was a rich supply of remarks in the literature. All of this was pretty well ignored by physicists and astronomers before 1965, except for some published work by Zel'dovich as well as Doroshkevich and Novikov in the Soviet Union, who referred to some of these calculations and suggested

the utility of measurements from artificial satellites. Zel'dovich misinterpreted some observations made by E.A. Ohm at the Bell Telephone Laboratories as limiting any background radiation from the cosmos to less than 1°K. Herman, Follin and I made a number of attempts from 1949 to 1955 to interest other physicists and radio astronomers in looking for a background radiation. In retrospect it should have been possible with existing technology, but we found no buyers. Even Gamow got in the act, for then-student Joseph Weber (later well known for his attempts to detect gravitational waves) was told that looking for the microwave background would be fruitless.

The year 1965 was a pivotal year for this subject, for Arno Penzias and Robert Wilson of Bell Telephone Laboratories reported observing a cosmic microwave background radiation at 7.3 cm corresponding to a temperature of about 3.5°K. They were not aware of our prior prediction or of the cosmological interpretation; their work was interpreted by a group including Dicke, Peebles, Roll and Willkinson at Princeton as the relict radiation from a primeval fireball (the Big Bang). The Princeton group had been setting up a Dicke radiometer to seek residual radiation from prior collapse of an oscillating cosmological model. They were able to verify quickly the work from the Bell Laboratories, and thus began a long series of observations by many scientists verifying the reality of this cosmic microwave background. This all culminated in the stunning observations over a period of several years by the COBE satellite, launched in 1989, of a nearly perfect Planck radiation distribution corres ponding to a temperature of 2.726°K, shown as Figure 7.

The back-to-back papers by Penzias and Wilson, and by the Princeton group, appeared in Astrophysical Journal in 1965 with no reference to the prior calculations by Herman and me. The only reference to our work or Gamow's work on the background radiation made in early Princeton papers was to the Alpher-Follin-Herman paper on conditions early in the universe. The more-than-eight references to the background were not listed.

I would remind you of several other COBE observations, namely confirmation of the motion of the observing system with respect to the surface of last scattering of the microwave background radiation, which puts a dipole component in the celestial background temperature data, measurable at an amplitude of several millikelvin. There are also small departures from uniformity in the background, at a level of about 10 parts per million, which appear to be residual fluctuations from the very early universe. These departures were a welcome observation, since they provide seeds for the later formation of structure in the expansion. These matters are outside the scope of this talk.

I want to comment briefly on a number of events associated with the microwave background, including observations prior to the Penzias-Wilson announcement, and the manner in which our prior work was ignored.

In 1940 and 1942, W.S. Adams of Mt. Wilson and A. McKellar of Dominion Astrophysical Observatory published observations in which they proposed a background radiation bath at about 2.3°K based on the occupation numbers of excited rotational states with assumed oscillator strengths of the CN molecule along the line of sight to the star ζ Ophiuchi. G. Herzberg mentioned these results later in his book on molecular spectra, with the comment that of course we do not understand their origin. The result was resurrected after the Penzias-Wilson publication, principally by N. Woolf and G. Field, who had knowledge of the observations, but lacked oscillator strength data to aid in interpretation. During the 1950s there were observations by Shmaonov in the Soviet Union, and by LeRoux in France, both of whom used captured German radar antennas to observe a background of several degrees Kelvin. There was no interpretation of the results, no cosmological connection, and I have seen no critique of their work. Finally, in the notebooks of a radio astronomer named William K. Rose, then at the Naval Research Laboratory, and now at the University of Maryland, there is a report of observation of a background radiation of 2.5–3°K, using an heterodyne receiver with a maser amplifier. The work was done in 1962, but Stephen Brush, science historian, has told me that Rose did not have an opportunity to verify his result, and did not publish. When informed years later, Penzias commented that the correction for a 15°K system background was questionable.

I will not comment in detail on the rocky road traveled by our work on primordial nucleosynthesis and particularly our CMBR prediction. In retrospect I still find it hard to believe most of happened. It gave us a jaundiced view of the level of scholarship exhibited by too many people. Herman and I, and occasionally Gamow, were torn between doing nothing, as the gentlemanly course, writing mild letters of protest, and on occasion sending strongly worded protests. However, our work now seems to have been widely accepted and recognized, for which we are grateful indeed.

Shortly before Gamow passed away, at his instigation he, Herman and I coauthored a paper (1967) trying to set straight the record of our involvement in cosmological matters. It appeared in the Proceedings of the National Academy of Sciences, which, as it turns out, is the wrong place to publish if the work is something you hope people will see.

In any event, I am pleased to have been allowed this time to go over the history of the Big Bang model, and of the role played by Herman, Gamow and me. I am sorry that I could not be at this meeting to express my personal thanks for my interactions with George Gamow and Robert Herman. They were fun while they lasted, which was not long enough.

Recommended reading list

(Admittedly incomplete)

Material with considerable technical content.

Alpher R.A. Gamow G. and Herman R.C. *Thermal Cosmic Radiation and the Formation of Protogalaxies, Proc. Nat. Acad. Sci.*, **58**, 2179 (1967)

Alpher R.A. and Herman R.C. *Reflection on Big Bang Cosmology*, and *Memories of Gamow, in Cosmology, Fusion and Other Matters* (F. Reines, Ed.), Colorado Associated University Press, 1972

Alpher R.A. *Large Numbers, Cosmology and Gamow, Amer. Scientist*, **61**, 52 (1973)

Alpher R.A. and Herman R.C. *Reflections on Early Work on Big Bang Cosmology, Physics Today*, **41** (8), 24 (1988)

Alpher R.A. and Marx G. *The Creation of Free Energy, Vistas in Astronomy,* **35**, 179 (1992)

Alpher R.A. and Herman R.C. *George Gamow and the Big Bang Model in The George Gamow Symposium*, *The Astronomical Society of the Pacific Conference Series* (E.Harper. W.C.Parke, and G.D.Anderson, eds.), **129**, 1997

Barrow J.D. and Tipler F.J. *The Anthropic Cosmological Principle* (Oxford University Press, New York, 1986)

Bernstein J. and Feinberg G. *Cosmological Constants: Papers in Modern Cosmology* (Columbia University Press, New York, 1986)

Bertotti B., Balbinot R., Bergia S. and Messina A. (Eds.) *Modern Cosmology in Retrospect* (Cambridge University Press, New York, 1990)

Coles P. and Lucchin F., *Cosmology: The Origin and Evolution of Cosmic Structure* (John Wiley & Sons, New York, 1995)

Einstein A. *The Meaning of Relativity* (Princeton University Press, Princeton, New Jersey, 1946

Hawley J.F. and Holcomb K.A. *Foundations of Modern Cosmology* (Oxford University Press, New York, 1998)

Hetherington N.S. (Ed.) *Encyclopedia of Cosmology* (Garland Publishing Co., New York, 1993)

Kolb E. and Turner M. *The Early Universe* (Addison-Wesley Pess, Reading, Massachusetts, 1990)

Kragh H. *Cosmology and Controversy: The Historical Development of Two Theories of the Universe* (Princeton University Press, Princeton, New Jersey, 1996)

Misner C.W., Thorne K.S. and Wheeler J.A. *Gravitation* (W.H.Freeman, San Francisco, 1973)

Partridge B. *3K: The Cosmic Microwave Background Radiation* (Cambridge University Press, New York, 1992)

Peebles P.J.E. *Principles of Physical Cosmology* (Princeton University Press, Princeton, New Jersey, 1993)

Sandage A.R., Kron R.G. and Longair M.S. (Contributors; edited by B.Binggeli and R.Buser) *The Deep Universe* (Springer-Verlag, Berlin, 1995)

Tolman R.C. *Relativity, Thermodynamics and Cosmology* (Clarendon Press, Oxford, 1934)

Weinberg S. *Gravitation and Cosmology: Principles and Applications of the General Theory of Relativity* (John Wiley & Sons, New York, 1972)

Books of More General Interest

Alpher R.A., Herman R. *Genesis of the Big Bang* (Oxford University Press), 2000 (in preparation)

Bartusiak M. *Thursday's Universe* (Times Books, New York, 1986

Bartusiak M. *Through a Universe - Darkly* (Harper Collins, New York, 1993

Chaisson E. *Cosmic Dawn: The Origins of Matter and Life* (W.W.Norton & Co., New York, 1981

Chown M. *Afterglow of Creation* (University Science Books, Sausalito, California, 1996

Ferris T. *The Whole Shebang: A State-of-the-Universe(s) Report* (Simon and Schuster, New York, 1997

Gamow G. *One Two Three....Infinity* (Viking Press, New York, 1947)

Gamow G. *The Creation of the Universe* (Viking Press, New York, 1952)

Gamow G. *My World Line-An Informal Autobiography* (Viking Press, 1970)

Guth A. *The Inflationary Universe* (Addison-Wesley Press, Reading, Massachusetts, 1997

Harrison E.R. *Cosmology: The Science of the Universe* (Cambridge University Press, New York, 1981

Kolb E.W. *Blind Watchers of the Sky: The People and Ideas that Shaped Our View of the Universe* (Addison-Wesley Publishing Co., Reading, Massachusetts, 1996)

Lankford J. (Ed.) *History of Astronomy: An Encyclopedia* (Garland Publishing Co., New York, 1997)

Lemaître G. *The Primeval Atom: A Hypothesis of the Origin of the Universe* (translated by B.H.Korff and S.A.Korff) (D.Van Nostrand Co., Inc., New York, 1950)

Mather J.C. and Boslough J. *The Very First Light* (Basic Books/Harper Collins, New York, 1996)

Munitz, M.K. *Theories of the Universe* (The Free Press, Glencoe, Illinois, 1957)

Narlikar J.V. *Seven Wonders of the Cosmos* (Cambridge University Press, 1999)

Silk J. *The Big Bang* - second edition (W.H. Freeman and Co., San Francisco, California, 1995)

Smoot G., and Davidson K. *Wrinkles in Time* (Wm. Morrow and Co., Inc., New York 1993)

Weinberg S. *The First Three Minutes* - updated edition (Basic Books/Harper Collins, New York, 1988)

SOME REFLECTIONS ON GEORGE GAMOW'S CREATIVE STYLE

I.B. Pustylnik

Department of Astrophysics, Tartu observatory
Tartu region, Toravere 61602, Estonia, *izold@aai.ee*

ABSTRACT. We discuss some aspects of the rich scientific legacy of George Gamow. Our analysis is based partly on Gamow's own scientific and popular books and articles, partly on reminiscences of his contemporaries. A special attention is given to G.Gamow's contribution to deciphering DNA genetic code and to the peculiarities of the "creative laboratory" of this unique figure in XXth century physics and cosmology.

Key words: history of astronomy, personalia: G.Gamow.

Distinguished guests, dear colleagues and friends.

Let me start with some remarks of a personal nature. It is a joy for me to be among the attendees of George Gamow's memorial conference. It is also a homecoming: almost forty years ago I graduated from the Mechnikov University in this charming city.

We have just heard a vivid and highly emotional talk presented by Professor of Colorado University, Igor Gamow who shared with us his impressions of an early childhood, reminiscences of his father accompanied by a touching amateur film commemorating George Gamow in a family circle. While I was watching so many young faces in this hall it seemed to me as if Georgij Antonovich's spirit was hovering somewhere inside these walls.

In my small contribution I will try to concentrate on some peculiarities of George Gamow's unique creative style without going into the technical details of his fundamental discoveries. This will be the subject of presentations prepared by cosmologists, specialists in relativity and theoretical physics. My modest analysis is based partly on Gamow's own books- "Thirty years that shook physics", "One, two, three... infinity", "Biography of Physics" and on two memorial volumes "Cosmology, Fusion and other Matters" and the most recent one - "The 1996 George Gamow Symposium"(held in Washington). It can be regarded as a continuation of my earlier article published three years ago in *Astronomical & Astrophysical Transactions* (see volume 10, p.167) and was based on my talk presented almost exactly five years ago at the first George Gamow international conference held in his home town. In that earlier publication we emphasized that Gamow's rich scientific legacy is being constantly reasessed because many recent spectacular achievements in space research and observational cosmology have brought about numerous confirmations of his prophetic forecasts.

One of the most amazing features of his talent is Gamow's lucid , transparent way of treating the most intricate problems of theoretical physics, visuality of his physical models, which manifests itself in the best way in his popular books still bringing his author a public recognition from world-wide audience after his earthy life. Let me illustrate this thought with just two examples. In his critical essay reviving Gamow's crucial role in elaborating the drop model of atomic nucleus American historian of science R.H.Stewer offers a straightforward explanation: "Possibly the very shape of the nuclear potential well - which when viewed from above resembles a volcanic cone containing energetic alpha particles inside it - sparkled his thoughts (The 1996 Gamow symposium, p.36). Here is another, perhaps, even more striking example of what S.Ulam defines as Gamow's urge " to find even in most abstract theories, motivations or similes, i.e. analogies with precisely understood models" (Cosmology, Fusion and other Matters, G.Gamow's memorial volume 1972, p.60). In his popular book "Biography of Physics" Gamow introduces an uninitiated reader to a rather intricate notion of quantum mechanics - penetration by alpha particle through a high potential barrier surrounding uranium nucleus. He uses a "visible simile", analogy between de Broglie waves and the waves of light. As always , he makes himlself illustration for his book and sketches the slab of glass reminding the reader a familiar in geometric optics phenomenon of the total internal reflection of light. Next making a mental experiment he draws another imaginary slab of glass supposedly only several wave-lengths away from the original one explaining through the Snail's law of refraction the difference between the geometric and wave optics thereby vividly illustrating how the photon can "jump" from one glass slab to the other without violating physical laws and thereby facilitating a comprehension of the mechanism leading to nuclear barrier penetration.

One cannot help feeling that this rare facet of

G.Gamow's numerous talents has something to do with his artistic perception of the world. Several following transparences demonstrate Gamow's abilities of a gifted artist. Of all these cartoons the illustrations of a jocular parody on Goethe's Faust chosen as an epilogue to his last book "Thirty Years That Shook Physics", a unique collective gallery of the portraits of the greatest physicists of our time , occupy a special place. As we argued in our earlier paper, in a sense it is symbolic because the book was completed only for years before the death of Gamow.

So looking at Gamow's cartoons and illustrations , reading picturesque stories narrating this or that amusing episode almost invariably accompanying his fundamental scientific accomplishments I have always had an impression that there is more behind the superficial fabric of events. Indeed, the following fragment taken from Alex Rich"s reminiscences of G.Gamow's substantial contribution to the solution of genetic code mistery is a tell-tale testimony of a rich "toolkit" in Gamow's creative laboratory. All of them served just one purpose to emanate the spirit of a "brain sturm". A.Rich recalls an early history of discovery of genetic code and resurrects an atmosphere of a great excitement and curiosity following the publication by J.Watson and F.Crick the idea of double-stranded structure of DNA molecule. This event catalyzed Gamow's interest in 1958 to an extent that he wrote a letter to J.Watson and F.Crick and explained these gentlemen without many preliminaries his keen interest and strong motivation for solving the problem of DNA detailed structure. With his characteristic intuitive instinct for the new Gamow immediately recognized that from the moment of Watson's and Crick's discovery biology in a broad sense had entered the realm of the exact science. And realizing the advent of this crucial moment he embarked upon the task of constructing the physical model of DNA structure and in a full accord with his artistic perception of the world in large also of illustrative model. Because of a novelty and a great complexity of the task he even departed from his self-proclaimed principle (voiced in "Thirty Years that Shook Physics"): "I never liked to work in crowded places". Apparently Gamow himself was not very enthusiastic about his early individual efforts to analyze relative abundances of aminoacids in proteins from tobacco mozaic virus (see his article "On Information Transfer from Nucleic Acids to Proteins", published in "Danish Biological Bulletin" and dedicated to the 70th anniversary of Porfessor Nils Bohr). So publishing a joint review paper with A.Rich and M.Ycas, Gamow with his coauthors creates a model in which they place DNA base-pairs, either adenine or thymine or guanine in a pair with cytosine along the DNA strand in a helical manner. In his own charismatic way of creating the atmosphere of improvised performance Gamow invents more or less during the same period the so-called RNA tie club. It was composed of 20 members - one for each amino acid. Gamow even visited the haberdrashery in Los Angeles and designed the ties depicting ring-like structures of purines and pyramidines, the bases of RNA. So the first printing of RNA structure was manifactured on linens ! The members of RNA club also had specially designed tie pins. Acting much as a producer or a stage director Gamow made a formal stationary for his club members. All of the members of the club were on the list of the stationary like actors in the stage production: Alex Rich was Lord Privy Seal, M.Ycas - archivist,F.Crick - the pessimist, Gamow himself - synthesizer. As in a good performance even minute details are important: even the pins with special engravings should not be distributed at random. One with inscription "Ala" belonged to Gamow himself (Why Ala ? "I always wanted to be a God and now I have a chance to be one"...) etc, etc. The status of honorary members of RNA club was introduced with four members one for each base of RNA molecule on rotating principle so that each member of the club finally could enjoy the privilege of becoming the honorary member. Gamow had an insatiable appetite for jokes especially for practical jokes (one of them is a mockery article on measuring the velocity of a moving body in a liquid using a snapshot of W.Pauli's body as a "test particle" submerged in the waters of Geneve lake, the transparence of which I demonstrated you a couple of minutes ago). As Dr.A.Rich recalls, once Gamow organized a meeting of his close associates - A.Rich, F.Crick and others but without his personal attendence. Together with his friend Max Delbrück he composed a fabricated letter from another colleague - a biologist announcing a complete deciphering of RNA structure including all minor details with angles and distances and amino acids polymerized, all as established and well-known facts. It took four hours of heated discussions with placing the different pieces of evidence on RNA structure this way or the other before one of the participants, as A.Rich recalls it, had a hunch that all of them once again became victims of Gamow's whimsical way of creating a "team spirit".

Let me finish this paragraph with the concluding quotation from the same article of Dr.A.Rich:"What Gamow did was to bring a kind of enthusiasm to the problem, and an intensity and focus. Likewise he pulled a large number of people from physical sciences into this kind of biology, later called molecular biology. I think this represented a kind of a turning point , because it changed the evolution of molecular biology, and pushed it forward into a field in which physical scientists could work closely and well with biological scientists and make a significant contribution." An intriguing question, which invariably emerges,whenever a scientific legacy of an eminent nuclear physicist is scrutinized, is an issue of the so-called Oppenheimer's syndrome. To what extent G.Gamow was prone to this

syndrome, how much reflections on devastative nature of the forces released from the "bottle" by him and his colleagues engaged in the chain reaction project preoccupied his inquisitive mind ? It is well-known that during the World War II Gamow worked at the American Navy high explosives laboratory with A.Einstein himself and with J. von Neumann. After the war Gamow was involved in the Bikini bomb test to study the effect of nuclear blast shock waves on the surface structure of ships and on hydrogen bomb project at Los Alamos jointly with E.Teller (for more details see the reminiscences of F.Saafeld in "The 1996 Gamow Symposium", p.26).

It seems to us that Gamow's famous cartoons to some extent betray his uneasy thoughts on this delicate issue. It's well known that during his work in the famous T-division Gamow sketched several mockery shields (reminding one the medieval courts of arms) dedicated to the project. One of them depicts the leader of T-division Mr.Carson Mark. The shield is encircled on all sides by motto "For he is a good, jolly fellow". Close to a portrait of a hero Gamow places a sinister atomic mushroom. Another corner of the same shield contains a number of figurines, presumably, the children of "jolly, good fellow" crawling out of something which look either as a belly of a whale or as a horn of plenty. Unwittingly, the whole picture emanates some apocalyptic-sarcastic or even sardonic expressiveness. Here is another (this time both amusing and ironical) example of G.Gamow's evasive style of treating the same ticklish subject. In his book "One,two, three... infinity" he muses: "In respect to nuclear energy we live (or rather lived until quite recently) in a world similar to that of Eskimo, dwelling in a subfreezing temperature for whom the only solid is ice and the only liquid alcohol. Such an Eskimo would never have heard about fire, since one cannot get fire by rubbing two pieces of ice against each other, and would consider alcohol as nothing but a pleasant drink ,since he would have no way of raising its temperature above the burning point. And the great perplexity of humanity caused by the recently discovered process of liberating on large scale the energy hidden in the interior of the atom can be compared to the astonishment of our imaginary Eskimo when shown ordinary alcohol burner for the first time"(One, two,three...infinity,p.168). Curiously enough, in the same book Gamow confides the principle of statistic disorder and even the burning question of the difference between living and non-living forms of matter again addressing the meaningful figure of alcohol. "We should have a much closer analogue of a biological process if, for example, the presence of a single alcohol molecule (C_2H_5OH) in a water solution of carbon dioxide gas should start a self-supporting synthesizing process that would unite one by one the H_2O molecules in the dissolved gas forming new molecules of alcohol. Indeed,if one drop of whiskey put into glass of ordinary soda water should begin to turn this soda into pure whiskey, we should be forced to consider alcohol as living matter"(One, two, three... infinity, p.236). And following this passage Gamow proceeds to a description of recent progress in studying the structure of the simplest living forms - viruses. So why spirituous after all ? Because it is as **contagious** as the virus or because G.Gamow himself brooding over the eternal questions of good and evil of his epoch, over the fate of his homeland, from time to time looked into the glass in a desperate search for an answer to questions tormenting him (see an article of D.I.Ivanenko in the supplement to Gamow's biography "My World Line" describing the difficult episodes in Gamow's life)...?

Close friends called him affectionately Geo. If one recalls the original meaning of the word for all of us, the inhabitants of this planet, it brings us once again to Goethe's immortal figure of doctor Faust. The concluding fragment (in Russian translation from Boris Pasternak) is equally applicable to an unique personality of Georgij Antonovich Gamow:

"On rvetsja v boj, i ljubit bratj pregrady, i vidit celj, manjashchuju vdali, i trebujet u neba zvezd v nagradu, i luchshih naslazhdenij u zemli, i vek jemu s dushoj ne budet sladu, k chemu by poiski ne priveli".

Acknowledgements. It's my pleasure to extend sincere expressions of gratitude to the SOC of Gamow's Memorial Conference for invitation to attend this Meeting, I acknowledge likewise support from the LOC of the Meeting and by Grant 2629 of Estonian Science Foundation.

References

Gamow G.: 1955, *"On Information Transfer from Nucleic Acids to Proteins, Biologiske Meddelelser*, bind **22**, nr.8, 1.

Gamow G.: 1961, *Biography of Physics*, Harper and Brothers Publishers, New York, 280.

Gamow G.: 1961, *In: One, two, three...infinity,* The Viking Press, New York.

Gamow G.: 1966, *Thirty Years That Shook Physics, the Story of Quantum Physics*, Heinemann, London.

Ivanenko D.D.: 1994, *"Gamow's Epoch Seen with the Eyes of His Contemporaries", In: G.Gamow, My World Line*, ed. Ju. Lisnevskij, VO Nauka, Moscow, 278.

Pustylnik I.: 1997, *Astron. & Astrophys. Trans.*, **10**, 167.

Rich A.: 1997, *"Gamow and Genetic Code", In: The 1996 Gamow Symposium*, ed. Harper E., Parke W.C., Anderson G.D., 115.

Ulam S.: 1972, *In: Cosmology, Fusion and Other Matters, G.Gamow Memorial Volume*, ed. Frederick Reines, London, 272.

WEAK-FIELD LIMIT OF THE CONFORMAL THEORY OF GRAVITY AND GALACTIC ROTATION CURVES

O. V. Barabash[1], Yu. V. Shtanov[2]

[1] Department of Physics, Shevchenko National University, Kiev 01022, Ukraine
[2] Bogolyubov Institute for Theoretical Physics, Kiev 03143, Ukraine
shtanov@ap3.bitp.kiev.ua

ABSTRACT. We study the weak-field limit of the static spherically symmetric solution of the locally conformally invariant theory, which is regarded as an alternative to Einstein's general relativity theory in explaining the flat galactic rotation curves. In contrast with the previous works, we consider the physically relevant case where the scalar field that breaks conformal symmetry and generates fermion masses is nonzero. In the physical gauge, in which this scalar field is constant in space-time, the solution reproduces the weak-field limit of the Schwarzschild–(anti) de Sitter solution modified by an additional term that, depending on the sign of the Weyl term in the action, is either oscillatory or exponential as a function of the radial distance. Such behaviour reflects the presence of, correspondingly, either a tachyon or a massive ghost in the spectrum, which is a drawback of the theory under discussion.

Key words: Gravity: conformal; galaxies: rotation curves.

One of the long-standing problems of modern cosmology is the so-called problem of dark matter [see, e.g., Peebles (1993)]. In general, this problem consists in the discrepancy between the amount of the observed luminous matter on various spatial scales and the assumption that this matter is the only essential source of gravitation. Thus, on very large scales, the amount of the present luminous matter is insufficient to account for the measured rate of expansion of the universe. On the galactic scales, the problem reveals itself, in particular, in a peculiar behaviour of the galactic rotation curves in spiral galaxies, which do not appropriately fall with the distance from the galactic centre. In a broad sense, the problem can be stated as the violation of the laws of the general relativity theory and can be expressed in the form of the inequality

$$G_{\mu\nu} \neq 8\pi T^*_{\mu\nu}\,, \qquad (1)$$

where $T^*_{\mu\nu}$ is the stress-energy tensor of the *observed* luminous matter and $G_{\mu\nu}$ is the Einstein tensor corresponding to the spacetime metric inferred from *observations* (we use the geometrized units, in which Newton's gravitational constant and the speed of light are equal to unity).

The common general solution of the above problem lies in the assumption that most of matter on the relevant spatial scales is invisible, so that an extra term should actually be present on the right-hand side of the above relation, thus restoring the equality. There exist several candidates for such dark matter, ranging from massive relic elementary particles (of known or predicted species) to compact objects of planetary type. The search for this dark-matter component is currently being continued.

In parallel to the above-mentioned common approach, some people consider another interesting possibility, namely, that it is not the right-hand side of Eq. (1) that is to be modified by the contribution from still undetected matter, but rather that it is its left-hand side that is to be somehow modified. In other words, it is assumed that the laws of the general relativity theory fail to be universally valid and must be replaced by some other laws. On this path, one certainly needs some guiding principles to decide how such a modification might be made.

Recently, Mannheim and Kazanas (1989) [see also Mannheim (1993, 1997, 1998), and references therein] explored the possibility that gravity is described by the conformally invariant theory with the key ingredient in the action being the Weyl term

$$\begin{aligned} I_{\rm W} &= -\alpha \int d^4x\sqrt{-g}\, C_{\lambda\mu\nu\kappa}C^{\lambda\mu\nu\kappa} \\ &= -2\alpha \int d^4x\sqrt{-g}\, \left(R_{\mu\nu}R^{\mu\nu} - R^2/3\right) \\ &\quad + \text{boundary terms}\,, \end{aligned} \qquad (2)$$

where $C^{\lambda}{}_{\mu\nu\kappa}$ is the conformal Weyl tensor and α is the purely dimensionless gravitational coupling constant. In particular, they obtained the complete *conformally* static spherically symmetric solution of the theory described by Eq. (2) with the line element given by

$$ds^2 = C^2(x)\left[-G(r)dt^2 + dr^2/G(r) + r^2 d\Omega\right], \qquad (3)$$

where $C(x)$ is an arbitrary nonzero function of the spacetime coordinates x, and $G(r)$ is given by

$$G(r) = 1 - \beta(2 - 3\beta\gamma)/r - 3\beta\gamma + \gamma r - \kappa r^2. \quad (4)$$

Here, β, γ, and κ are integration constants. Having tacitly assumed that test bodies move along the geodesics of the metric with the line element of Eq. (3) and with $C(x) \equiv 1$, Mannheim and Kazanas (1989) then claimed to recover the Newtonian term ($\propto 1/r$) in the potential of solution (4) of the conformal gravity theory and also suggested that the additional linear term γr in Eq. (4) might account for the flat galactic rotation curves without having to invoke dark matter.

It should be noted, however, that solution (3), (4) of the purely gravitational conformal theory defined by Eq. (2) is not quite relevant to the observations, since it is obtained without regard for the matter part of the theory that includes the mass-generation mechanism for the elementary particles and thereby for test bodies such as stars and planets. Such a feature of this solution is reflected in the unrestricted freedom of choosing the conformal factor $C(x)$ in Eq. (3) which clearly affects the timelike geodesics of the metric, but which is totally undetermined thus far. Moreover, the electrovac generalization of solution (3), (4) was previously obtained by Riegert (1984), who also asserted that one of the integration constants can be eliminated by further coordinate and conformal transformations. This property of the solution, with γ being such a constant, was noted and explicitly demonstrated by Schmidt (1984, 1999). All this makes very problematic the use of the metric given by the second expression in Eq. (3) and by Eq. (4) as an observable one.

Here, we consider this problem taking the matter to be represented by the generic conformally invariant action

$$I_{\rm M} = -\int d^4x\sqrt{-g}\left[\partial^\mu S\partial_\mu S/2 + \lambda S^4 - S^2R/12 + i\bar\psi\gamma^\mu(x)\nabla_\mu\psi - \zeta S\bar\psi\psi\right], \quad (5)$$

where ψ is the fermion field, S is the scalar field, R is the curvature scalar of the metric, and λ and ζ are dimensionless coupling constants. In the theory defined by Eqs. (2), (5), once the scalar field S is everywhere nonzero it can be gauged to an identical constant S_0 by a conformal transformation. In this gauge, the fermion part of the action acquires the standard form with constant mass, hence all physical effects receive the standard description; in particular, massive particles and test bodies move along the timelike geodesics of the metric as in the general relativity theory. It is clear that since conformal symmetry is broken and there are massive particles in the real world, one should take solutions with S being nonzero. The physical vacuum is then regarded as the state without excitations of the rest of the matter fields, in our case, the field ψ.

We consider solutions outside a compact source formed by the matter fields (represented in our model by the single field ψ). The equations of the theory have the form

$$4\alpha W_{\mu\nu} = T_{\mu\nu}, \quad (6)$$

where the two sides stem, respectively, from the variation of actions (2) and (5) with respect to the metric, and the expression of the stress-energy tensor $T_{\mu\nu}$ in the gauge $S \equiv S_0$ and with the ψ field being zero is given by

$$T_{\mu\nu} = -S_0^2\left(R_{\mu\nu} - g_{\mu\nu}R/2\right)/6 - \lambda S_0^4 g_{\mu\nu}. \quad (7)$$

Equations (6) with the right-hand side given by Eq. (7) are nothing but the Bach–Einstein equations with the cosmological constant term—the last term in Eq. (7). Note that the left-hand side of Eq. (6) is identically traceless, and it is convenient to rewrite system (6) as

$$4\alpha W_{\mu\nu} = \mathcal{T}_{\mu\nu}, \quad R = 24\lambda S_0^2, \quad (8)$$

where $\mathcal{T}_{\mu\nu} \equiv -S_0^2\left(R_{\mu\nu} - g_{\mu\nu}R/4\right)/6$ is the traceless part of the stress-energy tensor $T_{\mu\nu}$, and the second equation of system (8) is the trace of Eq. (6).

We restrict ourselves to the static spherically symmetric case. As we explained above, we are interested in the situation where $T_{\mu\nu}$ is given by Eq. (7) with constant nonzero S_0. In this gauge, a static spherically symmetric metric can be put in the form

$$ds^2 = -B(r)dt^2 + A(r)dr^2 + r^2d\Omega\,. \quad (9)$$

It appears to be difficult to obtain the exact general solution for $A(r)$ and $B(r)$. However, it is possible to obtain solution in the weak-field limit. Let the physical metric of Eq. (9) in the spatial region of interest be sufficiently close to the flat one, so that

$$A(r) = 1 + \epsilon a(r), \quad B(r) = 1 - \epsilon b(r), \quad (10)$$

where ϵ is an auxiliary small parameter to be set equal to unity in the end.

To obtain the system of equations for the functions $a(r)$ and $b(r)$, we must linearize the equations of system (8) for the metric of in the small parameter ϵ. We note that the scalar curvature R of this metric is of order ϵ. Hence, the second equation of system (8) implies that the dimensionless value of $\lambda S_0^2 r^2$ should also be at least of order ϵ in the spatial region under consideration. On observational grounds, this restriction on the value of $\lambda S_0^2 r^2$ is quite natural since this value represents the effect of the cosmological constant, which is believed to be small on the galactic and stellar spatial scales. However, from the theoretical viewpoint, such a restriction constitutes the fine-tuning problem of the cosmological constant. The solution of this long-standing problem is absent, so we formally replace λ by $\epsilon\lambda$, thus taking into account the smallness of the corresponding parameter.

Omitting the calculations, which can be found in Barabash and Shtanov (1999), we present here the resulting solution. We make the notation

$$p = \frac{S_0^2}{24\alpha}\,, \quad q = \lambda S_0^2\,, \tag{11}$$

and note that solution depends on the sign of the constant p that coincides with the sign of α. First, we consider the case where $p > 0$. We obtain

$$a(r) = 2m/r - 2qr^2 + n\left[\sin\left(kr+\phi\right)/r - k\cos\left(kr+\phi\right)\right]\,, \tag{12}$$

$$b(r) = \left[2m + 2n\sin\left(kr+\phi\right)\right]/r - 2qr^2\,, \tag{13}$$

where $k = \sqrt{p}$, and n and ϕ are integration constants. We see that in the Newtonian limit, apart from the universal term qr^2, there arises the additional gravitational potential

$$V(r) = -\frac{m + n\sin\left(kr+\phi\right)}{r}\,, \tag{14}$$

in which the constants m, n, and ϕ are to be related to the source. The constants $k = \sqrt{p}$ and q are universal and are given by Eq. (11).

We note that the linearized static spherically symmetric solutions in a generic (not conformally invariant) second-order gravitational theory without the cosmological constant were obtained by Stelle (1978). Their structure is similar to that of Eqs. (12), (13) and to solutions (25), (26) below. However, it is not possible to pass to the direct limit of conformal invariance in the solutions of Stelle (1978), because the case of conformal invariance is characterized by a nontrivial degeneracy, in particular, the massive scalar degree of freedom that is present in a generic case is missing here [see also Schmidt (1985*a*, 1985*b*, 1986) in this respect].

Now suppose that a static compact source is composed of identical "atoms" (these may be real atoms or elementary particles) and that each of these atoms produces static gravitational potential as given by Eq. (14) with identical constants m, n, and ϕ. In view of the weakness of the potential, we also assume the validity of the superposition principle. Then, if $\mu(\mathbf{r})$ is the spatial distribution of the "atoms" in the source, the total potential is given by the expression

$$\Phi(\mathbf{r}) = \int V\left(|\mathbf{r}-\mathbf{r}'|\right)\mu\left(\mathbf{r}'\right)d\mathbf{r}'. \tag{15}$$

This potential is the sum of two terms: $\Phi(\mathbf{r}) = \Phi_m(\mathbf{r}) + \Phi_n(\mathbf{r})$. They satisfy the equations

$$\Delta\Phi_m(\mathbf{r}) = 4\pi m\mu(\mathbf{r}), \tag{16}$$

$$\Delta\Phi_n(\mathbf{r}) + p\,\Phi_n(\mathbf{r}) = 4\pi n\sin\phi\,\mu(\mathbf{r}), \tag{17}$$

that, in the theory under investigation, correspond to the unique Poisson equation of the linearized general relativity theory.

For a spherically symmetric compact distribution $\mu(r)$, the potential given by Eq. (15) with the kernel given by Eq. (14) is easily calculated:

$$\Phi(r) = -\int_r^\infty \frac{M(r')}{r'^2}dr' - \frac{N\sin(kr+\phi)}{r} - \frac{4\pi n\sin\phi}{kr}\int_r^\infty \mu(r')\sin\left[k\left(r-r'\right)\right]r'dr', \tag{18}$$

where

$$M(r) = 4\pi m\int_0^r \mu(r')r'^2dr', \tag{19}$$

$$N = \frac{4\pi n}{k}\int_0^\infty \mu(r')\sin\left(kr'\right)r'dr'. \tag{20}$$

Thus, outside the source, the potential of the form (14) is reproduced with the same phase ϕ, but with different coefficients m and n. Moreover, while the coefficient m is additive (it plays the role of the gravitational mass of the source), the coefficient n is not: its new value N is given by Eq. (20). However, the coefficient n becomes approximately additive for a distribution whose spatial size is significantly less than $1/k$.

If the product $kr < 1$ in the region of interest (say, on galactic scales), one can expand the oscillatory part of Eq. (14) in powers of kr to obtain

$$V(r) = V_0 - \frac{M_0}{r} + \frac{\Gamma r}{2} + Qr^2 + \mathcal{O}\left[(kr)^3\right]\,, \tag{21}$$

where $V_0 = -nk\cos\phi$, $M_0 = m + n\sin\phi$, $\Gamma = nk^2\sin\phi$, and $Q = q + nk^3\cos\phi/6$. We thus recover the linear term in the potential of Eq. (21), similar to that which occurs in Eq. (4) and which was used by Mannheim and Kazanas (1989) to account for the flat galactic rotation curves. However, there exists an important observational bound that rules out the possibility for the linear term in expansion (21) to play a significant role on galactic scales. Note that the coefficients $-g_{00}(r)$ and $g_{rr}(r)$ of the metric of our solution are not mutually inverse, which is reflected in the fact that the functions $a(r)$ and $b(r)$, given, respectively, by Eqs. (12) and (13), are not equal to each other. At small enough distances, both functions reproduce the Newtonian potentials with the masses, respectively, $m_0 = m + n\sin\phi$ and $m_1 = m + (n\sin\phi)/2$, the difference between them being $\Delta m = (n\sin\phi)/2$. At the same time, the *Viking* spacecraft observations in the vicinity of the Sun indicate that the ratio $\Delta m/m \lesssim 2\times10^{-3}$ [see Will (1993)]. This implies the following observational bound for the Sun:

$$\frac{n\sin\phi}{m} \lesssim 4\times10^{-3}. \tag{22}$$

Since we assume that the parameter k is sufficiently small so that expansion (21) is legitimate on galactic scales, the values of both m and n are additive on such scales and estimate (22) is valid on galactic scales as

well. Now, the linear term in Eq. (21) formally becomes comparable in magnitude to the Newtonian one only at the distance $r \sim \sqrt{M/\Gamma} \approx \sqrt{m/(nk^2 \sin\phi)}$. But, for such distances, we would have $kr \sim \sqrt{m/(n \sin\phi)} \gtrsim 10$ because of estimate (22), which contradicts the original assumption $kr < 1$. Thus, the linear term in expansion (21) cannot play a significant role on galactic scales, and one should rather try the exact potential in the form (18) for a spherically symmetric source with the bounding condition (22) to account for the galactic rotation curves.

It is instructive to estimate the realistic value of the constant α in Eq. (2) for which the value of kr is of order unity on a typical galactic scale of 10 kpc, thus making the potential of the form (14) in principle relevant to the galactic rotation curves. Whatever scalar fields are present in the theory, they all contribute to the value of p given by Eq. (11). Thus, at least the scalar Higgs field of the standard model of strong and electroweak interactions should be taken into account. The mean value of this field is known to be $\eta \simeq 246$ Gev; this value will contribute to S_0 in Eq. (11) and, in order that $k \times (10 \text{ kpc}) \lesssim 1$ be valid, we must have

$$\alpha \gtrsim 10^{74}, \tag{23}$$

which, of course, is a severe restriction. It is difficult to conceive models in which this restriction is substantially weakened without fine-tuning.

On the other hand, if we take $\alpha \sim 1$, then the expectation value $\eta \simeq 246$ GeV of the standard model Higgs field leads to the spatial scale

$$1/k \sim 10^{-16} \text{ cm} \tag{24}$$

on which potential (14) oscillates. Its significance might only be manifest on the spatial scales of elementary particles, where, of course, the whole theory must be quantized.

In the case $p < 0$, which corresponds to $\alpha < 0$, the solution for $a(r)$ and $b(r)$ has the form

$$\begin{aligned} a(r) &= 2m/r - 2qr^2 \\ &+ n_1 (1 + kr) e^{-kr}/r + n_2 (1 - kr) e^{kr}/r, \end{aligned} \tag{25}$$

$$b(r) = 2m/r - 2qr^2 + 2n_1 e^{-kr}/r + 2n_2 e^{kr}/r, \tag{26}$$

where now $k = \sqrt{-p}$, and n_1 and n_2 are integration constants. Similar solutions in a generic second-order gravitational theory (not conformally invariant) without the cosmological constant were obtained by Stelle (1978). Solutions in the conformally invariant second-order theory with the Einstein term but without the cosmological-constant term were also obtained in Schmidt (1985*a*, 1985*b*, 1986). The physically meaningful solution is selected by imposing boundary conditions at infinity, which leads to the condition $n_2 = 0$. For sufficiently small values of k, the observational bound similar to condition (22) implies

$$\frac{n_1}{m} \lesssim 4 \times 10^{-3}, \tag{27}$$

and makes the extra exponential potential in Eq. (26) uninteresting.

Finally, we note that in the case $p < 0$, which corresponds to $\alpha < 0$, one also can obtain solutions by formally replacing the trigonometric functions in Eqs. (12), (13), and (14) by their hyperbolic counterparts and taking $k = \sqrt{-p}$. Equations (16), (17) will then remain valid in this case as well, with the replacement of $\sin\phi$ by $\sinh\phi$. The structure of the left-hand sides of Eqs. (16), (17) reflects, besides the presence of the massless graviton, also the well-known presence of a spin-two tachyon (in the case of $\alpha > 0$) or a spin-two massive ghost (in the case of $\alpha < 0$) on the background with $S \neq 0$ of the theory described by Eqs. (2), (5) [see, e.g., Stelle (1978)]. The presence of a tachyon in the case $\alpha > 0$ indicates instability of a large class of solutions, including the flat space-time solution in the case $\lambda = 0$; and the presence of a ghost in the case $\alpha < 0$ implies possible absence of perturbative unitarity in the corresponding quantum theory. This appears to be the main drawback of the conformal theory under discussion.

Acknowledgements. The authors are grateful to P. Mannheim for valuable discussions. This work was supported in part by the Foundation of Fundamental Research of the Ministry of Science of Ukraine under grant No. 2.5.1/003.

References

Barabash O.V., Shtanov Yu.V.: 1999, *Phys. Rev. D*, **60**, 064008.
Mannheim P.D., Kazanas D.: 1989, *Ap. J.*, **342**, 635.
Mannheim P.D.: 1993, *Ap. J.*, **419**, 150.
Mannheim P.D.: 1997, *Ap. J.*, **479**, 659.
Mannheim P.D.: 1998, *Phys. Rev. D*, **58**, 103511.
Peebles P.J.E.: 1993, *Principles of Physical Cosmology* (Princeton University Press, Princeton, N.J.).
Riegert R.J.: 1984, *Phys. Rev. Lett.*, **53**, 315.
Schmidt H.-J.: 1984, *Ann. Phys. (Leipz.)*, **41**, 435.
Schmidt H.-J.: 1985*a*, *Astron. Nachr.*, **306**, 67.
Schmidt H.-J.: 1985*b*, *Astron. Nachr.*, **306**, 231.
Schmidt H.-J.: 1986, *Astron. Nachr.*, **307**, 339.
Schmidt H.-J.: 1999, gr-qc/9905103, Report No. UNIPO-MATH-99-May-27.
Stelle K.S.: 1978, *Gen. Rel. and Grav.*, **9**, 353.
Will C.M.: 1993, *Theory and Experiment in Gravitational Physics* (Cambridge University Press, Cambridge).

POLYGONAL ARMS IN GRAND DESIGN SPIRALS

A.D. Chernin[1,2]

[1]Sternberg Astronomical Institute, Moscow University
Universitetskii Pr., 13, Moscow 119899 Russia, *chernin@sai.msu.ru*
[2]Tuorla Observatory, University of Turku
Piikkiö 21500 Finland

ABSTRACT. The phenomenon of polygonal arms in grand design spiral galaxies is reviewed. The Whirlpool Nebula, Messier 51 (NGC 5194) in Canes Venatici, is taken as an archetypical example. Optical photographs, H_α, UV and far-UV images, CO, 21 cm, sinchrotron emission maps, K_s-band mosaic of M 51 are used to recognize the global spiral pattern in M 51 which contains multiple straight arm segments and is presented by two polygons almost entirely. The polygons are almost identical, and the pattern has approximate twofold symmetry. The length of the straight arm segments is about the distance from the center of the disk. The segments intersect one another at the angle which is in average $\approx 2\pi/3$. A brief list of galaxies with straight segments (M101 including) is given. The wave nature of the phenomenon is argued. A gasdynamical approach is discussed which implies that the formation of straight arm segments might be due to the generic stability of flat shock fronts and the tendency of a slightly curved shock front to get flat. A quantitative flattening criterion, based on this assumption, enables to explain the geometrical properties of the arm patterns found in M 51 and some other grand design spirals. Same considerations seem to be applicable to the ring structures that have a form of almost regular hexagons in a dozen disk galaxies.

Key words: Galaxies: spiral; Stars: formation.

1. Introduction: M51

The nearly face-on giant Sbc spiral Messier 51 (NGC 5194), one of most photogenic, constitutes a textbook example of a spiral structure. I do not know exactly who gave this galaxy its name The Whirlpool; may be it was Lord Rosse who was the first to detect the spiral nature of certain nebulae, now known to be galaxies. The Whirlpool Galaxy is one of the most symmetrical galaxies in the sky. Spirals exhibiting this high degree of symmetry and large-scale regularuty are often called grand design spirals. Presumably, they have been formed by some global process that involves the whole galaxy.

The geometry and physics of the spiral pattern of M51 is in the focus of my discussion here.

2. Polygonal pattern

Photographs of M51, like ones made by Zwicky in the 50s, are dominated by the blue light from luminous, young O and B stars and the regions of ionized hydrogen (HII). Since O and B stars live less than 10 Myr (compared to the age of the galaxy 10 Gyr), they can be seen only in the regions of recent star formation. Spiral arms are no doubt regions of rapid and effective star formation. The HII regions are also young objects; in Baade's apt phrase, they are "strung out like pearls along the arms".

There are dark strips on the inside of each arm which are well recognizable on the photograph in "The Hubble Atlas of Galaxies"; as Sandage noted there, "the entire spiral pattern of M 51 is dominated by the dust lanes". The dark strips are believed to be caused by absorbtion of the galaxy's starlight in dense clouds of gas and dust.

Looking at the photographs of M51 and following the shape of the arms as it is traced by the dust lanes, one can realize that the major spiral arms of the galaxy contain segments of different forms. The images demonstrate almost perfectly curved arm elements near the center of the disk. It is also obvious at a glance that out of the very central area, several arm segments are fairly straight. More careful analysis (Chernin 1999) has been done with the use of not only optical photographs, but also H_α, UV and far-UV images, CO, 21 cm, sinchrotron emission maps, K_s-band mosaic of M 51. The analysis shows that:

* the spiral pattern of M 51 contains 5 fairly straight arm segments in the EN arm and 4 in the WS one;

* the segments form two polygons which represent each arm almost entirely;

* the polygons are almost identical, and the pattern has approximate twofold symmetry.

* the length of a straight segment is about its distance from the center of the disk;

* the segments intersect one another at the angle which is in average $\approx 2\pi/3$.

At least a dozen other grand design spirals seen face-on demonstrate a similar geometry of arm patterns. For more than 50 straight segments recognized in the galaxies of this sample, the characteristic angle is mostly around $2\pi/3$ and the lengths of the segments is about their distances to the centers of galaxy disk (Chernin *et al.* 2000a).

It seems instructive that the polygonal pattern in M51 (and also in other galaxies) is traced by the youngest populations of the arms which are gas/dust clouds of the dust lanes, H II regions and bright blue stars. If to look at the galaxy M51 in red light dominated by older disk stars, one may see that the red stars exhibit a spiral pattern similar to the blue stars, but with smoother and broader arms. The old disk population participates in the spiral pattern, but its space distribution is remarkably differnt from the distribution of the O and B stars or HII regions. No straight forms are seen in red light.

3. Vorontsov-Velýaminov: rows in arms

The discussion of straight arm segments dates back to Vorontsov-Velýaminov (1951, 1964, 1978). He called these features **rows** and described them as "straight-line segments of a spiral arm in the form of elongated star clouds" or "chains of knots that are consisted of hot giants and open clusters".

Several spirals with straight arm segments (but not M51!) were listed in his book "Extragalactic Astronomy" . The nearest giant galaxy M 101 was pointed out a typical example. Two very large and bright rows can easily be recognized in the Eastern major arm of M 101. They are seen in both a blue photograph and the distribution of the column density of HI. Rows are not only large, but also bright forms. In M 101, they are among the brightest (and bluest) elements of the spiral arms. Huge superassociations and giant HII regions prefer to settle in them, like NGC 5461 and NGC 5462 in M 101.

The discovery of rows has not attracted much attention for decades; perhaps this is partly because of some episodes in astronomy when geometrical interpretation of spatial patterns in the sky led to spurious conclusions (canals on Mars or ring configurations of stars on the Palomar Sky Survey images, *etc.*). Such misinterpretation may be due to the human eye's propensity to connect the dots in a regular manner and see patterns where none actually exist.

However, the interpretive difficulties of this type can be avoided in the case of Vorontsov-Vel'yaminovs's rows. The reality of the straight segments in the spiral structure of the archetype galaxy M 101 can be confirmed by comparing the features discovered in optical images with stellar and interstellar tracers at other wavelengths. The most impressive data on the spiral pattern of the galaxy M101 has recently been provided by the Shuttle-borne Ultraviolet Imaging Telescope. The deep FUV image has revealed that the spiral arm morphology consists of a dozen linear arm segments traced by a disk-wide system of bright knots (Waller *et al.* 1997). With the distance 7.4 Mpc and a radius 30 kpc, the largest outer straight segment in the Eastern arm is 23 kpc in length, being 2-3 kpc across. The other rows have the lengths in the interval of $5 - 13.6$ kpc. They intersect one another often at angle $\approx 2\pi/3$ (Waller *et al.* 1997). A polygon pattern may be recognized in two grand design arms of M 101 (Chernin 1998); a relatively small scale straight segments are found also in the irregular flocculent arms there (Waller *et al.* 1997).

More than 150 spirals with straight arm segments, including M 61, M 99, M 100, NGC 628, NGC 1232, NGC 1365, NGC 2997, NGC 3184, NGC 3631, NGC 4303, NGC 3310, NGC 3147, NGC 1179, NGC 1187, NGC 4535, NGC 5427, NGC 3938, NGC 6221, NGC 6946, NGC 7424, NGC 6744, NGC 7137, NGC 1313, are in the list which is now under preparation at Sternberg Institute (Arkhipova *et al.* 2000).

4. Polygonal pattern: tides or waves?

Do the polygonal pattern have material nature or wave nature? Waller *et al.* (1997) suggested that the straight segments in the arms of M101 had material nature and were due to tidal processes. On the contrary, I assumed (Chernin 1999) that these structures (at least in M51) were of wave nature.

Waller mention (in our personal exchange) that perhaps one of the best ways to determine whether tidal processes or wave processes are responsible for generating the straight-arm segments is to look for spatio-temporal evidence of propagating waves. For wave-dominated dynamics, there should be a spatial offset between tracers of the most recent star formation and tracers of more evolved stellar populations. If no offset is evident, then we are looking rather at material arms that have been drawn out by tidal action.

Waller did this sort of investigation in the center of M101, using CO emission and FUV emission as respective tracers of the current-epoch starbirth and the evolved blue supergiants $\simeq 3$ Myr downstream. In the inner galaxy, he found some spatial offsets (Waller *et al.* 1997). In the outer parts of M101 where the straight segments predominate, the image registration is trick, and so the work has not yet been completed. O'Connel has had some success comparing H_α and FUV in M51, finding some good offsets in the WS arm and inner EN arm (astro-ph/9706265), both of which show polygonal morphology.

The most impressive *prima facie* evidence for the off-

sets in M51 is given by the systematics in the positions of the dust lanes and bright stars along the polygonal arms there: the stars are regularily behind the dust lanes downstream. We can conclude that the wave nature of the polygonal grand design arms has all the grounds to be adopted.

However the nature of the small-scale straight segments in flocculent (not grand design) arms needs more studies.

5. Density waves and shock waves

The spiral structure in stellar disks is regarded as a density wave, a wave-like ascillation that propagates through the disk in much the same way that waves propagate through violin string or over the ocean surface. It was first recognized by C.C. Lin and F. Shu in the early 60s. As a wave parcel, the spiral structure rotates as a whole with a constant angular velocity, while the disks may rotate differentially. This is the basis of the current understanding of the phenomenon.

Propagating spiral waves should have their generator. In M 51, it is most probably the companion galaxy NGC 5195: it excites the wave pattern and supplies it with energy. In galaxies with bars, the spirals are most likely excited by the bars.

The profile of the density wave in M51 is directly seen in the distribution of the red old stars (Sec.2): the density wave ridges have a smooth round shape without any straight segments.

It has also long been recognized that the dust lanes are actually the fronts of spiral shocks seen edge-on when a galaxy is seen face-on. In the lanes, the interstellar gas is shocked into dense layers which obscure the starlight. This interpretation was suggested by W.W. Roberts and independently S.B. Pikelner in 1969. They argued that the fronts form when the gas of the galaxy disk passes through the gravitational potential of a density wave. The gravitational potential has minima along the spiral arms where the density of star distribution is higher. The gas falls into the potentiall well of a density wave and then leaves the well, but it loses its velocity partly in this process. The change of the velocity is rather sharp, and this means that the physics of the process is the same as in shock waves. It is this sharp decrease in the flow velocity that shocks the gas into the dense layers along the spiral arms. And just in these layers, new stars form.

When we look at the pattern of dust lanes (or the ridges of the synchrotron emission which practically coinside with the dust lanes) in M 51, we actually see adge-on two global shock fronts along the arms there. The shock fronts are curl in the central region of M51 and flat in the outer straight segmets. It means that the shock wave follows the lines of minima of the potential, but only in general. Withing the potential wells of the density wave, the shock fronts have their own spatial structure, and they may be flat where the potential well is round.

6. Why are they flat?

Why does a shock front get flat in the round potential wells of the spiral arms? I do not have an ultimate answer, and a conjecture can only be suggested. Perhaps this phenomenon is due to the generic propencity of any shock front for minimizing its surface. This tendency can be observed in a number of gasdynamical examples and may be perhaps formulated as a kind of theorem in the spirit of variation principles. From my discussions with V.M. Kontorovich and other experts in shocks, I learned that this may be probable, generally.

A more specific assumption about the flattening phenomenon implies that the formation of straight arm segments might be due to the gasdynamical effect of stability of flat shock fronts and the tendency of a slightly curved shock front to get flat. I suggest a quantitative flattening criterion, based on this assumption, which says that the size of the flattening shock front is near the local radius of curvature of the potential well of the arm where the shock forms (Chernin 1999). If so, one can explain why the length of a straight segment is about its distance from the center of the disk and why the segments intersect one another at the angle which is in average $\approx 2\pi/3$ (Sec.2). This follows simply from the shape of the gravitational potential well which may closely be described by a logarithmic (selfsimilar) spiral (with k ¡ 1).

Flattening is possible provided that the potential well of the arm is wide enough to contain a flat front of the size of the local radius of curvature of the well. Unfortunately, this is all I can now answer to the question why this galaxy has straight segments, but another one does not. The existence of the straight segments depends most probably on the width of the underlying gravitational potential wells. The width of the well may be related to such global physical characteristics of the disks as mean velocity dispersion in star distribution, etc. It would be interesting to try to find correlations between the existence of straight segments with these global properties of the disks.

7. Hexagonal rings

A considerable fraction of all disk galaxies reveal large-scale global structures which are described as rings, pseudorings or lenses (see Vorontsov-Vel'yaminov 1978, Buta and Combes 1996). In some of them, rings look rather like more or less regular hexagons with straight segments. This is, for instance,

NGC 7020 (Buta and Combes 1996). A list of hexagons one may found is not too long; together with NGC 7020 or NGC 4429, it includes NGC 3081, NGC 3351, NGC 4429, NGC 6782, NGC 6935, PGC 31551, UGC 12646, ESO 325-28, ESO 565-11.

It is interesting that a pseudoring with "a characteristic hexagonal shape" (Buta and Combes 1996, p.104) is put in the central sketch of the de Vaucouleurs and de Vaucouleurs's three-dimensional classification in the cross section near Sb. The galaxy NGC 4303 is mentioned as a model for this sketch; but it proves to be rather a spiral with polygonal arms: one can clearly see this, for instance, in the Atlas by Sandage and Berdke.

Better images for some of the galaxies with hexagons we listed will perhaps lead to a similar re-examination of their morphology. Nevertheless, one may expect that at least the galaxies NGC 3081, NGC 3151, PGC 3351, and UGC 12646 will survive as closed hexagons.

What is the place of hexagonal structures in the general variety of galaxy morphologies? Why they are just hexagonal, and no closed pentagons or septagons are observed? What may be their physical nature? In a recent note (Chernin *et al.* 2000b), we try to approach these questions by examining a possible relation of hexagons to the polygonal arm patterns.

The major similarity between hexagons and polygons is that both structures are made of straight segments. Another property is more special: in both patterns, the angle between two straight segments is about $2\pi/3$, and the length of a segments is near the distance from the center of the disk. If these geometrical properties are generic or crucial for the phenomenon of straight segments, this may explain why we see hexagons, but not, for instance, pentagons or septagons.

The similarity in geometry suggests that both phenomena may have a common physical nature. Arguing along this line, one may assume that the hexagons are also made of flat segments of shock fronts. Hydrodynamical simulations by Guivarch and Athanassoula (1996) seem to support this view: regular hexagons made of flat layers of shocked gas may appear as a reaction of interstellar gas to a (strong) bar. On the other hand, the same simulations may be considered also as an argument for our general gas-dynamical approach to the phenomenon of straight segments and polygonal patterns.

8. Conclusions: back to M51

The galaxy M51 with its large angular diameter and prominent spiral pattern has been a favorite target of astronomers for more than 150 years since the first observations by Lord Rosse. The phenomenon of polygonal pattern found in M51 shows the morphology, dynamics and evolution of spiral (and also ring) galaxies in a new light. The phenomenon is closely related to basic physical processes that make galaxies look as they do. A complex interplay of density waves in the distribution of stars and shock waves in the disk gas is behind the phenomenon.

In conclusion, I would like to note that the physics of polygonal arms reveals also in systematics in the location of brightest OB/H II complexes in the arms of M51. It may be demonstrated that the objects occupy predominantly the areas around the corners of the polygonal arms of this galaxy (Chernin 2000). An interpretation of the phenomenon assumes that complex gas flows around the corners of the polygonal arms must include additional shock fronts and tangential discontinuities, as it follow from the general gasdynamical theory of shock-front intersections. These flows can enchance star formation because of extra compression of gas in the additional shocks and/or turbulization of gas via decay of the tangential discontinuities.

A similar assumption for hexagonal rings is definitely supported by the gasdynamical simulations by Guivarch and Athanassoula (1996); it is essential that these simulations describe also star formation process: the process is evidently enchanced in some of the the corners of the hexagons.

Acknowledgements. I thank Yu.N. Efremov, A.V. Zasov and V.M. Kontorovich for suggestive discussions, V.P. Arkhipova and A.S. Kravtsova for cooperation, and W.H. Waller for interesting correspondence. A partial support from a grant "Universities of Russia: Fundamental Studies" is acknowleged.

References

Arkhipova V.P., Kravtsova A.S., Zasov A.V., Chernin A.D.: 2000 (in preparation).

Buta R., Combes F.: 1996, *Fund. Cosm. Phys.*, **17**, 95.

Chernin A.D.: 1998, *Astrofisica*, **41**, 609.

Chernin A.D.: 1999, *MNRAS*, **308**, 321.

Chernin A.D.: 2000, (in press).

Chernin A.D., Zasov A.V., Arkhipova V.P., Kravtsova A. S.: 2000a (in press).

Chernin A.D., Zasov A.V., Kravtsova A. S., 2000b (in press).

Guivarch B., Athanasoula E.: 1996, in *Barred Galaxies*, eds. R.Buta et al.,*ASP Conf.Ser.* **91**, 375.

Vorontsov-Vel'yaminov B.A.: 1951, *Astron. Zh.*, **28**, 43.

Vorontsov-Vel'yaminov B.A.: 1964, *Astron. Zh.*, **41**, 814 (English transl.: *Sov. Astron.*, **8**, 649, 1965).

Vorontsov-Vel'yaminov B.A.: 1978, *Extragalactic Astronomy*, Moscow, Nauka (English edition: New York, Harwood Academic Publishers, 1987).

Waller W.H., Bohlin R.C., Cornett R.H., et al.: 1997, *ApJ*, **481**, 169.

DENSITY PERTURBATIONS IN A REALISTIC UNIVERSE

M. Demiański[1], Z. Golda[2], A. Woszczyna[2]

[1] Institute of Theoretical Physics, University of Warsaw, Warsaw, Poland *mde@fuw.edu.pl*

[2] Astronomical Observatory, Jagiellonian University, Cracow, Poland *uowoszcz@cyf-kr.edu.pl*

ABSTRACT.

We analyze evolution of density perturbations in a flat or open universe filled in with matter, relativistic particles and possibly cosmological constant. Density perturbations grow very slowly in a universe filled in with low mass neutrinos.

Key words: Cosmology: Big Bang: Early Universe, Density Perturbations

1. Introduction

As we celebrate the 95-th birthday of George Gamow in Odessa, it is quite appropriate, I think, to reflect upon his two important moments of great desperation. It could be a legend that Gamow fled from Odessa to Turkey on a canoe, but even if it is a legend, it is a nice one, worth remembering. One can only imagine the level of desperation which forced him to flee. Several years later, while already in the United States, Gamow desperately tried to convince, first, his friends and associates, and later the whole astronomical community that the universe was created at the Big Bang (Gamow, 1946). After the discovery of the microwave background radiation by Arno Penzias and Robert Wilson in 1964 (Penzias and Wilson, 1965) the Big Bang scenario of the very early evolution of the universe has been universally accepted.

George Gamow was the early driving force of understanding physics of the evolving universe. His ambitious attempt to create all elements that exist in nature at Big Bang failed (Alpher, Bethe, Gamow 1948; Gamow 1948), but the theory of primordial nucleosynthesis later on turned out to provide very important information about the early universe and the constituents of matter. Comparing the observed abundance of light elements, in particular He^4, deuterium, and Li^7 with predictions of the theory of primordial nucleosynthesis we now determine the density of baryonic matter in the Universe (Schramm, Turner 1998). It was noticed by V. Shvartzman (Shvartzman 1969) that the final abundance of He^4 depends on the number of families of relativistic particles present at the epoch on nucleosynthesis. Using this idea it was possible to show that there are only 3 different kinds of weakly interacting neutrinos. Later this result was confirmed by laboratory experiments.

2. Main constituents of a realistic Universe

I think that Gamow would have joined us in the recent period of desperation in cosmology as we straggle to find out what are the main constituents of the Universe.

During the golden period of cosmology in the sixties and seventies it was generally assumed that the universe is filled in with radiation (I really mean with photons and neutrinos) and baryons with electrons (leptons) present to make the total electric charge of the universe equal to zero. As is well known since the time of Friedman, the expansion rate of the universe is determined by the equation

$$H^2(t) = (\frac{\dot{R}}{R})^2 = \frac{8\pi G}{3}\varrho - \frac{kc^2}{R^2} + \frac{\Lambda c^2}{3}, \qquad (1)$$

where R is the scale factor, ϱ is the average density, $k = +1, 0, -1$ is the curvature parameter, and Λ is the cosmological constant. The average matter density can be explicitly written down as $\varrho = \varrho_r + \varrho_m$, where ϱ_r is the average density of all relativistic particles and ϱ_m is the matter density. If matter does not interact with radiation we have

$$\varrho_r R^4 = \text{const}, \quad \text{and} \quad \varrho_m R^3 = \text{const}. \qquad (2)$$

It is useful to introduce so called critical density by the relation

$$H^2 = \frac{8\pi G}{3}\varrho_{crit},$$

where H is the Hubble constant, and the omega parameter $\Omega = \dfrac{< \varrho >}{\varrho_{crit}}$, where $< \varrho >$ is the average matter density. These two basic parameters determine the global properties of the Friedman type homogeneous and

isotropic Universe. Actually one can actually define several omega parameters, namely

$$\Omega_r = \frac{\varrho_r}{\varrho_{crit}}, \quad \Omega_m = \frac{\varrho_m}{\varrho_{crit}}, \quad \Omega_c = -\frac{kc^2}{R^2H^2},$$

$$\text{and} \quad \Omega_\Lambda = \frac{\Lambda c^2}{3H^2}. \tag{3}$$

The Friedman equation implies that

$$\Omega_r + \Omega_m + \Omega_c + \Omega_\Lambda = 1. \tag{4}$$

With the help of the omega parameters the Friedman equation can be rewritten as

$$H^2(z) = H_0^2(\Omega_{0r}(1+z)^4 + \Omega_{0m}(1+z)^3 + \Omega_{0c}(1+z)^2 + \Omega_{0\Lambda}), \tag{5}$$

where $1 + z = \frac{R_0}{R(t)}$ and corresponding Ω_0 parameters denote their present values.

Attempts to determine the average matter density of the Universe led to an important discovery that there is more matter in the Universe than allowed by the theory of primordial nucleosynthesis and that most baryons do not emit light. I do not want to spend more time discussing these issues since tomorrow Volodia Lukash will present a general overview of the basic cosmological parameters. Let me only mention that $\Omega_{stars} = 0.005 \pm 0.002$ is much smaller than $\Omega_B = 0.045 \pm 0.005$. The best data on average matter density of the universe is provided by flat rotation curves of spiral galaxies, study of motions of galaxies in galaxy clusters, x-ray radiation from clusters of galaxies, and lensing on clusters of galaxies. Large scale flows of galaxies provide an independent estimate of the average matter density. From such dynamical type measurements it follows that $\Omega_m = 0.25 \pm 0.06$.

After very precise measurements of temperature of the microwave background radiation by the COBE satellite $T = 2.726 \pm 0.005$ (Bennett *et. al.* 1994), and laboratory determination that there are only three different types of neutrinos (probably all of very small mass) we have $\Omega_r = 9.5 \cdot 10^{-5}$.

Recent measurements of the Hubble constant and other basic cosmological parameters from observations of distant Type Ia supernovae lead to $H_0 = 65 \pm 2$ km/sMpc and for the first time seriously established that we live in a universe with different from zero cosmological constant and $\Omega_\Lambda \approx 0.75$ (Pelmutter *et.al* 1999; Riess *et. al.* 1999). These measurements imply that the Universe is flat with $\Omega_c = 0$.

3. Evolution of density perturbations

The problem of stability of the Friedman universe was solved by E. M. Lifschitz in 1946 (Lifschitz, 1946). The general relativistic equations describing evolution of small perturbations have been extensively studied since then. I do not want to rederive these equations here. Let me concentrate on the equation describing evolution of density perturbations. Assuming that dark matter particles are non relativistic and pressureless the equation describing density perturbations is usually written in the following form

$$\frac{d^2\Delta}{dt^2} + 2H\frac{d\Delta}{dt} - 4\pi G\varrho_m\Delta = 0, \tag{6}$$

where $\Delta = \delta\varrho/\varrho$.

Using this equation Guyot and Zeldovich (1970) and later independently Meszaros (1974) noticed that radiation strongly suppresses growth of density perturbations in particular in open cosmological models. This fact creates problems since now we have observationally established limits on the amplitude of density perturbations at the epoch of recombination. When density perturbations are adiabatic (what we assume) fluctuations of temperature of the microwave background radiation observed by COBE $\frac{\delta T}{T} \sim 10^{-5}$ restrict the value of $\frac{\delta\varrho}{\varrho}$ at recombination since we have $\frac{\delta\varrho}{\varrho} \approx 3\frac{\delta T}{T}$. In order to create galaxies and large scale structure by $z \approx 10$ the density perturbations should grow during that period by a factor of $\approx 10^4$. This restriction is not a problem anymore since dark matter particles decoupled from thermal equilibrium much earlier than baryons and therefore amplitude of dark matter density perturbations at recombination could be much higher. When baryons cease to interact with radiation after recombination they rapidly fall into gravitational potential wells and soon after recombination we have that $(\frac{\delta\varrho}{\varrho})_B \approx (\frac{\delta\varrho}{\varrho})_{DM}$.

It turns out that equation (6) also holds when $\Lambda \neq 0$. In the general case equations (6) can be conveniently transformed into

$$x(\Omega_r + \Omega_m x + \Omega_c x^2 + \Omega_\Lambda x^4)\Delta'' + (\Omega_r + 3/2\Omega_r x + 2\Omega_c + \Omega_\Lambda x^4)\Delta' - \frac{3}{2}\Omega_m\Delta = 0, \tag{7}$$

where $x = \frac{R(t)}{R_0}$ and $'$ denotes differentiation with respect to x.

In a simpler case, when $\Omega_\Lambda = 0$ this equation was studied by Rozgacheva and Sunyaev (1981), and Rozgacheva (1983) among others. I am not aware of analytical solutions of this equation when $\Omega_\Lambda \neq 0$. Therefor let me present numerical solutions and discuss how the cosmological constant influences evolution of density perturbations. We have numerically solved the equation (7) with the initial condition $\Delta(x = 0.001) = 1$ and therefore the final answer gives the growth factor of density perturbations in their post recombination evolution. If there are three different kinds of

massless neutrinos, and the Hubble constant is $H_0 = 65km/(sMpc)$ then $\Omega_r = 0.0001$. Commonly accepted value of the averaged total matter density in the universe (including dark matter) gives $\Omega_m = 0.3$. To include the recent observational estimates of the value of the cosmological constant, we will consider two cases $\Omega_\Lambda = 0.7$, $\Omega_c = 0$ and $\Omega_\Lambda = 0$ and $\Omega_c = 0.7$. The results are shown in Fig. 1.

We enlarge the parameter space by taking into account recent estimates of the mass of neutrinos. The largest possible mass of neutrinos allowed by measurements is in the range 0.1 eV to 0.03eV (Kearns, Kajita and Tostsuka, 1999) so neutrinos are still relativistic particles what leads to Ω_r in the range of 0.002 to 0.007. In Fig. 2 we present results of numerical integration of equation (7) in a flat universe with $\Omega_c = 0$ but with different form zero cosmological constant and curves shown in Fig. 3 represent solutions in an open universe without cosmological constant but with $\Omega_c = 0.698$ and $\Omega_c = 0693$ correspondingly.

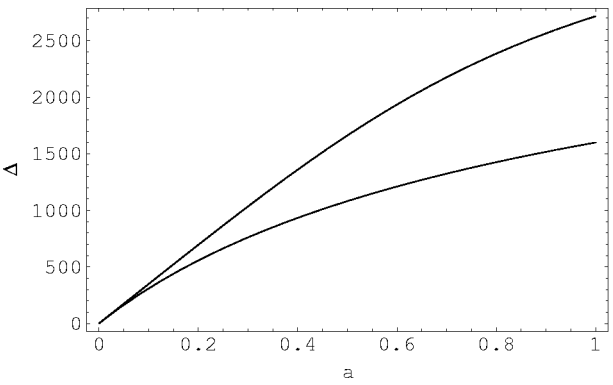

Figure 1: Growth of density perturbations in a Friedman universe with $\Omega_r = 0.0001$, $\Omega_m = 0.3$, and $\Omega_c = 0$, $\Omega_\Lambda = 0.6999$ upper curve, and $\Omega_c = 0.6999$, $\Omega_\Lambda = 0$ lower curve.

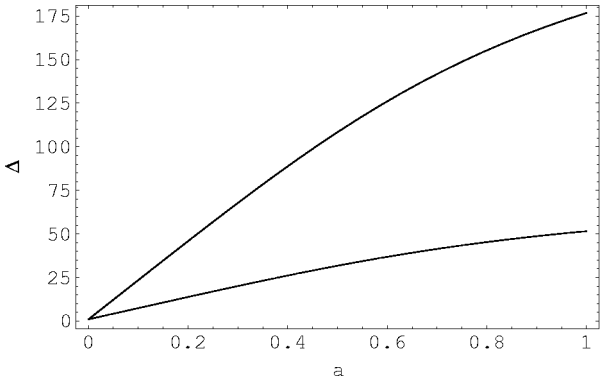

Figure 2: Growth of density perturbations in a Friedman universe with $\Omega_c = 0$, $\Omega_m = 0.3$, and $\Omega_r = 0.002$, $\Omega_\Lambda = 0.698$ upper curve, and $\Omega_r = 0.007$, $\Omega_\Lambda = 0.693$ lower curve.

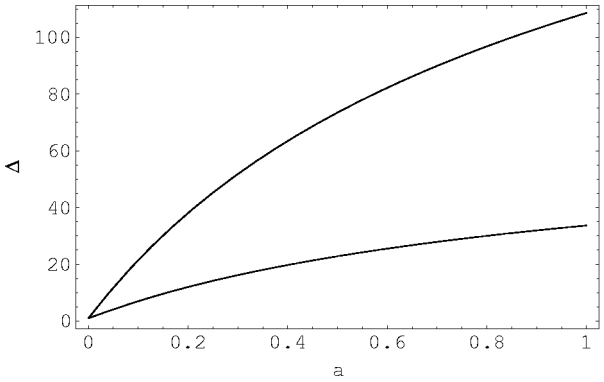

Figure 3: Growth of density perturbations in a Friedman universe with $\Omega_\Lambda = 0$, $\Omega_m = 0.3$, and $\Omega_r = 0.002$, $\Omega_c = 0.698$ upper curve, and $\Omega_r = 0.007$ and $\Omega_c = 0.693$ lower curve.

4. Conclusions

We confirm the previous results that the density perturbations grow slower in a radiation dominated universe. From Fig. 1, and comparing Fig. 2 and Fig. 3, it is apparent that, with the same Ω_r and Ω_m, density perturbations grow faster in a flat universe with the cosmological constant then in an open universe without the cosmological constant. With the present estimates of the mass of neutrinos the growth of density perturbation in the post recombination period is unacceptably slow.

Acknowledgements. This work was supported in part by the Polish State Committee for Scientific Research grant 2-P03D-022-10 and 2-P03D-014-17.

References

Gamow G.: 1946, *Phys. Rev.*, **70**, 572.
Penzias A., Wilson R.: 1965, *Astrophys. J.*, **142**, 419
Alpher R., Bethe H., Gamow G.: 1948, *Phys. Rev.*, **73**, 803.
Gamow G.: 1948, *Phys. Rev.*, **74**, 505.
Schramm D., Turner M.S.: 1998, *Rev. Mod. Phys.*, **70**, 303.
Shvartzman V.F.: 1969, *Pisma ZhETPh*, 9, 315.
Bennett, C. L., *et al.*: 1994, *Astrophys. J.*, **436**, 423.
Pelmutter S, *et al.*: 1999, *Astrophys. J.*, **517**, 565.
Riess A.G., *et al.*: 1999, *Astrophys. J.*, **517**, 707.
Lifschitz, E.M.: 1946, *ZhETPh*, **16**, 587.
Guyot M., Zeldovich Ya.B.: 1970, *As. Ap.*, **9**, 227.
Mészáros P.: 1974, *As. Ap.*, **37**, 225.
Rozgacheva I.K., Sunyaev R.A.: 1981, *Pisma A. Zh.*, **7**, 323.
Rozgacheva I.K.: 1983, *Astron. Zh.*, **60**, 823.
Kearns E., Kajita T., Totsuki Y.: 1999, *Sci. Amer.*, **281**, 2, 48.

GRAVITATIONAL WAVE TRACK IN THE EARTH'S ELECTROMAGNETIC FIELD

L.V. Grunskaya, V.V. Dorochzkov, V.V. Isakevich

Vladimir State University, Vladimir, Russia
grunsk-m2@vpti.vladimir.su

ABSTRACT. At present the idea of the extracting of the frequencies in the earth's electromagnetic field spectra corresponding to the gravitational radiation frequencies of the double star systems is based equally with the traditional approaches to solve the task of gravitational wave fields recording. In the theoretical plan of this task solving the known possible mechanisms of the electromagnetic fields of the ELF range in the Earth-ionosphere cavity being affected with the gravitational wave radiation of the astrophysical source were analyzed and the two-level model of the excitation oscillations in the near by earth's layer with the gravitational wave field is suggested. The catalogues of the spectra allowing to extract the frequencies associated with the global geodynamic processes and to analyze the type of the spectrum near by the frequencies of the astrophysical sources are arisen from the long- term continuos records of the earth's electromagnetic field with the multiple-response receiving complex of 1997 and 1998 enlisting the correlation and spectral analyses methods and the up-to-date ones of the simulation of the non-linear dynamical processes. The addition of the known methods of the direct recording of the gravitational wave radiation of the astrophysical objects to the suggested electromagnetic phenomena are very useful on account of the theoretically predicted low intensity gravitational wave radiation for the solving of the fundamental problem of the modern physics- the gravitational wave detection.

Key words: Gravitational wave, Electromagnetic field.

Intoduction

There has been realizing experimental investigation s of the Earth electromagnetic field in the ELF range (below 30 Hz) at the Department of Physics in the Vladimir State University since 1972. The ELF range electromagnetic fields are used for the investigation of ionosphere, magnetosphere, underground and underwater radio connection. The experimental results of the long-term watching of the Earth field can be used for the electromagnetic spectrum analysis near by the gravitational wave radiation frequencies of the binary star systems with the ELF radiation. Among the models of the electrical variations excitation in the Earth surface layer by the gravitational wave field one can extract the following model: a gravitational wave effects the Earth's crust and excitates ELF mechanical variations in it. These variations are passed to the Earth electrical field. The own frequencies of the Earth mechanical variations coincide with the gravitational wave radiation range of the binary star systems.

Recording Complex

The work provides using of broad possibilities of the unique experimental Vladimir University's base for making fundamental physical researches. The measuring ELF range complex consists of the surface and underground receiving channels located on the area of 4 hectares. The level of the measured fields is from $0,1mV/m$ to $100V/m$. The calibration system provides reliable functioning of the receiving complex. Recording of the Earth field electrical component is carried out synchronously in the continuous mode by all channels. The complex allows to record ELF range signals with some background interference to get daily and seasonal fluctuation, the law of the ELF range field distribution. Meteorological parameters are measured in the same way. The results are recorded by an electronic computer.

Experimental Data Processing

The received spectra analysis was done according to 3 directions. The first is the frequency analysis of the daily Earth rotation and harmonics of this frequency. The second is the analysis of the tide phenomena on the Earth which frequency display is in the ELF range. And the last is the frequency analysis of the gravitational wave radiation of the binary star systems.

Arising from continuous recordings of the electrical component of the Earth field with correlative and spec-

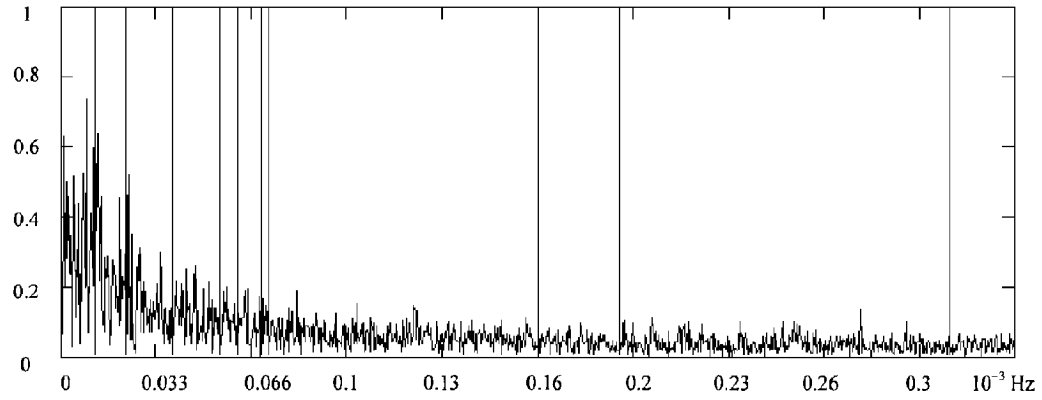

Figure 1: Common spectrum

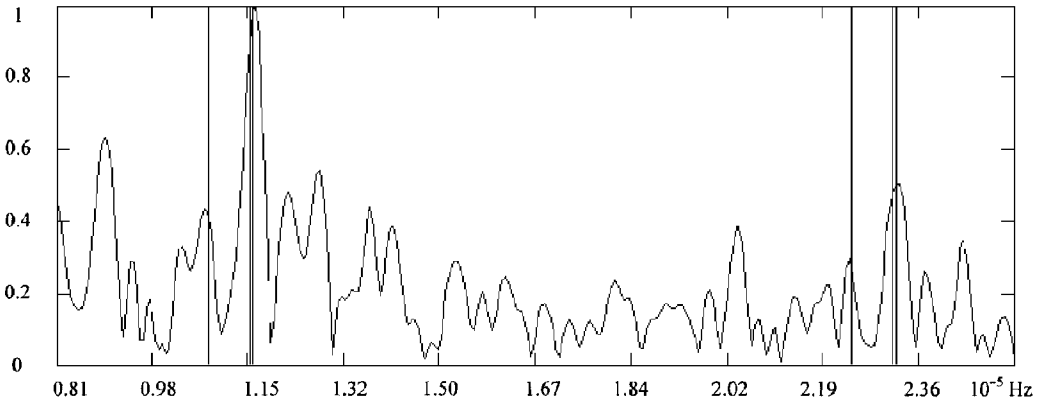

Figure 2: Tide effects' spectrum

tral analysis, the spectra- catalogues have been got allowing to extract frequencies connected with the global geodynamic processes and astrophysical sources frequencies. The duration of the continuous recording for two months in 1998 and a month in 1997 allows to get resolving according at a frequency $10 - 7Hz$. The total spectrum in the radiation range of the binary star systems is given in the fig.1 (lines show the frequencies of the sources). The total spectrum in the range of the tide phenomena is given in the fig.2 (lines show the tide frequencies). The harmonics of the Earth rotation frequency was extract up to ten members based on experimental results. Seven tide waves were analyzed and the closest spectral components according to the experiments of 1997 and 1998 were extracted. The spectra catalogues allowed to evaluate a probability of the pseudoalarm. The probability of the pseudoalarm of the tide effects is $0,07\%$. The probability of the pseudoalarm of the diurnal Earth rotation frequency is $0,1\%$. The probability of the pseudoalarm of the binary star systems frequencies is 8% in 1998. According to the results for tow years (1997 and 1998) could show the repetition of the signals near by the frequencies of the sources $J1012+5307, J1915+1606, J0024-7204J$. At present only the base of these investigations was done but preliminary results are optimistically enough.

Acknowledgement. The work is accomplished with the support of the Russian Fund of the Fundamental Investigations, project 98-05-64346.

References

Grunskaya L.V., Balakin A.B., Murzakhanov Z.G.: 1997, *Gravitation and Cosmology*, **3**, N 11, 233.

Bocaletti D, De Sabbata V., Fortini P., Gualdi C.: 1970, *Nuovo Cim.*, B. 70, N 2, 129.

Ginzburg V.L., Tsitovitch V.N. *Transition radiation and transition scattering.* - Moscow: Nauka, 1984, 360 p. (in Russian).

Grunskaya L.V., Dorozhkov V.V., Isakevich V.V.: 1999, *Theses of reports of 10th Russian Gravitational Conference. Theoretical and experimental problems of general relativity and gravitation.* Vladimir-Moscow.

Grunskaya L.V., Dorozhkov V.V., Vinogradov D.V.: 1999, *Ibid.*

Grunskaya L.V. 1996, *Abstracts of reports of 9th Russian Gravitational Conference*, Novgorod-Moscow. International seminar. *Theses of reporters.* Novgorod.

Kazarinov Y.M., Grishin Yu.P. *Radio-technical systems.* Moscow: Vysshaya Shkola, 1990 (in Russian).

INTERACTING GRAVITATIONAL EXCITONS AND OBSERVABLE EFFECTS FROM EXTRA DIMENSIONS

U. Günther[1], A.I. Zhuk[2]

[1] Gravitationsprojekt, Mathematische Physik I,
Institut für Mathematik, Universität Potsdam,
Am Neuen Palais 10, PF 601553, D-14415 Potsdam, Germany,
u.guenther@htw-zittau.de

[2] Department of Physics, University of Odessa,
2 Petra Velikogo St., Odessa 270100, Ukraine,
zhuk@paco.odessa.ua

ABSTRACT. It is supposed that a multidimensional manifold undergoes a spontaneous compactification $M \longrightarrow M^4 \times \prod_{i=1}^{n} M_i$, where M^4 is the 4−dimensional external space-time and M_i are compact internal spaces. Conformal excitations of the internal space metric can be observed as massive and massless scalar fields (gravitational excitons) in the external space-time. Specific interaction features of gravitational excitons with gravitons are considered.

Key words: Gravitation theory; cosmology: cosmological models; field theory.

1. Introduction

The large scale dynamics of the observable part of our present time universe is well described by the Friedmann model with 4-dimensional Friedmann-Robertson-Walker (FRW) metric. However, it is possible that space-time at short (Planck) distances might have a dimensionality of more than four and possess a rather complex topology. String theory (Green, Schwarz, Witten 1987) and its recent generalizations — p-brane, M- and F-theory (Strominger, Vafa 1996; Duff 1996) widely use this concept and give it a new foundation. From this viewpoint, it is natural to generalize the Friedmann model to multidimensional cosmological models (MCM) with topology (Ivashchuk, Melnikov, Zhuk 1989)

$$M = \mathbf{R} \times M_0 \times M_1 \times \ldots \times M_n \ , \qquad (1.1)$$

where for simplicity the $M_i \quad (i = 0, \ldots, n)$ can be assumed to be d_i−dimensional Einstein spaces. M_0 usually denotes the $d_0 = 3$ - dimensional external space.

One of the main problems in multidimensional models consists in the dynamical process leading from a stage with all dimensions developing on the same scale to the actual stage of the universe, where we have only four external dimensions and all internal spaces have to be compactified and contracted to sufficiently small scales, so that they are apparently unobservable. To make the internal dimensions unobservable at the actual stage of the universe we have to demand their contraction to scales $10^{-17}cm$ — $10^{-33}cm$ (between the Fermi and Planck lengths). This leads to an effectively four-dimensional universe.

In the present paper we briefly review some recent results connected with different aspects of multidimensional gravitational models (Günther, Zhuk 1997a,b, 1998; Günther, Starobinsky, Zhuk 1999).

1. We show that inhomogeneous fluctuations of the scale factors of internal factor spaces in MCMs can be interpreted as scalar particles (gravitational excitons) in our observable $(D_0 = 4)$−dimensional external space-time.

2. We point out some specific features of interaction and propagation of gravitational excitons and gravitons in the presence of inhomogeneous scale factor backgrounds.

3. A consideration of the interaction of gravitational excitons with abelian gauge fields allows us to indicate some specific astrophysical implications related to gravitational excitons as well as some possible observable consequences connected with their existence.

4. Starting from the fact that according to present day observations the dynamical behaviour of the universe after inflation is well described by the standard Friedmann model in the presence of a perfect fluid we show that this approach can be generalized to the description of the postinflationary stage in multidimensional cosmological models. We derive a class of models where, from one side, the internal spaces are stable compactified near Planck scales and, from the other side, the external universe behaves in accordance with

the standard Friedmann model.

2. Gravitational excitons

In this section we describe the basic features of our model and show how gravitational excitons necessarily occure in higher dimensional gravitational theories (Günther, Zhuk 1997a,b).

Let us consider a multidimensional space-time manifold

$$M = \bar{M}_0 \times M_1 \times \ldots \times M_n \tag{2.1}$$

with decomposed metric on M

$$g = g_{MN}(X) dX^M \otimes dX^N = g^{(0)} + \sum_{i=1}^{n} e^{2\beta^i(x)} g^{(i)}, \tag{2.2}$$

where x are some coordinates of the $D_0 = d_0 + 1$ - dimensional manifold $\bar{M}_0$ and

$$g^{(0)} = g^{(0)}_{\mu\nu}(x) dx^\mu \otimes dx^\nu. \tag{2.3}$$

Let manifolds M_i be d_i-dimensional Einstein spaces with metric $g^{(i)} = g^{(i)}_{m_i n_i}(y_i) dy_i^{m_i} \otimes dy_i^{n_i}$, i.e.,

$$R_{m_i n_i}\left[g^{(i)}\right] = \lambda^i g^{(i)}_{m_i n_i}, \qquad m_i, n_i = 1, \ldots, d_i \tag{2.4}$$

and

$$R\left[g^{(i)}\right] = \lambda^i d_i \equiv R_i. \tag{2.5}$$

In the case of constant curvature spaces parameters λ^i are normalized as $\lambda^i = k_i(d_i - 1)$ with $k_i = \pm 1, 0$. Internal spaces M_i $(i = 1, \ldots, n)$ may have nontrivial global topology, being compact (i.e. closed and bounded) for any sign of spatial topology (Wolf 1967, Fagundes 1992, 1993).

With total dimension $D = 1 + \sum_{i=0}^{n} d_i$, κ^2 a D-dimensional gravitational constant, Λ - a D-dimensional bare cosmological constant and S_{YGH} the standard York-Gibbons-Hawking boundary term (York 1972, Gibbons, Hawking 1977), we consider an action of the form

$$S = \frac{1}{2\kappa^2} \int\limits_M d^D X \sqrt{|g|} \left\{R[g] - 2\Lambda\right\} + S_{add} + S_{YGH}. \tag{2.6}$$

The additional potential term

$$S_{add} = -\int\limits_M d^D X \sqrt{|g|} \rho(x) \tag{2.7}$$

is not specified and left in its general form, taking into account the Casimir effect (Candelas, Weinberg 1984), the Freund - Rubin monopole ansatz (Freund, Rubin 1980), a perfect fluid (Gavrilov, Ivashchuk, Melnikov 1995; Kasper, Zhuk 1996) or other hypothetical potentials (Bleyer, Zhuk 1995; Günther, Kriskiv, Zhuk 1998). In all these cases ρ depends on the external coordinates through the scale factors $a_i(x) = e^{\beta^i(x)}$ $(i = 1, \ldots, n)$ of the internal spaces.

After dimensional reduction the action reads

$$\begin{aligned} S &= \frac{1}{2\kappa_0^2} \int\limits_{\bar{M}_0} d^{D_0} x \sqrt{|g^{(0)}|} \prod_{i=1}^{n} e^{d_i \beta^i} \times \\ &\times \left\{ R\left[g^{(0)}\right] - G_{ij} g^{(0)\mu\nu} \partial_\mu \beta^i \, \partial_\nu \beta^j + \right. \\ &+ \left. \sum_{i=1}^{n} R\left[g^{(i)}\right] e^{-2\beta^i} - 2\Lambda - 2\kappa^2 \rho \right\}, \end{aligned} \tag{2.8}$$

where $\kappa_0^2 = \kappa^2 / V_I$ is the D_0-dimensional gravitational constant and

$$V_I = \prod_{i=1}^{n} v_i = \prod_{i=1}^{n} \int\limits_{M_i} d^{d_i} y \sqrt{|g^{(i)}|} \tag{2.9}$$

defines the internal space volume corresponding to the scale factors $a_i \equiv 1, i = 1, \ldots, n$. $G_{ij} = d_i \delta_{ij} - d_i d_j$ $(i, j = 1, \ldots, n)$ is the midisuperspace metric (Ivashchuk, Melnikov, Zhuk 1989; Rainer, Zhuk 1996). The action functional (2.8) is written in the Brans-Dicke frame. A conformal transformation to the Einstein frame

$$g^{(0)}_{\mu\nu} = \Omega^2 \tilde{g}^{(0)}_{\mu\nu}, \tag{2.10}$$

with

$$\Omega = exp\left(-\frac{1}{D_0 - 2} \sum_{i=1}^{n} d_i \beta^i \right) \tag{2.11}$$

yields

$$\begin{aligned} S &= \frac{1}{2\kappa_0^2} \int\limits_{\bar{M}_0} d^{D_0} x \sqrt{|\tilde{g}^{(0)}|} \left\{ \tilde{R}\left[\tilde{g}^{(0)}\right] - \right. \\ &- \left. \bar{G}_{ij} \tilde{g}^{(0)\mu\nu} \partial_\mu \beta^i \, \partial_\nu \beta^j - 2U_{eff} \right\}. \end{aligned} \tag{2.12}$$

The tensor components of the midisuperspace metric (target space metric on $\mathbf{R}^n_T$) $\bar{G}_{ij}$ $(i, j = 1, \ldots, n)$, its inverse metric $\bar{G}^{ij}$ and the effective potential are respectively

$$\bar{G}_{ij} = d_i \delta_{ij} + \frac{1}{D_0 - 2} d_i d_j, \tag{2.13}$$

$$\bar{G}^{ij} = \frac{\delta^{ij}}{d_i} + \frac{1}{2 - D} \tag{2.14}$$

and

$$U_{eff} = \left(\prod_{i=1}^{n} e^{d_i \beta^i} \right)^{-\frac{2}{D_0 - 2}} \left[-\frac{1}{2} \sum_{i=1}^{n} R_i e^{-2\beta^i} + \Lambda + \kappa^2 \rho \right]. \tag{2.15}$$

We recall that ρ depends on the scale factors of the internal spaces: $\rho = \rho\left(\beta^1, \ldots, \beta^n\right)$. Thus, we are led to the action of a self-gravitating $\sigma-$model with flat target space $(\mathbf{R}^n_T, \bar{G})$ (2.13) and self-interaction described

by the potential (2.15). It can be easily seen that the problem of the internal spaces stable compactification reduces now to a search of models that provide minima of the effective potential (2.15). It is important to note that the conformal transformation (2.10) is performed with respect to the external metric $g^{(0)}$. Thus, stable configurations of the internal spaces do not depend on the choice of the frame. However, in the present paper the Einstein frame is considered as the physical one (Cho 1992; Litterio et al 1996).

As next step we bring midisuperspace metric (target space metric) (2.13) by a regular coordinate transformation

$$\varphi = Q\beta, \quad \beta = Q^{-1}\varphi \tag{2.16}$$

to a pure Euclidean form

$$\bar{G}_{ij}d\beta^i \otimes d\beta^j = \sigma_{ij}d\varphi^i \otimes d\varphi^j = \textstyle\sum_{i=1}^n d\varphi^i \otimes d\varphi^i,$$

$$\bar{G} = Q^T Q, \quad \sigma = \mathrm{diag}(+1, +1, \ldots, +1). \tag{2.17}$$

(The superscript ^{T} denotes the transposition.) An appropriate transformation $Q:\ \beta^i \mapsto \varphi^j = Q^j_i\beta^i$ is given e.g. by

$$\begin{aligned} \varphi^1 &= -A\textstyle\sum_{i=1}^n d_i\beta^i, \\ \varphi^i &= [d_{i-1}/\Sigma_{i-1}\Sigma_i]^{1/2}\textstyle\sum_{j=i}^n d_j(\beta^j - \beta^{i-1}), \end{aligned} \tag{2.18}$$

$i = 2, \ldots, n$, where $\Sigma_i = \sum_{j=i}^n d_j$,

$$A = \pm\left[\frac{1}{D'}\frac{D-2}{D_0-2}\right]^{1/2} \tag{2.19}$$

and $D' = \sum_{i=1}^n d_i$. So we can write action (2.12) as

$$\begin{aligned} S &= \frac{1}{2\kappa_0^2}\int\limits_{\bar{M}_0} d^{D_0}x\sqrt{|\tilde{g}^{(0)}|}\left\{\tilde{R}\left[\tilde{g}^{(0)}\right] - \right. \\ &- \left. \sigma_{ik}\tilde{g}^{(0)\mu\nu}\partial_\mu\varphi^i\,\partial_\nu\varphi^k - 2U_{eff}\right\} \end{aligned} \tag{2.20}$$

with effective potential

$$U_{eff} = e^{\frac{2}{A(D_0-2)}\varphi^1}\left(-\frac{1}{2}\sum_{i=1}^n R_i e^{-2(Q^{-1})^i{}_k\varphi^k} + \Lambda + \kappa^2\rho\right). \tag{2.21}$$

In this section let us for simplicity consider models with a constant scale factor background localized in one of the minima $\vec{\varphi}_c, c = 1, ..., m$ of the effective potential $\left.\frac{\partial U_{eff}}{\partial\varphi^i}\right|_{\vec{\varphi}_c} = 0$. Then, for small field fluctuations $\xi^i \equiv \varphi^i - \varphi^i_{(c)}$ around the minima the potential (2.21) reads

$$U_{eff} = U_{eff}\left(\vec{\varphi}_c\right) + \frac{1}{2}\sum_{i,k=1}^n \bar{A}_{(c)ik}\xi^i\xi^k + O(\xi^i\xi^k\xi^l), \tag{2.22}$$

where the Hessians

$$\bar{A}_{(c)ik} := \left.\frac{\partial^2 U_{eff}}{\partial\xi^i\,\partial\xi^k}\right|_{\vec{\varphi}_c} \tag{2.23}$$

are not vanishing identically. The action functional (2.20) reduces to a family of action functionals for the fluctuation fields ξ^i

$$\begin{aligned} S &= \frac{1}{2\kappa_0^2}\int\limits_{\bar{M}_0} d^{D_0}x\sqrt{|\tilde{g}^{(0)}|}\left\{\tilde{R}\left[\tilde{g}^{(0)}\right] - 2U_{eff}\left(\vec{\varphi}_c\right) - \right. \\ &- \left. \sigma_{ik}\tilde{g}^{(0)\mu\nu}\partial_\mu\xi^i\,\partial_\nu\xi^k - \bar{A}_{(c)ik}\xi^i\xi^k\right\}, \\ &\quad c = 1, ..., m. \end{aligned} \tag{2.24}$$

It remains to diagonalize the Hessians $\bar{A}_{(c)ik}$ by appropriate $SO(n)-$rotations S_c :
$\xi \mapsto \psi = S_c\xi, \quad S_c^T = S_c^{-1}$

$$\bar{A}_c = S_c^T M_c^2 S_c, \quad M_c^2 = \mathrm{diag}(m^2_{(c)1}, m^2_{(c)2}, \ldots, m^2_{(c)n}), \tag{2.25}$$

leaving the kinetic term $\sigma_{ik}\tilde{g}^{(0)\mu\nu}\partial_\mu\xi^i\,\partial_\nu\xi^k$ invariant

$$\sigma_{ik}\tilde{g}^{(0)\mu\nu}\partial_\mu\xi^i\,\partial_\nu\xi^k = \sigma_{ik}\tilde{g}^{(0)\mu\nu}\partial_\mu\psi^i\,\partial_\nu\psi^k, \tag{2.26}$$

and we arrive at action functionals for decoupled normal modes of linear $\sigma-$models in the background metric $\tilde{g}^{(0)}$ of the external space-time:

$$\begin{aligned} S &= \frac{1}{2\kappa_0^2}\int\limits_{\bar{M}_0} d^{D_0}x\sqrt{|\tilde{g}^{(0)}|}\left\{\tilde{R}\left[\tilde{g}^{(0)}\right] - 2\Lambda_{(c)eff}\right\} + \\ &+ \sum_{i=1}^n \frac{1}{2}\int\limits_{\bar{M}_0} d^{D_0}x\sqrt{|\tilde{g}^{(0)}|}\times \\ &\times \left\{-\tilde{g}^{(0)\mu\nu}\psi^i_{,\mu}\psi^i_{,\nu} - m^2_{(c)i}\psi^i\psi^i\right\} \\ &\quad c = 1, \ldots, m, \end{aligned} \tag{2.27}$$

where $\Lambda_{(c)eff} \equiv U_{eff}\left(\vec{\varphi}_c\right)$ plays the role of a D_0-dimensional effective cosmological constant and the factor $\sqrt{V_I/\kappa^2}$ has been included into ψ for convenience: $\sqrt{V_I/\kappa^2}\psi \to \psi$.

Thus, conformal excitations of the metric of the internal spaces behave as massive scalar fields developing on the background of the external space-time. By analogy with excitons in solid state physics where they are excitations of the electronic subsystem of a crystal, the excitations of the internal spaces were called gravitational excitons (Günther, Zhuk 1997a).

Different models which ensure minima of the effective potential were described in (Günther, Zhuk 1997a,b; Günther, Kriskiv, Zhuk 1998). Some of them (including the pure geometrical case with $\rho \equiv 0$) satisfy following physical conditions

$$\begin{array}{lccl} (i) & a_{(c)i} & = & e^{\beta^i_c} \gtrsim L_{Pl}, \\ (ii) & m_{(c)i} & \leq & M_{Pl}, \\ (iii) & \Lambda_{(c)eff} & \to & 0. \end{array} \tag{2.28}$$

The first condition expresses the fact that the internal spaces should be unobservable at the present time and stable against quantum gravitational fluctuations. This condition ensures the applicability of the classical gravitational equations near positions of minima of the effective potential. The second condition means that the curvature of the effective potential at minimum points should be less than the Planckian one. Of course, gravitational excitons can be excited at the present time if $m_i \ll M_{Pl}$. The third condition reflects the fact that the cosmological constant at the present time is very small: $|\Lambda| \leq 10^{-56}\mathrm{cm}^{-2} \approx 10^{-121}\Lambda_{Pl}$, where $\Lambda_{Pl} = L_{Pl}^{-2}$. Strictly speaking, in the multiminimum case ($c > 1$) we can demand $a_{(c)i} \sim L_{Pl}$ and $\Lambda_{(c)eff} \to 0$ only for one of the minima to which corresponds the present universe state. For all other minima it may be $a_{(c)i} \gg L_{Pl}$ and $|\Lambda_{(c)eff}| \gg 0$.

3. Interaction of gravitational excitons and gravitons

In this section we give a brief sketch of some of the basic features of the interaction between gravitational excitons and gravitons corresponding to fluctuations of the external metric $\tilde{g}^{(0)}$ (Günther, Starobinsky, Zhuk 1999). To simplify notations we shall drop the index (0) for the external metric: $\tilde{g}^{(0)}_{\mu\nu} \equiv \tilde{g}_{\mu\nu}$ and use the abbreviations

$$A_{ij} := \frac{\partial^2 U_{eff}}{\partial\beta^i \partial\beta^j}, \quad b_i := \frac{\partial U_{eff}}{\partial\beta^i} \ . \tag{3.1}$$

As starting point of our consideration we choose the Euler-Lagrange equations for the scale factors and the external metric derived by variation of the action functional (2.12)

$$\tilde{R}_{\mu\nu} - \frac{1}{2}\tilde{g}_{\mu\nu}\tilde{R} - T_{\mu\nu}\left[\beta, \tilde{g}\right] = 0 \tag{3.2}$$

and

$$\bar{G}_{ij}\Box\beta^j \equiv \bar{G}_{ij}\frac{1}{\sqrt{|\tilde{g}^{(0)}|}}\partial_\mu\left(\sqrt{|\tilde{g}^{(0)}|}\tilde{g}^{(0)\mu\nu}\partial_\nu\beta^j\right) = b_i(\beta)\,, \tag{3.3}$$

where

$$\begin{aligned} T_{\mu\nu}\left[\beta, \tilde{g}\right] &= \bar{G}_{ij}\partial_\mu\beta^i\partial_\nu\beta^j - \\ &\quad -\frac{1}{2}\tilde{g}_{\mu\nu}\left(\bar{G}_{ij}\tilde{g}^{\alpha\beta}\partial_\alpha\beta^i\partial_\beta\beta^j + 2U_{eff}\right) \\ &\equiv \bar{G}_{ij}\partial_\mu\beta^i\partial_\nu\beta^j + \tilde{g}_{\mu\nu}\kappa_0^2 L_\beta[\beta] \ . \end{aligned} \tag{3.4}$$

Assuming that there exists a well defined splitting of the physical fields $(\tilde{g}, \beta)$ into not necessarily constant background components $(\bar{g}, \bar{\beta})$ and small perturbational (fluctuation) components (h, η)

$$\begin{aligned} \tilde{g}_{\mu\nu} &= \bar{g}_{\mu\nu} + h_{\mu\nu}\,, \\ \beta^i &= \bar{\beta}^i + \eta^i \end{aligned} \tag{3.5}$$

we can perform a perturbational analysis of the interaction dynamics of our model splitting the field equations (3.2) and (3.3) into an equation set defining the dynamics of the background fields (zeroth order contribution of fluctuations)

$$\bar{R}_{\mu\nu} - \frac{1}{2}\bar{g}_{\mu\nu}\bar{R} - T_{\mu\nu}\left[\bar{\beta}, \bar{g}\right] = 0\,, \tag{3.6}$$

$$\Box\bar{\beta}^i = \left[\bar{G}^{-1}\right]^{ij} b_j(\bar{\beta}) \tag{3.7}$$

and a set of background depending linearized field equations for the fluctuational components (first order contribution)

$$\begin{aligned} \tfrac{1}{2}h_{\mu\nu;\lambda}{}^{;\lambda} &- h^\lambda{}_{(\mu;\nu);\lambda} + \frac{1}{2}h_{;\mu;\nu} + \\ + &\quad \frac{1}{2}\bar{g}_{\mu\nu}\left(h^{\alpha\lambda}{}_{;\alpha;\lambda} - h_{;\lambda}{}^{;\lambda}\right) + \frac{1}{2}h_{\mu\nu}\bar{R} - \\ - &\quad \frac{1}{2}\bar{g}_{\mu\nu}h^{\kappa\lambda}\bar{R}_{\kappa\lambda} + \kappa_0^2 L_{\bar{\beta}}h_{\mu\nu} + \\ + &\quad \frac{1}{2}\bar{g}_{\mu\nu}\bar{G}_{ij}\partial_\kappa\bar{\beta}^i\partial_\lambda\bar{\beta}^j h^{\kappa\lambda} + \\ + &\quad \bar{G}_{ij}\left(\partial_\mu\bar{\beta}^i\partial_\nu\eta^j + \partial_\mu\eta^i\partial_\nu\bar{\beta}^j\right) - \\ - &\quad \bar{G}_{ij}\bar{g}_{\mu\nu}\bar{g}^{\kappa\lambda}\partial_\kappa\bar{\beta}^i\partial_\lambda\eta^j - \bar{g}_{\mu\nu}b_j(\bar{\beta})\eta^j = 0 \end{aligned} \tag{3.8}$$

and

$$\begin{aligned} \Box\eta^i - \left[\bar{G}^{-1}\right]^{ij}A_{jk}(\bar{\beta})\eta^k = \frac{1}{\sqrt{|\bar{g}|}}\partial_\nu\left(\sqrt{|\bar{g}|}h^{\mu\nu}\partial_\mu\bar{\beta}^i\right) - \\ -\frac{1}{2}\bar{g}^{\mu\nu}\partial_\mu\bar{\beta}^i\partial_\nu h \ . \end{aligned} \tag{3.9}$$

Here $\bar{R}_{\mu\nu}$ and the semicolon denote the Ricci-tensor and the covariant derivative with respect to the background metric $\bar{g}_{\mu\nu}$. Additionally we have used the formula

$$\tilde{g}^{\mu\nu} = \bar{g}^{\mu\nu} - h^{\mu\nu} \tag{3.10}$$

which is valid up to linear terms in h. Indices in $h_{\mu\nu}$ are raised and lowered by the background metric $\bar{g}_{\mu\nu}$, e.g. $h = h_{\mu\nu}\bar{g}^{\mu\nu}$.

Let us now generalize the normal mode formalism applied in section 2 for the derivation of gravitational excitons over constant scale factor backgrounds to models with non-constant scale factor backgrounds (Günther, Zhuk 1998). For this purpose we diagonalize matrix $\left[\bar{G}^{-1}A\right]^i_k \equiv \left[\bar{G}^{-1}\right]^{ij}A_{jk}(\bar{\beta})$ by an appropriate background depending $SO(n)-$rotation $S = S(\bar{\beta})$

$$S^{-1}\bar{G}^{-1}AS \stackrel{def}{=} M^2 = \mathrm{diag}\left[m_1^2(\bar{\beta}), \ldots, m_n^2(\bar{\beta})\right] \tag{3.11}$$

and rewrite Eq. (3.9) in terms of generalized normal modes (gravitational excitons) $\psi = S^{-1}\eta$:

$$\begin{aligned} \bar{g}^{\mu\nu}D_\mu D_\nu\psi - M^2(\bar{\beta})\psi &= \left(h^{\mu\nu} - \frac{1}{2}\bar{g}^{\mu\nu}h\right)_{;\nu} D_\mu\bar{\varphi} + \\ &\quad + h^{\mu\nu}D_\mu D_\nu\bar{\varphi}\,, \end{aligned} \tag{3.12}$$

where $\bar{\varphi}$ are $SO(n)-$rotated background scale factors $\bar{\varphi} = S^{-1}\bar{\beta}$ and M^2 can be interpreted as background depending diagonal mass matrix for the gravitational excitons.

D_μ denotes a covariant derivative

$$D_\mu := \partial_\mu + \Gamma_\mu + \omega_\mu \ , \quad \omega_\mu := S^{-1}\partial_\mu S \tag{3.13}$$

with $\Gamma_\mu + \omega_\mu$ as connection on the fibre bundle $E(\bar{M}_0, \mathbf{R}^{D_0} \oplus \mathbf{R}^n_T) \to \bar{M}_0$ consisting of the base manifold $\bar{M}_0$ and vector spaces $\mathbf{R}^{D_0}_x \oplus \mathbf{R}^n_{Tx} = T_x\bar{M}_0 \oplus \left\{\left(\eta^1(x), \ldots, \eta^n(x)\right)\right\}$ as fibres. So, the background components $\bar{\beta}^i(x)$ via the effective potential U_{eff} and its Hessian $A_{ij}(\bar{\beta})$ play the role of a medium for the gravitational excitons $\psi^i(x)$. Propagating in $\bar{M}_0$ filled with this medium they change their masses as well as the direction of their "polarization" defined by the unit vector in the fibre space

$$\xi(x) := \frac{\psi(x)}{|\psi(x)|} \in S^{n-1} \subset \mathbf{R}^n, \tag{3.14}$$

where S^{n-1} denotes the $(n-1)-$dimensional sphere.

From (3.8), (3.9) and (3.12) we see that in the lowest order (linear) approximation of the used perturbation theory a non-constant scale factor background is needed for an interaction between gravitational excitons and gravitons. For constant scale factor backgrounds $\bar{\beta} = const$ the system is necessarily located in one of the minima $\bar{\beta} = \beta_{(c)}$ of the effective potential U_{eff} so that $b_i(\beta_{(c)}) = 0, \quad \kappa_0^2 L_{\beta_{(c)}} = U_{eff}(\beta_{(c)}) = \Lambda_{(c)eff}$ and gravitational excitons and gravitons can only interact via nonlinear (higher order) terms. In the linear approximation they decouple over constant scale factor backgrounds due to vanishing terms in (3.8), (3.9) and (3.12).

4. Interaction of gravitational excitons with abelian gauge fields and possible astrophysical implications

In this section we consider the zero mode case, i.e., the case of an abelian vector potential that depends only on the external coordinates: $A_M = A_M(x) \quad (M = 1, \ldots, D)$. Thus, for non-zero components of the field strength tensor we have: $F_{\mu\nu} = \partial_\mu A_\nu - \partial_\nu A_\mu \quad (\mu, \nu = 1, \ldots, D_0)$ and $F_{\mu m_i} = \partial_\mu A_{m_i} - \partial_{m_i} A_\mu = \partial_\mu A_{m_i} \quad (m_i = 1, \ldots, d_i; i = 1, \ldots, n)$.

Dimensional reduction of the action for the gauge field yields

$$\begin{aligned} S_{em} &= -\frac{1}{2}\int_M d^D X \sqrt{|g|} F_{MN}F^{MN} \qquad (4.1)\\ &= -\frac{1}{2}\int_{\bar{M}_0} d^{D_0}x \sqrt{|g^{(0)}|}\prod_{i=1}^n e^{d_i\beta^i}\left\{F_{\mu\nu}F^{\mu\nu} + \right.\\ &\left. + 2g^{(0)\mu\nu}\sum_{i=1}^n e^{-2\beta^i(x)}\bar{g}^{(i)m_in_i}\partial_\mu A_{m_i}\partial_\nu A_{n_i}\right\}, \end{aligned}$$

where we introduced the constant metric

$$\bar{g}^{(i)m_in_i} \equiv \frac{1}{v_i}\int_{M_i} d^{d_i}y\sqrt{|g^{(i)}|}g^{(i)m_in_i}(y^i) \tag{4.2}$$

and included the factor $\sqrt{V_I}$ into A_M for convenience: $\sqrt{V_I}A_M \to A_M$. In Eq. (4.1) we assumed $F^{\mu\nu} = g^{(0)\mu\kappa}g^{(0)\nu\delta}F_{\kappa\delta}$.

The exact field strength 2-form $F = dA$, $A = A_\mu dx^\mu$ with components $F_{\mu\nu}$ is invariant under gauge transformations $A \to A^f = A + df$, i.e., $A_\mu \to A^f_\mu = A_\mu + \partial_\mu f$, $F^f = dA + d^2 f = dA = F$, with $f(x)$ any smooth function. Gauge invariance of F implies a gauge invariance of the action functional (4.1).

Action functional (4.1) is written in the Brans-Dicke frame. After conformal transformation (2.10) and with an ansatz

$$A_\mu = \Omega^k \tilde{A}_\mu \tag{4.3}$$

for the vector potential, where $\Omega(x)$ is given by (2.11), the effective action in the Einstein frame reads

$$\begin{aligned} S_{em} = -\frac{1}{2}\int_{\bar{M}_0} d^{D_0}x\sqrt{|\tilde{g}^{(0)}|}\left\{\Omega^{2(k-1)}\bar{F}_{\mu\nu}\bar{F}^{\mu\nu} + \right.\\ \left. + 2\tilde{g}^{(0)\mu\nu}\sum\nolimits_{i=1}^n e^{-2\beta^i(x)}\bar{g}^{(i)m_in_i}\partial_\mu A_{m_i}\partial_\nu A_{n_i}\right\}, \end{aligned} \tag{4.4}$$

where

$$\bar{F}_{\mu\nu} := D_\mu\tilde{A}_\nu - D_\nu\tilde{A}_\mu \tag{4.5}$$

and

$$D_\mu := \partial_\mu + \partial_\mu(\ln\Omega^k)\,. \tag{4.6}$$

The external space indices are raised and lowered by the metric $\tilde{g}^{(0)}$. Explicitly we have in (4.4)

$$\begin{aligned} \bar{F}_{\mu\nu}\bar{F}^{\mu\nu} &= \tilde{F}_{\mu\nu}\tilde{F}^{\mu\nu} - \\ &-2\tilde{F}^{\mu\nu}\left[\tilde{A}_\mu\partial_\nu(\ln\Omega^k) - \tilde{A}_\nu\partial_\mu(\ln\Omega^k)\right]\\ &+2\tilde{g}^{(0)\mu\kappa}\partial_\mu(\ln\Omega^k)\partial_\kappa(\ln\Omega^k)\tilde{A}^\nu\tilde{A}_\nu - \\ &-2\left(\tilde{A}^\mu\partial_\mu(\ln\Omega^k)\right)^2, \end{aligned} \tag{4.7}$$

where $\tilde{F} = d\tilde{A}$.

In order to preserve the gauge invariance of the action functional when passing from the Brans-Dicke frame to the Einstein frame we have to keep the vector potential unchanged, i.e. we have to fix the conformal weight at $k = 0$ (Günther, Starobinsky, Zhuk 1999). As result we arrive at an action functional

$$\begin{aligned} S_{em} = -\frac{1}{2}\int_{\bar{M}_0} d^{D_0}x\sqrt{|\tilde{g}^{(0)}|}\times\\ \times\left\{e^{\frac{2}{D_0-2}\sum_{i=1}^n d_i\beta^i(x)}F_{\mu\nu}F^{\mu\nu} + \right.\\ \left. + 2\tilde{g}^{(0)\mu\nu}\sum\nolimits_{i=1}^n e^{-2\beta^i(x)}\bar{g}^{(i)m_in_i}\partial_\mu A_{m_i}\partial_\nu A_{n_i}\right\}, \end{aligned} \tag{4.8}$$

with a dilatonic coupling of the abelian gauge potential to the gravitational excitons. The components A_{m_i} play the role of additional scalar fields.

Similar to string cosmology models describing the dynamics of electromagnetic fields with dilatonic coupling (Gasperini, Giovannini, Veneziano 1995a,b) we can expect in theory (4.8) an amplification of electromagnetic vacuum fluctuations (due to the presence of a dynamical gravitational exciton background) which can result in the observable cosmic microwave background anisotropy.

Let us now discuss some astrophysical implications of the interaction between gravitational excitons and photons. For simplicity we consider the one internal space case ($i = 1$) and suppose that the scale factor background is localized in a minimum $a_{(c)} = \exp\beta^1_{(c)}$ of the effective potential (2.15). Then, for small scale factor fluctuations $\eta = \beta^1 - \beta^1_{(c)}$ action (2.6) with $S_{add} \equiv S_{em}$ (where S_{em} is described by Eqs. (4.1) and (4.8)) reads

$$S = \frac{1}{2\kappa_0^2}\int\limits_{\tilde{M}_0} d^{D_0}x\sqrt{|\tilde{g}^{(0)}|}\left\{\tilde{R}\left[\tilde{g}^{(0)}\right] - 2\Lambda_{(c)eff}\right\} + \\ + \frac{1}{2}\int\limits_{\tilde{M}_0} d^{D_0}x\sqrt{|\tilde{g}^{(0)}|}\left\{-\tilde{g}^{(0)\mu\nu}\psi_{,\mu}\psi_{,\nu} - m^2_{(c)}\psi\psi\right\} - \\ - \frac{1}{2}\int\limits_{\tilde{M}_0} d^{D_0}x\sqrt{|\tilde{g}^{(0)}|}\{F_{\mu\nu}F^{\mu\nu} - \\ - 2\sqrt{\frac{d_1}{(D_0-2)(D-2)}}\kappa_0\psi F_{\mu\nu}F^{\mu\nu}\Bigg\} + \dots\ , \quad (4.9)$$

where we used the notations of Eq. (2.27) and fluctuations η and ψ are connected with each other as follows:

$$\eta = \kappa_0\sqrt{\frac{D_0-2}{d_1(D-2)}}\psi\ . \quad (4.10)$$

As mentioned above, $\kappa_0^2 = 8\pi/M_{Pl}^2$ is the D_0-dimensional (usually $D_0 = 4$) gravitational constant. In Eq. (4.9) we normalize the electromagnetic field as: $(a_{(c)})^{d_1/(D_0-2)}F_{\mu\nu} \longrightarrow F_{\mu\nu}$ and the last term there describes the interaction between gravitational excitons and photons. In a tree-level approximation this term corresponds to the diagram at Fig.1 and describes a gravitational exciton decaying into two photons. For the probability of this decay we can easily get the estimate

$$\Gamma \sim \left(\frac{1}{M_{Pl}}\right)^2 m^3_{(c)} = \left(\frac{m_{(c)}}{M_{Pl}}\right)^3 \frac{1}{T_{Pl}}\ , \quad (4.11)$$

which results in a life-time of the gravitational excitons with respect to this decay

$$\tau = \frac{1}{\Gamma} \sim \left(\frac{M_{Pl}}{m_{(c)}}\right)^3 T_{Pl}\ . \quad (4.12)$$

This equation shows that for excitons with masses $m_{(c)} \leq 10^{-21}M_{Pl} \sim 10^{-2}GeV \sim 20m_e$ (where m_e is the electron mass) the life-time $\tau \geq 10^{19}sec > t_{univ} \sim 10^{18}sec$ is greater than the age of the universe. Thus, gravitational excitons are very weakly interacting particles and can be considered as Dark Matter (DM). The type of the DM depends on the DM particle masses. It is hot for $m_{DM} \leq 50 - 100eV$, warm for $100eV \leq m_{DM} \leq 10KeV$ and cold for $m_{DM} \geq 10 - 50KeV$. The gravitational exciton masses are defined by the scales of compactification: $m_{(c)} \sim \left(a_{(c)}\right)^{-(D-2)/(D_0-2)}$ (Günther, Zhuk 1997a,b). It is clear that it is hardly possible to use the diagram at Fig.1 to estimate from experiments the gravitational exciton masses and respectively the scale of the internal spaces compactification. The reason consists in the term $1/M_{Pl}$ in the vertex of the diagram. However, by analogy with axions (Gnedin 1997a,b, 1999) it is possible that in strong magnetic field there can occure oscillations between gravitational excitons and photons which are described by the diagram at Fig.2, which corresponds to an interaction term $L_{eff} \sim \kappa_0\psi F^{\mu\nu}_{ext}f_{\mu\nu}$. $F^{\mu\nu}_{ext}$ is an external magnetic field and $f_{\mu\nu}$ describes photons. The probability of magnetic conversion of gravitational excitons into photons (and vice versa) can be much greater then (4.11) and will result in observable lines in spectra of astrophysical objects.

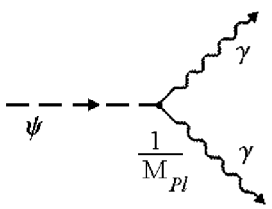

Figure 1: Decay of a gravitational exciton into two photons.

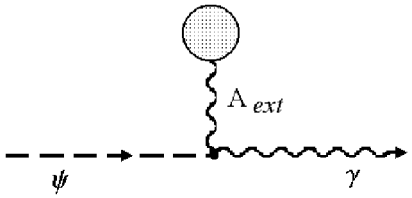

Figure 2: Conversion of a gravitational exciton into a photon in the presence of a strong magnetic background field.

5. Multidimensional perfect-fluid cosmology with stable compactified internal dimensions

Here we present a toy example of a multidimensional cosmological model (MCM) which shows the principal possibility to achieve a postinflational Friedmann-Robertson-Walker dynamics for the external ($D_0 = 4$)−dimensional space-time keeping the internal factor spaces stable compactified. This model is out of the scope of MCM with stable compactification found in (Günther, Zhuk 1997a,b). The main difference consists in an additional time-dependent term in the effective potential that provides the needed dynamical behaviour of the external space-time. This term is induced by a special type of fine-tuning of the parameters of a multicomponent perfect fluid. Although such a fine-tuning is a strong restriction on the matter content of the model, many important cases of physically interest are described by this class of perfect fluid. We note that a similar class of perfect fluids was considered in (Kasper, Zhuk 1996), where MCMs were integrated in the case of an absent cosmological constant and Ricci-flat internal spaces. As result particular solutions with static internal spaces had been obtained. In this section we show that these solutions are not stable and a bare cosmological constant and internal spaces with non-vanishing curvature are necessary conditions for their stabilization. With the help of suitably chosen parameters the model can be further improved to solve two problems simultaneously. First, the internal spaces undergo stable compactification. Second, the external space behaves in accordance with the standard Friedmann model.

To reach this goal let us start for simplicity from a homogeneous metric ansatz for the multidimensional cosmological model

$$\begin{aligned} g &= g_{MN} dX^M \otimes dX^N \qquad (5.1)\\ &= -\exp\left[2\gamma(\tau)\right] d\tau \otimes d\tau + \sum_{i=0}^{n} \exp\left[2\beta^i(\tau)\right] g_{(i)}, \end{aligned}$$

where we assumed the product manifold given by (1.1) with all factor spaces M_i, $i = 0, \ldots, n$ as Einstein manifolds and a foliated external space-time $\bar{M}_0 = \mathbf{R} \times M_0$. The scalar curvature corresponding to the metric (5.1) reads

$$\begin{aligned} R &= \sum_{i=0}^{n} R_i \exp\left(-2\beta^i\right) + \exp\left(-2\gamma\right) \times \qquad (5.2)\\ &\quad \times \sum_{i=0}^{n} d_i \left[2\ddot{\beta}^i - 2\dot{\gamma}\dot{\beta}^i + \left(\dot{\beta}^i\right)^2 + \dot{\beta}^i \sum_{j=0}^{n} d_j \dot{\beta}^j \right]. \end{aligned}$$

Matter fields we take into account in a phenomenological way as a m−component perfect fluid with energy-momentum tensor

$$T_N^M = \sum_{a=1}^{m} T^{(a)}{}_N^M, \qquad (5.3)$$

$$\begin{aligned} T^{(a)}{}_N^M &= \mathrm{diag}\left(-\rho^{(a)}(\tau), \underbrace{P_0^{(a)}(\tau), \ldots, P_0^{(a)}(\tau)}_{d_0 \text{ times}}, \ldots, \right. \\ &\quad \left. \ldots, \underbrace{P_n^{(a)}(\tau), \ldots, P_n^{(a)}(\tau)}_{d_n \text{ times}} \right) \qquad (5.4) \end{aligned}$$

and equations of state

$$P_i^{(a)} = \left(\alpha_i^{(a)} - 1\right) \rho^{(a)}, \quad i = 0, \ldots, n, \quad a = 1, \ldots, m. \qquad (5.5)$$

It is easy to see that physical values of $\alpha_i^{(a)}$ according to $-\rho^{(a)} \le P_i^{(a)} \le \rho^{(a)}$ run the region $0 \le \alpha_i^{(a)} \le 2$. The conservation equations we impose on each component separately

$$T^{(a)}{}_{N;M}^M = 0. \qquad (5.6)$$

Denoting by an overdot differentiation with respect to time τ, these equations read for the tensors (5.4)

$$\dot{\rho}^{(a)} + \sum_{i=0}^{n} d_i \dot{\beta}^i \left(\rho^{(a)} + P_i^{(a)}\right) = 0 \qquad (5.7)$$

and have according to (5.5) the simple integrals

$$\rho^{(a)}(\tau) = A^{(a)} \prod_{i=0}^{n} a_i^{-d_i \alpha_i^{(a)}}, \qquad (5.8)$$

where $a_i \equiv e^{\beta^i}$ are scale factors of M_i and $A^{(a)}$ are constants of integration. It is not difficult to verify that the Einstein equations with the energy-momentum tensor (5.3)-(5.8) are equivalent to the Euler-Lagrange equations for the Lagrangian (Ivashchuk, Melnikov 1995; Zhuk 1996)

$$\begin{aligned} L &= \frac{1}{2} e^{-\gamma+\gamma_0} G_{ij} \dot{\beta}^i \dot{\beta}^j - \qquad (5.9)\\ &\quad - e^{\gamma+\gamma_0} \left(-\frac{1}{2} \sum_{i=0}^{n} R_i e^{-2\beta^i} + \kappa^2 \sum_{a=1}^{m} \rho^{(a)} + \Lambda \right). \end{aligned}$$

Here we use the notation $\gamma_0 = \sum_0^n d_i \beta^i$.

The Lagrangian (5.9) can be obtained by dimensional reduction of the action functional (2.6).

Via conformal transformation of the external space-time metric from the Brans-Dicke to the Einstein frame:

$$g = g_{MN} dX^M \otimes dX^N$$

$$= \bar{g}^{(0)} + \sum_{i=1}^{n} \exp\left[2\beta^i(x)\right] g^{(i)}$$
$$= \Omega^2 \tilde{g}^{(0)} + \sum_{i=1}^{n} \exp\left[2\beta^i(x)\right] g^{(i)}, \quad (5.10)$$

with Ω^2 given by (2.11) we find that the external scale factors in the Brans-Dicke frame $a_0 = e^{\beta^0} \equiv a$ and in the Einstein frame $\tilde{a}_0 = e^{\tilde{\beta}^0} \equiv \tilde{a}$ are connected with each other by the relation

$$a = \left(\prod_{i=1}^{n} e^{d_i \beta^i} \right)^{-\frac{1}{D_0 - 2}} \tilde{a}. \quad (5.11)$$

The energy densities $\rho^{(a)}$ of the perfect fluid components are given by (5.8) and with the help of relation (5.11) can be rewritten as

$$\rho^{(a)} = \rho_0^{(a)} \prod_{i=1}^{n} a_i^{-\xi_i^{(a)}}, \quad (5.12)$$

where

$$\rho_0^{(a)} = A^{(a)} \frac{1}{\tilde{a}^{\alpha_0^{(a)} d_0}} \quad (5.13)$$

and

$$\xi_i^{(a)} = d_i \left(\alpha_i^{(a)} - \frac{\alpha_0^{(a)} d_0}{d_0 - 1} \right). \quad (5.14)$$

For the effective potential (2.15) we get accordingly

$$U_{eff} = \left(\prod_{i=1}^{n} e^{d_i \beta^i} \right)^{-\frac{2}{D_0 - 2}} \left[-\frac{1}{2} \sum_{i=1}^{n} R_i e^{-2\beta^i} + \right.$$
$$\left. + \Lambda + \kappa^2 \sum_{a=1}^{m} \rho^{(a)} \right]. \quad (5.15)$$

We now investigate MCMs containing a special subclass of this effective potential (5.15): potentials with separating scale factor contributions from internal and external factor spaces

$$U_{eff} = \underbrace{\left(\prod_{i=1}^{n} e^{d_i \beta^i} \right)^{-\frac{2}{D_0 - 2}} \left[-\frac{1}{2} \sum_{i=1}^{n} R_i e^{-2\beta^i} + \Lambda \right]}_{U_{int}} +$$
$$+ \underbrace{\kappa^2 \sum_{a=1}^{m} \rho_0^{(a)}}_{U_{ext}}. \quad (5.16)$$

We will show below, that such a separation on the one hand provides a stable compactification of the internal factor spaces due to a minimum of the first term $U_{int} = U_{int}(\beta^1, \ldots, \beta^n)$ as well as a dynamical behaviour of the external factor space due to $U_{ext} = U_{ext}(\tilde{\beta}^0)$. On the other hand this separation crucially simplifies the calculations and allows an exact analysis. The price that we have to pay for the separation is a fine-tuning of the parameters of the multicomponent perfect fluid

$$\alpha_0^{(a)} = \frac{2}{d_0} + \frac{d_0 - 1}{d_0} \alpha^{(a)}$$
$$\alpha_i^{(a)} = \alpha^{(a)}, \quad i = 1, \ldots, n, \quad a = 1, \ldots, m. \quad (5.17)$$

Only in this case we have

$$\xi_i^{(a)} = -\frac{2 d_i}{d_0 - 1} \quad (5.18)$$

yielding the compensation of the exponential prefactor for the perfect fluid term in the effective potential (5.15). The corresponding components $\rho_0^{(a)}$ read, respectively,

$$\rho_0^{(a)} = A^{(a)} \frac{1}{\tilde{a}^{2 + (d_0 - 1)\alpha^{(a)}}}. \quad (5.19)$$

Although the fine-tuning (5.17) is a strong restriction, there exist some important particular models that belong to this class of multicomponent perfect fluids. For example, if $\alpha^{(a)} = 1$ the a-th component of the perfect fluid describes radiation in the space M_0 and dust in the spaces $M_1, \ldots, M_n$. This kind of perfect fluid satisfies the condition $\sum_{i=0}^{n} d_i \alpha_i^{(a)} = D$ and is called superradiation (Liebscher, Bleyer 1985). If $\alpha^{(a)} = 2$ we obtain the ultra-stiff matter in all $M_i \, (i = 0 \ldots, n)$ which is equivalent, e.g., to a massless minimally coupled free scalar field. In the case $\alpha^{(a)} = 0$ we get the equation of state $P_0^{(a)} = \left[(2 - d_0) / d_0 \right] \rho^{(a)}$ in the external space M_0 which describes a gas of cosmic strings if $d_0 = 3 : P^{(a)} = -\frac{1}{3} \rho^{(a)}$ (Spergel, Pen 1997) and vacuum in the internal spaces $M_1, \ldots, M_n$. If $\alpha^{(a)} = 1/2$ and $d_0 = 3$ we obtain dust in the external space M_0 and a matter with equation of state $P_i^{(a)} = -\frac{1}{2} \rho^{(a)}$ in the internal spaces $M_i, \quad i = 1, \ldots, n$.

Let us first consider the conditions for the existence of a minimum of the potential $U_{int}(\beta^1, \ldots, \beta^n)$. According to (Günther, Zhuk 1997b) potentials U_{int} of type (5.16) have a single minimum if the bare cosmological constant and the curvature scalars of the internal spaces are negative $R_i, \Lambda < 0$. The scale factors $\left\{ \beta_c^i \right\}_{i=1}^{n}$ at the minimum position of the effective potential are connected by a fine-tuning condition

$$\frac{R_i}{d_i} e^{-2\beta_c^i} = \frac{2\Lambda}{D - 2} \equiv \widetilde{C}, \qquad i = 1, \ldots, n \quad (5.20)$$

and the masses squared of the corresponding gravitational excitons are degenerate and given as

$$m_1^2 = \ldots = m_n^2 = m_{exci}^2$$
$$= -\frac{4\Lambda}{D - 2} \exp\left[-\frac{2}{d_0 - 1} \sum_{i=1}^{n} d_i \beta_c^i \right]$$
$$= 2 \left| \widetilde{C} \right|^{\frac{D-2}{d_0 - 1}} \prod_{i=1}^{n} \left| \frac{d_i}{R_i} \right|^{\frac{d_i}{d_0 - 1}}. \quad (5.21)$$

Further it was shown in (Günther, Zhuk 1997b) that the value of the potential U_{int} at the minimum is connected with the exciton mass by the relation

$$\Lambda_{int} := U_{int}(\beta_c^1, \dots, \beta_c^n) = -\frac{d_0 - 1}{4} m_{exci}^2 \ . \quad (5.22)$$

From equations (5.20), (5.21) we see that exciton masses and minimum position $a_{(c)i} = \exp \bar{\beta}_c^i$ are constants that solely depend on the value of the bare cosmological constant Λ, the (constant) curvature scalars R_i and dimensions d_i of the internal factor spaces. This means that we have automatically $\Omega_c = \bar{M}_0$ from the very onset of the model. Hence the exciton approach in the present linear form breaks down only when the excitations become too strong so that higher order terms must be included in the consideration or the phenomenological perfect fluid approximation itself becomes inapplicable.

Let us now turn to the dynamical behaviour of the external factor space. For simplicity we consider the zero order approximation, when all excitations are freezed, in the homogeneous case: $\tilde{\gamma} = \tilde{\gamma}(\tilde{\tau})$ and $\tilde{\beta} = \tilde{\beta}(\tilde{\tau})$. Then the action functional (2.27) with

$$\begin{aligned} U_{(c)eff} &\equiv U_{eff}\left[\vec{\beta}_c, \tilde{\beta}(\tilde{\tau})\right] \\ &= U_{int}(\beta_c^1, \dots, \beta_c^n) + U_{ext}\left[\tilde{\beta}(\tilde{\tau})\right] \\ &\equiv \Lambda_{int} + \bar{\rho}_0(\tilde{\tau}) \end{aligned} \quad (5.23)$$

after dimensional reduction reads:

$$\begin{aligned} S &= \frac{1}{2\kappa_0^2} \int\limits_{\bar{M}_0} d^{D_0}x \sqrt{|\tilde{g}^{(0)}|} \left\{ \tilde{R}\left[\tilde{g}^{(0)}\right] - 2U_{(c)eff} \right\} \\ &= \frac{V_0}{2\kappa_0^2} \int d\tilde{\tau} \left\{ e^{\tilde{\gamma} + d_0\tilde{\beta}} e^{-2\tilde{\beta}} R[g^{(0)}] + \right. \\ &\quad + d_0(1 - d_0) e^{-\tilde{\gamma} + d_0\tilde{\beta}} \left(\frac{d\tilde{\beta}}{d\tilde{\tau}}\right)^2 - \\ &\quad \left. - 2e^{\tilde{\gamma} + d_0\tilde{\beta}} \left(\Lambda_{int} + \bar{\rho}_0\right) \right\} + \\ &\quad + \frac{V_0}{2\kappa_0^2} d_0 \int d\tilde{\tau} \frac{d}{d\tilde{\tau}} \left(e^{-\tilde{\gamma} + d_0\tilde{\beta}} \frac{d\tilde{\beta}}{d\tilde{\tau}} \right), \end{aligned} \quad (5.24)$$

where usually $R[g^{(0)}] = k d_0(d_0 - 1), \quad k = \pm 1, 0$. The constraint equation $\partial L / \partial \tilde{\gamma} = 0$ in the synchronous time gauge $\tilde{\gamma} = 0$ yields

$$\left(\frac{1}{\tilde{a}} \frac{d\tilde{a}}{d\tilde{t}}\right)^2 = -\frac{k}{\tilde{a}^2} + \frac{2}{d_0(d_0 - 1)} \left(\Lambda_{int} + \bar{\rho}_0(\tilde{a})\right), \quad (5.25)$$

which results in

$$\begin{aligned} &\tilde{t} + const \\ &= \int \frac{d\tilde{a}}{\left[-k + \frac{2\Lambda_{int}}{d_0(d_0-1)}\tilde{a}^2 + \frac{2\kappa^2}{d_0(d_0-1)} \sum_{a=1}^m \frac{A^{(a)}}{\tilde{a}^{(d_0-1)\alpha^{(a)}}}\right]^{1/2}} \ , \\ &= \int \frac{d\tilde{a}}{\left[-k + \frac{\Lambda_{int}}{3}\tilde{a}^2 + \frac{\kappa^2}{3} \sum_{a=1}^m \frac{A^{(a)}}{\tilde{a}^{2\alpha^{(a)}}}\right]^{1/2}}, \end{aligned} \quad (5.26)$$

where in the last line we put $d_0 = 3$.

Thus in the zero order approximation we arrived at a Friedmann model in the presence of negative cosmological constant Λ_{int} and a multicomponent perfect fluid. The perfect fluid has the form of a gas of cosmic strings for $\alpha^{(a)} = 0$, dust for $\alpha^{(a)} = 1/2$ and radiation for $\alpha^{(a)} = 1$. As $0 \le \alpha^{(a)} \le 2$, the cosmological constant plays a role only for large $\tilde{a}$ and because of the negative sign of Λ_{int} the universe has a turning point at the maximum of $\tilde{a}$. To be consistent with present time observation we should take

$$|\Lambda_{int}| \le 10^{-121} \Lambda_{Pl}. \quad (5.27)$$

We note that due to (5.26) and in contrast with (2.27) the minimum value $U_{(c)eff}$ of the effective potential in (5.23) cannot be interpreted as a cosmological constant, even as a time dependent one. Coming back to the gravitational excitons we see that according to (5.22) the upper bound (5.27) on the effective cosmological constant leads to ultra-light particles with mass $m_{exci} \le 10^{-60} M_{Pl} \sim 10^{-32} eV$. This is much less than the cosmic background radiation temperature at the present time $T_0 \sim 10^{-4} eV$. It is clear that such light particles up to present time behave as radiation and can be taken into account as an additional term $\rho_r = \frac{\kappa_0^2 A_r/3}{\tilde{a}^2}$ in (5.26). It can be easily seen that we reconstruct the standard scenario if we consider the one-component ($m = 1$) case with $\alpha^{(1)} = 1/2$, $\kappa^2 A^{(1)} \sim 10^{61}$ and $\kappa_0^2 A_r \sim 10^{117}$. Here we have at early stages a radiation dominated universe and a dust dominated universe at later stages of its evolution.

For completeness we note that via equations (5.21) and (5.22) the value of the effective cosmological constant has a crucial influence on the relation between the compactification scales of the internal factor spaces and their dimensions. In the case of only one internal negative curvature space $M_1 = H^{d_1}/\Gamma$ with $R_1 = -d_1(d_1 - 1)$ and compactification scale $a_{(c)1} = 10 L_{Pl}$ we have e.g. the relation $\Lambda_{int} = -(d_1 - 1) 10^{-2(d_1+2)} L_{Pl}$, so that the bound (5.27) implies a dimension of this space of at least $d_1 = 59$. Taking instead of one internal space a set of 2-dimensional hyperbolic $g-$tori $\left\{M_i = H^2/\Gamma\right\}_{i=1}^n$ (Lachieze-Rey, Luminet 1995) with compactification scale $a_{(c)i} = 10^2 L_{Pl}$ it is easy to check that we need at least $n = 29$ such spaces to satisfy (5.27).

Of course, other values of the cosmological constant lead to other exciton masses and compactification - dimensionality relations. So, it is also possible to get models with much more heavier gravitational excitons. For $\Lambda_{int} = -10^{-8} \Lambda_{Pl}$ we have e.g. $m = 10^{-4} M_{Pl}$ and the excitons are very heavy particles that should be considered as a cold dark matter. If we take the

one-component case $\alpha^{(1)} = 1$ we get at early times a radiation dominated universe with smooth transition to a cold dark matter dominated universe at later stages. But for this example it is necessary to introduce a mechanism that provides a reduction of the huge cosmological constant to the observable value $10^{-121}\Lambda_{Pl}$.

6. Conclusion

In the present paper we reviewed some recent results on inhomogeneous scale factor fluctuations as they necessarily occure in higher dimensional gravitational models after stable compactification of internal factor spaces. We showed that such scale factor fluctuations should be interpreted as massive or massless scalar particles propagating in the external space-time and interacting with other particles.

As simplest examples we considered lowest order approximations of the interaction of gravitational excitons with gravitons and photons.

Due to the specific gradient-like coupling terms of gravitational excitons and gravitons, in the used lowest order approximation of the theory an interaction between them occures only in the presence of a non-constant scale factor background. For constant scale factor backgrounds the system is necessarily located in one of the minima of the effective potential so that an interaction is only possible via nonlinear (higher order) coupling terms.

The analysis of the interaction between gravitational excitons and abelian gauge field showed that due to the high life-time of gravitational excitons with respect to the decay channel into photons the excitons should be interpreted as Dark Matter. Nevertheless, by analogy with axions it is possible that in strong magnetic fields there can occure oscillations between gravitational excitons and photons which will result in observable lines in spectra of astrophysical objects.

The last section of this review was devoted to the question of compatibility of the considered multidimensional gravitational models with the postinflational Friedman-Robertson-Walker dynamics of the observable part of our universe. For this purpose we considered a MCM with bare cosmological constant and a perfect fluid as matter source. It can be easily seen that there are only two classes of perfect fluids with stably compactified internal spaces. These kind of solutions are of utmost interest because an absent time variation of the fundamental constants in experiments (Marciano 1984; Kolb, Perry, Walker 1986) shows that at the present time the extra dimensions, if they exist, should be static or nearly static.

The first class (Günther, Zhuk 1997a,b) consists of models with $\alpha_0^{(a)} = 0$. It leads to the vacuum equation of state in the external space M_0. All other $\alpha_i^{(a)} (i = 1, \ldots, n)$ can take arbitrary values. This model can be used for a phemenological description of a muitidimensional inflationary universe with smooth transition to a matter dominated stage.

For models of the second class the stability is induced by a fine-tuning of the equation of state of the perfect fluid in the external and internal spaces (5.17). This class includes many important particular models and allows considerations of perfect fluids with different equations of state in the external space, among them also such that result in a Friedmann-like dynamics. Thus, this class of models can be applied for the description of the postinflationary stage in multidimensional cosmology. For the considered models we found necessary restrictions on the parameters which, from the one hand, ensure stable compactification of the internal spaces near Planck length and, from the other hand, guarantee dynamical behaviour of the external (our) universe in accordance with the standard scenario for the Friedmann model.

This toy model gives a promising example of a multidimensional cosmological model which is not in contradiction to observations. Although, a fine-tuning is necessary to get an effective cosmological constant in accordance with the present day observations.

Acknowledgements. We thank V. Frolov, V. Rubakov, V. Melnikov, V. Ivashchuk, M. Khlopov, V. Lukash, Yu. Gnedin and M. Rainer for stimulating discussions. The work was partially supported by DFG, grants 436 UKR 113, 436 RUS 113 and KON 1575/1999/GU 522/1.

References

Bleyer U., Zhuk A.: 1995, *Class. Quant. Grav.,* **12**, 89.

Candelas P., Weinberg S.: 1984, *Nucl. Phys.,* **B237**, 397.

Cho Y.M.: 1992, *Phys. Rev. Lett.,* **68**, 3133.

Duff M.J.: 1996, *Int.J.Mod.Phys.,* **A11**, 5623, (hep-th/9608117).

Fagundes H.V.: 1992, *Gen. Relativ. Gravit.,* **24**, 199.

Fagundes H.V.: 1993, *Phys. Rev. Lett.,* **70**, 1579.

Freund P.G.O., Rubin M.A.: 1980, *Phys. Lett.,* **B97**, 233.

Gasperini M., Giovannini M., Veneziano G.: 1995a, *Phys. Rev. Lett.,* **75**, 3796, (hep-th/9504083).

Gasperini M., Giovannini M., Veneziano G.: 1995b, *Phys. Rev.* **D52**, 6651, (astro-ph/9505041).

Gavrilov V.R., Ivashchuk V.D., Melnikov V.N.: 1995, *J. Math. Phys. (N.Y.),* **36**, 5829.

Gibbons G.W., Hawking S.W.: 1977, *Phys. Rev.,* **D15**, 2752.

Gnedin Yu.N. et al: 1999, *M. N. R. A. S.,* **306**, 117.

Gnedin Yu.N.: 1997a *Ap & SS,* **249**, 125.

Gnedin Yu.N.: 1997b *Ap & SS,* **252**, 95.

Green M.B., Schwarz J.H., Witten E.: 1987, *Superstring Theory,* (Cambridge: Cambridge Univ. Press.)

Günther U., Zhuk A.: 1997a, *Phys. Rev.,* **D56**, 6391, (gr-qc/9706050).

Günther U., Kriskiv s., Zhuk A.: 1998, *Gravitation & Cosmology,* **4**, 1, (gr-qc/9801013).

Günther U., Starobinsky A., Zhuk A.: 1999, *Interacting gravitational excitons from extra dimensions,* in preparation.

Günther U., Zhuk A.: 1997b, *Stable compactification and gravitational excitons from extra dimensions* (Proc. Workshop "Modern Modified Theories of Gravitation and Cosmology", Beer Sheva, Israel, June 29 - 30, 1997), 1998, *Hadronic Journal*, **21**, 279, (gr-qc/9710086).

Günther U., Zhuk A.: 1998, *Class. Quant. Grav.,* **15**, 2025, (gr-qc/9804018).

Ivashchuk V.D., Melnikov V.N.: 1995, *Class. Quant. Grav.,* **12**, 809.

Ivashchuk V.D., Melnikov V.N., Zhuk A.I.: 1989, *Nuovo Cimento,* **B104**, 575.

Kasper U., Zhuk A.: 1996, *Gen. Relativ. Gravit.,* **28**, 1269.

Kolb E.W., Perry M.J., Walker T.P.: 1986, *Phys. Rev.,* **D33**, 869.

Lachieze-Rey M., Luminet J.-P.: 1995, *Phys. Rep.,* **254**, 135.

Liebscher D.-E., Bleyer U.: 1985, *Gen. Relat. Gravit.,* **17**, 989.

Litterio M., Sokolowski L.M., Golda Z.A., Amendola L., Dyrek A.: 1996, *Phys. Lett.,* **B382**, 45.

Marciano W.J.: 1984, *Phys. Rev. Lett.,* **52**, 489.

Rainer M., Zhuk A.: 1996, *Phys. Rev.,* **D54**, 6186.

Spergel D., Pen U.-L.: 1997, *Astrophys. J.,* **491**, L67, (astro-ph/9611198).

Strominger A., Vafa C.: 1996, *Phys.Lett.,* **B379**, 99, (hep-th/9601029).

Wolf J.A.: 1967, *Spaces of constant curvature,* (McGraw-Hill, New York).

York J.W.: 1972, *Phys. Rev. Lett.,* **28**, 1082.

Zhuk A.: 1996, *Class. Quant. Grav.,* **13**, 2163.

COSMOARCHEOLOGY: ASTROPHYSICAL PROBES FOR NEW PHYSICS IN THE EARLY UNIVERSE

M.Yu. Khlopov

Centre for Cosmoparticle physics "Cosmion"
Miusskaya Pl.4, Moscow, 125 047, Russia *mkhlopov@orc.ru*

ABSTRACT. The original Gamov's Big Bang cosmology has evolved for the last decades to the modern cosmology, losing the direct relationship with the experimentally proven physical laws. It is the aim of cosmoparticle physics to study both the early Universe and the physics, governing its evolution, in the combination of their indirect cosmological, astrophysical and physical effects. Cosmoarcheology is the important branch of this research. It undertakes the Gedanken Experiment, tracing cosmological signatures for the new physics in the astrophysical data. The main ideas of the modern cosmology find their physical origin in the hypothetical processes in the early Universe: the total density is related to the result of inflation, the baryon density - to baryosynthesis and the dark matter - to primordial particles and/or fields generated before the 1 s of cosmological expansion. The physical mechanisms for these processes are based on predictions of particle theory. To specify the physical origin of the cosmological functions one needs the additional model-dependent cosmological effects, that can be referred to as the hidden functions of the modern cosmology. Cosmoarcheological analysis finds the spectrum of primordial black holes, inhomogeneous baryosynthesis and multicomponent dark matter as important signatures of the new physics in the early Universe, related to a wide class of physical realisations of cosmological models. Such analysis predicts new phenomena in the Universe, which can be the subject of astronomical discoveries in the next decades, such as mirror matter, 4th type of neutrino, or macroscopic antimatter in baryon asymmetrical Universe. In particular, it follows from this analysis, that the halo of our Galaxy can contain up to 100000 antimatter stars. Cosmoarcheological chains link the processes in the early Universe to the effects after the first second, which can be tested in the observations of the thermal background, of the baryon matter space distribution and chemical composition, of non-thermal electromagnetic backgrounds and cosmic rays. The important role of cosmoarcheological methods is illustrated on the example of the model of horizontal unification. The model proves that in no case the physically self-consistent realisation of inflation, baryosynthesis and dark matter can be reduced to these three phenomena only. Cosmoarcheological analysis of the additional cosmological consequences, following from such realisations, provides the principal possibility to reproduce the physics of early Universe in all its nontrivial complexity.

Key words: cosmology: inflation, baryosynthesis, dark matter, antimatter, black holes: primordial black holes; elementary particles: quarks, leptons: neutrino; cosmoparticle physics.

1. Introduction

The modern cosmology is based on the two observational facts, namely, that the Universe expands and that the Universe contains the electromagnetic black body background radiation. Putting them together one comes to the Gamov's ideas of big bang Universe. One inevitably comes to the conclusion, that at earlier stages of cosmological expansion the physical conditions in the Universe should have been much different from what we observe now. Extrapolating, or more precisely interpolating, the law of cosmological expansion to the past, one finds, that at much earlier stages of cosmological expansion energy density of radiation exceeded the matter density, so that the radiation dominance stage should have taken place. One can easily check that matter and radiation were in equilibrium, that there were no galaxies, stars, but the matter was in the form of nearly homogeneous plasma. Gamov's big bang scenario was a self-consistent combination of general relativity, thermodynamics and well prove n in laboratories laws of atomic and nuclear physics, successively applied to the evolution of the Universe as a whole, under the assumption that only baryon matter and electromagnetic radiation (and neutrinos) maintain its content (see review in Zeldovich, Novikov,1975). According to this scenario at the first three minutes nuclear reactions should have taken place, leading to the primordial chemical composition. This picture found qualitative confirmation in the comparison of predictions of big bang nucleosynthesis with the observed light element abundance. It gave qualitative explanation to the observed structure of inhomogeneities as a result of

gravitational instability in nearly homogeneous matter. However, quantitative disagreements turning to be more and more profound made the whole picture controversial, unless some additional fundamental elements are added to the basis of the whole construction. These additional elements found physical motivation in the development of parti cle theory.

In the Gamov's cosmology it was reasonable to take into account only electrons, nucleons, photons and neutrino from hundreds elementary particles, discovered at accelerators, since only stable particles are of cosmological importance. In particle theory stability reflects the conservation law, which from Noether's theorem follows from fundamental particle symmetry. Electron is stable owing to electric charge conservation and proton's stability reflects conservation of baryon charge. Though the standard model of weak, electromagnetic and strong interactions, built on the basis of the generalisation of gauge principle of Quantum Electrodynamics, finds no experimental contradictions, there are internal inconsistencies and esthetical reasons, which lead the particle theory beyond the standard model. New symmetries and mechanisms of their breaking result in new conservation laws and macroscopic phenomena, having important cosmological consequences - phase transitions in the early Universe, stable and metastable particles, topological defects etc.

The account for these consequences of particle theory made it possible to approach the principal questions: why the Universe expands? why its initial conditions were so close to flat Universe? why they were so similar in causally disconnected regions? why it contains matter and no antimatter? Does baryon matter dominate in the modern Universe?, which had no fundamental answers in the old cosmological picture. The modern cosmology retains the main spirit of Gamov's approach - to treat the Universe as the physical process, but physical laws governing this process also turn to be the subject of study. The exciting challenge to elaborate both the true theory of the Universe and the true physics, underlying it, is the topic of the present paper.

2. The modern description of big bang Universe – inflationary cosmology with baryosynthesis and dark matter

The first three questions found principal solution in inflationary cosmological models (Guth, 1981), assuming the existence of a stage of superluminous (in the simplest case exponential) expansion in the very early Universe. Such a stage can not be provided by matter, radiation or relativistic plasma dominance, but can be realised under some conditions as cosmological consequence of particle theory, c.f. in strong first order phase transition or by slow rolling down of scalar field to its true vacuum state. Simultaneously inflationary models found the physical mechanisms for generation of the spectrum of initial fluctuations. Most of these effects are related to experimentally inaccessible parts of particle theory, in particular, to the mechanisms of symmetry breaking at supehigh energy scales. One can also find, that different inflationary models follow from different theoretical grounds and in general may coexist in the complete cosmological scenario.

A.Sakharov (1967) and then V.Kuzmin (1970) were first, who related the observed baryon asymmetry of the Universe to the generation of baryon excess due to out-of-equilibrium CP violating effects in hypothetical baryon nonconserving processes at very early stages of the initially baryon symmetric Universe. Grand unified models have provided physical basis for these original ideas of baryogenesis, having the existence of baryon non conserving interactions among their predictions. The mechanisms of baryosynthesis found then some other grounds in supersymmetric models, where primordial condensate of scalar quarks is possible, resulting in baryon excess after scalar quarks decay on ordinary quarks, and even in the standard model, leading to baryon nonconservation at very high temperatures, provided that it is extended by larger Higgs sector and/or by inclusion of lepton number violating processes, related to neutrino Majorana mass generation mechanism.

The discrepancy between the estimated baryon density and the total density of the Universe is ascribed in the modern cosmology to the existence of non-baryonic dark matter. Namely, the level of initial fluctuations, needed in the old big bang scenario to provide the formation of the observed large scale structure of the Universe, turned to correspond to the expected effect in anisotropy of thermal electromagnetic background inconsistent with the observed level of its isotropy. On the other hand, low baryonic density, one needs to reproduce the observed light element abundance as a result of big bang nucleosynthesis (see review in Schramm,Copi,1996), was inconsistent with much higher density, one needs to provide the formation of the large scale structure as a result of development of gravitational instability on matter dominated stage. In the simplest cases dark matter is associated with primordial weakly interacting particles, originated from early Universe - massive neutrino (hot dar k matter, HDM), invisible axions or neutralino (cold dark matter, CDM) or unstable neutrino (UDM). However different are from the cosmological viewpoint the models of large scale structure formation by hot, cold, unstable dark matter, or more sophisticated models, implying cosmic strings plus hot dark matter, late phase transitions etc, they are not alternatives from the viewpoint of particle physics, having grounds in different and in general complementary parts of hidden sector of particle theory. So, in principle, the mixture of all of them should be considered as the general case.

So the modern cosmological picture reflects the prin-

ciple change in our understanding, what big bang cosmology is. From self-consistent but basically controversial and incomplete old big bang scenario we come to the picture of inflationary cosmology with baryosynthesis and (multicomponent?) nonbaryonic dark matter. Thus, directly or indirectly, Gamov's big bang theory is supplemented in the modern standard big bang Universe by at least three necessary elements (inflation, baryosynthesis and nonbaryonic dark matter), based on the physical laws, predicted by particle theory but having no experimental proofs. There is a wide variety of different physical mechanisms for inflation, baryosynthesis, various candidates on the role of dark matter particles and, since both the early Universe, when inflation and baryosynthesis should have taken place, and dark matter could not be observed directly by astronomical means, one should elaborate the system of indirect means to make the proper choice between these variants, corresponding to various cosmological scenarios and particle models, underlying them.

The problem is that the space of cosmological and physical parameters is, in general, multidimensional, since physical grounds for different mechanisms of inflation, baryosynthesis and different candidates for dark matter follow from different physical motivations and are not in general alternative but complementary. On the other hand, cosmological tests for particle models should, in general, account both for the particular realization of inflation, baryosynthesis and dark matter and for the additional modifications of cosmological scenarios, corresponding to the chosen realization. Cosmoarcheology, searching in the astrophysical data for the footprints of new physical phenomena in the Universe, may be viewed as already existing branch of proper CosmoParticle Physics (Khlopov,1999), in which all its components are mixed up in a nontrivial manner, resulting in a set of astrophysical probes for the existence and possible properties of hypothetical particles, fields, objects and phenomena predicted as cosmological consequences of particle theory.

Cosmoarchelogy treats the Universe as a unique natural accelerator laboratory, so that the astrophysical data play here the role of specific experimental sample in Gedanken Experiments, Cosmoarcheology undertakes. As in any experiment, to achieve meaningful result one should have precise understanding of the experimental device used, as well as to develop the methods of data sampling and analysis. The problem is, that in the Universal particle laboratory both the source and detectors are out of control. Astrophysical processes can not be directly reproduced in laboratories, but however complicated the combination of effects is, theoretical astrophysics uses, as a rule, in its analysis natural laws, proven in experiment. The trouble is, that in theoretical treatment of the Universe and its evolution the basic physical laws are not known. It makes selfconsitent formulation of cosmoarcheological approach to be, in general, model dependent. One should account for the relationship between the hypothetical particle or field, probed by the astrophysical data, and the physics, underlying inflation, baryosynthesis and nonbaryonic dark matter. And, since the latter is model dependent, one should consider cosmological consequences of the considered hypothesis refered to the picture of cosmological evolution, based on the chosen particle model, underlying these necessary elements of the modern cosmology. It means, that the cosmological trace of hypothetical particle or field may be multi-step, following the nontrivial cosmological path, the model implies.

On the other hand, one should expect, the real picture of cosmological evolution to be much more complicated, than the original Gamow's big bang scenario, and generally more sophisticated, than simple addition of inflation, baryosynthesis and nonbaryonic dark matter dominancy to the scenario of Gamov's Universe. The reason is, that any physically reasonable theoretical framework, giving rise to the necessary elements of cosmology, is generally much more extensive, supplementing these elements by a number of additional cosmologically viable details. Testing these details, cosmoarcheology extends the might of observational cosmology in its probe for the true theory of the Universe.

3. Cosmological probes for physical nature of inflation, baryosynthesis and dark matter

Assuming, that inflational baryon asymmetrical cosmology with nonbaryonic dark matter is more close to reality, than Gamow's original big bang scenario, one should face on the problem of observational evidences, specifying the choice for inflational model, mechanism of baryosynthesis and for the proper form of nonbarynic dark matter.

3.1. Tracers for the mechanism of inflation

One considers inflation as necessary element of cosmological picture. Inflational models explain, why the Universe expands. They provide solution for horizon, flatness, magnetic monopole etc problems (Guth,1981, see review in Khlopov,1999). The solution is based on superluminous expansion, taking place for equation of state $p < -frac\epsilon 3$. Neither matter, nor radiation dominance can provide such an equation of state. One needs some hypothetical phenomena to occur in the very early Universe, inducing unstable negative pressure stage of cosmological evolution. Such hypothetical processes may be related to R^2 effects in gravity, to strong first order phase transitions, or to slow rolling down of effective potential to the true vacuum state. To make the proper choice between these

possibilities, or, at least, to make some cut in their wide variety, additional traces of inflational mechanism should be considered. - Fluctuations on inflational stage induce the spectrum of initial density fluctuation, giving rise to galaxy and large scale structure formation in respective scales. The amplitude of these fluctuations is constrained by the observed isotropy of the thermal electromagnetic background. It rules out all the inflational models with high amplitude of predicted fluctuations, the most of GUT induced phase transition scenarios, in particular. In simplest models with quasi-De Sitter close to $p = -\epsilon$ equation of state on inflational phase flat Harrison-Zeldovich form of the spectrum is predicted. Then the estimated amplitude of initial fluctuations at the modern LSS scale provides some information on the possible inflaton properties, e.g. on the form and parameters of scalar field potential. - For more complicated inflational models, e.g. multicomponent inflation, the form of the predicted spectrum of fluctuations may differ from simple flat one. Phase transitions on inflational stage lead to specific peaks or plateaus in the spectrum with the position and amplitude defined by the parameters of the model. One should also account for phase transitions after the global inflational stage, in which the initial spectrum may be modified. - Both in R^2 and scalar field driven (c.f. chaotic) inflational scenarios long dust-like post-inflational stage appears, induced by coherent inflaton field oscillations. The duration of such stages defines the maximal temperature of the Universe after reheating, when radiation dominance stage starts. It also defines the specific entropy of the Universe after reheating. - Initial density fluctuations grow on postinflational dust-like stage, following the general law of development of gravitational instability on matter dominated stage in expanding Universe $frac\delta\rho rho = \delta_0 fractt_(0)^{2/3}$. If the ratio of cosmological timescales, corresponding to the end, t_1 , and the beginning, t_0, of the dust-like stage exceeds ${\delta_0}^{-frac32}$ where δ_0 is the amplitude of fluctuation, in the respective scale inhomogeneity is formed. Evolution of such inhomogeneity may lead to primordial black hole (PBH) formation. Spectrum of PBHs reflects the scales, at which inhomogeneities are formed as well as the mechanism of PBH formation. The minimal probability W_{PBH} of PBH formation is ${\delta_0}^{13/2}$, estimated for direct formation of PBHs in contraction of a very small fraction of configurations, evolved from specifically isotropic and homogeneous fluctuations (see Refs. in Khlopov, 1999). The account fo r PBH formation in a result of evolution of the bulk of inhomogeneities strongly increases the amount of expected PBHs. - Peaks in the spectrum of density fluctuations, produced at inflational stage, may also induce PBH formation even on radiation dominance stage with the probability $W_{PBH}\ exp-frac118{\delta_0}^2$.

3.2. Antimatter trace for inhomogeneous baryosynthesis

The generally accepted motivation for baryon asymmetric Universe is the observed absence of antimatter at macroscopic scales up to the scales of clusters of galaxies. In baryon asymmetric Universe the observed baryonic matter is originated from initial baryon excess, surviving after local nucleon-antinucleon annihillation, taking place at the first millisecond of cosmological evolution. The baryon excess is assumed to be generated in the process of baryogenesis (Sakharov,1967; Kuzmin,1970 see review in Khlopov,1999), resulting in baryon asymmetry of initially baryon-symmetrical Universe. It turned out, that practically all the existing mechanisms of baryogenesis may under some conditions lead to inhmogeneous baryosynthesis and even to generation of antibaryon excess in some places. So inhomogeneities of baryon excess distribution and even domains of antimatter in baryon asymmetric Universe may provide a probe for the mechanism of baryogenesis.

In the original Sakharov's scenario of baryosynthesis CP violating effects in out-of-equilibrium B-nonconserving processes, say decays of some particles X, generated in charge symmentric Universe with equal amount of X and their antiparticles baryon excess proportional to n_X and $Im\phi$, ϕ being CP violating phase. If sign and magnitude of $\phi(x)$ varies in space, the same out-of-equilibrium B-nonconserving processes, leading to baryon asymmetry, results in $B(x)$ and in $B(x) < 0$ in the regions, where $Im\phi(x) < 0$. Spatial dependence of ϕ is predicted in model of spontaneous CP violation or in models, where CP violating phase is associated with the amplitude of invisible axion field. The size and amount of antimatter in domains, generated in this case, is related to the parameters of models of CP violation and/or invisible axion (see review in Khlopov,1999; Khlopov, Chechetkin,1987; Chechetkin et al,1982, Khlopov,1992).

SUSY GUT motivated mechanisms of baryon asymmetry imply flatness of superpotential relative to existence of squark condensate. Such a condensate, being formed with B¿0, induces baryon asymmetry, after squarks decay on quarks and gluinos. However the mechanism doesn't fix the value and sign of B in the condensate, opening the possibilities for inhomogeneous baryon charge distribution and antibaryon domains (Khlopov,1999; Chechetkin et al,1982, Khlopov,1992).

New approach to baryosynthesis, based on electroweak baryon charge nonconservation at high temperatures, also imply the possibility of antimatter domains, e.g. due to spontaneous CP violation (Comelli et al, 1994).

So antimatter domains may appear in baryon asymmetric Universe and may be related to practically al

the mechanisms of baryosynthesis, to mechanisms of CP violation and to possible mechanisms for primordial baryon charge inhomogenity. The size of domains depends on the details of the respective phase transitions and initial distributions of spatial variable CP violating phase, what accounting for inflation may be as large as the modern horizon, being the case for the models of "island Universe" (Dolgov et al,1987) with very large scale inhomogeneity of baryon charge distribution.

General parameters of the averaged effect of the domain structure are the relative amount of antimatter $\Omega_a = frac\rho_a\rho_{crit}$, where ρ_a is the averaged over large scales cosmological density of antimatter and $\rho_{crit} = frac3H^28\pi G$ is the critical density, and the mean size of domains, l, (the characteristic scale in their distribution on sizes) or for small domains, t_{an}, the timescale of their annihillation with the surrounding matter.

Dense antimatter domain with the size exceeding the survival scale can form antimatter globular cluster in our Galaxy. It was recently shown (Khlopov,1998; Belotsky et al,1999) that the minimal mass of such cluster is determined by the survival scale and the maximal total mass of antimmatter stars in our Galaxy is constrained by the galactic gamma ray background. Such cluster should be the galactic source of antinuclear component of cosmic rays, which is accessible in all the allowed range to search for antimatter in AMS experiment on Alpha station (Battiston,1999).

3.3. Multicomponent dark matter

The main arguments favouring nonbaryonic nature of dark matter in the Universe are big bang nucleosynthesis (BBN) in inflational cosmology and formation of large scale structure of the Universe at the observed isotropy of relic radiation. The first line of arguments accounts for the reasonable fits of BBN predictions to the observed light element abundance at $\Omega_b < 0,20$ and the predicted by inflational cosmology $\Omega_{tot} = 1$, ascribing the difference to nonbaryonic dark matter. The second type of arguments is that one can not accommodate both the formation of the large scale structure and the observed isotropy of thermal electromagnetic background without some weakly interacting form of matter triggering structure formation with minor effect in relic radiation angular distribution (see review in Khlopov,1999). There are several scenarios of structure formation by hot (HDM), cold (CDM), unstable (UDM), mixed hot+cold (H+CDM), hierachical decaying (HDS) etc dark matter. These scenarios physically differ by the ways and succession in which the elements of structure are formed, as well as by the number of model parameters. But having in mind general independence of the motivations for each type of dark matter candidates, one finds from particle physics viewpoint hot, cold, unstable etc dark matter not as alternatives but as supplementary options to be taken together, accounting for the whole set of reasonable physical arguments.

Indeed, one considers the would be eV-(10eV)- neutrino mass as physical motivation for hot dark matter scenario. But massive neutralinos, predicted in supersymmetric models, or invisible axions, following from Peccei-Quinn solution of strong CP violation problem in QCD, being cold dark matter candidates, are based on physical grounds, which are in no case alternative to the physics of neutrino mass. So mixed hot+cold dark matter scenarios seem to be physically more reasonable, than simple one-parameter HDM or CDM models. However, all these motivations do not correlate with the problem of quark lepton families, of the existence of three types of neutrinos. Physical mechanisms of family symmetry breaking lead to new interactions, causing massive neutrino instability relative to decay on lighter neutrinos and light Goldstone boson, familon or singlet Majoron.

Neutrino instability, intimately related to family symmetry breaking, provides physical grounds for unstable dark matter (UDM) scenarios (Khlopov,1999). At the expense of additional parameter (unstable particles lifetime) UDM models remove the contradiction between the data on the total density within the inhomogeneities, $\Omega_{inhom} < 1$, and the prediction of inflational cosmology, $\Omega_{tot} = 1$ ascribing the difference in Ω to homogeneous background of unstable particles decay products. UDM models also recover the disadvantages of HDM scenarios, related to too rapid evolution of the structure after its formation. Owing to neutrino instability large scale structure, formed at redshifts corresponding to observed distant objects, survives after the major part of dark matter, having formed the structure, decayed.

The actual multicomponent content of dark matter may be extremely richer, if one takes into account the hypothesis on shadow matter, following from the need to recover the equivalence of left- and right- handed coordinate systems in Caluzza-Klein and superstring models. One meets the problem to account for the whole set of matter fields and interactions, arising from E_8' sector of heterotic string $E_8 x E_8'$ model. Mirror and shadow particles represent the nontrivial dissipational form of dark matter. In the contrary to the usual dark matter candidates - weakly interacting particles, being in the form of collisionless nondissipating gas, mirror and shadow matter can form dense star-like dark matter objects. Such objects, causing microlensing effects in our Galaxy, may be responsible for the observed MACHO events.

Even the above list of options, far from complete, poses the serious problem of the proper choice of the true combination of various dark matter candidates in

physically motivated multicomponent dark matter scenarios.

Thus, since physical grounds for all the nonbaryonic dark matter candidates are outside the standard model and loose the proper experimentally proven basis, we either have to take into account all the possible ways to extend the standard model, treating all the candidates as independent, or find a quantitatively definite way to estimate their relative contribution.

4. Cosmological probes for particle theory

The physical basis for inflation, baryosynthesis and dark matter candidates is associated with the new physics, following from the particle theory. One has to use all the indirect means to probe this new physics, and cosmological tests play important role in these methods. One needs cosmologically viable consequences of particle models for such tests, which are generally related to stable or sufficiently metastable particles or objects predicted in them. Since (meta)stability is based in particle theory on some (approximate) conservation law, reflecting respective fundamental symmetry and/or the mechanism of symmetry breaking, cosmoarcheology probes the most fundamental new laws of Nature, assumed by respective extension of standard model.

Indeed, new symmetries, extending the symmetry of standard model, imply new charges, conserved exactly or approximately, and the lightest particle posessing respective charge should be either stable or metastable. The new charges may be related to local or global, continuous or discrete symmetry. They may be topological, induced by the topology of respective symmetry group. In the most cases the mass of hypothetical particles and objects reflects the new fundamental physical scale, at which the assumed symmetry is broken. So let's give some examples, referring to the book (Khlopov,1999) for details. - In all the GUT models, unifying electromagnetism with other forces within compact group of symmetry magnetic monopole solutions appear as topological point object, bearing Dirac magnetic charge $g = hc/e$ and having the mass of the order Λ/e, where Λ is the scale, at which U(1) symmetry, corresponding to electromagnetism, separates from the rest of interactions. - Some specific GUT models imply topology of symmetry group, leading to the existence of domain wall (spontaneously broken discrete symmetry), cosmic string (spontaneously broken U(1) symmetry), wall-surrounded-by-strings etc topological solutions. The respective unit surface (unit length) energy density is of the order of the respective power of the scale Λ of symmetry breaking, i.e. Λ^3 for walls and Λ^2 for strings. - R symmetry (exact or approximate) protects in supersymmetric models (meta)stability of the lightest supersymmetric particle (LSSP). Its mass is generally related to the scale of supersymmetry breaking. In local supersymmetric models this scale also defines the mass of gravitino - supersymmetric partner of graviton, having semigravitational coupling to other particles, inversely proportional to the Planck scale m_{Pl}. - See-saw mechanism of neutrino mass generation implies heavy right-handed neutrino with the Majorana mass M_R related to the scale of lepton number nonconservation. The Majorana mass of the ordinary left-handed neutrino is given by $m_\nu = fracm_D^2 M_R$, where m_D is the Dirac mass of fermions (typically related to the mass of respective charged lepton). The lifetime of the heavy right-handed neutrino, determined by its mixing with the left-handed one ($fracm_D M_R$), turns to be inveresely proportional to mass of light left-handed neutrino. - Spontaneous breaking of Peccei-Quinn symmetry, used to remove the problem of strong CP violation in QCD, results in the existence of (pseudo)Goldstone boson, axion, with the mass $m_a = fracm_\pi f_\pi F$, where F is the scale of Peccei-Quinn symmetry breaking. Axion couplings to fermions are inversely proportional to F, and its lifetime relative to decay on 2γ is equal to $t_a = frac64\pi F^2 m_a^3$. - Equivalence of right- and left- handed coordinate systems implies the existence of mirror partners of ordinary particles. Mirror particles should not have ordinary gauge interactions and their own mirror interactions should be symmetric to the respective interactions of respective ordinary partners. Then mirror particles, having the same mass spectrum and the same internal mirror couplings as their ordinary partners, are coupled to the ordinary matter by gravity only. - Mirror particles can be included together with the ordinary particles into the unifying GUT. It leads, after the GUT symmetry is broken and the ordinary and mirror sectors, retaining the discrete symmetry between them, are separated, to the existence of Alice strings, cosmic strings, changing the relative mirrority of objects along the closed paths around them. - In superstring models initial mirror symmetry is broken due to combined action of compactification and gauge symmetry breaking, so that shadow matter appears, loosing the discrete symmetry with the ordinary partners. In heterotic string model the initial $E_8 x E_8'$ gauge symmetry, assuming exact symmetry between the ordinary (E_8) and mirror (E_8') worlds in 10 space-time dimensional string model, is reduced after compactification and gauge symmetry breaking to $(broken)E_6 x (broken?)E_8'$ 4-dimensional effective field model with the ordinary matter embraced by $(broken)E_6$ symmetry and the enormously extensive world of shadow particles and their interactions, corresponding to the $(broken?)E_8'$ gauge group. - The Wilson loop mechanism of E_6 symmetry breaking down to the symmetry of standard model implies in the superstring models the existence of at least one new (4th) quark-lepton family and of at least one new $U(1)$ gauge

charge. The measured width of Z boson puts lower limit on the possible mass of 4th neutrino $m > 45$GeV. If the new $U(1)$ charge is attributed to the 4th family and is strictly conserved, the 4th neutrino, being the lightest particle of the 4th family, should be absolutely stable. - The mechanism of gauge symmetry breaking in compactification onto Callaby-Yao manifolds or orbifolds, used in superstring models, implies homotopically stable solutions with the mass $M = fracr_c\alpha'$, where r_c is the radius of compactification and α' is the string tension. These objects are sterile relative to gauge interactions and may act on the ordinary matter by gravity only. These and many other examples of the particle zoo, induced by the extensions of the standard model of electroweak and strong interactions, are related to the new phenomena, direct experimental search for which is either very hard or principally impossible. So cosmological effects are important or even unique sources of information on their possible existence.

5. Detectors of the Universe

One may reduce the effect of new particles and fields in the Universe to the two principal possibilities:1) general dynamical influence on the cosmological expansion and 2) specific influence on particular astrophysical processes. In the first case the very presence of hypothetical particles and fields in the Universe, independent on their specific properties, causes some observational effect. In the second case to estimate the expected result some properties of the considered particles and fields should be specified. In the Universe, viewed as particle laboratory, these two types of effects may be compared with integral and differential detectors, used in particle experiment. One can refer to the two widely known cosmological probes of new particles -age of the Universe (the modern total density is restricted by the observational lower bounds on the age of the Universe) and -4He primordial abundance (the total density of the Universe in the period of big bang nucleosynthesis is restricted by the observational upper limit on primordial He abundance, or in more refined approaches by the set of primordial light element abundance constraints) as to the integral detectors, probing the contribution into the cosmological density of any form of the matter, irrespective to its particular properties. In the both cases the only thing we assume on the hypothetical forms of the matter is their existence in our space-time, resulting in their contribution into the total density of the Universe. The same holds true for - the condition of sufficient growth of density fluctuations, following from the existence of the observed large scale structure of the Universe and the observed isotropy of the thermal radiation background. This condition leads to the existence of dust-like stage of (dark) matter dominance sufficiently long to provide the formation of large scale structure from initial density fluctuations, small enough to satisfy the observed level of isotropy of the relic radiation. It excludes the range of parameters of unstable particles (or objects) leading to the dominance of their relativistic decay products in the period of large scale structure formation.

In the latter case one also does not specify the properties or decay modes of the unstable matter. All these methods, being universal, have rather rude sensitivity to the parameters of the hypothetical matter. Only the amount of such matter, comparative to or dominating in the total cosmological density, may be definitely excluded by the integral detectors. More refined and sensitive tools are available, once specific tracers of hypothetical matter are specified.

For stable charge-symmetric species, present in the halo of Galaxy, their weak annihilation, resulting in neutrino-antineutrino, gamma-ray, electron-positron or proton-antiproton production, provides the possibility to exclude the range of respective parameters from - the observed nonthermal electromagnetic backgrounds or observational upper limits on them - the observed gamma ray background - the observed electron-positron background - the data on the cosmic ray fluxes - the restrictions on high energy neutrino cosmic backgrounds which may be viewed as the "experimental" data from differential detectors for the hypothetical processes.

Note, that the EGRET data on galactic gamma background at $E > 1$GeV and the data on underground WIMP searches are consistent with the hypothesis on the existence of stable 4th neutrino with the mass 50GeV (Golubkov et al, 1999). Annihilation of primordial 4th neutrinos and antineutrinos in the halo of our Galaxy should lead to the signature in the spectrum of cosmic positrons, which can be tested in AMS experiment on ISS during the next decade.

For unstable species with the lifetime, smaller, than the age of the Universe, the same types of data trace the respective decay modes, if the Universe is transparent for decay products. For each type of decay product one may fix the redshift, starting from which the Universe is opaque for respective fluxes. Then the data on - the thermal background spectrum distortions and on - the light element abundance from nonequilibrium cosmological nucleosynthesis provides indirect information on the effects of interaction of the fluxes with plasma and radiation in the early Universe. The spectrum of relic radiation may be viewed as "electromagnetic calorimeter" of the early Universe, since any electromagnetic energy release, starting from 10^5 s, induces the distortions of the Planck form of the thermal microwave radiation background spectrum. Light element abundance turns to be even more sensitive probe for inequilibrium processes on the radiation dominance stage, owing to the strong possible change of concen-

tration for the less abundant light elements (D, ^3He, Li, Be, B,...) in nuclear reactions, induced by energetic particle fluxes from the hypothetical sources with comparatively small electromagnetic energy release.

Practically all the above mentioned differential detectors may probe the products of PBH evaporation, so that the restrictions on the sources of respective particle fluxes or effects may be recalculated in the terms of the constraints on the concentration of PBHs with the mass 10^9 - 10^{15} g, evaporating from the 1 s to the present time. Accounting for the possible mechanisms of PBH formation, one may use the data, sensitive to PBH evaporation effects, to probe the hypothetical processes in the very early Universe.

The relative sensitivity of the integral and differential detectors, discussed above, to the hypothetical particles with the relative abundance $\nu = fracnn_\gamma$ (n - concentration of particles and n_γ- concentration of relic photons) and the mass m, causing the respective effects in the period τ, is presented in the review (Khlopov,Chechetkin,1987; Khlopov,1999), where more detailed discussion of various detectors of the Universe and extensive bibliography may be found.

6. Cosmology of horizontal unification

To combine methods of cosmoparticle physics one can consider the approach, trying to incorporate the main properties of elementary particles and the cosmologically relevant parameters, corresponding to the physical mechanisms of inflation, baryosynthesis and dark matter, into the unique quantitatively definite theoretical framework.

Such approach may be illustrated by the model of horizontal unification (see Khlopov, Sakharov,1996 and Refs wherein). It was shown in these studies, that the extension of the standard $SU(2)xU(1)xSU(3)_c$ model of electroweak and strong (QCD) interactions of elementary particles to the gauge symmetry SU(3)H of quark and lepton families provides not only reasonable theoretical description of the established existence of three families of quarks and leptons (ν_e, e, u, d); (ν_μ, μ, c, s); (ν_τ, τ, t, b); but in its realisation turns to be the theoretical framework, incorporating in an unique scheme physical grounds for inflation, baryosynthesis and dark matter. Even at the present level of "minimal" horizontal unification the quantitatively definite choice of the parameters of the model in a result of a combined analysis of its physical, astrophysical and cosmological predictions has lead to reasonable dark matter models of cosmological large scale structure format ion, as well as to quantitatively definite scenario of cosmological evolution from Planck times to the period of galaxy formation and a set of predictions, open for experimental and observational tests.

This model, offering the alternative (horizontal) way to unification, is in no case alternative to the more popular GUT or supersymmetric extensions of the standard model. The internal problems of the minimal horizontal unification imply its further supersymmetric and GUT extensions, which are expected to give better consistency with the observations for its astrophysical and cosmological predictions. But even in the present form the model reflects the main principles of cosmoparticle physics. On the base of local gauge model with spontaneous symmetry breaking it provides the phenomenology of world system, putting together practically all the main known particle properties and the main necessary cosmological parameters, related to the hidden sector of particle theory. It offers the quantitatively definite correspondence between fundamental cosmological parameters (form of inflaton potential, lepton number violation, mass, spectrum and lifetime of dark matter particles and fields), astr ophysical effects (rate of stellar archion emittion, contributing significantly stellar energy losses and dynamics of stellar collapse) and particle properties (see-saw mechanism of mass generation, hierachy of masses and mixings of quark and lepton families, Majorana mass ratio of neutrinos, rates of archion decays, double neutrinoless beta decays). Finally, the amount of free parameters of the model turns to be much less, than the amount of its signatures in particle processes, astrophysics and cosmology, thus providing its definite test and exhibiting its completeness.

So, the model illustrates the might of cosmoparticle approach. Its fundamental scale of horizontal symmetry breaking is *a priori* unknown and corresponds to the hidden sector of particle theory, but complex analysis of the set of its physical, astrophysical and cosmological predictions makes it possible to fix the value of this scale in two rather narrow windows (around 10^6GeV and around 10^{10}GeV). The second solution, corresponding to higher energy scale, seem to reproduce all the main features of widely assumed as standard cosmological scenario with inflation, baryosynthesis and cold (axionic) dark matter. The practical realisation of such scenario, which in no case reflects complete physical basis, shows, that even the most simple reduced csmological scenario does contain some additional elements (e.g. post inflational dust-like stage, on which primordial black hole (PBH) formation is possible with successive PBH evaporation at RD stage after primordial nucleosyntheis, formation of primordial percollational structure of archioles etc). This example favours the conclusion, that in *no* cases new cosmological elements, based on the hypothetical effects of particle physics, are reduced to inflation, baryosynthesis and dark matter *only*.

The development of cosmoparticle physics will lead to great astronomical and physical discoveries. Such exciting phenomena as the existence of thousands antimatter stars in our Galaxy, of the 4th stable massive

neutrino, of matter or shadow matter can find experimental and observational proofs even in the next decade. One can expect that the future Millennium will uncover before the fundamental science the dark side of the Universe and its hidden physical mechanism. On this way the Gamov's idea of the Universe governed by the laws of fundamental physics will find proper realisation and physical content.

Acknowledgements. The work was partially performed in the framework of Section "Cosmoparticle physics" of Russian State Programme "Astronomy", International project "Astrodamus", collaborations AMS-Epicos and Cosmion-ETHZ. We are grateful to ETHZ for permanent support of the studies.

References

Battiston R.: 1999. *Gravitation and Cosmology, Supplement*, bf 5, 54.

Belotsky K.M. et al.: 1999, *Gravitation and Cosmology, Supplement.*, bf 5, 47.

Chechetkin V.M., Khlopov M.Yu., Sapozhnikov M.G.: 1982, *Riv. Nuovo Cimento*, **5**,N-10.

Comelli D., Pietroni M., Riotto A.: 1994, *Nucl. Phys.*, **B412**, 441.

Dolgov A.D.,Illarionov A.F., Kardashev N.S., Novikov I.D.: 1987, *ZhETF*, **94**, 1.

Golubkov Yu.A., Konoplich R.V., Mignani R., Fargion D., Khlopov M.Yu.: 1999, *JETP Lett.*, **69**, 434.

Guth A.: 1981, *Phys. Rev.*, **D23**, 347.

Khlopov M.Yu., Chechetkin V.M.: 1987, *Sov. J. Part. Nucl.*, **18**, 267.

Khlopov M.Yu., Sakharov A.S.: 1996, *Proc. Cosmion-94*, Eds. M.Yu.Khlopov et al., Editions Frontieres, 273.

Khlopov M.Yu.: 1992 *Sov. J. Nucl. Phys.*, **55**,765.

Khlopov M.Yu.: 1996, *Proc. Cosmion-94*, Eds. M.Yu.Khlopov et al., Editions Frontieres, 67.

Khlopov M.Yu.: 1998, *Gravitation and Cosmology*, **4**, 69.

Khlopov M.Yu.: 1999, *Cosmoparticle physics*, World Scientific.

Kuzmin V.A.: 1970, *JETP Lett.*, **12**, 335.

Sakharov A.D.: 1967, *JETP Lett.*, **5**, 17.

Schramm D.N., Copi C.: 1996, *Proc. Cosmion-94*, Eds. M.Yu.Khlopov et al., Editions Frontieres, 77.

Zeldovich Ya.B., Novikov I.D.: 1975, *Structure and evolution of the Universe*, Nauka, M.

PHYSICAL PROPERTIES OF A CLASS OF SPHERICALLY SYMMETRIC PERFECT FLUID DISTRIBUTIONS IN NONCOMOVING COORDINATES

H. Knutsen

Stavanger College, P.O. Box 2557, Ullandhaug, N-4091 Stavanger, Norway

ABSTRACT. The physical properties of an exact solution of Einstein's field equations are examined. This spherically symmetric perfect fluid solution contains expansion, acceleration and shear. There exist models with regions of spacetime where the pressure and the density are positive and the dominant energy condition and the causality condition are also fulfilled. Moreover, the pressure and the density gradients are equal. The mass function is zero at the origin where there is Lorentz-Minkowski geometry and no trapped surface exists.

Key words: Noncomoving coordinates; expansion; acceleration; shear.

1. Introduction and line element

An exact solution of Einstein's field equations which appear in simple form in non-comoving coordinates may show a bewildering appearance when transformed to a comoving system. Hence, McVittie and Wiltshire (1977) thought it worth while to examine the possibility of solving Einstein's equations in terms of noncomoving coordinates. However, they obtained their solutions by ancillary mathematical assumptions and abstained from a detailed physical analysis of their models. In this paper we examine a particular model given by McVittie and Wiltshire (1977). We shall examine the properties of the following line element

$$\begin{aligned} ds^2 &= P^{4/3}d\eta^2 - P^{2/3}e^{-2\varepsilon\eta/\eta_0}\left(\sin\frac{\xi}{2}\right)^{-4} \\ &\times \quad (d\xi^2 + \sin^2\xi d\Omega^2), \end{aligned} \tag{1}$$

where $P = 1 + Ae^{-2z}$, $e^z = \sin\frac{\xi}{2}e^{\varepsilon\eta/\eta_0}$, $\varepsilon = \pm 1$ and A is a constant which may be positive or negative and η_0 is one more constant. This metric is solution (8.11) in McVittie and Wiltshire (1977). Writing

$$R^2 = P^{2/3}e^{-2\varepsilon\eta/\eta_0}\left(\sin\frac{\xi}{2}\right)^{-4}\sin^2\xi, \tag{2}$$

metric (1) yields that the centre (R=0) is represented by $\xi = \pi$. Using Einstein's equations "in reverse", we now find after some calculations that the pressure p and the density ρ are respectively given by

$$\begin{aligned} 8\pi p &= \frac{28 - 20P - 35P^2}{9\eta_0^2 P^{10/3}} + e^{2\varepsilon\eta/\eta_0}\frac{(P-1)\sin^2\frac{\xi}{2}}{9P^{8/3}} \\ &\times \quad \left[4P + 5 + 5(P-1)\sin^2\frac{\xi}{2}\right], \end{aligned} \tag{3}$$

$$\begin{aligned} 8\pi\rho &= \frac{3(5P-2)^2}{9\eta_0^2 P^{10/3}} \\ &- \quad e^{2\varepsilon\eta/\eta_0}\frac{(P-1)\sin^2\frac{\xi}{2}}{9P^{8/3}}\left[4P + 5 + 5(P-1)\sin^2\frac{\xi}{2}\right] \\ &- \quad \frac{5}{18}e^{2\varepsilon\eta/\eta_0}\frac{(P-1)^2}{P^{8/3}}\sin^2\xi. \end{aligned} \tag{4}$$

For the centre ($\xi = \pi$) we have

$$8\pi p_c = \frac{28 - 20P_c - 35P_c^2}{9\eta_0^2 P_c^{10/3}} + e^{2\varepsilon\eta/\eta_0}\frac{P_c - 1}{P_c^{5/3}}, \tag{5}$$

$$8\pi\rho_c = \frac{3(5P_c - 2)^2}{9\eta_0^2 P_c^{10/3}} - e^{2\varepsilon\eta/\eta_0}\frac{P_c - 1}{P_c^{5/3}}, \tag{6}$$

where the suffix c denotes centre value. We now choose $P_c = 1 + Ae^{-2\varepsilon\eta/\eta_0}$ such that the following two conditions are fulfilled:

$$28 - 20P_c - 35P_c^2 > 0, \tag{7}$$

$$3(5P_c - 2)^2 > 28 - 20P_c - 35P_c^2. \tag{8}$$

It is easily seen that this will be the case if and only if

$$P_c \in \langle -1.225\ ,\ -0.241\rangle \cup \langle\ 0.604\ ,\ 0.653\ \rangle. \tag{9}$$

Next, let $e^{2\varepsilon\eta/\eta_0} \approx 0$ such that the first two terms of equations (5) and (6) will dominate the expressions for the pressure and the density. Hence, we have the important conclusion *there are classes of solutions for which there exist regions of spacetime in which these models are physically valid.* Moreover, these models are nonsingular close to the centre. From equations (3) and (4) it is further seen that the weak energy condition $\rho + p \geq 0$ yields

$$H \equiv \frac{16}{\eta_0^2}e^{-2\varepsilon\eta/\eta_0} - P^{2/3}\sin^2\xi \geq 0. \tag{10}$$

2. The four velocity and comoving coordinates

We choose the timelike component u^4 to be positive, and with our line element (1) we obtain

$$u^4 = \frac{4}{\eta_0} P^{-2/3} e^{-\varepsilon\eta/\eta_0} H^{-1/2}. \tag{11}$$

$$u^1 = -\varepsilon \sin\xi \sin^2\frac{\xi}{2} e^{\varepsilon\eta/\eta_0} H^{-1/2}. \tag{12}$$

We shall now examine if it is really possible to transform our metric (1) into comoving coordinates. The condition expressing orthogonality of the metric and the condition that the radial coordinate r is comoving yield the following two differential equations for the time coordinate t and for r

$$e^{2\mu} u^1 \frac{\partial t}{\partial \eta} + e^{2\lambda} u^4 \frac{\partial t}{\partial \xi} = 0, \tag{13}$$

$$u^1 \frac{\partial r}{\partial \xi} + u^4 \frac{\partial r}{\partial \eta} = 0. \tag{14}$$

Equation (13) simplifies beautifully and we obtain

$$t = e^{\varepsilon\eta/\eta_0} \sin\frac{\xi}{2}. \tag{15}$$

However, with the substitutions $x = e^{-2\varepsilon\eta/\eta_0}$ and $y = \sin\frac{\xi}{2}$ we find that equation (14) reads

$$(ay^2 + bx)^{2/3}(1-y^2) y^{5/3} \frac{\partial r}{\partial y} + x^2 \frac{\partial r}{\partial x} = 0, \tag{16}$$

where a and b are arbitrary nonzero constants. We have not been able to integrate equation (16). Hence, we can not write the solution in comoving coordinates. But we shall still be able to discuss several interesting physical aspects concerning this model.

3. Four velocity field

The expansion Θ is given by

$$\begin{aligned}
\Theta &= \varepsilon H^{-3/2}\{-\frac{64}{P^{5/3}}(5P-2)\frac{e^{-3\varepsilon\eta/\eta_0}}{\eta_0^4} \\
&+ \frac{8}{3}\left[(58 - 40\sin^2\frac{\xi}{2})\sin^2\frac{\xi}{2} - \frac{7}{P}\sin^2\xi\right]\frac{e^{-\varepsilon\eta/\eta_0}}{\eta_0^2} \\
&+ 2\sin^2\xi\left[\frac{1}{3P^{1/3}}\sin^2\xi\right. \\
&- \left.\frac{P^{2/3}}{3}\sin^2\frac{\xi}{2}(7 - 4\sin^2\frac{\xi}{2})\right] e^{\varepsilon\eta/\eta_0}\}.
\end{aligned} \tag{17}$$

The four-acceleration $\dot{u}_i$ reads

$$\dot{u}_1 = \frac{16}{\eta_0^2} e^{-2\varepsilon\eta/\eta_0} P^{2/3} \sin\xi \sin^2\frac{\xi}{2} H^{-2}, \tag{18}$$

$$\dot{u}_4 = \frac{4}{\eta_0}\varepsilon P^{4/3}\sin^2\xi\sin^4\frac{\xi}{2} H^{-2}. \tag{19}$$

The shear tensor σ_{ij} reads

$$\sigma_{11} = \frac{32\varepsilon}{9\eta_0^2} e^{-3\varepsilon\eta/\eta_0} P^{2/3} \frac{1}{\sin^2\frac{\xi}{2}} H^{-5/2} K, \tag{20}$$

$$\sigma_{14} = \frac{8}{9\eta_0} e^{-\varepsilon\eta/\eta_0} P^{4/3} \sin\xi H^{-5/2} K, \tag{21}$$

$$\sigma_{22} = -\frac{\varepsilon}{9} e^{-\varepsilon\eta/\eta_0} P^{2/3} \frac{\sin^2\xi}{\sin^2\frac{\xi}{2}} H^{-3/2} K, \tag{22}$$

$$\sigma_{44} = \frac{2\varepsilon}{9} e^{\varepsilon\eta/\eta_0} P^2 \sin^2\xi \sin^2\frac{\xi}{2} H^{-5/2} K, \tag{23}$$

where K is given by

$$\begin{aligned}
K &= \frac{16}{\eta_0^2}\left(1 - \sin^2\frac{\xi}{2}\right)\left(1 + \frac{2}{P}\right) e^{-2\varepsilon\eta/\eta_0} \\
&- \left[\left(1 + 2\sin^2\frac{\xi}{2}\right) P^{2/3} + \frac{2}{P^{1/3}}\left(1 - \sin^2\frac{\xi}{2}\right)\right]\sin^2\xi.
\end{aligned} \tag{24}$$

The shear invariant reads

$$\sigma_{ij}\sigma^{ij} = \frac{2}{27} e^{2\varepsilon\eta/\eta_0} \sin^4\frac{\xi}{2} H^{-3} K^2. \tag{25}$$

In Kramer et al. (1980) we find the following statement concerning the solutions given by McVittie and Wiltshire (1977), "not all of their solutions have nonzero shear!". With our new and previous results we can sharpen that statement and declare *the McVittie-Wiltshire solutions which are non static and not trivially conformally flat all have expansion, acceleration and shear.*

4. Sound speed and gradients

The speed of sound v_{sound} is given by

$$\begin{aligned}
v_{sound}^2 &= 2\{-e^{4\varepsilon\eta/\eta_0} P^{4/3}\sin^2\xi\sin^2\frac{\xi}{2} \\
&\times [P + 2 + 2(P-1)\sin^2\frac{\xi}{2}] \\
&+ 4\frac{e^{2\varepsilon\eta/\eta_0}}{\eta_0^2} P^{2/3}\sin^2\frac{\xi}{2} \\
&\times [-2P\sin^2\frac{\xi}{2} + 11P + 22(1 - \sin^2\frac{\xi}{2})] \\
&- \frac{112}{\eta_0^4}(P+2)\} \times \{e^{4\varepsilon\eta/\eta_0} P^{4/3}\sin^2\xi\sin^2\frac{\xi}{2} \\
&\times [7P - 4 - 4(P-1)\sin^2\frac{\xi}{2}] \\
&+ 8\frac{e^{2\varepsilon\eta/\eta_0}}{\eta_0^2} P^{2/3}\sin^2\frac{\xi}{2} \\
&\times [20P\sin^2\frac{\xi}{2} - 29P + 14(1 - \sin^2\frac{\xi}{2})] \\
&+ \frac{96}{\eta_0^4}(5P-2)\}^{-1}.
\end{aligned} \tag{26}$$

The sound speed at the centre ($\xi = \pi$) reads

$$v^2_{sound}(centre) = \left[28(P_c+2) - 9\eta_0^2 e^{2\varepsilon\eta/\eta_0} P_c^{5/3}\right] \times \left[-12(5P_c-2) + 9\eta_0^2 e^{2\varepsilon\eta/\eta_0} P_c^{5/3}\right]^{-1}. \quad (27)$$

We now follow the process we used to obtain physically valid regions of spacetime, *i.e.* we restrict spacetime to regions where $e^{2\varepsilon\eta/\eta_0} \approx 0$. For these regions we have

$$v^2_{sound}(centre) = -\frac{7(P_c+2)}{3(5P_c-2)}. \quad (28)$$

We demand the sound speed to be real and less than the speed of light in vacuum. The following conditions must then be fulfilled

$$0 < -\frac{7(P_c+2)}{3(5P_c-2)} < 1, \quad (29)$$

Remembering condition (9) we obtain the following restriction

$$P_c \in \langle -1.225\ ,\ -0.364\rangle. \quad (30)$$

The ratio of the gradients with respect to comoving radial coordinate r is given by

$$\left(\frac{\partial p}{\partial r}\right)\left(\frac{\partial \rho}{\partial r}\right)^{-1} = \left(e^{2\lambda}u^4\frac{\partial p}{\partial \xi} + e^{2\mu}u^1\frac{\partial p}{\partial \eta}\right) \times \left(e^{2\lambda}u^4\frac{\partial \rho}{\partial \xi} + e^{2\mu}u^1\frac{\partial \rho}{\partial \eta}\right)^{-1} \quad (31)$$

This expression simplifies beautifully and we find

$$\frac{\partial p}{\partial r} = \frac{\partial \rho}{\partial r}. \quad (32)$$

We thus have the remarkable fact that *the pressure gradient and the density gradient with respect to comoving radial coordinate are the same.*

5. Mass function

The mass function is given by

$$m = \frac{4}{3}\pi\rho R^3 + E, \quad (33)$$

where E is interpreted as pure gravitational field energy (not binding energy) within spheres of surface radius R. However, we also have

$$m = \frac{R}{2}\left[1 + g^{ij}(\frac{\partial R}{\partial x^i})(\frac{\partial R}{\partial x^j})\right]. \quad (34)$$

and we obtain

$$\begin{aligned} m &= \frac{4e^{-3\varepsilon\eta/\eta_0}(5P-2)^2}{9\eta_0^2 P^{7/3}}\cot^3\frac{\xi}{2} \\ &- \frac{4e^{-\varepsilon\eta/\eta_0}(4P-1)(P-1)}{9P^{5/3}}\cot\frac{\xi}{2} \\ &+ \frac{4e^{-\varepsilon\eta/\eta_0}(5P-2)(P-1)}{9P^{5/3}}\cot\frac{\xi}{2}\sin^2\frac{\xi}{2} \\ &- \frac{4e^{-\varepsilon\eta/\eta_0}(P-1)^2}{9P^{5/3}}\cot\frac{\xi}{2}\sin^4\frac{\xi}{2}. \end{aligned} \quad (35)$$

We further find

$$\begin{aligned} \frac{4}{3}\pi\rho R^3 &= \frac{4e^{-3\varepsilon\eta/\eta_0}(5P-2)^2}{9\eta_0^2 P^{7/3}}\cot^3\frac{\xi}{2} \\ &- \frac{4e^{-\varepsilon\eta/\eta_0}(14P-5)(P-1)}{27P^{5/3}}\cot\frac{\xi}{2} \\ &+ \frac{4e^{-\varepsilon\eta/\eta_0}(19P-10)(P-1)}{27P^{5/3}}\cot\frac{\xi}{2}\sin^2\frac{\xi}{2} \\ &- \frac{20e^{-\varepsilon\eta/\eta_0}(P-1)^2}{27P^{5/3}}\cot\frac{\xi}{2}\sin^4\frac{\xi}{2}. \end{aligned} \quad (36)$$

The gravitational field energy E, however, takes the simple form

$$E = \frac{8e^{-\varepsilon\eta/\eta_0}(P-1)^2}{27P^{5/3}}\cot\frac{\xi}{2}(1-\sin^2\frac{\xi}{2})^2, \quad (37)$$

and both the mass function m and the gravitational field energy E vanish at the centre of the matter distribution. We further obtain

$$\left(\frac{2m}{R}\right)_c = 0 \quad (38)$$

and we conclude that no apparent horizon or trapped surface exist close to the centre. The criterion to have Lorentz-Minkowski geometry at the origin is given by

$$B_c^2 = \left(\frac{\partial R}{\partial r}\right)_c^2. \quad (39)$$

We find

$$\left(\frac{\partial R}{\partial r}\right)^2 B^{-2} = \frac{16}{\eta_0^2}e^{-2\varepsilon\eta/\eta_0}\sin^4\frac{\xi}{2}H^{-1}. \quad (40)$$

Remembering definition (10) we find that *there is Lorentz-Minkowski geometry at the origin.*

References

Kramer D., Stephani H., MacCallum M.A.H., Herlt E.: 1980, *Exact Solution of Einstein's Field Equations* (Cambridge University Press, Cambridge).

McVittie G. C., Wiltshire R. J.: 1977, *Int. J. Theor. Phys.* **16**, 121.

The Models of Voids in the Friedman Universe

M.P. Korkina[1], A.N. Turinov[2]

Department of Theoretical Physics, Dnepropetrovsk State University
Nauchniy lane, Dnepropetrovsk 49005 Ukraine,
[1]*korkina@ff.dsu.dp.ua*, [2]*theorph@ff.dsu.dp.ua*

ABSTRACT. The astronomical observations of the last years show that there are the regions in the Universe with much lower density of matter, than their surroundings. Theoretical studies of the regions (voids) in the model of the expanding Universe are carried on different directions. In this paper the voids have been built by means of matching Tolman and Friedman solutions. The Lichnerovich-Darmois matching conditions are used. It is shown that in expanding Universe with flat space the voids can not exist. So we have Friedman Universe with voids, with described by the Tolman solution. The models of voids in the Friedman Universe with negative spatial curvature have been built.

Key words: Universe, void, Friedman solution, space-time, matching conditions, density of energy.

1. Introduction

The astronomical observations of last years shows that there are the regions in the Universe with much lower density of matter than their surroundings (Thompson and Vishniac 1987; de Lapparent, Geller and Huchra 1986). Theoretical studies of these region (voids) in the models of the expanding Universe are carried on different directions (Redmouth 1988; Suto, Sato, and Sato 1984): small perturbations of homogeneous Universe; use of the Einstein-Straus model; use of the Tolman solution for the nonhomogeneous dust; consideration of the boundary of the void as the thin wall.

In this paper we use the Tolman spherically symmetric dust solution for the description of voids space-time, and Friedman solution for the description of the space-time of the surrounding Universe.

2. The Tolman solution

The Tolman solution for nonhomogeneous dust has the following form:

$$ds^2 = dt^2 - \frac{r'^2(R,t)}{f^2(R)}dR^2 - r^2(R,t)(d\Theta^2 + \sin^2\Theta d\varphi^2)\ , \tag{1}$$

where

$$r(R,t) = \frac{m(R)}{1-f^2(R)}\begin{Bmatrix}\sin^2(\alpha/2)\\ -\sinh^2(\alpha/2)\end{Bmatrix}\text{for}\begin{cases}f^2(R)<1\\ f^2(R)>1\end{cases}; \tag{2}$$

$$t-t_0(R)=\frac{m(R)}{|1-f^2(R)|^{3/2}}\begin{Bmatrix}\alpha-\sin\alpha\\ \sinh\alpha-\alpha\end{Bmatrix}\text{for}\begin{cases}f^2(R)<1\\ f^2(R)>1\end{cases}; \tag{3}$$

$$r(R,t) = \left[\pm\frac{2}{3}m(R)^{1/2}(t-t_0(R))\right]^{2/3}\text{for } f^2(R)=1. \tag{4}$$

The velocity of light $c = 1$. The prime means ∂/∂_R. $m(R)$, $f(R)$ and $t_0(R)$ are the arbitrary functions of integration. $m(R)$ is the hole mass of the dust ball with radial coordinate R, $f(R)$ is the hole energy of the test particle, which is on the distance R from the centre. $t_0(R)$ determines the time of the collapse.

The density of the energy is given by

$$\varepsilon(R,t) = \frac{1}{8\pi\gamma}\frac{m'(R)}{r^2(R,t)r'(R,t)}, \tag{5}$$

where γ is the Newton gravitational constant.

Friedman solution for homogeneous dust is the particular form of the Tolman one:

$$m(R) = a_0\left\{\begin{array}{c}\sin^3(R)\\ \sinh^3(R)\\ R^3\end{array}\right\}\text{for}\left\{\begin{array}{l}f^2(R)=\cos^2(R)\\ f^2(R)=\sinh^2(R)\\ f^2(R)=1\end{array}\right., \tag{6}$$

$t_0(R) = 0$, $a_0 = const.$

3. The matching conditions

We use the Lichnerovicz-Darmous matching conditions, which consist in following: the first and the second differential forms of the matched metrics are the same on the matching hypersurface. We consider two different Tolman metrics and choose the hypersurface $R = R_b = const$ as the matching hypersurface. Then the matching conditions have the following form:

$$\begin{aligned} r_1(R_b, t_1) &= r_2(R_b, t_2), \\ f_1(R_b) &= f_2(R_b), \\ m_1(R_b) &= m_2(R_b), \end{aligned} \tag{7}$$

where index "1" and "2" mark the first and second matched metrics, respectively.

4. The voids, described by the flat space-time

Bonnor and Chamorro considered the voids as the Minkowski space-time (Bonnor, and Chamorro 1990; Bonnor, and Chamorro 1991). They have shown that such voids can not exist in the Friedman Universe. But it is possible to choose the definite Tolman Universe and such Universe can have the voids which are describe by the empty space-time. It was to be expected that this Tolman Universe must be sufficiently exotic.

Friedman Universe also can not have the voids which are described by the other Friedman space-time. Under this assumption the matching conditions are not fulfilled.

So we consider the Tolman space-time as the space-time of the "void", and Friedman space-time as the one of the surroundings.

5. Friedman model

Let us assume that the Universe have been described by the parabolic Friedman model. Under this condition the void is described by the parabolic Tolman model. The matching conditions demand the same spatial curvature of the void and of the surroundings space-time. The arbitrary function $f(R)$ determines the spatial curvature. So we choose the function $f(R)$ in the voids the the same, as it has been chosen in Friedman space-time $f^2(R) = 1$. Exactly this choice of $f^2(R)$ permit us to consider the space coordinate R as the same in the void and in the surrounding space-time. From the matching conditions we have obtained that on the matching hypersurface $t_T = t_F + t_0(R_b)$.

The average density of energy in the void is given by

$$\bar{\varepsilon} = \frac{M}{V} = \frac{\int\limits_0^{R_b} \varepsilon\sqrt{-g}\; dR\; d\Theta\; d\varphi}{\int\limits_0^{R_b} \sqrt{-g}\; dR\; d\Theta\; d\varphi} = \frac{\int\limits_0^{R_b} \dfrac{m'}{f(R)}\; dR}{\int\limits_0^{R_b} \dfrac{r^2 r'}{f(R)}\; dR}. \tag{8}$$

For the parabolic Tolman model with $f^2(R) = 1$ from (8) we obtain

$$\bar{\varepsilon} = \frac{\int\limits_0^{R_b} m'(R)\; dR}{\int\limits_0^{R_b} r^2 r'\; dR} = \frac{3m(R_b)}{r^3(R_b, t_T)}. \tag{9}$$

For the Friedman homogeneous model we can write the expression for the $\bar{\varepsilon}$ in the following form

$$\bar{\varepsilon} = \varepsilon(t) = \frac{m'(R)}{r^2 r'} = \frac{3m(R)}{r^3(R, t)}. \tag{10}$$

Because energy density (10) is independent from R, we can replace the value R in the expression (10) to the value R_b, then we obtain

$$\bar{\varepsilon} = \varepsilon(t) = \frac{3m(R_b)}{r^3(R_b, t_F)}. \tag{11}$$

¿From (7), (9) and (11) we can see that in parabolic Friedman model the voids can not exist, because the homogeneous energy density in the external space and the average density in the internal space are the same.

6. The voids in hyperbolic Friedman Universe

Let us consider the "voids" in the hyperbolic Friedman model. We take the mass function of the voids as

$$m_V = a_0 \frac{\sinh^{n+1} R}{\sinh^{n-2} R_b}, \tag{12}$$

where n is arbitrary whole number.

For the different n the observing mass M, the volumes V and the average density of the voids have been calculated. We have consider the possibility of the formation of the little and the big voids ($R_b \to 10^{-2}$, 10^{-1}, 1, 2). We have chosen $t_0(R) \to 0$, R_b, $\sinh R_b$. From calculation we have obtained that the Tolman time always is greater than Friedman one. There are not exist the voids when $t_0(R) = 0$. For $n \geq 3$ we have voids only in earlier Universe, now they can not exist.

The parameters of the models of the voids with $n = 1$ and $t_0(R_b) = R_b$ are given in the tables 1, 2, 3, and 4.

Table 1: Model of void for $R_b = 0.01$.

R_b	t_T	V_T/V_F	M_T/M_F	E_T/E_F
	0.01001	8.9		0.15
	0.0101	1.1		0.92
	0.011	1		1
	0.02	1		1
0.01	0.11	1.01	1	0.99
	0.26	1.13		0.88
	0.51	2.4		0.44
	0.76	7.26		0.13
	1.01	**22.14**		**0.05**
	1.51	156.8		0.0065

Table 2: Model of void for $R_b = 0.1$.

R_b	t_T	V_T/V_F	M_T/M_F	E_T/E_F
	0.10001	$8.5 \cdot 10^4$		$1.2 \cdot 10^{-5}$
	0.1001	$9.3 \cdot 10^2$		$1.1 \cdot 10^{-3}$
	0.101	11		0.09
	0.11	1.17		0.85
0.1	0.2	1.05	1	0.95
	0.35	1.12		0.89
	0.6	1.5		0.67
	0.85	2.86		0.35
	1.1	**5**		**0.2**
	1.6	24.5		0.041

Table 3: Model of void for $R_b = 1$.

R_b	t_T	V_T/V_F	M_T/M_F	E_T/E_F
	1.00001	$1.4 \cdot 10^9$		$7.4 \cdot 10^{-10}$
	1.0001	$1.5 \cdot 10^7$		$7 \cdot 10^{-8}$
	1.001	$1.5 \cdot 10^5$		$7 \cdot 10^{-6}$
	1.01	$1.6 \cdot 10^3$		$6.5 \cdot 10^{-4}$
1	1.1	29	1.04	0.038
	1.25	9.8		0.11
	1.5	4.2		0.11
	1.75	11.9		0.09
	2	**18.9**		**0.06**
	2.5	61		0.017

Table 4: Model of void for $R_b = 2$.

R_b	t_T	V_T/V_F	M_T/M_F	E_T/E_F
	2.00001	$4.5 \cdot 10^10$		$2.4 \cdot 10^{-9}$
	2.0001	$4.9 \cdot 10^8$		$2.4 \cdot 10^{-7}$
	2.001	$4.9 \cdot 10^6$		$2.4 \cdot 10^{-5}$
	2.01	$5.1 \cdot 10^4$		$2.4 \cdot 10^{-3}$
2	2.1	653.3	1.15	0.0017
	2.25	108.2		0.011
	2.5	101.8		0.011
	2.75	111.6		0.01
	3	**152.9**		**0.007**
	3.5	400		0.003

Note, that the masses of the voids (M_T in the tables) are the same as the Friedman mass (M_F in the tables) in the region limited by R_b. But the volumes of the voids are greater than the corresponding Friedman volume.

E_T is the average energy density in the voids, E_F — the same in the Friedman space-time. Present time corresponds to the marked line.

¿From the tables we can see, that the ratio E_T/E_F is changed. This value is very little near the beginning of the Universe, then it increases some time, and decreases again. So at present time the voids can exist.

Conclusions show that these models describe the voids of different size. The voids are changing in time.

References

Bonnor, W.B., Chamorro, A.: 1990, *Ap.J.*, **350**, 502.
Bonnor, W.B., Chamorro, A.: 1991, *Ap.J.*, **378**, 461.
de Lapparent, V., Geller, M.J., Huchra, J.P.: 1986, *Ap.J.(Letters)*, **302**, L1.
Redmouth, I.H.: 1988, *M.N.R.A.S.*, **235**, 1301.
Suto, Y., Sato, K., Sato, H.: 1984, *Prog. Theor. Phys.*, **72**, 1137.
Thompson, K.L., Vishniac, E.T.: 1987, *Ap.J.* **313**, 517.

THE KINEMATIC OF RELATIVISTIC MOTIONS IN ASTROPHYSICAL OBJECTS - KEY TO THE VERIFICATION OF THE TIME - COORDINATE TRANSFORMATIONS

M.G. Larionov

Sternberg Astronomical Institute Moscow State University,
Universitetskii Prospect 13, 119899 Moscow, Russia
mgl@sai.msu.ru

ABSTRACT. On the basis of the independent interpretation of Mickelson-Morley experiment the not Lorenz transformations were suggested. Astrophysical data on kinematic for relativistic outflows in galactic sources was investigated. It was shown that the differences between standard relativistic transformations and the suggested ones occur at the v^3/c^3 power. That does not allow to accept or to reject this or that kind of transformations. Peculiarities of the observational data being the result of suggested transformations were enumerated.

Key words: relativity theory

1. Introduction

The of principal assumption of the modern physics is symmetries. They are laid in many of its parts, in the special relativity (SRT) it's postulates, Lorenz transformations and invariants. Although these thesises do not contradict to the visible homogeneousity and isotropicity of the space-time on a very large scale one should keep in mind that symmetries and invariants were not set by nature apriori but they were introduced by researchers in general principles intentions for more convenient in description of physical phenomena.

Evidences of infringement of geometrical, internal, local and global symmetries appeared from the elementary particle physics where quantization processes show themselves especially clearly. Using the postulation of the electromagnetic (EM) radiation propagation without of the any matter environment and because not quantum the SRT lose in her physical essence. By increasing of the experimental accuracy they must inevitably to enter on contradiction with observational data.

On the basis of astrophysical data in previous papers (Larionov 1993,1999) we attempted to base our arguments on facts of the existence of a virtual substance in which the EM radiation could propagate. Qualities of that substance principally differ from the ones of the real matter: quantization on the scale $\Delta l = 0.8 \cdot 10^{-12} cm$, virtual form existence $\Delta t = 2,6 \cdot 10^{-23} sek$, the practical non compression (this to lead to high speed light propagation $c = \frac{\Delta l}{\Delta t}$). That means Δl is the size of the elementary "space-time-matter" (STM) cell at this epoch, Δt is the cell time existence with the energy $E = 1,9 \cdot 10^{-44} erg$ and effective mass $m = 2,1 \cdot 10^{-65} g$.

Connection with the barionic part of the matter is much one of the physical vacuum (PV) qualities probably. This may mean that the terrestrial laboratory experiments will not give any positive results for the PV substance revelation for the reason of the practical absence of the relative movement between the Earth and PV formatted by it. That's the way haw we came to idea of the enclosations of the terrestrial and solar PV one into another etc. In consequence quanta of the EM radiation propagate through the PV of the Metagalaxy on the background of the Universe expansion.

At the same time processes of the desintegrations and birth of about 10^{121} having new parameters PV cells take place unremittingly. For the reason of the PV stretching quanta themselves are suffering the redshift (not Doppler origin) at time spreading. If only follow of this ideology there is no exist the absolute system co-ordinate for reason of the absence of the absolute PV.

Having probably an electron-positron (EP) virtual structure the PV is becoming available for observations in cases of electrical charge creations. When a charge is on rest we have a common phenomenon of a PV polarisation. The even motion of the virtual polarised EP pairs, surrounding the charge, give the occurrence of a direct current and a direct magnetic field. The accelerative charges give rise to EM radiation, when the phasation of the PV is carried out harmonically. The EM radiation propagation is the visible display of the excited state of the PV. Consequently, a medium of virtual particles is necessary in order to EM radiation propagate.

Interaction of charges could be a co-ordinated action of accompanied their virtual "fura", where the orientation of virtual EP pairs is formed either by attraction (because of the disappearance of the cells in common parts of EP "fura"), or by repulsing (by appearance of additional STM quanta in the space between of charges). In other words, according to the principle of the minimum action we have the realisation of the energetically more profitable situation. In the one case this leads to the distruction of the part space between charges, in the other one we may "observe" the birth of additional STM cells.

Thus the electrical interaction in that conception could have a virtual-mechanical nature, but charges themselves and matter in general have a nature of the topological space-time peculiarity. And besides the course of time direction is setting by the expansion of the Universe.

The dependence of an inertial body quality from the speed may have a physical explanation in the plan of a PV medium resistance by body motion. The top speed is formed by parameters of the PA matter and equal to speed light $c = \frac{\Delta l}{\Delta t}$. Enumerating qualities of the PV in the case of their existence might show that in the principles of the electrodynamic and relativistic physic constriction effects of the influence of PV matter should be take into consideration, both in the case of time - co-ordinate transformation and in one of motion lows and the EM radiation propagation.

2. Postulates and time - coordinate transformations (TCT)

Implying the existence of PV medium providing EM radiation propagation we can construct the TCT on the known principles keeping in mind the top speed propagation interactions. Both the electrodynamical postulate and the one of the PV matter, invisible under unexcited state, should be set in the basis of TCT. In spite of the unusual parameters PV behave itself as physical environment when EM radiation propagate through it. In that sense if parameters PV not changed the speed of the EM radiation propagation is a constant.

Therefore this is enough to introduce the postulate of the existence of the virtual PV matter that is providing of the translation EM radiation through PV with the top speed c. But the electrodynamical postulate must be based on the high accurency experiments. The Mickelson-Morley type experiments are of that ones. They direct on the absence of a variation of a interferent pattern with a changing of the instrument orientation. The only independent from interpretations conclusion follow from it: in inertial co-ordinate system (IKS) (the terrestrial system, on the short time, for example) falling on a mirror and reflecting from it wavelengths are equal ($\lambda_1 = \lambda_2$) and do not depend on the device orientation. These two postulates form the foundation of the TCT, connecting coordinates and time intervals in the moving with speed v TCT and the one the immovable relatively PV TCT (Larionov 1993,1999).

$$x_0 = x_1 \pm \frac{c \mp v}{c \pm v} v t_1; \qquad y_0 = y_1; \qquad z_0 = z_1$$

$$t_0 = t_1 (1 \mp \frac{v}{c})$$

$$x_0 = c t_0; \qquad x_1 = (\frac{c \mp v}{c \pm v}) c t_1, \tag{1}$$

where index "1" relates to the moving IKS, "0" relates to the one on rest; the bottom sign correspond to the IKS moving in the direction of the light propagation, the top sign correspond to the IKS moving in the opposite one. The suggested TCT are not symmetrical firstly by time interval, length and angle transformations:

$$\Delta t_0 = \Delta t_1 (1 + \frac{v}{c} Cos\theta_1); \quad \Delta l_0 = \Delta l_1 (1 - \frac{v}{c} Cos\theta_1);$$

$$tg\theta_0 = \frac{tg\theta_1}{1 - \frac{v}{c} Cos\theta_1}, \tag{2}$$

where index "1" relates to the moving IKS, "0" relates to the one on rest also, θ is the angle between the direction to the observer and moving emitting object (IKS).

The TCT are not symmetrical relatively to angles between directions to an observer and a moving emitting object. They contain always in the general case sighchanging or trigonometrical functions. In a common case differences between standard relative expression and reduced ones for the Doppler shift (for example) are at the power of v^3/c^3 (for the linear shift). It means that the organisation of the consequence experiment for the examination of the expression validity is a problem.

3. Visible manifestations of the TCT

The sample analysis of formulas (1) directs that with the positive and negative $Cos\theta$ (direction of moving IKS to the observer and a wrong way round) we have different numeral quantity for Δt, Δl and $tg\theta$. It should be taken into account in constructions of kinematic models of relativistic sources in parameters of compact double systems (CDS) calculations.

As the consequence transformations of Δt and Δl visible speeds of moving IKS's transformate of the not symmetrical way also:

$$v_{vis} = v \frac{1 + \frac{v}{c} Cos\theta}{1 - \frac{v}{c} Cos\theta}, \tag{3}$$

where v is a groupal speed of movement.

Visible overlight speed of movements (VOSM), observed in some extragalactic and galactic sources, have the natural explanation in the sense of giving expressions. The effect of the VOSM in our case is realised in some low than Spacial Reletivity number data ($v/c = 0,43$ and $\theta = 20deg.$).

The symmetry absence in transformations leads to visible morphological peculiarities in relativistic object:
a) differences in corners of precession cone for jet and contrjet,
b) bend of lines connecting outflow in contrdirections,
c) not equal intervals between blobs in the jet and contrjet,
d) a high flux ratio from the jet and contrjet blobs, that give additional difficulties in contrjet observations.

A visible difference of intervals between blobs in opposite directions from the sources as a visible asymmetry in jet corners is confirmed by VLBI interferometry observations. These confirm also the dependence between corners of jets and sources energetic (Parma et al. 1987, Bridl 1989).

Morphological and energetic peculiarity in relativistic sources TCT predicted let us carry out experimental tests of their validity and in some cases to get a new information applying independent methods of astrophysical objects observations.

4. Experimental tests for validity TCT

1. On the optical data basis (Margon 1984) kinetic model parameters for CDS system SS433 were calculated (Larionov 1993). Doppler shift expression deduced by us were used, that differ from the standard relativistic one in number of power $v3/c3$. The obtained data for the model SS433 agree with the standard relativistic case by making small (about some percent) modifications of the relation v/c or ones for the corner and the inclination of the precession cone of CDS. Solving of this problem required independent methods of finding CDC parameters (Larionov, 1993,1999).

2. TCT morphological peculiarities in relativistic objects were tested also in CDS SS433. Because the source belongs to Galaxy the VLBI system may gives the structure of separate blobs from source. The asymmetry of lineal transformation suppose stretch of blobs moving towards an observer and compression of ones in the opposite direction. The isophotes analysis confirmed completely these peculiarities and gave the possibility to determine some model parameters with using of independent methods (the inclination and value the precession cone, the v/c ratio from the blobs fluxes relation). It is important especially in the cases when optical objects are invisible and radio methods only give possibility to determine kinematic model CDC (Larionov, 1999).

3. At the first sight, it seems quite conveniently to use pulsar observations for testing TCT. We have a case of moving receptor and one measure a difference or ratio of impulses periods in various points of the earth orbit. Doppler shift expression differed also from relativistic one at the level $v3/c3$ (Larionov 1999). But periods ratio coincide exactly with the relativistic one. Because of insufficient precision in the determination of the light speed and especially the speed of Earth in her orbit it is impossible to choose between the offered and standard relativistic expressions in spite of the high stability of pulsar period and earth generators.

5. Conclusions

1. We have examined the type of the symmetry violations introduced by existence of PV as virtual matter.

2. It is offered TCT based on the principle of the virtual environment existence necessary for EM radiation propagation. The top speed of the interactions spreading is implied.

3. Visible manifestations of TCT suppose the presence of morphological peculiarity in relativistic objects connected with the not symmetrical TCT with the corner between directions to the observer and the IKS (emitting object).

4. Experimental tests for TCT show that modern possibilities of astrophysical objects observations do not allow us to reject the offered TCT and therefore they have right for the existence.

5. Terrestrial experiments of the Mickelson-Morley type do not reject the existence of the virtual matter necessering for the EM radiation propagation. The invariable interferent pattern in this case is evidence of invariable wavelengths in interferometers arms ($\lambda_1 = \lambda_2$) both as in the case of reflection from the mirror so in the case of the orientation changing in the space. The direct conclusion of this experiment is basis for the second (electrodynamical) postulate of TCT.

References

Bridle A.H.: 1984, *Astron. J.*, **89**, 979.
Larionov M.G.: 1993, *Astron. Tsirc.*, N1554, p.13.
Larionov M.G.: 1997a, in: *XXVII radio astronomical conference, St.-Peterburg,* **1**, 215.
Larionov M.G.: 1997b, *Astrophys. Space Sci.*, **252**, 140.
Larionov M.G.: 1999, in: *Astrophysika na rubezhe vekov*, publ. ASC FIAN, Moskow, in press.
Margon B.A.: 1984, *Rev. Astr. Astrophys.,* **22**, 507.
Parma P.: 1981, *Astron. and Astrophys*, **181**, 244.

THE KOTOV-LYUTY EFFECT: THE NEW COSMOLOGICAL INVARIANT?

M.G. Larionov
Sternberg Astronomical Institute Moscow State University,
Universitetskii Prospect 13, 119899 Moscow, Russia
mgl@sai.msu.ru

ABSTRACT. The analysis of the complete variation of the global constants using the world model with the positive cosmological constant, basis on radio astronomical data, was carried out. It was shown that, the simultaneous variations of the global constants are fulfilled in the limits of the self-confirmed solution, and the new cosmological invariant $T = \lambda/c$ appears. This allows to explain the existence of the 160-min period of the active galactic nuclei and quasars intensity variations independent of the redshift.

Key words: cosmological constants

1. Introduction

The dependence of numerical values of principle interaction constants from the interaction energy is predicted by theories. Because the energetic universe parameters may change in course of evolution, modifications of strong, electromagnetic, weak and gravitational quality of interactions should be expected also. As soon as the interaction constants, that contain the charge e, the Plank constant h, the speed light c, the gravitational constant G, are changing, then e, h, c, G changing with epoch should be expected as well.

On the other hand, there are known limitations on possible deviation range of interaction constants, connected with the existence of structural formations in the Universe with their actual set, with the formation of elements in the early epoch etc. That way, a solution of this problem in its full capacity is connected with considerable difficulties of the joint analysis of astrophysical data, results of cosmological investigations, elementary particles physic achievements. Hence, in treatment of this problem we cannot get by without certain assumptions.

Additionally, the appearance and accumulation of observant facts, that do not find a natural explanation in terms of modern astrophysical conceptions, lead us to the idea about the possibility of their solutions by manner of the secular "drift" of the global constants. The typical example of the such strange phenomenon is the Kotov-Lyuty effect (Kotov- Lyuty 1987), i.e. the availability of the 160-min period of fluxes variations in the active galactic nuclei and quasars independent of redshift of the observed object. Apparently, no satisfactory explanation of this effect exist at present, probably.

Authors themselves hold on the opinion, that the effect reflects cosmological conformity to natural lows. But we do not know of a natural cosmological explanation of this phenomenon for the reason of obviously contradictions of experimental data to modern scientific opinions.

Supposing the great cosmological importance of these questions we made the attempt to consider of the case of the global constants joint variation for the explanation of this effect using the world model with the positive cosmological constant on basis of radio astronomical, optical data and on the conception of the physical vacuum quantization (Larionov, 1997, 1999).

2. The possible global constants "DRIFT"

The closed Universe model with non-zero cosmological constant, deceleration parameter $q_0 = 0$ was used for determination of the principal cosmological correlations (Larionov 1997):

$$\frac{c}{R_0} = \frac{H_0}{\sqrt{2}} = Const; \quad \frac{c}{R_0} = \sqrt{\frac{4\pi G\rho_0}{3}};$$

$$\Lambda = \frac{4\pi G\rho_0}{c^2} = \frac{3}{R_0^2} = \frac{3H_0^2}{2c^2}; \quad l_{kv} = \frac{8\pi Gh}{3H_0c^2}. \quad (1)$$

The given correlation leads to dependencies showed in the table 1.

It is saw from the table, that the lows of changing m_{fot} and m_{pv} with epoch are the same, although the relations from which they were obtained are different ones. It is naturally because these effective masses have the identical roots: m_{fot} - a indignation in the PV matter, but the same PV environment have a characteristic of the effective mass m_{pv} of the STM sell including electron-positron virtual pairs (Larionov, 1997, 1999).

Table 1.

c=Const $\cdot R$	$E_{ph} = m_{ph}c^2 = Const/R^3$
$\lambda = Const \cdot R$	$l_{pv}^3 = Const/R^2$
$p = Const \cdot R^3$	$t_{pv} = Const/R^{5/3}$
$G = Const \cdot R^3$	$l_{pv}/t_{pv} = c = Const \cdot R$
$\Lambda = Const/R^2$	$t = Const/R$
$\sqrt{\Lambda} \cdot h \cdot c = Const/R^3$	$m_{pv} = Const/r^5$
$h = Const/R^3$	$e = Const/R$
$m_{ph} = Const/R^5$	

where c - the speed light, λ - the quantum wavelength, ρ_o - the matter density,
G - the gravitational constant, Λ - the cosmological constant,
$\sqrt{\Lambda} \cdot h \cdot c$ - the energy of the CTM cell,
h - the Plank constant, m_{fot} - the photon effective mass,
l_{kv} - the size of the STM cell, t_{kv} - the time existence of the STM cell having energy $\sqrt{\Lambda} \cdot h \cdot c$, t - the accompany system time, $m_{pv} = 2 \cdot 10^{-65} g$ - the effective mass of the STM cell,
e-the elementary charge.

The character of dependence of constants from the radius curvature of the Universe (R) give the possibility to determine of invariants (constants that do not depended of the epoch), from that we picked out, at the first time, $T = \lambda/c$ (the table 2).

Table 2.

$T = \lambda/c = Const$	$\sqrt{\Lambda} \cdot c = Const$
$G \cdot p = Const$	$E_{ph} \cdot G - Const$
$G \cdot h = Const$	$\rho_0/\rho_{cr} = Const$
$\sqrt{\Lambda} \cdot h \cdot c \cdot G = Const$	$(h/m) \cdot \Lambda = Const$
$G \cdot \Lambda/c = Const$	$(G \cdot h)/(m \cdot c) = Const$
$p/h = Const$	

The becoming invariant explain formally the cosmological nature of the phenomenon. This invariant is the direct consequence of the closed universe model and the introducing of the quantum PV matter.

The principal point is the interpretation of the redshift (z) by stretching PV environment, but not Doppler explanation (Larionov 1997). This is permitted to connect z with the scale factor or curvature radius R and physically comprehended of the itself constant $T = \lambda/c$.

Finally, the dependence $t = Const/R$ means, that processes in accompanying co-ordinate systems are passing according to the terrestrial clock with proportional coefficient R.

3. Conclusion

1. On the basis of the closed universe model with the positive cosmological constant, deceleration parameter $q_0 = 0$ and the quantum PV matter conception we get dependencies the principal constants on the epoch.

2. It is leads to the determination of invariants from them we examined $T = \lambda/c$.

3. The availability of the connection $T = \lambda/c$, do not depending on the epoch, given the possibility to state the cosmological nature of this invariant and the 160-min periods of the fluxes variable for quasars and galactic nuclei.

It is still necessary to find out the reason of the 160-min period changing of the global cosmological parameters, that is leading to the origin of this period.

References

Kotov V.A., Lyuty V.M.: 1987, *Izv. Krimsk. Astrofiz. Obs.*, **77**, 89.

Larionov M.G.: 1997, *Astrophys. and Space Sci.*, **252**, *140.*

Larionov M.G.: 1999, article in this issue.

THE STATE OF THE COSMOLOGICAL MODEL: OBSERVATIONS AND THEORY

V.N. Lukash

Astro Space Center of Lebedev Physical Institute
Profsoyuznaya 84/32, 117810 Moscow Russia

ABSTRACT. The main points and trends of observational and theoretical cosmology that influence and form the understanding of the Universe are reviewed.

Key words: cosmology

1. Introduction

The modern situation in revealing the true cosmology is considered. The investigation of the anisotropy of the relic CMB radiation ensures a basic channel of the information about our World. The continuing progress in the technology of deep-sky galactic surveys has resulted in impressive knowledge on the large scale structure in the Universe as well as its evolution back to high redshifts. Both $\Delta T/T$ and LSS experiments complement on supercluster scales and thus disclose the underlying cosmological model. To be brief, the model is found today up to accuracy 10-20 % which is a great progress since what we had 10-15 years ago when the discussions were at best on the level of a factor two. A great hope of the cosmologists is related with the development of ground and space based $\Delta T/T$ and far Universe observations which will help to delimit and determine the cosmological model up to a few per cent in the nearest future.

2. Basics of the LSS Formation

The seeds of the visible *Large Scale Structure* in the Universe are the *Cosmological Density Perturbations* which grow due to gravitational instability in the late, cold period of the Universe history when the expasion is dominated by *Cold Dark Matter* ($z < 10^5$). These primordial CDPs must have been created at the inflationary Big Bang epoch, as after the end of inflation the Universe was radiationally dominated and hence absolutely gravitationally stable against small perturbations of matter density and gravitation field. The CDPs existed in the hot Universe evolution period like the longwave 'gravitating sound waves' propagating across the relativistic matter with a constant amplitude. The CDPs started growing only after the equality epoch when the matter pressure decayed. The required CDP amplitude for galaxy clusters could form by now has therefore been predicted on the level $\delta \sim 10^{-5}$ which was finally confirmed by COBE (Bennet et al. 1996) on this same level but at two orders of magnitude larger scale (that in turn appeared to be in a successful consistency with another famous prediction known as the *Harrison-Zel'dovich* scale-invariant perturbation spectrum).

This optimistic situation has produced a great impetus for the observational and theoretical cosmology extending dramatically by continuing progress in the improved technology of deep-sky surveys and CMB temperature detections. The ultimate goal was to reconstruct the model parameters and CDP power spectrum from Mpc up to the horizon scale, the scope straighforwardly related to the high energy physics at inflation thus capable of being observationally tested today.

Three points should be emphasised in connection with the problem of LSS formation: theoretical, model, and observational.

The first point means that the LSS formation in the Universe is as fundamental problem as the creation of the Universe as a whole: both features, the small CDPs and the Friedmann background (the *Cosmological Principle*), were produced in the unique process of inflation in the very early Universe. The theory works at very high energies ($\sim 10^{13}$ GeV) whereas the observations occur in a low-energy limit ($\sim 10^{-4}$ eV). To provide a fair comparison in such a situation we need a model to know how perturbations evolved during the whole history of the Universe. Therefore, any confrontation in cosmology between theory and observations appears model dependent.

To determine the model we need priorities and parameters. The former assumes gravitational instability as the principal mechanism of the CDP dynamics on large scale, and Gaussian primordial perturbations with random spatial phases. The latter assumes knowledge of the current time when the structure is observed (H_0), the abundance of cosmic matter components (Ω_m, Ω_Λ, Ω_ν, Ω_b) and *Cosmic Gravitational Waves* (T/S), and the nature of dark matter (e.g. relic scalar field, cold/hot dark matter, the number of

species of massive neutrinos and relativistic particles). Today, cosmologists venture the following approach: if the dark matter model is postulated as fairly simple (with just a few model parameters) then the recovering of both the CDP power spectrum and the cosmological parameters can be provided by observational data on $\Delta T/T$ and LSS.

Below, I discuss the model under such a conventional probability sense. There is no principal restrictions on the way: any theory could be tested to the limit if we had enough data. The more data are available the less uncertainties remain in the theory and more parameters can be determined. Actually, we are now in the beginning of data collection. Cosmologists have started the model restoration exercise taking simple theories and confronting them with the observational data available. The development progresses with an increasing number of model parameters. Theory goes from simplicity, however Nature appears complex.

3. Dark Matter Models

Until recently there were two basic theories claiming to approach the corner stones of the LSS formation: inflation and defects. While being very much different in their grounds on galaxy seeds – the linear Gaussian scalar perturbations in one case and the non-linear non-Gaussian cosmic defects (strings, monopoles, textures) in other case – both models presented the fundamental inevitable perturbations produced in the very early Universe: the parametrically amplified quantum vacuum fluctuations of the inflaton and the topological defects left after phase transitions in the early Universe, respectively.

However, the simplest defect model normalised by the CMB fluctuations proved to fail to meet the LSS formation (Watson 1997). The reason is that the non-linear matter perturbations generate all three types of the metric fluctuations - *Scalar, Vortex* and *Tensor* ones, which all contribute to the Sachs-Wolfe $\Delta T/T$ anisotropy on large angular scale, so the resulting S-mode amplitude proved to have had insufficient power to develop the observed galaxy distribution.

By now only the inflation theories have got through ordeals of fitting the LSS and $\Delta T/T$ requirements. The principal quest here is the predicted Gaussian nature of small CDPs, which faces a satisfactory consistency with the real distribution of galaxies on scales $\sim 20\ h^{-1}$ Mpc (e.g. Juszkiewicz & Bouchet 1996). The only obstacle to testing reliably this important feature of the CDP seeds is the restricted depth of the available galaxy surveys.

Deep galaxy surveys would also be highly welcome for clarifying another challenge of the modern cosmology: the fractal model attacking persistently the cosmological principle. The point is that huge voids seen in the galaxy distribution spatial fields extend up to scales $\sim 100\ h^{-1}$ Mpc which is close to catalogues' sizes, thus leaving a room for discussions on the value of the homogeneity scale (Sylos Labini et al. 1997). Nevertheless, I would like to stress that the fractal challenge is still a question for the distribution of optical galaxies rather than for the total mass of the Universe. The latter should be pretty homogeneous on scales larger than tens of Mpc to fit the beautiful Hubble diagrams, to say nothing on the uniform microwave and X-ray backgrounds testifying the cosmic homogeneity on larger scales.

Thus, we consider only models backed on the inflationary theories. The main tool for the Gaussian perturbations is the second moment of their spatial distribution related to the power spectrum:

$$\langle \delta^2 \rangle = \int_0^\infty P(k) k^3 dk = \int_0^\infty \Delta_k^2 \frac{dk}{k}. \qquad (1)$$

The dimensionless CDP spectrum Δ_k^2 has a simple meaning of the variance of density contrast in the scale k (the wave number) within the scale band $dk \sim k$, it is evidently additive ($\delta^2 \sim \Sigma \Delta_k^2$).

Before passing to discussion on the spectrum observational reconstruction let me sketch briefly the situation with the model parameters.

4. Cosmological Parameters

It seems that the longstanding strong debate on H_0 is approaching to its end and we are going to learn the value of the Hubble constant during nearest years. Today, two methods seem very promising: measuring Cepheids in distant galaxies and the supernovae type Ia method. I would not like to fix here the number since it is not yet time for any consensus between the groups about systematic and selection bias effects for all methods employed. For us, it is important to note that the matter dominated cosmological models (with the critical dynamical density, $\Omega_m = 1$, and negligible Λ-term) are consistent only with small Hubble constant ($H_0 < 65\, km\, s^{-1} Mpc^{-1}$) regarding the low limit for the age of the Universe coming from globular clusters.

A more optimistic point stands for determination of the matter content in the Universe. At the first glance the situation looks similar: again we have two groups of experiment resulting in different conclusions. However, here the consensus is possible.

The first experiment deals with megaparsec scales – galaxy halos, groups and X-ray clusters, – $l < l_D$ where the dynamical scale in the Universe is $l_D \sim 10 h^{-1} Mpc$ (the scale of the richest collapsing clusters). The assumption on the hydrostatic equilibrium within cluster cores yields a low dynamical mass responsible for the formation of the gravitational potential on Mpc scale:

$\Omega_m \sim 0.3$. Another important observation is a large fraction of baryons inside X-ray clusters reaching somehow $\sim 20\%$ within scale ~ 1 Mpc:

$$\frac{M_b}{M_m} \sim 0.2, \qquad (2)$$

which is also consistent with the low matter density involved dynamically in small scales (as $\Omega_b \leq 0.1$ due to the primordial nucleasynthesis, and M_b/M_m may be $\sim \Omega_b/\Omega_m$ on the dynamical scale).

Another experiments dealing with LSS ($l > l_D$) hints that the Universe may be matter dominated ($\Omega_m > 0.5$). There are few arguments for it (still more model dependent ones in comparison with the small-scale arguments):

- the existence of substructures in the majority of galaxy clusters evidencing that the clusters are just forming systems, which is possible only in the Universe dynamically close to the critical density;
- the large coherence velocities obviously of the cosmological origin, allowing the reconstruction of the total density contrast (and as a consequence, consistency with the 'standard' model $\Omega_m > 0.5$ and the galaxy biasing factor $b \simeq 1$);
- the essentially Gaussian nature of the linear primordial cosmological perturbation pattern when it is recovered (by returning back in time from the actual non-linear distribution of matter density and velocity) in a matter-dominated universe ($\Omega_m \sim 1$);
- the weak gravitational lensing confirming high dynamical mass abundance around some X-ray clusters;
- the lensing argument on the fraction of splitting quasars, (still much dependent on the model assumptions);
- the evolutionary argument on the galaxy clusters number density (still under discussion);
- the geometrical argument from the distant supernovae type Ia, (still much to be clarified on systematic effects);
- the point coming from $\Delta T/T$ anisotropy (mainly, the location of the first acoustic peak).

The last three points got some important turns in the recent time which I cannot help mentioning here.

It is the ENACS identification of the nearby galaxy clusters (by the dispersion velocities of their optical galaxies, Mazure et al.1996) that has shown the previous underestimation of the Abell cluster abundance. At the moment we may state the consistency of the cluster number density evolution with redshifts for the $\Omega_m/sim1$ Universe. At least, the low evolution argument that for many years has been considered as a basic argument in favour of the low density Universe, is not any more as strong as it has seemed.

The breakthrough in the problem of the model geometry restoration is being done today using the classical Hubble diagrams (the redshifts *vs* apparent magnitudes) composed for distant supernovae of type Ia (Perlmutter et al. 1998). Contrary to galaxies, such sources look amazingly standard candles which is well supported by the distance measurements to nearby supernovae. Tested by distant supernovae, the deviations of the Hubble diagram from the linear law hint upon the real geometry of the Universe. Currently, the predictions are close to a halh-to-half matter-vacuum Universe ($\Omega_m \sim \Omega_\Lambda \sim 0.5$). However, this supernovae method is still young and careful analysis of the systematic effects is required to make it trustable.

Reconstruction of the cosmological parameters from CMB temperature fluctuations reminds one an exercise since the strongest effect comes from the location and amplitude of the first acoustic peak (the Sakharov oscillation) whose observational detection leaves much to be desired. However, without discussing here the numbers, it is worthwhile recalling the *tendency* for the model parameter constraints resulting from all $\Delta T/T$ data available in the literature (e.g. Lineweaver & Barbosa 1997): they favor low H_0 (~ 0.5) and high Ω_b (~ 0.1) and Ω_0 (> 0.5 , $\Omega_0 = \Omega_m + \Omega_\Lambda$). The low density open Universe ($\Omega_0 < 0.3$) is rejected by current $\Delta T/T$ data. It is also interesting that the high Ω_0 values are welcome by the Ly_α forest data.

Finally, a possible reconciliation between the DM experiments on small and large scales can be the following: some fraction of dark matter in the Universe is distributed on large scales and does not enter the galaxy halos and groups.

How can it be arranged?

Today we have purely theoretical ideas on such a possibility. The most frequently discussed are models with *Mixed Dark Matter* (cold+hot, with the hot particles like massive neutrinos with a few eV rest mass and the corresponding density parameter $\Omega_\nu \in (0.2, 0.4)$), non-zero Λ-term ($\Omega_\Lambda \in (0.5, 0.7)$), and a combination of both (the ΛMDM models). In all cases CDM particles form a dynamic structure on Mpc scales, while on large scales there is an additional contribution coming from light neutrinos or/and vacuum density (the Λ-term affects the cosmological expansion rate). A sceptical point concerning these and other cosmology models which are considered today as possible candidates for the real Universe is as follows: all of them are multi-parameter and thus non-minimal models; the more parameters is involved, the better comes the situation with data confrontation.

Does the latter tell us that we miss something important in our discussion on the formation of the Universe

structure? May be. I can only conclude here saying than none of the models under discussion meets all the observational tests. Say, regarding previous examples, for $\Lambda \neq 0$ models one can expect a large fraction of old (relaxed) galaxy clusters and lensed quasars, whereas the MDM models require $H_0 < 65\, km\, s^{-1} Mpc^{-1}$ and too a small abundance of X-ray clusters and high-redshift quasars. Probably, the dark matter can exist in the form of relic scalar field left after inflation or in some other exotic form which requires special analysis.

In such a situation the observational verifications become extremely important. The principal test here is the LSS evolution in the early Universe.

5. The spectrum of density perturbations

The cosmological models of LSS formation discussed today are aimed to fit the observational data at $z = 0$. Thus we cannot distinguish between the models without going into their evolution at medium and high redshifts where the models demonstrate their essential difference.

Two main experiments promote a snow ball progress in the reconstruction of the CDP spectrum, which was impossible in previous years: $\Delta T/T(\theta > 1')$ and direct investigation of the evolution and hierarchy of LSSs. The reason for stimulating such a progress is that these two experiments confront and overlap each other: the $\Delta T/T$ investigations go nowadays to small comoving scales up to $l \sim 10\, h^{-1}$ Mpc (recall the corresponding angular scale in arcmin $\theta \sim lh$), and, at the same time, we observe a developed structure of clusters, filaments, voids, and superclusters reaching the scales $\sim 100\, h^{-1}$ Mpc.

Any reasonable assumption on the "formation" of large voids and superclusters in Gaussian perturbation theories inevitably leads to $\Delta T/T$ predictions at $\sim 1^0$ capable of current detection. It is a great puzzle that namely this scale specifies the horizon at the decoupling era and therefore the angular scale of the first acoustic peaks. Its existence was predicted by theory long ago. Now, the time for observations came: it is just on agenda, a matter of the improved instrument's technology and foreground separations that will precisely determine the acoustic peak parameters and ultimately prove and determine the theory.

We are aware of the cosmological temperature anisotropy on large scale and have some information on the whole spectrum of the CMB fluctuations (Hancock et al. 1998). Fortunately, the small angular scales ($\theta < 1^0$) can be effectively tested from the Earth's surface. A hope is that such terrestrial instruments as SK, CAT, VSI, TOCO, BUMERANG, RATAN-600, combined with balloon experiments as well as the MAP and Planck Surveyor satellites, will provide a sensitivity advance sufficient for the cosmological model reconstruction.

Meanwhile, the situation with the CDP spectrum looks rather dramatic. On large scales ($\sim 1000\, h^{-1}$ Mpc) the fundamental spectrum is small in amplitude and consistent with the HZ slope:

$$\Delta_k^2 \sim k^{3+n_S}, \quad n_S = 1.1 \pm 0.1. \tag{3}$$

However, on smaller scales ($\leq 100\, h^{-1}$ Mpc) the power should be boosted as we observe rich structures in spatial distribution of galaxies, clusters, Ly_α systems, and distant sources like quasars. The latter is especially important. We live in the period of decay of quasar and star formation activities (Boyle & Terlevich 1998). We thus have a unique opportunity to observe these numerous early sources tracing the past dynamics of LSS formation. This would be extremely informative as the LSS perturbation amplitude, being still less than unity today at $l \sim 100\, h^{-1}$ Mpc, was ever lower in the past, which predicts a strong inverse evolution of such huge systems as superclusters and voids.

It seems that quasars, the active galactic nuclei of distant galaxies, form the LSS at medium redshifts ($z \sim 1 - 2$) which is provided by their correlation function and the existence of large QSO groups recalling in properties (the comoving size and abundance) the local superclusters (Komberg et al. 1996). Actually, distant bright quasars may originate in merging galaxies in protoclusters, and thus can trace the sites of enhanced matter density at medium and high redshifts analogous to how galaxy clusters trace them in the near space. In case of matter dominated Universe the dynamical formation of these early LSSs suggests that the spectral amplitude on superclusters scale ($\sim 100\, h^{-1}$ Mpc) should be comparable and pretty close to that on cluster scale ($\sim 10\, h^{-1}$ Mpc), i.e. the CDP spectrum is nearly flat between those scales (Komberg & Lukash 1994):

$$\Delta_k^2 \sim k^{0.9 \pm 0.2}. \tag{4}$$

This estimate for the spectrum shape is also backed by the local observations of galaxy and galaxy cluster distributions (Guzzo 1991, Peacock 1996, Einasto et al. 1997).

A strong break in the spectrum slope from the HZ asymptotic (3) to the flat part (4) should have happened at supercluster scale ($\sim 100 - 150\, h^{-1}$ Mpc) which is obviously a real feature of the fundamental CDP spectrum. This 'signature of the God' in the primordial spectrum demands its explanation in physics of the very early Universe.

I cannot help mentioning another connection of the very early Universe with the primordial perturbation spectrum. This is a possibility to have high abundance of cosmic gravitational waves contributing to large-scale CMB anisotropy.

There are at least two reasons for such discussion.

The first one is theoretical. Inflation theory is not discriminative to any of the perturbation modes if inflation occurs at GUT energies (Lukash & Mikheeva 1997): both S (CDP) and T (CGW) modes can be produced with similar amplitudes and thus comparable contribution to the CMB anisotropy,

$$\left(\frac{\Delta T}{T}\right)^2_{10^0} = S + T. \quad (5)$$

The second reason comes from observations. If the scalar perturbation spectrum is 'blue' ($n_S > 1$) then a non-zero T/S¿0 is required to reconcile the COBE $\Delta T/T$ measurement with the galaxy cluster abundance.

The problem of T/S is fundamental but can be treated at the moment only theoretically. A serious discussion on the observational detection of T/S could be launched after CMB polarization measurements, which would require the instrumental sensitivity $\sim 1\mu K$ currently non-reachable.

6. Conclusions and Tendencies

As never before, the cosmologists are close to recovering the real model of our Universe and the post-recombination CDP spectrum directly from observations, both $\Delta T/T$ and LSS, and to creating an exciting link to the physics of the very early Universe. We are going to gain the data from the advanced ground and space based CMB explorers as well as huge surveys of spatial distribution of galaxies, to delimit the cosmological model with unprecedented precision.

The list of current conclusions may be incomplete:

- the extreme open models ($\Omega_0 < 0.3$) are rejected by CMB and cluster evolution data;
- the distant supernovae Ia may be used to restoring the spatial geometry of our Universe;
- the current data on the acoustic peak indicate small H_0 ($\leq$ 65 $km\ s^{-1}\mathrm{Mpc}^{-1}$) and large Ω_b (~ 0.1) and Ω_0 (> 0.5);
- the slope of the fundamental CDP spectrum is consistent with HZ ($n_S \simeq 1$);
- the CMB and LSS data indicate a break in the CDP spectrum slope at scale $\sim 100 - 150$ Mpc, which requires *new physical* explanation;
- the T/S problem cannot be ignored and needs careful treatment.

Acknowledgements. The work was supported in part by INTAS (97-1192).

References

Bennet C.L. et al.: 1996, *ApJ*, **464**, L1.
Boyle B.J., Terlevich R.J.: 1998, *MNRAS*, **293**, L49.
Einasto J. et al.: 1997, *Nature*, **385**, 139.
Guzzo L.: 1991, *ApJ*, **382**, L5.
Hancock S. et al.: 1998, *MNRAS*, **294**, L1.
Juszkiewicz R., Bouchet F.R.: 1996, *astro-ph/ 9602134.*
Komberg B.V., Lukash V.N.: 1994, *MNRAS*, **269**, 277.
Komberg B.V., Kravtsov A.V., Lukash V.N.: 1996, *MNRAS*, **282**, 713.
Lineweaver C.H., Barbosa D.: 1997, *astro-ph/9706077.*
Lukash V.N., Mikheeva E.V.: 1997, *http://www.mrao.cam.ac.uk/ppeuc/astronomy/papers/lukash/lukash.html*
Mazure A. et al.: 1996, *As.Ap.*, **310**, 31.
Peacock J.: 1996, *astro-ph/9608151.*
Perlmutter S. et al.: 1998, *Nature*, **391**, 51.
Sylos Labini F., Montuori M., Pietronero L.: 1997, *astro-ph/9711073.*
Watson A.: 1997, *Science*, **278**, 574.

BEST-FIT COSMOLOGICAL PARAMETERS FROM OBSERVATIONS OF THE LARGE SCALE STRUCTURE OF THE UNIVERSE

B. Novosyadlyj[1], S. Apunevych[1], R. Durrer[2], S. Gottloeber[3], V. Lukash[4]

[1] Astronomical observatory, I.Franko State University of Lviv
Kyryla i Mephodia, 8, Lviv 290005, Ukraine,
novos@astro.franko.lviv.ua, apus@astro.franko.lviv.ua

[2] Department of Theoretical Physics, University of Geneva
Quai Ernest Ansermet 24, CH-1211 Geneva 4, Switzerland, *ruth.durrer@physics.unige.ch*

[3] Astrophysikalisches Institut Potsdam
An der Sternwarte 16, D-144482 Potsdam, Germany, *sgottloeber@aip.de*

[4] Astro Space Center of Lebedev Physical Institute of RAS
Profsoyuznaya 84/32, 117810 Moscow, Russia, *vladimir@lukash.asc.rssi.ru*

ABSTRACT. The possibility to determine cosmological parameters on the basis of a wide set of observational data including the Abell-ACO cluster power spectrum and mass function, peculiar velocities of galaxies, the distribution of Ly-α clouds and CMB temperature fluctuations is analyzed. Assuming a flat universe, $\Omega_\Lambda + \Omega_m = 1$, with purely scalar perturbations, we show that a χ^2 minimization method applied on this data set determines quite precisely the values of the spectral index n of the primordial power spectrum, the baryon and massive neutrino density Ω_b and Ω_ν respectively, the Hubble constant $h \equiv H_0/(100\mathrm{km/s/Mpc})$ and the value of the cosmological constant, Ω_Λ.

Varying all parameters we find that a tilted ΛMDM model with one species of massive neutrinos and the parameters $n = 1.13 \pm 0.10$, $\Omega_m = 0.41 \pm 0.11$, $\Omega_\nu = 0.06 \pm 0.028$, $\Omega_b = 0.039 \pm 0.014$ and $h = 0.70 \pm 0.12$ matches the observational data best.

Key words: Cosmology: theory: large scale structure of the Universe: dark matter; galaxies: clustering.

1. Introduction

The goal of this paper is to determine cosmological parameters on the basis of observational data on large scale structure (LSS) of the Universe obtained during last years. We consider a scale free power spectrum of purely scalar primordial perturbations which evolve in a multicomponent medium to form the large scale structure of the Universe. Today it is understood that models with a minimal number of free parameters, such as scale independent ($n = 1$) standard cold dark matter model (SCDM) or standard mixed (cold plus hot) dark matter model (SMDM), match observational data only marginally. Better agreement between predictions and observational data can be achieved in models with a larger number of parameters, e.g. cold dark matter (CDM) or mixed dark matter (MDM) with baryons, tilted primordial power spectra and cosmological constant (Valdarnini et al. 1998, Primack & Gross 1998).

The determination of cosmological parameters from some observational characteristics of the LSS of the Universe was carried out in many papers (e.g. Atrio-Barandela et al. 1997, Lineweaver & Barbosa 1998, Tegmark 1998, Bridle et al. 1999, Novosyadlyj 1999 and references therein). These papers differ by the number of parameters and the set of observational data included into the analysis. In this paper a total of 23 measurements from sub-galaxy scales (Ly-α clouds) over cluster scales up to the horizon scale (CMB quadrupole) is used to determine eight cosmological parameters, namely the tilt of the primordial spectrum n, the densities of cold dark matter Ω_{cdm}, hot dark matter Ω_ν, and baryons Ω_b, the density parameter of cosmological constant Ω_Λ, and the Hubble parameter h, the biasing parameter b_{cl}, the number of massive neutrino species N_ν.

Here we restrict ourselves to the analysis of spatially flat cosmological models with $\Omega_\Lambda + \Omega_m = 1$, where $\Omega_m = \Omega_{cdm} + \Omega_b + \Omega_\nu$, and to an inflationary scenario without tensor mode. It reduces the number of search parameters to seven. We also neglect the effect of a possible early reionization which could reduce the

amplitude of the first acoustic peak in the CMB anisotropy spectrum.

2. Experimental data set and method

2.1. Observational data

We use the power spectrum of Abell-ACO clusters (Einasto et al. 1997, Retzlaff et al. 1998), measured in the range $0.03 \leq k \leq 0.2h$/Mpc, as observational input. Its amplitude and slope at lower and larger scales are quite sensitive to baryon content Ω_b, Hubble constant h, neutrino mass m_ν and number species of massive neutrinos N_ν (Novosyadlyj 1999). The total number of Abell-ACO data points with their errors used for minimization is 13, but not all of these points can be considered as independent measurements. Since we can accurately fit the power spectrum by an analytic expression depending on three parameters only (the amplitude at large scales, the slope at small ones and the scale of the bend); we assigned to the power spectrum 3 effective degrees of freedom.

The second observational data set which we use are the position and amplitude of first acoustic peak derived from data on the angular power spectrum of CMB temperature fluctuations. To determine the position and amplitude of the first acoustic peak we use a 6-th order polynomial fit to the data set on CMB temperature anisotropy, accumulated and compiled by Tegmark on his homepage with the new TOCO points added (Miller et al. 1999), 49 data points in total. The amplitude A_p and position ℓ_p of first acoustic peak determined from this fit are $80.81 \pm 18.0\mu$K and 256 ± 83 correspondingly. The statistical errors are estimated by edges of the χ^2-hyper-surface in the space of polynomial coefficients which corresponds to 68.3% (1σ) probability level under the assumption of Gaussian statistics. Also the mean weighted bandwidth of each experiment around l_p is added to obtain total $\Delta\ell_p$.

A constraint on the amplitude of the matter density fluctuation power spectrum at cluster scale can be derived from the cluster mass and X-ray temperature functions. It is usually formulated in terms of the density fluctuation in a top-hat sphere of $8h^{-1}$ Mpc radius, σ_8, which can be easily calculated for the given initial power spectrum. According to the recent optical determination of the mass function of nearby galaxy clusters (Girardi et al. 1998) and taking into account the results from other authors (see for references Borgani et al. 1999) we use the value $\tilde{\sigma}_8\tilde{\Omega}_m^{0.49-0.09\Omega_m} = 0.60 \pm 0.08$ Another constraint on the amplitude of the linear power spectrum of density fluctuations in our vicinity comes from the study of galaxy bulk flow, the mean peculiar velocity of galaxies in sphere of radius $50h^{-1}$ Mpc around our position. We use the data given by Kolatt & Dekel 1997, $\tilde{V}_{50} = (375 \pm 85)$ km/s.

An essential constraint on the linear power spectrum of matter clustering at galactic and sub-galactic scales $k \sim (2-40)h$/Mpc can be obtained from the Ly-α forest of absorption lines seen in quasar spectra (Gnedin 1998, Croft et al. 1998 and references therein). Assuming that the Ly-α forest is formed by discrete clouds of a physical extent near Jeans scale in the reionized inter-galactic medium at $z \sim 2-4$ Gnedin 1998 has obtained a constraint on the value of the r.m.s. linear density fluctuations $1.6 < \tilde{\sigma}_F(z=3) < 2.6$ (95% CL) at Jeans scale for $z = 3$ equal to $k_F \approx 38\Omega_m^{1/2}h$/Mpc (Gnedin 1999).

The procedure to recover the linear power spectrum from the Ly-α forest has been elaborated by Croft et al. 1998. Analyzing the absorption lines in a sample of 19 QSO spectra they have obtained the following constraint on the amplitude and slope of the linear power spectrum at $z = 2.5$ and $k_p = 1.5\Omega_m^{1/2}h$/Mpc, at (95% CL)

$$\tilde{\Delta}^2_\rho(k_p) \equiv k_p^3 P(k_p)/2\pi^2 = 0.57 \pm 0.26, \qquad (1)$$

$$\tilde{n}_p \equiv \frac{\Delta log\ P(k)}{\Delta log\ k}\ |_{k_p} = -2.25 \pm 0.1, \qquad (2)$$

.

In addition to the power spectrum measurements we use the constraints on the value of Hubble constant $\tilde{h} = 0.65 \pm 0.15$ which is a compromise between measurements made by two groups: Tammann & Federspiel 1997 and Madore et al. 1998. We also employ the nucleosynthesis constraints on the baryon density of $\tilde{\Omega_b h^2} = 0.019 \pm 0.0024$ (95% CL) given by Burles et al. 1999.

2.1. Method

In order to find the best fit model we must evaluate theoretical counterparts of above mentioned values.

For the solution of our searching problem we use the accurate analytic approximations of the MDM transfer function $T(k;z)$ depending on the parameters Ω_m, Ω_b, Ω_ν, N_ν, h by Eisenstein & Hu 1999.

The linear power spectrum of matter density fluctuations is

$$P(k;z) = Ak^n T^2(k;z) D_1^2(z)/D_1^2(0), \qquad (3)$$

where A is the normalization constant and $D_1(z)$ is the growth factor, useful analytical approximation for which has been given by Carreta et al. 1999.

We normalize the spectra to the 4-year COBE data (Bennett et al. 1996) according to (Liddle et al. 1996, Bunn and White 1997).

The Abell-ACO power spectrum is connected with the matter power spectrum at $z = 0$ by a linear and scale independent cluster biasing parameter b_{cl}, which we include as a free parameter

$$P_{A+ACO}(k) = b_{cl}^2 P(k;0). \qquad (4)$$

For a given set of parameters n, Ω_m, Ω_b, h, Ω_ν, N_ν and b_{cl} the theoretical value of $P_{A+ACO}(k_j)$ can be calculated for each observed scale k_j. Let's denote these values by y_j $(j = 1, ..., 13)$.

The dependence of the position and amplitude of the first acoustic peak in the CMB power spectrum on cosmological parameters has been investigated using the public code CMBfast by Seljak & Zaldarriaga 1996. As expected, these characteristics are independent on the hot dark matter content.

We determine values ℓ_p and A_p for given parameters (n, h, Ω_b and Ω_Λ) on a 4-dimensional grid for parameter values inbetween the grid points we determine ℓ_p and A_p by linear interpolation. We denote ℓ_p and A_p by y_{14} and y_{15} respectively.

The theoretical values of the other experimental constraints are obtained as follows: the density fluctuation σ_8 is calculated according to

$$\sigma_8^2 = \frac{1}{2\pi^2}\int_0^\infty k^2 P(k;0) W^2(8\text{Mpc } k/h)dk, \quad (5)$$

with $P(k;z)$ from Eq. (3). We set $y_{16} = \sigma_8 \Omega_m^{0.49-0.09\Omega_m}$ and $y_{17} = \sigma_8 \Omega^\alpha$, where $\alpha = 0.24$ for $\Omega_\Lambda = 0$ and $\alpha = 0.29$ for $\Omega_\Lambda > 0$, respectively.

The r.m.s. peculiar velocity of galaxies in a sphere of radius $R = 50h^{-1}$Mpc is equal

$$V_{50}^2 = \frac{1}{2\pi^2}\int_0^\infty k^2 P^{(v)}(k) e^{-k^2 R_f^2} W^2(50\text{Mpc } k/h)dk, \quad (6)$$

where $P^{(v)}(k)$ is the density-weighted power spectrum for the velocity field (Eisenstein & Hu 1999), $W(50\text{Mpc } k/h)$ is a top-hat window function, and $R_f = 12h^{-1}$Mpc is a radius of Gaussian filter used for smoothing of the raw data. For the scales considered $P^{(v)}(k) \approx (\Omega^{0.6} H_0)^2 P(k;0)/k^2$. We denote the r.m.s. peculiar velocity by y_{18}.

The value of the r.m.s. linear density perturbation from the formation of Ly-α clouds for corresponding z and k_F is given by

$$\sigma_F^2(z) = \frac{1}{2\pi^2}\int_0^\infty k^2 P(k;z) e^{(-k/k_F)^2} dk. \quad (7)$$

It is denoted by y_{19}.

The corresponding values of the $\Delta_\rho^2(k_p, z)$ and slope $n(z)$ were obtained as defined in Eq. (1) and Eq. (2) at $z = 2.5$ and $k_p = 0.008H(z)/(1+z)(\text{km/s})^{-1}$, and are denoted by y_{20} and y_{21} accordingly.

For all tests excluding Gnedin's Ly-α test we used the density weighted transfer function $T_{cb\nu}(k, z)$ from Eisenstein & Hu 1999. For σ_F the function $T_{cb}(k, z)$ is used according to the prescription by Gnedin 1998. Note, however, that even in the model with maximal Ω_ν (~ 0.2) the difference between $T_{cb}(k, z)$ and $T_{cb\nu}(k, z)$ is $\leq 12\%$ for $k \leq k_p$.

Finally, the values of $\Omega_b h^2$ and h are denoted by y_{22} and y_{23} respectively.

Under the assumption that the errors on the data points are Gaussian, the deviations of the theoretical values from their observational counterparts can be characterized by χ^2:

$$\chi^2 = \sum_{j=1}^{23} \left(\frac{\tilde{y}_j - y_j}{\Delta\tilde{y}_j}\right)^2, \quad (8)$$

where $\tilde{y}_j$ and $\Delta\tilde{y}_j$ are the experimental data and their dispersions, respectively. The set of parameters n, Ω_m, Ω_b, h, Ω_ν, N_ν and b_{cl} can be determined by minimizing χ^2 using the Levenberg-Marquardt method (Press et al. 1992). The derivatives of the predicted values w.r.t the search parameters required by this method are calculated numerically using a relative step size of 10^{-5}.

This method has been tested and has proven to be reliable, independent on the initial values of parameters and it has good convergence.

3. Results and conclusions

The determination of the parameters n, Ω_m, Ω_b, h, Ω_ν, N_ν and b_{cl} by the Levenberg-Marquardt χ^2 minimization method is realized in the following way: we vary the set of parameters n, Ω_m, Ω_b, h, Ω_ν and b_{cl} and find the minimum of χ^2, using all observational data described in previous section. Since the N_ν is discrete value, we repeat this procedure three times for N_ν=1, 2, and 3. The lowest of the three minima is the minimum of χ^2 for the complete set of free parameters.

The results are presented in the Table 1. The errors in the determined parameters are calculated as root square from diagonal elements of covariance matrix of the standard errors.

One can see the model with one sort of massive neutrinos provides the best fit to the data, $\chi^2_{min} \approx 4.6$. Note, however, that there are only marginal differences in χ^2_{min} for $N_\nu = 1, 2, 3$. Therefore, with the given accuracy of the data we cannot conclude whether – if massive neutrinos are present at all – their number of species is one, two, or three.

The number of degrees of freedom is $N_F = N_{\text{exp}} - N_{\text{par}} = 7$. The χ^2_{min} for all cases is within the expected range, $N_F - \sqrt{2N_F} \leq \chi^2_{\text{min}} \leq N_F + \sqrt{2N_F}$ for the given number of degrees of freedom. This means that the cosmological paradigm which has been assumed is consistent with the data.

We summarize, that the observational data on LSS of the Universe considered here can be explained by a tilted ΛMDM inflationary model without tensor mode. The best fit parameters are: $n = 1.13 \pm 0.10$, $\Omega_m = 0.41 \pm 0.11$, $\Omega_\nu = 0.06 \pm 0.028$, $\Omega_b = 0.039 \pm 0.014$ and $h = 0.70 \pm 0.12$. All predictions of measurements are close to the real experimental values mentioned above and within the error bars of data. The CDM density

Table 1: Cosmological parameters determined for the tilted ΛMDM model with one, two and three species of massive neutrinos.

N_ν	χ^2_{min}	n	Ω_m	Ω_ν	Ω_b	h	b_{cl}
1	4.55	1.13±0.10	0.41±0.11	0.060±0.028	0.039±0.014	0.70±0.12	2.22±0.33
2	4.74	1.14±0.10	0.49±0.13	0.104±0.042	0.039±0.015	0.70±0.13	2.32±0.36
3	5.02	1.14±0.10	0.56±0.14	0.133±0.053	0.040±0.015	0.69±0.13	2.44±0.37

parameter is $\Omega_{cdm} = 0.31 \pm 0.12$ and Ω_Λ is moderate, $\Omega_\Lambda = 0.59 \pm 0.11$. The neutrino matter density corresponds to a neutrino mass $m_\nu = 94\Omega_\nu h^2 \approx 2.7 \pm 1.2$ eV. The value of Hubble constant is close to measurements made by Madore et al. 1998. The age of the Universe for this model equals 12.3 Gyrs which is in good agreement with the age of the oldest objects in our galaxy. The spectral index coincides with the COBE prediction. Relation between matter density Ω_m and cosmological constant Ω_Λ agrees well with measurements of cosmic deceleration and global curvature based on the SNIa observation (Schmidt et al. 1998).

The coincidence of the values of cosmological parameters obtained by different methods indicates that a wide set of cosmological measurements are correct and that their theoretical interpretation is consistent. However, we must also note that the accuracy of present observational data on the large scale structure of the Universe is still too modest to determine a set of cosmological parameters at high confidence level.

References

Atrio-Barandela F., Einasto J. Gottlöber S., et al.: 1997, *Pis'ma Zh. Eksp. Teor. Fiz.*,**66**, 373.

Bahcall N.A., Fan X.: 1998, *ApJ*, **504**, 1.

Bennett C.L., Banday A.J., Gorski K.M., et al.: 1996, *ApJL*, **464**, L1.

Borgani S., Girardi M., Carlberg R.G., et al.: 1999, *astro-ph/9907323*.

Bridle S.L., Eke V.R., Lahav O., et al.: 1999, *astro-ph/9903472*.

Burles S., Nollett K.M., Truran J.N., Turner M.S.: 1999, *astro-ph/9901157*.

Bunn E.F., White M.: 1997, *ApJ*, **480**, 6.

Carreta E., Gratton R.C., Clementini G., et al.: 1999, *astro-ph/9902086*.

Croft R.A.C., Weinberg D.H., Pettini M., et al.: 1998, *ApJ*, **495**, 44.

Einasto J., Einasto M., Gottlöber S., et al.: 1997, *Nature*, **385**, 139.

Eisenstein D.J., Hu W.: 1999, *ApJ*, **511**, 5.

Girardi M., Borgani S., Giuricin G., Mardirossian F., Mezzetti M.: 1998, *ApJ*, **506**, 45.

Gnedin N.Y.: 1998, *MNRAS*, **299**, 392.

Gnedin N.Y.: 1999, *private communication*.

Kolatt T., Dekel A.: 1997, *ApJ*, **479**, 592.

Liddle A.R., Lyth D.H., Viana P.T.P., White M.: 1996, *MNRAS*, **282**, 281.

Lineweaver C.A., Barbosa D.: 1998, *ApJ*, **496**, 624.

Madore B.F., Freedman W., Silbermann N., et al.: 1998, *astro-ph/9812157*.

Miller A.D., Caldwell R., Devlin M.J., et al.: 1999, *astro-ph/9906421*.

Novosyadlyj B.: 1999, *Journal of Physical Studies*, **V.3**, No 1, 122.

Press W.H., Flannery B.P., Teukolsky S.A., Vettrling W.T.: 1992, *Numerical recipes in FORTRAN*. New York: Cambridge Univ. Press

Primack, J.R., Gross, M.A.: 1998, *astro-ph/9810204*.

Retzlaff J., Borgani S., Gottlöber S., Klypin A., Müller V.: 1998, *New Astronomy*, **v.3**, 631.

Seljak U., Zaldarriaga M.: 1996, *ApJ*, **469**, 437.

Schmidt B.P. et al.: 1998, *astro-ph/9805200*.

Tammann G.A., Federspiel M.: 1997, in "The Extragalactic Distance Scale", eds. M.Livio, M.Donahue, N.Panagia (Cambridge Univ. Press).

Tegmark M.: 1998, *astro-ph/9809201*.

Tegmark M.: *http://www.sns.ias.edu/∼max/*.

Valdarnini R., Kahniashvili T., Novosyadlyj B.: 1998, *As.Ap.*, **336**,11.

MODERN TREND OF THE GRAVITATIONAL WAVE DETECTION

V.N. Rudenko

Sternberg Astronomical Institute of Moscow State University
Universitetskii Prospect 13, 119899 Moscow, Russia

ABSTRACT. A brief review of the gravitational wave detection is presented and some modern approach in the gravitational wave experiment is considered. In addition to the old method of searching for coincident reactions of two separated gravitational antennae it was proposed to seek perturbations of the gravitational detector noise background correlated with astrophysical events such as neutrino and gamma ray bursts which can be relaibly registered by correspondent sensors. The problem of optimal algorithms for this approach is discussed. The importance of the question is demonstrated in reanalysis of the old data concerning the phenomenon of neutrino-gravity correlation registered during of SN1987A explosion.

Key words: Gravitational waves

A conventional scheme of the gravitational wave experiment on searching for stochastic bursts of gravitational radiation from astrophysical sources supposes a registration of coincident reactions of two or more spatially separated gravitational detectors. It was considered as only way to establish a global nature of the detected signal which probably could be a metric perturbation associated with gravitational wave if the detector's isolation was good enough (Weber, 1960). A realization of this scheme requires at least two identical gravitational antennae located in different points of the globe with good synchronized clocks, good communication etc. Although this ideology is known already thirty years the coincident experiment in automatic regime was performed only by J.Weber during his first observation with room temperature bar detectors located in Chicago and Maryland (Weber, 1969, 1970). Later the "coincidence searching" episodically have been done by several groups as a rule in the form of joint data analysis of the electronic records of both setups *a posteriori* but not on line. The recent example of such procedure with cryogenic antennae EXPLORER and ALLEGRO is presented in the paper (Astone et.al., 1994). A reason why the detection of coincidences "on line" was replaced with analysis *a posteriori* is obvious. The "on line" regime (although it's very convenient and effective) requires an additional electro- communication equipment. Besides it could be easy realized if the same research group would have two equivalent detectors in disposal (like it was in "time of room temperature bar detectors") but a complication and large cost of modern cryogenic and interferometrical set up makes it difficult in general. In nearest future the automatic selection of coincidences probably will be realized with two large scale interferometric antennae which are under construction now in the LIGO project (Abramovici et.al., 1992). At present however the coincidence analysis *a posteriori* is considered as the only way of investigation stipulated by a presence of two gravitational antennue in simultaneous operation with equivalent sensitivity.

In last years another type of gravitational wave experiment was discussed. The idea is to search weak perturbations of the gravitational detector's noise background correlated with some astrophysical events such as neutrino and gamma ray bursts (Bemporad, 1995; Michelson, 1995; Modestino & Pizzella; Gusev et.al., 1998). The reason of this approach lies in the understanding that last stages of star evolution (such as supernova explosion, binary coalescence, collapse etc.) traditionally considered as the gravitational burst sources have to be accompanied also by neutrino and very likely gamma radiation. It means in general that a detection of neutrino or gamma ray bursts by appropriate sensors defines time marks around which one might hope to find also exitations of the gravitational detectors. An advatage of this method consists first of all in a remarkable reduction of the observational time interval and second in a potential opportunity to accumulate weak signals. The last point is especially interesting taking into account a deficit of required sensitivity of the gravitational detectors available at present in the world laboratories.

The theoretical presentation of the neutrino bursts produced by collapsing stars at the end of stellar evolution is well known, see for example (Nadezhin & Otrochenko, 1980; Browers & Wilson, 1982; Bethe, 1982). According to the theory a total energy released in the form of neutrino radiation of all flavors has the order of value $0.1 M_{\odot} c^2$ and a time scale of several seconds (2-20 s) This radiation can be detected (mainly due to

the inverse β-decay reaction) if a source is located not too far from the Earth $(10 \div 100)kpc$. Correspondent experimental programms ("Supernova Watcher") are accepted and carried out by the all neutrino groups having appropriate liquid scintillation detectors (Aglietta et.al.1986; Alexeyev, 1988) or water cherenkov detectors (Bienta et.al, 1983; Hirata et.al., 1988). Moreover the first registration of neutrino flux from supernova as it believes was fixed during of SN1987A explosion (Aglietta et.al.1987; Hirata et.al., 1987; Bionta et.al.1987; Alexeyev et.al.1989). All this programms are orientated on the search of collapsing stars in the Galaxy and close local groups i.e. expected average rate of events is 3 per 100 years (Aglietta et.al., 1987). It is unlikely to wait a large increasing of penetrating power from the neutrino telescopes in nearest future. So Super Kamiokande detector with effective mass in ten times larger allows a detection of 150 neutrino events per year from LMC but only one event from Andromeda (Takita, 1993). It is unrealistic to relay on a detection neutrino from supernova in the Virgo Claster $(15 - 20Mpc)$ which considered as one of the principal sources of a signal for gravitational detectors. Thus a search of correlations between noise backgrounds of neutrino and gravitational wave detectors is limited by the condition of very low event rate $(3 - 10)10^{-2}y^{-1}$ and an opportunity of "signal-noise enhancing" through some integrating procedure practically is absent. Although an expected amplitude of a solitary gravitaional pulse signal might be relatively large up to 10^{-18} in term of metric perturbation from a source in the center of Galaxy.

The other astrophysical phenomenon of our interest, gamma-ray bursts, looks more propitious although it still remains to be confused (Fishman 1993). The main attractive feature of this phenomenon is a relatively high event rate, on average one per day. The large energy emission evaluated for some registered gamma bursts up to the $0,1M_{\odot}c^2$ together with amplitude short time variations on order of $0,1s$ implies to relativistic stars as burst sources. In process of study of this phenomenon two principal scenarios have been considered in respect of the gamma-ray bursts nature. The first one suggests its galactic origin associated with high velocity pulsars distributed not only in the galactic disc but also in the Halo (Belli, 1997). The second scenario appeals to a cosmological picture in which gamma bursts are produced during catastrophic processes with relativistic stars such as collapses, binary coalescences, supernova explosions in distant galaxies (Wijers, 1998). Thus the both scenarios deal with objects that have been considered also as sources of gravitational radiation. Galactic pulsars could produce only very weak GW-bursts as a result of "starquakes" with equivalent metric perturbation on the Earth of order of $10^{-23} \div 10^{-24}$ (Thorn, 1995) for a source in center of Galaxy. However authors of the papers (Bisnovatyi-Kogan, 1995; Komberg & Kompaneets, 1997) believe that even a more close pulsar population in vicinity $100pc$. might provide an observable rate of gamma events ~ 5 per month through mechanizm of "starquake". Then a correspondent GW burst amplitude would be awaited on the level of $10^{-21} \div 10^{-22}$. In the cosmological picture, if one includes into consideration binaries with back hole components the astrophysical forecast gives the GW-burst event rate up to 30 per year at a metric amplitude level of 10^{-21} in the solar vicinity of 50-100 Mpc (Lipunov et.al. 1995; Lipunov et.al, 1997). This estimation was found supposing that only 10^{-4} part of stellar rest mass energy could be converted into gravitational radiation. A more optimistic value of the convertion coefficient 10^{-2} used in the other papers (Sazhin et.al. 1996; Imshennik, 1992) would increase the expected metric amplitude up to 10^{-20}. The recent results obtained with BeppoSAX satellite and Keck II telescope permitted to confront the gamma-ray burst GRB971214 with a galaxy having the redshift of $z = 3.4$. The other case is the burst GRB970508 with an optical counterpart at $z \geq 0.835$ (Kulkarni et.al., 1998). That is the strong evidence of the cosmological nature at least for a part of the registered bursts. Along with these very far sources (1-10) Gpc. more close events were registered. For example the burst GRB980425 probably was associated with an optical object type of supernova explosion at the distance 40 Mpc. $(z = 0,08)$ (Galama et. al., 1998). It is not completely clear how the gamma radiation could penetrate through envelope of supernova, how the black hole coalescence could release the gamma burst, but the energetic of observable events definitely requires scenarios with a crash of relativistic stars and therefore an expectation of the gravitational radiation accompaniment seems reasonable. Moreover the energetic estimation of the GRB971214 burst $\sim 2 \cdot 10^{53}erg$ even exceeds a conventional theoretical electromagnetic energy release $10^{51}erg$ for supernova or neutron star binary merging (Ramprakas, 1998). It makes the models of black hole binary mergers or rapidly rotating massive black hole with accretion, so called "hypernova" (Pachinski, 1998), more attractive and at the same time they are more promissing in respect of the gavitational wave output.

Thus there are serious theoretical prerequisites to search for gravitational bursts around time marks defined by correspondent events of neutrino and gamma-ray detectors. Now lists of desirable events can be provided by the four world neutrino telescops and cosmic CGRO (BATSE) and BepoSAX satellites. In this situation the key question is a sensitivity of the gravitational detectors which are in operation at present. In fact this is only supercryogenic resonance detector "NAUTILUS" (INFN, Frascati) and similary set up "AURIGA" (INFN, Legnaro) could achieve the sensitivity level 10^{-21} for short bursts $\sim 10^{-3}sec$ (Astone

et.al., 1997). The two cryogenic detectors mentioned above "ALLEGRO" and "EXPLORER" have the short burst sensitivity $6 \cdot 10^{-19}$ i.e. of 2, 5 orders less the desirable value. However it worth to note here that for more long signals the estimation of its sensitivity must be increased up to 10^{-21} for burst duration close to $1sec$ due to accumulation of signal cycles (see detailes in Gusev et.al. 1997).

Generally an improvement of detection sensitivity depends on our knowledge of the signal structure, arrival time etc. In this sense a theory does not provide us a large assortiment of models for gravitational signal. Mostly its energetic part might be presented by a short pulse with several cycles of carrier frequency $(10^2 - 10^3)$ Hz (Thorn, 1995). There is a deficit of models with joint description of the gravitational, neutrino, and gamma radiation output. Some examples one can find in the papers (Thorn, 1995; Sazhin et.al. , 1996; Imshennik, 1992; Zakharov, 1996) where multistage scenarios of gravitational collapse were considered in the processes of neutron star formation and star remnants coalescence. In such approach a packet of the neutrino pulses separated by time intervals from few seconds up to several days accompanied by gravitational bursts was predicted with a total energy release up to one percent of the rest mass. The multi-stage scenario is also typical for collapse of massive star with large initial angular momentum (Thorn, 1995). A radial matter compression there might be interrupted by repulsing bounces, fragmentation, fragments mergers or ejection of one of them etc. In principle each of these stage could produce gravitational, electromagnetic and neutrino bursts but a detaile description of such models has not yet been developed. Entirely inspite of obvious uncertainty of joint scenarios and unknown event rate of complex collapses in the Universe an expectation of the multi-pulse structure for a gravitational signal associated with a packet of neutrino and gamma ray bursts is enough grounded at present.

The argumentation above stimulates one to define an optimal data processing of the gravitational detector output in parallel with a record of astrophysical events registered by neutrino or gamma ray observatories. A simple comparison with an attempt to find coincidences is insufficient due to an inevitable unknown time delay between events of different nature but mainly due to a deficit of gravitational and neutrino detector sensitivity. Partly for this reason the attepmts of searching for correlation between neutrino-gamma data (Aglietta et.al., 1995) and gamma-gravity data (Astone et.al., 1999) were not successful. It has to be done according to the optimal filtration theory taking into account all available information concerning of noise background and conceivable model of signal (Helstrom, 1968).

Thus the one actual problem of GW-experiment is to formulate some optimal algorithm of searching for a correlation of neutrino as well as gamma-ray events with stochastic background of gravitational detectors. The example of solution this problem was given by the RTM-collaboration when this group reported about the "neutrino-gravity correlation effect" registered by two room temperature bar detectors in Roma and Maryland and Torino neutrino scintillator under Mont Blanc (Amaldi et.al., 1987; Aglietta et.al., 1989, 1991).

The RTM-algorithm consisted in composing the following variable

$$Z = \sum_{k=1}^{n} (1/2)(R^2(t_k + \tau)/\sigma^2) \qquad (1)$$

which was the sum of quadratic values of the overlope of output antenna process (in fact the detector energy variations) taken in times of astrophysical events i.e. registered neutrino time marks t_k, with some small shift τ ; the sum was accumulated on the interval of observation which *aposteriori* contained n events. (A physical sense of this variable becames clear after normalization (1) on the total number of the events: then it is a "selected mean value" of the detector energy variations corresponded to the astrophysical events.) Thus the RTM group having deal with Z-variable (1) have found under a special shift $\tau = 1.2sec$ the relatively large experimental value $Z/n = 72.3K$ fixed in the night Feb 22-23 when SN1987A was exploded. To estimate a chance probability this value was compared with an empirical statistics extracted from the gravitational data according to simulated neutrino piossonian time marks. This procedure resulted in the extremely small chance probability for the registered Z-value on order of 10^{-6}. It was interpreted as a fixation of the remarkable (νg)-correlation produced by SN1987A.

However later in our paper (Rudenko et.al., 1999) it was shown that a formal application of the Maximum Likelihood Principal to the problem leaded to some correction of the optimal variable. It was recommended to find an absolute maximum of Z through variation of the shift τ , i.e. to get over a new so called "absolute maximum -variable"

$$Z_{max} = max_{\tau} Z(\tau), \quad \tau \in [\tau_{min}, \tau_{max}] \qquad (2)$$

A value of τ_{opt} which provides a maximum of $Z(\tau)$ should be taken as MLP-evaluation of the real time shift between astrophysical event and gravitational signal (in our simple approach the shift is supposed to be the same for all events, - a hypothesis of "homogenity of events"). It was remarked in [44] that there was no a definition of the τ-interval limits inside of the statistical model; it has to be choosed on a base of additional physical arguments, astrophysical scenarios etc.

In our reanalysis of the RTM data we confirmed the same experimental value of Z variable (72.3 K). However according to the developed MLP-algorithm the estimation of the chance probability now had to be done on the base of Z_{max} statistics (2) instead of Z.

Such method takes into account an increase the chance probability due to selection of the "optimal time shift" between gravitation and astrophysical (neutrino) data. As we found a new estimation of the chance probability was reduced to the value 10^{-3} which was also not too large. Unfortunately a reliabilty of this estimation occasionally was suffered from the fact that sampling times of gravitational (1 sec) and neutrino (0.01 sec) data were different and neccessity of some interpolation procedure introduced an additional uncertainty resulted in the value 10^{-2} for the chance probability. Thus our MLP-algorithm have shown that the available experimental data of RTM group were insufficient to make a robust conclusion in favour of (νg)-correlation effect.

The example with SN1987A gave enough presentation how the MPL-algorithm could work exhibiting clearly at the same time its weak point: a dependence on the unknown range of time shift between astrophysical and "gravitational" events. An *apriori* estimation of it on physical arguments is desirable to provide an efficiency of the algorithm. Any attepmts to limit this range appealing to specific of the experimental data or particular manner of opreator behaviour under searching for the "signal exitation Z_{exp}" do not lead to "objective boundaries" for time shift variations and thus a correspondent evaluation of the chance probability remains to be suspended. Only an apriori knowledge of the time shift range could introduce some certainty (deterministic elements) in this ill posed problem. In the extremely favourable case when the value of shift is known exactly the estimation of chance probability can be taken just from Z-distribution which is much more robust then Z_{max}-distribution.

In the case of gamma ray bursts the problem of "optimal algorithm" probably will be more difficult due a complex structure of gamma pulses, uncertaties in its time position, duration , unhomogenious form etc. and unclear nature of this phenomenon itself. Nevertheless as a final remark we should like to emphasize that the modern approach to gravitational wave experiment discussed in this talk stimulates a research activity in two directions: the first is a development of more detailed joint scenarios for neutrino-gamma-gravity radiation sources, the second is an elaboration of more robust filtering data processing procedures which could be free from subjective elements in estimation of statistical errors.

References

Abramovici A. et.al.: 1992, *Science*, **256**, 281.

Aglietta M. et.al.: 1986, *Nuovo Cimento*, **9C**, N2, 185.

Aglietta M. et.al.: 1987, *Europhys .Lett.*, **3**, 1315.

Aglietta M. et.al.: 1989, *Nuovo Cimento*, **12C**, N1, 75.

Aglietta M. et.al.: 1995, *24-ICPC*, **2**, 73, Roma, Italy.

Aglietta M. et.al.: 1991, *Nuovo Cimento*, **14C**, N2, 171.

Alexeyev E. et.al: 1988, *Phys. Lett.*, **B205**, 209.

Alexeyev E. et.al. 1989, *Pis'ma v JETPh***49**, 480.

Astone P. et.al. 1994, in *Gen. Rel. Grav. Phys.*, 551, W.Sci.

Astone P. et.al. 1997, *Astroparticle Physics*, **7**, 231.

Astone P. et.al. 1999, *Astron. Astrophys.*, **352**, 612.

Belli B.M.: 1997, *Ap. J.*, **479**, L31.

Bemporad C.: 1995, in *Proc. First E. Amaldi Conf.*, 18, W.Sci.

Bethe H.: 1985, in: *Proc. SIF, Course XCI*, **181**, North Holland, Amsterdam.

Bionta R.M.: et.al.: 1983, *Phys. Rev. Lett*, **51**, 27.

Bionta R.M.: et.al.: 1987, *Phys. Rev. Lett*, **58**, 1494.

Bisnovatyi-Kogan G.S.: 1995, *Ap. J. S. S.*, **97**, 185.

Bowers R., Wilson J.R.: 1982, *Ap. J.*, **263**, 366.

Fishman G.J., Meegan C.A.: 1993, *Ann. Rev. Astron. Astrophys.*, **33**, 415.

Galama T.J. et.al.: 1998, *Nature*, **395**, 670.

Gusev A.V.et.al.: 1997, *Astronomy Reports*, **41**, N2, 245.

Gusev A.V.et.al.: 1998, in *Proc. Second E. Amaldi Conf.*, 512, W.Sci.

Helstrom C.W.: 1968, in *Statistical Theory of Signal Detection*, Perg. Press, NY.

Hirata K.S. et.al.: 1987, *Phys. Rev. Lett.*, **58**, 1490.

Hirata K.S. et.al.: 1988, *Phys. Rev.*, **D38**, 448.

Imshennik V.S.: 1992, *Pisma v Astr. Zhurn.*, **18**, 489.

Komberg B.V., Kompaneets D.A.: 1997, *Astronomy Reports*, **41**, N5, 611.

Kulkarni S.R. et.al.: 1998, *Nature*, **393**, 35.

Lipunov V.M. et.al.: 1995, *A& A*, **298**, 677.

Lipunov V.M., Postnov K.A., Prokhorov M.E.:1997, *New Astronomy*, **2**, 43.

Michelson P.: 1995, in *Proc. First E. Amaldi Conf.*, 37, W.Sci.

Modestino G., Pizzella G.: 1997, *Nota Interna LNF 97/038 IR*, (Italy).

Nadyozhin D.K., Otrochenko I.V.: 1980, *Sov. Asrtron.*, **24**, 47.

Pachinski B. : 1998, *Ap.J.*, **494**, L45.

Ramaprakash A.N. et.al.: 1998, *Nature*, **393**, 43.

Rudenko V.N. et.al: 1999, *atro-ph/9903365*, 24 March.

Sazhin M.V., Ustyugov S.D., Chechetkin V.M.: 1996, *JETP Lett*, **64**, (iss.12), 25.

Takita M.: 1993, in *Frontier of Neutrino Astrophysics*, **5**, 135, Univ.Ac.Press Inc., Tokyo, Japan.

K.S.Thorn : 1995, in *Particles and Nuclear Astrophysics and Cosmology in the next Millenium*, 160, W.Sci.

Weber J.: 1960, *Phys.Rev*, **117**, 306.

Weber J.: 1960, *Phys.Rev.Let.*, **22**, 1320; 1970, **24**, 276.

Wijers R.: 1998, *Nature*, **393**, 13.

Zakharov A.F.: 1996, *Astron. Zhurnal*, 73, N4, 605, (in Russ.).

THE ONLY NON-CONTRADICTORY MODEL OF UNIVERSE

V. Skalský

Faculty of Materials Science and Technology of the Slovak Technical University,
917 24 Trnava, Slovakia, E-mail: skalsky@mtf.stuba.sk

ABSTRACT. The Friedmannian model of the flat expansive non-decelerative isotropic and homogeneous universe with the zero gravitational force state equation is the only model of universe, which does not contradict to the theory of relativity and the quantum mechanics.

Key words: Theoretical cosmology, observational cosmology

1. Introduction

The mathematical-physical basis of the present relativistic cosmology represent *the Friedmann general equations of isotropic and homogeneous universe dynamics* (Friedmann 1922, 1924). Using *the Robertson-Walker general metrics of isotropic and homogeneous universe* (Robertson, 1935, 1936a, 1936b, Walker 1936) they can be written in the form:

$$\dot{a}^2 = \frac{8\pi G\rho a^2}{3} - kc^2 + \frac{\Lambda a^2 c^2}{3}, \qquad (1a)$$

$$2a\ddot{a} + \dot{a}^2 = -\frac{8\pi G p a^2}{c^2} - kc^2 + \Lambda a^2 c^2, \qquad (1b)$$

$$p = K\varepsilon, \qquad (1c)$$

where a is the gauge factor, ρ is the mass density, k is the curvature index, Λ is the cosmological member, p is the pressure, K is the state equation constant and ε is the energy density.

The Friedmannian equations (1a), (1b) and (1c) – without introducing of any restrictive supplementary assumptions – describe infinite number of *the Friedmannian models of universe*.

Individual Friedmannian models of universe are determined by the Friedmannian equations (1a), (1b) and (1c) with the values: $k = +1,\ 0,\ -1$; $\Lambda > 0, = 0, < 0$; and $K > 0, = 0, < 0$.

The Friedmannian equations (1a), (1b) and (1c) represents an application of *the Einstein equations of gravitational field* (Einstein 1915) to the whole isotropic relativistic universe in a Newtonian approximation, under the hypothetical supplementary assumptions, introduced into the relativistic cosmology by Einstein (Einstein 1917), de Sitter (de Sitter 1917) and Friedmann (Friedmann 1922, 1924) and generalised by Friedmann (Friedmann 1922, 1924).

The Friedmannian equation (1a), (1b) and (1c) contain the supplementary assumptions in the mathematically generalised form, therefore, they contains and its factually negation, too. It means that they described the Friedmannian models of universe which are solution of the Einstein equations of gravitation field in the Newtonian approximation with the hypothetical supplementary assumptions and without they, too (i.e. with all possible combinations its non-zero and zero values). Therefore, under assumption that the mathematical-physical description of our observed *expansive and isotropic relativistic Universe* not require an introduction of any next supplementary assumptions, the Friedmannian equations (1a), (1b) and (1c) must immanently contained and the Friedmannian model of universe, which described our observed Universe, too (Skalský 1997).

2. The model properties of the expansive and isotropic relativistic Universe

In the observed expansive and isotropic relativistic Universe the gravitation and expansion of matter objects cause the relativistic effects, which for the observers in any co-ordinate systems have different values and in the largest distances, in which the velocity of its expansion approximates to the boundary velocity of signal propagation, they gain extremely values, which approximate to the limit (i.e. zero and infinite) values. Therefore, **the global parameters of the observed expansive and isotropic relativistic Universe (with non-limit values) principally cannot be possibly expressed relativistically!** We can express them only in the non-relativistic approximation, i.e. only using such a theory of gravity in which we abstract from observed relativistic effects.

There exists only one theory of gravitation:

- *The Einstein general theory of relativity,*

  which exactly describes the macro-physical reality, and has only one special partial solution in which we abstract from all relativistic effects:

- *The Newton theory of gravitation (the classical*

mechanics).

The general theory of relativity is the macro-physical (relativistic) theory of (inertial and non-inertial) co-ordinate systems, which describes the relativistic properties of the physical objects from point of view of any co-ordinate systems; the global relativistic point of view does not exist. Therefore, from point of the general theory of relativity the concepts *whole of universe* and *whole parameters of universe* have not a concrete physical sense!

From point of view of the general theory of relativity about 'the whole of Universe' and about 'the whole parameters of Universe' we can consider only limitly. However, the limit relativistic parameters of the expansive and isotropic relativistic Universe have non-physical (i.e. zero and infinite) values.

We cannot describe the whole of the expansive and isotropic relativistic Universe and its global parameters in a relativistic non-limit way just because the general theory of relativity precisely describes the macro-physical (relativistic) reality.

What it is not possible in the general theory of relativity (because it precisely describes all parts of relativistic reality), becomes trivial in the Newton theory of gravitation. It is because in the Newton theory of gravitation we abstract just from the relativistic effects which in the general theory of relativity such a non-limit description make impossible. Therefore, we can state:

1. The global parameters of expansive and isotropic relativistic Universe with finite (non-limit) values of the physical quantities can be expressed only in the Newtonian approximation.

The whole parameters of the expansive and isotropic relativistic Universe in the Newtonian approximation (projection) are equivalent to the parameters of the Newtonian-Euclidean expansive homogeneous matter sphere.

This fact has a significant influence on the model properties of observed expansive and isotropic relativistic Universe, because **the Euclidicity of space in the Newton theory of gravitation principally excludes any consideration on curvature of space in the Newtonian approximation of the expansive and isotropic relativistic Universe!**

The shown facts have these results:

2a. The expansive and isotropic relativistic Universe in the Newtonian model projection (approximation) is flat (Euclidean), irrespective of actual relativistic matter-space-time properties it has.

2b. From the fact 2a reciprocally results that the actual observed expansive and isotropic relativistic Universe principally is not, and cannot be, flat.

The fact that the global parameters of the expansive and isotropic relativistic Universe can be non-limitly expressed only in the Newtonian model projection, however, it does not mean that the Universe is Newtonian. The observed Universe is relativistic, it means that the Universe in the Newtonian model approximation must consider these relativistic facts:

As a consequence of the finite velocity of signal propagation we can optically observe the Universe up to the beginning of matter era, when – as a result of *"the recombination" of hydrogen atoms* – the matter and the radiation were separated and the Universe became transparent for the photons. Using *the neutrino observing technology* we could see even further, and using *the hypothetical graviton observing technology* we could see up to the cosmological time $t \sim 10^{-43}$ s. Theoretically (using the retrospective extrapolation), we can "reach" even into the beginning of Universe expansive evolution, i.e. up to *the initial limit cosmological singularity.* This means that we are contemporaries of the expansive evolution of Universe at any physically real cosmological times t and theoretically (in the mathematical-physical sense) we are also contemporaries of the initial limit cosmological singularity.

According to Einstein (Einstein 1921), in the finite area no choice of co-ordinates can exclude the gravitational field, however, infinitely small area of space can be considered as flat, in which the laws of the special theory of relativity are valid. Therefore, the theoretical initial limit cosmological singularity with zero dimensions – from the point of view of the general theory of relativity – behaves in two ways:

- As a gravitational object with the limit matter-space-time values in which the motion stopped.
- As an inertial system with the limit matter-space-time values, which expands towards all observers at the boundary velocity of signal propagation.

These facts in the Newtonian model approximation are considered only by the model of Newtonian-Euclidean homogeneous matter sphere, expanding at the constant velocity $v = c$. It means:

3. The expansive and isotropic relativistic Universe in the Newtonian model approximation is non-decelerative and during the whole expansive evolution it expands at the constant boundary velocity of signal propagation c.

Therefore, for the gauge factor of universe a, i.e. for the radius of Euclidean homogeneous matter sphere r and the cosmological time t in the Newtonian model

approximation of the expansive and isotropic relativistic Universe are valid the relations (Skalský 1989):

$$a = r = ct. \tag{2}$$

According to the general theory of relativity, *the gravitational forces* are determined by the sum of the energy density ε and three-multiple of the pressure p.

4. In the Newtonian model approximation of the expansive and isotropic relativistic Universe (represented by the Newtonian-Euclidean homogeneous matter sphere, expanding at the boundary velocity of signal propagation c), the gravitation is not manifested because it is precisely compensated by the expansion.

Therefore, for the sum of the energy density ε and three-multiple of the pressure p in the Newtonian model approximation of the expansive and isotropic relativistic Universe is valid the relation (Skalský 1991):

$$\varepsilon + 3p = 0. \tag{3}$$

The Friedmannian models of the flat expansive universe are determined by the equations (1a), (1b) and (1c) with $k = 0$, $\Lambda = 0$ and $K > 0, = 0, < 0$. These models *de facto* represent the Newtonian-Euclidean expanding homogeneous matter sphere with the radius $r = a$ with the critical mass density ρ.

The Newtonian-Euclidean homogeneous matter sphere expanding at the velocity $v = c$ has the radius

$$r = r_g = \frac{2Gm}{c^2}, \tag{4}$$

where r_g is the Schvarzschild gravitational radius and m is the mass.

From the infinite number of the Friedmannian models of the flat universe – determined by the equations (1a), (1b) and (1c) with $k = 0$, $\Lambda = 0$ and $K > 0$, $= 0$, < 0 – only one model can fulfil *the relativistic restrictive assumptions*, expressed by the relations (2), (3) and (4).

The general theory of relativity and *the quantum mechanics* are the complementary theories. The macrophysical relativistic universe is in finite result represented by the micro-physical quantum-mechanical objects (by the particles and the fields) and on the contrary, the quantum-mechanical objects can really exist only in the relativistic macro-world (universe).

It means that the Friedmannian model of universe with assumptions, which result from the general theory of relativity, simultaneously must also fulfil the assumptions, which result from the quantum mechanics (*the quantum theory*).

According to *the Planck quantum hypothesis*, it has a sense to think about the physical parameters of the observed expansive Universe from the moment when its dimensions reach the values, which correspond to the Planck length $l_P = (hG/c^3)^{1/2} = ct_P$, i.e. at the *Planck time* $t_P = (hG/c^5)^{1/2} = l_P/c$ (Planck (1899)).

At present time *the Planck units* are shown with *the Planck (reduced) constant* $= h/2\pi$:
the Planck length

$$l_P = \sqrt{\frac{G}{c^3}} = ct_P = 1.616\,05(10) \times 10^{-35}\,\mathrm{m}, \tag{5}$$

the Planck time

$$t_P = \sqrt{\frac{G}{c^5}} = \frac{l_P}{c} = 5.390\,56(34) \times 10^{-44}\,\mathrm{s}. \tag{6}$$

From definitions of the Planck length (5) and the Planck time (6) it results unambiguously that – according to the Planck quantum theory – the expansive universe could begin its expansive evolution at only one possible velocity $v = c$ and at the cosmological time $t = t_P$ (6) for the gauge factor $a = l_P$ (5) the relations (2) were valid in it. It means that:

From infinity numbers of Friedmannian models of flat universe – determined by the equations (1a), (1b) and (1c) with $k = 0$, $\Lambda = 0$ and $K > 0, = 0, < 0$ – only one model (i.e. only with one from the values of the state equation constant K) can fulfil *the relativistic and quantum-mechanical restrictive assumptions*, expressed by the relations (2) (Skalský 1999).

3. The Friedmannian model of the expansive and isotropic relativistic universe

The retrospective extrapolation of the evolution of expansive and isotropic relativistic universe leads to the theoretical initial limit cosmological singularity, therefore, in the Newtonian model approximation of the universe could begin its expansive evolution only at one possible velocity: *the boundary velocity of signal propagation c.*

According to the special theory of relativity, with the boundary velocity of signal propagation c the time-flow will stop, therefore, the expansive and isotropic relativistic universe, which started its expansive evolution at the boundary (limit) velocity (at which the time was stopped), in the Newtonian model approximation (at which the time flow equally with an arbitrary velocity) it must during the whole expansive evolution expand at the constant velocity $v = c$ (Skalský 1989).

In the Newtonian model projection of the expansive and isotropic relativistic universe (i.e. in the Newtonian-Euclidean homogeneous matter sphere, expanding at the constant velocity $v = c$), all parameters are mutually linearly bound, therefore, **the relation between its two arbitrary model parameters can be used as a restrictive assumption for**

the unambiguously determination of the Friedmannian model universe, which describes our Universe.

The Friedmannian equations (1a), (1b) and (1c) with $k = 0$ and $\Lambda = 0$ fulfil the relativistic and quantum-mechanical restrictive assumption of the relations (2) (and the relativistic and the quantum-mechanical restrictive assumptions of the relations (3), (4), (5) and (6), too) only with the value of the state equation constant $K = -1/3$, i.e. only with *the zero gravitational force state equation* (Skalský 1991):

$$p = -\frac{1}{3}\varepsilon. \tag{7}$$

Using the Friedmannian equations (1a) and (1b) with $k = 0$ and $\Lambda = 0$, the state equation (7), the Newtonian relations for the Euclidean homogeneous matter sphere and the Hubble relation (Hubble 1929) we can determine the relation between next parameters of the expansive and isotropic relativistic universe, in the Newtonian approximation, i.e. between other parameters of the Friedmannian model of *the* (flat) *expansive non-decelerative* (isotropic and homogeneous) *universe* (ENU) (Skalský 1991, 1993, 1994):

$$a = ct = \frac{c}{H} = \frac{2Gm}{c^2} = \sqrt{\frac{3c^2}{8\pi G\rho}}, \tag{8}$$

where H is the Hubble coefficient ("constant").

The space-time properties of the ENU you can see in the paper: V. Skalský: "The space-time properties of the Universe" in this publication.

4. Conclusions

The Friedmannian model of the ENU, determined by the Friedmannian equations (1a), (1b) and (1c) with $k = 0$, $\Lambda = 0$ and $K = -1/3$, is the only model of universe, which does not contradict to: 1. the Einstein general theory of relativity (and its special partial solutions: the Einstein special theory of relativity and the Newton theory of gravity), and 2. the quantum mechanics (Skalský 1999).

References

De Sitter, W.: 1917, *Proc. Acad. Wetensch. Amsterdam*, **19**, 1217.
Einstein, A.: 1915, *Sitzber. Preuss. Akad. Wiss.* **48**, 844.
Einstein, A.: 1917, *Sitzber. Preuss. Akad. Wiss.* **1**, 142.
Einstein, A.: 1921, *The meaning of relativity*, Princeton, New York.
Friedmann, A.: 1922, *Z. Phys.* **10**, 377.
Friedmann, A.: 1924, *Z. Phys.* **21**, 326.
Hubble, E.: 1929, *Proc. U.S. Nat. Acad. Sci.* **15**, 168.
Planck, M.: 1899, *Sitzber. Preuss. Akad. Wiss.* **26**, 440.
Robertson, H. P.: 1935, *Astrophys. J.* I, **82**, 284.
Robertson, H. P.: 1936a, *Astrophys. J.* II, **83**, 187.
Robertson, H. P.: 1936b, *Astrophys. J.* III, **83**, 257.
Skalský, V.: 1989, *Astrophys. Space Sci.* **158**, 145.
Skalský, V.: 1991, *Astrophys. Space Sci.* **176**, 313. (Corrigendum: 1992, **187**, 163.)
Skalský, V.: 1993, *Astrophys. Space Sci.* **201**, 3. (Corrigendum: 1994, **219**, 303.)
Skalský, V.: 1994, *Astrophys. Space Sci.* **219**, 275.
Skalský, V.: 1997, *DYNAMICS OF THE UNIVERSE in the Consistent and Distinguished Relativistic, Classically-Mechanical and Quantum-Mechanical Analyses*, STU, Bratislava.
Skalský, V.: 1999, http://www.cosmology.sk
Walker, A. G.: 1936, *Proc. Lond. Math. Soc.* **42**, 90.

GLOBULAR CLUSTERS AS GRAVITATIONAL LENSES. OBSERVATIONAL TEST

A.V. Yushchenko

Astronomical observatory of Odessa State University
T.G.Shevchenko Park, Odessa 270014 Ukraine,
yua@lens.tenet.odessa.ua

ABSTRACT. Let us suppose that globular clusters in the halos of distant galaxies can act as a gravitational lenses. The observational test for this hypothesis is the overdensity of star-like images near foreground galaxies. We analyzed USNO A2.0 catalog in the vicinity of 35862 galaxies with redshifts 0.01-0.33 and found that mean overdensity of objects brighter than 21^m is near 100 objects per galaxy.

Key words: quasi-stellar objects; galaxies: redshifts - gravitational lensing

1. Introduction

The first who proposed gravitational lensing for explanation of quasars was Barnotti (1965). But it was shown that neither galaxies, nor stars in the halos of galaxies cannot explain all properties of Arp's objects. Burbidge et al. (1990) found near 500 associations of quasars with foreground galaxies.

In a series of papers - Baryshev, Raikov, Yushchenko (1993), Baryshev & Ezova (1997), Yushchenko, Baryshev, Raikov (1998) - it was shown that quasar-galaxy associations can be explained by gravitational lensing by cores of globular clusters and dwarf galaxies. These globular clusters in the halos of foreground galaxies and dwarf galaxies can explain all associations. The properties of globular clusters as gravitational lenses were investigated by Yakovlev et al. (1983). In the above mentioned papers we extend the Yakovlev's results for sources with non-zero sizes. It was shown that amplification of small background sources by cores of globular clusters can reach 5-10 magnitudes. The angular sizes of amplified image is equal to the angular size of the core of globular cluster in the halo of foreground galaxy - this is star-like image for our optical telescopes.

Yushchenko & Raikov (1998) proposed, that significant part or all quasi-stellar objects can be explained by this effect. This hypothesis can work if the cores of globular clusters are transparent. The necessary condition are also the existence of distant Seyfert nuclei with spectral properties similar to that of quasars. Typically only one globular cluster per foreground galaxy can act as a gravitational lens - the number of background Seyfert nuclei is too small.

2. Hypothesis

Let us suppose that there are not only Seyfert nuclei at high redshifts, but galaxies of all types. It is known that the number of Seyfert galaxies is of order of 1% of all galaxies. If all types of galaxies will be gravitationally amplified by cores of globular clusters and dwarf galaxies by 5-10 magnitudes we can expect the excess of number density of star-like images near foreground galaxies. We know that the usual number of globular clusters per galaxy is near 10^2 or more.

That is why the expected number density of high redshift galaxies, gravitationally amplificated by globular clusters, must be two orders higher than the number density of quasi-stellar objects. The last catalogs of quasars contain near 10^4 objects. We can expect near 10^6 high redshifts star-like objects situated near foreground galaxies. The expected spectral properties of these objects will be similar to spectral properties of usual galaxies (with correction for redshift and evolution). In any case their colors will be more redder than quasars.

2. Observed number densities

For checking the validity of this hypothesis we used digitized Palomar survey with extension to south sky - USNO A2.0 catalog (Monet et al., 1998) - as a catalog of star-like images. This catalog contain more than 500 millions of objects brighter than 21^m. We used CfA catalog (Huchra et al, 1995) as a catalog of foreground galaxies. We selected 35862 galaxies with redshifts more than 3000 km/s from CfA catalog. We calculated the number density of all objects in the concentric rings around each galaxy up to 1.5 degree in diameter. The similar calculations were made for four

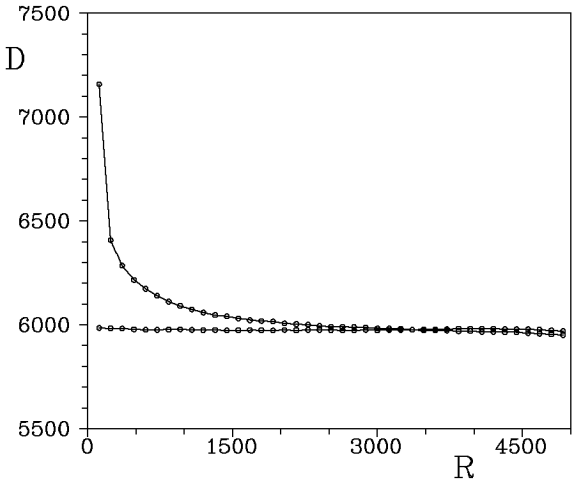

Figure 1: The mean density of objects in concentric rings around 35862 galaxies (the upper line), and around random centers. The axes are the radii of concentric rings in arc seconds and mean density of objects per square degree.

random centers around each galaxy.

The mean results are shown on fig. 1. We can see a well detected over-density of objects around galaxies in comparing with random centers. The overdensity is near 100 objects per galaxy. It should be noted that the mean density of objects in the investigated regions is near 6000 objects per square degree. 100 objects is near 1.5% over-density. Only mean results for 35862 galaxies permit us to claim that this overdensity exist. This means that near 35862∗100 or more than 3 millions objects in USNO A2.0 are star-like images of distant galaxies amplified by cores of globular clusters or dwarf galaxies by 5-10 magnitude.

The statistics is sufficient and we were able to plot the overdensity as a function of galaxies types and redshifts, the plots of the numbers of lensed images as a functions of their magnitudes and colors. The overdensity is insignificant for objects brighter than 15^m, and became more pronounced for fainter objects. The maximum of the distribution of B-R colors of discovered objects is located near B-R=1.5-2. These data confirm our hypothesis.

2. Conclusion

We predicted and found the overdensity of star-like images around galaxies. These star-like images are the images of high redshift galaxies, amplificated by cores of globular clusters (or dwarf galaxies).

The overdensity of objects near galaxies is an observational fact and it is necessary to investigate this problem. Part of this overdensity can be explained by usual images of galaxies - USNO A2.0 catalog do not resolve stellar and galaxy images.

It should be noted that there were surveys for detecting galaxies about quasars, for detecting quasars, but there were no surveys for detecting star-like images (with spectral properties different than spectral properties of quasars) around galaxies.

References

Barnotti J.M.: 1965, *Astron. J.,* **70**, 666

Baryshev Yu.V., Raikov A.A., Yushchenko A.V.: 1993, Proc. of 31 Liege Astrophys. Coll. *Gravitational lenses in the Universe,* P. 307.

Baryshev Yu.V., Ezova Yu.L.: 1997, *Astronomy reports,* **74,** 497

Burbidge G., Hewitt A., Narlikar J.V., Das Gupta P.: 1990, *Astrophys. J. Suppl. Ser.*, **74,** 675.

Huchra J.P., Geller M.J., Clemens C.M., Tokarz S.P., Michel A.: 1995, *ADS CD ROM*, Vol.**3**.

Monet D., et al.: 1998, USNO A2.0. A catalog of astrometric standards (CD edition).

Yakovlev D.G., Mitrofanof I.G., Levshakov S.A., Varshalovich D.A.: 1983, *Astrophys. and Space Sci.*, **91,** 133.

Yushchenko A.V., Baryshev Yu.V., Raikov A.A.: 1998, *Astron. Astroph. Transactions,* **17,** 9.

Yushchenko A.V., Raikov A.A.: 1998, Proc. of the II conf. *Selected problems of astronomy and astrophysics*, Lviv, Ukraine, p. 185.

THE MASSIVE STELLAR POPULATION IN THE DWARF STARBURST GALAXIES

N.G. Guseva[1]

[1] Main Astronomical Observatory, Ukrainian National Academy of Sciences
Goloseevo, Kiev 03680 Ukraine, *guseva@mao.kiev.ua*

ABSTRACT. The analysis of the long-slit spectral observations of 39 Wolf-Rayet (WR) galaxies with heavy element mass fraction ranging over 2 orders of magnitudes from $Z_\odot/50$ to $2Z_\odot$ are presented. We derive the number of O stars from the luminosity of the Hβ emission line, the number of early carbon Wolf-Rayet stars (WCE) from the luminosity of the red bump (broad CIV λ5808 emission) and the number of late nitrogen Wolf-Rayet stars (WNL) from the luminosity of the blue bump (broad emission near λ4650). We identified some of weak WR emission lines, most often the N III λ4512 and Si III λ4565 lines, which have very rarely or never been seen and discussed before in WR galaxies. A new technique for deriving the number of WNL stars (WN7-WN8) from the N III λ4512 and the number of WN9-WN11 from Si III λ4565 emission lines has been proposed. This technique is potentially more precise than the blue bump method because it does not suffer from contamination of WCE and early WN (WNE) stars and nebular gaseous emission. We find that the fraction of WR stars relative to all massive stars increases with increasing metallicity, in agreement with predictions of evolutionary synthesis models. The relative number ratios N(WC)/N(WN) and the equivalent widths of the blue and red bumps derived from observations are also in satisfactory agreement with theoretical predictions, except for the most metal-deficient WR galaxies. A possible source of disagreement is too low a line emission luminosity adopted for a single WCE star in low-metallicity models.

Key words: Blue compact galaxies: starburst galaxies: Wolf-Rayet stars: Wolf-Rayet galaxies: HII regions: galaxies abundance.

1. Introduction

The dwarf galaxies with starburst activity (so-called blue compact galaxies) have high star formation rate during short episodes. Such burst of star formation results in a large population of hot massive stars. The total number of O stars responsible for the blue continua and strong narrow emission lines in these galaxies can reach 10^2-10^5 (Kunth & Sargent 1983; Vacca & Conti 1992). The most massive stars evolve through the WR phase.

Galaxies with Wolf-Rayet star features in their spectra have long been known, beginning with 1976 (Allen, Wright & Goss, 1976). Individual WR stars cannot be usually observed as single stars in distant galaxies. They have been observed only in our Galaxy and in some members of the Local Group. WR stars in more distant objects are detected indirectly by observing integrated galaxy spectra.

Osterbrock & Cohen (1982) and Conti (1991) introduced the concept of WR galaxies, defining them to be those galaxies which show broad stellar emission lines in their integrated spectra mainly in a broad emission excess in the blue region near λ4650, so called "blue bump".

More than 130 WR galaxies are now known (Conti 1999; Schaerer, Contini & Pindao 1999). We present a uniform, high signal-to-noise sample of WR galaxies, selected from a large sample of a low-metallicity blue compact galaxies. Our main goal is to search for WR (WN and WC) stars in these galaxies, compare the relative number of WR stars to all massive stars with predictions from evolutionary synthesis models and test massive stellar evolution models in a wide range of metallicities.

2. Results of observations and comparison with evolutionary synthesis models

2.1. Observations

We analyze long-slit spectral observations of 39 Wolf-Rayet (WR) galaxies. These spectra were obtained at the Kitt Peak National Observatory (KPNO) 4m and 2.1m telescopes. Recently the WR stars were discovered in 2 galaxies with extremely low metallicity, I Zw 18 ($Z = Z_\odot/50$) (Izotov et al.(1997) and Legrand et al. (1997)) and SBS 0335-052 ($Z = Z_\odot/40$) (Izotov et al. (1999). The spectrum of I Zw 18 was obtained with the Multiple Mirror Telescope (Izotov et al. 1997). The spectrum of SBS 0335-052 was obtained with the Keck

telescope (Izotov et al. 1999a). All observations and data reduction were performed in the same way with the IRAF software package.

While some of these objects are known to contain WR stars from previous studies, the majority are newly discovered WR galaxies.

2.2. Wolf-Rayet stellar population

All spectra in our sample have high signal-to-noise ratio and therefore allow to detect WR features not only in the blue region, but also in the rarely observed C IV λ5808 region, so-called "red bump". The broad WR emission in the blue region of the spectrum at λ4650 (the blue bump), an unresolved blend of N V λ4605, 4620, N III λ4634, 4640, C III λ4650, C IV λ4658 and He II λ4686 emission lines, is present in 37 galaxies and is suspected in 2 more. The red bump mainly produced by the emission of broad C IV λ5808 is detected in 30 galaxies. The WR population in the majority of our galaxies is dominated by late WN and early WC stars. However, a nonnegligible population of early WN stars can be present in the highest-metallicity galaxies in our sample.

We detected also several new lines in the spectra some of our WR galaxies which have rarely or never been seen before in the spectra of WR galaxies. The N III λ4512 and Si III λ4565 lines are most often present and they are tracers of WN7-WN8 and WN9-WN11 stars respectively. These features have been detected in particular in the most metal-deficient blue compact galaxy known, I Zw 18 (Izotov et al. 1997). Those new line identifications constitute one of the most important results of our work. We revealed C III λ5696 in 3 of our galaxies. This emission line is seen mainly in late-type WC stars (WC7-WC9). In some of our galaxy we detected C II λ4267 emission line, which are seen only in the spectra of central stars of planetary nebular and are classified as [WC10]-[WC12] (e.g. Leuenhagen &Hamann, 1994, 1998 and Leuenhagen, Hamann & Jeffery, 1996).

We derive the number of late nitrogen Wolf-Rayet stars (represented by WN7 stars) from the luminosity of the blue bump, the number of early carbon Wolf-Rayet stars (represented by WC4) from the luminosities of the red bump, and the number of O stars from the luminosity of the Hβ emission line.

We also propose a new technique for deriving the numbers of WNL stars (WN7-WN8) from the fluxes of the N III λ4512 emission line and the number of WN9-WN11 from the fluxes of the Si III λ4565 emission line. This technique is potentially more precise than the blue bump method because it does not suffer from contamination of WCE and WNE stars and nebular gaseous emission. All three determinations of WNL stars (blue bump, N III λ4512 and Si III λ4565) well agree. However, a more precise calibration of the N III λ4512 and Si III λ4565 emission lines in WR stars are necessary.

2.2. Comparison with evolutionary synthesis models

The luminosity of the blue bump decreases with decreasing metallicity. This decrease is expected from massive stellar evolution models (Maeder 1991; Meynet 1995; Schaerer & Vacca 1998). The earlier observations of WR galaxies had no galaxies with abundance less 7.9. A possible exception was the galaxy Zw 0855+06, although there was some controversy about its oxygen abundance (from 7.72 to 8.40) (Vacca & Conti, 1992; Kunth & Joubert, 1985).

The discovery of WR stars in the most metal-deficient galaxies I Zw 18 ($Z_\odot/50$, Izotov et al. 1997; Legrand et al. 1997) and SBS 0335–052 ($Z_\odot/40$, Izotov et al. 1999a) implies that the luminosity of the blue bump likely becomes not equal to zero for these low metallicities, as predicted by evolutionary synthesis models.

Good general agreement is found between the relative numbers of WR stars N(WR)/N(O+WR) infered from observations and those predicted by evolutionary systhesis models (N(WR)=N(WN)+N(WC)). The relative numbers of WR stars decrease with decreasing metallicity in the whole metallicity range ($Z_\odot/50$ - $2Z_\odot$), in agreement with predictions of massive stellar evolution models with enhanced stellar wind (Maeder & Meynet 1994).

The relative numbers N(WC) / N(WN) of WR stars of different subtypes in the galaxies of our sample can be explained by the bursting nature of star formation and are in general good agreement with predictions of evolutionary synthesis models by Schaerer & Vacca 1998. The N(WC) / N(WN) ratio derived for the galaxies in our sample is very different from that expected in the case of continuous star formation as derived empirically by observations of individual WR stars (Massey & Johnson, 1998) in the Local Group galaxies.

The relative numbers N(WR) / N(O+WR) and observed equivalent widths of the blue and red bumps also compare favorably with predictions of evolutionary synthesis models by Schaerer & Vacca 1998 for metallicities larger than $\sim 1/10$ solar. However, the agreement is not so good for galaxies at the low-metallicity end, where N(WC) / N(WN), EW(λ4650) and EW(λ5808) derived from observations are several times larger compared to model predictions. Part of the disagreement may come from the poor statistics of WR stars in these low-metalicity WR galaxies. In the case of I Zw 18 ($Z_\odot/50$) however, the difference between observations and models may be explained by too low single WCE star line luminosities adopted in the Schaere & Vacca 1998 models, or by an additional contribution by WR

stars in binaries. In any case high signal-to-noise ratio two-dimensional spectroscopic mapping necessary to exclude the possibility that we are observing (Izotov et al. 1997) in I Zw 18 a region with a locally enhanced number of WCE stars.

Acknowledgements. It is pleasure to thank Daniel Schaerer for the use of his evolutionary synthesis models and useful comments. This international collaboration was possible thanks to the partial financial support of INTAS grant No. 97-0033. The observations were performed by Y.I.Izotov and T.X.Thuan thank the partial financial support of NSF grant AST-9616863.

References

Allen D.A., Wright A.E., & Goss W.M.: 1976, *MNRAS,* **177**, 91.
Conti P.S.: 1991, *ApJ,* **377**, 115.
Conti P.S.: 1999, *PASP,* **111**, 251.
Izotov Y.I., Chaffee F.H., Foltz C.B., Green R.F., Guseva N.G., & Thuan T.X.: 1999, *ApJ,* 20 December.
Izotov Y.I., Foltz C.B., Green R.F., Guseva N.G., & Thuan T.X.: 1997, *ApJ,* **487**, L37.
Kunth D., & Joubert M.: 1985, *A&A,* **142**, 411.
Kunth D., & Sargent W.L.W.: 1981, *A&A,* **101**, L5.
Legrand F., Kunth D., Roy J.-R., Mas-Hesse J.M., & Walsh J.R.: 1997, *A&A,* **326**, L17.
Leuenhagen U., & Hamann W.-R.: 1994, *A&A,* **283**, 567.
Leuenhagen U., & Hamann W.-R.: 1998, *A&A,* **330**, 265.
Leuenhagen U., Hamann W.-R., & Jeffery C.S.: 1996, *A&A,* **312**, 167.
Maeder A.: 1991, *A&A,* **242**, 93.
Maeder, A., & Meynet, G. 1994, *A&A,* **287**, 803.
Massey P., & Johnson O.: 1998, *ApJ,* **505**, 793.
Meynet G.: 1995, *A&A,* **298**, 767.
Osterbrock D.E., & Cohen R.D.: 1982, *ApJ,* **261**, 64.
Schaerer D., Contini T., & Pindao M.: 1999, *A&AS,* **136**, 35.
Schaerer D., & Vacca W.D.W.: 1998, *ApJ,* **497**, 618.
Vacca W.D., & Conti P.S.: 1992, *ApJ,* **401**, 543.

THE IMAGES OF EXTRAGALACTIC RADIO SOURCES IN THE DIFFUSION MODEL

F.M. Kolesnikov[1], V.M. Kontorovich[1,2]

[1] Department of Radio Phisics, Kharkov State University,
4 Independency square, Kharkov 310066 Ukraine,
[2] Institute of Radio Astronomy NANU
4 Krasnoznamennaya St., Kharkov 310002 Ukraine, *vkont@ira.Kharkov.ua*

ABSTRACT. The distribution of the spectral index and radio lobes' isophots were derived by numerical methods in the diffusion model of extragalactic radio sources. The kinetic equation for the distribution function of relativistic electrons is considered. Regions of electron injection, associated with hot spots, are considered as moving. Velocities of hot spots and the diffusion velocity of electrons determined the correlation of transverse and longitudinal lobes' sizes. Observed changes of lobes at various frequencies accord with the diffusion model. The reabsorption in the lobes leads to the asymmetry of them, depending on source's rotation relatively to the line of sight.

Key words: extragalactic radio sources: hot spots, lobes, diffusion model, spectral indexies, asymmetry.

1. Introduction

Spatial structures of extragalactic radio sources (ERS) have been detected due to their numerous observations. Images of ERS (Leahy, Bridle, and Strom, 1995) demonstrate four basic morphological components: core, jets, hot spots and lobes. The physical model explaining these four morphological structures is known as the jet model (Begelman, Blandford, and Rees, 1984). The radio core corresponds to the AGN. Jets extend from the core and end at hot spots. Energy from the AGN is transported by jets to the radio-emitting lobes and at hot spots jets convert some of their kinetic energy into relativistic particles, and magnetic fields. We assume that the hot spots are sources of relativistic electrons (accelerated by shock waves). Electrons propagate due to the diffusion, lose the energy because of the synchrotron emission, and form the lobes. We introduce the motion of the injection regions which naturally explains the lobes size asymmetry and the displacement of the hot spots with respect to the center of the lobes (Valtaoja, 1982, Gestrin, Kontorovich and Kochanov, 1987).

2. The diffusion model with moving sources of relativistic electrons

The distribution function N for the relativistic electrons satisfies to the kinetic equation with moving source:

$$\frac{\partial N}{\partial t} - \frac{\partial}{\partial E}\left(\beta E^2 N\right) - D_0\left(\frac{E}{E_D}\right)^{\mu}\Delta N = \qquad (1)$$

$$= Q\delta\left(x - x_0(t)\right)\delta(y)\delta(z)E^{-\gamma_0}\Theta(t)\Theta\left(E_2 - E\right)\Theta\left(E - E_1\right)$$

The second term $\frac{\partial}{\partial E}\left(\beta E^2 N\right)$ describes the synchrotron and Compton losses:

$$\beta = \left(\frac{32\pi}{9}\right)\left(\frac{e^2}{mc^2}\right)\frac{\omega_H + \omega_r}{m^2c^3},$$

where $\omega_H + \omega_r$ is the energy density of the random magnetic field and the radiation.

To simplify the model, disregard the possible coordinate dependence of the diffusion coefficient D, and the magnetic field H, the power-law dependence on the energy is taken for the diffusion coefficient:

$$D = D_0\left(\frac{E}{E_D}\right)^{\mu}.$$

The right side in the kinetic equation (1) corresponds to the point source $(x_0(t), 0, 0)$ of relativistic electrons (the hot spot) moving along the x-axis; the injection spectrum is taken as the power-law dependence on the energy $E^{-\gamma_0}$ in the range $E_1 < E < E_2$ and zero outside it.

To derive the distribution function, apply the Laplace transformation with respect to time to the kinetic equation (1):

$$N^*(E, \vec{r}, p) = \int_0^{+\infty} exp(-pt)\, N(E, \vec{r}, t)\, dt.$$

Then this equation for $N^*(E, \vec{r}, p)$ can be reduced to the diffusion equation. The expression for the

$N^*(E,\vec{r},p)$ is used with the Melline transformation to derive the distribution function $N(E,\vec{r},t)$ for $x_0 = vt$ (GKK 87):

$$N\big(E,t,\vec{r}\big) = \frac{Q_0 E^{-2}}{8\pi^{3/2}\beta}\big(1-\mu\big)* \qquad (2)$$

$$*\left(\frac{\beta\big(1-\mu E_D{}^{\mu}\big)}{D_0}\right)^{\big(\gamma_0-1\big)\big(1-\mu\big)} *$$

$$* \int\limits_{\lambda^2(E)}^{\lambda^2(E_2)} d\lambda_0^2 \frac{\lambda_0^{2\big(\gamma_0-1\big)\big(1-\mu\big)-2}}{\big(\lambda^2-\lambda_0^2\big)^{3/2}}\Theta\big(D_0 t-\big(\lambda^2-\lambda_0^2\big)\big)$$

$$exp\left(\frac{-\left(x-vt+\frac{v}{D_0}\left(\lambda^2-\lambda_0^2\right)\right)^2-y^2-z^2}{4\left(\lambda^2-\lambda_0^2\right)}\right).$$

In this expression for the distribution function, $\lambda^2 = \frac{D_0 E^{\mu-1}}{(1-\mu)E_D^{\mu}\beta}$ is the square of the diffusion length (Berezinskiy, Bulanov, Ginzburg, et al., 1984).

The radio spectrum for electrons is found from the formulas for the synchrotron emission (Ginzburg, 1987):

$$I(\nu) = \int\limits_{-\infty}^{s_0} dsdEN(E,t,\vec{r})\,p(E,\nu), \qquad (3)$$

where the integration corresponds to the integration along the line of sight, s_0 is the observation point. And $p(E,\nu)$ is the synchrotron radiation flux density from single electron. With the accuracy sufficient for comparison with observations the synchrotron radiation flux density can be put (σ_T is the Thomson cross section):

$$p(\nu) = \frac{\sqrt{2}\sigma_T mc^2 H}{12\sqrt{3}\,0.29\pi e r^2}\nu\delta\left(\nu-\nu(E)\right),$$

$$\nu(E) = \frac{0.29\sqrt{3}eH}{2\pi\sqrt{2}mc^2}\left(\frac{E}{mc^2}\right)^2.$$

In the case when the reabsorbtion is considered, we have the radio spectrum of the lobe (with $N^*(E,\vec{r},p)$ from (2)):

$$I(\nu) = \int\limits_{-\infty}^{s_0} ds_1 dEN(E,t,\vec{r})\,p(E,\nu)\,exp\left(\frac{1}{c}\int\limits_{s_0}^{s_1} ds_2\mu\right).$$

where μ is the reabsorbtion factor. The common expression for μ (Ginzburg and Syrovatskii, 1964, Zheleznyakov, 1997):

$$\mu(\nu) = -\frac{c^2}{32\pi^2\nu^2}\int\frac{\partial N}{\partial E}p(\nu,E)\,dE.$$

3. Numerical calculatons' results and conclusion

As it has been shown in (GKK 87) the dependence of the radio flux on the distance to the hot spot (transverse to the motion direction) of the source 3C 196 is close to theoretical one from the diffusion model.

We see from expressions for the distribution function (2) and the radio spectrum (3) that the external shape of radio lobes is determined by the relation between the electron diffusion velocity $v_{diff} = \frac{D_0}{\lambda}$ and the velocity $v_\perp$ of the source in the mapping plane (the longitudinal component vanishes on the integration along the line of sight), both of these are appearing in the expression for the distribution function.

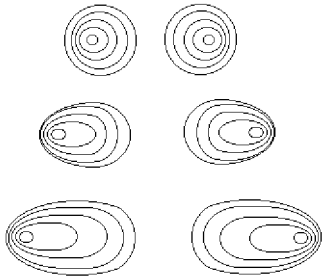

Figure 1: Radio sources' isophots produced by the diffusion of relativistic electrons for various correlations of hot spots' velocities in the mapping plane and the electron diffusion velocities: $v_\perp/v_{diff} = 1,\ 4,\ 8$. $\gamma_0 = 2$.

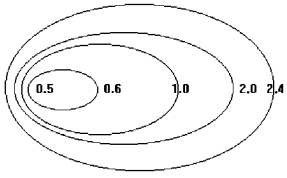

Figure 2: The distribution of the spectral index for $\gamma_0 = 2$ and $v_\perp = 8v_{diff}$.

For $v_\perp \ll v_{diff}$, one has approximately a sphere with diameter $l \approx 4\lambda$ and the hot spot near the center, while for $v_\perp \geq v_{diff}$, the lobe is an ellipsoid with the major axis $L \approx \left(\frac{v_\perp}{D_0}\right)\lambda^2 + 4\lambda$ and the minor axis $l \approx 4\lambda$, while the hot spot is near the outer edge. For $v_\perp \gg v_{diff}$, the lobe has a broad tail and a relatively narrow head, in which the hot spot lies. The

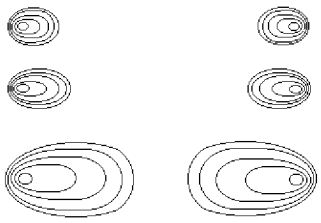

Figure 3: Radio source isophotes derived at three frequencies: 150 Mhz, 450 Mhz, 900 Mhz. $\gamma_0 = 2$, $v_\perp / v_{diff} = 8$.

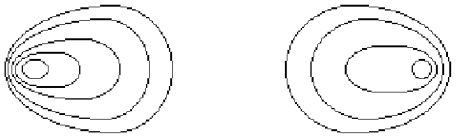

Figure 4: Isophots of the rotated at 10 degrees radio source (the left lobe is closer to the observation point). The reabsorbtion is taken into account. $\gamma_0 = 2$, $v_\perp / v_{diff} = 8$.

external pressure (neglected in this model) will undoubtedly alter lobe's configuration, but the main characteristics should persist. Figure 1 shows examples of radio sources for various correlations of $v_\perp$ and v_{diff} derived numerically. The distribution of the spectral index (Carilli and Barthel, 1996) show that relativistic particles lose energy the more faster the more energy they have. Figure 2 shows the distribution of the spectral index α ($I(\nu) \propto \nu^{-\alpha}$) derived numericaly in the diffusion model.

The longitudinal size L and transvers one l of the lobe provide estimations for $D(E)$ and $v_\perp$:

$$v_\perp \approx \beta E (L - l),$$

$$D = D_0 \left(\frac{E}{E_D} \right)^\mu = \frac{l^2 \beta E}{4(1-\mu)} \propto v_{diff} \frac{l}{4},$$

where E is the electron energy corresponding to the observation frequency $\nu = \nu(E)$.

The increase of lobes' size when the observation frequency is reduced agrees with predictions of the model, which shows that the transverse size varies as $\nu^{-1/4}$ for $D =$ constant. The variation of the L and l correlation we explain by various correlations of $v_\perp$ and v_{diff} at various observation frequencies. As we see from expresion for $N(E, \vec{r}, t)$ and $I(\nu)$ only electrons with the ehergy more than the energy corresponding to the observation frequency $\nu = \nu(E)$ make contribution to the radiation. Therefore, the square of the diffusion length decreases and effective v_{diff} increases (figures 3).

Figure 4 show the example of the source (isophots) derived with account for the reabsorbtion. This leads to the asymmetry of radio lobes.

The diffusion model thus describes the situation close to the observation data, the account for the reabsorbtion and simple incorporation of hot spot's motion relativly to the medium provides conclusions applicable to the real extended extragalactic radio sources, where the model can explain the major observed characteritics.

References

Begelman M.C., Blandford R.D., Rees M.J.: 1984, *Rev.Mod.Phys.*, **165**, 395.

Berezinskiy V.S., Bulanov S.V., Ginzburg V.L., et al.: 1984, *Astrophisics of cosmic rays.* -Moscow, Nauka.

Carilli C.L., Barthel P.D.: 1996, *As. Ap. Rev.*, **7**, 1.

Gestrin S.G., Kontorovich V.M., Kochanov A.E.: 1987, *Kinem. i Fiz. Neb. Tel.*, **3**, N 4, 57.

Ginzburg V.L.: 1987, *Theoretical Physics and Astrophysics.*-Moscow, Nauka.

Ginzburg V.L., Syrovatskii S.I.: 1964, *Origin of cosmic rays.* -Pergamon Press.

Kaiser C.R., Alexander P.: 1999, in: *Observational Cosmology: The development of galaxy systems,* eds. G.Giuricin, M.Mezetti, P.Salucci, *ASP Conf. Ser.,* **176**, 377.

Leahy J.P., Bridle A.H., Strom R.G.: 1996, *IAU*, **175**, 157.

Valtaoja E.: 1982, *As. Ap.,* **111**, 213.

Zheleznyakov V.V.: 1997, *Radiation in astrophysical plasma.* -Moscow.: Yanus-K.

A SHOCK WAVE THEORY OF "SUPER-LUMINAL" OUTBURST FROM AGN

V.M. Kontorovich[1,2], V.N. Pasyuga[1,3]

[1] Department of Mecanics and Mathematics, Kharkov State University,
4 Independency square, Kharkov 310066 Ukraine,
[2] Institute of Radio Astronomy NANU
4 Krasnoznamennaya St., Kharkov 310002 Ukraine, *vkont@ira.Kharkov.ua*,
[3] Research and Technological Institute of TTR, P.O.Box 589,
3 Kolomenskaya St., Kharkov 310166 Ukraine, *zhuck@insurance.kharkov.ua*

ABSTRACT. Dynamics is investigated of relativistic blast waves in the neighborhood of active galactic nuclei (AGN). The inverse cubic decrease of the density is considered corresponding to the hydrostatic equilibrium of the relativistic media with the equation of state $p \propto \rho^{4/3}$ in the vicinity of a big point mass. For the off-center ultra-relativistic point explosion the Lorentz factor of the leading point of the shock front is proved to have an asymptotically constant value that explains the observed super-luminal relativistic velocities of jets' components of 3C 345(Babadjanjanz, Belokon',1985; Belokon', 1991). It is also found that for the leading point moving at small angles to the direction of sight the apparent super-luminal velocity linearly depends on the energy of explosion, which is in a good agreement with the observations for 3C 273(Babadjanjanz, Belokon',1993).

Key words: AGN: bursts, superluminal jets; shocks: ultra relativistic, blast wave.

1. Introduction. Off-Center Relativistic Adiabatic Explosion

Among objects of the contemporary radio astronomy explosion processes with extremely high energies are of particular interest such as Supernova (or even Hypernova) explosions (Waxman & Loeb, 1998), gamma-bursts (Paczynski, 1999) and outbursts from AGN — jets (Begelman, Blandford & Rees, 1984). In these cases motions have relativistic or even ultra-relativistic velocities (see for example the review by Vermeulen and Cohen, 1994 for the super-luminal sources, where the velocities of jet components are given): that boosts interest in investigations of dynamics of relativistic blast waves (Blandford and McKee, 1976, 1977). As follows from the conditions of the hydrostatic equilibrium the density decrease in the vicinity of AGN obeys the inverse cubic law. The adiabatic model of explosions is considered — the medium believed non-viscous, with no thermal conductivity and no interaction with magnetic field or radiation. This work is based on the Kompaneets approximation for the relativistic motion (Shapiro, 1979, 1980). The Kompaneets equation for SF is generally speaking (nonlinear) integro-differential one due to the volume of spreading hollow within the SF it contains. The volume expression contains time depending coordinates of the leading points limiting the SF in the direction of the density gradient. In non-relativistic case (Kompaneets, 1960; see also the review of Bisnovatyi-Kogan and Silich, 1995 and Kontorovich and Pimenov, 1997, 1998) the volume is only as multiplier at time derivative and can be by including in the new variable ("Kompaneets time") removed from the coefficients of the equation. In the relativistic case the similar volume exclusion is impossible, the equation is essentially integro-differential. But in ultra-relativistic limit, when the SF movement proceeds at a speed rather close to the velocity of light, the SF form is quite close to the sphere of the radius ct and the hollow volume present in the equation is thus known. In this case however the aim of the calculation is Γ-factor, which can be expressed through the media density in the point crossed by the SF (see below). For a strong explosion the relation is valid $p_2/n_2 \gg p_1/n_1$, where $n_{1,2}$ and $p_{1,2}$ are the concentration and pressure before and after the shock front in the comoving reference frame of the fluid, correspondingly. According to this relation the average kinetic energy of particles is much greater behind the shock front (SF) than it is in front of it. Consequently, the pressure in front of the SF can be neglected. As the density at the explosion point is finite, the Sedov's stage of deceleration exists for early stages of expansion with the uniform distribution of flow parameters and Lorentz factor. At later stages the value of the Lorentz factor can change essentially along the SF.

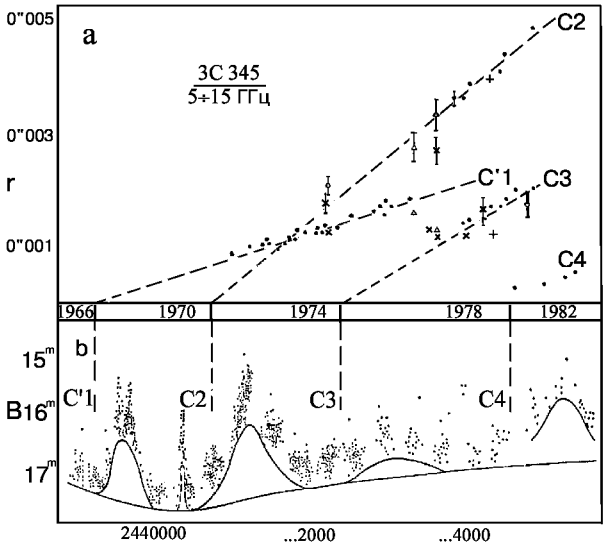

Figure 1: A correlation is seen between the super-luminal velocity components and the optical bursts that can witness their explosion origin (BB85). The jet components are observed moving at constant ultra-relativistic velocities in accordance to the result below.

2. Observational Data of Super-Luminal Velocity Components in Quasars

Yet the authors of VLBI observations, who revealed the occurrence of "super luminal components", were searching for (and would never found) the events in RADIO variability (for the total radio flux from the object), which would correspond to the component formation in millisecond jets (3 273 3 120, 3 345). Such evidences were first found (though for variability in OPTICS) at 3 345, 3 120, 3 273, OJ 287 Babadjanjanz and Belokon' (BB85). Later similar relations was found both in optics and in radio: Bregman, et al., 1986, 3C 345 (radio, mm), Krichbaum, et al., 1990, (IR-optical flare), Mutel, et al., 1990, (BL Lac, radio), Zenzus, et al., 1990, 3 273 (radio), etc. Recently the correlation of formation of super luminal components with gamma bursts has been reported (see as example Pohl, et al., 1995, 0528+134, etc). Therefore, it is possible, that some sources release their most energy of bursts, which accompany the components, in the X- and gamma-ranges. The evaluation of burst energy release are impeded also by their complex structure. Below we will rely upon the Leningrad team's data with allowance for the made reservations.

The interpolation trajectories are shown in Fig.1 of ultra-relativistic velocity components of the jet 3 345. Their apparent velocities can be explained by relativistic effects of motion at the small angles to the direction of sight.

Apparently, the only result, which argues in favour of correlation between the burst energy release and the speed of the flare-related component, is yet adduced in the article on 3 273 (Fig. 4 and Fig. 5 in BB93). On the fig 4 for 3C273 from BB93 the dependence is clearly seen: the greater the intensity of optical radiation at the initial stage, the greater the apparent super-luminal velocity. In Fig.2 the dependence of the apparent super-luminal velocity on the optical activity and, correspondingly, the optical flux density F at the stage of separation of components from the nucleus is presented for the components 2 – 9 of the millisecond radio jet 3 273 (BB93).

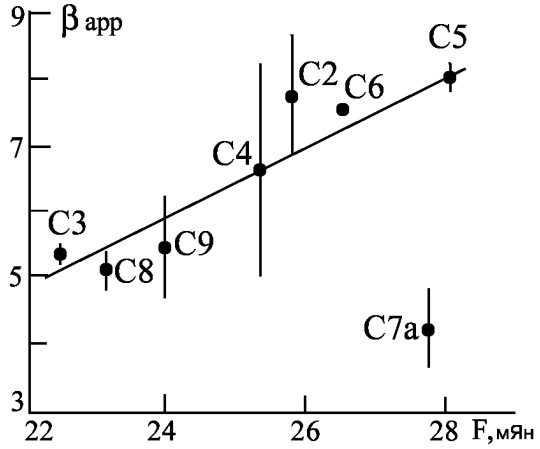

Figure 2: The linear dependence is observed of the apparent super-luminal velocity on the energy density of the optical radiation flux (BB93).

3. The Ultra-Relativistic Blast Shock Wave

The necessary condition for the motion to be relativistic is given by the expression $E \gg \rho_1 V c^2$, i.e. the energy of explosion is much more than the rest energy of gas within the envelope. For the adiabatic explosion the following relations are true at the SF (Blandford R.D. & McKee C.F., 1976):

$$p_2 = e_2/3 = 2\Gamma^2 w_1 c^2, \quad n_2' \equiv \gamma_2 n_2 = 2\Gamma^2 n_1, \qquad (1)$$

$$\gamma_2^2 = \Gamma^2/2, \quad \Gamma = 1/\sqrt{1 - v^2/c^2}.$$

Here p_2, e_2, n_2 are the pressure, the density of energy and the concentration of particles in the reference frame of pre-shock and post-shock flows, correspondingly. The values n_2', γ_2, w_1 , are the concentration of particles, the Lorentz factor of the flow behind the SF and the density of external media in the frame of the unshocked gas, accordingly (for a cool gas $w_1 = n_1 m_1$). For the explosion processes in question the values of parameters are sensitive to a small difference between of the velocity of light and the SF one. There is the Lorentz factor of the SF that characterizes this difference and describes observational values. That is why it is important to know the time dependence of the Lorentz factor along the SF.

4. The Relativistic Kompaneets Approximation.

This approximation describes the qualitative dynamics of SF adequately at the exponent $n \leq 3$ (Shapiro P.R., 1980) in the law of density decrease. The pressure behind the SF in the reference frame of post-shock is suggested uniform along the SF and proportional to the average density of the explosion energy.

$$p_2 = \lambda E/V \tag{2}$$

where E is the explosion energy, V is the volume restricted by the envelope and λ = const that is taken from the self-similar solutions (Shapiro P.R., 1979).

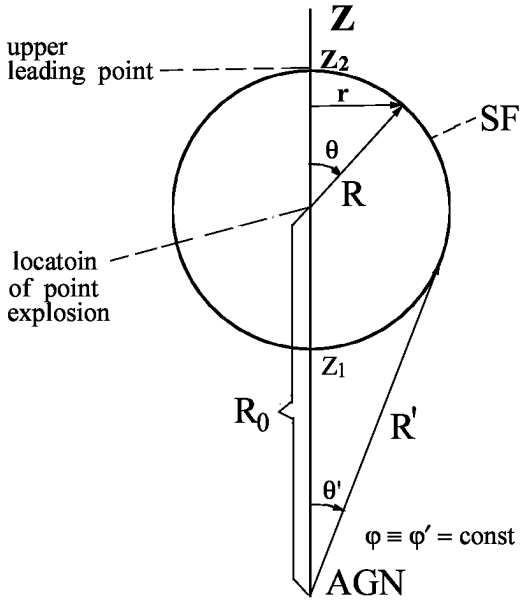

Figure 3: The shock front and the reference frame

Analytically the velocity $\beta = v/c$ of the SF motion is described in the cylindrical coordinates (r, z) as follows

$$\beta = \dot{r}/c\sqrt{1 + r_z^2}, \quad r_z \equiv \partial r/\partial z. \tag{3}$$

From the relations at the SF (1) and the Kompaneets approximation condition (2) the equation of the SF motion follows (Blandford and McKee 1976):

$$\dot{r}/\sqrt{1 + r_z^2} = c\left[1 - \frac{2w_1(r,z)V(t)c^2}{3\lambda E}\right]^{1/2}. \tag{4}$$

5. The Ultra-Relativistic Explosion in the Vicinity of AGN

In the spherical coordinates $(R', \theta'$) with the center in the AGN the density of external media is $w_1 = a/R'^3$, a =const > 0 in the range $R_* < R' \ll R_{ef}$ where R_* is a radius of the galactic nucleus, R_{ef} — is such a distance from the nucleus for which either the mass of the external medium inside the sphere of this radius is equal to the nucleus mass or the media becomes non-relativistic. Note that in this consideration we completely neglect the movement of media due to accretion on the central compact object (Blandford 1999, Shakura 1974) or ejection in the jet or wind that can affect as directly as through the density distribution.

In the reference frame of the nucleus the coordinates of the explosion point are $(R_0, 0)$. Consider a new system of spherical coordinates (R, θ) with the center at the explosion point and the polar axis directed towards the upper leading point of the SF. The shape of the SF is close to a sphere at least for $t < t_* \leq R_0/c$ where t_* is the time since that the motion of the lower leading point can not be ultra-relativistic. We can estimate the volume $V \approx 4\pi t^3/3$ restricted by the SF and the density of external medium w_1:

$$w_1 \approx a(t^2 + R_0^2 + 2tR_0\cos\theta)^{-3/2}. \tag{5}$$

From the conditions (1) and (2) the explicit expressions for the Lorentz factor of the SF can be written as

$$\Gamma^2 \approx \frac{(t^2 + R_0^2 + 2tR_0\cos\theta)^{3/2}}{2Bt^3}, \quad B = \frac{4\pi ac^2}{9\lambda E}. \tag{6}$$

At larger times as the SF lower leading part approaches the radius of the nucleus R_* this part decelerates and the shock front becomes non-spherical (cf. Kontorovich, Pimenov, 1997, 1998). Nevertheless, at least for the SF upper leading part the relation (6) remains true. It can be proved that if the size of the central mass is negligible compared to the size of the envelope than the relative deviation of the volume of its estimation is small enough $\Delta V_s/V = O(\Gamma^{-4/3})$.

Instead of the Kompaneets approximation any version of the sector approximation can be used (Laumbach and Probstein 1969, Shapiro 1979, Gnatyk 1987, Gnatyk and Petruk 1996). It can be shown that because the shape of the SF in the vicinity of the upper leading point is close to a part of a sphere the expressions of the Lorentz factor found in Blandford and McKee 1976 and Shapiro 1979 coincides with (6).

If time t approaches infinity the relation (6) gives an asymptotically constant value of the Lorentz factor of the upper leading part of the SF.

$$\Gamma^2 \overset{t\to\infty}{\longrightarrow} \frac{1}{2B}. \tag{7}$$

Note that the asymptotic expression (7) is an intermediate one because time is restricted by the inequality $t \ll R_{ef}/c$.

6. The Dependence of Ultra-Relativistic Velocities on the Energy of Explosion

It is known (see Begelman M.C., Blandford R.D. & Rees M., 1984) that the apparent super-luminal velocity of a source moving at a small angle to the line of sight is equal to

$$\beta_{app} = \frac{\beta \sin\alpha}{1-\beta\cos\alpha} \stackrel{\alpha\ll 1}{\longrightarrow} \frac{2\alpha}{1/\Gamma^2+\alpha^2}, \qquad (8)$$

where β is the real velocity of motion

$$1-\beta \approx 1/2\Gamma^2 \ll 1.$$

Considering the energy of explosion E as a parameter the relation in the vicinity of the upper leading point can be reduced to the expression

$$\beta \approx 1 - \frac{4\pi a t^3 c^2 (t^2+R_0^2+2tR_0\cos\theta)^{-3/2}}{9\lambda E}. \qquad (9)$$

At larger times due to the asymptotic approach of the Lorentz factor to a constant value the multiplier at E^{-1} in (9) can be considered constant as well that allows representing the relation (9) as follows

$$\beta \approx 1 - \frac{A}{E}, \quad A = \frac{4\pi a c^2}{9\lambda}, \quad (\Gamma^2 \approx \frac{E}{2A}). \qquad (10)$$

For small enough angles $\alpha \ll 1/\Gamma$ Lorentz factor defined by the relation (10) can be substituted into the right side of the equation (8). The final expression for the apparent super-luminal velocity of the motion is

$$\beta_{app} \approx \alpha A^{-1} \cdot E. \qquad (11)$$

Thus, the apparent super-luminal velocity of the SF upper leading point is proportional to the explosion energy. In the case of nonconstancy (variability) of the angle α or the necessity of the averaging on it the energy dependence of the apparent component velocity has to change. As example for simple integrating on the angle this dependence will be logarithmic: $\beta_{app} \propto \ln E$.

7. Conclusion

1. For the model of the ultra-relativistic explosion in the vicinity of an AGN the Lorentz-factor of the SF leading point is proved to approach asymptotically to a constant. This result is in a good agreement with the observational data of ultra-relativistic velocities of jets' components (BB85, BB94, Belokon', 1991).
2. In the same model at the assumption that the leading part of the ultra- relativistic SF moves at a small angle to the line of sight the linear dependence is found of the apparent ultra-relativistic velocity of the leading part on the explosion energy. This result explains the observational values of apparent velocities of jets' components (BB93) at the suggestion about a proportionality between the optical energy flux at the moment of the components' origin and the explosion energy.

Acknowledgements. The authors are kindly grateful to M.K.Babadzhanyanz and E.T.Belokon' for useful comments and references and S.F.Pimenov for discussion and help in the text translation.

The more complete paper is to be published in Radio Physics and Radio Astronomy Journal.

References

Babadzhanyanz M.K., Belokon' E.T.: 1993, *Astron. Zh.,* **70,** 241 (BB93).

Babadzhanyanz M.K., Belokon' E.T.: 1985, *Astrofizika,* **23,** 459 (BB85).

Babadzhanyants M.K., Belokon' E.T.: 1994, In: *Multi-wavelength Continuum Emission of AGN / Eds. T.J.-L. Courvoisier and A. Blecha. Kluwer AP.,* 390 (BB94).

Begelman M.C., Blandford R.D., Rees M.: 1984, *Rev. Mod. Phys.,* **56,** 255.

Belokon' E.T.: 1987, *Astrofizika,* **27,** 429.

Belokon' E.T.: 1991, *Astron. Zh.,* **68,** 1.

Bisnovatyi-Kogan G.S., Silich S.A.: 1995, *Rev. Mod. Phys.,* **67,** 661.

Blandford R.D.: 1999, Relativistic Accretion (astro-ph/ 9902001).

Blandford R.D. and McKee C.F.: 1976, *Phys. of Fluids,* **19,** 1130.

Blandford R.D., McKee C.F.: 1977, *Mon. Not. R. Astr. Soc.,* **180,** 343.

Bregman J.N., Glassgold A.E., Huggins P.J., et al.: 1986, *ApJ,* **301,** 708

Gnatyk B.I.: 1987, *Astrofizika,* **26,** 113.

Gnatyk B.I., Petruk O.L.: 1996, *Kinematika i Fizika Nebesnykh Tel,* **12,** 44.

Kompaneets A.S.: 1960, *Doklady AN SSSR,* **130,** 1001.

Kontorovich V.M., Pimenov S.F.: 1998, *Izv. VUZ'ov, Radiofizika,* **41**, 683.

Kontorovich V.M., Pimenov S.F.: 1997, *Solar Physics*, **172**, 93.

Krichbaum T.P., Hummel C.A., Quirrenbach A., et al.: 1990, *A.Ap,* **237,** 3

Laumbach D.D., Probstein R.F.: 1969, *J. Fluid Mech.,* **35,** 53.

Mutel R.L., Phillips R.B., Su B., Bucciferro R.R.: 1990, *Ap.J,* **352,** 81

Paczynski B.: 1999, Preprint (astro-ph/9909048).

Pohl M., Reich W., Krichbaum T.P., et al.: 1995, *A.Ap,* **303,** 383

Shakura N.I.: 1974, *Astron. Zh.,* **15,** 74.

Shapiro P.R.: 1979, *Ap.J.,* **233,** 831; 1980, **236,** 958.

Vermeulen R.C., Cohen M.H.: 1994, *Ap.J.,* **430,** 467.

Waxman E., Loeb A.: 1998, Preprint (astro-ph/ 9808135).

Zenzus J.A., Unwin S.C., Cohen M.H., Biretta J.A.: 1990, *AJ,* **100,** 1777

JETS IN 20 AGNS WITH STRONG LONG-TERM VARIABILITY OF 1–22 GHZ SPECTRA

Yu.A. Kovalev[1], A.B. Berlin[2], Y.Y. Kovalev[1], N.A. Nizhelsky[2]

[1] Astro Space Center of the Lebedev Physical Institute
Profsoyuznaya 84/32, 117810 Moscow, Russia, *ykovalev@dpc.asc.rssi.ru*
[2] Special Astrophysical Observatory
Nizhny Arkhyz, Karachaevo-Cherkessia, 357147 Russia

ABSTRACT. Results of multifrequency broad band spectra observations and their interpretations by the Hedgehog relativistic jet model are presented for 20 strong variable radio sources. The many years strong variability of well known objects, including BL Lac and OJ 287 for 20 years, is analyzed. Instantaneous 5–7 frequency spectra were measured at the RATAN–600 radio telescope over the period from 1979 to 1999. The strong long-term variability of the spectra is explained by the variability of a continuous relativistic jet with a variable ejection of it from an active nucleus in quasi radial magnetic field.

Key words: galaxies: active — galaxies: jets — BL Lacertae objects: general — quasars: general

1. Introduction

The general final aim of any experiments is a study of an origin of processes, which give rise to the observational phenomenon. For the given case it is a study of an origin of variable extragalactic radio sources. The phenomenon of the variability can be qualitatively interpreted in terms of an activity of a central nucleus of a galaxy or a quasar. Nevertheless the problems exist for a quantitative explanation of the variability by a concrete physical model: the longer the temporal and the wider the frequency intervals of an analysis (as well as the more a number of frequencies), the worse the quantitative fit to the observational data, as a rule.

Earlier we had fitted a relativistic jet model of variable extragalactic radio sources to the instantaneous 1–22 GHz spectra at 6–7 frequencies for 79 variable sources at 1–2 epochs, as well as the similar explanation had been done for the observational shapes of about 200 VLBI-compact extragalactic objects (Kovalev & Kovalev, 1996, 1997). Now we report on successful results of a comparison of the same model with our multi epochs observations of instantaneous 1–22 GHz spectra for 20 well known variable radio sources.

2. Observations and the Model

Observations were carried out at the RATAN–600 radio telescope during 1979–1999 in the framework of our monitoring program to study the long-term spectra variability of extragalactic radio sources. Each individual spectrum was measured during several minutes at all frequencies and averaged on the set for a few spectra measurements. Observations were done with 3–4 sets per year, excluding several years because of modernizations of the antenna and other reasons. Duration of each set was 1–3 weeks. 1–22 GHz spectra were measured at 5-7 wave lengths of the following: 1.00/1.38, 2.08/2.7. 3.9, 6.0, 7.6, 8.2, 13 and 31 cm. The part of the presented data was published earlier. Details see in Kovalev (1998), Kovalev et al. (1999).

The following sources with strong long-term variability are included in the analysis:

1. BL Lac and OJ 287 (for 20 years), 3C 84, 3C 120, 3C 273, 3C 279, 3C 345, 3C 454.3, 4C 39.25, 1510−08, 2134+00 for 1979–1999;
2. CTA 102, 0528+13 (Nimfa), 1055+01, 1124−18, 1219+04, 1730−13, 1749+09, 2209+23 for 1989–1999;
3. 0109+22 for 1979–1999.

The typical amplitude of variability during the presented period was several times more than the minimal value of the flux density for these objects.

The Hedgehog jet model (Kardashev, 1969) is used to study an origin of these variable sources (full references see in Kovalev & Kovalev, 1996, 1997). To explain the observed quantities of the polarization by the model, we assume that the observed emission is strongly depolarized — for an example, by the Faraday rotation in the ambient magnetized plasma of the jet, an envelope or a lobe along the line of sight.

3. Results

Presented well known variable radio sources (quasars, galaxies, BL Lacs) with strong long-term radio variability from our many years multi epochs multifrequency measurements:

1. show the natural wave-like changes of the instantaneous spectra in centimeter-decimetre wave lengths on the scales from a few weeks to several years;
2. have one/two component shapes of the instantaneous spectra, the high frequency component of which is variable, and the low frequency component, if it is detected, is not variable;
3. can be explained in the framework of the Hedgehog relativistic jet model (with an accuracy about or more than 90%) by a variable persistent flow of relativistic particles from an active nucleus of an object in the strong quasi radial magnetic field.

The jet in the model is associated with the observed high frequency component of the spectra. The time scale of the spectra variability at higher frequencies is equal to the scale of the variability of the flow of relativistic particles from an active nucleus. Any short scale can be in the model, including the variability during a day, if it is permitted by a mechanism of the variability for the flow of the particles from the nucleus.

Acknowledgements. Observations are partly supported by the State Program of Science and Technology "Astronomy" (grant 1.2.5.1) in 1997–1999 and by the Russian Foundation for Basic Researches (grant 99–02–17799) in 1999. YAK thanks also his wife Zina for the partly support of travels to do the observations in 1994–1998 from the family budget.

References

Kardashev N.S.: 1969, Epilogue to the russian edition of the book Burbidge J., Burbidge M., *Quasars*, Mir, Moscow.

Kovalev Yu.A., & Kovalev Y.Y.: 1996, *Odessa Astron. Publ.*, **9**, 163.

Kovalev Yu.A. & Kovalev Y.Y.: 1997, *Astrophys. Space Sci.*, **252**, 133.

Kovalev Yu.A.: 1998, *Bull SAO*, **44**, 50.

Kovalev Y.Y., Nizhelsky N.A., Kovalev Yu.A., Berlin A.B., Zhekanis G.V., Mingaliev M.G., Bogdantsov A.V.: 1999, *Astron. Astrophys. Suppl.*, **139**, 545.

ON THE POSSIBILITY FOR MEASURING THE HUBBLE CONSTANT FROM OPTICAL-TO-NIR VARIABILITY TIME DELAY IN AGNS

V.L. Oknyanskij

Sternberg Astronomical Institute,
Universitetskij Prospect 13, 119899 Moscow, Russia, *oknyan@sai.msu.ru*

ABSTRACT. The Optical-to-Near-infrared variability time delay have already been reported for a small number (~ 7) of AGNs and has been firmly established only for 5 of them. The time delay is probably increasing with the IR wavelengths. The most naturally this time delay can be interpreted by the model where IR emission is attributed to circumnuclear dust heated by the nuclear radiation. In given model a suggestion on narrowness of the near-infrared (NIR) emission region is quite natural, as far as the dust can be not saved on distances from the nucleus closer then some critical value, on which it is reached the sublimation temperature for graphite particles (Barvainis, 1987). For NGC 4151 case it has been shown that the NIR region has a form of thin ring or torus. The radius of this ring correlates with level of the nucleus activity (Oknyanskij et al. 1999). This dependency of radius of the NIR emission region from luminosity reveals itself as under object variability (as in the case of NGC4151), and also when objects with high and low luminosity are considered. We assume that the observed time delays allow us to derive a redshift independent luminosity distances to AGNs and estimate a Hubble constant.

Some problems of using this strategy for the Hubble constant determination are discussed.

Key words: AGNs: Sy1Gs, QSOs; individual: NGC4151, 7469, 3786, 3783, Fairal 9, GQ Comae; Cosmolgy: H_0 determination.

1. Introduction

H_0 - the Hubble constant is fundamental parameter in standard cosmology, measuring the rate at which the Universe is expanding. H_0 connected with many other significant values in cosmology and first of al age of Universe and distance scale. The value of the Hubble constant is still subject of intensive discussions in many publications.

There are 2 different groups of methods for the Hubble constant determinations can be noted:

1. Traditional or *"non direct"* methods, which use some directly measured distance in our Galaxy, for example till Hiades, then extrapolate it some way till other galaxies. In this group of methods are well known:

(i) using period-luminosity dependence for variable stars (a recent successful example of this is HST Key project (Freedman et al., 1994));

(ii) using the principle that a sample of nearby spirals of specific Hubble type represents a "fair" sample of intrinsic population (Sandage 1996; Goodwin, 1997); and some others.

Current estimates of H_0 using methods from this group are in range $\sim 60 - 90\ kms^{-1}Mpc^{-1}$

2. *"Direct methods"*:

(i) Using Sunyaev-Zel'dovich effect (Syunyaev & Zeldovich 1980);

(ii) Using gravitationally lensed QSOs (Refsdal 1964);

(iii) Time delay between variability of AGN in different UV-Optical-NIR wavelengths (Collier et al., 1999);

(iv) and some others, for example, using motions and line-of-sight accelerations of water maser emission (Miyoshi et al. 1995).

Current estimates of H_0 using methods from this group are in range $\sim 30 - 80\ km\ s^{-1}\ Mpc^{-1}$. "Direct" methods give systematically smaller values for H_0 than "non direct". Meanwhile these 'direct' methods are more model dependent.

We propose here a new method that utilizes the redshift-independent luminosities of AGNs obtained from observed optical-to-near IR time delay.

In chapter 2 we discuss the theory of the method. In chapter 3 we present our published and new results of the optical-to-NIR time delay determinations for several AGNs NGC4151 (Oknyanskij 1993, Oknyanskij et al. 1999), QSO PQ Comae and NGC7469 and combine them with other published results on the optical-to-NIR time delays in several other AGNs. Then we apply our method for determination of H_0 using the

observation results.

2. Theory

2.1. First step idea of the method

2.1.1. Basic assumptions

(i) NIR emission is attributed to circumnuclear dust heated by the nuclear radiation.

(ii) The dust is spherically symmetric and smoothly distributed.

(iii) NIR emission region has a form of a smooth spherical shell.

(iii) The dust (graphite grains) can be not survived on distances from the nucleus closer then some critical value, on which it is reached the sublimation temperature for graphite particles (Barvainis, 1987, next times here B1)

(iv) The time delay between UV (optical) and NIR variations caused by simple light travel time effects.

This critical distance, "evaporation radius" is given by (following to B1):

$$r_{evap} = 1.3\ L_{UV,4}^{0.5}\ T_{1500}^{-2.8} pc \qquad (1)$$

where T is the grain evaporation temperature in units of 1500 K and L is ultraviolet luminosity in units $10^{46} ergs\ s^{-1}$ and r_{evap} is the radius in parsecs.

2.1.2. Core of the idea

From the observations we can get the time delay between UV (or optical) and near IR variations in some AGN, which give us r_{evap} and estimation of L^*_{UV}. Then we can use observed flux in UV to get independent from z distance to the object and estimate the H_0. If we have already got the estimation of the $L_{UV,H=50}$ for $H_0 = 50\ km\ s^{-1}\ Mpc^{-1}$ then we can get estimation

$$H_0 = 50\ (L_{UV,H=50}/L^*_{UV})^{0.5}\ km\ s^{-1}\ Mpc^{-1} \qquad (2)$$

2.1.3 Problems

1. From the observations we have found that the NIR emission region should have form of thin ring or torus, but not spherical shell (Oknyanskij, 1999).

2. If the grains are depleted when the UV luminosity peaks, and cannot reform, then a dust-free hole surrounding the central source will be created with radius corresponding to the sublimation distance at the UV peak. This hole can be a problem in explanation of NIR variability.

3. The nature of the grain is unknown. The evaporation temperature can be significantly higher then 1500 K considered in B1 and probably can reach 2000 K (Sanders et al 1989). The size of the grains also can be bigger then 0.05 μ used for deriving (1) .

2.2. Next step model

Barvanis (1992) has considered the "survival" and "reformation" models. The reason for this is that clouds might serve to either protect the grain from sublimation, allowing them to serve when the UV flux high, or provide a medium in which grains can reform. So the model thus assumes that dust is located into clouds.

For next step we can use small improvements: we will assume that

(i) dust is clumped into clouds with UV optical depth $\tau_{UV} \geq 1$;

(ii) the dust region geometry has disklike form.

Thus model assumes clouds existing at radii well inside the sublimation radius for the peak UV flux given by (1).

In place of (1) we will use here improvement of it with 2 additional parameters given by Sitko et al. (1993):

$$r_{evap} = 9{\times}10^8\ L_{UV,46}^{0.5}\ T^{-2.8}\ [0.05/A_\mu]^{0.5}\ e^{-\tau/2} pc \qquad (3)$$

where A_μ is graphite grain size in μ, τ - is optical depth of the clouds in UV. We will use following to Sitko et al. the same values of parameters: $T = 1700$ K, $A_\mu = 0.15$, $\tau = 1$.

3. Observational data on the Optical-to-NIR time delays in AGNs

By now, the time delay between optical (UV) and NIR variations has been detected in several AGNs. The data on these objects (including our results) are given in the Table 1. The data which are not quite reliable (for example, results for IIIZw2 (Lebofsky and Reike 1980) and NGC 1566 (Baribaud et al. 1992) were not included in the table. The objects where NIR radiation has nonthermal origin (BLACs) and objects with a peculiar orientation, presence of superluminal radio components (for example, 3C273) were not considered in the paper too.

4. Estimation of H_0

Observed data are very good following to the theoretical relation (3) for $H_0 = 50\ km\ s^{-1}\ Mpc^{-1}$ (see Fig.1).

So using (2) we have got the estimation

$$H_0 \sim\ 50\ km\ s^{-1}\ Mpc^{-1}. \qquad (4)$$

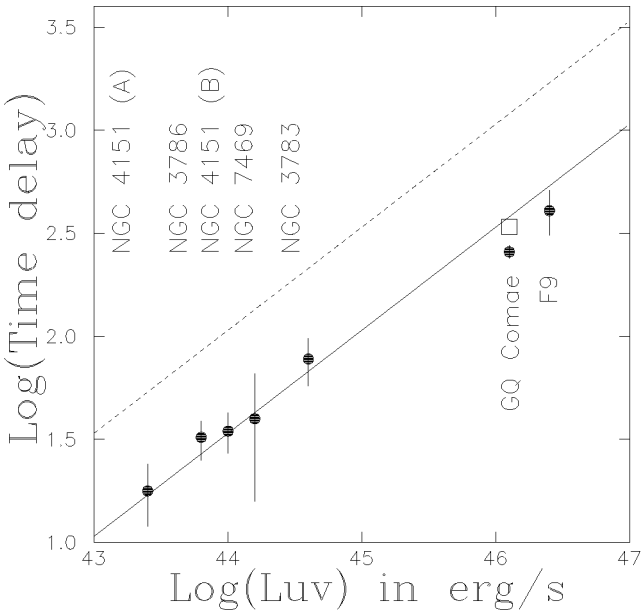

Figure 1: Dependence luminosity – time delay in logarithmic scale. Line corresponds to the theoretical dependence (3), dashed line - to the (1). Points correspond to the time delay data (for filter K) from Table 1 and UV luminosities estimated for $H_0 =$ 50 km s^{-1} Mpc^{-1} from the observed fluxes. A box corresponds to the time delay for GQ Comae corrected for the red shift (z=0.165).

Table 1: AGNs with detected lag between the IR and optical or UV variations

Object	Δt, lag days (1 from 2)	Band (1 - 2)	References
NGC4151	$30 \div 60$	$L(UBV)$	Penston et al., 1994
	18 ± 6	$K(U)$	Oknyanskij 1993
	35 ± 8	$K(UBV)$	Oknyanskij
	97 ± 10	$L(UBV)$	et al.,1999
	8 ± 4	$H(UBV)$	
	~ 6	$J(UBV)$	
NGC3786	32 ± 7	$K(V)$	Nelson,1996)
NGC3783	~ 78	$K(U)$	Glass,1992
F9	410 ± 110	$L(UV)$	Clavel
	385 ± 100	$K(UV)$	et al.,1989
	250 ± 100	$H(UV)$	
	-20 ± 100	$J(UV)$	
NGC7469	–	JHLK	Glass,1998
	0 ± 25	$J(U)$	This paper
	41 ± 25	$K(U)$	
	≥ 65	$L(U)$	
	40 ± 20	$K(J)$	
	73 ± 15	$L(J)$	
	30 ± 20	$H(J)$	
GQ Comae	~ 250	$K(UV)$	Sitko
	~ 700	$L(UV)$	et al.,1993
	260 ± 20	$K(V)$	This paper
	750 ± 20	$L(V)$	

Summary

We have combined published data on the optical-to NIR time delay in AGNs. We have made cross-correlation analysis of published data using own code and have found the new values of time delays for NGC4151, 7469, GQ Comae.

We show that the observed time delays allow us to derive an estimate of the Hubble constant value, however it is model dependent.

The results presented here will be used as the groundwork for more detailed paper which is in preparation.

Acknowledgements. The author are thankful to Prof. K.Horn for useful discussions.

References

Baribaud T., Aloin D., Glass I. S., Pealat D.: 1992, *Astron. Astrophys.,* **256**, 375.
Barvainis R.: 1987, *Ap.J.,* **320**, 537.
Barvainis R.: 1992, *Ap.J.,* **400**, 502.
Clavel J., Wamsteker W., Glass I. S.: 1989, *Ap.J.,* **337**, 236.
Collier S., Horn K., Wanders I., Peterson B. M.: 1999, *MNRAS*, **302**, L24.
Glass I.S.: 1992, *M.N.R.A.S.,* **256**, 23P.
Glass I.S.: 1998, *M.N.R.A.S.,* **297**, 18.
Goodwin S.P., Gribbin J., Hendry M.A.: 1997, *A.J.,* **114**, 2212.
Freedman W. et al.: 1989, *Ap.J.Suppl.Ser.,* **69**, 763.
Lebofsky M.J., Reike G.H.: 1980 *Nature,* **284**, 410.
Miyoshi M. et al.: 1995 *Nature,* **373**, 127.
Nelson B.O.: 1996, *Ap.J.,* **465**, 87.
Oknyanskij V.O.: 1994, *Astron. Lett.,* **19**, 416.
Oknyanskij V.O.: 1999, *Astron. Lett.,* **25**, 483.
Penston M.V., Balonek, T. J., Barker, E. S. et al.: 1974, *M.N.R.A.S,* **159**, 357.
Refsdal S.: 1964 *MNRAS,* **128**, 295.
Sandage A. et al.: 1996, *Ap.J.,* **460**, L15.
Sanders D.B. et al.: 1989, it Ap.J., **347**, 29.
Sitko M.L., Sitko A.K., Siemiginowska A., Szczerba R.: 1993, *Ap.J.,* **409**, 139.
Syunyaev R.A., Zel'dovich Y.B.: 1980, *Ann. Rev. Astron. Ap.,* **18**, 537.

ON THE EVOLUTIONARY STATUS OF LOW-METALLICITY BLUE COMPACT GALAXIES

L.S. Pilyugin

Main Astronomical Observatory of National Academy of Sciences of Ukraine
Goloseevo, Kiev, 03680, Ukraine, *pilyugin@mao.kiev.ua*

ABSTRACT. A remarkably small scatter in the N/O ratios for the HII regions in low-metallicity blue compact galaxies (BCG) has been found recently by Izotov and Thuan. They have concluded that these galaxies are presently undergoing their first burst of star formation, and that nitrogen measured in these galaxies is produced by massive stars in the current star formation burst only. Here it has been tested whether this interpretation is compatible with other observational data and with the existing ideas on the chemical evolution of galaxies.

It has been found that the existence of systems (damped Lα absorbers) in which the N/Si ratios are lower than in low-metallicity BCGs and the chemical homogeneity of star-forming BCGs are in conflict with conclusion that the massive stars from current star formation event are responsible for the nitrogen abundance measured in low-metallicity BCGs. The low-metallicity BCGs seem to be systems with a small amount of old underlying stellar population over which the current star formation burst is superposed; only the stars from the previous star formation event(s) are responsible for the observed chemical composition in the giant HII regions in these galaxies.

Key words: Galaxies: irregular: evolution

1. Introduction

Assumption that BCGs can be young systems is widely discussed after it was initially suggested by Searle & Sargent (1972). In order to reproduce the observed properties of low-metallicity BCGs, only a few (in some cases only one or two) star formation bursts during their life are required (Tosi 1994). Papaderos et al (1998) have found that the spectrophotometric properties of SBS 0335-052, the second most metal-poor known BCD, can be accounted for by a stellar population not older than $\sim$ 100 Myr. The possibility of an underlying old stellar population with mass not exceeding $\sim$ 10 times that of young stellar population mass however cannot be definitely ruled out on the basis of the spectrophotometric properties. Then, in addition to the spectrophotometric properties, the element abundance ratios (in particular the N/O abundance ratios) are used in order to establish the evolutionary status of galaxies.

It is believed that both the massive and intermediate mass stars make contributions to the nitrogen production, but the mass range of the nitrogen-producing stars and the predicted amount of freshly produced nitrogen depend on poorly known parameters (Renzini and Voli, 1981; Marigo et al 1996; Marigo et al 1998; van den Hoek and Groenewegen 1997). The time variation of N/O ratio in the interstellar medium of the system after star formation burst has the characteristic feature. Since the bulk of oxygen is produced by short-living massive stars and part of nitrogen is produced by relatively long-living intermediate-mass stars, there is a temporary decrease of the N/O ratio after star formation event. The value of N/O decrease depends on the contribution of intermediate-mass stars to the nitrogen production and on the initial metallicity of gas where the star formation event takes place. The N/O ratio corresponding to the early stage (before ejecta of intermediate - mass stars) of the first star formation event is a lower limit for the global N/O ratios. The best way to find the lower limit of N/O ratio and hence the amount of nitrogen produced by massive stars would be an undisputable determination of the N/O ratios in galactic halo stars. Unfortunately, at the present state their N/O ratios cannot be determined with a precision better than a factor 2 or 3 (Carbon et al 1987).

Izotov and Thuan (Thuan et al 1995; Izotov and Thuan 1999) have found a remarkably small scatter ($\pm$ 0.02 *dex*) in the N/O ratios of the HII regions in low-metallicity (with 12+logO/H $\leq$ 7.6) BCGs. They concluded that these galaxies are presently undergoing their first burst of star formation, and that nitrogen in these galaxies is produced by massive stars only. (Strictly speaking, the constancy of N/O ratio during the early stage of the first star formation event will takes place if stellar nitrogen yields $Y_N(M_S)$ and oxygen yields $Y_O(M_S)$ are related by the following equation $Y_N(M_S) = const \times Y_O(M_S)$ for star of every mass M_S out of mass range $M_S \geq 10\ M_\odot$.) If low-metallicity BCGs galaxies are presently undergoing their first burst of star formation, the N/O ratio

observed in these galaxies would be a lower limit for the global N/O ratios. This is in conflict with the fact that the nitrogen to α-element abundance ratios measured in some DLAs are well below than the value observed in low-metallicity BCGs (Lu et al 1998 and references therein). (Since oxygen abundance measurements are not available for DLAs, $[N/S]$ or $[N/Si]$ ratios are considered instead of $[N/O]$. This is justified by the fact that there is no reason to believe that the relative abundances of O, S and Si which are all produced in Type II supernovae are different from solar in DLAs.)

Thus the question arises whether the constancy of the N/O ratios in low-metallicity BCGs and the scatter of the N/Si ratios in DLAs are compatible with each other and with the existing ideas on the chemical evolution of galaxies.

2. Possible interpretation of nitrogen abundances in BCGs and DLAs

Here we will demonstrate that the constancy of the N/O ratios in low-metallicity BCGs and the scatter of the N/Si ratios in DLAs can be reconciled under the assumptions that a significant part of nitrogen is produced by intermediate-mass stars, and the previous star formation events are responsible for heavy element abundances observed in the HII regions of the BCGs.

Assumption that previous star formation events are responsible for the observed heavy element abundances in BCGs is equivalent to say that the element abundances of HII regions in BCGs are not yet polluted by the stars of the present star formation event, and that their abundances reflect the average N/O in the galaxy, which results from cumulative previous star formation. Martin (1996) has found that the current event of star formation in the most metal-poor known blue compact galaxy I Zw 18 started 15-27 Myr ago. The duration of current star formation burst in another extremely metal-poor blue compact galaxy SBS 0335-052 (Papaderos et al 1998) is also in excess of the lifetime of the most massive stars. Therefore, a selection effect in favor of observations of young HII regions in which the massive stars had not yet have time to explode as supernovae cannot be reason why the HII regions are not observed as self-enriched. Massive stars in the current star formation burst have often had time to synthesize heavy elements and to eject them via stellar winds and supernova explosions into the surrounding interstellar gas. Kunth and Sargent (1986) suggest that the heavy elements produced by massive stars in the current star formation burst mix immediately into H II region, i.e. the giant H II regions are self-enriched. Given the time delay between the injection of nitrogen by intermediate-mass stars and that of oxygen by shorter lived massive stars (the time – delay hypothesis: Edmunds & Pagel 1978) and the hypothesis of self-enrichment of star formation regions (Kunth & Sargent 1986), models for the chemical evolution of dwarf galaxies predicting the large scatter in N/O at fixed O/H in low-metallicity dwarf galaxies have been constructed (Garnett 1990; Pilyugin 1992, 1993; Marconi et al 1994).

However, it is possible that the nucleosynthetic products of massive stars are in high stages of ionization and do not make appreciable contribution to the element abundance as derived from optical spectra (Kobulnicky and Skillman 1997; Kobulnicky 1999). Indeed, the oxygen abundance in SBS 0335-052 has been measured within the region of 3.6 kpc (Izotov et al 1997). There is a supershell of radius $\sim$ 380 pc. There is no significant difference in oxygen abundances inside and outside the supershell as it should be expected since $\sim$ 1500 supernovae are required to produce this supershell (Izotov et al 1997). Other star-forming galaxies, which are chemically homogeneous despite the presence of multiple massive star clusters, are reported by Kobulnicky and Skillman (1998). This can be considered as evidence that the nucleosynthetic products of massive stars in giant HII regions are hidden from optical spectroscopic searches because they are predominantly found in a hot, highly – ionized superbubble. It should be noted however that some fraction of supernova ejecta can mix with dense clouds changing their chemical composition. If such cloud survives and produces a subgroup of stars shortly, the star formation region will have sub-generations of stars with different chemical composition. This seems to be the case in the Orion star formation region (Cunha and Lambert 1994; Pilyugin and Edmunds 1996).

If the suggestion that the heavy elements ejected by massive stars are in hot superbubble for a some time and do not mix immediately into the giant HII region is correct, the time variation of the N/O ratio in the warm gas phase after star formation event does not agree with the time variation of the N/O ratio in the interstellar medium as a whole. Hot and warm gas phases have different chemical compositions. The chemical composition of warm gas within star formation region remains unaltered and is equal to the initial chemical composition of gas where the star formation event takes place. A temporary decrease of the N/O ratio takes place in cold gas phase after that the bubble disappeared and the nucleosynthetic products of massive stars mix with ambient interstellar medium.

With this behaviour of the N/O ratio, the nitrogen abundances measured in BCGs and DLAs can be interpreted in the following way (Pilyugin 1999). The low-metallicity BCGs are systems with a small amount of old underlying stellar population over which the current star formation burst is superposed; only the stars from the previous star formation event(s) are responsible for the observed chemical composition in the

giant HII regions in these galaxies. In other words, the abundances mesured in giant HII regions in BCGs reflect the average N/O in the galaxy, which results from cumulative previous star formation. The DLA observations sample the general ISM at random times along random lines of sight and may or may not see a region where a star formation event occured in a recent past. The DLAs with low nitrogen to α-element ratios correspond to systems probed less than around 1 Gyr after the last local star formation event, but after a time sufficient for disappearance of the superbubble and mixing of the freshly produced heavy elements in the interstellar medium. Conversely, the DLAs with nitrogen to α-element ratios close to that in low-metallicity BCGs correspond to systems in which the time interval after last star formation event is sufficiently large for intermediate-mass stars to have substantially enhanced the nitrogen to α-element abundance ratios.

3. Conclusions

It has been found that the existence of systems (damped Lα absorbers) in which the N/Si ratios are lower than in low-metallicity BCGs and the chemical homogeneity of star-forming BCGs are in conflict with conclusion that the massive stars from current star formation event are responsible for the nitrogen abundance measured in low-metallicity BCGs.

The low-metallicity BCGs seem to be systems with a small amount of old underlying stellar population over which the current star formation burst is superposed; only the stars from the previous star formation event(s) are responsible for the observed chemical composition in the giant HII regions in these galaxies.

Acknowledgements. I would like to thank Drs. N.G. Guseva and Y.I. Izotov for fruitful discussions. I thank the Organizing Committee of the Gamow Memorial International Conference for the financial support of my participation in the meeting. This research was supported in part by INTAS grant No 97-0033.

References

Carbon D.F., Barbuy B., Kraft R.P., Friel E.D., Suntzeff N.B.: 1987, *P.A.S.P.*, **99**, 335
Cunha K., Lambert D.L.: 1994, *Ap.J.*, **426**, 170
Edmunds M.G., Pagel B.E.J.: 1978, *M.N.R.A.S.*, **185**, 77p
Garnett D.R.: 1990, *Ap.J.*, **363**, 142
Izotov Y.I., Lipovetsky V.A., Chaffee F.H., Foltz C.B., Guseva N.G., Kniazev A.Y.: 1997, *Ap.J.*, **476**, 698
Izotov Y.I., Thuan T.X.: 1999, *Ap.J.*, **511**, 639
Kobulnicky H.A.: 1999, *astro-ph* 9901260
Kobulnicky H.A., Skillman E.D.: 1997, *Ap.J.*, **489**, 636
Kobulnicky H.A., Skillman E.D.: 1998, *Ap.J.*, **497**, 601
Kunth D., Sargent W.L.W.: 1986, *Ap.J.*, **300**, 496
Lu L., Sargent W.L.W., Barlow T.A.: 1998, *Ap.J.*, **115**, 55
Marconi G., Matteucci F., Tosi M.: 1994, *M.N.R.A.S.*, **270**, 35
Marigo P., Bressan A., Chiosi C.: 1996, *As.Ap.*, **313**, 545
Marigo P., Bressan A., Chiosi C.: 1998, *As.Ap.*, **331**, 564
Martin C.L.: 1996, *Ap.J.*, **465**, 680
Papaderos P., Izotov Y.I., Fricke K.J., Thuan T.X., Guseva N.G.: 1998, *As.Ap.*, **338**, 43
Pilyugin L.S.: 1992, *As.Ap.*, **260**, 58
Pilyugin L.S.: 1993, *As.Ap.*, **277**, 42
Pilyugin L.S.: 1999, *As.Ap.*, **346**, 428
Pilyugin L.S., Edmunds M.G.: 1996, *As.Ap.*, **313**, 792
Renzini A., Voli M.: 1981, *As.Ap.*, **94**, 175
Searle L., Sargent W.L.W.: 1972, *Ap.J.*, **173**, 25
Thuan T.X., Izotov Y.I., Lipovetsky V.A.: 1995, *Ap.J.*, **445**, 108
Tosi M.: 1994, in *Dwarf Galaxies*, Eds. Meylan G., Prugniel P., (Garching: Europen Southern Observatory), p. 465
van den Hoek L.B., Groenewegen M.A.T.: 1997, *As.Ap.S.S.*, **123**, 305

ON ANOMALOUS DIELECTRIC FUNCTION OF INTERSTELLAR GRAIN IN FAR INFRARED

I.S. Altman[1], P.V. Pikhitsa[2]

[1] Physical Department, Odessa State University
Dvoryanskaya 2, Odessa, 65026 Ukraine, *ialtman@tm.odessa.ua*
[2] Physics Institute of Odessa State University
Pasteur's 27, Odessa, 65026 Ukraine, *pvp@dtp.odessa.ua*

ABSTRACT. We show that the fact that the thermal radiation from small particles follows the Wien law instead of the Planck one should lead to the anomalous wavelength dependence of the far-infrared emission efficiency of interstellar grain substance. We claim that photoconductivity of interstellar grains induced by the ultraviolet radiation from a hot star may account for this dependence.

Key words: dust, extinction.

1. Introduction

Interstellar dust plays important role in evolution of both the entire Universe and separate astrophysical objects (galaxies, nebulae, stars). It is the reason for a great number of papers on investigation of properties of various dust conglomerates to appear (see, for example, (Dwek & Arendt 1992; Siebenmorgen 1993; Williams 1997; Hughes, Dunlop & Rawlings 1997; Mathis 1998; Duley & Poole 1998; Howk & Savage 1998) and references therein).

The information about the spectral dependence of extinction of optically thin dust clouds and their radiation spectra is usually obtained from experiment. It is assumed that by this information one can reconstruct the composition, temperature and mass of dust conglomerates in the following way (Spitzer 1978; Bochkarev 1990). Indeed, the spectral dependence of extinction in the visual and UV range allows one to estimate the sizes of dust grains. The peculiarities of extinction in near IR region give the information about the spectra of absorption of the dust matter (what gives a possibility to identify the dust material). The IR spectrum of radiation informs us about the temperature of dust grains. The total IR luminosity of a dust conglomerate can be used for estimation of its mass.

This seemingly perfect scheme for investigation of interstellar dust must be changed if one takes into account that for the description of radiation of small dust grains one should use instead of the Planck formula (with the Rayleigh-Jeans tail in IR) the Wien one (Altman 1999).

In the present paper we will analyze the known far-infrared spectra of interstellar grains illuminated by a hot star as a rule. The use of the Wien formula will allow us to reveal the anomalous spectral dependence of the interstellar grain dielectric function. In order to explain this dependence we predict the photoconductivity mechanism of light absorption in grains of interstellar dust.

2. Anomalous dielectric function of dust

Specifically, the observed radiation flux at a given wavelength λ from a dust conglomerate takes the form (Pipher, Duthie & Savedoff 1978):

$$F_\lambda = 3D\Omega B_\lambda\left(T_g\right)\tau, \tag{1}$$

where Ω is the beam size, $B_\lambda\left(T_g\right)$ is the Planck function, T_g is the grain temperature and the optical depth of the dust cloud τ (which is considerably less than unity) is proportional to the grain absorption efficiency at the wavelength λ (Bohren & Huffman 1983):

$$Q_{abs}\left(\lambda\right) = 3D\frac{8\pi a}{\lambda}\mathrm{Im}\frac{\epsilon-1}{\epsilon+2}. \tag{2}$$

Here a is the radius of a grain (which is considered spherical) and $\epsilon = 3D\epsilon' + i\epsilon''$ is the complex dielectric function of the grain substance at the wavelength λ. Eq.(2) can be transformed into

$$Q_{abs}\left(\lambda\right) = 3D\frac{24\pi a}{\lambda}\frac{\epsilon''}{\left(\epsilon'+2\right)^2+\left(\epsilon''\right)^2}. \tag{3}$$

Since usually $\epsilon'' \ll \epsilon'$ and within the IR range $\epsilon' \approx const$ it is considered that it is possible to reconstruct the spectral dependency of ϵ'' by the observed flux F_λ, taking into account that in the IR the Planck function is given by the Rayleigh-Jeans tail $B_\lambda\left(T_g\right) \propto \lambda^{-4}$.

Therefore

$$Q_{abs}(\lambda) \propto \frac{F_\lambda}{B_\lambda(T_g)} \propto F_\lambda \lambda^4 \equiv \lambda^{-\beta} \qquad (4)$$

In different experiments (Pipher et al. 1978; Thronson & Harper 1979; Rowan-Robinson 1979; Chini et al. 1984; Rengarajan et al. 1985; Hughes et al. 1997; Eyres et al. 1997) the exponent β (which is defined in accordance with Eq.(4)) has been obtained to be ≈ 1 and therefore $\epsilon'' \propto Q_{abs}(\lambda)\,\lambda \approx const$.

We, however, think that this result can not be correct. Indeed, as it is shown in (Altman 1999) the intensity of thermal radiation from a small grain should contain the Wien function $B_\lambda^W(T_g)$ instead of the Planck one:

$$B_\lambda^W(T_g) = 3DB_\lambda(T_g)\left[1-\exp\left(-\frac{hc}{\lambda k T_g}\right)\right]. \qquad (5)$$

This function should replace $B_\lambda(T_g)$ in Eq.(1) and Eq.(4). Then, because the IR asymptotic behavior of the Wien function is $B_\lambda^W(T_g) \propto \lambda^{-5}$ the correct spectral dependency of ϵ'' which corresponds to the experimentally observed β should be $\epsilon''(\lambda) \propto \lambda \sim 1/\nu$.

Such a behavior of ϵ'' against frequency ν indicates the conductivity mechanism of light absorption at low frequencies, specifically (Landau & Lifshitz 1982),

$$\epsilon'' = 3D\frac{\sigma_e}{2\pi\epsilon_0\nu}, \qquad (6)$$

where σ_e is the conductivity of the substance and ϵ_0 is the dielectric permittivity of vacuum. The prevailing of the conductivity mechanism of light absorption over the phonon one (the latter would give

$\epsilon''(\lambda) \propto \nu$ (Seki & Yamamoto 1980)) at the grain temperature (~ 50 K) can not be due to the thermal induced conductivity. On our opinion this conductivity mechanism is due to the photoconductivity induced by the external high-energy radiation from the hot nucleus of the duct conglomerate.

3. Photoconductivity of a dust grain

Let us estimate the equilibrium concentration of photoconductivity electrons in a grain. Assume that the grain substance be solid dielectric with the energy gap E_g. We will consider that a photon of the energy above E_g, colliding the grain, creates an electron-hole pair with probability one (Bonch-Bruevich & Kalashnikov 1977). If the central region of the dust conglomerate has the temperature T_s and the radius R_s, and the grain is located at the distance R_g from the center then the generation rate of electron-hole pairs in the grain may be estimated as

$$\frac{dN}{dt} = 3D\int_0^{hc/E_g} \frac{\pi B_\lambda(T_s)}{(hc/\lambda)}\left(\frac{R_s}{R_g}\right)^2 \pi a^2 d\lambda. \qquad (7)$$

Performing integration in Eq.(7) we obtain

$$\frac{dN}{dt} \approx \frac{15\sigma T_s^3}{\pi^4 k_B}\left(\frac{R_s}{R_g}\right)^2 \pi a^2 f(x), \qquad (8)$$

where k_B is the Boltzmann constant, σ is the Stefan-Boltzmann constant, $x = 3DE_g/(k_B T_s)$ and $f(x) \equiv \left(x^2+2x+2\right)\exp(-x)$.

Taking into account that the equilibrium electron concentration n_e corresponds to the situation when the generation rate is equal to the rate of electron-hole recombination we can write (see, for example, (Bonch-Bruevich & Kalashnikov 1977))

$$\frac{dN}{dt} = 3D\sigma_c v\frac{4\pi}{3}a^3 n_e^2, \qquad (9)$$

where σ_c is the recombination cross section and v is the electron velocity at the grain temperature. Then we find

$$n_e = 3D\left[\frac{45\sigma T_s^3}{4\pi^4 k_B}\left(\frac{R_s}{R_g}\right)^2 \frac{f(x)}{\sigma_c v a}\right]^{1/2}. \qquad (10)$$

For typical values $T_s = 3D30000$ K, $E_g = 3D6$ eV, $(R_s/R_g)^2 = 3D10^{-12}$, $a = 3D10^{-8}$ m, $\sigma_c = 3D10^{-22}$ m^2 and $v_e = 3D5\times10^4$m s^{-1} we get $n_e \approx 6\times10^{20}$m^{-3}. The electron conductivity of the grain substance can be calculated by the formula $\sigma_e = 3Den_e\mu_e$, where e is the electron charge and μ_e is the electron mobility. Choosing $\mu_e = 3D0.01$m^{2}V^{-1}s^{-1} (which is appropriate for wide energy gap dielectrics) we obtain $\sigma_e \approx 1\Omega^{-1}$m^{-1}. For $\lambda = 3D150\mu$m this conductivity gives a contribution to ϵ'' of order of 10^{-2} and for longer wavelengths ϵ'' due to photoconductivity overcomes the phonon part (which, for instance, for possible grain substance - MgO (Mathis 1996) is of order 10^{-3} at this wavelength (Jasperse et al. 1966)) and becomes the leading term so that Eq.(6) holds.

Note, that the value of ϵ'' restored from the typical mass-absorption coefficient 0.15 m^{2}kg^{-1} (Hughes et al. 1997) of a grain at wavelength 800μm with the help of Eq.(3) is of order 10^0. Such a big value of ϵ'' can be explained only on the base of the conductivity mechanism of absorption (Bohren & Huffman 1983).

4. Summary

Summarizing we point out that when the IR spectra of interstellar dust grains are under investigation one should use the Wien formula for restoration of dust substance properties. For the known experimental spectra it brought us to the conclusion that the interstellar grain substance is characterized by the anomalous dielectric function. To explain this anomaly we put forward the assertion that the dielectric losses in interstellar dust, in the IR at least, are due to the photoconductivity of dust grains induced by strong ultraviolet

radiation from the hot central star. The estimation we made showed the possibility of such a mechanism. We also think that the existence of the hot photoinduced electrons in the dust substance may lead to some peculiarities of dust extinction in visual and UV regions.

References

Altman I. S.: 1999, *Phys. Lett. A*, **256**, 122.

Bochkarev N. G.: 1990, *Basics of Interstellar Medium Physics,* Moscow: MGU Publishers.

Bohren C. F., Huffman D. R.: 1983, *Absorption and Scattering of Light by Small Particles,* New York: Wiley.

Bonch-Bruevich V. L., Kalashnikov S. G.: 1977, *Physics of Semiconductors*, Moscow: Nauka.

Chini R., Kreysa E., Mezger P. G., Gemund H.-P.: 1984, *As. Ap.*, **137**, 117.

Duley W. W., Poole G.: 1998, *ApJ*, L113.

Dwek E., Arendt R. G.: 1992, *ARAA*, **30**, 11.

Eyres S. P. S., Evans A, Geballe T. R., Davies J. K., Rawlings J. M. C.: 1997, *ApSS*, **251**, 303.

Howk J. C., Savage B. D.: 1998, *astro-ph/9810442.*

Hughes D. H., Dunlop J. S., Rawlings S.: 1997, *MNRAS*, **289**, 766.

Jasperse J. R., Kahan A., Plendl J. N., Mitra S. S.: 1966, *Phys. Rev.*, **146**, 526.

Landau L. M., Lifshitz E. M. 1982, *Electrodynamics of Continuous Media*, Moscow: Nauka.

Mathis J. S.: 1996, *ApJ*, **472**, 643.

Mathis J. S.: 1998, *ApJ*, **497**, 824.

Pipher J. L., Duthie J. G., Savedoff M. P.: 1978, *ApJ*, **219**, 494.

Rengarajan T. N., Fazio G. G., Maxson C. W., McBreen B., Serio S., Sciortino S.: 1985, *ApJ*, **289**, 630.

Rowan-Robinson M.: 1979, *ApJ*, **234**, 111.

Seki J., Yamamoto T.: 1980, *ApSS*, **72**, 79.

Siebenmorgen R.: 1993, *ApJ*, **408**, 218.

Spitzer L.: 1978, *Physical Processes in the Interstellar Medium*, New York: Wiley.

Thronson H. A., Jr., Harper D. A.: 1979, *ApJ*, **230**, 133.

Williams P. M.: 1997, *ApSS*, **251**, 321.

THE CYCLOTRON EMISSION OF ANISOTROPIC ELECTRONS IN THE X-RAY PULSARS

A.N. Baushev[1], G.S. Bisnovatyi-Kogan[2]

[1] Space Research Institute, Profsoyuznaya, 84/32, Moscow 117810, Russia, *abaushev@mx.iki.rssi.ru*

[2] Space Research Institute, Profsoyuznaya, 84/32, Moscow 117810, Russia, *gkogan@mx.iki.rssi.ru*

ABSTRACT. The spectrum of cyclotron radiation is calculated for anisotropically distributed relativistic electrons with a nonrelativistic velocity scattering across the magnetic field. It is shown that if such electrons are responsible for a formation of the "cyclotron" line in the spectrum of Her X-1, then the value of its magnetic field $(3-6)\cdot 10^{10}$ Gs following from this interpretation is in a good agreement with some other observations and theoretical estimations. Observations of a time dependence of the energy of this "cyclotron" line in the spectra of several X-ray pulsars is explained by a variability of the average longitude energy of the electrons, decreasing with increasing of the liminocity due to radiational braking of the accretion flow.

Key words: X-ray pulsars; cyclotron emission.

1. Introduction

There are a lot of observations of the cyclotron resonance structure in the X-ray spectrum of pulsar Her X-1 (Tueller et al. (1984), Trümper et al. (1978), Voges et al. (1982), Gruber et al. (1980), Ubertini et al. (1980), Sheepmaker et al. (1981)) at 39-58 KeV (see Table 1, was taken from Tueller et al. (1984). This singularity is interpreted as a cyclotron line, and the magnetic field intensity was usually calculated from the non-relativistic formula

$$H = \frac{mc\omega}{e}, \tag{1}$$

where ω is the cycle frequency of the photons, m is the mass of the electron. It was obtained to be of the order of $(3-5)\cdot 10^{12}$ Gs. But as large as this value comes into conflict with some theoretical reasonings like interpretation of the observations of pulsar spin acceleration (Bisnovatyi-Kogan & Komberg, 1973), condition for the transparency for the outgoing of the directed radiation (Bisnovatyi-Kogan, 1973; Bisnovatyi-Kogan, 1974) consideration of the interrelation between radio and X-ray pulsars Bisnovatyi-Kogan & Komberg (1974), simulation of the 35-days cycle variability (Sheffer et.al., 1992).

It seems likely that the reason of this conflict is an unsuitability of the non-relativistic formula in this case. According to Bisnovatyi-Kogan & Fridman (1969), the temperature of the electrons emitting a cyclotron line could be $\sim 10^{11}K$, and therefore they are ultrarelativistic. By this means the mean energy of the cyclotron line is broadened and shifted relativistically by a factor of $\gamma \simeq \frac{kT}{mc^2}$. In this article the spectrum profile of the cyclotron line is calculated for various electrons distributions. Furthermore, the model of the hot spot on the pulsar is considered and it is shown that the overall observed X-ray spectrum (from 0.2 to 120 KeV) can arise under the fields near the pulsar surface ($\approx 5\cdot 10^{10}$ Gs) which are well below then those, obtained from (1).

2. The cyclotron radiation of the anisotropic relativistic electrons

According to Gnedin & Sunyaev (1973) and Bisnovatyi-Kogan (1973), in the magnetic field near the pulsar the cross component of a momentum emits rapidly, while the parallel component remains constant. Hence the momentum distribution of the electrons is anisotropic

$$p_\perp^2 \ll p_\parallel^2, \tag{2}$$

where $p_\perp \ll mc$, $p_\parallel \gg mc$. In this article we assume for simplicity that the transverse electron distribution is two-dimensional Maxwellian

$$dn = \frac{N}{T_1}\exp\left(-\frac{mu^2}{2T_1}\right) d\frac{mu^2}{2}, \tag{3}$$

where $T_1 \ll mc^2$. Let us calculate the cyclotron emission of N such particles that move at a rate V along the magnetic field.

For a single particle, having the transverse velocity u, we find (Ginzburg, 1975):

$$j(\theta) =$$

$$\frac{e^4H^2u^2(1-\frac{V^2}{c^2})^2[(1+\cos\theta)(1+\frac{V^2}{c^2})-4\frac{V}{c}\cos\theta]}{8\pi c^5m^2(1-\frac{V}{c}\cos\theta)^5}, \tag{4}$$

where θ is an observational angle in a laboratory frame of reference. Integrating over the distribution (3), we obtain for N particles:

$$J(\theta)=\int j(\theta)dn,$$

$$J(\theta)=$$

$$=N\frac{e^4H^2T_1(1-\frac{V^2}{c^2})^2[(1+\cos\theta)(1+\frac{V^2}{c^2})-4\frac{V}{c}\cos\theta]}{4\pi c^5m^3(1-\frac{V}{c}\cos\theta)^5}. \tag{5}$$

For the spectrum we find:

$$\omega(\theta)=\omega_H\frac{\sqrt{1-\frac{V^2}{c^2}}}{1-\frac{V}{c}\cos\theta},\quad \omega_H=\frac{eH}{mc}. \tag{6}$$

When $V\simeq c$ the cyclotron radiation is highly directed and diagram has a pencil beam along V ($\theta\simeq 0$). Under these conditions ($\theta=0, V\simeq c$) we obtain from (5),(6):

$$J(0)=\frac{2Ne^4H^2T_1}{\pi c^5m^3(1-\frac{V}{c})}, \tag{7}$$

$$\omega(0)=\omega_H\sqrt{\frac{1+\frac{V}{c}}{1-\frac{V}{c}}}\approx 2\omega_H\frac{E_\parallel}{m_ec^2}, \tag{8}$$

what gives

$$1-\frac{V}{c}=\frac{2\omega_H^2}{\omega^2}. \tag{9}$$

Let us consider the parallel momentum distribution of the electrons as:

$$dn=f(p_\parallel)\,dp_\parallel. \tag{10}$$

Substituting of dn for N and using

$$p_\parallel=\frac{mc}{2}\frac{\omega}{\omega_H};\quad 1-\frac{V}{c}=\frac{2\omega_H^2}{\omega^2}, \tag{11}$$

we obtain for the spectral density:

$$J_\omega=\frac{e^2T}{2\pi c^2\omega_H}\omega^2 f\left(-\frac{mc}{2}\frac{\omega}{\omega_H}\right)d\omega. \tag{12}$$

Let us consider two important cases. When f is a relativistic Maxwell:

$$f=\frac{n_0c}{T_2}\exp\left(-\frac{p_\parallel c}{T_2}\right),\quad T_2\gg mc^2\gg T_1, \tag{13}$$

where n_0 is a number of emitting electrons. Then the spectrum is:

$$J_\omega=\frac{n_0e^2}{2\pi c\omega_H}\frac{T}{T_2}\omega^2\exp\left(-\frac{mc^2\omega}{2\omega_HT_2}\right)d\omega. \tag{14}$$

This spectrum has a single maximum at

$$\frac{\omega}{\omega_H}=\frac{4T_2}{mc^2}. \tag{15}$$

In the second case consider the function f as

$$f=\frac{n_0}{\sqrt{\pi}\sigma}\exp\left(-\frac{(p_\parallel-a)^2}{\sigma^2}\right). \tag{16}$$

The spectrum of radiation is

$$J_\omega=\frac{n_0e^2}{2\pi c^2\omega_H}\omega^2\exp\left(-\frac{(\frac{mc}{2}\frac{\omega}{\omega_H}-a)^2}{\sigma^2}\right)d\omega. \tag{17}$$

When $\sigma\ll a$ this spectrum has a single maximum at

$$\omega\simeq\frac{2a}{mc}\omega_H. \tag{18}$$

Notice that in all cases the maximum is shifted to

$$\frac{\omega}{\omega_H}\sim\frac{\bar{E}_e}{mc^2}. \tag{19}$$

It is a common property of relativistic cyclotron line, that is independent of the particular form of f. We had approximated experimental spectrum taken from Mihara et al. (1990) (solid line) by (14),(17), and spectrum McCray et al. (1982) by (17) only. Setting (in accordance with Bisnovatyi-Kogan & Fridman (1969)) the longitude electron temperature as $\sim 2\cdot10^{11}$ K, that is $T_2=2\cdot10^{11}$ K and $a=7\cdot10^{-4}$ $\frac{\text{eV}\cdot\text{s}}{\text{cm}}$, we obtain for the magnetic field strength $B=4\cdot10^{10}$ Gs, $8\cdot10^{10}$ Gs, and $4\cdot10^{10}$ Gs respectively. Here we estimate the spectral form of the cyclotron line averaged over the pulsar period, supposing uniform distribution of $f(p\parallel)$ over the polar cap. In this model the beam of the cyclotron feature is determined by the number distribution of the emitting relativistic electrons, moving predominantly along the magnetic field, over the polar cap.

3. Model of the X-ray spectrum of Her X-1.

In order to obtain the whole experimental spectrum of the Her X-1 the following model of the hot spot is considered. A collisionless shock wave is generated in the accretion stream nearby the surface on the magnetic pole of a neutron star. In it's front the ultrarelativistic electrons are generated. It's worth mentioning that according to Bisnovatyi-Kogan (1973) and Gnedin & Sunyaev (1973) these electrons when generated can possess only small pitch-angle values and the condition (2) is fullfilled automatically. Under the shock there is a hot turbulent zone with a temperature T_e, and optical depth τ_e, and under this zone a heated spot on the surface of the neutron star with a smaller temperature is situated.

Table 1: Cyclotron resonance structure in the X-ray spectrum of pulsar Her X-1

Date	Article	$\omega_{\max}$(KeV)	Width(KeV)
1978,May	1	58	11^{+26}_{-11}
1977,Sep.	2	51	21^{+9}_{-7}
1978,Feb.	3	48	28 ± 7
1980,Apr.	3	54	11^{+14}_{-11}
1980,May.	4	49.5	18^{+6}_{-3}
1980,Sep.	5	39	27^{+21}_{-20}

Articles:
1 – Trümper et al. (1978)
2 – Voges et al. (1982)
3 – Gruber et al. (1980)
4 – Ubertini et al. (1980)
5 – Tueller et al. (1984).

The whole X-ray spectrum of pulsar Her X-1 was taken from McCray et al. (1982). There are three main regions in it: a quasi-Plankian spectrum between 0,3 and 0,6 KeV, that is generated near the magnetosphere of the X-ray pulsar; power-law spectrum $(0.6 \div 20)$ KeV with a rapid decrease at 20 KeV, and the cyclotron feature.

The power-law spectrum area appears as follows. A surface emits the black-body spectrum with a temperature T_s. Travelling through the turbulent zone this radiation is comptonized. This comptonized spectrum has been calculated according to Sunyaev & Titarchuk (1980) Setting the neutron star radius equal to 10 km, distance from the X-ray pulsar 6 Kps, hot spot area $S = 2 \cdot 10^{12}$ cm^2, we have found the best approximation conditions at $T_s = 1$ KeV, $T_e = 8$ KeV, $\tau_e = 14$. The best approximation of the X-ray spectrum of the pulsar Her X-1 agrees nicely with the experimental curve.

4. Discussion.

The observation of the variability of the cyclotron line is reported in Mihara et al. (1997) Ginga detected the changes of the cyclotron energies from 4 pulsars. The change is as much as 40 % in the case of 4U 0115+63. Larger luminosity of the source corresponds to smaller average energy of the cyclotron feature. These changes might be easily explained in our model. The velocity of the accretion flow decreases with increasing of the pulsar's luminosity because localy the luminosity is close to the Eddington limit. As a result the shock wave intensity drops as well as the energy of the ultrarelativistic electrons in it's front. The cyclotron energy decreases in accordance with (19).

5. Conclusion.

X-ray pulsar Her X-1 is one of the most interesting and most investigated of this kind of objects. In the spectra of the other pulsars there is also observed the cyclotron line, but these observations were less reliable. In all of these cases the magnetic field intensity turned out to be too large, if it is calculated according to the non-relativistic formula. The way to overcome this difficulty is proposed in this article. So the relativistic formula for the cyclotron line yields for the magnetic fields the value that is consistent with other observational data and many theoretical estimates.

References

Basko M.M., Sunyaev R.A.: 1976, *M.N.R.A.S.,* **175**, 395.

Bisnovatyi-Kogan G.S.: 1973, *Astron. Zhurn.*, **50**, 902.

Bisnovatyi-Kogan G.S.: 1974, *Astron. Zhurn.*, **51**, 443.

Bisnovatyi-Kogan G.S., Fridman A.M.: 1969, *Astron. Zhurn.*, **46**, 721.

Bisnovatyi-Kogan G.S., Komberg B.V.: 1973, *Astron. Tsirk.*, No. 784, 721.

Bisnovatyi-Kogan G.S., Komberg B.V.: 1974, *Astron. Zhurn.*, **51**, 373.

Ginzburg V.L.: 1975, *Theoretical physics and astrophysics*, "Nauka", Moscow.

Gnedin Yu.N., Sunyaev R.A.: 1973, *Astron. Astrophys.*, **25**, 233.

Gruber D.E., et al.: 1980, *Ap.J.(Letters)*, **240**, L27.

McCray R.A., Shull J.M., Boynton P.E., et al.: 1982, *Ap.J.*, **262**, 301.

Mihara T., Makishima K., Ohashi T. et al.: 1990, *Nature*, **346**, 250.

Mihara T., Makishima K., Nagase F.: 1997, *Proceedings of an international Workshop "All-sky X-ray Observations in the Next Decade",* 135.

Sheepmaker T., Jansen F.A., Deerenberg A.J.M., et al.: 1981, *Space Sci. Rev.*, **30**, 325.

Sheffer E.K., Kopaeva I.F., Averintsev M.B., et.al.: 1992, *Astron. Zhurn.*, **69**, 82.

Sunyaev R.A., Titarchuk L.G.: 1980, *Astron. Astrophys.*, **86**, 121.

Trümper J., Pietsch W., Reppin C., et al.: 1978, *Ap.J.*, **219**, 105.

Tueller J., Cline T.L., Teegarden B.J. et al.: 1984, *Ap.J.*, **279**, 177-183.

Ubertini P., Bazzano A., LaPadula C.D., et al.: 1980, *Proc. 17th Int. Cosmic-Ray Conf.*, Paris, **1**, 99.

Voges W., Pietsch W., Reppin C. et al.: 1982, *Ap.J.*, **263**, 803.

Zel'dovich Ya.B., Shakura N.I.: 1969, *Astron. Zhurn.*, **46**, 225.

INVESTIGATION OF THE IONIZED COMPONENT OF THE LOCAL INTERSTELLAR MEDIUM

N.G. Bochkarev[1], M.I. Ryabov[2], E.A.Isaeva[2]

[1] Sternberg Astronomical Institute, Moskow State University Moskow 119899 Russia, *boch@sai.msk.su*

[2] Odessa Observatory URAN-4, Radioastronomical Institute ... hb Pushkinskaya Str.37 Odessa 270011 Ukraine *astro@te.net.ua*

ABSTRACT. Based upon numerous observational data of variability in extragalactic radiosources of the southern sky at low frequences the possibility of obtaining information on ionized component structure in the Local Interstellar Medium (LISM) is investigate. The model of anisotropic structure of LISM developed by Bochkarev (1987) is compared with investigational results of extragalactic radio sources scintillation of the soutern sky at 80 and 160 MHz (Slee, Siegmen, 1988). In the direction where scintillation indices increase, regions of interaction of interstellar wind with large scale structure of LISM are located. Decrease region of scintillation indices are observed wherein on towards the third galactic quadrant (near $l = 240°$), there is a gas free tunnel. On the basis of the theory refraction scintillation the estimations of characteristic time of changes of flows of radiosources on frequency 100 MHZ for the mentioned above areas LISM are considered. In view of high importance of speed of movement inhomogenius of electronic concentration and their sizes for the given areas LISM, reaching 500 km/sec and 20-70 a.u., the characteristic times variability turn out equal 0.1-0.7 years, that will be coordinated to the data of supervision.

Key words: Interstellar medium: Local Interstellar medium: ionized component: interstellar radiosources scintillation.

1. Introduction

Interstellar scintillations of radio sources resulting from small-scale inhomogeneities of interstellar matter's refractive coefficient (Rickett, 1986) can yield information about plasma turbulence near shock fronts (Pikelner and Tsytovich, 1969). Here, the thin scattering screen approximation may be applied.

We used Culgoora (Australia) 1970–1984 array observations of extragalactic radio sources at 80 and 160 MHz (Slee and Siegman, 1988). During 15 years, 412 sources covering homogeneously most of the sky (with the exception of a northern sky section) were observed repeatedly, in two or more 4-week-long series. 190 sources proved variable at least at one frequency and only 27, at both frequencies. [**?**] give many arguments in favor of interstellar origin of the variations. They published measured scintillation variability indices m for the time scale of 1 month ($m1$) and from one to several years ($m12$). In all cases, the main maxima are present for the majority of the data combinations and conserve their positions within our angular resolution (about $20° - 30°$), with slight variations of sizes and positions of the mapped structures.

2. Results and interpretation

We found 3 clear maxima, virtually independent of the data combinations and ways of averaging, in the all-sky distribution of interstellar scintillation indices (Table 1). Three other maxima, though probably real, are not as definite as the three first ones. In all the cases, a minimum of m is present near the galactic longitude $l = 240°$ in the Southern hemisphere, but the data for this direction is too scarce to allow definite conclusions.

We assume that the revealed maxima of m can be identified with maxima of the soft X-ray background radiation distribution (B, C, and M bands in the survey by McCammon et al., 1983). The maxima 1 and 2 from Table 1 are overlapping a considerable part of the two brightest X-ray filaments in the M1 band (440–930 eV) map corresponding to Loop I, the old SNR expanding inside the coronal gas in a cavern formed around the Sco–Cen stellar association (Bochkarev, 1987b, 1990).

Another marked m maximum (number 3) obviously coincides with a soft X-ray background bright spot observed in the Southern hemisphere in B (130–188 eV) and C bands. According to Bochkarev (1987ab, 1990), the spot corresponds to the area of interaction of the outer part of the Local Cloud with the envelope surrounding the Sco–Cen association, namely to the position

Table 1: Galactic coordinates and possible identifications of the features in the map of interstellar scintillation index distribution

	Features	Identification
	Clear maxima	
1.	$0° < l < 30°; 0° < b < 30°$	Loop I
2.	$300° < l < 330°; 0° < b < 30°$	Loop I
3.	$-20° < l < 20°; -60° < b < -40°$	Southern maximum of soft X-ray BG (B and C bands, McCammon et al., 1983)
	Other possible maxima	
4.	$170° < l < 220°; 30° < b < 45°$	Northern maximum of soft X-ray BG (B and C bands, McCammon et al., 1983)
5.	$180° < l < 200°$; $-20° < b < 0°$	Orion star-formation region
6.	$l \approx 120°$ and $300°$ $b > 75°$	Soft X-ray BG filament near NGP (B and C bands, McCammon et al., 1983)
	Minimum of m	
7.	$l \approx 240°$ low southern b	Tunnel free of interstellar extinction (Bochkarev 1987b, 1990)

where the line of sight meets the relatively dense coronal gas near the shock front boundaries of the Sco–Cen superbubble. A similar northern maximum of m probably exists (number 4), but there is insufficient data for its direction in the Culgoora survey.

The maximum 5 is uncertain because its position and shape vary with data combinations. It might be identified with the densest northern part of the Ori–Eri superbubble, namely with the Orion star formation region.

The minimum 7 corresponds to a very old bubble, spread by differential rotation of the Galaxy within the Galactic quadrant III.

3. Discussion of time scale of interstellar scintillations

In accordance with the interpretation discussed in Section 3, the distance L to the maxima 1,2 (Loop I) is about 150 pc (Cox and Reynolds 1987; Bochkarev, 1987b, 1990). The velocity of the shock wave is 530–580 km/s (Bochkarev, 1990). Adopting typical angular sizes of the point components of extragalactic radio sources at 100 MHz $\theta = 0.2 - 0.5$ arcsec (see Janardhan and Alurkar, 1993 and references in Slee and Siegman, 1988), we find, in accordance with [**?**], $\tau = L\theta/v = 0.1 - 0.7$ years, and the size of the scattering inhomogeneities $a = 20 - 70$ A.U.

For the maxima 3, 4, we assume the distance $L = 20-40$ pc (Bochkarev, 1987ab, 1990) and v equal to the thermal velocity in coronal gas with the temperature $T = 10^6$ K: $v = 130$ km/s. In this case, $\tau = 0.1 - 0.3$ year.

In both cases (for all most definite m maxima), the estimated time scale of refractive interstellar scintillations is considerably shorter than that of the average scattering screen in the Galaxy (Rickett 1986; Slee and Siegman, 1988) and is in good agreement with the observed radio-source variations.

3. Conclusions

A) Areas of the sky are found with intensified extragalactic radio-source interstellar scintillation at low radio frequencies (80 – 160 MHz), at time scales from months to years.

B) A correspondence between the areas mentioned in Conclusion A and soft X-ray background details of large angular size is found: two Loop I bright X-ray filaments; high Galactic latitude brightest spots in soft (B and C bands) X-ray background radiation. The direction of the "interstellar absorption-free tunnel" at the galactic longitude $l = 240°$ probably corresponds to a minimum of interstellar scintillation.

C) The estimated time scales $\tau = 0.1 - 0.7$ year at 100 MHz for interstellar scintillation in hot LISM structures are shorter than those for a typical scattering screen and correspond to Slee & Siegman (1988) observations.

References

Bochkarev N.G.: 1987a, *Soviet Astron.,* **31** , 1

Bochkarev N.G.: 1987b, *Astrophys. Space Sci.,* **138**, 229.

Bochkarev N.G.: 1990, *Local Interstellar Medium*, Moscow, Nauka Publ.

Cox D.P., Reynolds, R.J.: 1987, *Ann. Rev. Astron. Astrophys.,* **25**, 303

Janardhan P., Alurkar S.K.: 1993, *As.Ap.* **269**, 119

McCammon D. et al.: 1983, *Ap.J.* **269**, 107

Pikelner S.B., Tsytovich V.N.: 1969, *Sov. Astron.*, **13**, N. 1

Rickett B.J.: 1986, *Ap.J.*, **307**, 564

Slee O.B., Siegman B.C.: 1988, *M.N.R.A.S.*, **235**, 1313.

CLOUD STRUCTURE OF INTERSTELLAR MATTER. OBSERVATIONAL PARAMETERS

I.V. Gosachinskij[1], V.V. Morozova[2]

[1] Sankt-Petersburg branch of Special Astrophysical observatory, Pulkovskoe Shosse, 65, S-Petersburg,196140, Russia, *gos@fsao.spb.su*

[2] Special Astrophysical observatory, Nizhnij Arkhys, Karachaevo-Cherkesia, 357147, Russia, *vvm@ratan.sao.ru*

ABSTRACT. Parameters of 7600 HI clouds were determined on the base of HI RATAN-600 Survey in the second and third quadrants of galactic longitudes. The spectra of cloud linear diameters, HI densities and masses are obtained first for such huge population of clouds. Mass spectrum of HI clouds shows that, in middle mass range, the process of coalescence in cloud–cloud collisions predominates, but the clouds with low masses are probably evaporated due to the very hot ISM component. It is found that mean clouds linear diameters along Galactic plane are 2.5 times greater than in transverse direction. The relation between HI concentrations and cloud diameters is obtained in the f of $n_H \propto d^{-1.25\pm0.01}$ probably regardless of selec effects. It is shown that velocity dispersion does depend on cloud diameters, as distinct from molec clouds. It is found that 16% of HI clouds have syste tic velocity gradients across cloud disks that is ma due to clouds rotation. Mean clouds angular rotati velocity is about $5 \cdot 10^{-14} s^{-1}$ and observable quant of clouds with opposite directions of rotation are e within 5% in both galactic quadrants investigated

Key words: Interstellar matter, clouds, HI

1. Introduction

The characteristics of interstellar gas clouds main role in any theories of star formation. The d molecular cloud cores are probably immediate par of stars. However, the molecular clouds themse arise obviously from some structures of atomic c ponent of interstellar medium, because namely in the atomic gas may arise two-phase system: clouds and intercloud medium, namely neutral atomic clouds are able to increase their masses and densities due to inelastic collisions and rapid cooling. So the neutral atomic clouds may be named as "grand parents" of stars and their properties play genetic role for whole chain of matter transformations in the galaxies.

2. Equipment and methods

The RATAN-600 radio telescope has greatly high sensitivity to low contrast details of emission observed on the bright complex background. That's why we were able to create the unique database of HI clouds on the base of HI RATAN-600 Survey. The angular resolution of this Survey was $2.4' \times 130'$, velocity resolution was 6.3 km/s, r.m.s. fluctuations of antenna temperature (T_a) were 0.25 K. A detailed description of equipment, technique and antenna parameters can

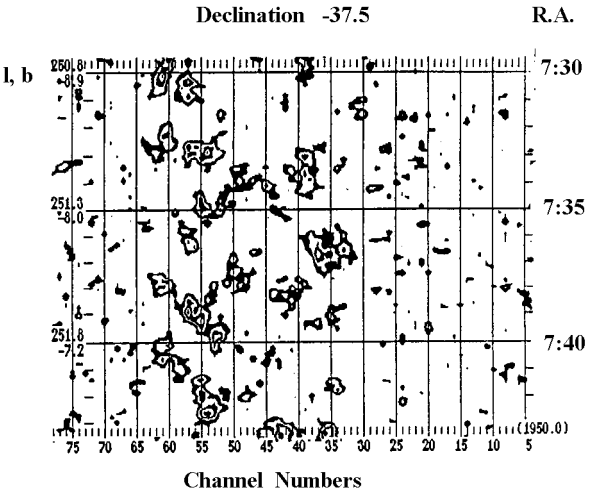

Figure 1: The HI details after removing of wide spread background emission.

In all drift curves of each cross-section the details of HI emission narrower than 0.5° were filtered with a simple second-order difference filter. Then the parameters of each details were determined with a help of a Gauss-analysis code and tabulated. For computing cloud distances, we accepted the Galactic rotation model of Kerr and Linden-Bell (1986) with $R_\odot$=8.5 kpc.

An example of HI details in function of right ascension and velocity (channel numbers) is represented on Fig. 1. About 1000 square degrees have been observed on the Sky, that correspond about 20 cubic kilo parsec at these regions of Galaxy.

All clouds with kinematical distances r ¡ 1.0 kpc were rejected because their relative distance errors are very high. Moreover, clouds with $T_a < 0.75$ K (3 times r.m.s. errors) and line widths $\Delta V < 6.3$ km/s were rejected too. Diameters, masses, gas densities and velocity dispersions of about 7600 HI clouds were determined in the second and third quadrants of galactic longitudes in $180° < l < 260°$, $-15° < b < +15°$ $100° < l < 150°$, $-10° < b < +10°$. Some selection effects were discovered and our statistic results were corrected for them.

3. Selection effects

It is obvious that any statistical results are very sensitive to selection effects, arising due to limited possibilities of equipment and methods. The obvious selection effect is demonstrated in Fig. 2 where a dependance is presented between cloud linear diameters (d) and their distances (r). The inclined lines show our limits on the angular dimension of a cloud due to antenna resolution, sensitivity and methods of filtering employed.

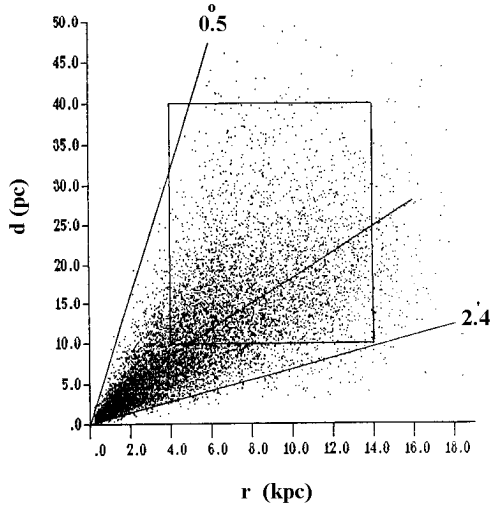

Figure 2: The diameters of HI clouds as a function of their distance. The inclined lines show the limitations of cloud survey.

We correct our cloud statistics for this effect by restriction of the ranges of d and r as shown in Fig. 2 by rectangle in which there is no dependence between d and r. The second method of correction supposes that characteristics of the cloud structure are uniform in the investigated regions of the Galaxy. So a number of cloud with particular diameter may be corrected. The first method may be applied to correlation dependances of parameters, but for spectra both methods can be applied.

The final estimates of measuring errors of the main cloud parameters are the next: linear dimension $\pm 1.0pc$, integral intensity $\pm 40\%$, HI density up to factor 1.5 and HI mass up to factor 3.

4. The spectra of parameters

It is obtained that maximum volume fraction occupied by HI clouds is $2 \cdot 10^{-4}$ in the Galactic plane and decreases with z. The mass density of the cloud component is about $8 \cdot 10^4 M_\odot$ kpc^{-3} in the plane and dec-

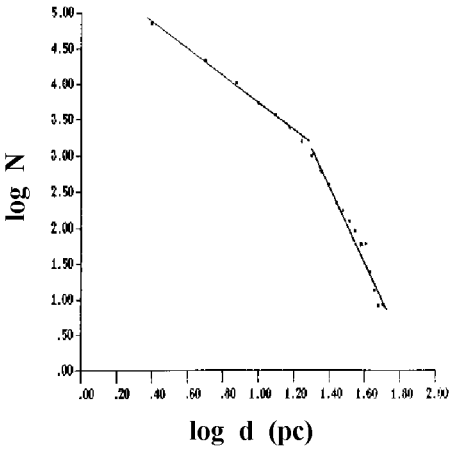

Figure 3: The diameters spectrum of HI clouds.

It is found that mean clouds linear diameters along Galactic plane are 2.5 times greater than in transverse direction. The cloud diameter spectrum (Fig. 3) has a bimodal power shape with spectral indexes of –1.9 ± 0.5 between 1 – 16 pc, and –3.9 ± 0.5 between 16 – 45 pc.

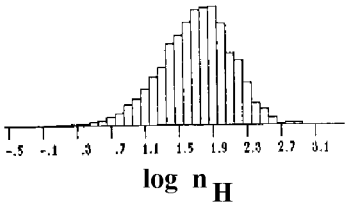

Figure 4: The distribution of HI cloud densities.

A HI gas density spectrum in the range of 1.0 to 400 cm^{-3} (Fig. 4) has not a power form, but it has a maximum at $n_H = 10 - 40$ cm^{-3} depending of galactic latitude. The lowest and highest density observed in the clouds are the very important parameters for theories of thermal instability and formation of molecules. These are about 1 cm^{-3} and about 400 cm^{-3} respectively. The first value shows that according to Suchkov and Shchekinov (1981) the rate of primary ionization

of hydrogen is rather low at about $10^{-17} - -10^{-18} s^{-1}$ and abundance of heavy elements in the interstellar medium is close to the solar one.

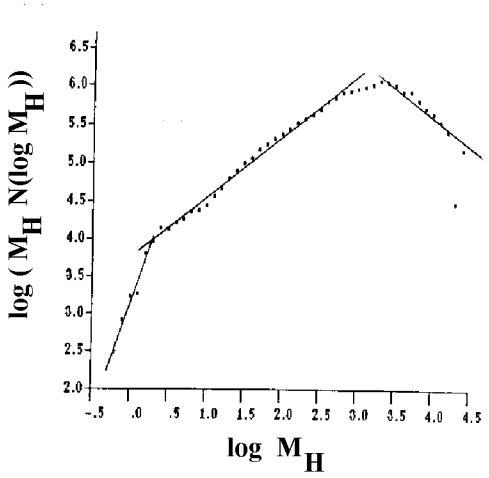

Figure 5: The mass spectrum oh HI clouds.

The mass spectrum in the form of M·N(log M) was obtained in the mass range of 0.6 to $2.5 \cdot 10^4$ $M_\odot$ (Fig. 5). It consists of at least three parts. In the range of 2 to 600 $M_\odot$ the spectrum has a spectral index of 0.8 ± 0.1, in the range of 0.6 to 2 $M_\odot$ the spectral index is 3.0 ± 1 , and in the range of 600 to $2 \cdot 10^4$ $M_\odot$ the spectral index is -0.7 ± 0.3. A theoretical computation of mass spectra for colliding clouds was made by Cheeze and Lazareff (1980). They show that a rather high spectral index of 0.8 can occur only if the processes of coalescence dominate in the cloud–cloud collision. Clouds with low masses may be evaporated probably due to very hot ISM component. In the very high mass range the number of neutral gas clouds may be decreased because of gravitational instability or/and molecularization.

5. The relations between cloud parameters

There are wellknown empirical power-law scaling relation for internal velocity dispersion, Δv, gas particle density, n and cloud diameter d and mass M, first pointed by Larson (1981) for population of molecular clouds. These relation is generally interpreted as evidence for mechanical equilibrium in self-gravity, turbulent molecular clouds. For lower density atomic (HI) clouds self-gravitation is unessential and Fleck (1996) supposed phenomenological model of compressible turbulence. It is interesting to note however that there is dozen papers on investigation of the scaling relation in molecular clouds but only one - for atomic clouds.

The relation between HI concentrations and cloud diameters presented in Fig. 6 for more than 7700 clouds. The linear regression give the dependence in the form of $n_H \propto d^{-1.25 \pm 0.01}$ regardless of selection effects. The correlation coefficient between *log* n_H and *log* d is equal –0.87. This is nearly the same as obtained by many authors (see Falgarone, Puget, 1986, Vasquez-Semadeny et al. 1997) for molecular clouds. Fleck (1996) has shown that for atomic clouds $\rho \propto d^{-3\alpha}$, where α is a measure of the degree of compression at each level of compressible turbulence. So our data give $\alpha = 0.42$, that is about 2.5 times greater than from Fleck(1996).

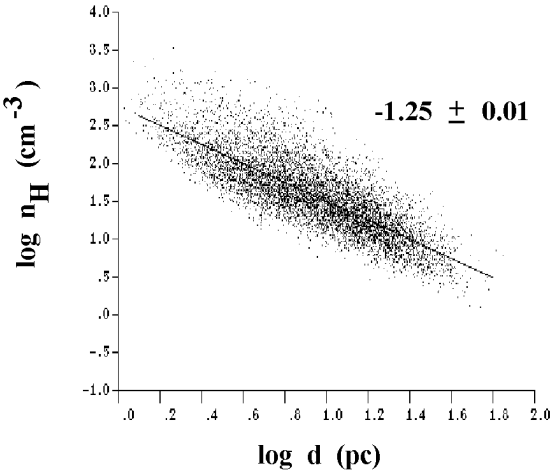

Figure 6: Relation between HI clouds diameters and densities.

It is shown that other important dependence – velocity dispersion versus cloud diameters, that is well defined for molecular clouds in the form of $\Delta v \propto d^{-0.4}$ – is completely absent in the case of HI clouds with large significance level (see Fig. 7, where instead of velocity dispersion half widths of observable emission profiles are presented). Probably this is due to negligible role of intrinsic turbulence in the HI clouds but may be that atomic and molecular clouds represent distinct populations.

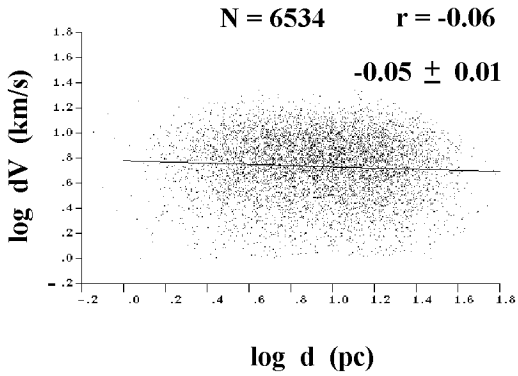

Figure 7: Relation between HI cloud diameters and profile widths.

6. The rotation of the HI clouds

It has been found that 16% of HI clouds have significant systematic velocity gradients across cloud disks that may be due to rotation of clouds (Fig. 8). This phenomenon may explain rather high velocity widths of HI line profiles in the observable clouds. These gradients have been approximated by straight lines and for those objects, where values of slope were greater than 3 times r.m.s., angular rotational velocities were determined. The mean value of clouds angular rotational velocity obtained with these gradients is about $5 \cdot 10^{-14}$ s^{-1}.

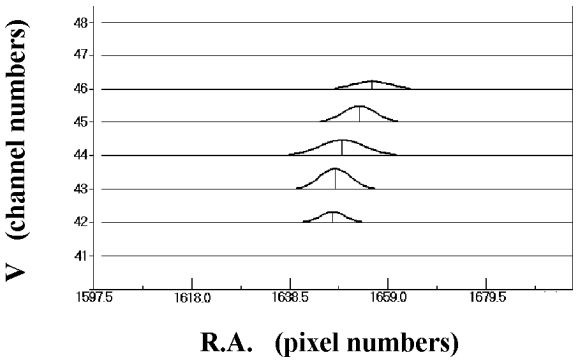

Figure 8: R.A. of maximum cloud emission in function of channel number.

The distribution of absolute values of rotational velocities is presented on the Fig. 9. It may be seen that the range of values is rather narrow. This may be due to some methodical restriction (selection effects) therefore the mean value of rotational velocities is only tentative. With these data mean rotational energy of clouds is about 10^{48} ergs, that is comparable to the

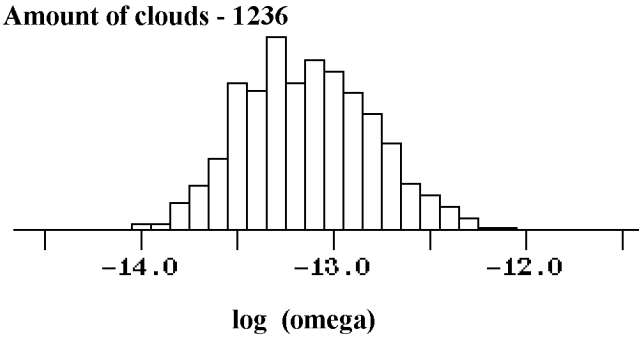

Figure 9: Distribution of measured cloud angular velocities.

Finally, observable quantities of clouds with opposite directions of rotation are equal within 5% in both galactic quadrants investigated.

It is interesting to note that in the recent paper of Phillips (1999) some results on rotation of molecular clouds are reported. Part of them corresponds to our results on atomic clouds, in particular, that part of clouds with rotation is very large and that directions of rotation axes are mainly arbitrarily.

7. Concluding remarks

High angular resolution and high sensitivity of the RATAN–600 to low contrast details of emission allowed us to create the unique collection of HI cloud parameters in the Second and Third Galactic Quadrants. It is now not necessary to use so-called "standard cloud" for computation of any theoretical models. It is possible to use our results in the straightforward manner for further investigation like Khersonsky (1997) who try to connect the interstellar gas cloud mass spectrum with stellar mass spectrum in star-forming regions.

These results are published in the next paper: Gosachinskij I.V., 1989, Pisma v A.Zh. **15**, 788, Gosachinskij I.V. and Morozova V.V., 1996, Astron. Astrophys. Transactions, **11**, 215, and will be published in Gosachinskij I.V., Morozova V.V., 1999, Astron. Zh. (in press).

Acknowledgments. The authors are very grateful to their colleagues who provided the RATAN-600 HI Survey during many years: N.A.Yudaeva, M.E.Makrosova, Z.A.Alferova and T.V.Monastyreva.

This work was supported with RFFI grant 96-02-16565.

References

Cheeze J.P., Lazareff B.: 1980, *As. Ap.*, **91**, 290.
Falgarone E., Puget J.-L.: 1986, *As. Ap.*, **162**, 235.
Fleck Jr. R.C.: 1996, *Ap. J.*, **458**, 739.
Kerr F.D., Linden-Bell D.: 1986, *Mon. Not. Roy. Astron. Soc.*, **221**, 1023.
Khersonsky V.K.:1997, *Ap. J.*, **475**, 594.
Larson R.B.: 1981, *Mon. Not. Roy. Astron. Soc.*, **194**, 809.
Phillips J.P.:1999, *As. Ap. Suppl.*, **134**, 241.
Suchkov A.A., Shchekinov Yu. A.: 1981, *Pisma v A.Zh.*, **7**, 617.
Venger A.P., Gosachinskij I.V., Grachev V.G., Ryzhkov N.F.: 1979, *Izvestia SAO*, **14**, 118.

INTERACTION OF SUPERNOVA BLAST WAVES WITH WIND-DRIVEN SHELLS: FORMATION OF "JETS", "BULLETS", "EARS", ETC

V.V. Gvaramadze[1,2,3]

[1] Abastumani Astrophysical Observatory, Georgian Academy of Sciences, A.Kazbegi ave. 2-a, Tbilisi, 380060, Georgia, *vgvaram@mx.iki.rssi.ru*
[2] Sternberg State Astronomical Institute, Moscow, Russia
[3] Abdus Salam International Centre for Theoretical Physics, Trieste, Italy

ABSTRACT. Most of middle-aged supernova remnants (SNRs) have a distorted and complicated appearance which cannot be explained in the framework of the Sedov-Taylor model. We consider three typical examples of such SNRs (Vela SNR, MSH 15-52, G 309.2-00.6) and show that their structure could be explained as a result of interaction of a supernova (SN) blast wave with the ambient medium preprocessed by the action of the SN progenitor's wind and ionized emission.

Key words: ISM: bubbles; ISM: supernova remnants.

1. Introduction

Most of middle-aged SNRs have a distorted and complicated appearance which cannot be explained in the framework of the standard Sedov-Taylor model. Three possibilities are usually considered to describe the general structure of such remnants:
– the SN blast wave interacts with the inhomogeneous (density stratified and/or clumpy) interstellar medium;
– the SN ejecta is anisotropic and/or clumpy;
– the stellar remnant (e.g. a pulsar) is a source of the relativistic wind and/or collimated outflows (jets) which power the central synchrotron nebula (plerion) and/or interact with the SNR's shell.

For example, all above possibilities were considered to explain the structure of the Vela SNR. Namely, the general asymmetry of this remnant (the northeast half of the Vela SNR faced towards the Galactic plane has a nearly circular boundary, whereas the opposite half is very distorted) as well as its patchy appearance in soft X-rays were attributed to the expansion of the SN blast wave in the inhomogeneous (large-scale cloud + a multitude of cloudlets) interstellar medium (e.g. Kahn et al. 1985, Bocchino et al. 1997). One of consequences of this suggestion is the proposal that the origin of optical filaments constituting the shell of the remnant is due to the slowing and cooling of parts of the SN blast wave propagating into dense clumps of matter (cloudlets). A number of radial structures (most prominent in soft X-rays) protruding far outside the main body of the remnant was interpreted as bow shocks produced by fragments of the exploded SN star ("bullets") supersonically moving through the interstellar medium (Aschenbach et al. 1995). An elongated X-ray structure stretched from the Vela pulsar position to the center of the brightest radio component of the Vela SNR (known as Vela X) was interpreted as a one-sided jet emanating from the Vela pulsar and transferring the pulsar's slow-down energy to the Vela X (e.g. Markwardt & Ögelman 1995). This interpretation supports the proposal of Weiler & Panagia (1980) that the Vela X is a plerion. A nebula of hard X-ray (2.5-10 keV) emission stretched nearly symmetrically for about 1° on either side of the pulsar in the northeast-southwest direction was also interpreted as a plerion (Willmore et al. 1992).

The first and third possibilities were considered in connection with the SNR MSH 15-52 (G 320.4-01.2). The radio map of this remnant given by Caswell et al. (1981) shows the elongated shell consisting of two bright components stretched parallel to the Galactic plane and separated by a gap of weak emission. The brightest X-ray emission of this remnant comes from two components, one of which centres on the position of the pulsar PSR B1509-58 (located close to the geometrical center of the MSH 1509-58), while the second one coincides with the maximum of emission of the brightest (closer to the Galactic plane) radio component and with the bright optical nebula (known as RCW 89). It was suggested that the central X-ray component of the MSH 15-52 is a plerion (e.g. Seward et al. 1984) and that the general structure of this remnant is affected by one (Tamura et al. 1996, Brazier & Becker 1997) or two (Manchester 1987, Gaensler et al. 1999) jets emanating from the pulsar.

And the third example is the SNR G 309.2-00.6, which consists (at radio wavelengths) of a nearly circular shell and two "ears" – arclike filamentary structures protruding from the shell in the opposite directions (nearly parallel to the Galactic plane). It was suggested, by analogy with the well-known system SS433/W50, that the distorted appearance of the G 309.2-00.6 is due to the interaction between a pair of jets produced by the central (unvisible) stellar remnant and the originally spherical shell of the SNR (Gaensler et al. 1998). It was also suggested that one of linear filaments in the northeast "ear" represents one of the proposed jets.

The goal of this paper is to show that the structure of at least three above-mentioned SNRs could be explained as a result of interaction of a SN blast wave with the ambient medium preprocessed by the action of the SN progenitor's wind and ionized emission.

2. Interaction of SN blast waves with wind-driven shells

It is known that progenitors of most of SN stars are massive ones (e.g. van den Bergh & Tammann 1991). Such stars are sources of intense stellar winds and ionizing emission which strongly modify the ambient interstellar medium. The ionizing radiation of the progenitor star creates an H II region, the inner, homogenized part of which gradually expands due to the continuous photoevaporation of density inhomogeneities in stellar environs (McKee et al. 1984). If the mechanical luminosity of the stellar wind L is much smaller than some characteristic wind luminosity, $L^* \simeq 10^{34}(S_{46}^2/n)^{1/3}\,\mathrm{ergs\,s^{-1}}$, where S_{46} is the stellar ionizing flux in units of 10^{46} photons $\mathrm{s^{-1}}$ and n is the mean density the ambient medium would have if were homogenized, the stellar wind flows through a homogeneous medium and creates a bubble of radius (e.g. Weaver et al. 1977) $R(t) = 11 L_{34}^{1/5} n^{-1/5} t_6^{3/5}$ pc, where $L_{34} = L/(10^{34}\,\mathrm{ergs\,s^{-1}}), t_6 = t/(10^6\mathrm{years})$. Initially the expanding bubble is surrounded by a thin, dense shell of swept-up interstellar gas, but eventually the gas pressure in the bubble becomes comparable to that of the ambient medium, and the bubble stalls, while the shell disappears. The radius of the stalled bubble is $R_\mathrm{s} = 5.5 L_{34}^{1/2} n^{-1/2}$ pc. Since the star continues to supply the energy in the bubble, the radius of the bubble continues to grow, $\propto t^{1/3}$, until the radiative losses in the bubble interior becomes comparable to L. Then the bubble recedes to some stable radius R_r, at which radiative losses exactly balance L (D'Ercole 1992): $R_\mathrm{r} = 2.2\, L_{34}^{6/13} n^{-7/13}$ pc. Before a massive star exploded as a supernova it becomes for a relatively short time, $t_\mathrm{RSG} \simeq 10^6$ years, a red supergiant (RSG). The ionized gas outside the bubble rapidly cools off because the central star cannot keep it hot. At the same time the rarefied interior of the bubble remains hot as the radiative losses there are negligible on time-scales of t_RSG. As a result, the bubble supersonically reexpands in the external cold medium and creates a new dense shell (D'Ercole 1992; cf. Shull et al. 1985). Two main factors could significantly affect the structure of the shell. The first one is the regular interstellar magnetic field (generally it is parallel to the Galactic plane). This factor leads to the matter redistribution over the shell and to its concentration near the magnetic equator: the column density at the equator is increased about ten times (Ferrière et al. 1991). The second factor is the large-scale density gradient. It is known (Landecker et al. 1989, Gosachinskij & Morozova 1999) that molecular clouds tend to be stretched along the Galactic plane, therefore one might expect that due to the interaction with a nearby cloud one of two sides of the shell (not necessary the nearest to the Galactic plane) could be more massive than the opposite one. These two factors naturally define two symmetry axes (parallel and perpendicular to the Galactic plane) of the future SNR.

During the RSG stage a massive star lost most of its mass (e.g. a $20M_\odot$ star loses about two thirds of its mass) in the form of slow, dense wind. This material expands in the interior of the reexpanded main-sequence (MS) bubble and occupies a compact region surrounded by a dense shell. The size of this region is determined by the counter-pressure of the external hot gas and is equal to about few parsecs (e.g. Chevalier & Emmering 1989, D'Ercole 1992). Most probably that this region is far from the spherical symmetry (it is believed that the wind of a RSG is concentrated close to the stellar equatorial plane).

After the SN exploded, the blast wave interacts with the dense RSG wind. This interaction continues few hundreds years and determines the appearance of young SNRs (e.g. Cas A, see Borkowski et al. 1996). Then the blast wave propagates through the low-density interior of the MS bubble until it catches up the dense shell. During this period (lasting about one thousand years) the blast wave is unobservable. The subsequent evolution of the blast wave (i.e. the SNR) depends on the mass of the shell. If the mass of the shell is smaller than about 50 times the mass of the SN ejecta the blast wave overruns the shell and continues to expand adiabatically as a Sedov-Taylor shock wave. For more massive ones, the blast wave merges with the shell, and the reaccelerated shell evolves into a momentum-conserving stage (e.g. Franco et al. 1991). The impact of the blast wave with the shell causes the Rayleigh-Taylor and other dynamical instabilities. The inhomogeneous mass distribution over the shell affects the development of instabilities and results in the asymmetry of the resulting SNR. The more massive half of a shell created in the density-stratified medium is less sensitive to the impact of the SN blast wave, while the opposite (less massive) one becomes

strongly deformed and sometimes even disrupted. The effect of the regular magnetic field is twofold: first, it leads to the bilateral appearance of SNRs (cf. Ferrière et al. 1991, Gaensler 1998), second, it results in the elongated form of remnants (because of reduced inertia of shells at the magnetic poles).

3. Three examples

Let us consider the SNRs mentioned in Sect. 1.

3.1. Vela SNR

We suggest that the Vela SNR is a result of type II SN explosion in a cavity created by the wind of a 15-20 $M_\odot$ star and propose that the general structure of the remnant is determined by the interaction of the SN blast wave with the massive shell created around the reexpanded MS bubble (see Sect. 2; for details see Gvaramadze (1999a)). The impact of the blast wave with the shell causes the development of Rayleigh-Taylor deformations of the shell ("blisters"), which appear as arclike and looplike filaments when our line of sight is tangential to their surfaces. The optical emission is expected to come from the outer layers of the shell, where the transmitted SN blast wave slows to become radiative, while the soft X-ray emission represents the inner layers of the shell heated by the blast wave up to X-ray temperatures. The origin of some radial protrusions (labelled by Aschenbach et al. (1995) as "bullets" A,B,C, and D/D') could be connected with the shell deformations, while the "bullets" E and F could be interpreted as outflows of a hot gas escaping through the breaks in the SNR's shell (Gvaramadze 1998a, Bock & Gvaramadze 1999). As to the X-ray "jet" discovered by Markwardt & Ögelman (1995), an analysis of the radio, optical, and X-ray data suggested that it is a dense filament in the Vela SNR's shell (projected by chance near the line of sight to the Vela pulsar), and that its origin is connected with the nonlinear interaction of the shell deformations (see Gvaramadze 1999a). The nature of the radio source Vela X is considered in the paper by Gvaramadze (1998b), where it is shown that the Vela X is also a part of the shell of the Vela SNR, but not a plerion. In conclusion one should be noted that the slow, dense RSG wind lost by the progenitor star and subsequently reheated and reaccelerated by the passage of the SN blast wave could be responsible for the origin of a hard X-ray nebula discovered by Willmore et al. (1992) (Willmore et al. mentioned that their data do not allow to discern the thermal and nonthermal forms of the spectrum of this nebula).

3.2. SNR MSH 15-52

The SNR MSH 15-52, associated with the pulsar PSR B1509-58, is usually classified as a composite SNR. This is because of it consists of an extended nonthermal radio shell (at the distance of $\simeq$ 5 pc (e.g. Gaensler et al. 1999) the diameter of the remnant $\geq$ 40 pc) and a central elongated X-ray nebula ($\simeq$ 7 pc $\times$12 pc) which is thought to be a synchrotron pulsar-powered nebula (a plerion). The spin-down age of the pulsar is $\simeq$ 1700 years (i.e. nearly the same as that of the Crab pulsar), while the size and general appearance of the MSH 15-52 suggest that this system should be much older (few times 10^4 years). To reconcile the ages of the pulsar and remnant, Seward et al. (1983) considered two possibilities: 1) MSH 15-52 is a young SNR, and 2) PSR B1509-58 is an old pulsar. The first one implies (in the framework of the Sedov-Taylor model) that the SN explosion was very energetic and occured in a tenuous medium (see also Bhattacharya 1990). This point of view is generally accepted (e.g. Gaensler et al. 1999). The second possibility was reexaminated by Blandford & Romani (1988), who suggested that the pulsar spin-down torque grew within the last $\simeq 10^3$ years (due to the growth of the pulsar's magnetic field) and therefore the true age of the pulsar could be as large as it follows from the age estimates for the SNR. We propose an alternative explanation (Gvaramadze 1999b) and suggest that the high spin-down rate of the pulsar is inherent only for a relatively short period of the present spin history and that the enhanced braking torque is connected with the interaction of the pulsar's magnetosphere with a dense clump of circumstellar matter (whose origin is connected with the late evolutionary stages of the progenitor star). This suggestion implies that the central X-ray nebula could be interpreted as a dense material lost by the progenitor star during the RSG stage and reheated to high temperatures by the SN blast wave. The existance of a hot plasma (of mass of about few $M_\odot$) around the pulsar follows from the IR observations of the MSH 15-52 by Arendt (1991), who discovered an IR source near the position of the pulsar. We believe that the thermal emission of this plasma is contaminated by the hard nonthermal emission from a (much smaller) compact nebula powered by the pulsar (similar to the $1'(\simeq 4\times10^{17}$ cm) nebula discovered by Harnden et al. (1985; see also de Jager et al. 1996) around the Vela pulsar), and that this is the reason why the spectrum of the whole central nebula is usually described by a nonthermal model (e.g. Greiveldinger et al. 1995, Tamura et al. 1996).

The shell of the MSH 15-52 remainds that of the Vela SNR (cf. Fig.8 of Gaensler 1998 and Fig.1 of Gvaramadze 1999a). In both remnants the halves faced towards the Galactic plane are brighter and more regular than the opposite ones. We suggest that the MSH 15-52 is a result of interaction of the SN blast wave with the wind-driven shell created in the inhomogeneous interstellar medium: the northwest half of the shell interacts

with the region of enhanced density (that results in the origin of bright radio, optical and X-ray emission), and therefore is less affected (distorted) by the impact of the SN blast wave than the southeast half. The bilateral and elongated appearance of the shell could be connected with the effect of the large-scale interstellar magnetic field (cf. Gaensler 1998, Gaensler et al. 1999).

3.3. SNR G 309.2-00.6

We suggest that the "ears" of this SNR were blown up in the polar regions of the (former) wind-driven shell created in the interstellar medium with regular magnetic field (oriented nearly parallel to the Galactic plane). The origin of the "jet" and other filamentary structures visible in the remnant (see Fig.2 of Gaensler et al. 1998) we connect with projection effects in the Rayleigh-Taylor unstable shell. We suggest also that the SN explosion site[1] should be marked by a hard X-ray nebula and predict that the angular size of the nebula (for the distance to the remnant of 5-14 kpc (Gaensler et al. 1998)) is about $1.5^{'} - 2^{'}$.

References

Arendt R.G.: 1991, *A. J.*, **101**, 2160.

Aschenbach B., Egger R., Trümper J.: 1995, *Nat.*, **373**, 587.

Bhattacharya D.: 1990, *JA&A*, **11**, 125.

Blandford R.D., Romani R.W.: 1988, *M.N.R.A.S.*, **234**, 57.

Bocchino F., Maggio A., Sciortino S.: 1997, *Ap. J.*, **481**, 872.

Bock D.C.-J., Gvaramadze V.V.: 1999, in preparation.

Borkowski K.J., Szymkowiak A.E., Blondin J.M., Sarazin C.L.: 1996, *Ap. J.*, **466**, 866.

Brazier K.T.S., Becker W.: 1997, *M.N.R.A.S.*, **284**, 335.

Caswell J.L., Milne D.K., Wellington K.J.: 1981, *M.N.R.A.S.*, **195**, 89.

Chevalier R.A., Emmering R.T.: 1989, *Ap. J.*, **342**, L75.

D'Ercole A.: 1992, *M.N.R.A.S.*, **255**, 572.

de Jager O.C., Harding A.K., Strickman M.S.: 1996, *Ap. J.*, **460**, 729.

Ferrière K.M., Mac Low M.-M., Zweibel E.G.: 1991, *Ap. J.*, **375**, 239.

Franco J., Tenorio-Tagle G., Bodenheimer P., Różyczka M.: 1991, *P.A.S.P.*, **103**, 803.

Gaensler B.M.: 1998, *Ap. J.*, **493**, 781.

Gaensler B.M., Green A.J., Manchester R.N.: 1998, *M.N.R.A.S.*, **299**, 812.

Gaensler B.M., Brazier K.T.S., Manchester R.N., Johnston S., Green A.J.: 1999, *M.N.R.A.S.*, **305**, 724.

Greiveldinger C., Caucino S., Massaglia S., Ögelman H., Trussoni E.: 1995, *Ap. J.*, **454**, 855.

Gvaramadze V.V.: 1998a, in: *The Local Bubble and Beyond*, eds. D.Breitschwerdt, M.Freyberg, J.Trümper, Springer-Verlag, Heidelberg, p.141.

Gvaramadze V.V.: 1998b, *Astronomy Letters*, **24**, 178.

Gvaramadze V.V.: 1999a, *Astron. Astrophys.*, in press.

Gvaramadze V.V.: 1999b, submitted to *Astron. Astrophys.*.

Gosachinskij I.V., Morozova V.V.: 1999, *Astronomy Reports*, in press.

Harnden F.R., Grant P.D., Seward F.D., Kahn S.M.: 1985, *Ap. J.*, **299**, 828.

Kahn S.M., Gorenstein P., Harnden F.R., Seward F.D.: 1985, *Ap. J.*, **299**, 821.

Landecker T.L., Pineault S., Routledge D., Vaneldik J.F.: 1989, *MNRAS*, **237**, 277.

McKee C.F., Van Buren D., Lazareff R.: 1984, *Ap. J.*, **278**, L115.

Manchester R.N.: 1987, *Astron. Astrophys.*, **171**, 205.

Markwardt C.B., Ögelman H.: 1995, *Nat*, **375**, 40.

Seward F.D., Harnden Jr., F.R., Murdin P., Clark D.H.: 1983, *Ap. J.*, **267**, 698.

Seward F.D., Harnden Jr., F.R., Szymkowiak A., Swank J.: 1984, *Ap. J.*, **281**, 650.

Shull P., Dyson J.E., Kahn F.D., West K.A.: 1985, *M.N.R.A.S.*, **212**, 799.

Tamura K., Kawai N., Yoshida A., Brinkmann W.: 1996, *P.A.S.P.*, **48**, L33.

van den Bergh S., Tammann G.A.: 1991, *ARA&A*, **29**, 363.

Weaver R., McCray R., Castor J., Shapiro P., Moore R.: 1977, *Ap. J.*, **218**, 377.

Weiler K.W., Panagia N.: 1980, *Astron. Astrophys.*, **90**, 269.

Willmore A.P., Eyles C.J., Skinner G.K., Watt M.P.: 1992, *M.N.R.A.S.*, **254**, 139.

[1]Note that it could be shifted from the geometrical centre of the SNR due to the proper motion of the SN progenitor star.

STELLAR WIND IN THE ISM

T.A. Lozinskaya

Sternberg Astronomical Institute, Moscow, Russia,
lozinsk@sai.msu.su

ABSTRACT. After a brief review of the modern understanding of stellar wind's action on the ISM we consider two aspects of its "global" collective effect from observational viewpoint. First, stellar winds from OB associations do provide favorable conditions for triggering star formation. Second, the entire history of an active star-forming complex does regulate the nature of a wind-blown bubble or a SNR.

Key words: ISM: SNR, wind-blown bubbles; stars: WR, OB-associations, star formation

1. Introduction

Stellar wind's and SNe' collective action are the dominant factors regulating the structure and dynamics of the ISM. Deep high-resolution images of nearest galaxies in $H\alpha$ and 21-cm lines look just like "layers of foam" of neutral and ionized shells and supershells that are believed to be created by stellar winds and SNe.

The wind from early-type Main Sequence stars was discovered in 1967; and since then we know that all OB stars (earlier than B2) are characterized by powerfull winds.

The physics of wind's action on the ambient gas has been understood immediately. According to the classical theory (Pikelner, 1968; Avedisova, 1971; Steigman et al., 1975; Castor at al., 1975; Weaver et al., 1977) strong stellar wind in the homogeneous ambient gas creats a multilayer system, so called "wind-blown bubble". Starting from inside it consists of the cental cavity filled with a freely expanding wind; the geometrically thick layer of hot wind material, heated by the reflected shock, and mixed with evaporated interstellar gas; and the outermost dense shell of the interstellar gas that is swept-up and heated by the shock wave.

The general concepts of the classical theory have remained unchanged for three decades. Modern theory has added radiative losses and instabilities, outflow changes over the lifetime of stars, inhomogeneities of the ISM (large-scale density gradients and cloudy structure) and, finally, clumpy structure of stellar winds.

The idea has recently been put forward that the standard "wind-blown bubble model" is not consistent with observations: kinematic ages of wind-swept shells appear to be lower than ages of related stellar populations or expansion velocities are higher than the model predicts (see Oey, Massey 1994; Oey 1996, and references therein).

I would say that it is not completely clear so far. In many cases we may have been oversimplifying the nature of real shells. Actually, pure, "constant density wind-blown bubbles" just do not exist. In terms of modern understanding of massive stars evolution three types of shells must exist around each WR star: 1 – wind-blown bubbles, 2 – stellar ejecta and 3 – shell-like HII regions. In some cases, indeed, they are clearly seen together. Two best studied examples are the following (Lozinskaya, 1992 contains the images and further references to the literature). The Of star HD148937 and its bright ejected shell NGC6164-5 are surrounded by very faint filaments of a wind-blown bubble and both are located at the center of an extended shell-like HII region and the outermost shell of dust.

The prototype of a wind-blown bubble: the nebula NGC6888 around WR WR has been shown to represent the stellar ejecta material, perhaps shocked by stellar wind, while surrounding system of very faint [OIII] filaments is swept-up by the wind of WR star. Both are located in the center of an extended IR shell, probably created by the wind at MS stage (Marston, 1995; Lozinskaya et al., 1997), or alternatively by SN-explosion of a close companion star (Nichols-Bohlin, Fesen, 1993). And all the system, in its turn, belongs to the multishell complex around OB association Cyg OB1.

What is more important: if there is no ring nebula around a WR star with strong wind we do understand why not. Because of evacuation of surrounding gas by common winds of the parent OB-association, we observe a rind nebula around a WR provided that there is an ejected material, and as long as its emission is detectable.

The general approach to the problem of the wind action on the ISM has been changing. Today we do understand that the nature of an "individual" wind-blown bubble (or a SNR) strongly depends on the entire history of the interaction of stars and the ISM in an active star-forming complex. In terms of the new

approach each giant molecular complex must be considered as an ecosystem. Collective winds and SNe create expanding supershells around rich stellar groups, and that triggers a new wave of star formation.

I'll illustrate two aspects of the new approach basing on recent results of our investigations:

First, stellar winds from OB associations do indeed provide favorable conditions for triggering star formation.

Second, the entire history of an active star-forming complex does indeed regulate the nature of a wind-blown bubble or a SNR.

2. Star formation triggered in supershells around OB associations

One of the best studied multishell complex in the Galaxy is that related to the Cyg OB1 association (see Lozinskaya, Sitnik, 1988; Lozinskaya *et al.* 1998a; Lozinskaya, 1998 and references herein). The shell-like structure of this region is revealed by optical lines and by radio continuum, by the infrared emission and by neutral hydrogen.

Lozinskaya and Sitnik (1988) identify here an extended elongated shell (we will refer to it as *the supershell*) and several inner shells of different sizes. The kinematics of the multi-shell complex has been studied in a long lasting set of H_α Fabry-Perot observations (Lozinskaya *et al.* 1998a and references herein).

It has been found that the dominant kinematic structure of the shell as a whole exhibits bright emission at low velocities 2-20 km/s and also weaker emission at both high negative up to -100– -90 km/s, and positive, up to +60–+80 km/s, velocities.

To summarize the observational material, following Lozinskaya *et al.* 1998a; Lozinskaya, 1998, 1999, we can conclude the following.
1 – The multishell system appears to be formed by a rich OB association in a dense molecular complex.
2 – It clearly exhibits a hyerarchical structure and "two-component" kinematics: the bulk of the gas is unaccelerated (the supershell's expansion velocity ≤ 10 km/s) while faint features correspond to fast motions.

The two-component kinematics of this supershell is not unique. Complexes of this type have been distinguished around Car OB1/OB2, Ori OB1/λ Ori, and Sco OB1, see Table. Note, that two sets of velocities in these supershells have been detected from interstellar absorption lines in spectra of WR and O stars. Our detailed observations of the Cyg OB1 supershell confirm, that faint high-velocity features are not local to the stars with strong stellar winds. They really characterize a supershell as a whole.

The major properties of the supershells are rather similar: they have similar sizes of about 100-300 pc, the shells reveal a two-component kinematics; the characteristic velocities are 5-25 km/s for the bright line components and around 100 km/s for the weak ones. (Kinematic age of the slow shells is $\approx 5 \times 10^6$ yrs, that of fast features is $\approx 5 \times 10^5$ yrs.) And, finally, they all are related to dense molecular complexes.

Therefore the phenomenon of two-component kinematics seems to be fairly common for supershells around rich OB associations in the dense ISM.

A possible scenario for the formation of two-component kinematics suggest a new insight to the problem of triggered star formation. An interpretation of the phenomenon assumes that two-component kinematics is entirely consistent with the classical theory of the interaction of the winds from OB associations with the interstellar gas (Lozinskaya (1998, 1999). Two different shells are formed by the winds of an OB association: one is massive and expanding slowly, while the other (or several others), inside the first one, are less massive and expanding with relatively high velocity. The key point here is that the shells develop in a totally different ambient gas: the massive slow one is created before the most massive stars leave the MS in the dense quasy-homogeneous parent gas; the fast shells are formed by strong winds from WR stars and, perhaps, by SNe in the tenuous cavity surrounded by dense walls. According to Lozinskaya, Chernin (in preparation) dynamical structures of this type provide very favorable conditions for triggering star formation.

The idea that activity of OB associations can trigger star formation in the surrounding interstellar medium is not a new one, see for example a detailed analytical treatment by McCray and Kafatos (1987); a review by Elmegreen (1998) and references therein. Multiple SN explosions have been considered as the major agent of propagating star formation.

Lozinskaya and Chernin argue that multiple collisions of the fast inner shells with the massive slow one trigger the process of star formation regulated by a combine action of gravitational fragmentation in the slow shells and shock compression of the fragments by the fast shells. Stellar wind plays an important role in the vicinity of rich OB associations in the dense ISM.

The way in which the process develops depends on the ambient density: fragmentation of the shells occurs before (or after) its termination, before (or after) WR stars appear if the density is relatively high (low).

Two sequences of the events are possible. (1) It may be that the slow shell is near the state of termination with the expansion velocity about its isothermal sound speed; and this shell remains stable against gravitational fragmentation. Then first impacts by the fast inner shells are able to compress the gas of the slow shell, initiating the onset of instability.

(2) In the dense ISM the slow shell may come to the state of gravitational fragmentation before its termination and before WR stars appear. In that case the fast shells collide with individual fragments and it's able

Table 1: Supershells with two-component kinematics.

supershell	size, pc	slow shell		fast features		reference
		V(exp) km/s	kinematic age, yrs	V km/s	kinematic age, yrs	
Cyg OB1, Cyg OB3	80 – 100	$\leq$ 10	$\geq 3 \cdot 10^6$	-85 -55	$4 \cdot 10^5$	1
Car OB1, Car OB2	200	10	$6 \cdot 10^6$	100	$6 \cdot 10^5$	2 – 6
Ori OB1, λ Ori	280	15 – 25	$4 \cdot 10^6$	100 – 120	$3 \cdot 10^5$	2, 7 – 9

REFERENCES:
1 - Lozinskaya et al. (1998a);
2 - Lozinskaya, 1992 and references therein
3 - Cowie et al. (1981); 4 - Walborn and Hesser (1981)
5 - Walborn et al. (1984); 6 - Seward, Chlebowski (1982)
7 - Goudis (1982); 8 - Reynolds, Ogden (1979)
9 - Cowie et al. (1979)

to compress these clouds and accelerate their gravitational collapse.

In both cases the typical parameters of the massive shell's fragments are favorable for molecularization in their cores.

The result of the combine action of two major mechanisms of triggering star formation – gravitational fragmentation and shock compression – may be much more significant, than in other cases, when they act separately. In this sense, rich OB associations seem to be most effective agents of induced star formation, at least on the 500 pc scale dimensions.

3. The origins of an "individual" wind-blown bubble (or a SNR) strongly depends on the entire history of an active star-forming complex

Our recent observations of the galaxy IC1613 clearly illustrate this approach (Lozinskaya et al., 1998b; Afanasiev, Lozinskaya, Moiseev, Blanton (in press). This irregular dwarf galaxy represents a relatively clean case: we know of only one WR star (and that one of a rare subclass WO), only one SNR, and only one recent star-forming region.

Six WO stars have been identified in the Local Group galaxies (compared to about 600 WRs): three are in our Galaxy, two are in the Magellanic Clouds and one is in IC1613. WOs occur in the very short final stage in the massive stars evolution, the stage of a nearly naked CO core, immediately preceding the supernova explosion. These stars are characterized by a very powerful wind, the wind's mechanical luminosity 10 times higher than that for usual WRs; and they are extremely hot, $T_{eff} \simeq 100,000$ K.

Figure 1(a) shows a deep monochromatic H_α image of the neighborhood of the WO star in IC1613 we obtained with the Interferometer Fabry=Perot at 6-m telescope SAO RAN (Afanasiev et al., in press). The WO star is in the center of the previously known bright nebula S3 – an HII region $29 \times 9''$ in size, with strong HeII 4686 emission near the star (Hodge et al. 1990; Hunter et al. 1993; Garnett et al. 1991). Two extended, weak, shell-like formations 100 and 300 pc in size are clearly seen both sides of the bright elongated core. I have already declared several times that there is a huge bipolar structure related to the WO star (see Lozinskaya, 1997) but it was at the level of my suspicion.

Our measurements indicate on the expansion of both shells: the lower limit of expansion velocity is around 50 km/s for the brighter lobe and at least 70 km/s for the faint one (Afanasiev et al., in press).

A possible explanation of the structure is that these two shells are formed by the powerful wind on either sides of a dense layer of gas. The origin of the layer may be related to a previous stellar activity in the area. The large-scale neutral gas distribution in IC1613 seems to confirm the suggestion.

The image of the galaxy in the 21 cm line obtained by Lake, Skillman (1989) displays two most prominent features: a "supercavity" and a brightest spot – a dense giant complex of the neutral gas. The sizes of both features are about 700 pc.

Deep H_α images of the dense giant cloud's area displays an extended complex of interlocked ionized shells and supershells (see Meaburn et al., 1988; Lozinskaya et al., 1998b) around a group of young stellar associations. The sizes of the shells are 100–300 pc, expansion velocities of 30-50 km/s according to Meaburn at al.,

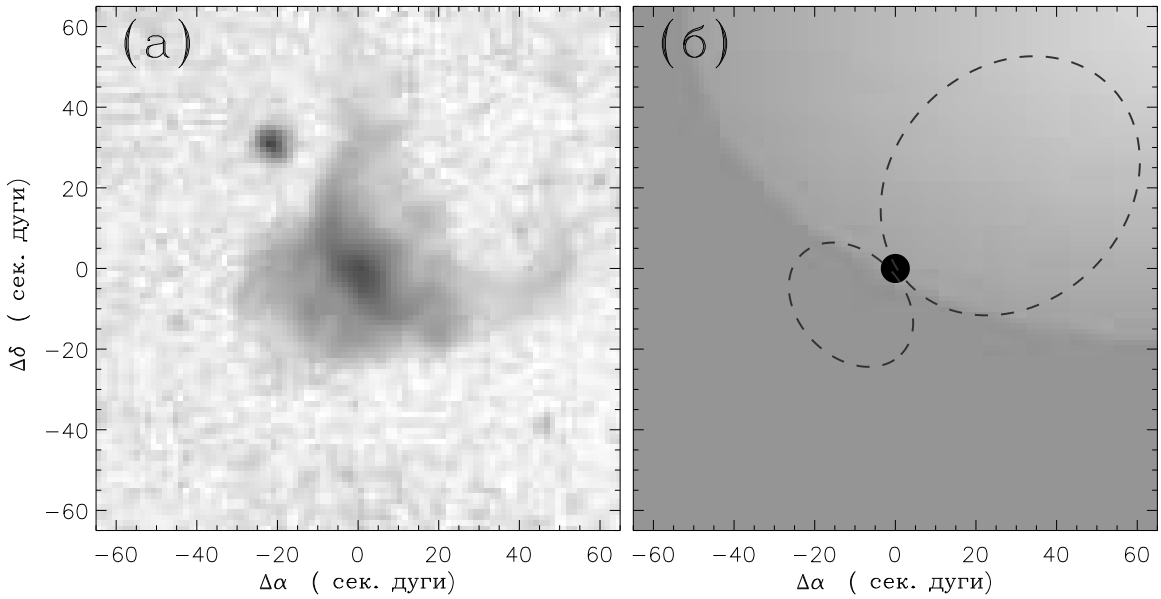

Figure 1: (a): Deep monochromatic H_α image of the bipolar shell related to the WO star in IC1613 obtained with the Interferometer Fabry=Perot at 6-m telescope SAO RAN (Afanasiev et al., in press). The brightness is in the logarithmic scale. (b): The scheme of the bipolar structure superimposed on the one-quarter sector of the "supecavity" in the neutral gas distribution from 21 cm line observations by Lake, Skillman, 1989.

1988. This is the only recent star-forming region in the galaxy.

It is interesting to note that the single known SNR in IC1613 is located in this star-forming complex. We proposed for ROSAT observations, and we identified the brightest X-ray source in the galaxy IC1613 with its single known SNR (Lozinskaya et al., 1998b) This SNR appears to be peculiar. It is one of the brightest nebulae in the galaxy. At the same time, this is one of the most luminous X-ray SNR in the Local Group, including Milky Way – like Crab Nebula and Cass A. To explain the coexistence of the hot X-ray plasma and cool, dense optical gas we proposed that the supernova explosion took place inside a cavity surrounded by a dense shell. And the SNR is just at the stage of encountering the dense wall of the cavity. The cavity's origin is most probably related to the previous activity of the parent OB-association.

Now, let us return to the WO star and its bipolar shells. What is an expected future of a star-forming complex like one just mentioned? In about 10^8 yrs we'll find here a supercavity surrounded by a dense neutral shell, similar to the above mentioned superhole.

Therefore, the two most prominent large-scale structures in IC1613: the superhole in 21 cm distribution and the giant complex of star formation appear to represent two stages of evolution of a giant molecular cloud.

The bipolar shell's location at the edge of the supercavity, and orientation of the larger and fainter lobe in the direction of the low-density interior of the cavity, and the shapes of the large lobes (see Fig. 1b) - all seem to be in agreement with the scenario of the WO star in the dense core of a layer of the interstellar gas with large-scale density gradient, proposed by Lozinskaya, 1997. The cavity and the wall seems to be created by a previous burst of star formation in the galaxy, similar to previously mentioned one.

Therefore our observations of the two peculiar objects in IC1613: the bipolar shell around WO star and the SNR provide a clear demonstration of the statement that the entire history of an active star-forming complex dictates the nature of each individual SNR or wind-swept shell.

Acknowledgements. Our investigations described here have been supported by the Russian Foundation for Basic Research under grants 95-02-03781 and 98-02-16032.

References

Afanasiev V.L., Lozinskaya T.A., Moiseev A.V., Blanton E.: *Astron.Zh.Lett.,* (in press)

Avedisova V.S.: 1971, *Sov.Astron.,* **15**, 708. (1972, Transl. from *Astron.Zh.,* **48**, 894.)

Castor J., McCray R., Weaver R.: 1975, *ApJ,* **200**, L107.

Cowie, L.L., Hu, E.M., Taylor, W., York, D.G.: 1981, *ApJ Lett.,* **250,** L25.

Cowie, L.L., Songaila, A., York, D.G.: 1979, *ApJ,* **230,** 469.

Elmegreen G.B." 1998, *ASP Conf. Ser.*, **148**, 149.

Garnett, D. R., Kennicutt, R. C., Chu, Y.-H., Skillman, E. D.: 1991, *ApJ,* **373,** 458.

Goudis, C.: 1982, *Astrophys. Space Sci.*, **90,** 1.

Hodge, P., Lee, M. G., Gurwell, M.: 1990, *PASP,* **102,** 1245.
Hunter D.A., Hawley W.N., Gallagher J.S.: 1993, *A.J.,* **106,** 1797.
Lake G., Skillman E.D.: 1989, *Astron.J.,* **98,** 1274.
Lozinskaya, T.A.: 1992, *Supernovae and Stellar Wind in the Interstellar Medium,* New York: AIP.
Lozinskaya T.A.: 1997, *Astrophys. and Space Sci.,* **252,** 199.
Lozinskaya T.A.: 1998, *Astronomy Letters*, **24**, 237. (Transl. from it Pis'ma Astron.Zh., **24**, 285.)
Lozinskaya T.A.: 1999, in *PASP, Confer. Ser. "New perspectives on the Interstellar Medium."* eds A.R.Taylor, T.L.Landecker, G.Joncas., **168**, 427.
Lozinskaya T. A., Sitnik T.G.: 1988, *Pisma Astron.Zh*, **14**, 240. (*Astronomy Lett.*)
Lozinskaya T.A., Pravdikova V.V., Gosachinskij I.V., Trushkin S.A.: 1997, *Astron.Zh.*, **74**, 376.
Lozinskaya T.A., Pravdikova V.V., Sitnik T.G., Esipov V.F., Melnikov V.V.: 1998a, *Astronomy Reports*, **42**, 453. (transl. from *Astron.Zh.,* **75**, 514.)
Lozinskaya T.A., Silchenco O.K., Helfand D.J., Goss W.M.: 1998b, *Astron.J.,* **116**, 2328.
Lozinskaya T.A., Chernin A.D.: (in preparation)
Marston A.P.: 1995, *Astron.J.*, **109**, 2257.
McCray R., Kafatos M.: 1987, *ApJ*, **317**, 190.
Meaburn J., Clayton C.A., Whitehead M.G.: 1998, *MNRAS,* **235**, 479.
Nichols-Bohlin J., Fesen R.A.: 1993, *Astron.J.,* **105**, 672.
Oey M.S., Massey P.: 1994, *Astrophys.J.,* **425**, 635.
Oey M.S.; 1996, *Astrophys.J.,* **467**, 666.
Pikelner S.B.: 1968, *Astrophys.Lett.,* **2**, 97.
Reynolds R.J., Ogden P.M.: 1979, *ApJ,* **229**, 942.
Seward F.D., Chlebowski T.: 1982, *ApJ,* **256**, 530.
Steigman G., Strittmatter P.A., Williams R.E., et al.: 1975, *ApJ*, **198**, 575.
Walborn N.R., Hesser J.E.: 1981, *ApJ,* **252**, 156.
Walborn N.R., Heckathorn J.N., Hesser J.E.: 1984, *ApJ,* **276**, 524.
Weaver R., McCray R., Castor J., et al.: 1977, *ApJ,* **218**, 377.

IMF AND EVOLUTION OF CLOSE BINARIES AFTER STARFORMATION BURSTS

S.B. Popov[1], M.E. Prokhorov[1], V.M. Lipunov[1,2]

[1] Sternberg Astronomical Insitute
Universitetskii pr. 13, Moscow 119899 Russia, *polar@xray.sai.msu.su*
[2] Department of physics, Moscow State University, *lipunov@sai.msu.su*

ABSTRACT. This paper is a continuation and development of our previous articles (Popov et al., 1997, 1998). We use "Scenario Machine" (Lipunov et al., 1996b) – the population synthesis simulator (for single binary systems calculations the program is available in WWW: **http://xray.sai.msu.ru/** (Nazin et al., 1998)) – to calculate evolution of populations of several types of X-ray sources during the first 20 Myrs after a starformation burst.

We examined the evolution of 12 types of X-ray sources in close binary systems (both with neutron stars and with black holes) for different parameters of the IMF – slopes: $\alpha = 1$, $\alpha = 1.35$ and $\alpha = 2.35$ and upper mass limits, M_{up}: 120 $M_\odot$, 60 $M_\odot$ and 40 $M_\odot$. Results, especially for sources with black holes, are very sensitive to variations of the IMF, and it should be taken into account when fitting parameters of starformation bursts.

Results are applied to several regions of recent starformation in different galaxies: Tol 89, NGC 5253, NGC 3125, He 2-10, NGC 3049. Using known ages and total masses of starformation bursts (Shaerer at al., 1998) we calculate expected numbers of X-ray sources in close binaries for different parameters of the IMF. Usually, X-ray transient sources consisting of a neutron star and a main sequence star are most abundant, but for very small ages of bursts (less than ≈ 4 Myrs) sources with black holes can become more abundant.

Key words: Stars: binary: evolution;

1. Introduction

Theory of stellar evolution and one of the strongest tools of that theory – population synthesis – are now rapidly developing branches of astrophysics. Very often only the evolution of single stars is modeled, but it is well known that about 50% of all stars are members of binary systems, and a lot of different astrophysical objects are products of the evolution of binary stars. We argue, that often it is necessary to take into account the evolution of close binaries while using the population synthesis in order to avoid serious errors.

Initially this work was stimulated by the article Contini et al. (1995), where the authors suggested an unusual form of the initial mass function (IMF) for the explanation of the observed properties of the galaxy Mrk 712 . They suggested the "flat" IMF with the exponent $\alpha = 1$ instead of the Salpeter's value $\alpha = 2.35$. Contini et al. (1995) didn't take into account binary systems, so no words about the influence of such IMF on the populations of close binary stars could be said. Later Shaerer (1996) showed that the observations could be explained without the IMF with $\alpha = 1$. Here we try to determine the influence of the variations of the IMF on the evolution of compact binaries and apply our results to seven regions of starformation (Shaerer et al., 1998, hereafter SCK98).

Previously (Lipunov et al., 1996a) we used the "Scenario Machine" for calculations of populations of X–ray sources after a burst of starformation at the Galactic center. Here, as before in Popov et al. (1997, 1998), we model a general situation — we make calculations for a typical starformation burst. We show results on twelve types of binary sources with significant X-ray luminosity for three values of the upper mass limit for three values of α.

2. Model

Monte-Carlo method for statistical simulations of binary evolution are now widely used in astrophysics: for analysis of radio pulsar statistics, for formation of the galactic cataclysmic variables etc. (see the review in van den Heuvel 1994).

Monte-Carlo simulations of binary star evolution allows one to investigate the evolution of a large ensemble of binaries and to estimate the number of binaries at different evolutionary stages. Inevitable simplifications in the analytical description of the binary evolution that we allow in our extensive numerical calculations, make those numbers approximate to a factor of 2-3. However, the inaccuracy of direct calculations giving

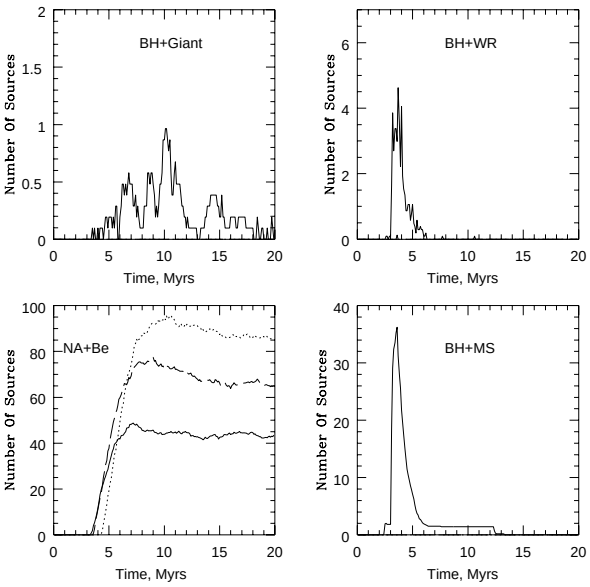

Figure 1: Evolution of numbers of binary systems after a burst of starformation. $\alpha = 1.35$. BH+Giant – A BH with a He-core Star (Giant). BH+WR – A BH with a Wolf–Rayet Star. NA+Be – An Accreting NS with a Main Sequence Star (Be-transient). BH+MS – A BH with a Main Sequence Star

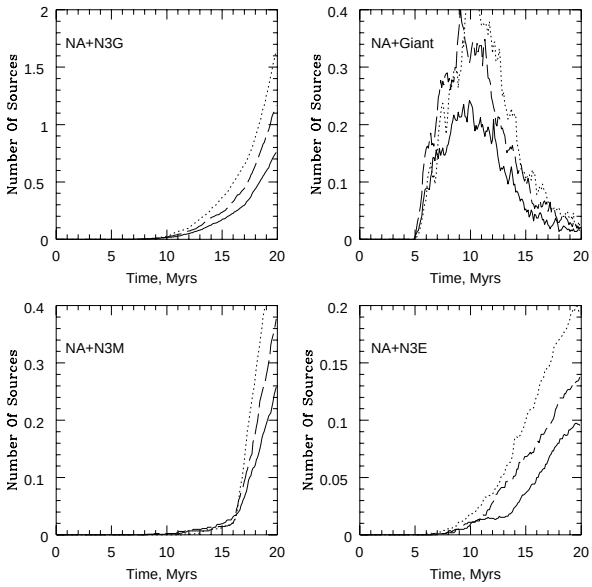

Figure 2: Evolution of numbers of binary systems after a burst of starformation. $\alpha = 1.35$. NA+N3G – An Accreting NS with a Roche-lobe filling star, when the binary loses angular momentum due to gravitational radiation. NA+Giant – An Accreting NS with a He-core Star (Giant). NA+N3M – An Accreting NS with a Roche-lobe filling star, when the binary loses angular momentum due to magnetic wind. NA+N3E –An Accreting NS with a Roche-lobe filling star (nuclear evolution time scale).

the numbers of different binary types in the Galaxy (see e.g. van den Heuvel 1994) seems to be comparable to what follows from the simplifications in the binary evolution treatment.

In our analysis of binary evolution, we use the "Scenario Machine", a computer code, that incorporates current scenarios of binary evolution and takes into account the influence of magnetic field of compact objects on their observational appearance. A detailed description of the computational techniques and input assumptions is summarized elsewhere (Lipunov et al. 1996b; see also: **http://xray.sai.msu.ru/˜ mystery/articles/review/**), and here we briefly list only principal parameters and initial distributions.

We trace the evolution of binary systems during the first 20 Myrs after their formation in a starformation burst. Obviously, only stars that are massive enough (with masses $\geq 8 - 10$ $M_\odot$) can evolve off the main sequence during the time as short as this to yield compact remnants: neutron stars (NSs) and black holes (BHs). Therefore we consider only massive binaries, i.e. those having the mass of the primary (more massive) component in the range of $10\,M_\odot - M_{up}$.

We assume that a NS with a mass of 1.4 $M_\odot$ is formed as a result of the collapse of a star, whose core mass prior to collapse was $M_* \sim (2.5 - 35)$ $M_\odot$. This corresponds to an initial mass range $\sim (10 - 60)$ $M_\odot$, taking into account that a massive star can lose more than $\sim (10 - 20)\%$ of its initial mass during the evolution with a strong stellar wind. The most massive stars are assumed to collapse into a BH once their mass before the collapse is $M > M_{cr} = 35$ $M_\odot$. The BH mass is calculated as $M_{bh} = k_{bh} M_{cr}$, where the parameter k_{bh} is taken to be 0.7.

The mass limit for NS (the Oppenheimer-Volkoff limit) is taken to be $M_{OV} = 2.5$ $M_\odot$, which corresponds to a hard equation of state of the NS matter.

We made calculations for several values of the coefficient α:

$$\frac{dN}{dM} \propto M^{-\alpha}$$

We calculated 10^7 systems in every run of the program. Then the results were normalized to the total mass of binary stars in the starformation burst. We also used different values of the upper mass limit, M_{up}.

3. Results

On the figures we show some of the results of our calculations (full results can be found in the electronic preprint (Popov et al. 1999)). On all graphs on the X-

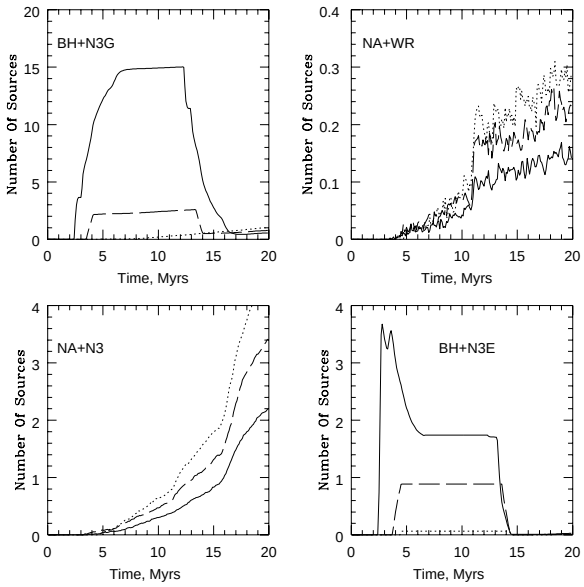

Figure 3: Evolution of numbers of binary systems after a burst of starformation. $\alpha = 1.35$. BH+N3G – A BH with a Roche-lobe filling star, when the binary loses angular momentum by gravitational radiation. NA+WR – An Accreting NS with a Wolf–Rayet Star. NA+N3 – An Accreting NS with a Roche-lobe filling star (fast mass transfer from the more massive star). BH+N3E – A BH with a Roche-lobe filling star (nuclear evolution time scale).

axis we show the time after the starformation burst in Myrs, on the Y- axis — number of the sources of the selected type that exist at the particular moment.
On the figures results are shown for three values of upper mass limits: $120M_\odot$ – solid lines, $60M_\odot$ – dashed lines, $40M_\odot$ – dotted lines.

The calculated numbers were normalized for $10^6\,M_\odot$ in binary stars. We show on the figures and in tables only systems with the luminosity of compact object greater than 10^{33} erg/s.

Curves were not smoothed so all fluctuations of statistical nature are presented. We calculated 10^7 binary systems and then the results were normalized.

We apply our results to seven regions of recent starformation (see the tables, the full set can be found in (Popov et al., 1999)). Ages, total masses and some other characteristics were taken from SCK98 (we used total masses determined for Salpeter's IMF even for the IMFs with different parameters, which is a simplification). We made an assumption, that binaries contain 50% of the total mass of the starburst. Numbers were rounded off to the nearest integer.

As far as for several regions ages are uncertain, we made calculations for two values of the age.

Different types of close binaries show different sensitivity to variations of the IMF. When we replace $\alpha = 2.35$ by $\alpha = 1$ the numbers of all sources increase. Systems with BHs are more sensitive to such variations.

When one try to vary the upper mass limit, another situation appear. In some cases (especially for $\alpha = 2.35$) systems with NSs show little differences for different values of the upper mass limit, while systems with BHs become significantly less (or more) abundant for different upper masses. Luckily, X-ray transients, which are the most numerous systems in our calculations, show significant sensitivity to variations of the upper mass limit. But of course due to their transient nature it is difficult to use them to detect small variations in the IMF. If it is possible to distinguish systems with BH, it is much better to use them to test the IMF.

Table 1: He 2-10; age 5.5 Myrs; total mass $10^{6.8}M_\odot$

Slope	2.35	2.35	2.35	1.35	1.35	1.35
Up.mas.	120	60	40	120	60	40
bh+ms	0	0	0	16	0	0
bh+giant	0	0	0	0	0	0
bh+n3e	1	0	0	9	4	0
bh+n3g	4	1	0	62	10	0
bh+wr	0	0	0	1	0	0
na+ms	24	22	15	187	241	165
na+n3	0	0	0	0	0	0
na+wr	0	0	0	0	0	0
na+n3m	0	0	0	0	0	0
na+n3e	0	0	0	0	0	0
na+n3g	0	0	0	0	0	0
na+giant	0	0	0	0	0	0

Table 2: He 2-10; age 6.0 Myrs; total mass $10^{6.8}M_\odot$

Slope	2.35	2.35	2.35	1.35	1.35	1.35
Up.mas.	120	60	40	120	60	40
bh+ms	0	0	0	9	0	0
bh+giant	0	0	0	1	0	0
bh+n3e	1	0	0	9	4	0
bh+n3g	4	1	0	65	11	0
bh+wr	0	0	0	0	0	0
na+ms	29	30	22	198	283	233
na+n3	0	0	0	0	1	1
na+wr	0	0	0	0	0	0
na+n3m	0	0	0	0	0	0
na+n3e	0	0	0	0	0	0
na+n3g	0	0	0	0	0	0
na+giant	0	0	0	0	1	0

4. Discussion and conclusions

The results of our calculations can be easily used to estimate the number of X- ray sources for different parameters of the IMF if the total mass of stars

Table 3: NGC5253A; age 3.0 Myrs; total mass $10^{6.6} M_\odot$

Slope	2.35	2.35	2.35	1.35	1.35	1.35
Up.mas.	120	60	40	120	60	40
bh+ms	0	0	0	5	0	0
bh+giant	0	0	0	0	0	0
bh+n3e	1	0	0	10	0	0
bh+n3g	1	0	0	11	0	0
bh+wr	0	0	0	0	0	0
na+ms	0	0	0	0	0	0
na+n3	0	0	0	0	0	0
na+wr	0	0	0	0	0	0
na+n3m	0	0	0	0	0	0
na+n3e	0	0	0	0	0	0
na+n3g	0	0	0	0	0	0
na+giant	0	0	0	0	0	0

Table 4: NGC5253B; age 5.0 Myrs; total mass $10^{6.6} M_\odot$

Slope	2.35	2.35	2.35	1.35	1.35	1.35
Up.mas.	120	60	40	120	60	40
bh+ms	1	0	0	21	0	0
bh+giant	0	0	0	1	0	0
bh+n3e	1	0	0	7	3	0
bh+n3g	2	1	0	36	7	0
bh+wr	0	0	0	3	0	0
na+ms	11	10	5	92	112	58
na+n3	0	0	0	0	0	0
na+wr	0	0	0	0	0	0
na+n3m	0	0	0	0	0	0
na+n3e	0	0	0	0	0	0
na+n3g	0	0	0	0	0	0
na+giant	0	0	0	0	0	0

Table 5: Tol 89; age 4.5 Myrs; total mass $10^{5.7} M_\odot$

Slope	2.35	2.35	2.35	1.35	1.35	1.35
Up.mas.	120	60	40	120	60	40
bh+ms	0	0	0	4	0	0
bh+giant	0	0	0	0	0	0
bh+n3e	0	0	0	1	0	0
bh+n3g	0	0	0	4	1	0
bh+wr	0	0	0	0	0	0
na+ms	1	1	0	9	9	2
na+n3	0	0	0	0	0	0
na+wr	0	0	0	0	0	0
na+n3m	0	0	0	0	0	0
na+n3e	0	0	0	0	0	0
na+n3g	0	0	0	0	0	0
na+giant	0	0	0	0	0	0

Table 6: NGC3125; age 5.0 Myrs; total mass $10^{6.1} M_\odot$

Slope	2.35	2.35	2.35	1.35	1.35	1.35
Up.mas.	120	60	40	120	60	40
bh+ms	0	0	0	7	0	0
bh+giant	0	0	0	0	0	0
bh+n3e	0	0	0	2	1	0
bh+n3g	1	0	0	12	2	0
bh+wr	0	0	0	1	0	0
na+ms	3	3	1	29	36	18
na+n3	0	0	0	0	0	0
na+wr	0	0	0	0	0	0
na+n3m	0	0	0	0	0	0
na+n3e	0	0	0	0	0	0
na+n3g	0	0	0	0	0	0
na+giant	0	0	0	0	0	0

and age of a starburst are known (in (Popov et al., 1997, 1998) analytical approximations for source numbers were given). And we estimate numbers of different sources for several regions of recent starformation.

Here we tried to show, that populations of close binaries are very sensitive to the variations of the IMF. One must be careful, when trying to fit the observed data for single stars with variations of the IMF. And, vice versa, using detailed observations of X-ray sources, one can try to estimate parameters of the IMF, and test results, obtained from single stars population.

Acknowledgements. We want to thank K.A. Postnov for discussions and G.V. Lipunova and I.E. Panchenko for technical assistance. SBP also thanks organizers of the conference for support and hospitality.

This work was supported by the grants: NTP "Astronomy" 1.4.2.3., NTP "Astronomy" 1.4.4.1 and "Universities of Russia" N5559.

References

Contini T., Davoust E., Considere S.: 1995, *As. Ap.*, **303**, 440

Lipunov V.M., Ozernoy L.M., Popov S.B., Postnov K.A. Prokhorov M.E.: 1996a, *Ap.J.* **466**, 234

Lipunov V.M., Postnov K.A., Prokhorov M.E.: 1996b, *Ap. Space Phys. Rev.* **9**, part 4.

Nazin S.N., Lipunov V.M., Panchenko I.E., Postnov K.A., Prokhorov M.E., Popov S.B.: 1998, *Grav. Cosmology,* **4**, suppl. "Cosmoparticle Physics", pt. 1, 150 (astro-ph 9605184).

Popov S.B., Lipunov V.M., Prokhorov M.E., Postnov K.A.: 1997, *astro-ph/9711352.*

Popov S.B., Lipunov V.M., Prokhorov M.E., Postnov K.A.: 1998, *AZh*, **75**, 35 (astro-ph/9812416).

Popov S.B., Prokhorov M.E., Lipunov V.M.: 1999, *astro-ph/9905070.*

Schaerer D.: 1996, *Ap.J.*, **467**, L17

Schaerer D., Contini T., Kunth D.: 1998, *As. Ap.* **341**, 399 (astro-ph/9809015) (SCK98).

van den Heuvel, E.P.J.: 1994, in: "Interacting Binaries", Eds. Shore, S.N., Livio, M., van den Heuvel, E.P.J., Berlin, Springer, 442.

ON VARIABILITY OF OBSERVED POLARIZATION PARAMETERS OF GALACTIC RADIO EMISSION AT METER WAVES

V.A. Razin, A.I. Teplykh

Radiophysical Research Institute (NIRFI)
25, B.Pecherskaya, Nizhnij Novgorod 603600 GSP-51 Russia
tepl@nirfi.sci-nnov.ru

ABSTRACT. The polarization temperature T_p variations, which exceeded errors of measurements were observed already during the initial (1958-1962) and then the following measurements of linear polarization of galactic radio emission at meter waves. The long term regular polarizations observations carring out at NIRFI Radio Astronomical Observatory "Staraya Pustyn'" in the range 150-290 MHz, prove the existences of variability of available polarization temperature T_p and also position angle χ_0, in the broad time intervals. Data analyses shows that variations of T_p and χ_0 are not connected directly with solar activity because there are no correlations with indices R9 and C9. Cross-correlation analyses of T_p variations and galactic cosmic rays intensity I_c testify to there statistical dependence. Since 1981 till 1984 at 290 MHz nine time intervals has been found, each of them lasting about one month, within the limits of which correlation coefficients $R(T_p, I_c)$ are in interval $0.5 \pm 0.2 < |R| < 0.8 \pm 0.1$. Among possible reasons of polarization parameter variability there are effects of propagation of radio waves in inhomogeneous magnetoactive plasma of geleosphere, emission of non-stationary fluxes of high energy electrons in the interplanetary medium, and also linearly polarized component of radioemission, caused by Thompson scattering of solar radio emission.

Key words: Galactic radio emission, linear polarization, variability, metre band, cosmic rays.

1. Introduction

Already during initial (1958-1962) measurements of linear polarization of galactic radio emission at metre waves the polarization temperature (T_p) variations, which exceeded errors of measurements were observed. There were irregular and very large (up to 100%) daily variations of T_p and also slowly changes of T_p according the time scale about several months and years depending on phases of solar activity (Razin 1958, 1964). T_p variations also observed during further polarization measurements carried out at the NIRFI Radioastronomical Observatory "Staraya Pustyn'" at 210 MHz (Kapustin et al. 1973), in the frequency interval 195-215 MHz (Teplykh et al. 1980) and at 150 MHz (Teplykh et al. 1985).

2. Results of measurements and dicussion.

In the course of long-term regular observations of the Galactic radio emission linear polarization at 290 MHz at "Staraya Pustyn'" it has been obtained a large amount of data testifying to noticeable variations of the brightness polarization temperature T_p and polarization plane position angle χ_0.

The data on T_p and χ_0 variations of linearly polarized radio emission for the region of strong polarization with Galactic coordinates $l = 147^\circ$, $b = +8^\circ$ (PGA147 + 8) and for North Celestial Pole region (NSP) at 290 MHz are given in (Teplykh et al. 1990) for the period 1977-1988. There have been significant T_p variations for these regions in a wide spectrum of time intervals: short-term (with a period of several days), sometimes very strong (nearly two times) as well as yearly recurrent seasonal T_p variations. Special attention must be given to synchronous T_p variations of both $GPA147 + 8$ and NCP regions observed simultaneously in 1980-1981 with a period of about a year (Kovalchuk O.M., Teplykh A.I. 1991).

The values of χ_0 have also temporal variations. For NCP they are from -30° up to -10° in the equatorial coordinate system with the mean value $< \chi_0 >= -22^\circ \pm 2^\circ$. However, from april to July 1984 and in May-June 1985 we observed values $+20^\circ$ and $+10^\circ$, respectively, where in the second case it was registered a smooth change of χ_0 by 30° for a period of one month. It should be noted that during these two very intervals we have registered the strongest short-term fluctuations accompanying the growth of T_p.

To clear up the reasons of polarization characteristic

variability we have compared T_p with the geomagnetic activity index $C9$ and solar activity index $R9$ fore the period 1980-1984. The analysis of the data has shown that there is not any definite dependence of T_p on $C9$ and $R9$ although monthly average values of T_p increased gradually with the growth of the solar activity starting with the minimum of solar activity in 1983-1984 up to 1988 approximately by $(15 \div 20)\%$ per year.

Seaking the reasons of polarization parameters variability we tried to find out the correlation between T_p and daily average values of cosmic ray intensity I_c. For this purpose we used the measurement results of T_p obtained at "Staraya Pustyn'" ($\lambda = 43°.63$, $\varphi = 55°.66$) at 290 MHz in period of 1980-1984 and neutron monitoring data obtained at stations Huankayo ($\lambda = 248°.67$, $\varphi = -12°.03$) and Tokio ($\lambda = 139°.72$, $\varphi = 35°.75$) and published in the monthly journal "Solar-Geophysical Data". These stations were chosen for the analysis as those having the highest energy detection threshold ($13.01GV$ for Huankayo and $11.50GV$ for Tokyo) which registered the events associated mainly with high-energy cosmic rays of Galactic origins (so the events associated with solar cosmic rays were practically excluded). The cosmic ray intensity for these data is characterized by a number of events in hour (cts/h) divided by scale factor 100 for Huankayo and 256 for Tokyo. The correlation coefficient $R(T_p, I_c)$ and its error σR were calculated by the standard formulas. Correlation coefficient R can be both positive when T_p increases with growth of I_c and negative when T_p decreases with the growth of I_c.

At the early stage of analysis we have plotted the dependencies $T_p(I_c)$ for $PGA147 + 8$ (42 points) and NCP (20 points) for the period October 1980 - December 1981 using Huankayo station data. The correlation coefficients turned to be $+0.44 \pm 0.12$ and $+0.36 \pm 0.19$, respectively.

We did not carry out regular observations of $PGA147 + 8$ since the end of 1981, so the further results are related only to NCP region observations. We have plotted $T_p(I_c)$ for the period September 1980 - December 1984 for Huankayo station data (152 points) and for Tokyo station data (213 points). The correlation coefficients are -0.51 ± 0.06 and -0.47 ± 0.05 respectively.

The fact that at the positive correlation coefficient related to only a part of the time interval taken the correlation coefficient related to the whole period of observation is negative suggests that at the shorter time intervals one can expect lager values of the correlation coefficients both positive and negative ones. To prove this suggestion we calculated then the "sliding" correlation coefficient R on time intervals of about $20 \div 30$ days: each recurrent value of R refers to the following interval the beginning and end of which are shifted by one or several days ahead. We have got in this way the sign-alternating dependence of R on time. The Table 1 gives the values of R corresponding to maxima of this dependence and exceeding module 0.5.

Table 1.

R	ΔR	Period	Year
-0.50	0.24	02-28.09	1980
-0.73	0.16	28.04-25.05	1981
+0.51	0.23	29.09-06.10	1983
+0.54	0.24	05-19.12	1983
+0.53	0.18	09.02-03.03	1984
+0.72	0.14	19.05-26.06	1984
+0.58	0.20	28.06-26.07	1984
-0.61	0.16	21.08-14.09	1984
-0.81	0.11	26.09-25.10	1984

Then we have compared the values T_p and I_c averaged over the time intervals given in Table 1. The correlation coefficient calculated on the basis of these values is equal to $R = -0.69 \pm 0.17$.

Thus, the observational data make it possible at this step of work to make a conclusion on a relation between the temperature of linearly polarized component of the cosmic radio emission T_p in the metre radio wave band and the cosmic ray intensity I_c. This relation is rather complicated. There are intervals with significant correlation coefficients of T_p and I_c values being both positive or negative one. Between these intervals there are periods where the correlation coefficient is small and as a rule changes its sign. Some periodicity of about $1.5 \div 2$ months can be seen in the change of the correlation coefficient sign.

The next stage of the work should involve a further treatment of experimental data on T_p after 1984 up to 1998 using the data on cosmic ray intensity I_c obtained during ground-based experiments as well as on board the spaceships and earth satellites.

3. Conclusion

It is apparent the variability of cosmic radiation polarization parameters in the metre wave band is associated with the processes occurring in the near space: possibly in the interplanetary medium or in a local interstellar medium and the region of its interaction with the Solar system. This is testified first by short-term fluctuations of T_p and as well as by their seasonal behaviour. Besides, the linearly polarized radio emission from far Galactic regions is depolarized in the metre band due to the difference of polarization plane Faraday rotation along the line of sight. Nondepolarized radiation remains only what is generated nearly the Solar system and the linear size of the generation area along the line of sight is contracted with the wavelength making it possible "to sound" the interstellar medium along the

line of sight (Razin V.A., Hizhnyakova I.P. 1969). This effect is to be particularly pronounced in the regions where the Galactic magnetic field is parallel to the line of sight.

In this connection NIRFI has planned at a number of frequencies in the metre band and has started this year at 290 MHz the observations of the regions with coordinates $\alpha = 22^h, \delta = 55^\circ$ and $\alpha = 19^h$, $\delta = 14^\circ$, as well as the apex region $\alpha = 18^h$, $\delta = 30^\circ$.

To create a physical model explaining the reasons of polarization parameter variability it is also necessary to consider the effects of radiowaves propagation in inhomogeneous magnetoactive plasma of heliosphere, the radiation of high-energy nonstationary electron currents in the interplanetary medium, as well as the possibility of radio emission linearly polarized component generation in an inhomogeneous interplanetary medium due to the Thompson effect.

Acknowledgements. The authors are thankful to Russia State Scientific Program "Fundamental Cosmic Research. Astronomy" for financial support.

References

Razin V.A.: 1958, *A.J.*, **35**, 241.

Razin V.A.: 1964, *Izvestiya Vuzov. Radiofizika*, **7**, 395

Razin V.A., Hizhnyakova I.P.: 1969, *Izvestiya Vuzov. Radiofizika*, **12**, 479.

Kapustin P.A., Petrovskij A.A., Pupysheva L.V., Razin V.A.:1973, *Izvestiya Vuzov. Radiofizika*, **16**, 1325

Teplykh A.I. et al.: 1980, *Reports of NIRFI*, number of state registration **76019925**, 27.

Teplykh A.I. et al.: 1985, *Reports of NIRFI*, number of state registration **81039598**, 40.

Kovalchuk O.M., Teplykh A.I.: 1991, *XXIII radio-astronomical conference. Ashkhabad.* Thesisses, 67.

CALCULATION OF CHEMICAL EQUILIBRIUM IN THE INTERSTELLAR CLOUD

I. Shmeld[1], J. Freimanis[1], N.G. Bochkarev[2]

[1] Institute of Astronomy, Latvian University
Raina Blvd 19, Riga, LV–1586 Latvia *shmeld@latnet.lv*
[2] Sternberg Astronomical Institute
Universitetskij Prosp. 13, 119899 Moscow, Russia *boch@sai.msu.ru*

ABSTRACT. In order to calculate the molecular concentrations in the interstellar cloud and to obtain their spatial distribution we have made a computational code to solve the set of equations for chemical equilibrium and equations of charge and atom balance. Now 109 molecules and 1070 chemical reactions are included. Besides, the gas phase reactions with neutrals and ions, formation of molecular hydrogen on grains and the ionization and dissociation due to cosmic rays and UV radiation were taken into account. In order to calculate the photodissociation rates of H_2 and CO molecules we take into consideration: i) extinction due to H_2 Lyman and Werner series bands, ii) extinction due to atomic H Lyman series lines — up to n=1 → n=51, iii) extinction due to 33 CO bands and dust continuum extinction. Only UV continuum for photodissociation of all other species was taken into account.

Key words: Interstellar medium: abundances

1. Introduction

One of the most powerful methods to investigate the interstellar medium, particularly the interstellar clouds and inhomogenities near the star forming regions, is the observation of molecular lines. To obtain the physical characteristics of the region, where molecular lines are born, it is necessary to know the distribution of molecular concentrations throughout the cloud. The problem is rather complicated because these concentrations are determined by set of chemical reactions between a great amount of the molecules and atoms. As a result almost all concentrations are mutually dependent. Besides, in many cases the necessity to account for the photochemical reactions leads to modelling of the radiation transfer throughout the cloud. The amount of known interstellar molecules exceeds one hundred. So, the calculations of molecular concentrations in the molecular cloud lead to the set of differential equations if the problem is time–dependent and to the set of algebraical equations for the steady state problem. The latest assumes that the cloud dynamics is unimportant, i.e., that the cloud is stable over the period larger than the chemical timescale. Usually the equilibrium problem is solved, but the unequilibrium approach becomes more and more important in astrophysics. Our experience leads to conclusion that steady state is reached after approximately 10^7 — 10^8 years even for diffuse clouds with total density about 10 cm^{-3}, which is comparable with the clouds' lifetime.

In order to calculate the molecular concentrations in the interstellar cloud with great amount of molecules (more than 100) and chemical reactions (about 1000) it is necessary to have the computer code for solving the set of equations of chemical equilibrium or kinetics with photochemical reactions and radiation transfer, included. There are some such programs in the world, but they are not available in the east European and post Sovietic region (recent exception by Shematovich, Shustov and Wiebe as part of code for calculating the dynamics of protostellar medium). In order to fill up this gap we have made a program package to solve the set of equations of chemical kinetics and equations of charge and atom balance. Now 109 molecules and 1070 chemical reactions are included.

2. The model of the cloud

We assume that the cloud is a plane–parallel slab immersed into Draine's(1978) interstellar ultraviolet radiation field from both sides. It is assumed that no radiaton falls onto cloud shortwards of atomic Lyman limit $\lambda = 911.763$ Å. The cloud is homogenous, isothermic, and the excitation temperatures of all species are equal to the kinetic temperature.

3. Chemical and physical processes taken into account

2.1. Gas phase reactions

The set of chemical reactions by Viala (1986) is used

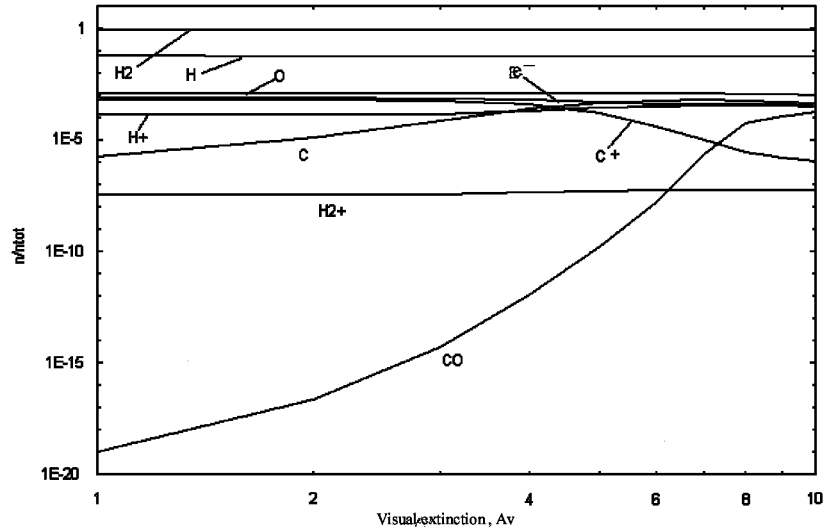

Figure 1: Relative abundances of some species n/n_{total} as function of visual extinction for cloud with total extinction 20, total density 100 cm^{-3} and T_{kin} = 50K.

and 1014 reactions with ions and neutrals are included.

2.2 Formation of the molecular hydrogen on grains

The expression by Viala (1986) is used for the rate R of H_2 formation on grains per H atom:

$$R = 3.6 \cdot 10^{-18} n T^{1/2}\ \mathrm{s}^{-1}$$

where $n = n_H + 2n_{H_2}$ and T is the gas temperature.

2.3 The cosmic rays ionisation rates

They are also taken from Viala's database and all 8 reactions of ionisation H, H_2, He, C, N and O are included.

2.4 The photodissociation, photoionization and radiative transfer

The cloud is assumed to be a plane–parallel slab and exposed in interstellar UV field, approximated by Draine (1978). For all cases except the photodissociation of H_2 and CO only the photodissociation in UV continuum was taken into account, and following Sternberg and Dalgarno (1995) we used the approximation formula:

$$\Gamma_i = 2 \cdot 10^5 C_i \exp(-\alpha_i A_\nu - \beta_i A_\nu^2) s^{-1}$$

where Γ_i is the dissociation rate and C_i, α_i and β_i are the coefficients given in paper by Roberge *et al* (1991). 50 photodissociation reactions are included.

Only the photoionization of atomic carbon and silicon was accounted for. Photoionization rates of Sternberg and Dalgarno (1995) for unattenuated Draine's (1978) UV field were used, multiplying them by attenuation coefficient on dust calculated as in section 2.5.

2.5 Photodissociation of H_2 and CO

In order to calculate the photodissociation rates of H_2 and CO molecules, we assume that the cloud is a plane–parallel slab immersed into Draine's (1978) interstellar ultraviolet radiation field from both sides. It is assumed that no radiation falls onto cloud shortwards of atomic H Lyman limit $\lambda = 911.763$Å. For the purpose of calculation of the mean UV radiation intensity at a given point inside cloud, we account for i) extinction due to H_2 Lyman and Werner series bands, ii) extinction due to atomic H Lyman series lines – up to n=1 → n=51, iii) extinction due to 33 CO bands mentioned by Dishoeck and Black (1988), see Tables I and IV) dust coninuum extinction. The excitation temperatures of all gaseous species are assumed equal to the kinetic temperature, the latter being homogenous throughout the cloud. No scattering in atomic and molecular lines is accounted for; we assume that all the photons absorbed in the ultraviolet are reradiated in the optical and infrared region through cascade processes. Of course, this is not true regarding atomic hydrogen line Ly$_\alpha$, but we use this approximation at the present stage.

Scattering on dust is treated in forward–only scattering approximation, in a manner as by Viala (1986), and we adopted uniform optical properties of dust grains through all the spectral region with UV lines: 911.763Å$\leq \lambda \leq 1250\mathring{A}$. As the interstellar extinction curve in far ultraviolet is still quite uncertain, we assume a constant ratio of ultraviolet to visual extinction efficiency, namely, $Q_{UV}^{ext}/Q_V^{ext} = 2.73$ — a little more as in Federman, Glassgold and Kwan (1979), crudely evaluating the curve of Roberge et al. (1991) (see Fig. 1 of this paper). The true dust albedo a_{eff} is assumed to be $a = 0.6$ as by Lillie and Witt (1976), and the effective albedo in forward–only scattering approxima-

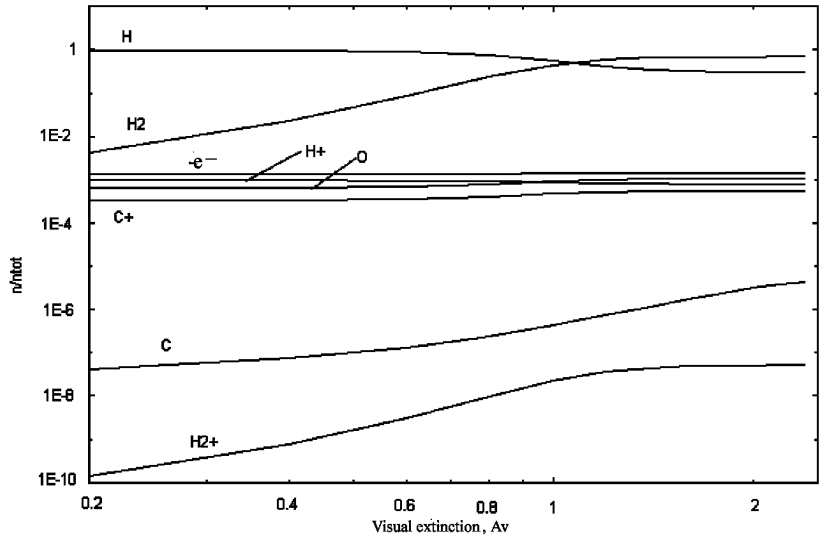

Figure 2: Relative abundances of some species n/n_{total} as function of visual extinction for cloud with total extinction 4.8, total density 20 cm^{-3} and T$_{kin}$ = 50K.

tion:

$$1 - a_{eff} = (1 - a)^{1/2}$$

So, the intensity of ultraviolet radiation in pure dust cloud would be described by the formula:

$$I = I_0 \exp(-\tau_V Q_{UV}^{ext}(1 - a_{eff})/\mu Q_V^{ext}))$$

where I_0 is the intensity of interstellar UV radiation, τ_V optical depth in the visual region, μ cosine of the angle between the direction of radiation propagation and perpendicular to the slab boundary.

We assume that the mechanism of photodissociation of H_2 is through absorption of UV photons in Lyman and Werner bands, with subsequent dissociation. For H_2 molecular bands each rotational transition line is treated separately, 750 lines in total, assuming Foight profiles for them. Their oscillator strengths and radiative lifetimes were taken from Abgrall and Roueff (1989). For the ground level, 16 lowest rotational sublevels are accounted for, assuming their population to be in accordance with Boltzmann distribution. No collisional processes and turbulence were accounted for i.e. only the thermal motion of gas particles was accounted for to obtain the Doppler widths of line cores for hydrogen and CO.

We calculated the spectral parameters for atomic H lines by exact non–relastivic quantum mechanical treatment (the radial integrals were calculated using method by Hoang–Binh (1990), and Foight profiles were assumed for them, too.

CO molecular bands are treated using more crude approximation, because we have not at our disposal the transition probabilities for individual rotational lines. We use the spectral data of Dishoeck and Black (1988) where the oscillator strengths and radiative lifetimes for vibrational bands as a whole are given, and approximate each of them by Foigt profile of corresponding width.

4. The first results

On to day only a limited set of calculation results with limited number of molecules (36) including only H, O and C is available. Two examples are displayed to show the region of formation of CO (Fig 1) and the region of transition of atomic hydrogen to molecular (Fig 2).

Acknowledgements. This contribution was supported by the Program "Astronomy" of Russian Ministerium of Science (project 1.3.3.1) and the Latvian Council of Science (grant 096.0036).

References

Abgrall H., Roeff E.: 1989, *As. Ap. Suppl.,* **79**, 313.
Dishoeck E.F.,Black J.H.: 1988, *Ap. J.*, **334**, 771.
Draine B.T.: 1978, *Ap.J.Suppl.*, **36**, 595.
Federman S.R., Glassgold A.E., Kwan J.: 1979, *Ap. J.*, **227**, 466.
Hoang–Binh D.: 1990, As. Ap., **238**, 449.
Lillie C.F., Witt A.N.: 1976, *Ap. J.*, **208**, 64.
Roberge V.G., *et. al.*: 1991, *Ap. J. Suppl.*, **77**, 287.
Shematovich V.I., Shustov B.M., Wiebe D.S.,: 1997, *Mon. Not. Roy. Astron. Soc.*, **262**, 601.
Sternberg A., Dalgarno A.: 1995, *Ap. J. Suppl.*, **99**, 565.
Viala Y.P.: 1986, *As. Ap. Suppl.,* **64**, 391.

BUBBLES IN THE NORMAL AND STARBURST GALAXIES

S.A. Silich

Main Astronomical Observatory NAS of Ukraine,
03680, Kyiv-127, Golosiiv, Ukraine, *silich@mao.kiev.ua*

ABSTRACT. A kinetic feedback from massive stars on the interstellar medium (ISM) in normal and starburst (SB) galaxies is reviewed. Hot bubbles and expanding shells observational manifestations, and recent results from the numerical models are discussed. The possible reasons for hydrodynamic and X-ray discrepancies between the standard bubble model predictions and observations are analyzed.

Key words: Interstellar medium: Galaxies: Shock waves: Stellar winds: Supernova remnants.

1. Introduction

20 years have passed since the discovery by Heiles (1979) large empty cavities in the Milky Way neutral hydrogen distribution. Later on the study of interstellar bubbles has been extended to many nearby galaxies (see recent reviews by van der Hulst, 1996; Brinks & Walter 1998). The optical counterpart of these objects are the H_α ring-shaped nebulae (e.g. Meaburn 1980; Lozinskaya & Sitnik 1988). The similar structures have been also traced in the IR (Lozinskaya & Repin, 1990), and X-ray (Chu & Mac Low, 1990; Walter et al., 1998) emissions.

During the last two decades the major role of the radiative and kinetic feedback from massive stars on the distribution and physical conditions found in the ISM of the star forming galaxies has been well established. It is a general consensus (Tenorio-Tagle & Bodenheimer, 1988) that a majority of the observed structures originate from the combined action of stellar winds (SW) and supernova (SN) explosions in the massive star clusters (for the discussion of some potential problems see Gosachinskii, 1993; Rhode et al., 1999).

The observed shells can be tentatively classified into three distinct categories: small wind-blown or supernova produced bubbles around single individual stars (type S), moderate size bubbles, which result from the correlated action of a few to several hundreds of stars constituted a typical OB-association (type M), and huge superbubbles resulted from a violent, space correlated star forming activity in the SB galaxies (type H).

Table 1: Bubble classification.

Type	Progenitor	log(E/1 erg)	Size (pc)
S	single star	51	$\sim$10
M	OB association	52-53	> 10
H	SB galaxy	≥ 54	≥ 1000

Our review will focus on the recent studies of the large-scale M and H type objects. A comprehensive discussions of the different aspects of the S bubble evolution one may found in the proceedings of the recent IAU Symposium N193 (e.g. Marston, 1999; Dopita et al. 1999).

A variety of different physical processes controls large bubbles evolution and observational manifestations: interstellar gas distribution, galaxy gravity and gaseous disc differential rotation, hot interior metal enrichment and cooling, hydrodynamical instabilities and effects of projection. Fast growth of our knowledge in this frontier field of the galaxy astrophysics was inconceivable without development of the suitable 2D and 3D numerical methods that are easy to work with, fast, and could give reasonable accuracy. Therefore I first briefly discuss one of the method based on the thin layer approximation we have developed during the last decade. Then I discuss the effects of projection, Large Magellanic Cloud (LMC) M-bubbles growth rate discrepancy, the origin of the Lyα profiles in the starburst galaxies. At the end of the presentation I turn to the bubble X-ray emission, a particularly exiting topic in view of the new AXAF and XMM missions.

2. Thin layer approximation

An impressive progress in our knowledge of the energetic processes that make up ISM, has been made with the development of the multidimensional hydrodynamical methods. First analytic approximation for a two-dimensional adiabatic shock wave propagation within an exponential, plane-stratified gas density distribution, has been proposed by Kompaneets (1960). Later on Kompaneets approach has been improved to take

into account the inertia of the post-shock expending shell (Andriankin et al., 1962). This version of the Kompaneets method is known as a thin layer approximation, and is widely used in a number of astrophysical applications (see for review Bisnovatyi-Kogan & Silich, 1995).

First 2D numerical scheme based on the thin layer approximation has been developed by Bisnovatyi-Kogan & Blinnikov (1982), who has applied this method for SNRs resulting from asymmetric, plane concentrated supernovae ejecta. Later on Tenorio-Tagle & Palouš (1987), Mac Low & McCray (1988) have used a similar approach to discuss M-type bubble evolution in a plane-stratified, differentially rotating galaxy disk. Mac Low et al. (1989), Bisnovatyi-Kogan et al. (1989) have compared the thin layer approximation results with the analytic and full numerical calculations and did confirm their good accuracy.

3D numerical schemes based on the thin layer approach have been developed independently by Bisnovatyi-Kogan & Silich (1991), Silich (1992) and Palouš (1992) (see for review Bisnovatyi-Kogan & Silich, 1995). In this approach shock is approximated with a number of Lagrangian elements. If m is the mass, $\mathbf{r}$ is the radius-vector, $\mathbf{u}$ is the velocity of the particular Lagrangian element, and $\rho(x,y,z) = \rho_0 f(x,y,z)$ is the ambient gas density, then equations of the mass and momentum conservation may be written as follows:

$$\frac{dm}{dt} = \rho(x,y,z)(\mathbf{u}-\mathbf{V})\mathbf{n}\Sigma, \tag{1}$$

$$\frac{d}{dt}(m\mathbf{u}) = \Delta P\mathbf{n}\Sigma + \mathbf{V}\frac{dm}{dt} + m\mathbf{g}, \tag{2}$$

$$\frac{d\mathbf{r}}{dt} = \mathbf{u}, \tag{3}$$

where $\mathbf{n}$ is the normal to the shock front unit vector, $\mathbf{g}$ is the acceleration of the external gravitational field, $\mathbf{V}$ is the velocity field of the external gas flow, Σ is the surface area of the Lagrangian element, $m = \sigma\Sigma$, σ is the surface density, and $\Delta P = P_{in} - P_{ext}$ is the pressure difference between the hot interior and rather cold external gas. The pressure P_{in} is a function of the bubble thermal energy E_{th} and remnant volume Ω:

$$P_{in} = (\gamma - 1)E_{th}/\Omega. \tag{4}$$

The motion of any Lagrangian element is then described by seven ordinary differential equations. For N Lagrangian elements one gets a system of $7N$ differential equations of the mass and momentum conservation. This set of equations is coupled by the equation (4) for the gas pressure within a cavity, and the energy conservation equation. Numerical integration of these equations gives time evolution of a shell shape, expansion velocity, and surface density distribution. The results of the calculations for the superbubble evolution in the M31 and HoII galaxies are shown in figure 1 (Silich et al., 1996).

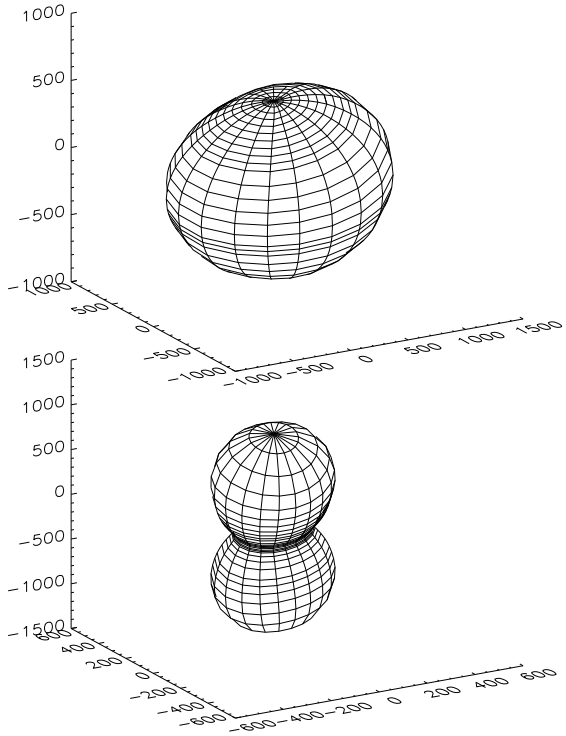

Figure 1: Bubble morphology for HoII (top), and M31 (bottom) galaxies.

2. The projection effects

The growing bulk of observational data and fast progress in numerical methods led to a new understanding of the ISM as a dynamic system regulated by a number of local energy sources. However, the development of the *quantitative* theory has required to provide numerous calculations and compare their results with observational data.

As soon as most of the objects were found in the external galaxies, a principal problem arisen: how to distinguish between the distortion effects of projection and bubble real 3D morphology? Silich et al. (1996), Mashchenko & Silich (1997) incorporated effects of projection into their 3D numerical scheme, and provided a careful analysis of the problem for neutral hydrogen shells. From the observational point this problem was analysed by Thilker et al. (1998). Later on Mashchenko et al. (1999) have incorporated the thin layer numerical model into Thilker et al. (1998) method for automated identification and classification of supershells in the spiral galaxies.

Search for the neutral hydrogen shells in the external spiral and irregular galaxies includes analysis both of integrated, and single velocity neutral hydrogen maps. For example, it was found that in IC 2574 neutral

hydrogen holes are more prominent in the single velocity channels, whereas in the HoII it is easier to identify the same objects in the integrated column density map (Brinks & Walter, 1998).

Let us define the galaxy reference system (x,y,z), and the coordinate system (x',y',z') in the plane of view. The HI column density along any line of sight follows from the equation:

$$N(x', y') = \sum_l N_l + \int n(x', y', z')\,\mathrm{d}z', \qquad (5)$$

where index l denotes different Lagrangian elements along line of sight, and N_l is the contribution of each Lagrangian element to the total column density. The last term represents the galactic cold ISM contribution. The value of shell contribution, N_l, depends on the shell column density, N_{sl}, shell thickness, d, and angle, α, between,the line of sight and the normal to the shell surface (Silich et al., 1996):

$$N_l = \frac{N_{s,l}}{\delta} \times \begin{cases} F_1(\alpha,\beta) - F_2(\alpha,\beta)\,, & \alpha < \alpha_{cr}, \\ 2\,F_1(\alpha,\beta)\,, & \alpha \geq \alpha_{cr}, \end{cases} \qquad (6)$$

where $\delta = d/R_s$ was assumed to be constant, d and R_s are the shell thickness and radius.

$$F_1(\alpha,\beta) = \sqrt{\cos^2\alpha + \delta + \frac{\delta^2}{4}}, \qquad (7)$$

$$F_2(\alpha,\beta) = \sqrt{\cos^2\alpha - \delta + \frac{\delta^2}{4}}, \qquad (8)$$

A careful analysis of more than 10000 models reveals that projection effects are highly dependant not only on the inclination angle i, but also on the bubble position in the plane of a galaxy. A projection distortion is negligible nearby galaxy major and minor axes, but dominates hole orientations in the intermediate sectors. These results made it possible to propose a new method which can distinguish between the two possible directions (towards and outwards of observer) of the galactic angular momentum vector, the problem which is close related with the physical conditions at the epoch of galactic formation.

Mashchenko & Silich (1997) extended this study on the different velocity channels. They introduced Gaussian sensitivity curves for spectral filters:

$$W(U,\sigma_f) = \frac{1}{\sigma_f\sqrt{2\pi}} \exp\left\{-\frac{1}{2}\left[\frac{U-V}{\sigma_f}\right]^2\right\}. \qquad (9)$$

where V is the central velocity, and σ_f is dispersion of a particular filter. Then number of neutral hydrogen atoms on the line of sight reads as:

$$N_j = \frac{1}{\sigma_*\sqrt{2\pi}} \int_{-\infty}^{\infty} n(z') \exp\left\{-\frac{1}{2}\left[\frac{V(z')-V_j}{\sigma_*}\right]^2\right\}\mathrm{d}z', \qquad (10)$$

Where $\sigma_* = \sqrt{\sigma_f^2 + \sigma_g^2}$, σ_g^2 is the ISM gas random motion one-dimensional velocity dispersion. Finally, to imitate radiotelescope spatial resolution, this value was smoothed with a two-dimensional Gaussian function. New algorithm was applied for several supershells in the M31 and HoII galaxies. The calculations revealed a principal role of the ISM gas random motion, and an interesting effect of the hole center displacement at the different velocity channels. These results have to be taken into account at any analysis of observational data to avoid misinterpretation of the same object as several intersecting or overlapping shells.

4. Bubble dynamic discrepancy

Due to it's proximity and almost face-on position the Large Magellanic Cloud (LMC) provides an excellent possibility to study a multi-shell structure of the ISM, and interstellar hydrodynamic state around individual OB-associations. It is important to note, that the LMC internal and foreground extinction is so small, that detailed studies of the LMC OB-associations stellar contents are now easy possible (Saken et al., 1992; Oey 1996a). These photometric and spectral observations in combination with the stellar evolution models constrain all input model parameters one needs to compare the observed objects with the bubble model predictions: bubble sizes, expansion velocities, and mechanical energy input rate.

This comparison (Oey, 1996b) indicates, that the standard spherical model cannot reproduce the observed properties of a number of shells. In particular, the collection of bubbles observed in the LMC exhibit two different sets of objects with expansion velocities that are either too high or too low to be explained by the standard model. For the low velocity objects, the discrepancy could probably be explained by errors in the estimation of the input wind power or ambient gas density (Oey 1996b). For the high velocity shells, however, the observed expansion velocities ($V_{exp} \geq 25$ km s^{-1}) are at least a factor of two larger than the expected values (Oey 1996b). These objects are rather young. Their radii fall in the range 25 - 50 pc, and lifetimes are several Myrs. Neither the density gradient in the disk of the LMC nor possible variations of the initial stellar population can resolve this discrepancy (Oey 1996b).

A possible solution to this problem has been suggested by Silich & Franco (1999). It is based on the fact that the LMC has a moderate inclination angle, and therefore LMC shells are viewed with a nearly face-on orientation. It is well-known, that in the plane-stratified gas density distribution shock wave exhibits at first a continuous deceleration, and only when top radius exceeds several characteristic scales of gaseous

disc thickness, top expansion changes towards the increasing speed. It is clear that LMC bubble large expansion velocities cannot be related to a large-scale density gradient. The observed shells are too small to blowout of the LMC gaseous layer. Shell acceleration could be pronounced only if one takes into account the presence of a giant molecular cloud (GMC) which gives birth to the parental stellar cluster and controls the initial bubble expansion. The high initial mass concentration induces strong changes in the young bubble dynamics. There is a bulk of the observational evidences which indicate that GMCs are rather flat than spherically symmetric objects (e.g. Gosachinskii, this volume). Therefore a simple two-dimensional model for a GMC surrounded by a homogeneous ISM was considered:

$$\rho = \begin{cases} \rho_c, & F(r,z) \leq 1, \\ F(r,z)^{-w/2}, & F(r,z) \leq \xi^{2/w}, \\ \rho_{ISM}, & F(r,z) > \xi^{2/w}, \end{cases} \qquad (11)$$

where $F(x,z) = \left(\frac{r}{R_c}\right)^2 + \left(\frac{z}{Z_c}\right)^2$, $\xi = \rho_c/\rho_{ISM}$ is the ratio of the cloud core density to the ISM gas density, w is the power-law index, and R_c and Z_c are the characteristic scale heights for the cloud density distribution in the r and z-directions, respectively. The appropriate range of values for the cloud parameters was derived from observational data, and cloud flatness $Z_c = R_c/2$ was assumed.

Figure 2 presents the results of the calculations for 2×10^4 $M_\odot$ cloud with different mass concentrations at the cloud center (a low-density cloud with $n_c = 10$ cm^{-3}, and high density cloud with $n_c = 10^2$ cm^{-3}).

These results indicate that bubbles blowing out of the flattened clouds can reach a high degree of asymmetry on a short time scale (during the first million years of expansion), with z-velocities in the range of the observed high-velocity cases. The model considered predicts a remarkable difference in the bubble kinematics for a face-on and edge-on galaxies, and is in line with the semi-analytical results for a sharp density contrast discussed by Oey & Smedley (1998).

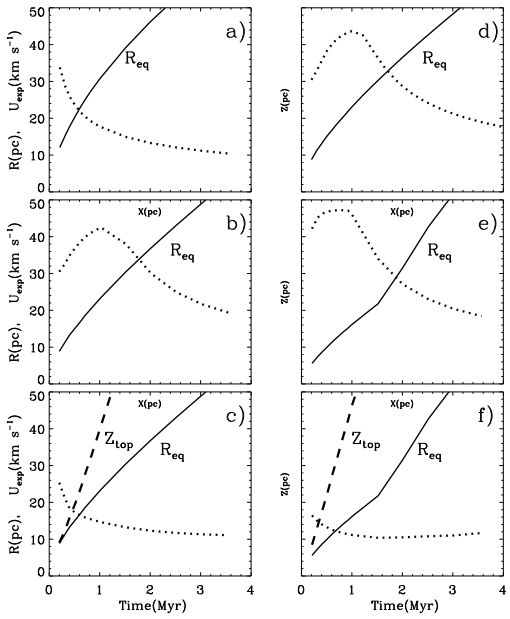

Figure 2: Bubble expansion from a GMC. a) Spherical cloud. b) Low density cloud as seen in a face-on galaxy. c) Low density cloud as seen in an edge-on galaxy. d) Low density cloud with shell fragmentation due to R-T instability. e) High density cloud for a face-on galaxy. f) High density cloud for an edge-on galaxy. The solid lines are the shell radii along the plane of the galaxy, and the dashed lines are the top z-extensions. Dotted lines for panels a, b, d and e are the top expansion velocities along the z-axis. Dotted lines for panels c and f are the expansion velocities at the bubble equator.

5. Lyα profiles in the SB galaxies

It has been long proposed that primordial galaxies have to be easy detected from their Lyα emission. However ultraviolet (UV) observations of high redshifted galaxies show that many of them present weak, or sometimes none Lyα emission at all (Lowenthal et al., 1997). This problem puzzled the astronomical community for more than a decade, and stimulated many discussions and new observational programs. Resent HST data on star-forming galaxies (see e.g. Kunth et al., 1998) revealed three typical Lyα profiles: broad damped absorption, pure emission, and emission with P Cygni type blueshifted absorption. Sometimes the additional details like emission within a damped absorption, or redshifted emission are also observed. P Cygni absorptions have rather large (several hundred km s^{-1}) offset with respect to the parent galaxy. These observations lead to suggestion, that the velocity field and ISM density distribution along line of sight, rather than dust absorption alone, are the dominant factor for the escape of the Lyα photons from these galaxies.

A qualitative scenario for different Lyα profile origin was proposed by Tenorio-Tagle et al. (1999). The model is based on the synthetic properties of starbursts, as derived by Leitherer & Heckman (1995), and considers the galaxy ISM hydrodynamic response on the SB mechanical energy deposition $L_{SB} = 10^{38} - 10^{42}$ erg s^{-1}. The ISM gas distribution was approximated with the two isothermal components related to the central dense molecular core, and low density extended gaseous halo

$$\rho_g = \rho_{core} + < \rho_{halo} > \qquad (12)$$

retained in an equilibrium state by rotation, random gas motion, and gravity from the stellar and dark mat-

ter components. It was assumed, that ISM constitutes 10% of the total mass of the galaxy, and ranges from 5×10^7 $M_\odot$ for smallest dwarf galaxies to the 10^{10} $M_\odot$ for the massive spiral ones.

The numerical code described in the section 2, was completed with the algorithms which define a shell thickness, and Stromgren zone extension. The Stromgren zone radii were calculated in the equilibrium on-the-spot, radial approximation with account for gas concentration within a high density shell:

$$\Delta(R) = N_{UV} - 4\pi \left(\int_{R_1}^{R_2} n^2(r)\alpha_B r^2 \mathrm{d}r - \int_{R_2}^{R} n^2(r)\alpha_B r^2 \mathrm{d}r \right), \quad (13)$$

where R_1 and R_2 are the inner and outer shell cross points along line of sight, $\alpha_B = 2.59\times10^{-13}\, cm^3\, s^{-1}$ is the recombination coefficient of the hydrogen atoms to all levels but the ground state. If value of Δ is positive

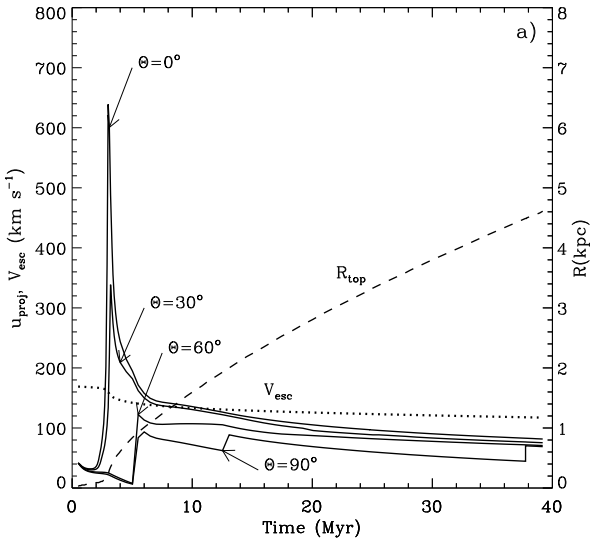

Figure 3: Bubble time evolution. Solid lines represent the expansion velocities along different line of sights. Dotted line indicates the local escape velocity. Bubble pole position is indicated by the dashed line.

at the galaxy boundary R_G, there are enough UV photons to ionize neutral hydrogen shell, all interstellar gas along line of sight, and escape of the galaxy. If value of $\Delta(R_G)$ is negative, the number of UV photons is not sufficient to ionize all the halo. The radius of the HII region follows from the condition $\Delta(R) = 0$, and lies between the shock front and the galaxy outer boundary R_G. Note, that the characteristic recombination time $\tau_{rec} = 1/n_e\alpha_A \approx 10^5/n_{halo}$ yr of the low density halo may exceed bubble expansion time t. This causes the ionized halo to become temporarily transparent to the Lyα photons, even upon dramatic drop of the central UV flux, which is expected after 4 - 5 Myr in the instantaneous SB model. The hydrodynamical evolution of the typical model is shown in the figure 3.

The shell expansion shows at first continuous deceleration, followed after 1 - 2 Myrs by a sudden blowout with rapid acceleration and Rayleigh-Taylor disruption of the pole sections. Later on the shock builds a new shell of swept-up halo matter. The remnant speed begins to decline, and ends up well below the galaxy escape velocity. Nevertheless, after 20 - 40 Myr a SB forms a huge, several kiloparsec size remnant filled with a low density ($10^{-3}-10^{-4}$ cm^{-3}) hot gas, which is surrounded by a massive, rather cold shell.

Before the blowout the dense, slowly expanding shell preserves interstellar gas of the powerful ionizing radiation, which escape of the central star forming region. However, after blowout UV photons escape of the disrupted pole segments, and produce a cone of ionized interstellar gas around the symmetry axis Z. This cone becomes rapidly broader, and reaches its maximum opening angle after 2.5 - 3 Myr (figure 4).

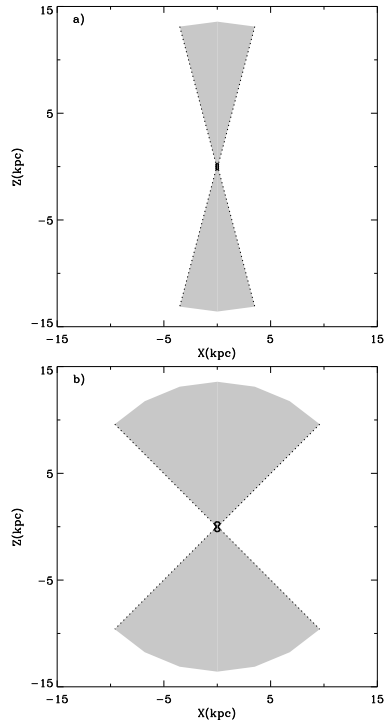

Figure 4: The development of the conical HII region in the low density galaxy halo.

The rapid changes in the ionization state of the galaxy ISM have a profound impact on the transport of the Lyα emission, and lead to a sequence of the Lyα profiles. This sequence starts with a broad damped absorption, which followed after blowout by a pure emission. Recombinations in a totally ionized new-formed shell produce a secondary blue-shifted emission. However, if the shell column density grows to $\sim 10^{19}$ cm^{-2}, it

traps the ionization front, and forms a multiple structure with a photoinized inner edge, a central neutral zone, and outer collisionally ionized layer. This is promoted also by the rapid decrease in the UV production rate after 3 - 4 Myrs, and UV flux geometrical dilution. Once the neutral hydrogen zone is formed, the recombinations within a shell become increasingly more important, leading to a P Cygni Lyα profile and eventually again to a full saturated absorption.

5. Hot gas and X-ray emission

Search for hot gas within the neutral hydrogen shells is an important test of the standard (space correlated supernova explosions within a young stellar cluster) model. LMC provided an excellent laboratory for this purpose during Einstein and ROSAT observatories epoch. With the AXAF and XMM launch this research will be extended on a number of the nearby galaxies, and new exiting results are expected in the forthcoming few years.

Interstellar bubbles with cold radiative shells and adiabatic interiors have four zone structure (Weaver et al., 1977). A central zone containing a freely expanding wind matter. Hot interior zone which is filled with a gas heated at the inner reverse shock. This zone is bounded with a cold shell, which is separated by a contact discontinuity and accumulates swept-up interstellar gas. This zone is bounded with a leading shock front, which separates a bubble shell of the external ISM. Second zone covers most of the bubble volume. It contains mixture of the heated at the reverse shock ejecta and evaporated from a cold shell interstellar gas. This mixture has temperatures of $10^6 - 10^7$ K, and produce bulk of the X-ray emission. Note, that in the low density environment (or at a very high energy input rate) bubble shell remains adiabatic for a long time, and also contributes to a bubble total X-ray luminosity.

A simple analytic model for X-ray luminosity L_x from a spherically symmetric, energy dominated bubble with a cold radiative shell, has been developed by Chu & Mac Low (1990) for a constant energy input rate, and Silich (1995) for a power law energy deposition. This model is based on the self-similar hot inner gas temperature and density distributions (Weaver et al., 1977), accounts for a X-ray emission cut-off temperature $T_{cut} \sim 5 \times 10^5$ K, and approximates X-ray emissivity within the 0.1 - 2.4 keV energy band by a constant value $\Lambda_x = 3\xi \times 10^{-23}$ erg cm^3 s^{-1}, where ξ is the hot gas metallicity in the solar units. A simple analytic expression may be derived for a constant ambient gas density n_0, and constant mechanical energy input rate L_w:

$$L_x = 10^{36} \xi I(\tau) L_{38}^{33/35} n_0^{17/35} t_7^{19/35} \, erg\, s^{-1} \qquad (14)$$

where L_{38} is wind mechanical luminosity in the 10^{38} erg s^{-1} units, and t_7 is the elapsed time in the 10^7 yr unites. $I(\tau)$ is a dimensionless integral:

$$I(\tau) = \frac{125}{33} - 5\tau^{1/2} + \frac{5}{3}\tau^3 - \frac{5}{11}\tau^{11/2}, \qquad (15)$$

and τ is the ratio of the X-ray cutoff temperature to the bubble central one. More comprehensive numerical models, which account for bubble deviation of the spherical symmetry, and use equilibrium Raymond & Smith (1977) model for the X-ray emissivity, have been developed for Milky Way bubbles by Silich et al. (1996), and SB bubbles by Suchkov et al. (1994), Silich & Tenorio-Tagle (1998), Strickland & Stevens (1999).

To date X-ray emitting, shocked stellar wind bubble from a single star has been unambiguously detected in the only one object NGC 6888 (Bochkarev, 1988, Wrigge et al., 1994) while a number of the X-ray emitting M and H-type objects grows continuously.

Chu & Mac Low (1990) have examined Einstein Observatory archives, and revealed diffuse X-ray emission around 15 LMC OB-associations. The regions with X-ray excess correlate with the Hα emission, and best can be associated with the hot M-type bubbles. Bubble X-ray luminosities range from 7×10^{34} to 7×10^{36} erg s^{-1}. The comparison of the observed values with the model predicted ones revealed an intrigue result: X-ray bright bubbles have X-ray luminosities more than an order of magnitude higher than model predicted ones. Later on this result has been confirmed with the ROSAT data (Chu et al., 1993). Several X-ray dim M-bubbles were also found (DEM 31, DEM 105, DEM 106, and DEM 137) in the LMC survey (Chu et al., 1995). In these cases 3σ upper limits are comparable with the model predicted ones, but deeper exposure, or more sensitive observations are needed to determine their real X-ray luminosities.

30 Dor, the most spectacular HII nebula in the Local Group of galaxies, provides an excellent possibility for understanding massive star origin and its interaction with the ISM. The central OB-association, NGC 2070, was formed 1 - 2 Myr ago, and emits $\sim 10^{52}$ UV photons every second. HII filaments extend more than 100 pc away of the cluster, and coincide with the regions of the diffuse X-ray emission. Two high mass binaries and supernova remnant N157B have been revealed in the 30 Dor core region (Wang, 1999). However, X-ray emission is predominantly diffuse, and ASCA data confirm its thermal origin. The best estimation of the emitting gas temperature in the two-component model gives value in the 2 - 9 $\times 10^6$ K range, and intrinsic X-ray luminosity in the 0.5 - 2 keV energy band of $L_x \approx 9 \times 10^{37}$ erg s^{-1} (Wang, 1999). This low temperature indicates on the additional mass ejection into a cavity, which is likely to be an effective erosion of the parent molecular cloud via photoevaporation from the central compact star cluster.

Several huge (kiloparsec scale) regions of the diffuse X-ray emission in the LMC coincide with the well known HII giant shells LMC-4 and LMC-2 (Bomans et al., 1996, Caulet & Newell, 1996). Walter et al. (1998) have revealed a similar (1000×500 pc) in size object in the nearby dwarf galaxy IC 2574. An X-ray excess coincides with the HI shell in the northeast part of this galaxy, and the region of the star-forming activity as traced by the Hα emission. The observed X-ray luminosity in the 0.1 - 2.4 keV energy band is $L_x \approx 1.6 \times 10^{38}$ erg s^{-1}. It is suggested that main contribution comes from the hot gas embedded within a shell, although contamination from the X-ray binaries cannot be ruled out. Simple estimations show that this luminosity is about an order of magnitude higher than those, which predicted by the theoretical model (14). The same problem, as has been discussed above for the most X-ray emitting bubbles in the LMC.

ROSAT observations one of the most X-ray luminous ($L_x \sim 10^{40}$ erg s^{-1}) dwarf galaxy HoII present opposite problem. Despite of violent ISM structure with a number of neutral hydrogen holes and expending shells (Puche et al., 1992), main X-ray emission comes from a single unresolved region, which coincides with a large HII region. A high X-ray variability supports accretion into a compact object rather than extended bubble model (Zezas, 1999).

Star formation activity gets its extreme value in the starburst galaxies. These systems are between the brightest sources of the IR emission, present obvious evidences for the powerful gas outflow in the visible wave length band, and also often present the extended (tens of kiloparsecs) diffuse X-ray emission. To date only several dwarf and peculiar galaxies have definite detection of extended, thermal X-ray emission (Martin, 1999). There are NGC 1569 NGC 4449, M82. Several others, NGC 5253, NGC 4214, NGC 1705, I Zw18, have been also detected in the X-ray band, but interpretation of the existing data is controversial (for a comprehensive analysis see Stricland & Stevens, 1998). For a example, Martin & Kennicutt (1995) found, that the observed X-ray luminosity of NGC 5253 ($L_x \sim 6.5 \times 10^{38}$ erg s^{-1}) exceeds standard bubble model predictions more than an order of magnitude.

6. Conclusions

Interstellar bubbles present direct manifestation of massive star cluster feedback on the galaxy ISM, and have profound importance to the global galaxy structure, star formation history, chemical evolution, energy balance, and relationship between different gaseous phases.

Several potential problems with this hypothesis, however, are waiting for their intensive discussion. The basic ones may be formulated as follows:

- A comprehensive study of the stellar population within the large (M and H-types) bubble regions. Search for the excess of the late (A, F) type stars, the debris of the initial massive star clusters.
- Extension of the LMC analysis of the bubble kinematics on the another nearby face-on and edge-on galaxies. The comparison of the coherent SNe model predictions with a variety of observational data.
- A detailed analysis of the different mechanism which may be responsible for superbubbles X-ray emission: off-center SN explosions, mass-loading flows, hot gas metal enrichment, etc. New series of the X-ray observations of the nearby normal and SB galaxies with better sensitivity and space resolution.

Acknowledgements. It is my please to acknowledge support from a Royal Society grant for joint projects with the former Soviet Union states. I am also greatly appreciate many useful discussions of the reviewed problems with my colleagues and friends: G. Bisnovatyi-Kogan, J. Franco, T. Lozinskaya, R. Terlevich and E. Terlevich, G. Tenorio-Tagle.

References

Andriankin, E.I., Kogan, A.M., Kompaneets, A.S. and Krainov V.P.: 1962, *Zh. Prikl. Mekh. Tekh. Fis.*, **6**, 3.

Bisnovatyi-Kogan G.S., Blinnikov S.I.: 1982, *Astron. Zh.*, **59**, 876.

Bisnovatyi-Kogan G.S., Blinnikov S.I., Silich S.A., 1989, *Ap&SS*, **154**, 229.

Bisnovatyi-Kogan G.S., Silich S.A.: 1991, *Astron. Zh.*, **68**, 749.

Bisnovatyi-Kogan G.S., Silich S.A.: 1995, *Rev. Mod. Phys*, **67**, 661.

Bochkarev N.G. 1988, *Nature*, **332**, 518.

Bomans D.J., De Boer K.S., Koornneef J., Grebel E.K.: 1996, *Astron. Astrophys.,* **313**, 101.

Brinks, E., Walter, F.: 1998, in *The Magellanic Clouds and Other Dwarf Galaxies*, ed. T. Richtler & J. Braun (Aachen: Shaken Verlag), p.1.

Caulet A., Newell R.: 1996, *Astrophys. J.,* **465**, 205.

Chu Y.-H., Mac Low M.-M.: 1990, *Astrophys. J.,* **365**, 510.

Chu Y.-H., Mac Low, M.-M., Garsia-Segura G., Wakker B., Kennicutt R.C.: 1993, *Astrophys. J.,* **414**, 213.

Chu Y.-H., Chang H.-W., Su Y.-L., Mac Low M.-M. 1995, *Astrophys. J.,* **450**, 157.

Dopita M.A., Kim M.S., Oey M.S., Lozinskaya T.A. 1999, in IAU Symposium N193 *Wolf-Rayet phenomena in massive stars and starburst galaxies*, eds. K.A. van der Hucht, G. Koenigsberger & P.R.J. Eenens, p.441.

Gosachinskij I.V.: 1993, in ASP, **66**, *Physics of the gaseous and stellar disks of the Galaxy*, ed. I.R. King, 257.
Heiles C.: 1982, *Astrophys. J.,* **262**, 135.
Kompaneets A.S.: 1960, *Doklady Akad. Nauk SSSR*, **130**, 1001.
Leitherer C., Heckman T.M.: 1995, *Astrophys. J. S.*, **96**, 9.
Kunth D., Mas-Hesse J.M., Terlevich E., Terlevich R.,
Lequeux J., Fall M.: 1998, *Astron. Astrophys.,* **334**, 11.
Lozinskaya T.A., Sitnik, T.G.: 1988, *Astron. Zh. Letters*, **14**, 240
Lozinskaya T.A., Repin S.V.: 1990, *Astron. Zh.*, **67**, 1152
Mashchenko S.Ya., Silich S.A., 1997, *Astron. Zh.*, **74**, 25.
Mashchenko S., Thilker D., Braun, R.: 1999, *Astron. Astrophys.,* **343**, 352.
Mac Low M.-M., McCray R.: 1988, *Astrophys. J.,* **324**, 776.
Mac Low M.-M., McCray R., Norman N.L.: 1989, *Astrophys. J.,* **337**, 141.
Marston A.P.: 1999, in IAU Symposium N193 *Wolf-Rayet phenomena in massive stars and starburst galaxies*, eds. K.A. van der Hucht, G. Koenigsberger & P.R.J. Eenens, p.306.
Martin C.L., Kennicutt R.C.: 1995, *Astrophys. J.,* **447**, 171.
Martin C.L.: 1999, *Astrophys. J.,* **513**, 156.
Meaburn, J. 1980, *Mon. Not. R. Astron. Soc.,* **192**, 365.
Oey M.S.: 1996a, *Astrophys. J.,* **465**, 231.
Oey M.S., 1996b, *Astrophys. J.,* **467**, 666.
Oey M.S., Smedley S.A.: 1998, *Astron. J.,* **116**, 1263.
Palouš, J., 1992, in *Evolution of Interstellar Matter and Dynamics of Galaxies*, edited by J. Palouš, W. B. Burton, and P. O. Lindblad (Cambridge Univ. Press, Cambridge), 65.
Puche, D., Westpfahl, D., Brinks, E. and J-R. Roy, 1992, *Astron. J.,* **103**, N6, 1841.
Raymond J.C., Smith B.W.: 1977, *Astrophys. J.S*, **35**, 419.
Rhode K.L., Salzer J.J., Westpfahl D.J., Radice L.A., 1999, *Astron. J.,* **118**, 323.
Saken J.M., Shull J.M., Garmany C.D., Nichols-Bohlin J., Fesen, R.A.: 1992, *Astrophys. J.,* **397**, 537.
Silich S.A., Fomin P.I.: 1983, *Dok. Acad. Nauk SSSR*, **268**, 861.
Silich S.A.: 1992, *Ap&SS* **195**, 317.
Silich S.A., Mashchenko S.Ya., Tenorio-Tagle G., Franco J., 1996, *Mon. Not. R. Astron. Soc.,* **280**, 711.
Silich S.A., Franco J.: 1999, *Astrophys. J.,* **522**, 863.
Silich, S.A.: 1996, *Atron. Astrophys. Transactions*, **9**, 85.
Stricland D.K., Stevens I.R.: 1998, *Mon. Not. R. Astron. Soc.,* **297**, 747.
Tenorio-Tagle G., Palouš J.: 1987, *Astron. Astrophys.,* **186**, 287.
Tenorio-Tagle G, Bodenheimer P.: 1988, *Ann. Rev. Astron. Astrophys.* **26**, 145.
Tenorio-Tagle G, Silich S.A., Kunth D., Terlevich E., Terlevich R.: 1999, *Mon. Not. R. Astron. Soc.,* **309**, 332.
Thilker D.A., Braun R., Walterbos R.: 1998, *Astron. Astrophys.,* **332**, 429.
van der Hulst J.M.: 1996, in ASP Conf. Ser., **106**, *The Minnesota Lectures on Extragalactic Neutral Hydrogen*, ed. E.D. Skillman, p. 47. Walter F.,
Kerp J., Duric N., Brinks E., Klein U.: 1998, *Astrophys. J. Lett.*, **502**, L143.
Wang Q.D.: 1999, *Astrophys. J., Letters* **510**, L139.
Weaver R., McCray R., Castor J., Shapiro P., Moore, R.: 1977, *Astrophys. J.,* **218**, 377.
Wrigge M., Wendker H.J., Wisotzki L.: 1994, *Astron. Astrophys.,* **286**, 219.
Zezas A.L., Georgantopoulos I., Ward M.J.: 1999, *Astro-ph 9903335.*

RADIO SPECTRA OF COMPLETE SAMPLE OF GALACTIC SUPERNOVA REMNANT

S.A. Trushkin

Special astrophysical observatory
Nizhnij Arkhyz, 357147, Russia *satr@sao.ru*

ABSTRACT. We present radio continuum spectra for 192 Galactic supernova remnants (SNRs) from 220 known and included in Green's (1998) catalog. These spectra include most of measurements available in literature, as well as multi-frequency measurements of nearly 120 SNRs with the RATAN-600 radio telescope.

The measurements have been placed on the same absolute flux density scale of Baars (1977). The presented compilation has given a possibility of plotting quite accurate spectra accounting for the thermal plasma free–free absorption in fitting the spectra accounted for.

From 190 spectra seventy eight (41%) have clear frequency turnover caused, apparently, by absorption in the thermal foreground within Milky Way. Frequencies of ($\nu_{\tau=1}$) are distributed from 5 to 365 MHz, with medium value : 32 MHz.

There are no correlations between Galactic coordinates, spectral index and $\nu_{\tau=1}$ in the sample of SNRs, but there is significant correlation of the frequency $\nu_{\tau=1}$ and distances, estimated from $\Sigma - D$ relation.

Key words: ISM: supernova remnants; radio continuum: ISM

1. Introduction

The non-thermal radio spectrum is a key property distinguishing SNRs from extended Galactic plane radio sources. The current catalog of SNRs (Green, 1998) contains 220 Galactic SNRs and some dozens of possible or probable ones, named SNR candidates here. While it contains information about the spectral index and flux densities at 1 GHz, there is no complete collection of the available data on flux density measurements, scattered over hundreds of publications and catalogs. Reviews of radio spectra of a few dozen SNRs are given in many early papers and the recent papers by Kassim (1989a,b), Kovalenko et al. (1994a, 1994b) and the papers on Galactic plane sources (Reich et al., 1988) based on the 11 cm and 21 cm Effelsberg Galactic plane surveys (Reich et al., 1990a, 1990b).

The results of new all-sky surveys with a resolution of about $1'$ are presently available, which comprise much more data on extended sources in the Galactic plane.

We used our measurements of the flux densities of nearly 120 SNRs (Trushkin, 1986, 1996ab, 1997; Trushkin et al., 1988). Thus the flux densities of half of the SNRs were measured at several (up to six) frequencies, which corrected and complemented essentially the spectra of many SNRs.

We collected all these data and make them accessible in the CATS database (Verkhodanov et al., 1997). The spectrum plotting procedure of the SNRs with optional fitting is designed to simplify the statistical investigation of radio properties of these SNRs by providing easy and public access to the available data.

While there are no significant correlations of global SNR parameters with the spectral indices (Caswell and Clark, 1975; Lerche, 1980), Weiler (1983) proposed an extremely important classification which divided the SNRs into groups: shells, plerions, and composite SNRs. Probably the SNRs are intimately related with the basic type classification of supernova: SNIa, SNIb and SNII. The SNIb and SNII are the birthplace of neutron stars and black holes and thus lead to production of plerions or, in dense ISM, composite SNRs with appearance of filled-center and shell structure in the X-rays and radio emission, respectively. On the other hand, the classical shells are created by SNIa, as is the case with the historical SN 1604 Tycho. Besides the morphology differences in radio emission, these three classes of SNRs have different mean spectral indices ($S_\nu \propto \nu^\alpha$) (Weiler, 1983, 1985).

Accurate spectra are very important for the classification "shell/plerion", recognition of the mechanism of generation of relativistic particles, search for possible high- or low-frequency turnovers of spectra. The theoretical calculations of evolution of radio spectra and possible correlation between spectral index and surface brightness ("$\Sigma - D$", "$\alpha - \Sigma$" planes) should be confirm by observational data of the total samples to draw conclusions concerning the physical evolution of SNRs.

2. Flux density measurement data

The catalog of the flux measurements contains nearly 2300 entries, which is a base for plotting the spec-

tra of 200 SNRs and candidates. We have used our measurements of the flux densities of about 120 SNRs (Trushkin, 1986, 1996a,b, 1997; Trushkin et al., 1988). We added to the list of SNRs four first detected SNRs: G3.2−5.2, G11.2−1.1, G16.2−2.7, G16.0+2.7 and G356.2+4.4, and also the SNR candidates G4.7+1.3, G4.8+1.2, G4.8+6.2, G9.7−0.1 and G85.2−1.2 from Duncan et al. (1997). Detailed paper about G16.2-2.7 have been submitted by the author in A&A in 1999. The complete list of RATAN-600 data contains 350 multi-frequency measurements.

The thermal absorption of the foreground describes well the spectra of most SNRs:

$$S_\nu = [S_{408}(\nu/408)^\alpha]\ \mathtt{exp}[-\tau_{408}(\nu/408)^{-2.01}].$$

Kassim (1989b) used the low-frequency data to derive spectra for 32 SNRs, and their turnovers at low frequencies (< 100 MHz) to indicate the presence of extended ionized medium along the line of sight.

For fitting we used, as a rule, an approximation formula, $y = A + Bx + C\,\mathtt{exp}(Dx)$, or a simple linear case, $y = A + Bx$, where $x = \log\nu$, $y = \log S_\nu$, ν — frequency (MHz), S_ν — flux density (Jy), $D = \pm 1$ or $D = -4.83$. Clearly the latter case is adequate to real thermal absorption at low frequencies and steady in fitting the spectra with a few points. The inverse squares of relative flux errors, $(\Delta S_\nu/S_\nu)^{-2}$, are used as formal weights of their flux points. Often we used the option "without errors" for the spectrum plotting, when the scattering of points of spectrum is larger than the values of errors.

For fitting the curve we give two spectral indices at 0.4 and 4 GHz if these frequencies are within the fitting range. The first one is closer to $\tau = 1$ since the spectra have maxima near 10–100 MHz, while $\nu_{max} \simeq 3\,\nu_{\tau=1}$. The second one is the spectral index of an optically thin spectrum and is not influenced by propagation conditions, but there is a high-frequency turnover of spectra because of the properties of synchrotron radiation.

Trushkin (1998) presented atlas of spectra of 200 SNRs: 192 SNRs, included in Green's catalog and the spectra of eight new SNRs or SNR candidates.

3. Analysis of spectra

The sample mean spectral indices at 0.4 and 4.0 GHz are $\alpha_{0.4} = -0.45 \pm 0.2$ and $\alpha_4 = -0.50 \pm 0.21$. The distributions of the low- and high-frequency spectral indices ($\alpha_{0.4}$ and α_4, respectively) for 192 SNRs are shown in Fig. 1. For comparison we present the best gaussian fit of the distribution with a dispersion $\sigma = 0.3$. There is no significant difference in the distributions of both spectral indices.

Spectral index do not correlate with the Galactic coordinates. In Fig.2 and Fig.3 $\alpha - l$ and $\alpha - b$ dependences are given.

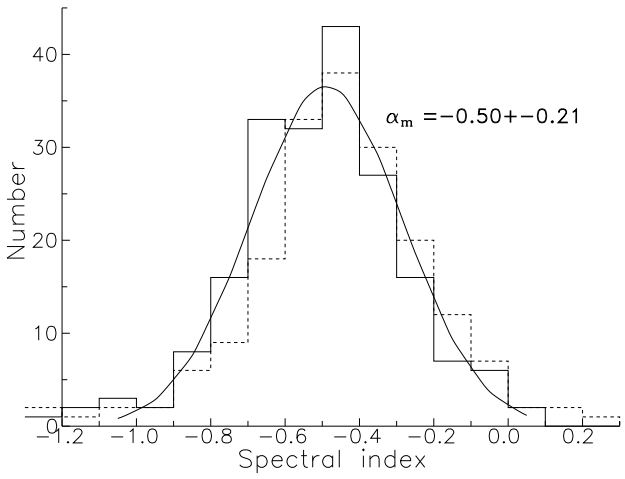

Figure 1: Distribution of α_4 (solid line) and $\alpha_{0.4}$ (dashed line) for 192 SNRs

As Lerche (1980) has shown, Bell's (1978a,b) mechanism (as a variant of the Fermi acceleration of the first order) of repowering is attractive because it provides a simple explanation of the observed spread of spectral indices: from acceleration whether on a strong adiabatic shock wave with a compression factor $\chi = 4$ or on a strong isothermal shock with $\chi = 2.4$. Thus the spectral index of relativistic electrons, $\gamma = \frac{2+\chi}{\chi-1}$, varies from 2 to 3.1. Therefore the spectral indices may vary from -0.5 to -1.1 if the equation of state in SNR is described by strong adiabatic or isothermal shocks.

An analysis of 190 spectra showed that 78 SNRs (41 %) have clear low-frequency turnover caused, apparently, by absorption in the thermal foreground of the Milky Way. Fig. 7 shows the distribution of the turnover frequency ($\tau = 1$) for these SNRs.

These frequencies $\nu_{\tau=1}$ do not correlate with the Galactic coordinates, while $\nu_{\tau=1}$ in Anticenter direction are below than in Galactic Center direction. In Fig.5 and Fig.6 $\nu_{\tau=1} - l$ and $\nu_{\tau=1} - n$ are given. Thus most SNRs have frequency of turnover ($\nu_{\tau=1}$) below 80 MHz. We could search for considerable correlation between a turnover frequency and distance of SNRs. Because the distance d estimates for individual SNRs are very uncertain, d we could only use $\Sigma - D$ relation for estimate of distances to SNRs. A new refined $\Sigma - D$ relation was obtained by Case & Bhattachatya (1998) for a sample of 36 Galactic shell SNRs: $\Sigma_{1\mathrm{GHz}}(\mathrm{W\,Hz^{-1}m^{-2}sr^{-1}}) = 2.07^{+3.10}_{-1.24} \times 10^{-17}\,D_{\mathrm{pc}}^{-2.38\pm0.26}$. They also give table for all SNRs from Green's catalog, where the size and flux density at 1 GHz could be estimated.

From 16 SNRs with active neutron stars (Frail, 1998), the spectra of 15 ones have no low-frequency turnover at $> 20-50$ MHz which is logically associated with the contribution of neutron stars (or pulsars) inside SNRs. Pulsars as a rule have steeper spectra than

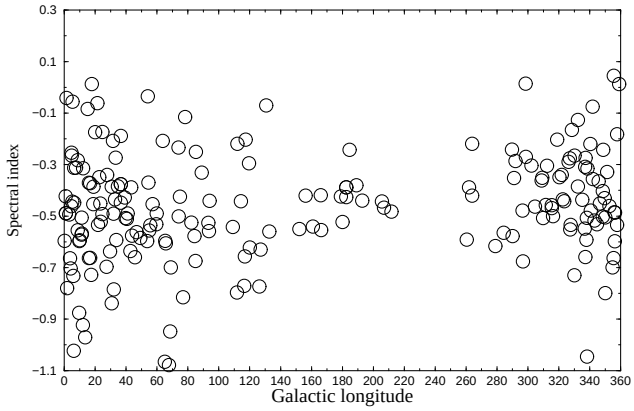

Figure 2: The spectral index via Galactic longitude.

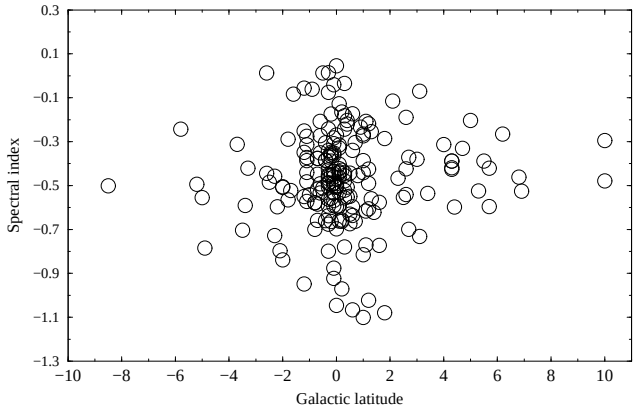

Figure 3: The spectral index via Galactic latitude.

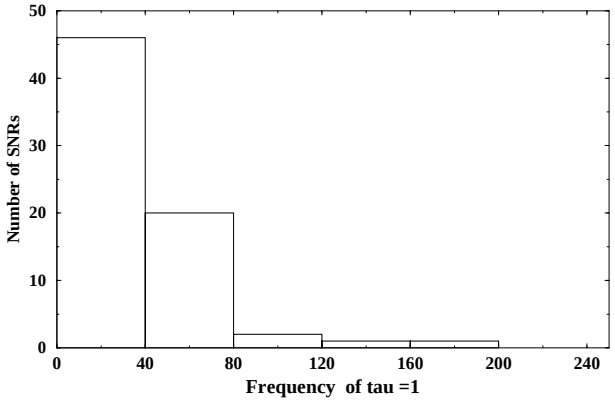

Figure 4: Distribution of turnover frequency ($\tau = 1$) for 78 SNRs

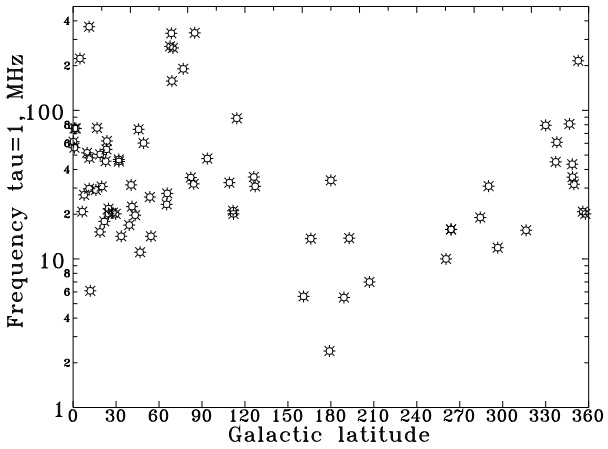

Figure 5: Frequency of turnover ($\tau = 1$) via Galactic longitude (78 SNRs)

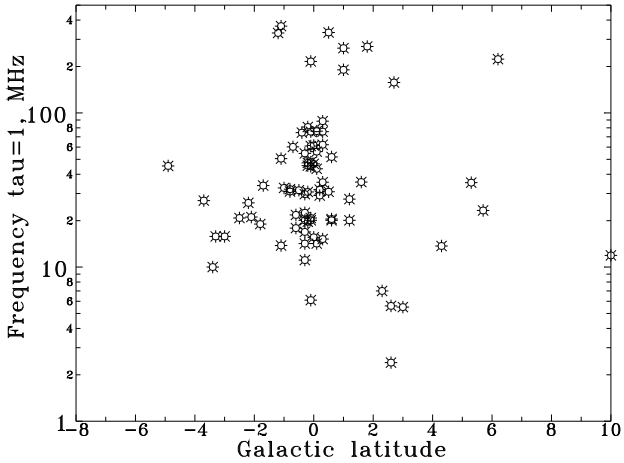

Figure 6: Frequency of turnover ($\tau = 1$) via Galactic latitude (78 SNRs)

SNRs, thus their contribution will be higher at low frequencies.

The catalog of SNR spectra has ten cases of clear turn-up at low frequencies. It is interesting that five (50 %!) such SNRs contain radio pulsars (Kaspi, 1998). Of course, it is probable that there is discrepancy of flux scales in low- and high-frequency measurements of flux densities. But in further observations we should pay special attention to the sample of SNRs without turnover or even with turn-up at low frequencies for search for pulsars or active stellar supernova remnants. There is significant correlation of the frequency $\nu_{\tau=1}$ and distances, estimated from $\Sigma - D$ relation ($\rho = 0.61 \pm 0.05$). It could be easily explained by either increasing the probability to catch at line of sight the absorbing HII region or increasing of the path in absorbing interstellar medium.

There are few data for SNR with large angular size at frequencies higher than 10 GHz in our catalog. Only

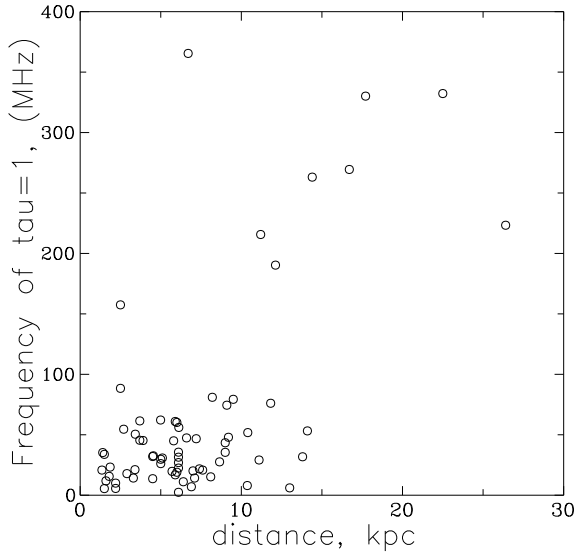

Figure 7: Turnover frequency ($\tau = 1$) for 70 SNRs via estimated distance $d_{\Sigma-d}$.

in these SNRs with big ages such turnovers are due to synchrotron losses. Thus the high-frequency surveys of the SNRs are needed.

4. Conclusions

We present radio continuum spectra for 192 Galactic supernova remnants (SNRs) from 220 known and included in Green's (1998) catalog. We added eight SNR candidates detected in the Galactic survey carried out with the RATAN-600 radio telescope (Trushkin, 1996) and in the investigations of 1997–1998. The catalog contains about 2200 flux density measurements. The spectra can be plotted only for 200 SNRs because about 20 other new and weak SNRs (Whiteoak and Green, 1996; Gray, 1994) have only one–frequency flux density measurements.

The procedure of spectrum plotting based on this catalog is "on-line" in the CATS data base *http://cats.sao.ru/C* (Verkhodanov et al., 1997).

These spectra include most flux density measurements from literature and our measurements of flux densities of nearly 120 SNRs with the RATAN-600 radio telescope in 1, 2, and 4 Galactic quadrants and from the Galactic plane survey at 0.96 and 3.9 GHz (Trushkin 1988, 1996).

Where it was possible, the flux measurements were reduced to the common flux scale of Baars (1977), as it was done in the work of Kassim (1989a). The correcting coefficients from the compiled catalog of Kuhr et al. (1981) were used.

The presented compiled catalog of flux density measurements enables one to plot spectra of SNRs with allowance made for their turnover at low frequencies due to thermal absorption in the Galaxy.

Acknowledgements. The author is grateful to his colleagues O.V. Verkhodanov, V.N. Chernenkov and H. Andernach who created the CATS database and to the Russian Foundation for Basic Research for financial support of the CATS project (grant No 96-07-89075).

References

Baars J.W.M., Genzel R., Pauliny-Toth I.I.K., et. al.: 1977, *As. A.p*, **61**, 99.
Bell A.R.: 1978a, *M.N.R.A.S.*, **182**, 147.
Bell A.R.: 1978b, *M.N.R.A.S.*, **182**, 443.
Case, G. L., Bhattacharya, D., 1998, ApJ, 504, 761
Clark D.H., Caswell J.L.: 1976, *M.N.R.A.S.*, **174**, 267.
Duncan A.R., Stewart R.T., Haynes R.F., Jones K.L.: 1997, *M.N.R.A.S.*, **287**, 722.
Gray A.D.: 1994, *M.N.R.A.S.*, **270**, 847.
Green D.A.: 1998, A Catalogue of Galactic Supernova Remnants (*1998 Sept. vers.*), MRAO, UK (available on the WWW at "http://www.mrao.cam.ac.uk/surveys/snrs/").
Kaspi V.M.: 1998, Adv. in Space Research, **21**, 167.
Kassim N.E.: 1989a, *Ap.J.*, **347**, 915.
Kassim N.E.: 1989b, *Ap. J. S.*, **71**, 799.
Kassim N.E.: 1992, *A. J.*, **103**, 943.
Kovalenko A.V., Pynzar' A.V., Udal'tsov V.A.: 1994, *A.R.*, **38**, 95.
Kovalenko A.V., Pynzar' A.V., Udal'tsov V.A.: 1994, *A.R.*, **38**, 110.
Kuhr H., Witzel A., Pauliny-Toth I.I.K., Nauber U.: 1981, *As. Ap. S.*, **45**, 367.
Lerche I.: 1980, *A. & A.*, **85**, 141.
Reich W., Fürst E., Reich P., Reif K.: 1990a, *As. Ap. Suppl.*, **85**, 633.
Reich W., Fürst E., Reich P., Junkes N.: 1988, in: "Supernova remnants and the Interstellar Medium", *IAU*
Colloquium N **101**, eds.: Roger R.S & Landecker T.L. Cambridge University Press, 293.
Reich W., Reich P., Fürst E.: 1990b, *As.Ap.Suppl.*, **83**, 539.
Trushkin S.A.: 1986, *Astron. Tsirk.*, **1453**, 4.
Trushkin S.A.: Vitkovskij V.V., Nizhelskij N.A., 1988, Astrofiz. Issled. (Izv. SAO), **25**, 84.
Trushkin S.A.: 1996a, *Bull. SAO*, **41**, 64.
Trushkin S.A.: 1996b, Astron. Astrophys. Trans., **11**, 225.
Trushkin S.A.: 1998, *Bull. SAO*, **46**, 65.
Verkhodanov O.V., Trushkin S.A., Andernach H., Chernenkov V.N.: 1997, *in: "Astronomical Data Analysis Software Systems VI",* eds.: G.Hunt & H.E.Payne., *ASP Conference Series*, **125**, 322.
Whiteoak J.B.Z., Green A.: 1992, *A.& A. S.*, **118**, 329.
Weiler K.W.: 1983, *Observatory*, **1054**, 85.
Weiler K.W.: 1985, *in: "Crab Nebula and related supernova remnants",* eds.: M.C. Kafatos & R.B.C. Henry, Cambridge Un. Press., 227.

ON THE EVOLUTION OF RADIO EMISSION OF THE TYCHO BRAHE'S SUPERNOVA REMNANT (3C10)

E.N. Vinyajkin

Radiophysical Research Institute (NIRFI)
25, B.Pecherskaya st., Nizhnij Novgorod, GSP-51, 603600, Russia,
evin@nirfi.sci-nnov.ru

ABSTRACT. Basing on long-term (1966-1998) measurements at the frequency 86 MHz the mean rate of the secular decrease of Tycho Brahe's supernova remnant (SNR) radio emission flux density has been estimated as $(0.92 \pm 0.70)\%\,\mathrm{yr}^{-1}$. The decrease of Tycho Brahe's SNR radio emission is not uniform in time. The rate of the secular decrease of this SNR radio emission is frequency independent in the limits of the errors. The weighted mean value of the rate of the secular decrease of the Tycho Brahe's SNR radio emission in the frequency range 86-5000 MHz is $(0.41 \pm 0.02)\%\,\mathrm{yr}^{-1}$.

Key words: Supernova remnants; individual: Tycho Brahe, 3C10.

1. Introduction

The supernova 1572 remnant (Tycho Brahe's SNR) is a well known shell radio source 3C10 with an angular diameter of $8'$ (Strom and Duin 1973, Duin and Strom 1975, Strom et al. 1982, Klein et al. 1979, Vinyajkin et al. 1987). The source spectrum is straight in the interval 12.6-15000 MHz with the spectral index $\alpha = 0.61 \pm 0.03$, flux density $S_\nu \propto \nu^{-\alpha}$, $S_\nu(370\ \mathrm{MHz}) = 100 \pm 7$ Jy (Vinyajkin et al. 1987). The secular decrease of the radio emission of Tycho Brahe's supernova remnant was investigated by Stankevich et al. (1973) at 952 MHz, Dickel and Spangler (1979) at 1400 MHz, Ivanov et al. (1982) at 952 MHz, Strom et al. (1982) at 1415 MHz, Vinyajkin et al. (1987) at 86 MHz and Stankevich et al. (1997) at 5000 MHz. In these papers the values of the secular decrease rate

$$d = S_\nu^{-1} dS_\nu/dt \qquad (1)$$

of the radio flux density S_ν were obtained by two-three different epochs measurements separated by intervals from 8 up to 27 years.

The aim of this work is to estimate the value of d at 86 MHz according a more long than in the paper of Vinyajkin et al. (1987) interval between the first and final epochs of measurements. A more reliable value of d at 86 MHz will be useful for study of possible frequency dependence of the secular decrease rate of 3C10 radio emission. Such dependence is observed in the radio emission of another young SNR Cassiopeia A (Dent et al. 1974, Stankevich 1977, Baars et al. 1977, Vinyajkin et al. 1980, Ivanov and Stankevich 1987, O'Sullivan and Green 1999).

2. Observations

The measurements of Tycho Brahe's SNR flux density at 87 MHz relative to radio galaxy 3C20 (this is a steady radio source) were carried out in August 1998 at Pushino radio observatory (PRAO) using the DKR-1000 east-west antenna. This antenna was divided into two equal parts (with dimensions of about 500×40 m), which then made a two-element correlation interferometer. The interference fringes of both 3C10 and 3C20 were registered near their upper culminations. The upper culmination zenith angles of 3C10 and 3C20 at the latitude of Pushino are equal correspondingly to $\approx 9^\circ$ and $\approx 3^\circ$. Such measurements are described in more detail by Vinyajkin et al. (1987). A little alteration of frequency (87 MHz instead of 86 MHz) was caused by man-made interference. Both sources 3C10 and 3C20 were observed on 5 consecutive nights during 1998 August with registration of signal in both sine and cosine channels of correlation receiver. For each night the ratio

$$\frac{A_{3C10}}{A_{3C20}} \equiv r \qquad (2)$$

(where A_{3C10} is an amplitude of 3C10 interferometric response and A_{3C20} is an amplitude of 3C20 interferometric response) was computed for both sine and cosine channels. As a result the mean value of $r = 2.75 \pm 0.09$ for the epoch 1998.6 was derived from these measurements (a little correction was made to obtain the value of r for $\nu = 86$ MHz). For the epoch 1966.7 $r = 3.48 \pm 0.16$ (Artukh et al. 1968) and for the epoch 1983.6 $r = 3.64 \pm 0.09$ (Vinyajkin et al. 1987).

It should be stressed that the values of r for all three epochs (1966.7, 1983.6 and 1998.6) were derived from

measurements of r using the same radio telescope and the same method. The values of r are plotted against epoch in Fig.1, where the straight line shows weighted least-squares fit. The straight line corresponds to the following mean rate of the secular decrease for $S^{3C10}_{86\,\mathrm{MHz}}$ for the time period 1966.7-1998.6.

$$d^{3C10}_{86\,\mathrm{MHz}} = -(0.92 \pm 0.70)\%\,\mathrm{yr}^{-1} \qquad (3)$$

We can see from Fig.1 that the decrease of the flux

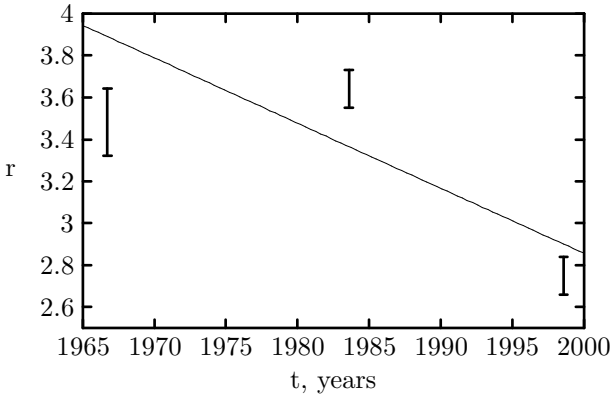

Figure 1: Amplitude of 3C10 interferometric response relative to that of 3C20 at 86 MHz. The straight line shows weighted least-squares fit.

density of 3C10 with time is not uniform. In 1966-1983 $S^{3C10}_{86\,\mathrm{MHz}}$ was constant in the limits of errors. Since 1983 up to 1998 the decrease of radio emission of 3C10 was occurring: $S^{3C10}_{86\,\mathrm{MHz}}(1998.6)$ is $(24 \pm 4)\%$ lower than $S^{3C10}_{86\,\mathrm{MHz}}(1983.6)$. It should be noted that the amplitude of interferometric response slightly decreases with time due to the expansion of Tycho Brahe's SNR but this effect provides only a small decrease near 1% for 15 years for our observations. The temporal nonuniformity of the 3C10 flux density decrease was observed at 952 MHz by Stankevich et al. (1973) and Ivanov et al. (1982): $d^{3C10}_{952\,\mathrm{MHz}}(1964-1972) = -(0.8 \pm 0.1)\%\,\mathrm{yr}^{-1}$, $d^{3C10}_{952\,\mathrm{MHz}}(1964-1981) = -(0.5 \pm 0.15)\%\,\mathrm{yr}^{-1}$.

It should be noted that the measurements of the flux density of Cas A relative to that of Cyg A were made by the author using the same radio telescope at the same frequency on the same nights. The ratio of the flux densities of Cyg A and 3C20 $S^{CygA}_{87\,\mathrm{MHz}}/S^{3C20}_{87\,\mathrm{MHz}} = 216 \pm 11$ was derived from these measurements (a correction for different angular sizes of Cyg A and 3C20 was made and it increased the measured ratio by 1.5 %). This may be compared with the ratio 228 ± 20 which can be computed from the value of $S^{CygA}_{87\,\mathrm{MHz}} = 15500 \pm 700$ Jy (Baars et al. 1977) and the value of $S^{3C20}_{87\,\mathrm{MHz}} = 68 \pm 5$ Jy (Kuhr et al. 1981). One can see a good agreement between these two values of the ratio of the flux densities of two steady radio sources Cyg A and 3C20.

3. Discussion

Let us compare the measured value (3) 3C10 radio flux density secular decrease rate at 86 MHz with the values of d at a more higher frequencies. Table 1 lists and Fig.2 shows values for d at 5 frequencies including (3).

Table 1

ν, MHz	Period, years	$-d$, $\%\,\mathrm{yr}^{-1}$	Ref.
86	1966.7-1998.6	0.92 ± 0.70	This paper
952	1964-1981	0.5 ± 0.15	Ivanov et al. 1982
1400	1963-1978	0.4 ± 0.5	Dickel and Spangler 1979
1415	1971-1979	0.23 ± 0.19	Strom et al. 1982
5000	1967.4-1994.8	0.41 ± 0.03	Stankevich et al. 1997

The weighted mean of d from Table 1 is

$$d_{wm} = -(0.41 \pm 0.02)\%\,\mathrm{yr}^{-1} \qquad (4)$$

The straight line in Fig.2 is determined by weighted

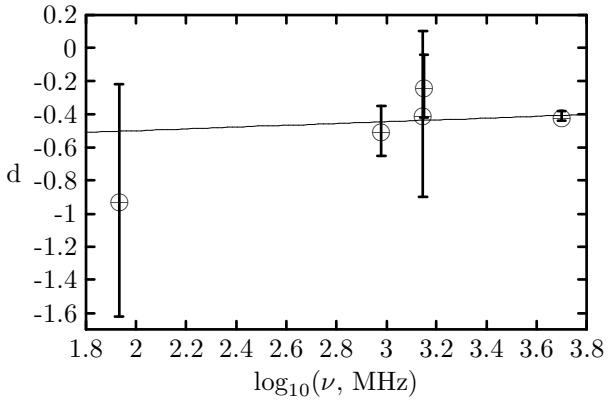

Figure 2: The variation of 3C10 radio flux density secular decrease rate $d(\%\,\mathrm{yr}^{-1})$ with $\log_{10}$(frequency, MHz). The straight line shows weighted least-squares fit.

least-squares fit to the data from Table 1 and is described by the following equation

$$d = (0.05 \pm 0.12)\log_{10}\frac{\nu(\mathrm{MHz})}{1000} - (0.445 \pm 0.08) \qquad (5)$$

We can see from (5) that the rate of 3C10 radio flux density secular decrease is frequency-independent within errors.

Let us compare the value (4) with the prediction of Shklovsky's (1960) model. According to the model of

Shklovsky (1960)

$$d = -p\frac{4\alpha + 2}{T}, \qquad (6)$$

where p-is a power index in a dependence of a source radius R from an age T of a source ($R \propto T^p$), α is a spectral index of a source ($S \propto \nu^{-\alpha}$). Substituting the values of $p = 0.462 \pm 0.024$ (Tan and Gull 1985), $\alpha = 0.61 \pm 0.03$ (Vinyajkin et al. 1987) and $T = 411$ years (411 years is the age of Tycho Brahe's SNR for the mean epoch 1983 of the observations) into Eq.(6) yields the value of $d = -(0.50 \pm 0.02)\%\,\mathrm{yr}^{-1}$ which coincides with (4) in the limits of near 2σ.

4. Conclusion

As a result of long-term measurements of the radio flux density of 3C10 relative to 3C20 at 87 and 86 MHz using a single radio telescope DKR-1000 and the same method we find the following mean secular decrease rate of the radio flux of 3C10

$$d^{3C10}_{86\,\mathrm{MHz}} = -(0.92 \pm 0.70)\%\,\mathrm{yr}^{-1}$$

Based on this value of d and the values of d at 952, 1400, 1415 and 5000 MHz of other authors the weighted mean value of d

$$d_{wm} = -(0.41 \pm 0.02)\%\,\mathrm{yr}^{-1}$$

is obtained that can be understood in the framework of Shklovsky's (1960) model.

Acknowledgments. The author is grateful to Mr. V.I.Kostromin and Mr. B.S.Formozov for assistance with the observations. This work has been supported by Russian Fund of Basic Research (Project code 97-02-16256a).

References

Artukh V.S, Vitkevich V.V., Dagkesamanskij R.D., Kozhukhov V.N.: 1968, *Astron. Zh.*, **45**, 712.

Baars J.W.M., Genzel R., Pauliny-Toth I.I.K., Witzel A.: 1977, *Astron. and Astrophys.*, **61**, 99.

Dent W.A., Aller H.D., Olsen E.T.: 1974, *Astrophys.J.*, **188**, L11.

Dickel J.R., Spangler S.R.: 1979, *Astron. and Astrophys.*, **79**, 243.

Duin R.M., Strom R.G.: 1975, *Astron. and Astrophys.*, **39**, 33.

Ivanov V.P., Bubukin I.T., Stankevich K.S.: 1982, *Pis'ma v Astron.Zh.*, **8**, 83.

Ivanov V.P., Stankevich K.S.: 1987, *Austral.J.Phys.*, **40**, 801.

Klein U., Emerson D.T., Haslam C.G.T., Salter C.J.:1979, *Astron. and Astrophys.*, **76**, 120.

Kuhr H., Witzel A., Pauliny-Toth I.I.K., Nauber U.: 1981, *Astron. and Astrophys. Suppl.Ser.*, **45**, 367.

O'Sullivan C., Green D.A.:1999, *M.N.R.A.S.*, **303**, 575.

Shklovsky I.S.: 1960, *Astron.Zh.*, **37**, 256.

Stankevich K.S., Ivanov V.P., Torkhov V.A.: 1973, *Astron. Zh.*, **50**, 645.

Stankevich K.S.: 1977, *Pis'ma v Astron.Zh.*, **3**, 349.

Stankevich K.S., Aslanyan A.M., Ivanov V.P., Durasov V.E., Kozlov A.N., Podvojskaya O.A.: 1997, *XXVII Radioastronomical conference. S.Petersburg. Thesisses*, **1**, 130.

Strom R.G., Duin R.M.: 1973, *Astron. and Astrophys.*, **25**, 351.

Strom R.G., Goss W.M., Shaver P.A.: 1982, *M.N.R.A.S.*, **200**, 473.

Tan S.M., Gull S.F.: 1985, *M.N.R.A.S.*, **216**, 949.

Vinyajkin E.N., Razin V.A., Khrulev V.V.: 1980, *Pis'ma v Astron.Zh.*, **6**, 620.

Vinyajkin E.N., Volodin Yu.V., Dagkesamanskij R.D., Sokolov K.P.: 1987, *Astron. Zh.*, **64**, 271.

MULTI-TIME-SCALE VARIABILITY OF STARS

I.L. Andronov

Department of Astronomy, Odessa State University
T.G.Shevchenko Park, Odessa 65014 Ukraine
il-a@mail.ru, http://www.paco.odessa.ua/~il-a

ABSTRACT. Physical mechanisms and corresponding mathematical models for different types of stellar variability are reviewed with applications to concrete stars. Special attention is attributed to the following topics: *cataclysmic variables* (synchronous and synchronizing magnetic systems, non-magnetic nova-like stars, dwarf novae; magnetic activity of the red companion, third body around), *pulsating variables* (additional classification criteria of variability, multi-parameter correlation analysis of the characteristics of the mean light curves of groups of long-period stars and of the multi-parameter correlation analysis of the individual characteristics of their pulsations), *mathematical models* (multi-periodic, multi-harmonic, multi-shift variations with possible trends, mono- and multi- cyclic variations of low coherence and the frequency changing/switching signals, "red noise" variability. Some original papers and links may be found at *http://ila.webjump.com*

Key words: stars: cataclysmic variables; stars: pulsating: Mira, semi-regular; stars: individual: TT Ari, UV Aur, BY Cam, PZ Cas, EM Cyg, AF Cyg, V792 Cyg, V1329 Cyg, AM Her, DQ Her, V533 Her, S Per, RX J0558.0+5353, RX J2107.9-0518, QQ Vul; data analysis.

Introduction

This self-review is based on the highlights of the results obtained during recent years in the group "Periodic and aperiodic processes in variable stars" in the main directions: cataclysmic variables at different stages of the influence of the magnetic field onto accretion; pulsating variables showing complicated multi-periodic and quasi-periodic behaviour; photometric classification of newly discovered or poorly studied variables; methods of mathematical modeling adequately satisfying the statistical conditions of the input data and approaching the asymptotic "signal/noise" ratio.

In *magnetic cataclysmic variables,* the variability is present at the time scale of seconds ("boiling column"), dozens of seconds ("shot noise", flare), hours (spin), days (spin-orbit beat, switches between a high and low states), years ("swinging dipole" and other mechanisms); $10^2 - 10^5$ years - spin period variations of the white dwarf;

non-magnetic nova-like: seconds to dozens of minutes (red noise); minutes to hour (quasi-periodic oscillations); hours (positive and negative superhumps, orbital variations); days (superhump-orbit beat); years (luminosity switches);

non-magnetic dwarf novae: cycle-to-cycle and season-to-season changes of characteristics of outbursts;

magnetic activity of the red companion: year-scale variations of the luminosity of systems with magnetic (polars and intermediate polars) and non-magnetic (nova-likes of VY Scl and UX UMa subtypes) white dwarfs; brightness variations at low states in dwarf novae and old classical novae; smooth variations and abrupt switches of the seasonal outburst cycle length in dwarf novae;

Asynchronous magnetic cataclysmic variables

The magnetic field of the white dwarf, if strong enough, leads to the synchronization of the spin with the orbital motion with a characteristic time $\tau = (P_{orb} - P_{spin})/\dot{P}_{spin} \lesssim 10^3$ yrs (Andronov, 1987). As this stage is very short as compared with the evolution time, only 3 nearly synchronous systems are discovered yet with a period difference about one per cent. This model predicted also a switching of the accretion stream from one pole to another in the asynchronous polars.

To check the observational evidence of the asynchronism between the spin and orbital motion, the international campaign "The Noah project" was organized (Silber et al., 1997) for observations of BY Cam. This title based on the Bible was preferred, as the duration of the project was suggested to be 40 days with a huge "flow" of the data. Further more detailed analysis of the results was published by Mason et al (1998).

The photometric variability has few periods. The largest amplitude corresponds to the sidelobe frequency $f = 2\omega - \Omega$, where ω is the spin frequency and Ω is the orbital frequency. This corresponds to the model that the accretion switches from one pole to another

during "idling" of the white dwarf in respect to the secondary. The accretion columns at both poles are nearly equal, as the amplitude of the variations with the spin frequency is ≈ 4 times smaller than that with the sidelobe (primary) frequency. The amplitude of the orbital variability is ≈ 2.5 times smaller than that of the primary variations.

The observed characteristic time of the synchronization obtained from the period derivative (Mason et al., 1998) is $\tau \approx 880 \pm 34$ yrs in an excellent agreement with the theoretical expectation (Andronov, 1987).

This behaviour is distinctly different from that of the intermediate polar RX J0558.0+5353 which shows variations of the circular polarization with a period twice the photometric period (Shakhovskoy and Kolesnikov 1997). This again argues for the magnetic axis of the white dwarf being relatively close to the spin equator. Another intermediate polar showing circular polarization is RX J2107.9-0518 (Shakhovskoy and Kolesnikov 1993).

Synchronous magnetic cataclysmic variables

After synchronization, the white dwarf becomes phase-locked to the red dwarf, and the spin and orbital periods become equal. However, there may be excited some orientation changes of the magnetic axis in respect to the rotating binary system, as was predicted by the "swinging dipole" model (Andronov, 1987). Such "swingings" are seen in the O–C variations of the extrema of two systems being studied for decades - AM Her and QQ Vul. Several mechanisms affect the accelerating/decelerating torgue with a complicated nonlinear overlap.

This torgue is dependent on the orientation of the magnetic axis of the white dwarf and on the accretion rate. The latter is dependent on the irradiation of the secondary by the flux from the accretion column with variable orientation, magnetic and spot activity of the red dwarf itself, minor variations of the orbital separation owed to the third body. Even in a simplest case of the accretionless dipole-dipole interaction, the orientation changes are very complicated, and even in this case different magnetic poles may be seen from the red dwarf.

This makes variations of the luminosity and the orientation very complicated and not periodic, with few characteristic time scales. This is well seen both in the long–term light curve (Andronov et al., 1997) and the changes of the longitude and latitude of the magnetic axis (Shakhovskoy et al., 1992).

The accreted plasma blobs become longer and more thin while falling onto the red dwarf causing few types of instability of the accretion column (cf. Andronov, 1987). One of the most important characteristic of this "rain" of plasma "spaghetties" is the characteristic time τ_e of penetration of such a blob through the shock front above the white dwarf. Usually this parameter is in the range from 40 to 120 seconds.

However, an interesting phenomenon was detected in BY Cam. It shows a dependence between the τ_e and the mean polarization which is obviously dependent on the orientation of the accretion column. This dependence is splitted into two parts possibly indicating a switch of the accretion pole from one to another. No splitting is seen for the same diagram for synchronous system QQ Vul (Shakhovskoy et al., 1999).

A comparison of the properties of the unprecedented UV Cet–type flare of AM Her (Shakhovskoy et al., 1993) with the small outbursts owed to accretion of plasma blobs was recently discussed by Bonnet–Bidaud et al. (2000).

The temperature estimate of the flare region at the red dwarf is $T \approx 12\,000$K with an effective radius of $R \approx 9\,000$km which is comparable with the radius of the white dwarf but the corresponding surface is only 0.5 per cent of the surface of the red dwarf. The modeling of the energy distribution of the white dwarf allowed to estimate its temperature of 20 000K (Silber et al., 1996), whereas the temperature of the accretion column is of $\approx 10^6 - 10^8$K.

Slow variations of the characteristics of cataclysmic binaries

Cataclysmic variables of different types show variations of characteristics with cycles of few years (cf. Bianchini, 1990; Andronov and Shakun, 1990). They may be seen in the luminosity changes between the "high" and "low" states of nova-like variables, polars and intermediate polars; in the lower amplitude changes of luminosity of these objects and in the variability of the cycle length between the outbursts of the dwarf novae.

In the addition to the usual interpretation of this variability as the accretion rate changes owed to a magnetic activity of the convective red dwarf companion, one may expect significant changes of the accretion rate caused by minor changes of the orbital separation owed to the gravitational interaction with a third body (light star or a heavy planet).

Chinarova et al. (1996) have found a 3000^d cyclicity of the mean brightness which is highly correlated with the effective amplitude of the outbursts. The brightness at the seasonal maximum is not statistically dependent on the mean brightness, thus the changes of the luminosity are caused mainly by the variability of the depth of the minima. Unexpectedly, no correlation was found between the mean seasonal outburst cycle length and luminosity or amplitude. However, the additional wavelet analysis of the individual cycles shows similar 3000^d wave in the duration.

Another example of drastic change of the seasonal mean cycle length shows V 792 Cyg seen on the SAI

photographic plate collection. This characteristic has switched from 25–29^d to $\approx 39^d$ between 1967 and 1973 yrs (Chinarova and Andronov, 2000). Unfortunately, the available data are not sufficient to study the possible cyclicity of the outburst behaviour.

Chinarova and Andronov (1999) reported on the possible waves of low coherency in RU Peg. The wavelet analysis shows characteristic times of 800^d, 2000^d and 22000^d either in the peak outburst brightness and in the interval between the successive outbursts.

The luminosity variability at a similar time scale of few years was found in the old novae V533 Her and DQ Her in their inactive state (Andronov et al., 1998).

The model of the modulation of the accretion rate by changing orbital separation in a triple system was indirectly confirmed by North (1999), who suggested a third body in EM Cyg, the star from our sample. Thus one may suggest that this mechanism may be one of complementary acting in at least some cataclysmic variables.

Positive and negative superhumps in nova-like variables

The SU UMa–type stars exhibit so-called superhumps during their superoutbursts which are interpreted as the precession of the eccentric accretion disk. The photometric period P_{sh} is larger than the orbital one P_{orb} in these stars, thus $P_{sh} - P_{orb} > 0$. For some nova-like variables (VX Scl–type stars), the difference $P_{sh} - P_{orb} < 0$. These objects may be called "negative superhumpers" (cf. Skillman et al., 1998). The most studied object of this type in our sample is TT Ari (Tremko et al., 1996; Andronov et al., 1999b) which recently underwent an unprecedented switch from a negative to positive superhump. Results of the international campaign "TT Ari-88" are published separately in this volume (Andronov et al., 1999a).

Variations of the light curves of symbiotic binaries

Symbiotic stars show variations of the phase light curves either if they belong to the group with a pulsating Mira-type component (UV Aur, Chinarova et al., 1994, Chinarova, 1998; R Aqr, Chinarova et al., 1996) or to the group of symbiotic novae (V 1329 Cyg, Chochol et al., 1999).

In UV Aur, a significant decrease both of the mean brightness and of the amplitude occurred near JD 2444900. The periodogram analysis showed the characteristic time of variations of 6800 ± 46^d with an approximation $dm_{max}/dm_{min} = 2.3 \pm 0.5$ which is opposite in sign as compared with the dwarf nova EM Cyg (see above). One of the possible explanations of the long-term light curve variations is the possible beat between the pulsations and the orbital motion.

In the symbiotic nova V 1329 Cyg, the secondary period of 553 ± 2^d and a longer cycle of 5300 ± 160^d are suggested which could be explained by systematic changes in geometry and location of the emitting region.

Wavelet analysis of irregularly spaced data

Irregularity of many astronomical signals leads to drastic deformations of a wavelet map making impossible the inverse wavelet transform and thus making lost the initial sense of the wavelet transform. A comparative analysis of the different modifications of the wavelet analysis based on the Morlet function was presented by Andronov (1998). An algorithm was proposed for use of the wavelet analysis based on the least squares method with supplementary weights, which extends the "weighted wavelet transform" proposed by Foster (1996). Spectral and statistical properties of the test- and smoothing functions were studied, the optimal values of the argument and frequency step were proposed. For the argument step, one may use a shift, at which the autocorrelation function corresponding to the response function crosses zero. Results are illustrated by application to continuous functions, numerical models of regular and irregular signals, including autoregressive processes, observations of the dwarf nova star SS Cygni.

The optimal wavelet smoothing algorithm was proposed by Andronov (1999b). For fixed time, the peak corresponding to the maximum of the test function WWZ is determined. Then the period is corrected to maximize the correlation coefficient between the data and the local wavelet fit. Then the corresponding test–function $S(f)$, mean value of the harmonic function, amplitude and smoothing value are computed.

Precise analytic expressions for these parameters as well as for the weighted wavelet transform are derived and illustrated on numerical examples of the harmonic, multi-frequency signals, autoregressive models, real data and the "running parabola" fits. The response functions corresponding to different basic (ordinary and trigonometric polynomials) and weight (rectangular, Gaussian and intermediate $p(z) = (1 - z^2)^2$) functions are compared by Andronov (1999b).

The wavelet analysis is effective for studies of signals with significantly variable period, mean value and amplitude, i.e. quasi–periodic oscillations in cataclysmic binaries, mode switchings in semi–regular variables etc.

The effective width of the Morlet-type wavelet corresponding to the width of a rectangular filter producing the same frequency resolution, is equal to $\Delta T = (3/8\pi^2 c)^{1/2} P \approx 1.74(1/80c)^{1/2} P$, where c is the only free parameter in this type of wavelet, and is set to $c = 1/80$ by default (cf. Foster, 1996).

For the first–order autoregressive model, the corrected shape of the autocorrelation function is presented.

The are applied to the stars of different types - cataclysmic, semi-regular, symbiotic - as well as to the

numerical models.

Scalegram analysis of the "Red noise"

The method of "running parabolae" is an effective tool for smoothing of aperiodic astronomical signals. The statistical and spectral properties of the fit for arbitrary weight and basic functions were described by Andronov (1997).

However, this method has an important application to irregular signals which are characterized by the "red noise" (cf. Andronov 1999a) caused either by the "shot noise" or by the dynamical chaos.

Such type of variability may be effectively described by the test function σ_{O-C} (i.e. the unbiased estimate of the data from the fit corresponding to the filter half–width Δt). For the noise superimposed onto the smooth variations, this test function has a standstill while Δt is small enough to produce systematic differences between the signal and the fit. With increasing systematic difference, the test-function σ_{O-C} increases with Δt to some asymptotic value corresponding to the parabolic fit.

For the flickering in cataclysmic variables, there is no standstill at the dependence $\sigma_{O-C}(\Delta t)$. Moreover, this dependence has a linear branch in a double logarithmic scale, which corresponds to a power law $\sigma_{O-C} \propto (\Delta t)^{\gamma_\sigma}$. This is caused by a presence of systematic differences at all characteristic times and by the accumulation of these differences with increasing Δt.

It may be recommended to introduce more complicated characteristics of fast variability, e.g. σ_{O-C} and the slope γ_σ at a fixed argument Δt. If computing σ_{O-C} for 3 fixed values of Δt, one may additionally determine the contribution of the uncorrelated observational noise.

If the power spectrum $S(f) \propto f^{\gamma_S}$, then one may expect that $\gamma_\sigma = (\gamma_S - 1)/2$. For the signals with a fractal dimension D, one may obtain $\gamma_\sigma = 0.5 - D$.

For AM Her, Andronov et al. (1997) have obtained $\gamma_\sigma = 0.18$, in excellent agreement with previously found value $\gamma_S = 1.36$. The corresponding value $D = 0.32$.

Periodogram analysis of the Hipparchos-Tycho suspected variables

The search for possible periodicities in 455 newly discovered suspected variables from the Hipparchos-Tycho observations was carried out by using several complementary methods. The main method was to compute the periodograms $S(f)$ corresponding to trigonometric polynomial (TP) fits of orders 1, 2 and 3 separately for B and V observations. Then the combined periodograms $S = (S_B S_V)^{1/2}$ have been computed indicating the peaks occurring at both colors. Results of this preliminary photometric classification are presented by Andronov et al. (1999).

To increase the "signal/noise" ratio, the periodic splines with *variable* degree have been proposed. To find periods of stars with asymmetric one-wave light curves, we have applied the *"RR-catcher"*, which is a 5-parameter fit: the descending branch is fitted by a parabola, and the ascending branch by a cubic parabola, keeping the smoothing curve and its first derivative continuous.

For the Algol–type variables (*"EA-catcher"*), the phase diagram is splitted into two minima of equal duration opposite in phase with an unknown depth, and a constant level outside minima. Both these methods need non–linear 3D optimization for each candidate period (characteristic phase width, phase shift and period correction). Then the stars are classified according to the phase light and color curves corresponding to the best "TP", "EA" and "RR" candidates.

Nonparametric methods of periodogram analysis

These methods are slow, but effective for the period search if there are the branches of fast signal variations with phase, e.g. in EA or RR– type stars. General approach to these methods based on the effective proximity of the points subsequent in phase was reviewed by Pel't (1980) and Terebizh (1992). Andronov and Chinarova (1997) studied statistical properties of 9 modifications of non-parametric methods nad concluded that they may be subdivided into two main groups - that similiar to the method by Lafler and Kinman (1965) and that by Deeming (1970).

The method has been extended to data with different weights by replacing the difference $|x_{k+1} - x(k)|$ in the test function by the weighted difference $|x_{k+1} - x(k)|/(\sigma^2_{k+1}+\sigma^2_k)^{1/2}$. The corresponding computer programs have been applied to the Hipparchos–Tycho observations of known and suspected variable stars.

Effective colors of correlated flickering

For cataclysmic variables, we approximate the signal by the sum of a slow non-linear trend (orbital or superhump variations), correlated flickering or quasi-periodic oscillations and uncorrelated photon counting noise. Initially we have applied the method to TT Ari (Tremko et al., 1996) where the U-B colors correspond to increasing temperature from the mean flux through superhump variability to 15-25 min QPOs.

For highly noisy signals, the method should be improved in the following way: the covariation matrix $R_{ij} = \langle (O-C)_i (O-C)_j \rangle$ is computed for different color pairs i, j for the residuals $(O-C)$ of the data from the "orbital/superhump" curve, than the mathematical expectation may be written as $R_{ii} = \sigma_i^2 = \sigma_{si}^2 + \sigma_{ni}^2$ for $i = j$ and $R_{ij} = \sigma_{si}\sigma_{sj}$ for $i \neq j$. Here σ_{si}^2 and σ_{ni}^2 are $2m$ variances of correlated signal and of an uncor-

related noise, respectively, where m is the number of simultaneously used filters. The number of independent equations is equal to $m(m+1)/2$, because the matrix is symmetrical: $R_{ij} = R_{ji}$.

For 3 colors, the solution is simple: $\sigma_{s1}^2 = R_{12}R_{13}/R_{23}$, $\sigma_{n1}^2 = R_{11} - R_{12}R_{13}/R_{23}$, and for the rest colors by using a cyclical index shift.

For more colors, one could minimize the weighted sum of the residuals from the equation $\rho_{ij} = R_{ij}/(R_{ii}R_{jj})^{1/2} = \rho_i\rho_j$, where $\rho_i = \sigma_{si}/\sigma_i$ is the correlation coefficient between the deviation from the fit of the correlated signal and of the observed (noisy) signal. Here the unknowns are ρ_i. The final parameters are $\sigma_{si} = R_{ii}^{1/2}\rho_i$ and $\sigma_{ni} = (R_{ii}(1-\rho_i^2))^{1/2}$.

This approach is slightly different from the minimization of the residuals of the equation $\eta_j\eta_j = \rho_{ij}^{-2}$ with the weights $(1-\rho_{ij}^2)^{-1}$, as was proposed by Tremko et al. (1996). Here the unknowns are $\eta_i = 1 + \sigma_{ni}^2/\sigma_{si}^2$. Obviously, both solutions for σ_{ni} and σ_{si} are equal for 3 colors.

The relative effective amplitudes of the correlated signal may be converted to stellar magnitudes by using a differential color $\Delta(m_i - m_j) = 2.5\lg(\sigma_j/\sigma_i)$ which is valid for $\sigma_i \ll 1$. However, for relatively large amplitudes, this "color correction" may also characterize an effective color of the flickering/QPO.

Long-period variables: additional classification criteria of variability

The studies of the pulsating variables are carried out in few directions.

At first, the multi-parameter correlation analysis of the characteristics of the *mean* light curves of groups of Mira-type stars. Results are briefly summarized by Kudashkina and Andronov (1996). The study of the "main sequencies" at the diagrams of the parameters of the mean light curves and of the "outstanding objects" is still in progress.

Second, the multi-parameter correlation analysis of the *individual* characteristics of long-period stars. The methods and 35 parameters of the individual light curve were described by Marsakova and Andronov (1998). Based on these methods, the Mira–type stars best covered by the observations from the AFOEV and VSOLJ databases have been analyzed.

The *"Catalogue of main characteristics of individual pulsational cycles of 35 Mira–type stars"* was published by Marsakova and Andronov (1998). The catalogue contains only the moments and brightness of the extrema and the inverse slopes $\mathrm{d}t/\mathrm{d}m$ of the light curves and the corresponding error estimates. One of the stars, Y Per, showed intervals of variability of different types - Mira or semiregular. Four stars show a secular period variations in a good agreement with the theoretical evolutionary track at the helium flash stage. Other stars show cycle-to-cycle variations, and very often the characteristic time is of order 15 000–20 000 days. The stars are clustered into groups showing correlations between different groups of parameters.

Some results of the analysis of this catalogue were published separately by Marsakova (1999, 2000).

At third, pulsating variables are studied as components of *symbiotic* variables, as was mentioned above.

The fourth direction is the study of *semiregular* pulsating variables based on own photographic observations and on the AFOEV and VSOLJ databases. Among most recent results one may note the necessity of the subdivision of the type SRc into at least two subtypes (Kudashkina and Andronov, 2000): a) SRca – supergiant stars with multi–periodic pulsations and regular light curve similar to the Mira–type, sometimes disturbed by the switching mode intervals (prototype S Per); b) SRcb – supergiant stars with a quasi–periodic light curve and intervals of brightness constancy (PZ Cas).

A phenomenological classification of semi–regular stars was proposed by Andronov et al. (1998). It is based on the arbitrary *stability* of their (multi-periodic) components of variability and, particularly, on the *switches* of pulsation mode in these stars (eg. AF Cyg). The used method is the periodogram analysis by using the least squares harmonic approximation with subsequent prewhitening (cf. Andronov, 1994). The classification was made according to the relative frequencies and number of the peaks at the periodograms. Despite the cycle–to–cycle changes of the light curve, some stars show only one main frequency; second subgroup consists of "multiharmonic" stars with frequencies close to integer multiplies of the main frequency; the third group collects the "multiperiodic" stars with 2 or more periods; the fourth group may be called "chaotic": after removal of the waves corresponding to 3 highest peaks at the periodogram, the periodogram of the residuals still contains a lot of peaks being statistically significant. The distribution of the SR stars in these groups does not usually coincide with the subtypes from the "General catalogue of variable stars". This study is continued for more wide sample of stars.

Other mathematical models:

The software package has been elaborated to study *multi-periodic* variations with possible periodic and aperiodic *trends* in the data and *shifts* between the sets owed to difference in the instrumental systems or run-to-run slow changes. The main expressions are described by Andronov (1994). The methods allow to study *mono-* and *multi- cyclic* variations of low coherence and the *mode switching* stars; aperiodic variability, e.g. corresponding to the *"shot noise"* and *"red noise"* types; secular period variations.

The algorithms for "running appoxinations" are based on the extension of the method of least squa-

res to the case of *unequal weights* of the data and an additional weight *(filter)* function making the models wavelet-like, being both dependent on time and a characteristic time scale. *Non-parametric* periodograms are extended to a case of unequal weights. These algorithms are compared according to a statistical significance of the results. More detailed descriptions and some papers may be found at our WWW pages *http://ila.webjump.com* and (briefly mirrored) *http://paco.odessa.ua/~il-a*.

References

Andronov I.L.: 1987, *Ap. Sp. Sci.,* **131**, 557.

Andronov I.L.: 1994, *Odessa Astron. Publ.,* **7**, 49.

Andronov I.L.: 1998, *Kinematics and Phys. Celestial Bodies*, **14**, N 6, 490.

Andronov I.L.: 1999a, *A.S.Pacif.Conf.Ser.,* **169**, 326.

Andronov I.L.: 1999b, in: *"Self-Similar Systems",* eds. V.B.Priezzhev, V.P.Spiridonov, JINR, Dubna, 57.

Andronov I.L.: 1997, *As. Ap. Suppl.,* **125**, 207.

Andronov I.L., Antoniuk K.A., Apeltauer T., Chinarova L.L., Galis R., Hric L., Kolesnikov S.V., Niarchos P.G., Novak R., Patkos L., Shakhovskoy D.N., Shakhovskoy N.M.: 1999a, *Odessa Astron. Publ.,* **12**, 157.

Andronov I.L., Arai K., Chinarova L.L., Dorokhov N.I., Dorokhova T.A., Dumitrescu A., Nogami D., Kolesnikov S.V., Lepardo A., Mason P.A., Matumoto K., Oprescu G., Pajdosz G., Passuelo R., Patkos L., Senio D.S., Sostero G., Suleimanov V.F., Tremko J., Zhukov G.V., Zola S.: 1999, *Astron.J.*, **117**, 574.

Andronov I.L., Chinarova L.L.: 1997, *Kinematics and Phys. Celestial Bodies,* **13**, N6, 67.

Andronov I.L., Chinarova L.L., Poyner G., Simon V., Szentasko L., Verdenet M.: 1998, in: *"Prospects of Astronomy and Astrophysics for the New Millennium, JENAM. Late Abstr.",* Praha, Czechia, 10.

Andronov I.L., Cuypers J., Piquard S.: 1999, in: *IAU Coll. No. 176 "The impact of large-scale surveys on pulsating star research. Abstracts",* Budapest, 46.

Andronov I.L.: 1998, *Kinematics and Phys. Celestial Bodies,* **14**, N 6, 490.

Andronov I.L., Kolesnikov S.V., Shakhovskoy N.M.: 1997, *Odessa Astron. Publ.,* **10**, 15.

Andronov I.L., Shakun L.I.: 1990, *As.Sp.Sci.*, **169**, 237.

Andronov I.L., Shapovalova L.L., Tsimaenko O.V.: 1998, in: *"Prospects of Astronomy and Astrophysics for the New Millennium, JENAM. Late Abstr.",* Praha, Czechia, 9.

Bianchini A.: 1990, *A.J.,* **99**, 1941.

Bonnet-Bidaud J.M., Mouchet M., Shakhovskoy N.M., Somova T.A., Somov N.N., Andronov I.L., de Martino D., Kolesnikov S.V., Kraicheva Z.: 2000, *As. Ap.* (in press).

Chochol D., Andronov I.L., Arkhipova V.P., Chinarova L.L., Mattei J., Shugarov S.Yu.: 1999, *Contr.Astron.Obs.Skalnate Pleso,* **20**, 31.

Chinarova L.L.: 1998, in: *Proc. 29th Conf. Variable Star Res.,* eds. J.Dusek, M.Zejda, Brno, 38.

Chinarova L.L., Andronov I.L.: 1999, in: *"The Universe of Gamow: Original ideas in astronomy and cosmology",* Odessa, 64.

Chinarova L.L., Andronov I.L.: 2000, in: *"B.V. Kukarkin: Variable Stars as a Key to Galactic Structure and Evolution",* Moscow (in press).

Chinarova L.L., Andronov I.L., Schweitzer E.: 1994, *Odessa Astron. Publ.,* **7**, 103.

Chinarova L.L., Andronov I.L., Schweitzer E.: 1996, *Odessa Astron. Publ.,* **9**, 100.

Deeming T.J.: 1970, *M.N.R.A.S.,* **147**, 365.

Foster G.: 1996, *Astron. J.,* **112**, 1709.

Kudashkina L.S., Andronov I.L.: 1996, *Odessa Astron. Publ.,* **9**, 108.

Kudashkina L.S., Andronov I.L.: 2000, *Astron. Soc. Pacif. Conf. Ser.* (in press).

Lafler J., Kinman T.D.: 1965, *Ap.J.Suppl.Ser.,* **11**, 216.

Marsakova V.I.: 1999, *Odessa Astron. Publ.,* **12**, 205.

Marsakova V.I.: 2000, *A.S.Pacif.Conf.Ser.* (in press).

Marsakova V.I., Andronov I.L.: 1998, *Odessa Astron. Publ.,* **11**, 79.

Mason P.A., Ramsay G., Andronov I., Kolesnikov S., Shakhovskoy N., Pavlenko E.: 1998, *Mon. Not. Roy. Astr. Soc.*, **295**, 511.

North R.C.: 1999, in: *Warner Symp. on Cataclysmic Variables,* Cambridge, 63.

Pelt J.: 1980, *Frequency Analysis of the Astronomical Time Series* (in Russian), Tallinn, Valgus.

Silber A.D., Raymond J.C., Mason P.A., Andronov I.L., Borisov N.V., Shakhovskoy N.M.: 1996, *Ap.J.,* **460**, 939.

Silber A.D., Szkody P., Hoard D.W., Hammergren M., Morgan J., Fierce E., Olsen K., Mason P.A., Rolleston R., Ruotsalainen R., Pavlenko E.P., Shakhovskoy N.M., Shugarov S., Andronov I.L., Kolesnikov S.V., Naylor T., Schmidt E.: 1997, *M.N.R.A.S.*, **290**, 25.

Shakhovskoy N.M., Alexeev I.Yu., Andronov I.L., Kolesnikov S.V.: 1993, *Ann.Israel Phys.Soc.,* **10**, 237.

Shakhovskoy N.M., Andronov I.L., Kolesnikov S.V., Halevin A.V.: 1999, *Odessa Astron. Publ.,* **12**, 242.

Shakhovskoy N.M., Kolesnikov S.V: 1993, *IAUC*, **5891**.

Shakhovskoy N.M., Kolesnikov S.V: 1997, *IAUC*, **6760**.

Shakhovskoy N.M., Kolesnikov S.V., Andronov I.L.: 1992, -in: *"Stellar Magnetism",* St.Petersburg, 148.

Skillman D.R., Harvey D.A., Patterson J., Kemp J., Jensen L., Fried R.E., Garradd G., Gunn J., van Zyl L., Kiyota S., Retter A., Vanmunster T., Warhurst P.: 1998, *Ap.J.,* **503**, L67.

Terebizh V.Yu.: 1992, *Time Series Analysis in Astrophysics* (in Russian), Moscow, Nauka, 1992.

Tremko J., Andronov I.L., Chinarova L.L., Kumsiashvili M.I., Luthardt R.,Pajdosz G., Patkos L., Roessiger S., Zola S.: 1996, *As. Ap.,* **312**, 121.

TT ARIETIS: UNPRECEDENTED SWITCHING FROM NEGATIVE TO POSITIVE SUPERHUMPS

I.L. Andronov[1], K.A. Antoniuk[1], T.Apeltauer[2], L.L. Chinarova[1], R. Gális[3], L. Hric[3], S.V. Kolesnikov[1], P.G. Niarchos[4], P. Novák[2], L. Patkos[5], D.N. Shakhovskoy[6], N.M. Shakhovskoy[6]

[1] Department of Astronomy, Odessa State University, T.G.Shevchenko Park, Odessa 270014, Ukraine, il-a@mail.ru
[2] N.Copernicus Observatory Brno, Kraví hora 2, Brno 61600, Czech Republic, rudolfn@sci.muni.cz
[3] Astronomical Institute of the Slovak Academy of Sciences, Tatranska Lomnica 05960, Slovakia, hric@ta3.sk
[4] Section of Astronomy, Astrophysics and Mechanics, Department of Physics, University of Athens, Panepistimiopolis, Zografos, Athens 15784, Greece, pniarcho@atlas.cc.uoa.gr
[5] Konkoly Observatory of the Hungarian Academy of Sciences, P.O. Box 67, Budapest 1525, Hungary, patkos@konkoly.hu
[6] Crimean Astrophysical Observatory, Nauchny 334413, Ukraine, shakh@crao.crimea.ua

ABSTRACT. Results of the international observational campaign "TT Ari–98" are presented. Altogether 11 336 observations have been obtained in the "positive superhump" state during 18 runs in 6 observatories, partially in UBV, UBVR (switching filters). During one night, 1027 simultaneous UBVRI data have been obtained. No significant shifts between the times of extrema in different colors have been found. The asymmetry is 0.44±0.01 is present showing more abrupt brightness increase than a decrease. The smoothed U-B color varies from -0.$^{\rm m}$65 to -0.$^{\rm m}$86, whereas the B-V=0.$^{\rm m}$03 is remarkably constant. Sometimes the maxima have larger amplitude and a sharp shape corresponding to flares with a duration of $\sim$ 5 minutes. One may note a significant decrease of the mean magnitude by 0.$^{\rm m}$35 on JD 2251069. The moments of 21 maximum and 18 minima are listed. They correspond to the period for the 1997 data obtained by Skillman et al. (1998) showing no period change from one season to the next. The "test function - frequency" dependence in a double logarithmic scale has a linear trend in the range (90–370 c/d) and a very large slope 2.3–3.1 corresponding to QPOs rather than to the flickering.

Key words: Stars: cataclysmic, individual: TT Ari

Introduction

Photometric period of TT Ari has been recently switched from its usual "negative superhump" value from 0.$^{\rm d}$1326 to 0.$^{\rm d}$1331 (Andronov et al., 1999) to the "positive superhump" value $P = 0.^{\rm d}14926$ (Skillman et al., 1998), which is in an excellent agreement (within 0.3%) with the value predicted by Tremko et al. (1996) based on the empirical "orbital period - superhump period" relation by Andronov (1990).

Such switch from a negative to a positive superhump without significant luminosity change is an unprecedented one, and the star should be carefully monitored to study details of such a process. Here we present some results of the international campaign "TT Ari-98". Owed to the paper size limitation, we will present the extrema timings based on the data from all observatories, whereas the fast variability will be discussed on the run of simultaneous UBVRI observations obtained in the Crimean observatory (fig. 1).

Characteristic time scales of the variability

Suggesting that the variability of TT Ari is not strictly periodic, the light curve was approximated by using the method of "running parabolae" (Andronov, 1997). Two maxima at the dependence of the signal/noise ratio vs. Δt were detected at $\approx 0.^{\rm d}065$ (superhump variability) and $\approx 0.^{\rm d}0054$ (quasi–periodic oscillations (QPOs) and flares).

Moments of extrema

By using the "running parabola" fit with the filter half-width $\Delta t = 0.^{\rm d}065$, we have computed the mo-

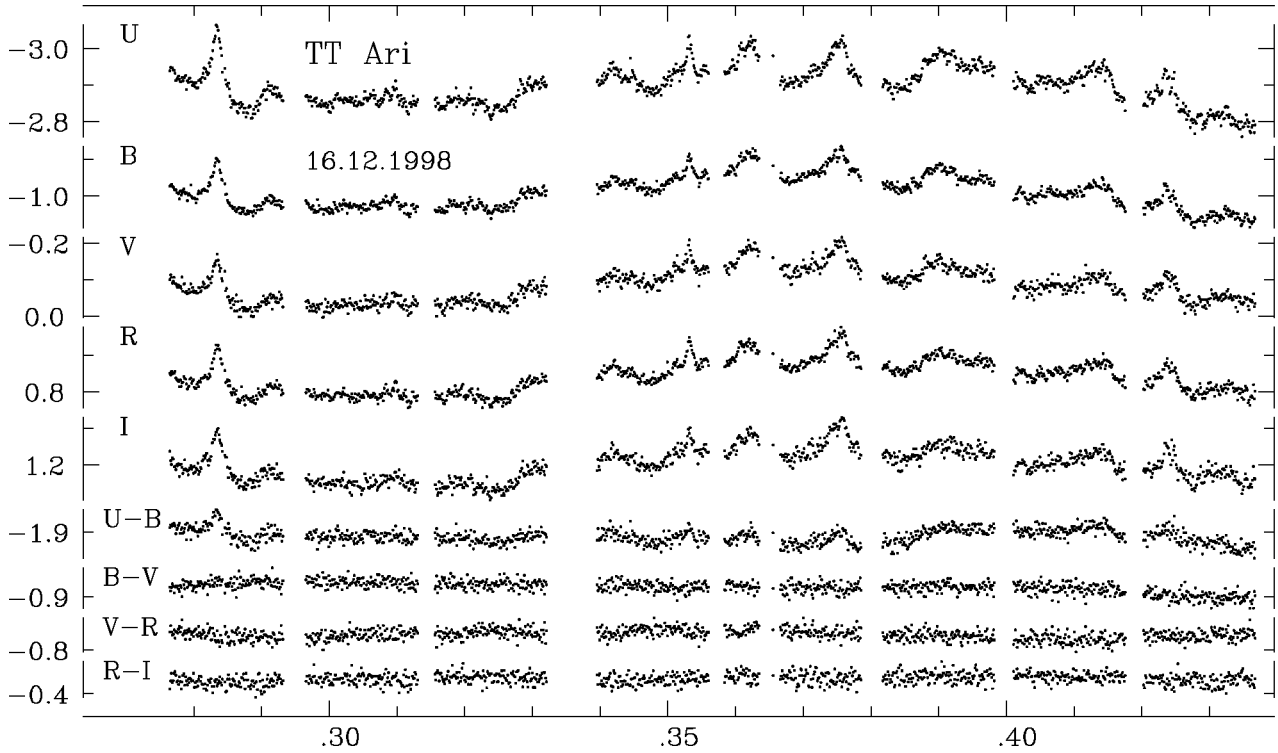

Figure 1. Instrumental UBVRI light curves of TT Ari (var-comp) and corresponding color differences. The vertical scale is the same for all graphs. The abscissa is decimal part of BJD.

Table 1. Moments of extrema

Max		Min	
BJD, 2451...	Obs	BJD, 2451...	Obs
066.4757 0.0018	Br W	051.5037 0.0010	Od B
069.5511 0.0011	Od B	051.5037 0.0010	Od B
069.5511 0.0011	Od B	066.5236 0.0036	Br W
097.4361 0.0029	Kr U	097.3786 0.0025	Kr B
097.4395 0.0025	Kr B	097.3793 0.0025	Kr V
097.4411 0.0024	Kr V	097.5183 0.0035	Kr U
100.4481 0.0009	Br V	097.5122 0.0048	Kr B
102.3859 0.0011	Br V	097.5244 0.0027	Kr V
104.4654 0.0043	Kr U	104.5588 0.0024	Kr U
104.4802 0.0036	Kr V	110.4165 0.0016	Bu B
104.4834 0.0031	Kr B	110.5574 0.0024	Bu B
110.3368 0.0023	Bu B	125.5303 0.0018	Br R
110.4770 0.0017	Bu B	125.6818 0.0012	Br R
125.4453 0.0014	Br R	164.3024 0.0005	Cr U
125.5984 0.0012	Br R	164.3025 0.0004	Cr B
125.7473 0.0023	Br R	164.3023 0.0005	Cr V
164.3696 0.0015	Cr U	164.3030 0.0004	Cr R
164.3670 0.0007	Cr B	164.3043 0.0004	Cr I
164.3677 0.0008	Cr V		
164.3684 0.0009	Cr I		
164.3714 0.0010	Cr R		

Here BJD is barycentric Julian date of the extremum and the corresponding error estimate. "Obs" marks the place of the institute/observatory, i.e. "Od" (Odessa), "Br" (Brno), "Bu" (Budapest), "Cr" (CrAO), "Kr" (Kryonerion), and the filter UBVRI or "W" (white, unfiltered).

ments of maxima and minima which are listed in Table 1.

No statistically significant difference between the times of extrema in different spectral bands was detected. The period derived from these extrema is in an excellent agreement with that published by Skillman et al. (1998).

"Red noise"

The periodograms in the double logarithmic scale show linear parts corresponding to the "red noise" fit $\lg S(f) = -a - \gamma(\lg f - \langle \lg f \rangle)$, where $\langle \lg f \rangle = 2.63$. To make a direct comparison with the results presented for the "negative superhump" state (Tremko et al., 1996; Andronov et al., 1998), we have used the same frequency interval 90-900 c/d. However, for the present data, the linear part finishes at the frequency $f \approx 370$c/d with a corresponding change of the best fit parameters. The values of a_{900}, γ_{900} and γ_{370} and the mean error estimate σ are listed in the following table:

filter	U	B	V	R	I	σ
a_{900}	2.95	2.95	2.99	2.92	2.92	0.008
γ_{900}	1.82	1.69	1.56	1.58	1.42	0.024
γ_{370}	2.40	2.32	2.67	2.64	3.13	0.063

Thus one may conclude that the coefficients γ_{900} are very similiar to that obtained during another state of the "negative superhump", whereas the maximal slope in the narrower range 90–370 c/d is much more larger and even exceeds 3.

The periodogram S(f) shows a peak at $f = 85.5$ c/d which is very close to the edge of the interval 90 c/d, contrary to the "negative superhump" data (Tremko et al., 1996; Andronov et al., 1999). Thus the "linear part" may be a "wing" of the peak rather than a "continuum" at the power spectrum. Such behaviour may be interpreted by a relatively small flickering as compared with the quasiperiodic oscillations and flares.

Scalegram analysis

The "scalegram" test function $\sigma_{O-C}(\Delta t)$ (Andronov, 1997) is an effective tool to study aperiodic "red noise"- like and chaotic processes, as it may be representer in some intervals by a power law $\sigma_{O-C}(\Delta t) \propto (\Delta t)^{\gamma_\sigma}$. E.g. for the magnetic cataclysmic variable AM Her, this fit is valid for the range differing by 7.5 orders of magnitude (Andronov et al., 1997).

Contrary to this, the scalegram for TT Ari is very complicated, showing branches of rapid increase with Δt corresponding to increasing systematic differences between the variability at ≈ 17 minutes and ≈ 3.6 hours and the fit.

Variability excess in the ultraviolet

The amplitude of ≈ 17 min variability is much larger in U than in other colors, in qualitative agreement with the the "negative superhump" data (Tremko et al., 1996; Efimov et al., 1998). This type of variability seems to be originated from the hotter inner parts of the accretion disk.

References

Andronov I.L.: 1990, *Astr. Tsirk.,* **1535**, 15.

Andronov I.L.: 1997, *As. Ap. Suppl.,* **125**, 207.

Andronov I.L., Arai K., Chinarova L.L., Dorokhov N.I., Dorokhova T.A., Dumitrescu A., Nogami D., Kolesnikov S.V., Lepardo A., Mason P.A., Matumoto K., Oprescu G., Pajdosz G., Passuelo R., Patkos L., Senio D.S., Sostero G., Suleimanov V.F., Tremko J., Zhukov G.V., Zola S.: 1999, *Astron.J.*, **117**, 574.

Andronov I.L., Kolesnikov S.V., Shakhovskoy N.M.: 1997, *Odessa Astron. Publ.,* **10**, 15.

Efimov Yu.S., Shakhovskoy N.M., Andronov I.L., Kolesnikov S.V.: 1998, *Izv. Krym. Ap. Obs.*, **94**, 263.

Skillman D.R., Harvey D.A., Patterson J., Kemp J., Jensen L., Fried R.E., Garradd G., Gunn J., van Zyl L., Kiyota S., Retter A., Vanmunster T., Warhurst P.: 1998, *Ap.J.,* **503**, L67.

Tremko J., Andronov I.L., Chinarova L.L., Kumsiashvili M.I., Luthardt R.,Pajdosz G., Patkos L., Roessiger S., Zola S.: 1996, *As. Ap.,* **312**, 121.

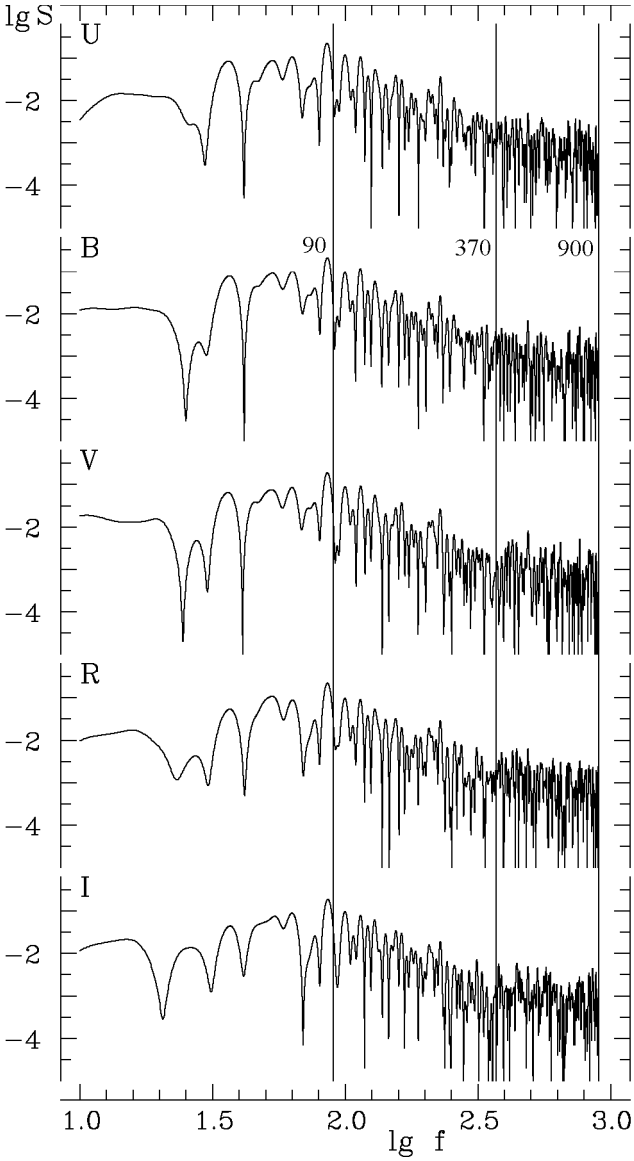

Figure 2. The periodograms for the residuals of the instrumental UBVRI observations of TT Ari from the smoothed superhump curve fitted by using the method of "running parabolae" with the filter half-width $\Delta t = 0^{\rm d}.065$. A double logarithmic scale is used. Vertical lines mark the border frequencies f =90, 370 and 900 cycles/day corresponding to the linear branches of the $\lg S - \lg f$ dependence. The range was 90–900 c/d for the "negative superhump" state (Tremko et al., 1996; Andronov et al., 1998) and seems to be much smaller 90–370 c/d for the present data. The highest peak at the periodogram occurs at the frequency $f = 85.5 \pm 0.2$ c/d corresponding to the "period" $P = 16.84 \pm 0.04$ minutes. The frequency estimates are coinciding within the accuracy estimates. The mean semiamplitudes of the variations are 22 (U), 15 (B,V) and 16 (R,I) mmag (± 1 mmag), i.e. significantly larger in U than in other colors.

PHOTOGRAPHIC STUDY OF ECLIPSING BINARIES BW CAS AND AT MON

K.A. Antoniuk
Department of Astronomy, Odessa State University
T.G.Shevchenko Park, Odessa 65014 Ukraine

ABSTRACT. Photometric elements for BW Cas and AT Mon, brightness of the comparison stars and moments of 15 weakenings are determined. The period of BW Cas is twice than that previously published by Diethelm (1997).

Key words: Stars - binary - eclipsing: Individual: BW Cas, AT Mon

The investigated stars were measured on the photographic plates of the Sky Patrol of the Astronomical Observatory of the Odessa State University. The brightness of the comparison stars was determined by linking to the standards in the NGC 654 (BW Cas) and NGC 2323 (AT Mon). The brightness of the standard stars was published by Kazanasmas et al. (1979). The finding charts are shown in Fig.1. The brightness of the comparison stars is listed in Table 1. For the periodogram analysis, we have used the method described by Lafler and Kinman (1965) and realized among other algorithms in the set of computer programs by Andronov (1994). The phase curves are shown in Fig. 2-3. The moments of weakenings with corresponding magnitudes are listed in Table 2.

BW Cas. Number of pg observations $n = 184$. The ephemeris is $Min.HJD = 2445580.806 + 2.525630 \cdot E$. No period variations are detected. The secondary minimum is doubt, the range is $12\overset{m}{.}8 - 13\overset{m}{.}3$. Our value of the period is two times larger than that published by Diethelm (1997).

AT Mon was measured on 168 negatives. The elements are $Min.HJD = 2443596.225 + 4.29405 \cdot E$, the range $10\overset{m}{.}95 - 11\overset{m}{.}30$, the depth of the secondary minimum is $\leq 0\overset{m}{.}06$.

Acknowledgement. The author is thankful to I.L.Andronov for helpful discussions.

The photometric elements:

Star	P	T_0
AT Mon	4.29405 ± 0.00015	43596.225 ± 0.003
BW Cas	2.52563 ± 0.00064	45580.806 ± 0.002

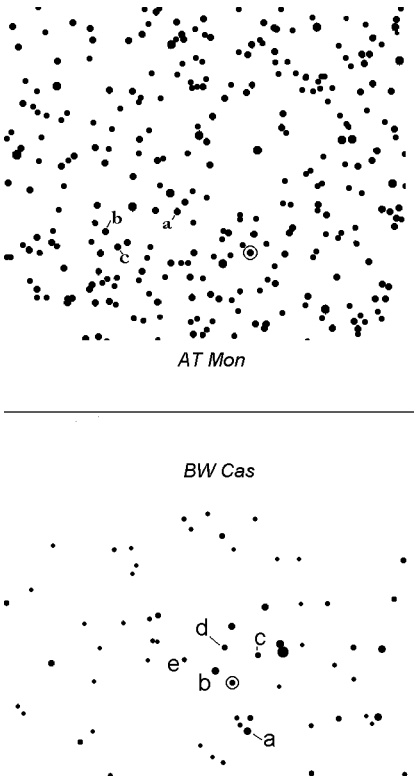

Figure 1. Finding charts for the investigated stars

Table 1. Brightness of the comparison stars.

Star	a	b	c	d	e
BW Cas	12.43	12.73	12.84	12.97	13.41
AT Mon	10.59	11.21	11.60	–	–

Table 2. Moments of weakenings and corresponding brightness.

HJD, 24.....	m_{pg}	HJD, 24.....	m_{pg}
BW Cas		BW Cas	
42331.4344	12.81	48183.4246	13.19
42801.2109	12.93	48539.4707	13.29
44109.5496	13.25	AT Mon	
44114.5420	13.10	41652.5258	11.29
45589.5185	13.24	41682.4476	11.16
46324.5416	13.26	41708.4231	11.08
46708.4750	12.79	45023.2773	11.29
47097.4057	13.06	47917.3599	10.96

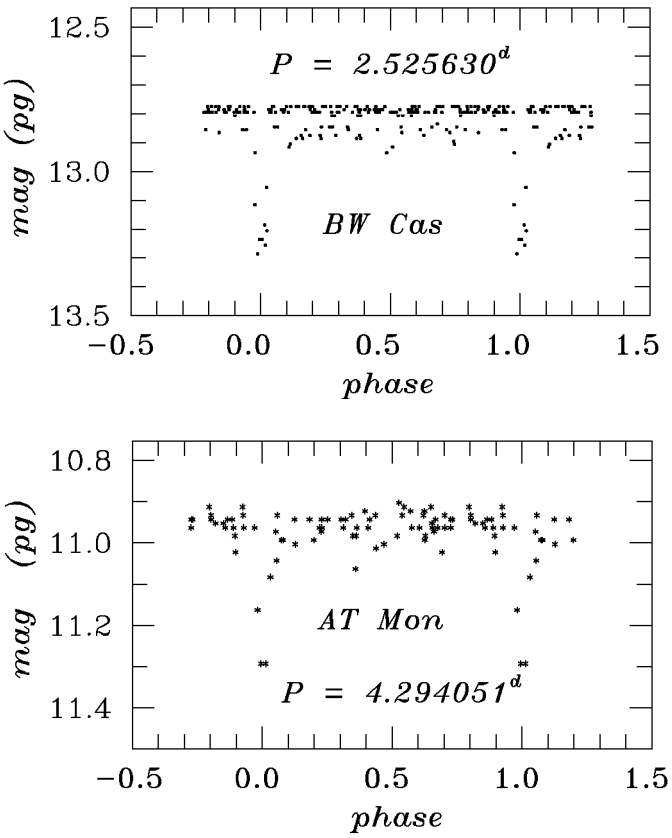

Figure 1. Phase light curves for BW Cas and AT Mon.

References

Andronov I.L.: 1994, *Odessa Astron. Publ.,* **7**, 49.

Lafler J., Kinman T.D.: 1965, *Ap. J. Suppl.,* **11**, 216.

Diethelm R.: 1997, *I.B.V.S.*, **4531**.

Kazanasmas M.S., Zavershneva L.A., Tomak L.F.: 1982, *Atlas of the photometric standards of stellar fields*, Kiev, Naukova Dumka.

ISOTOPIC ANOMALIES IN CP STARS

A. Aret, A. Sapar

Tartu Observatory, Tõravere 61602, Estonia
aret@aai.ee, sapar@aai.ee

ABSTRACT. In the present paper we analyze the anomalies in the atmospheres of HgMn stars. The abundance anomalies include both overabundances and underabundances of heavy elements. Recent observations show strongly anomalous isotopic composition of Hg, Pt, Tl and of He. Generation of abundance anomalies in quiescent atmospheres of CP stars is successfully explained by the mechanism of diffusional segregation of elements due to oppositing gravitational and radiative forces, but the formation of isotopic anomalies is not yet well explained. New diffusion mechanism called light-induced drift (LID), added to the one of radiative acceleration, successfully explains the observed isotopic anomalies. We have refined the theory of LID and applied it to CP star atmospheres. The results of computations confirm the important role of LID for diffusive segregation of isotopes.

Key words: diffusion; stars: abundances; stars: chemically peculiar

1. Introduction

Elemental abundances of about 15 % of atmospheres of main sequence stars of spectral classes B5–F5 are anomalous. Generation of these anomalies in quiescent atmospheres of CP (chemically peculiar) stars are ascribed to elemental diffusion due to radiative acceleration (Michaud 1970). In the present paper we analyze the anomalies in the atmospheres of mercury–manganese (HgMn) stars. The HgMn stars have T_{eff} between 10 000 and 16 000 K. Their abundance anomalies include both overabundances (Mn, Sr, Pt, Hg, Ga et al.) and underabundances (Al, Ni, Co et al.). Recent observations show strongly anomalous isotopic composition for Hg, Pt, Tl (overabundancy of heavier isotopes) and He (overabundancy of ^{3}He). The HgMn stars have low rotational velocities ($v\sin i = 1 - 20$ km s^{-1}) and no detected magnetic fields. The adopted values of parameters of MnHg stars χ Lup and HR7775 are given in Table 1 as an example (Adelman 1994, Jomaron et al. 1998, Kalus et al. 1998, Smith & Dworetsky 1993, Wahlgren et al. 1994, 1995). The element abundances are given relative to the solar system values by Anders & Grevesse (1989).

Table 1: The adopted parameters of HgMn stars

	χ Lup A	HR7775	
T_{EFF}	10 650	10 800	
log g	3.9	3.95	
Vsin i (km/s)	0	1	
[Hg/H]	+5.0	+5.2	
[Mn/H]	+0.3	+0.8	
[Pt/H]	+4.2	+4.7	
[Au/H]	+4.6	+3.8	
Isotopic composition, %			Terrestrial
Hg204	98.8	61.7	6.87
Hg202	1.1	37.2	29.86
Hg201	0.1	0.4	13.18
Hg200	–	0.3	23.10
Hg199	–	0.2	16.87
Hg198	–	0.2	9.97

In general the theory of radiatively driven diffusion describes adequately the observed abundances of elements. It resulted that for line–rich metals the expelling radiative force highly exceeds the gravity, being thus the dominant factor for formation of observed metal overabundances in the CP stellar atmospheres. However, essential discrepancies between observed isotopic anomalies and predictions of the theory still remain. The situation can be changed by taking into account additional diffusion mechanism called light–induced drift.

2. Light-induced drift (LID)

The important role of LID in segregation of elements in CP stellar atmospheres was proposed about a decade ago by Atutov and Shalagin (1988). LID can be considered as an additional effect to radiative acceleration due to selective transfer of photon momentum to an atomic particle in the line absorption process. Let us consider absorption in a spectral line with asymmetrical wings (due to overlapping with a line of some other element or due to local slope of continuum). As a result of this asymmetry there appears also an asymmetry in the excitation rates of atoms and ions with different Doppler shifts of thermal velocities. If the flux in the

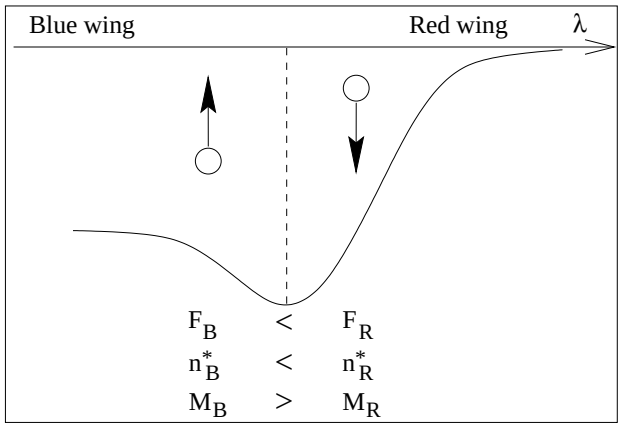

Figure 1: Scheme of the LID generation

red wing F_R is larger than the flux in the blue wing F_R (Fig. 1), there will be more excited ions moving downwards in atmosphere than moving upwards. The collisional cross–section is larger for atomic particles in the excited (upper) states than in the ground (lower) state and thus the mobility of particles in the excited states is lower than in the ground state. In Fig. 1 the mobility of particles moving downwards M_R is lower than the mobility of particles moving upwards M_B, causing thus an effective upward flow of particles. The drift direction depends on asymmetry in spectral line: larger flux in the red wing produces upward drift, large flux in the blue wing — downward drift.

Isotopes with slightly shifted energy levels have overlapping spectral lines giving systematically similar asymmetry in line profiles. Thus, the LID is most effective for diffusive segregation of isotopes. Consider, for example, a heavy element with only two isotopes. Its lighter isotope has the blueward spectral lines and heavier isotope has the redward ones. As a result, one isotope induces a drift of another. Lighter isotope with larger flux in the blue wing drifts downwards and heavier isotope with larger flux in the red wing drifts upwards. For light elements (say, for He) the isotopic line shift and thus the LID direction are opposite. This means that the overabundance of ^{3}He isotope and of the heaviest isotopes of Hg, Pt and some other heavy elements is expected.

2.1. Equations for LID

Let the lower state of atomic particle be l and the higher (upper) bound state u. In the result of photon absorption the radiation flux acts on particles in state u with force density

$$\vec{f}^{\vec{r}}_{ul} = \frac{\pi}{c} \int\limits_{-\infty}^{+\infty} n_l \, \sigma_0 W(u_\nu, a) \, \vec{F}_\nu \, d\nu \ , \qquad (1)$$

where $\pi\vec{F}_\nu$ is the total monocromatic flux, n_l – the number density of particles in state l and σ_0 – the cross–section of photon absorption in transition $l \to u$. The normalized frequency distribution in a spectral line or the Voigt function is the convolution of Lorentz and Doppler profiles, i.e.

$$W(u_\nu, a) = \int\limits_{-\infty}^{\infty} W(u_\nu, a, y) dy \ , \qquad (2)$$

where the integrand of the Voigt function

$$W(u_\nu, a, y) = \frac{a}{\pi^{3/2}} \frac{e^{-y^2}}{(u_\nu - y)^2 + a^2} \ . \qquad (3)$$

The Voigt function parameters are $u_\nu = (\nu - \nu_0)/\Delta\nu_D$, $a = \Gamma_{ul}/(4\pi\Delta\nu_D)$ and $y = v/v_D$, where $v_D = \sqrt{2kT/M}$ and M is the mass of the light–absorbing ion.

The light–induced drift starts with the process of transfer of thermal momentum from atomic particle in lower state to the particle in upper state induced by photon absorption. The momentum transferred in this way per unit volume and unit time interval $\vec{f}^{D}_{ul}$ is proportional to the volume density of particles n_l and the photon flow $\vec{i}I_\nu/h\nu$, to the momentum of particle in the direction of photon propagation Mv and to the photon absorption cross–section in line $\sigma_0 W(u_\nu, a, y)$, namely:

$$\vec{f}^{D}_{ul} = \int\limits_0^{+\infty} \int\limits_{-\infty}^{+\infty} \int\limits_{4\pi} n_l M v \sigma_0 W(u_\nu, a, y) \vec{i} \frac{I_\nu}{h\nu} d\nu dy d\Omega \ . \quad (4)$$

Taking into account, that $v = v_D y$, $\int_{4\pi} \vec{i} I_\nu d\Omega = \pi \vec{F}_\nu$ and that from Eqs.(2) and (3) follows

$$\partial W(u_\nu, a)/\partial u_\nu = -2 \int\limits_{-\infty}^{+\infty} y W(u_\nu, a, y) dy$$

we find expression for the transferred force density

$$\vec{f}^{D}_{ul} = -q \frac{\pi}{c} \int\limits_0^{+\infty} n_l \sigma_0 \frac{\partial W(u_\nu, a)}{\partial u_\nu} \vec{F}_\nu d\nu \ , \qquad (5)$$

where $q = \frac{M v_D}{2} \frac{c}{h\nu}$. The ratio of mean thermal momentum of atomic particle M to the momentum of absorbed photon is about 10^4. That is why LID is important even in the case of moderate asymmetry of radiative flux in the spectral line profile.

LID appears due to difference of collision rates of ions in upper and lower states ν_u and ν_l. The corresponding correction factor to $\vec{f}^{D}_{ul}$ is $1 - \nu_l/\nu_u$.

The LID efficiency reduces due to spontaneous radiative transitions by factor $1 - A_u/(A_u - \nu_u)$, where A_u is the frequency (probability) of spontaneous transitions.

The final correction factor to $\vec{f}^{D}_{ul}$ is

$$D = \frac{\nu_u - \nu_l}{A_u + \nu_u} \ . \qquad (6)$$

The value of D can be found only with rather low exactness. For rough estimates we may take $A_u = 10^8\ s^{-1}$, for upper layers of the CP star atmospheres $\nu_u = 10^6\ s^{-1}$ and for lower layers $\nu_u = 10^8\ s^{-1}$. Additionally we assume $\nu_u/\nu_l = 2$. In this approximation the characteristic values of the correction factor D are about $5 \cdot 10^{-3}$ in the upper atmospheric layers of CP stars and about 0.25 in the lower layers. Thus, the effective value of Dq reduces to 50 in the upper atmospheric layers and conserves large values in the deeper layers.

The total effective force on atomic particle due to both the radiative force and LID is given by

$$\vec{f}^t_{ul} = \vec{f}^r_{ul} - D\vec{f}^D_{ul}\ . \qquad (7)$$

Thus, the effect of light–induced drift can be included by substituting the Voigt function $W(u,a)$ in the radiative force expression Eq.(1) by

$$w(u_\nu, a) = W(u_\nu, a) + qD\frac{\partial W(u_\nu, a)}{\partial u_\nu}\ . \qquad (8)$$

This means that LID can be treated as an additional specific force.

3. Computations

We elaborated computer codes to calculate the accelerations to chemical elements and their isotopes in stellar atmosphere, extensively modifying the codes from CD–ROM18 by R. Kurucz for model atmospheres and synthetic spectra. Both the usual radiative acceleration in spectral lines due to the transfer of photon momentum to the stellar matter and the equivalent acceleration due to the light–induced drift have been taken into account (Eq.(7)).

Accelerations for mecury isotopes (Hg 198, 199, 200, 202, 204) have been calculated in model stellar atmosphere with $T_{eff} = 10750$ K, $\log g = 4$, $v \sin i = 0$. Three different abundances of mercury were used: solar abundance ($log\frac{N_{Hg}}{N_H} = -10.95$), solar abundance + 5 dex (both with terrestrial mixture of isotopes) and the HR7775 isotope mixture given in Table 1.

The Kurucz CD–ROM18 line lists have been used. The number of used HgI spectral lines was 27 including 2 resonance lines and the number of HgII spectral lines was 31 including 5 resonance lines. Our computations showed that the dominant contribution in LID is given by resonance lines.

We adopted the relative isotope shifts as the mean values found by Striganov & Dontsov (1955): we have taken $[198-200] = -0.94$, $[199-200] = -0.80$, $[201-200] = 0.30$, $[202-200] = 1$, $[204-200] = 1.98$. In wavenumbers $[202-200] = 0.179$ cm^{-1} for HgI and $[202-200] = 0.508$ cm^{-1} for HgII.

The computations were carried out for the spectral interval from 800 to 12 000 Å with resolution $R = 5 \cdot 10^6$. Such a high resolution is needed because spectral lines of mercury are narrow and their isotopic shifts are small.

4. Results

The effective acceleration on mercury isotopes due to LID cannot be expected to be large in the case of solar abundances of isotopes because the blending with strong neighbouring lines is more important than the mutual influence of very weak lines of mercury isotopes. Nevertheless it turned out, that although the usual radiative acceleration plays the dominant role in this case, the value of LID is of the same order of magnitude reducing upwards directed total acceleration for ^{198}Hg and increasing it for ^{204}Hg.

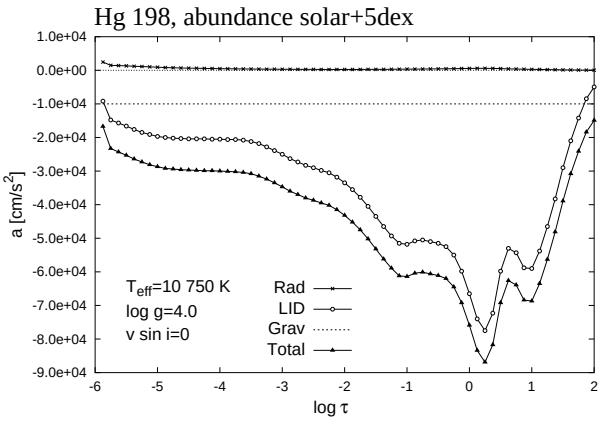

Figure 2: Accelerations on ^{198}Hg ions due to radiative force, LID, gravity and the total acceleration

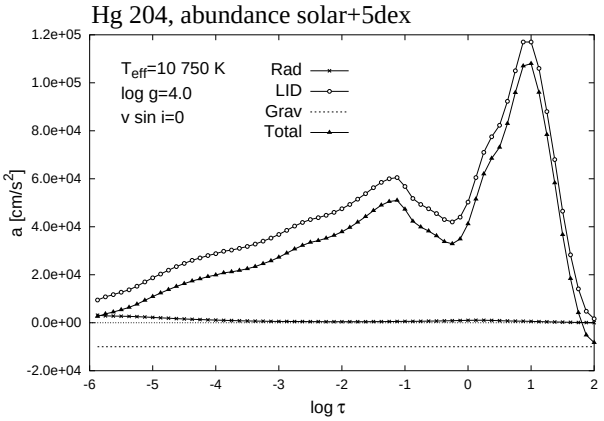

Figure 3: Accelerations on ^{204}Hg ions due to radiative force, LID, gravity and the total acceleration

The situation is drastically different in the atmosphere with high mercury abundance (solar + 5 dex). The mercury lines in such an atmosphere are strong

and the mutual influence of overlapping isotope lines is dominant generating large drift. Effective acceleration due to LID exceeds radiative accelaration up to two orders of magnitude, determining the total acceleration on mercury isotopes due to radiative force, LID and gravity. As expected, the acceleration on lightest isotope ^{198}Hg is directed downwards (Fig.2) and the acceleration on heaviest isotope ^{204}Hg is directed upwards (Fig.3). Total acceleration on the second heavy isotope ^{202}Hg is also directed upwards, being smaller than ^{204}Hg acceleration. Thus, LID causes sinking of lighter isotopes and rising of heavier ones leading to the segregation of isotopes.

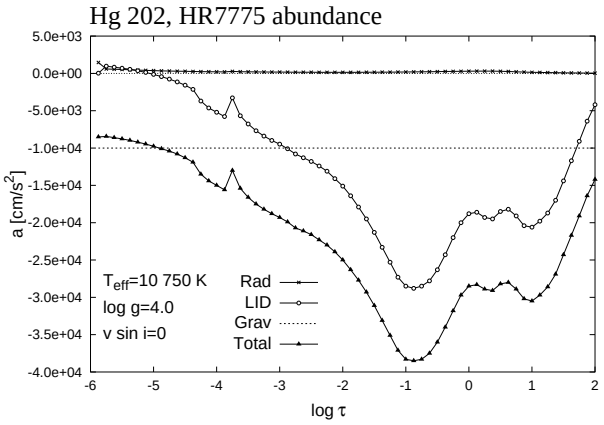

Figure 4: Accelerations on ^{202}Hg ions due to radiative force, LID, gravity and the total acceleration

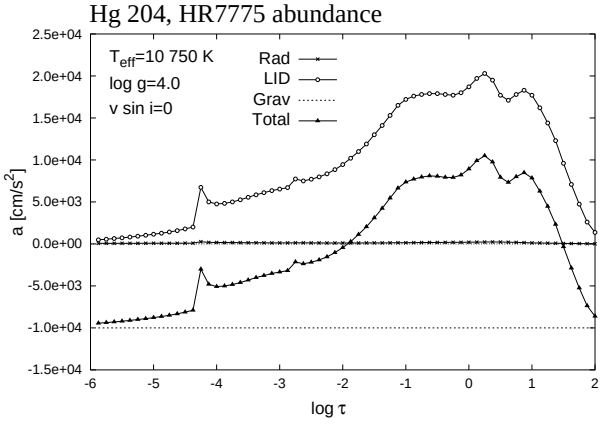

Figure 5: Accelerations on ^{204}Hg ions due to radiative force, LID, gravity and the total acceleration

In the atmosphere of HR7775 the abundance of mercury exceeds solar abundance by 5 dex, at the same time the isotopic structure differs drastically from terrestrial (Table 1). As a result of segregation of isotopes only two heaviest isotopes remained and the segregation due to LID continues. Lighter of remained isotopes ^{202}Hg which rised in atmosphere with solar mixture of isotopes now sinks (Fig.4). Accumulation of ^{204}Hg continues (Fig.5).

Basing on our results we may conclude that isotopic composition in mercury–manganese stars evolves from solar mixture to mixture in HR7775 and further to extreme isotopic structure of χ Lup.

5. Concluding remarks

Light–induced drift turned out to be of the same order of magnitude as the usual radiative acceleration in atmospheres of the main–sequence A–stars for line–rich elements (such as iron and manganese). This means that the LID cannot be neglected in the evolutionary calculations of element abundances in atmospheres of CP–stars (Sapar & Aret 1995, Aret & Sapar 1998).

Computations of the isotope segregation need the extremely high spectral resolution, exact and complete line databases, where also the isotopic and hyperfine structure splitting are taken into account.

The LID is much smaller for ionized than for neutral elements since the dominating component of the collision cross–section for ionized particle is Coulomb cross–section which is almost the same in the excited and in the ground state. The effective cross–section of two colliding charged particles is about 2 dex larger than of two colliding neutral particles or a neutral particle and an ion. This circumstance reduces efficiency of LID for ions almost proportsionally to the mean degree of ionization.

Acknowledgments. The authors are thankful to Estonian Science Foundation for support by grant No. 2629.

References

Adelman S.J.: 1994, *MNRAS*, **266**, 97

Anders E., Grevesse N.: 1989, *Geochim. Cosmochim. Acta*, **53**, 197.

Aret A., Sapar A.: 1998, *Contrib. Astron. Obs. Skalnaté Pleso*, **27**, 329.

Atutov S.N., Shalagin A.M.: 1988, *Sov. Astron. Lett.*, **14**, 284.

Jomaron C.M., Dworetsky M.M., Bohlender D.A.: 1998, *Contrib. Astron. Obs. Skalnaté Pleso*, **27**, 324.

Kalus G., Johansson S., Wahlgren G.M., Leckrone D.S., Thorne A.P., Brandt J.C.: 1998, *ApJ*, **494**, 792.

Michaud G.: 1970, *ApJ*, **160**, 641.

Sapar A., Aret A.: 1995, *Astron. Astroph. Transactions*, **7**, 1

Smith K.C., Dworetsky M.M.: 1993, *A&A*, **274**, 335.

Wahlgren G.M., Adelman S.J., Robinson R.D.: 1994, *ApJ*, **434**, 349.

Wahlgren G.M., Leckrone D.S., Johansson S.G., Rosberg M., Brage T.: 1995, *ApJ*, **444**, 438.

MAGIC NUMBERS: SUPPLEMENT, DESCRIPTION AND CLASSIFICATION

V.P. Bezdenezhnyi

Astronomical observatory, Odessa State University
T.G.Shevchenko Park, Odessa 65014 Ukraine, *astro@paco.odessa.ua*

ABSTRACT. New magic numbers are added to the early known ones, two sequences (large and small) are distinguished which are described in recurrent formulas (1) and (2). Due to the increase of magic number quantity some of the nuclear isotopes which were not considered to be magic have been attributed to such ones. As to isotopes C(6,6), Ca(20,20), Si(14,14), Ni(28,28) and Zr(40,50) they have been referred to twice magic ones. This enabled us to qualitatively explain all the peaks in the curve of isotope abundance. Small twice peaks at magic numbers of neutrons 28, 40, 70, 112 have been added to twice peaks of r-, s-processes of neutron capture at magic numbers 50, 82, 126. Three areas of relative stability at close twice magic isotopes X(112,168), Y(126,184), Z(168,258) and (or) Z'(168,240) are predicted.

Key words: nuclear astrophysics, r-, s-processes, Mendeleev's periodic system, magic numbers

Atomic nuclei containing definite numbers (2, 8, 20, 28, 50, 82, 126) of protons (p) or neutrons (n) show an enhanced stability that makes them distinguished among other nuclei neighbouring to them. These numbers of protons and neutrons are called "magic numbers". Their explanation lies in the envilope nucleus model. In explaining the valence and other properties for atoms in the periodic system of elements the ilectron states in them can be divided into groups at filling up each of them and transferring to the next group the electron energy bond decresses. The same holds true for the nuclei wherein the nuclons form filled envelopes separately for p and n.

According to the model of nucleus envelopes the nuclon energetic levels with close values of energy are grouped into series far apart from each other which are called nuclon envelopes.

According to the Pauli priciple a certain number of nuclons of the given kind can be placed on each envelope. Whenever an envelope is filled, it corresponds to the magic nucleus formation with the respective magic number. Nuclon envelopes of protons and neutrons are filled independently. The simultaneous filling up of proton and neutron envelopes is followed by a corresponding formation of particularly stable twice magic nucleus.

In the present work, Table (117.8) from "Quantum Mechanics" (Landau and Lifshits, 1963) is analyzed. In this table (see Table 1), the nuclon states in the nucleus are distributed as the following six groups. Designations: entire numbers are the main quantum numbers of the states; letters s, p, d, f, g, h, i are meanings of the orbiting momentum l; and fractional numbers j denote spin of nuclon. For each group is given total number n of proton or neutron vacancies. Numbers n are derived as the sum for states by the formula: $n = \sum (2j + 1)$. We added the following magic numbers M in the last column of the table.

In "Experimental Nucleus Physics" (Mukhin, 1974) is given a series of magic numbers with number 20 instead of 28. In literature such magic numbers as 40, 114 and 184 can be found. These divergencies make us suggest that these groups should not rather strictly correspond to nuclon envelopes in the nucleus. These groups contain envelopes as parts. As is noted by Landau and Lifshits, "though different states each of the groups enumerated consequently according to their constant filling in the series of nuclei, however, in the course of this filling considerable irregularities are noticed." They also show that state $1f_{7/2}$ are sometimes attributed to a special group. Then the remaining states in the group exhibit an envelope and magic number 20 whereas the state $1f_{7/2}$ adjoined to them gives the following stable envelope and magic number 28.

Unfortunately, in Table 1, six groups are presented and there is no possibility for us to estimate it further to see whether numbers 184 (given in literature) and 152 (was displayed from peculiatities of α-decay) are magic number indeed.

Therefore, a bypassing way had to be used: that of checking up if there is any analytical relation between members of a series of magic numbers. Two recurrent formulas have been found connecting all the set of magic numbers and isolating two their sequences: large and small ones.

$$M_i = M_{i-1} + \sum J(k) + J(i), \quad \text{for i=1,2,..., k=1,...,i-2} \tag{1}$$

$$m_{i-2} = M_i - J(i), \quad \text{for i=3,4,...} \tag{2}$$

We have the following relations: $J_j = 2j + 1 = 2\mathrm{i} = J_i$ and $\mathrm{j} = [2i - 1]/2$. Table 2 facilitates to make calculations from these formulas and straightens out the

Table 1: Groups of the nuclon states in the nucleus

No	The state in the group						n	M
1	$1s_{1/2}$						2	2
2	$1p_{3/2}$,	$1p_{1/2}$					6	8
3	$1d_{5/2}$,	$1d_{3/2}$,	$2s_{1/2}$,	$1f_{7/2}$			20	28
4	$2p_{3/2}$,	$1f_{5/2}$,	$2p_{1/2}$,	$1g_{9/2}$			22	50
5	$2d_{5/2}$,	$1g_{7/2}$,	$1h_{11/2}$,	$2d_{3/2}$,	$3s_{1/2}$		32	82
6	$2f_{7/2}$,	$1h_{9/2}$,	$2i_{13/2}$,	$2f_{5/2}$,	$3p_{3/2}$,	$3p_{1/2}$	44	126

Table 2: Calculations of magic numbers

i	1	2	3	4	5	6	7	8	9	10	11
M(i)	2	6	14	28	50	82	126	184	258	350	462
m(i-2)	-	-	8	20	40	70	112	168	240	330	440
j	1/2	3/2	5/2	7/2	9/2	11/2	13/2	15/2	17/2	19/2	21/2
J(i)	2	4	6	8	10	12	14	16	18	20	22
$\sum J(i)$	2	6	12	20	30	42	56	(72)	(90)	(110)	(132)

data.

Sums in brackets have not been used in calculating the first 16 magic numbers. As is seen from the Table 2, magic numbers M_2=6 and M_3=14 are added to the large sequence; and M_8=184 is confirmed. In the small sequence, besides magic numbers m_1=8, m_2=20, m_3=40, m_5=112 (instead of 114), numbers m_4=70, m_6=168 (not mentioned earlier) are added. All these numbers fit the peaks in the curve of abundance of isotopes with the atomic number Z. According to the above classification 152 is rather not a magic number, it is a number of α-particle configurations. Besides, it is a sum of two magic numbers of small sequence: m_3=40 and m_5=112.

Thus, in order to explain a series of magic numbers, some permutations in sequences of filling states in Table 1 are needed. If we refer the state $1d_{5/2}$ into a special subgroup, an additional magic number 14 can be obtained. In order to obtain magic number 40 which sometimes is found in literature, the states from group four $2p_{3/2}$, $1f_{5/2}$, $2p_{1/2}$ should be separated. The remaining state $1g_{9/2}$ with its $2j + 1 = 10$ gives the following magic number 50. Group five with its 32 nuclons produces magic number 50+32=82 and group six (44 nuclons) results in magic number 82+44=126. The first three members (states) of this group isolated separate envelope yield 32 nuclons and magic number 112 (instead of 114 which is found in literature).

If we permutate the state $1h_{9/2}$ and $2f_{7/2}$ in group 6 of Table 1, then after a stable state with magic number 82 a relatively stable state with Z=92 arises: M=82+10=92 (a number of α-particle configurations of uranum region). The states $2i_{13/2}$ and $3p_{1/2}$ in group 6 should be interchanged too. In group 5, the state $1h_{1/2}$ should be put in the end after the state $3s_{1/2}$. The revised Table 1 of filling the nuclon states makes a good agreement with two sequences of magic numbers. Besides, two subgroups are distinguished within each of the group starting from the second.

As the quantity of magic numbers increases, the quantity of magic and twice magic nuclei increases too. We add C(6,6), Si(14,14), Ca(20,20), Ni(28,28), Zr(40,50) and Sn(50,70) to twice magic isotopes known earlier: He(2,2), O(8,8), Pb(82,126). All they have high peaks in the curve of isotope abundance (see Fig.1).

C(6,6) corresponds to a high peak close to a twice magic oxygen O(8,8). The nucleus of magnesium Mg(12,12) with α-particle configuration gives a higher peak than aluminium Al(13,14) with its magic number N=14. Then follows a high maximum of a twice magic nucleus of silicon S(16,16) with its two numbers of α-particle combinations. After minimum of chlorine Cl and argon Ar at the ascent close to maximum of twice magic nucleus of calcium Ca(20,20) there is a magic nucleus of potassium K(19,20) with its N=20. Then a small peak of vanadium V(23,28) and chromium Cr(24,28) with magic number N=28 goes and further on - a mighty peak of iron with a magic isotope Fe(26,28). Then follows a twice magic isotope of nickel Ni(28,28), then - a small peak of germanium Ge(32,40) with its magic number N=40, and then - a peak of a magic isotopes of stroncium Sr(38,50) and ittrium Y(39,50) with N=50. Further on go small peaks of a twice magic nucleus of circonium Zr(40,50), rhutenium Ru(44,56) and palladium Pd(46,60) with their numbers of α-particle configurations. Then the peak of a twice magic isotope of tin Sn(50,70) follows, further - the peak of barium Ba(56,82) with magic number N=82 and α-particle Z=56.

After this a slow decrease in abundance isotopes of lanthanum (La), tserium (Ce), prazeodim (Pr) and

neodim (Nd) follows. Then small peak of α-particle isotope of samarium Sm(62,88) appear, as well as the peak of itterbium Y(70,103) with magic number Z=70. And finally, the platinum peak Pt(78,116) with α-particle N=116 and the peak of a twice magic nucleus of lead Pb(82,126) are noticed, as well as small peaks of thorium (Th) and uranium (U) of even-numbered and α-particle nuclei. Thus, the given classification of magic numbers explains all the peaks of an isotope abundance curve.

Theoretical interpretation of elemental abundance is one of the most important problems of nuclear astrophysics. Rather high is the abundance of elements from carbon C(6,6) to calcium Ca(20,20) the nuclei of which can contain a whole number of α-particles and some of them are magic nuclei. These elements are formed as a result thermonuclear reactions (α-processes) in the interior of giant stars. The iron peak arises due to e-process - the reaction preceeding the supernovae flare. The abundance of elements heavier than iron (Fe) can be explained by processes of neutron capture by nuclei. These processes in stars can be slow (s-process) and rapid (r-process). Twice maxima in the known curve of elemental abundance (Zyuss and Yuri) at magic numbers N=50, N=82 and N=126 convincingly confirm the existence of these two capture processes. Are there any twice r- and s-peaks at other magic numbers of neutrons: 28, 40, 70 and 112? Yes, there are as is seen from the curve of isotope abundance. Twice peaks at Z=23-25 with N=28, Z=31-32 (N=40), Z=50-52 (N=70) and Z=75-78 (N=112-114) are present too.

In literature a problem is considered of isotope existence of transuranium elements and the periodical system limit. It was Fermi who calculated the limit at Z=137. With the grouth of Z because of enormous nucleus charge, an instantaneous electron capture from the envelope takes place that brings about Z decrease. These calculations were made for a nigligible nucleus size. Allowance for the nucleus size and the distribution of charges in it shift the limit to Z=150. Theoreticians put forward brave hypotheses pertaining the nucleus Z=114 and N=184 should be stable with respect to spontaneous nuclear fission. In neutron - proton (see Fig.2) diagram one can notice an area of high stability with Z=82 and N=126 (to bismuth). Here is the region of twice magic nucleus of lead (Pb).

In the area of transbismuth isotopes, two "archipelagoes" of relative stability are suggested: the first one with Z=90-96 presented with known isotopes (the region of uranium) and the second hypothetical transcurie "archipelago" with its "islands" of stability at Z=114-126 and N=184. We assume that there are two "islands" (1 and 2) in the second "archipelago" at the following pairs of magic numbers: Z=112, N=168 and Z=126, N=184. The bravest theoreticians predict one more "island" with Z=168 (without N). This "island" seems to be present at Z=168 and N=240 (or 258). Twice magic isotopes X(112,168), Y(126,184) and Z(168,258) or Z'(168,240) will correspond to "islands" 1, 2 and 3.

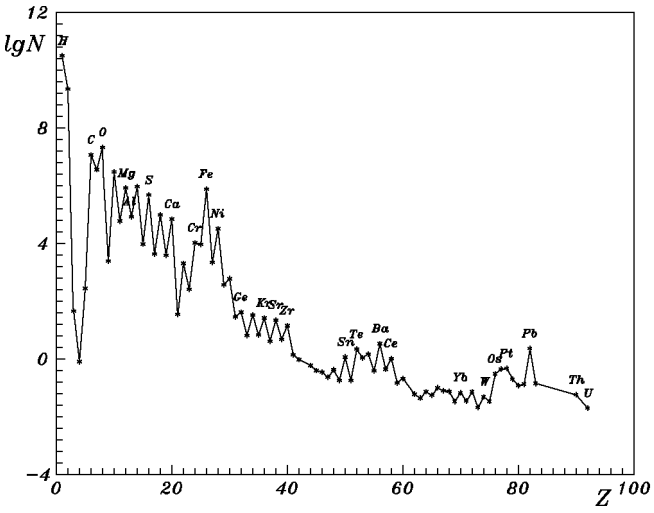

Figure 1: The curve of isotope abundance from data of sampling according to Lang (1978)

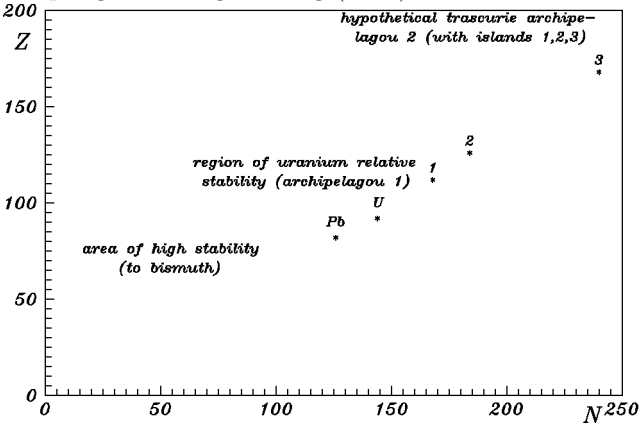

Figure 2: N-Z diagram (areas of stability)

The mean value Z=92 and N=144 correspond to "archipelago" 1. These are not magic numbers. These nuclei are apparently stable because of twice α- particle configuration. For this uranium area the ratio k_2=N_2/Z_2= 144/92=1.56; for the area of high stability of lead (Pb) k_1=126/82=1.54; and for three hypothetical "islands": k_3=168/112=1.5, k_4=184/126=1.46 and k_5=240/168=1.43 or k'_5=258/168=1.54 (coincides with k_1).

Acknowledgement. The author is thankful to I.V. Gabestro for translation of this work into English.

References

Landau L.D., Lifshits E.M.: 1963, *Quantum Mechanics,* Moscow, V.1, 523.

Mukhin K.N.: 1974, *Experimental Nuclear Physics,* Moscow, V.1, 48.

Lang K.R.: 1978, *Astrophysical formulae,* V.2, 14.

ACCRETION DISCS AROUND BLACK HOLES: DEVELOPEMENT OF THEORY

G.S. Bisnovatyi-Kogan[1]

[1] Space Research Institute, Russian Academy of Sciences
Profsoyuznaya 84/32, Moscow 117810 Russia, *gkogan@mx.iki.rssi.ru*

ABSTRACT. Standard accretion disk theory is formulated which is based on the local heat balance. The energy produced by a turbulent viscous heating is supposed to be emitted to the sides of the disc. Sources of turbulence in the accretion disc are connected with nonlinear hydrodynamic instability, convection, and magnetic field. In standard theory there are two branches of solution, optically thick, and optically thin. Advection in accretion disks is described by the differential equations what makes the theory nonlocal. Low-luminous optically thin accretion disc model with advection at some suggestions may become advectively dominated, carrying almost all the energy inside the black hole. The proper account of magnetic filed in the process of accretion limits the energy advected into a black hole, efficiency of accretion should exceed $\sim 1/4$ of the standard accretion disk model efficiency.

Key words: Stars: accretion discs; black holes.

1. Introduction

Accretion is a main source of energy in binary X-ray sources, quasars and active galactic nuclei (AGN). The intensive development of accretion theory began after discovery of X-ray sources and quasars. Accretion into stars is ended by a collision with an inner boundary, which may be a stellar surface, or outer boundary of a magnetosphere for strongly magnetized stars. All gravitational energy of the falling matter is transformed into heat and radiated outward.

In black holes matter is falling to the horizon, from where no radiation arrives. All luminosity is formed on the way to it. The efficiency of accretion is not known from the beginning, and depends on angular momentum of the falling matter, and magnetic field embedded into it. It was first shown by Schwartsman (1971) that during spherical accretion of nonmagnetized gas the efficiency may be as small as 10^{-8} for sufficiently low mass fluxes. He had shown that presence of magnetic field in the accreting matter increase the efficiency up to about 10%, and account of heating of matter due to magnetic field annihilation rises the efficiency up to about 30% (Bisnovatyi-Kogan and Ruzmaikin, 1974) In the case of a thin disc accretion, when matter has large angular momentum, the efficiency is about 1/2 of the efficiency of accretion into a star with a radius equal to the radius of the last stable orbit. In the case of geometrically thick and optically thin accretion discs the situation is approaching the case of spherical symmetry, where presence of a magnetic field plays a critical role.

Advection dominated accretion flow (ADAF) was suggested by Narayan and Yu (1995), and used as a solution for some astrophysical problems. The suggestions underlying ADAF: ignorance of the magnetic field annihilation in heating of a plasma flow, electron heating only due to binary collisions with protons (ions) had been critically analyzed in papers of Bisnovatyi-Kogan and Lovelace (1997, 1999), Bisnovatyi-Kogan (1999), Quataert (1997). There are contradictions between ADAF model and observational data in radioemission of elliptical galaxies (Di Matteo et al., 1999), and X-ray emission of Seyfert galaxy NGC4258 (Cannizzo, 1998). Account of processes connected with a small-scale magnetic field in accretion flow, strongly restricts solution. Namely, the efficiency of the accretion flow cannot become less then about 1/4 of the standard accretion disc value.

2. Development of the standard model

Matter falling into a black hole forms a disc when its angular momentum is sufficiently high. It happens when matter comes from the star companion in the binary, or from a tidal disruption of the star which trajectory approaches close to the black hole. The first situation is observed in many galactic X-ray sources (Cherepashchuk, 1996). A tidal disruption happens in quasars and active galactic nuclei (AGN) in the model of supermassive black hole surrounded by a dense stellar cluster.

Equations of a standard accretion disk theory had been first formulated by (Shakura, 1972); some corrections and generalization to general relativity (GR)

had been done by Novikov and Thorne (1973). Observational aspects of accretion disks have been analyzed by Shakura and Sunyaev (1973). Note, that all authors of the accretion disc theory from USSR were students (N.I.Shakura) or collaborators (I.D.Novikov and R.A.Sunyaev) of academician Ya.B.Zeldovich, who was not among the authors, but whose influence on them hardly could be overestimated. The main idea of this theory is to describe a geometrically thin non-self-gravitating disc of a mass M_d, much smaller then the mass of a black hole M, by hydrodynamic equations averaged over the disc thickness $2h$.

2.1. Equations

The small thickness of the disc in comparison with its radius $h \ll r$ means small importance of the pressure gradient ∇P in comparison with gravity and inertia forces. Radial equilibrium equation in a disc is a balance between the last two forces with an angular velocity equals to the keplerian one $\Omega = \Omega_K = \left(\frac{GM}{r^3}\right)^{1/2}$. Note, that just before a last stable orbit around a black hole this suggestion fails, but in the "standard" accretion disc model this relation is supposed to hold all over the disc, with an inner boundary at the last stable orbit. The equilibrium equation in the vertical z-direction is determined by a balance between the gravitational force and pressure gradient $\frac{dP}{dz} = -\rho\frac{GMz}{r^3}$. For a thin disc this differential equation is substituted by an algebraic one, determining the half-thickness of the disc in the form

$$h \approx \frac{1}{\Omega_K}\left(2\frac{P}{\rho}\right)^{1/2}. \qquad (1)$$

The balance of angular momentum, related to the ϕ component of the Euler equation has an integral in a stationary case, written as

$$\dot{M}(j - j_{in}) = -2\pi r^2\, 2h t_{r\phi}, \quad t_{r\phi} = \eta r\frac{d\Omega}{dr}. \qquad (2)$$

Here $j = v_\phi r = \Omega r^2$ is a specific angular momentum, $t_{r\phi}$ is a component of the viscous stress tensor, $\dot{M} > 0$ is a mass flux per unit time into a black hole, j_{in} is equal to the specific angular momentum of matter falling into a black hole. In the standard theory the value of j_{in} is determined from physical considerations. For accretion into a black hole it is suggested, that on the last stable orbit the gradient of the angular velocity is zero, corresponding to zero viscous momentum flux. In that case $j_{in} = \Omega_K r_{in}^2$, corresponding to the Keplerian angular momentum of the matter on the last stable orbit.

The choice of the viscosity coefficient is the most speculative problem of the theory. In the laminar case at low microscopic (atomic or plasma) viscosity the stationary accretion disc must be very massive and thick, and before its formation the matter is collected by disc leading to a small flux inside. It contradicts to observations of X-ray binaries, where a considerable matter flux along the accretion disc may be explained only when viscosity coefficient is much larger. It was suggested by Shakura (1972), that matter in the disc is turbulent, what determines a turbulent viscous stress tensor, parametrized by a pressure

$$t_{r\phi} = -\alpha\rho v_s^2 = -\alpha P, \qquad (3)$$

where v_s is a sound speed in the matter. This simple presentation comes out from a relation for a turbulent viscosity coefficient $\eta_t \approx \rho v_t l$ with an average turbulent velocity v_t and mean free path of the turbulent element l. It follows from the definition of $t_{r\phi}$ in (2), when we take $l \approx h$ from (1)

$$t_{r\phi} = \rho v_t h r\frac{d\Omega}{dr} \approx \rho v_t v_s = -\alpha\rho v_s^2, \qquad (4)$$

where a coefficient $\alpha < 1$ is connecting the turbulent and sound speeds $v_t = \alpha v_s$. Presentations of $t_{r\phi}$ in (3) and (4) are equivalent, and only when the angular velocity differs considerably from the Keplerian one the first relation to the right in (4) is more preferable. That does not appear in the standard theory, but may happen when advective terms are included.

Development of a turbulence in the accretion disc cannot be justified simply, because a Keplerian disc is stable in linear approximation to the development of perturbations. It was suggested by Ya.B.Zeldovich, that in presence of very large Reynolds number $\mathrm{Re} = \frac{\rho v l}{\eta}$ the amplitude of perturbations at which nonlinear effects become important is very low, so a turbulence may be developed due to nonlinear instability even when the disc is stable in linear approximation. Viscous stresses may arise from a magnetic field, it was suggested by (Shakura, 1972), that magnetic stresses cannot exceed the turbulent ones. It was shown by Bisnovatyi-Kogan and Blinnikov (1976), that inner regions of a highly luminous accretion discs where pressure is dominated by radiation, are unstable to vertical convection. Development of this convection produce a turbulence, needed for a high viscosity.

With alpha- prescription of viscosity the equation of angular momentum conservation is written in the plane of a disc as

$$\dot{M}(j - j_{in}) = 4\pi r^2\alpha P_0 h. \qquad (5)$$

When angular velocity is far from Keplerian one the relation (2) is valid with a coefficient of a turbulent viscosity $\eta = \alpha\rho_0 v_{s0} h$, where values with the index "0" denote the plane of the disc.

In the standard theory a heat balance is local, all heat produced by viscosity in the ring between r and

$r + dr$ is radiated through the sides of disc at the same r. The heat production rate Q_+ related to the surface unit of the disc is written as

$$Q_+ = h\, t_{r\phi} r \frac{d\Omega}{dr} = \frac{3}{8\pi}\dot{M}\frac{GM}{r^3}\left(1 - \frac{j_{in}}{j}\right). \quad (6)$$

Heat losses by a disc depend on its optical depth. The standard disc model (Shakura, 1972) considered a geometrically thin disc as an optically thick in a vertical direction. That implies energy losses Q_- from the disc due to a radiative conductivity, after a substitution of the differential equation of a heat transfer by an algebraic relation

$$Q_- \approx \frac{4}{3}\frac{acT^4}{\kappa\Sigma}. \quad (7)$$

Here a is a constant of a radiation energy density, c is a speed of light, T is a temperature in the disc plane, κ is a matter opacity, and a surface density $\Sigma = 2\rho h$. Here and below ρ, T, P without the index "0" are related to the disc plane. The heat balance equation is represented by a relation $Q_+ = Q_-$. A continuity equation in the standard model is used for finding of a radial velocity v_r

$$v_r = \frac{\dot{M}}{4\pi r h \rho} = \frac{\dot{M}}{2\pi r \Sigma}. \quad (8)$$

Completing these equations by an equation of state $P(\rho, T)$ and relation for the opacity $\kappa = \kappa(\rho, T)$ we get a full set of equations for a standard disc model. For power low equations of state of an ideal gas $P = P_g = \rho\mathcal{R}T$ ($\mathcal{R}$ is a gas constant), or radiation pressure $P = P_r = \frac{aT^4}{3}$, and opacity in the form of electron scattering κ_e, or Karammers formulae κ_k, the solution of a standard disc accretion theory is obtained analytically. Checking the suggestion of a large optical thickness confirms a self-consistency of the model. Note that solutions for different regions of the disc with different equation of states and opacities are not matched to each other.

2.2. Optically thin solution

It was found by Shapiro et al. (1976) that there is another branch of the solution for a disc structure with the same input parameters M, $\dot{M}$, α which is also self-consistent but has a small optical thickness. That implies another equation of energy losses, determined by a volume emission $Q_- \approx q\,\rho\,h$. The emissivity of the unit of a volume q is connected with a Planckian averaged opacity κ_p by a relation $q \approx acT_0^4\kappa_p$. In the optically thin limit the pressure is determined by a gas $P = P_g$. In the optically thin solution the thickness of the disc is larger then in the optically thick one, and density is lower.

While heating by viscosity is determined mainly by heavy ions, and cooling is determined by electrons, the rate of the energy exchange between them is important for a structure of the disc. The energy balance equations are written separately for ions and electrons. For small accretion rates and lower matter density the rate of energy exchange due to binary collisions is so slow, that in the thermal balance the ions are much hotter then the electrons. That also implies a high disc thickness. In the highly turbulent plasma the energy exchange between ions and electrons may be strongly enhanced due to presence of fluctuating electrical fields, where electrons and ions gain the same energy. In such conditions difference of temperatures between ions and electrons may be negligible. The theory of relaxation in the turbulent plasma is not completed, but there are indications to a large enhancement of the relaxation in presence of plasma turbulence, in comparison with the binary collisions (Galeev and Sagdeev, 1983; Quataert, 1997).

2.3. Accretion disc structure from equations describing continuously optically thin and thick regions

Equations of the disc structure smoothly describing transition between optically thick and optically thin disc, had been obtained using Eddington approximation. The expressions had been obtained (Artemova et al., 1996) for the vertical energy flux from the disk F_0, and radiation pressure in the symmetry plane

$$F_0 = \frac{2acT_0^4}{3\tau_0\Phi},\ \ P_{rad,0} = \frac{aT_0^4}{3\Phi}\left(1 + \frac{4}{3\tau_0}\right), \quad (9)$$

where $\tau_{\alpha 0} = \kappa_p\rho h = \frac{1}{2}\kappa_p\Sigma_0$, $\tau_* = (\tau_0\tau_{\alpha 0})^{1/2}$, $\Phi = 1 + \frac{4}{3\tau_0} + \frac{2}{3\tau_*^2}$. At $\tau_0 \gg \tau_* \gg 1$ we have (7) from (9). In the optically thin limit $\tau_* \ll \tau_0 \ll 1$ we get

$$F_0 = acT_0^4\tau_{\alpha 0}, \quad P_{rad,0} = \frac{2}{3}acT_0^4\tau_{\alpha 0}. \quad (10)$$

Using F_0 instead of Q_- and equation of state $P = \rho\mathcal{R}T + P_{rad,0}$, the equations of accretion disc structure together with equation $Q_+ = F_0$, with Q_+ from (6), have been solved numerically by Artemova et al. (1996). Two solutions, optically thick and thin, exist separately when luminosity is not very large. They intersect at $\dot{m} = \dot{m}_b$ and there is no global solution for accretion disc at $\dot{m} > \dot{m}_b$. It was concluded by Artemova et al. (1996) that in order to obtain a global physically meaningful solution at $\dot{m} > \dot{m}_b$, account of advectivion is needed. For the calculated case $M_{BH} = 10^8\ M_\odot$, $\alpha = 1.0$ at $\dot{m} = \dot{m}_b$ luminosity of the accretion disk is less than the critical Eddington one.

3. Accretion discs with advection

Standard model gives somewhat nonphysical behavior near the inner edge of the accretion disc around a black hole, with a zero heat production at the inner edge of the disk. It is clear from physical ground, that in this case the heat brought by radial motion of matter along the accretion disc becomes important. In presence of this advective heating (or cooling) term, depending on the radial entropy S gradient, written as $Q_{adv} = \frac{\dot{M}}{2\pi r} T \frac{dS}{dr}$, the equation of a heat balance is modified to

$$Q_+ + Q_{adv} = Q_-. \tag{11}$$

In order to describe self-consistently the structure of the accretion disc we should also modify the radial disc equilibrium, including pressure and inertia terms

$$r(\Omega^2 - \Omega_K^2) = \frac{1}{\rho}\frac{dP}{dr} - v_r \frac{dv_r}{dr}. \tag{12}$$

Appearance of inertia term leads to transonic radial flow with a singular point. Conditions of a continuous passing of the solution through a critical point choose a unique value of the integration constant j_{in}. First approximate solution for the advective disc structure have been obtained by Paczyński and Bisnovatyi-Kogan (1981). Attempts to find a solution for advective disc had been done by Abramovicz et al. (1988), Matsumoto et al. (1984). For moderate values of $\dot{M}$ a unique continuous transonic solution was found, passing through singular points, and corresponding to a unique value of j_{in}. The number of critical point in the radial flow with the gravitational potential ϕ_g (Paczyński and Wiita, 1980) $\phi_g = \frac{GM}{r - r_g}$, $r_g = \frac{2GM}{c^2}$. may exceed unity. Appearance of two critical points for a radial flow in this potential was analyzed by Chakrabarti and Molteni (1993). Using of equations averaged over a thickness of the disc changes a structure of hydrodynamic equations, leading to a position of singular points not coinciding with a unit Mach number point.

4. Amplification of the magnetic field at a spherical accretion

A matter flowing into a black hole is usually magnetized. Due to more rapid increase of a magnetic energy the role of the magnetic field increases when matter flows inside. It was shown by Schwartsman (1971), that magnetic energy density E_M approaches a density of a kinetic energy E_k, and he proposed a hypothesis of *equipartition* $E_M \approx E_k$, supported by continuous annihilation of the magnetic field in a region of the main energy production. This hypothesis is usually accepted in the modern picture of accretion (Narayan and Yu, 1995). Account of the heating of matter by magnetic field annihilation was done by Bisnovatyi-Kogan and Ruzmaikin (1974). For a spherical accretion with $\mathbf{v} = (v_r, 0, 0)$ the equations describing a field amplification in the ideally conducting plasma reduce to (Bisnovatyi-Kogan, Ruzmaikin, 1974)

$$\frac{d(r^2 B_r)}{dt} = 0, \quad \frac{d(r v_r B_\theta)}{dt} = 0, \quad \frac{d(r v_r B_\phi)}{dt} = 0, \tag{13}$$

where $\frac{d}{dt} = \frac{\partial}{\partial t} + v_r \frac{\partial}{\partial r}$ is a full Lagrangian derivative. Consider a free fall case with $v_r = -\sqrt{\frac{2GM}{r}}$. The initial condition problem is solved separately for poloidal and toroidal fields. For initially uniform field $B_{r0} = B_0 \cos\theta$, $B_{\theta 0} = -B_0 \sin\theta$ we get the solution (Bisnovatyi-Kogan, Ruzmaikin, 1974)

$$B_r = \frac{B_0 \cos\theta}{r^2} \Phi_1^{4/3}, \quad B_\theta = -\frac{B_0 \sin\theta}{\sqrt{r}} \Phi_1^{1/3}, \tag{14}$$

where $\Phi_1 = r^{3/2} + \frac{3}{2} t \sqrt{2GM}$. The radial component of the field is growing most rapidly. It is $\sim r^{-2}$ for large times, $\sim t^{4/3}$ at given small radius, and is growing with time everywhere. For initially dipole magnetic field

$$B_{r0} = \frac{B_0 \cos\theta}{r^3}, \quad B_{\theta 0} = -\frac{B_0 \sin\theta}{2r^3}$$

we obtain the following solution

$$B_r = \frac{B_0 \cos\theta}{r^2} \Phi_1^{-2/3}, \quad B_\theta = -\frac{B_0 \sin\theta}{2\sqrt{r}} \Phi_1^{-5/3}. \tag{15}$$

Here the magnetic field is decreasing everywhere with time, tending to zero. That describes a pressing of a dipole magnetic field to a stellar surface. The azimuthal stellar magnetic field if confined inside the star. When outer layers of the star are compressing with a free-fall speed, then for initial field distribution $B_{\phi 0} = B_0 r^n f(\theta)$ the change of B_ϕ with time is described by a relation $B_\phi = -\frac{B_0 f(\theta)}{\sqrt{r}} \Phi_1^{n+1/3}$.

5. Two-temperature advective discs

In the optically thin accretion discs at low mass fluxes the density of the matter is low and energy exchange between electrons and ions due to binary collisions is slow. In this situation, due to different mechanisms of heating and cooling for electrons and ions, they may have different temperatures. First it was realized by Shapiro et al. (1976), where advection was not included. It was noticed by Narayan and Yu (1995), that advection in this case is becoming extremely important. It may carry the main energy flux into a black hole, leaving rather low efficiency of the accretion up to $10^{-3} - 10^{-4}$ (advective dominated accretion flows

- ADAF). This conclusion is valid only when the effects, connected with heating of matter by magnetic field annihilation are neglected.

In the ADAF solution the ion temperature is about a virial one $kT_i \sim GMm_i/r$, what means that even at high initial angular momentum the disc becomes thick, forming a quasi-spherical accretion flow. When energy losses by ions are low, some kind of a "thermo-viscous" instability is developed, because heating increases a viscosity, and viscosity increases a heating. Development of this instability leads to formation of ADAF.

A full account of the processes, connected with a presence of magnetic field in the flow, is changing considerably the picture of ADAF. It was shown by Schwarzman (1971), that in the region of the main energy production, the condition of equipartition takes place, and efficiency of a radiation increase enormously from $\sim 10^{-8}$ up to ~ 0.1 due to magneto-bremstrahlung. To support the condition of equipartition a continuous magnetic field reconnection and heating of matter due to Ohmic dissipation takes place. It was shown by Bisnovatyi-Kogan and Ruzmaikin (1974), that due to Ohmic heating the efficiency of a radial accretion into a black hole may become as high as $\sim 30\%$. The rate of the Ohmic heating in the condition of equipartition was obtained in the form

$$T\frac{dS}{dr} = -\frac{3}{2}\frac{B^2}{8\pi\rho r}. \qquad (16)$$

In the supersonic flow of the radial accretion equipartition was suggested in a form (Schwartsman, 1971) $\frac{B^2}{8\pi} \approx \frac{\rho v_r^2}{2} = \frac{\rho GM}{r}$. For the disc accretion equipartition between magnetic and turbulent energy was suggested by Shakura (1972), what reduces with account of "alpha" prescription of viscosity to a relation $\frac{B^2}{8\pi} \sim \frac{\rho v_t^2}{2} \approx \alpha_m^2 P$, where α_m characterizes a magnetic viscosity in a way similar to the turbulent α viscosity. It was suggested by Bisnovatyi-Kogan and Ruzmaikin (1976) the similarity between viscous and magnetic Reynolds numbers, or between turbulent and magnetic viscosity coefficients $Re = \frac{\rho v l}{\eta}$, $Re_m = \frac{\rho v l}{\eta_m}$, where the turbulent magnetic viscosity η_m is connected with a turbulent conductivity $\sigma = \frac{\rho c^2}{4\pi\eta_m}$. Taking $\eta_m = \frac{\alpha_m}{\alpha}\eta$, we get a turbulent conductivity

$$\sigma = \frac{c^2}{4\pi\alpha_m h v_s}, \quad v_s^2 = \frac{P_g}{\rho} \qquad (17)$$

in the optically thin discs. For the radial accretion the turbulent conductivity may contain mean free path of a turbulent element l_t in (17) instead of h. In ADAF solutions, where ionic temperature is of the order of the virial one two above suggestions for magnetic equipartition almost coincide at $\alpha_m \sim 1$.

The heating of the matter due to an Ohmic dissipation may be obtained from the Ohm's law in radial accretion

$$T\frac{dS}{dr} = -\frac{\sigma\mathcal{E}^2}{\rho v_r} \approx -\sigma\frac{v_E^2 B^2}{\rho v_r c^2} = -\frac{B^2 v_E^2}{4\pi\rho\alpha_m v_r v_s l_t}, \qquad (18)$$

what coincides with (16) when $\alpha_m = \frac{4rv_E^2}{3v_r v_s l_t}$, or $l_t = \frac{4rv_E^2}{3v_r v_s \alpha_m}$. Here a local electrical field strength in a highly conducting plasma is of the order of $\mathcal{E} \sim \frac{v_E B}{c}$, $v_E \sim v_t \sim \alpha v_s$ for a radial accretion.

Equations for a radial temperature dependence in the accretion disc, separately for the ions and electrons are written as

$$\frac{dE_i}{dt} - \frac{P_i}{\rho^2}\frac{d\rho}{dt} = \mathcal{H}_{\eta i} + \mathcal{H}_{Bi} - Q_{ie}\ , \qquad (19)$$

$$\frac{dE_e}{dt} - \frac{P_e}{\rho^2}\frac{d\rho}{dt} = \mathcal{H}_{\eta e} + \mathcal{H}_{Be} + Q_{ie} - \mathcal{C}_{ff} - \mathcal{C}_{cyc}\ , \qquad (20)$$

A rate of a viscous heating of ions $\mathcal{H}_{\eta i}$ is obtained from (6) as

$$\mathcal{H}_{\eta i} = \frac{2\pi r}{\dot{M}}Q_+ = \frac{3}{2}\alpha\frac{v_K v_s^2}{r}, \quad \mathcal{H}_{\eta e} \le \sqrt{\frac{m_e}{m_i}}\mathcal{H}_{\eta i}. \qquad (21)$$

Combining (1),(8),(5), we get

$$v_r = \alpha\frac{v_s^2}{v_K\mathcal{J}}, \quad h = \sqrt{2}\frac{v_s}{v_K}r, \quad \rho = \frac{\dot{M}}{4\pi\alpha\sqrt{2}}\frac{v_K^2\mathcal{J}}{r^2 v_s^3}, \qquad (22)$$

where $v_K = r\Omega_K$, $\mathcal{J} = 1 - \frac{j_{in}}{j}$. The rate of the energy exchange between ions and electrons due to the binary collisions was obtained by Landau (1937). Neglecting pair formation for a low density accretion disc, we may write an exact expression for a pressure $P_g = P_i + P_e = n_i kT_e + n_e kT_p = n_e k(T_e + T_i)$, and an approximate expression for an energy, containing a smooth interpolation between nonrelativistic and relativistic electrons. The bremstrahlung $\mathcal{C}_{ff}$ and magneto-bremstrahlung $\mathcal{C}_{cyc}$ cooling of maxwellian semi-relativistic electrons, with account of free-bound radiation in nonrelativistic limit, may be written as interpolation of limiting cases (Bisnovatyi-Kogan and Ruzmaikin, 1976).

In the case of a disk accretion there are several characteristic velocities, v_K, v_r, v_s, and $v_t = \alpha v_s$, all of which may be used for determining "equipartition" magnetic energy, and one characteristic length h. Consider three possible choices of $v_B^2 = v_K^2$, v_r^2, and v_t^2 for scaling $B^2 = 4\pi\rho v_B^2$. The expression for an Ohmic heating in the turbulent accretion disc also may be written in different ways, using different velocities v_E in the expression for an effective electrical field $\mathcal{E} = \frac{v_E B}{c}$. A self-consistency of the model requires, that expressions for a magnetic heating of the matter $\mathcal{H}_B$, obtained from the condition of stationarity of the flow (16), and from the Ohm's law (18), should be identical. It happens

at $\frac{\alpha}{\mathcal{J}\alpha_m}\frac{v_E^2}{v_r^2} = \frac{3\sqrt{2}}{4}$. That implies $v_E \sim v_r \sim \frac{\alpha v_s^2}{v_K\sqrt{\mathcal{J}}} \simeq \frac{v_t v_s}{v_K\sqrt{\mathcal{J}}} < v_t$. In the advective models $\mathcal{J}$ is substituted by a function which is not zero at the inner edge of the disc. The heating due to magnetic field reconnection $\mathcal{H}_B$ in the equations (19), (20) may be written with account of (21) as $\mathcal{H}_B = \frac{3}{16\pi}\frac{B^2}{r\rho}v_r = \frac{1}{2\mathcal{J}}\mathcal{H}_{\eta i}\left(\frac{v_B}{v_K}\right)^2$. At $v_B = v_K$ the expressions for viscous and magnetic heating are almost identical. Observations of the magnetic field reconnection in the solar flares show (Tsuneta, 1996), that electronic heating prevails over the ionc one. Transformation of the magnetic energy into a heat is connected with the change of the magnetic flux, generation of the vortex electrical field, accelerating the particles.

The equations (19), (20) have been solved by Bisnovatyi-Kogan and Lovelace (1997) for nonrelativistic electrons, at v_B=v_K. The combined heating of the electrons and ions were taken as $\mathcal{H}_e = (2-g)\mathcal{H}_{\eta i}$, $\mathcal{H}_e = g\mathcal{H}_{\eta i}$. The results of calculations for $g = 0.5 \div 1$ show that almost all energy of the electrons is radiated, so the relative efficiency of the two-temperature, optically thin disc accretion cannot become lower then 0.25. Increase of the term Q_{ie} due to plasma turbulence may restore the relative efficiency to a value, corresponding to the optically thick disc.

6. Discussion

Observational evidences for existence of black holes inside our Galaxy and in the active galactic nuclei (Cherepashchuk, 1996; Ho, 1999) make necessary to revise theoretical models of the disc accretion. The improvements of a model are connected with account of advective terms and more accurate treatment of the magnetic field effects. Account of the effects connected with magnetic field annihilation does not permit to make a relative efficiency of the accretion lower then ~ 0.25 from the standard value. Strong relaxation connected with the plasma turbulence may increase the efficiency, making it close to unity. For explanation of underluminous galactic nuclei two possible ways may be suggested. One is based on a more accurate estimations of the accretion mass flow into the black hole, which could be overestimated. The second is based on existence of another mechanisms of the energy losses in the form of accelerated particles, like in the radiopulsars, where these losses exceed strongly a radiation. This is very probable to happen in a presence of a large scale magnetic field which may be also responsible for a formation of the observed jets (Bisnovatyi-Kogan, 1999; Blandford and Begelman, 1999). We may suggest, that underlumilnous AGN loose main part of their energy to the formation of jets, like in SS 433. The search of the correlation between existence of jets and lack of the luminosity could be very informative.

Acknowledgements. The author is grateful for partial support to RFBR, grant 99-02-18180, and GPNT "Astronomy", grant 1.2.6.5.

References

Abramovicz M.A., Czerny B., Lasota J.P., Szuszkiewicz E.: 1988, *ApJ*, **332**, 646.

Artemova I.V., Bisnovatyi-Kogan G.S., Björnsson G., Novikov I.D.: 1996, *ApJ*, **456**, 119.

Bisnovatyi-Kogan G.S.: 1999, in *"Observational evidences for black holes in the universe"*, ed. S.Chakrabarti, Kluwer, p.1.

Bisnovatyi-Kogan G.S., Blinnikov S.I.: 1976, *Pisma Astron. Zh.*, **2**, 489.

Bisnovatyi-Kogan G.S., Lovelace R.V.L.: 1997, *ApJL*, **486**, L43.

Bisnovatyi-Kogan G.S., Lovelace R.V.L.: 1999, *ApJ* (accepted), astro-ph/9902344.

Bisnovatyi-Kogan G.S., Ruzmaikin A.A.: 1974, *Ap. and Space Sci.*, **28**, 45.

Bisnovatyi-Kogan, G.S., Ruzmaikin, A.A., 1976, *Ap. and Space Sci.*, **42**, 401.

Blandford R.D., Begelman M.C.: 1999, *Month. Not. R.A.S.*, **303**, 1.

Cannizzo J.K. et al.: 1998, *AAS Abstracts*, **192**, 4103C.

Chakrabarti S.K., Molteni D.: 1993, *ApJ*, **417**, 671.

Cherepashchuk A.M.: 1996, *Uspekhi Fiz. Nauk.*, **166**, 809.

Di Matteo T., Fabian A.C., Rees, M.J. et al.: 1999, *Month. Not. R.A.S.*, **305**, 492.

Galeev A.A., Sagdeev R.Z.: 1983, Chap. 6, in *Handbook of Plasma Physics*, Vol. 1, eds. Rosenbluth M.N., Sagdeev R.Z. (Amsterdam: North-Holland Pub.), Ch. 6.1

Ho L.: 1999, in *"Observ. evidences for b. h. in the Universe"*, ed. S.Chakrabarti, Kluwer, p.157.

Landau L.D.: 1937, *Zh. Exp. Theor. Phys.* **7**, 203.

Matsumoto R., Sato Sh., Fukue J., Okazaki A.T.: 1984, *Publ. Astron. Soc. Japan*, **36**, 71.

Narayan R., Yu I.: 1995, *ApJ*, **452**, 710.

Novikov I.D., Thorne K.S.: 1973, in *Black Holes* eds. C.DeWitt, B.DeWitt (New York: Gordon & Breach), p.345

Paczyński B., Bisnovatyi-Kogan G.S.: 1981, *Acta Astron.*, **31**, 283.

Paczyński B., Wiita P.J.: 1980, *A&A*, **88**, 23.

Pringle J.E., Rees, M.J.: 1972, *A&A*, **21**, 1.

Quataert E.: 1997, *astro-ph/9710127*.

Schwartsman V.F.: 1971, *Soviet Astron.*, **15**, 377.

Shakura N.I.: 1972, *Astron. Zh.*, **49**, 921; (1973, Sov. Astron., 16, 756)

Shakura N.I., Sunyaev R.A.: 1973, *A&A*, **24**, 337.

Shapiro S.L., Lightman A.P., Eardley D.M.: 1976, *ApJ*, **204**, 187.

Tsuneta S.: 1996, *ApJ*, **456**, 840.

BLACK HOLE X-RAY BINARIES

A.M.Cherepashchuk

Sternberg State Astronomical Institute, Universitetski pr.,13, Moscow, 119899, Russia

ABSTRACT. Masses of black holes in 13 X-ray binary systems determined by different authors are summarized and compared with those of WR stars in close binary systems, which can be considered as progenitors of relativistic objects.

Average mass of CO cores of WR stars is $\sim (8-12)\ M_\odot$ which is close to that of black holes $\sim (8-10)\ M_\odot$. Distribution of masses of WR stars $M_{WR} = 5-55\ M_\odot$ is continuous but not bimodal in contrast with distribution of masses of neutron stars ($M_{NS} = 1.35 \pm 0.15\ M_\odot$) and black holes ($M_{BH} \approx 8 \div 10\ M_\odot$).

Key words: Black hole, neutron star, Wolf-Rayet star, binary system, X-ray, accretion.

1. Introduction

Black holes were predicted by Einstein's general relativity theory. Strong energy release from accreting black holes was predicted by Zeldovich (1964) and Salpeter (1964). The theory of disk accretion onto black holes was developped by Shakura (1972), Shakura and Sunyaev (1973), Pringle and Rees (1972) and Novikov and Thorne (1973). Binary systems as tracers of relativistic objects were proposed by Novikov and Zeldovich (1966) and Guseinov and Zeldovich (1966); see also Trimble and Thorne (1969). The discovery of compact X-ray sources in close binary systems (e.g. Tananbaum et al., 1972) confirmed all these theoretical predictions. Recent 3D gas-dynamic calculations of gaseous flows in close binary systems confirm basic suggestions about mass transfer (e.g. Bisikalo et al., 1998, Matsuada et al., 1999). Advectional solutions in the theory of disk accretion have been considered (e.g. Paczynski and Bisnovatyi-Kogan, 1981, Narayan et al., 1996). The influence of ohmic heating on advection dominated accretion flows calculated recently (Bisnovatyi-Kogan and Lovelace, 1997, Bisnovatyi-Kogan, 1999) suggests a much higher efficiency of conversion of the accretion energy to radiation than in the theory of advection-dominated disks. Thousands of compact X-ray sources in our Galaxy and in nearby galaxies have been discovered. Most of them are X-ray binary systems containing an optical star - the donor of matter and accreting relativistic object. Accretion of matter onto a relativistic object implies strong X-ray luminosities of about $10^{36} \div 10^{39}$ erg/s.

The first optical identification of X-ray binary systems allowed us to understand the basic origins of their optical variability: the X-ray heating effect (Cherepashchuk et al., 1972, Bahcall and Bahcall, 1972) and ellipticity effect of optical star (Lyuty et al., 1973, 1974). It is now widely known that the X-ray heating effect ("reflection effect") and ellipticity effect are typical for X-ray binary systems. Observations of optical variability caused by these effects enable reliable optical identification of X-ray binaries: coincidence of periods and phases of X-ray and optical variability as well as coincidence of X-ray and optical flashes, prove the correctness of identification. A method for estimating the orbital plane inclination i from the optical light curve of X-ray binary Cyg X-1, due mainly to ellipticity effect, was proposed by Lyuty et al. (1973). Now this method is widely used to estimate the masses of black holes in X-ray novae during quuiescence from their optical and infrared light curves (see reviews of Cherepashchuk, 1996a, 1997, 2000, Charles, 1999, Chakrabarti, 1999, and references therein).

In our review we summarize recent results about mass determination of 13 black holes in X-ray binaries and compare the distribution of the masses of relativistic objects with that of Wolf-Rayet stars.

2. Masses of black holes in X-ray binaries.

The investigation of motion, deformation and heating of the normal star in an X-ray binary system, as well as of eclipsing effects and the rotational broadening of absorption lines in the spectrum of optical star, allow to estimate mass function of the optical star

$$f_v(m) = \frac{m_x^3 sin^3 i}{(m_x + m_v)^2} = 1.038 \cdot 10^{-7} K_v^3 p (1-e^2)^{3/2}, \quad (1)$$

inclination of orbit plane i, mass ratio $q = m_x/m_v$ and other parameters of the X-ray binary (m_x and m_v are the masses of black hole and optical star respectively). Mass function $f_v(m)$ is absolute lower limit for the mass of black hole m_x. Value of m_x is determined by the formula:

$$m_x = f_v(m)\left(1+\frac{1}{q}\right)^2 \frac{1}{\sin^3 i}. \qquad (2)$$

Results of investigation of influence of non-zero dimensions of optical star as well as ellipticity and X-ray heating effects on the shape of absorption lines and corresponding radial velocity curve are published by Cherepashchuk (1996a), Antokhina and Cherepashchuk (1997) and Shahbaz (1998). For more details about methods of determination of the masses of black holes in X-ray binaries see Cherepashchuk (1996a), Charles (1999). Recently new method of determination of the values of q, i and masses of black holes from orbital variability of the profiles of absorption lines in the spectra of optical stars in X-ray binaries has been developped (Antokhina and Cherepashchuk, 1997, Shahbaz, 1998).

Up to now, the masses of 13 black holes have been estimated in the X-ray binary systems containing hot massive O–B or WR stars (Cyg X-1, LMC X-3, LMC X-1, Cyg X-3) as well as low mass M ÷ A stars (V616 Mon, V404 Cyg, XN Mus 1991, QZ Vul, V518 Per, XN Sco 1994, XN Oph 1977, XN Vel 1993, HL Lup). The basic parameters of 13 black hole X-ray binary systems are summarized in table 1 (see recent reviews of Charles (1999) and Cherepashchuk (2000) and references therein).

At present we have 13 black holes in X-ray binary systems with known values of the masses m_x (see fig.1). Therefore, the problem of black hole investigation is now becoming not only a theoretical, but an observational one, too. Taking into account recent direct dynamical determinations of the masses of nuclei of the set of galaxies: M87 $(2.4\cdot 10^9 M_\odot)$,NGC4258$(3.6\cdot 10^7 M_\odot)$, NGC7052$(3\cdot 10^8 M_\odot)$, NGC4261$(4.9\cdot 10^8 M_\odot)$ (Ford et al., 1994, Miyoshi et al., 1995, Ferrarese et al., 1996, van den Marel and van den Bosch, 1998), and the Galactic Center Sgr A (Eckart and Genzel, 1996)$(2.4\cdot 10^6 M_\odot)$, the same conclusion may be drawn about supermassive black holes (Ho, 1999).

The masses of black holes as well as masses of X-ray and radiopulsars are presented in fig.1. There is no correlation between the masses of the relativistic objects and their companions in close binary systems. Black holes in binary systems can have both high-mass and low-mass companions. The same situation is for the neutron stars in binary systems. Evolutionary considerrations of the origin of the black holes in binary systems were published by (Tutukov and Cherepashchuk,1985, 1993, 1997, Brandt et al., 1995, Wijers, 1996). A very important result has been obtained up to now: in all the cases when the mass of an X-ray or radiopulsar (i.e. rapidly rotating magnetizied neutron star) has been determined (17 objects) it does not exceed $3M_\odot$, the theoretical upper limit for the mass of a neutron star predicted by the Einstein General Relativity theory. On the other hand, none of the 13 known massive compact X-ray souces with $m_x > 3M_\odot$ (black holes) has regular X-ray pulsation or X-ray bursts of the first type. Therefore, the X-ray souces in binary systems are distinguished from each other not only by masses but also by observational appearences in full agreement with Einstein General Ralativity theory. Due to high number of mass determinations (17 neutron stars and 13 black holes) the statistical significance of this conclusions is high. The X-ray spectra of accreting neutron stars and black holes on average are also different from each other (e.g. Tanaka, 1989, 1999, Greiner et. al., 1991, Sunyaev et al., 1992, 1993, Asai et al., 1998). Highly collimated relativistic jets ($v \approx 0.92c$) have been discovered recently from three galactic black hole X-ray binary systems: 1E1747 - 2942, GRS1915-105 and GROJ1655-40 (Mirabel et al., 1992, Mirabel and Rodriguez, 1994, Hjellming and Rupen, 1995).

In all the cases where the optical star is a hot massive O–B or WR star the X-ray source is persistent. But in all the cases where the optical star is a cool low-mass M-A star, the X-ray source is transient (X-ray nova). The relatively low mass accretion rate as well as X-ray heating effects are important for generation of quiet and active state of accretion disks in X-ray novae (e.g. Narayan and Yi., 1995, Chen et al., 1997, Esin et al., 1997, King et al., 1997). In particular, King et al. (1997) pointed out that heating by irradiation of the accretion disk is much weaker if the accreting object is a black hole rather than a neutron star (see also Sunyaev and Shakura, 1973).

Two peculiarities of the transient X-ray binaries may be important for understanding of their nature: the activity of the cool low-mass star, caused by its deep convective envelope, which may be a trigger stimulating the formation of turbulent viscosity of plasma in the disk around black hole, and the high mass ratio of the components $q = m_x/m_v = 2 \div 20$, which implies a relatively high dimension of the accretion disk around the black hole. For such a high-dimension disk, the tidal interaction from the optical star is important (e.g. Sawada and Matsuda,, 1992). The theory of instability of accretion disks and related problems for X-ray novae were considered by Hameury et al. (1986, 1990), Goutikakis and Hameury (1993), Mineshige and Wheeler (1989), Narayan et al. (1996) (see also recent book by Kato et al. (1998) and references therein).

3. Distribution of masses of relativistic objects and Wolf-Rayet stars.

Wolf-Rayet (WR) stars are considered to be bare cores of massive stars which lost most of their hydrogen envelopes (Paczynski, 1973, Conti, 1976). Note that Gamov (1943) was the first who suggested that

Table 1. Parameters of black hole binary systems.

System	Spectrum of optical star	P_{orb} (days)	$f_v(m)$ $(M_\odot)$	m_x $(M_\odot)$	m_v $(M_\odot)$	V_{pec} (km/s)	Remaks
Cyg X-1 (V1357 Cyg)	O9.7 Iab	5.6	0.24 ± 0.01	16 ± 5	33 ± 9	2.4 ± 1.2	pers.
LMC X-3	B3 III-V	1.7	2.3 ± 0.3	9 ± 2	6 ± 2	–	pers.
LMC X-1	O (7–9) III	4.2	0.14 ± 0.05	7 ± 3	22 ± 4	–	pers.
Cyg X-3	WN 3–7	0.2	~ 2.3	7–40	5–20	–	pers.
A0 620-00 (V616 Mon)	K4 V	0.3	2.91 ± 0.08	10 ± 5	0.6 ± 0.1	-15 ± 5	trans.
GS 2023+338 (V404 Cyg)	K0 IV	6.5	6.08 ± 0.06	12 ± 2	0.7 ± 0.1	8.5 ± 2.2	trans.
GRS 1124-68 (GU Mus)	K2 V	0.4	3.01 ± 0.15	6 (+5,-2)	0.8 ± 0.1	26 ± 5	trans.
GS 2000+25 (QZ Vul)	K5 V	0.3	4.97 ± 0.10	10 ± 4	0.5 ± 0.1	–	trans.
GRO J0422+32 (V518 Per)	M2 V	0.2	1.13 ± 0.09	10 ± 5	0.4 ± 0.1	–	trans.
GRO J1655-40 (XN Sco1994)	F5 IV	2.6	2.73 ± 0.09	7 ± 1	2.5 ± 0.8	-114 ± 19	trans.
H 1705-250 (V2107 Oph)	K5 V	0.5	4.86 ± 0.13	6 ± 1	0.4 ± 1	38 ± 20	trans.
4U 1543-47 (HL Lup)	A2 V	1.1	0.22 ± 0.02	5 ± 2.5	~ 2.5	–	trans.
GRS 1009-45 (MM Vel)	(K6–M0) V	0.3	3.17 ± 0.12	$3.6 - 4.7$	$0.5 - 0.7$	–	trans.

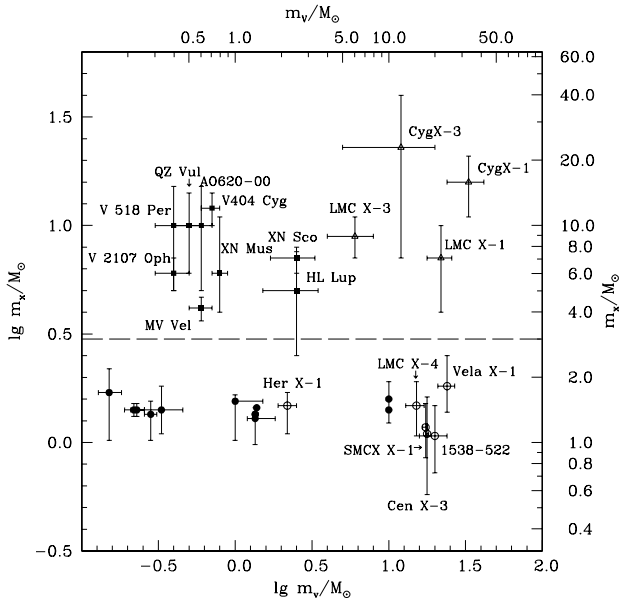

Figure 1: Dependence of the masses m_x of neutron stars (circles) and black holes (triangles and rectangles) on the masses of their companion starts m_v in close binary systems. Filled circles correspond to radio pulsars, filled rectangles correspond to black holes in X-ray novae. For the details see (Cherepashchuk, 2000).

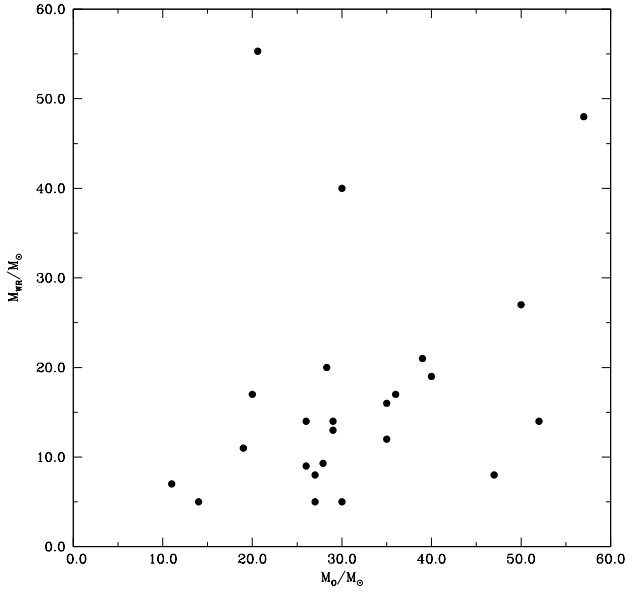

Figure 2: Dependence of the masses of WR stars in WR+O binary systems on the masses of the O-companion stars. This figure should be compared with the fig.1

WN and WC stars display at their surfaces products of different phases of thermonuclear processing. Recent determinations of radii and effective temperatures of some WR stars in binary systems (e.g. Cherepashchuk, 1996b, Cherepashchuk and Moffat, 1994, St.-Louis et al., 1993, Moffat and Marchenko, 1996) are in agreement with the model of WR stars as helium remnants which are formed from hot massive stars. Due to clumping of WR winds (Cherepashchuk et al., 1984, Moffat et al., 1988) values of mass loss rate $\dot{M}$ for WR stars determined from IR and radio observations seems to be overestimated at least by factor 2–4 (Antokhin et al., 1988, 1992, Hillier, 1991, Cherepashchuk,1992, Nugis et al., 1998). Therefore, we can neglect effect of decreasing of mass of WR stars by stellar wind mass loss during their evolution. Because WR stars are supposed to be progenitors of relativistic objects let us compare the distribution of masses of WR stars with that of neutron stars and black holes in close binary systems (Cherepashchuk, 1998, 2000) - see fig.1,2.

Distribution of the masses of relativistic objects may be suggested as bimodal (Baylin et al., 1998, Cherepashchuk, 1998). Average mass of neutron stars is $(1.35 \pm 0.15)\ M_\odot$ and average mass of black holes is $\sim (8-10) M_\odot$ (the ranges of the masses of neutron stars and black holes are $(1 \div 2)\ M_\odot$ and $(5 \div 15)\ M_\odot$ respectively). The gap in the distribution of the masses of relativistic objects between 2 $M_\odot$ and 5 $M_\odot$ can not be explained by observational selection effects (Bailyn et al., 1998). In contrast with relativistic objects (fig.1), the distribution of the masses of WR stars is continuous but not bimodal (fig.2).

Average mass of WR stars (23 stars) in WR+O binaries is 17.8 $M_\odot$ (Cherepashchuk, 1998, 2000). Masses of individual WR stars lie in wide range: from 5 $M_\odot$ to 48 $M_\odot$ and even 55.3 $M_\odot$ (HD 92740). The average mass of WN stars is 21.1 $M_\odot$ (12 stars), that of WC stars is 13.4 $M_\odot$ (9 stars). Average mass of CO cores of WC and WN stars is $(8 \div 12)\ M_\odot$ which is close to average mass of black holes $\sim (8 \div 10)\ M_\odot$. For more details about WR stars in binary systems see Catalog of Hifgly Evolved Close Binary Stars (Cherepashchuk et al., 1996a,b), and review of Cherepashchuk (1995).

Observed difference in the distribution of the masses of WR stars and relativistic objects allow us to suggest that origin and nature of newly formed relativistic object is determined not only by the mass of presupernova but also by some other stellar core parameters: its rotation, magnetic field and so on (Tutukov and Cherepashchuk, 1985, Ergma and van den Heuvel, 1998).

One WR SB1 binary and eleven suspected WR+c binaries are selected (Cherepashchuk, 1998, 2000) which could be considered as progenitors of black hole or neutron star low-mass X-ray binary systems containing low-mass M–A optical companions.

Acknowledgments. This work was supported by the Russian Foundation of Basic Research through the grant No 99-02-17589.

References

Antokhin I.I., Kholtygin A.F., Cherepashchuk A.M.: 1988, *Astron.Zh.* **65**, 558.

Antokhin I.I., Nugis T., Cherepashchuk A.M.: 1992, *Sov.Astron.* **36**, 260.

Antokhina E.A., Cherepashchuk A.M.: 1997, *Astronomy Letters* **23**, 773.

Asai K., Dotani T., Hoshi R., *et al.*: 1998, *Publ. Astron. Soc. Japan* **50**, 611.

Bahcall J.N., Bahcall N.A.: 1972, *Ap.J.* **178**, L1.

Bailyn C.D., Jain R.K., Coppi P., Orosz J.A.: 1998, *Ap.J.* **499**, 367.

Bisikalo D.V., Boyarchuk A.A., Kuznetsov O.A., Chechetkin V.M.: 1998, *Monthly Notices Roy. Astron. Soc.* **300**, 39.

Bisnovatyi-Kogan G.S., Lovelace R.V.: 1997, *Ap.J.* **486**, L43.

Bisnovatyi-Kogan G.S.: 1999, in: S.K.Chakrabarti (ed.), *Observational Evidence for Black Holes in the Universe*, Dordrecht: Kluwer, L1.

Chakrabarti S.K.: 1999, *Indian Journal of Physics*, in press (astro-ph/98032, 19 Mar 1998).

Charles P.A.: 1999, in: M.Abramovich *et al.* (eds.), *Theory Black Holes Accretion Disks*, CUP, 1, (astro-ph/9806217).

Chen W., Shrader C.R., Livio M.: 1997, *Ap.J.* **491**, 312.

Cherepashchuk A.M.: 1992, in: Y.Kondo *et al.* (eds.), *Evolutionary Processes in Interacting Binary Stars, IAU Symp. N 151*, Dordrecht: Kluwer, 123.

Cherepashchuk A.M.: 1995, *Space Sci. Rev.* **74**, 313.

Cherepashchuk A.M.: 1996a, *Physics–Uspekhi* **39**, 759.

Cherepashchuk A.M.: 1996b, in: J.M.Vreux *et al.* (eds), *Wolf-Rayet Stars in the Framework of Stellar Evolution, Proc. 33d Liege Intern. Astrophys. Coll.*, Liege: Univ. de Liege, 155.

Cherepashchuk A.M.: 1997, *Astrophys. Space Sci.* **252**, 375.

Cherepashchuk A.M.: 1998, in: D.S.Wiebe (ed.), *Modern Problems of Stellar Evolution, Proc. Internat. Conf. in Honor prof. A.G.Massevich, Zvenigorod,* Moscow: Geos Edition, 198.

Cherepashchuk A.M.: 2000, *Space Sci. Rev., in press.*

Cherepashchuk A.M., Eaton J.A., Khaliullin Kh.F.: 1984, *Ap.J.* **281**, 774.

Cherepashchuk A.M., Efremov Yu.N., Kurochkin N.E., *et al.*: 1972, *IBVS* No **720**, 1.

Cherepashchuk A.M., Katysheva N.A., Khruzina T.S., Shugarov S.Yu.: 1996a, *Highly Evolved Close Binary Stars: Catalog.*, vol.1, Brussels: Gordon and Breach Science Publishers.

Cherepashchuk A.M., Katysheva N.A., Khruzina T.S., Shugarov S.Yu.: 1996b, *Highly Evolved Close Binary Stars: Finding Charts*, vol.2, Brussel: Gordon and Breach Science Publishers.

Cherepashchuk A.M., Moffat A.F.J.: 1994, *Ap.J.* **424**, L53.

Conti P.: 1976, *Mem. Soc. R. Sci. Liege* **9**, N6, 193.

Eckart A., Genzel R.: 1996, in: R.Gredel (ed.), *The Galactic Center*, ASP Conf. Ser., **102**, 196.

Ergma E., van den Heuvel E.P.J.: 1998, *As.Ap.*, **331**, L29.

Esin A.A., McClintock J.M., Narayan R.: 1997, *Ap.J.*, **489**, 865.

Ferrarese L., Fors H.C., Jaffe W.: 1996, *Ap.J.* **470**, 444.

Ford H.C., Harm R.J., Tsvetanov Z.I., *et al.*: 1994, *Ap.J.* **435**, L27.

Gamov G.: 1943, *Ap.J.* **98**, 500.

Goutikakis C., Hameuery J.-M.: 1993, *As.Ap.* **271**, 118.

Greiner J., Egger R., Hartber G., *et al.*: 1991: in S.Brandt et al. (eds.), *Proc. of Workshop on Nova Muscae 1991*, Lyngby: Danish Space Res. Inst., 79.

Guseinov O.Kh., Zel'dovich Ya.B.: 1966, *Astron.Zh.* **43**, 313.

Hameury J.-M., King A.R., Lasota J.-P.: 1986, *As.Ap.* **162**, 71.

Hameury J.-M., King A.R., Lasota J.-P.: 1990, *Ap.J.* **353**, 585.

Hillier D.J.: 1991, *Astron.J.* **247**, 455.

Hjellming R.M., Rupen M.P.: 1995, *Nature* **375**, 464.

Ho L.C.: 1999, in: S.K.Chakrabarti (ed.), *Observational Evidence for Black Holes in the Universe*, Dordecht: Kluwer.

Kato S., Inagaki S., Fukue J., Mineshige S.: 1998, *Basic Physics of Accretion Disks*, Gordon and Breach Publ.

King A.R., *et al.*: 1997, *Ap.J.* **488**, 89.

Lyutyi V.M., Sunyaev R.A., Cherepashchuk A.M.: 1973, *Astron.Zh.* **50**, 3.

Lyutyi V.M., Sunyaev R.A., Cherepashchuk A.M.: 1974, *Astron.Zh.* **51**, 1150.

Matsuda T., Makita M., Boffin H.M.J.: 1999, in: S. Mineshige and J.C.Wheeler (eds.), *Disk Instabilities in Close Binary Systems*, Tokyo: Univ. Acad.Press INC, 129.

Mineshige S., Wheeler J.C.: 1989, *Ap.J.* **343**, 241.

Mirabel I.F., Rodrigues L.F., Cordier B., Paul J., Lebrun F.: 1992, *Nature* **358**, 215.

Mirabel I.F., Rodrigues L.F.: 1994, *Nature* **371**, 46.

Miyoshi M., Moran J.., Herrnstein J., *et al.*: 1995, *Nature* **373**, 127.

Moffat A.F.J., Drissen L., Lamontagne R., Robert C.: 1988, *Ap.J.* **334**, 1038.

Moffat A.F.J., Marchenko S.V.: 1996, *As.Ap.* **305**, L29.

Narayan R., McClintock J.E., Yi I.: 1996, *Ap.J.* **457**, 821.

Narayan R., Yi I.: 1995, *Ap.J.* **452**, 710.

Novikov I.D., Zel'dovich Ya.B.: 1966, *Nuovo Cim. Suppl.* **4**, 810.

Novikov I.D., Thorne K.S.: 1973, *Black Holes*, New York: Gordon and Breach.

Nugis T., Growther P.A., Willis A.J.: 1998, *As.Ap.* **333**, 596.

Paczynski B.: 1973, in M.Barry and J.Sahade (eds.), *Wolf-Rayet and High Temperature Stars*, IAU Symp. N 49, Dordrecht: Reidel, 143.

Paczynski B., Bisnovatyi-Kogan G.S.: 1981, *Acta Astron.* **21**, 283.

Pringle J.E., Rees M.: 1972, *As. Ap.* **21**, 1.

Salpeter E.E.: 1964, *Ap.J.* **140**, 796.

Sawada K., Matsuda T.: 1992, *Monthly Notices Roy. Astron. Soc.* **255**, 17P.

Shahbaz T.: 1998, *Monthly Notices Roy. Astron. Soc.* **298**, 153.

Shakura N.I.: 1972, *Astron.Zh.* **49**, 945.

Shakura N.I., Sunyaev R.A.: 1973, *As.Ap.* **24**, 337.

St.-Louis N., Moffat A.F.J., Lapointe L., *et al.*: 1993, *Ap.J.* **410**, 342.

Sunyaev R.A., Churazov E., Gilfanov M., *et al.:* 1992, *Ap.J.* **389**, L75.

Sunyaev R.A., Kaniovsky A.S., Borozdin K.N., *et al.*: 1993, *Astron.Astrophys.* **280**, L1.

Tanaka Y.: 1989, in: J.Hunt and B.Battrick (eds.), *23d ES LAB Symp.*, Nordwijk ESA, v.1, 3.

Tanaka Y.: 1999, in: S.Mineshige and J.C.Wheeler (eds.), *Disk Instabilities in Close Binary Systems*, Tokyo: Univ. Acad.Press INC, 21.

Tananbaum H., Gursky H., Kellog E.M., *et al.*: 1972, *Ap.J.* , **174**, L143.

Trimble V.L., Thorne K.S.: 1969, *Ap.J.* **156**, 1013.

Tutukov A.V., Cherepashchuk A.M.: 1985, *Astron.Zh.* **62**, 1124.

Wijers A.M.J.: 1996, in: A.M.J.Ralph *et al.* (eds.), *Evolutionary Processes in Binary Stars, NATO ASI Series C*, **477**, 327.

Van der Marel R.P., van den Bosch F.C.: 1998, *Astron.J.* **116**, 2220.

Zel'dovich Ya.B.: 1964, *Docl.Acad. Nauk USSR*, **155**, 67.

ON THE EVOLUTION OF WOLF-RAYET STARS IN CLOSE BINARY SYSTEMS

A.M. Cherepashchuk[1], V.G. Karetnikov[2]

[1] Sternberg Astronomical Institute, Moscow, 119899, Russia
[2] Odessa Astronomical Observatory, Odessa, 270014, Ukraine

ABSTRACT. The statistical study of the mass ratios of the components and eccentricities of close binary systems was made. Relations between these characteristics are obtained.

Results of the analysis allows to conclude that at least 70% of all known WR+O binary systems (with orbital period $P < 20^d$) where formed as a result of mass transfer in massive close binary systems.

Therefore, mass transfer through Roche lobe overflowing in massive close binary systems is an important mechanism of evolution in these interacting binaries.

Key words: Stars: binary: Wolf-Rayet.

1. Introduction

A good progress has been achieved in the understanding of the nature and evolution of Wolf-Rayet (WR) stars in close binary systems (Paczynski, 1973, Tutukov and Yungelson, 1973, Van den Heuvel and Heize, 1972). It is clear now that WR stars in close binaries can be considered as bare cores of initially more massive stars which lost up to 50phase of evolution (e.g. see the books of Shore et al., 1994 and Cherepashchuk et al., 1996 and references therein).

Recent increasing of observational data about WR stars in WR+O binary systems, especially, information on the masses of WR and O companions, allowed to suggest that mass transfer is insignificant, probably as a result of constantly present stellar winds and their collision in massive star close binaries, especially after the WR stage is reached for the primary component (e.g. Moffat, 1995).

Basic arguments for such a suggestion are the following:

1. There is no anticorrelation between masses of WR stars and O components in WR+O binaries, which could be suggested in the case of conservative mass exchange in massive close binaries. Moreover, some rough correlation between the masses of WR and O stars in WR+O binaries may be suggested (Cherepashchuk, 1991). Also, the mass of WR star decreases monotonically as one goes from cool to hot subtypes, whereas the mass of O companion is independent of the WR star subtype or its mass.

2. Among WR+O binaries there are systems with long periods, which have high values of eccentricity of the orbit, which can be considered as an argument against mass transfer (Massey, 1981). In this letter we compare the masses of companions in WR+O binaries with those of semi-detached close binary systems containing subgiants where mass transfer with no doubt occured. Also we compare the eccentricities of the orbits of WR+O binaries with those of detached and semi-detached close binary systems. For our investigation we use the data of Catalog of eclipsing binaries, containing data about 303 systems (Karetnikov and Andronov, 1989). We applie only photometrical values of the eccentricities of orbits which are much more reliable than spectroscopic. Results of the paper of Karetnikov and Cherepashchuk (1998) concerning statistical investigation of eclipsing binaries were used too.

2. Correlation between the masses of companion in WR+O and semi- detached close binaries with subgiants.

Dependence of the masses of WR stars MWR on the masses of O companion MO in WR+O binaries is presented on Fig.1a (the observational data are taken from Catalog of Cherepashchuk et al., 1996). Some rough correlation can be suggested in this case, but no anticorrelation exists.

Dependence between the masses of companions in semi-detached (SD) close binaries is presented in Fig.1b. There is clear correlation (but not anticorrelation) between the masses of M_1 and M_2 in semi-detached close binaries which went through Roche-Lobe overflowing mass transfer phase. In the paper of Karetnikov and Cherepashchuk (1998) this correlation was explained as a results of influence of initial conditions in the formation of close binaries. Average value of mass ratio in detached close to unity (~ 0.8, according to Karetnikov and Cherepashchuk, 1998). Mass exchange in semi-detached close binaries can not suppress

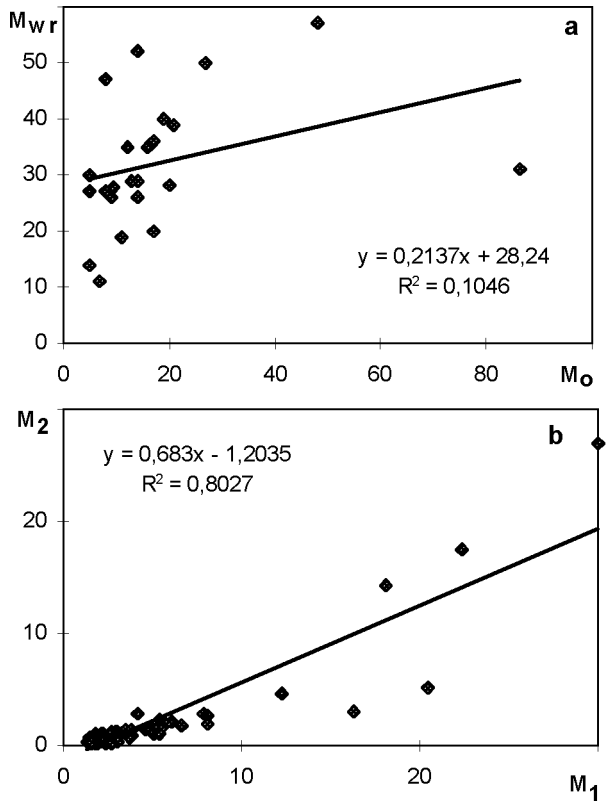

Figure 1: Dependence between stellar masses WR (a) and SD (b) binaries.

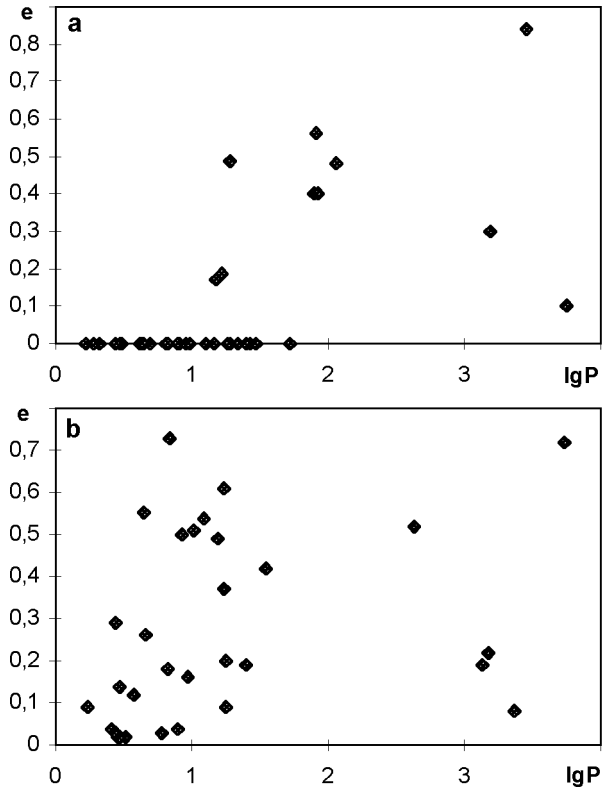

Figure 2: Dependence between stellar masses WR (a) and SD (b) binaries.

the influence of the initial condition for formation of close binaries.

Because there is no anticorrelation between the masses of the companions in semi-detached close binaries, absence of anticorrelation between masses of WR and O companions in WR+O binaries can not be considered as serious argument against mass transfer. Correlation between the masses of WR and O companions in WR+O binaries can be explained by influence of initial condition in the formation of massive close binary systems as well as by the fact that initial mass ratio is close to unity.

3. Comparison of the eccentricities of the orbits for WR+O binaries and detached and semi-detached binaries.

On the Fig.2a dependence of the eccentricities of the orbits e on the orbital periods P for WR+O binary systems is presented. For $P < 14^d$, $e = 0$ for all known WR+O binaries. On the Fig.2b dependence of $e(P)$ for all eclipsing binaries is presented. In this case $e = 0$ for $P < 2d$. For $P > 2d$, $e \neq 0$.

Therefore, for WR+O binaries $e = 0$ for much more higher values of orbital periods, up to 15 days is contrast to classical eclipsing binary systems. Among all known semi-detached eclipsing binaries with subgiants $e = 0$, which implies that mass transfer results in effective circularization of the orbits. Therefore, because in WR+O binaries $\sim 70\%$ systems have circular orbits, we can conclude that most of WR+O binaries were formed as a result of mass transfer in massive close binary systems. Only small parts of WR+O binaries ($< 30\%$) with longest orbital periods ($P > 14^d - 20^d$) may be formed without mass transfer mainly due to mass loss through stellar wind and wind-wind collision.

4. Examples of massive close binary system with mass transfer

Let us note some massive close binaries in which mass transfer is directly observed.

1. RY Sct: this massive O+O binary belongs to the well known W Ser type of close binary systems. Intensive mass transfer in this system occures and geometrically thick opaque disk around more massive companion is formed. This system may be considered as progenitor of WR+O binaries (Antokhina and Cherepashchuk, 1988).

2. SS 433: in this massive close binary containing relativistic object and Roche-Lobe filling optical star intensive secondary mass transfer occures in thermal

Table 1. Data of Close Binary with Wolf-Rayet Stars (Cherepashchuk et al., 1996).

Name	Spectra	P	e	M_{WR}	$M_\odot$
HD 63099	WC5+O7	14.305	0	7	25.0-11.0
γ^2 Vel	WC8+O9I	78.5002	0.4	21	39
HD 90657	WN4+O5	8.255	0	17	36
HD 92740	WN7+O6.5-O8.5	80.34	0.56	86.4	31
HD 94305	WC6+O6-8V	18.82	0	19	40
HD 94546	WN4+O7	4.9	0	9	26
HD 97152	WC7+O7V	7.886	0	11	19
HDE 311884	WN6+O5V	6.34	0	48	57
θ Mus	WC6+O9.5I	18.341	0		
HD 137603	WC8+B0Ia	26.9	0	> 5	> 27
HD 152270	WC7+O5	8.893	0	5	14
HDE 320102	WN4+O7	12.6	0		
CV Ser	WC8+O8-9V-III	29.707	0	14	29
HD 186943	WN4+O9V	9.555	0	16	35
HD 190918	WN5+O9.5I	112.8	0.48	13	29
V444 Cyg	WN5+O6	4.212424	0	9.3	27.9
HD 193793	WC6+O4V	2900	0.84	27	50
CX Cep	WN5+O5V	2.1267	0	7.0-20.0	16-28.3
HD 211853	WN6+O?	6.6884	0	14	26
CQ Cep	WN6-7+O9II-Ib	1.641246	0	40-17	30-20
B 22	WC6+O5-6V-III:	14.926	0.17	12	35
B 31	WC4+O?+O8I:	3.03269	0		
B 32	WC4+O6V-III:	1.91674	0	5	30
SK 188=AB8	WO4+O4V	16.644	0.19	14	52
HD 5980	WN4+O7I	19.266	0.49ph	8	27
AB 6	WN3+O7	6.681	0	8	47
HD 62910	WN6+WC4	85.37:	0.4:		
HD 192641	WC7+abs	5680	0.1:		
HD 193077	WN5+abs+?	1538	0.3		
HD 193928	WN6+?	21.64	0		
AS 422	WN+WC+?	22	0		
B 26	WN7+?	1.9075	0		
B 65	WN7+?	3.0032	0		
B 72	WN6+B1Ia	4.3092	0		
B 82	WN6+O5V	4.377	0		
B 86	WNL/Of	52.7	0		
B 87	WN6+?	2.7596	0		
B 90	WN77+?	25.17	0		

Table 2. Data of SD Close Binary Systems (Karetnikov and Andronov, 1989).

Name	P	M_1	M_2	Name	P	M_1	M_2
V453 Sco	12.004	30	27	U Sge	3.380619	5.7	1.9
V448 Cyg	6.519733	22.4	17.5	RS Vul	4.477661	4.65	1.45
XZ Cep	5.097227	18.1	14.2	RW Gem	2.865497	5.35	1.6
V356 Sgr	8.896099	12.3	4.7	DM Per	2.727742	5.5	1.65
SZ Cam	2.698438	20.4	5.1	TX UMa	3.063317	3.7	1.1
RZ Sct	15.1907	16.3	3.1	U Crb	3.452204	4.8	1.4
U Cep	2.493099	4.2	2.8	λ Tau	3.952948	6.6	1.75
Z Vul	2.454926	5.4	2.25	IZ Per	3.687662	5.2	1.35
FW Mon	3.873583	3.8	1.45	TU Mon	5.049029	8.1	2
u Her	2.051026	7.9	2.85	QS Aql	2.5133	3.85	0.85
RS Sgr	2.415683	6.1	2.2	GG Cas	3.758719	5	1.1
GT Cep	4.908749	8.1	2.75	β Per	2.867324	3.7	0.8
WW Cyg	3.317746	4.85	1.65	UX Mon	5.9045	3.5	1.5
ZZ Cas	1.243527	4.9	1.65	V505 Sgr	1.182875	2.1	1.15

Table 3. Data of Close Binary Systems [14].

Name	Spectra	P	e
AI Phe	F7V+K0IV	24.5923	0.19
RY Per	B5V+F6IV	1515.6	0.22
τ Per	G4III+A4V	6.8636	0.73
γ Per	G8III+A3V	5350	0.72
β Per	B8V	2.86773	0.02
RW Tau	B8V+K0III	2.7688	0.29
VV Mon	K0IV+F6	6.0506	0.03
RY Gem	A0V+K0IV	9.3009	0.16
p Vel	F3IV+F0V	10.2104	0.51
HD133822	G5IV+G5IV	17.8336	0.2
ε Lup	B3IV+B3V	4.5598	0.26
α CrB	B9.5IV+G	17.3599	0.37
W UMi	A3+G9IV	1.7012	0.09
HD153890	F3IV-V+F3V	34.8189	0.42
MM Her	G2V+K2IV	7.9604	0.04
96 Her	B3IV+B3IV	12.4573	0.54
V Sge	B7.5V+G4III-IV	1370	0.19
ψ Cyg	G8III-IV+G8III-IV	434.086	0.52
HD191201	B0III+B0III	8.3343	0.5
θ Aql	B9III+B9III	17.1243	0.61
HD197649	F6IV-V+G8V	18.0668	0.09
Y Cyg	B0IV+B0IV	2.9963	0.14
HD206874	F2IV+F2IV	3.2295	0.02
2 Lac	B6IV+B6V	2.6164	0.04
BW Aqr	F8IV+F7IV	6.7197	0.18
W Cru	F6IV+F6IV	2.9685	0.02
NY Cep	B0IV+B0IV	15.2765	0.49
CW Cep	B0.5IV-V+B0.5IV-V	2.7291	0.03
94 Aqr	G5IV+K2V	2323.6	0.08
HD22005	B3IVn+B3Ivn	4.4151	0.55
Y Psc	A3V+K0IV	3.7659	0.12

time scale with a rate $\sim 10^{-4}$ $M_\odot$/year (Cherepashchuk, 1981).

3. Cyg X-1: in this short period ($P \cong 4.8$ hours) X-ray binary system, the optical star is WR star, which is formed most probably through spiral-in mass loss mechanism during common envelope stage of evolution of massive close binary system (Cherepashchuk and Moffat, 1994). All these examples give us direct observational evidences for importance of mass transfer through Roche-Lobe overflowing in massive close binary systems.

5. Conclusion

Results of our investigations allow us to conclude that at least 70% of all known WR+O binary systems (with orbital period $P < 20^d$) where formed as a result of mass transfer in massive close binary systems.

Therefore, mass transfer through Roche lobe overflowing in massive close binary systems is an important mechanism of evolution in these interacting binaries.

References

Antokhina E.A., Cherepashchuk A.M.: 1988, *Pis'ma Astron. Zhurn.,* **14**, 252.

Cherepashchuk A.M.: 1981, *MNRAS*, **194**, 761.

Cherepashchuk A.M.: 1991, in: Van der Hucht K., Hidayat B. (eds.) *Wolf-Rayet Stars and Interrelation with other Massive Stars in Galaxies*, IAU Symp. No. **143**, Dordrecht, Kluwer, 187.

Cherepashchuk A.M., Katysheva N., Khruzina T.S., Shugarov S.Yu.: 1996, *Highly Evolved Close Binary Stars: Catalogue*, Gordon & Breach, Brussels.

Cherepashchuk A.M., Moffat A.F.J.: 1994, *Ap.J.,* **424**, L 53.

Karetnikov V.G., Andronov I.L.: 1989, *Statistical properties of eclipsing binary stars in the stage of initial mass exchange,* Manuscript in Ukr. NIINTI, Kiev, No. **2629-89**, 41 pp.

Karetnikov V.G., Cherepashchuk A.M.: 1998, *Astronomy Reports,* **42**, 476.

Massey Ph.: 1981, *IAU Symp.,* **120**.

Moffat A.F.J.: 1995, in: Van der Hucht K.A., Williams P.M. (eds). *Wolf-Rayet Stars: Binaries, Colliding Winds, Evolution*, IAU Symp. No. **163**, Dordrecht, Kluwer, 213.

Paczynski B.: 1973, in: Barry M., Sahade J. (eds.) *Wolf-Rayet and High Temperature Stars*, IAU Symp. No. **40**, Dordrecht, Reidel, p.143.

Shore S., Livio M., Van den Heuvel E.P.J.: 1994, *Interacting Binaries,* Berlin-Budapest, Springer-Verlag.

Tutukov A.V., Yungelson L.R.: 1973, *Nauchn. Inform.,* **27**, pp. 58, 70, 86.

Van den Heuvel E.P.J., Heize J.: 1972, *Nat. Phys.Sci.,* **239**, 67.

Table 2 (continued).

Name	P	M_1	M_2
RY Per	6.863566	5.4	1.1
TV Cas	1.8126	2.75	1.3
AI Dra	1.198814	2.3	1.05
TW Cas	1.428325	2.55	1.15
W UMi	1.701158	2.9	1.25
δ Lib	2.327353	3	1.3
XZ Pup	2.192306	3	1.2
RW Mon	1.906091	2.55	1
V548 Cyg	1.80524	3.05	0.95
IM Aur	1.247335	3.1	0.9
SW Cyg	4.572839	2.35	0.65
RW Tau	2.768844	2.95	0.8
AQ Peg	5.548503	2.2	0.55
Y Psc	3.765876	2.14	0.52
TT Hya	6.953429	2.05	0.55
S Cnc	9.484551	2.33	0.17
QY Aql	7.22959	2.15	0.65
RY Gem	9.300525	2.8	0.59
VV UMa	0.687378	2.1	0.48
KO Aql	2.864022	2.5	0.5
AB Per	7.16025	2.4	0.5
W Del	4.806043	2.3	0.46
UU Oph	4.396766	2.7	0.5
TW Lac	3.037494	2.1	0.4
ST Per	2.648325	2.25	0.4
T LMi	3.019912	2.35	0.33
TY Peg	3.092234	2.3	0.3
S Equ	3.436066	3	0.37
AS Eri	2.664151	1.93	0.21
DN Ori	12.96626	2.65	0.18
X Tri	0.971527	1.75	1
DL Vir	1.315475	1.8	0.95
RZ Dra	0.550877	1.5	0.72
AT Peg	1.146079	1.7	0.8
TW Dra	2.806834	1.7	0.8
U Sct	0.954985	1.9	0.75
SX Hya	2.895697	1.65	0.58
RZ Cas	1.195252	1.75	0.6
Y Leo	1.686081	1.8	0.6
RW Crb	0.726411	1.5	0.4
UX Her	1.548842	2	0.5
Z Dra	1.357439	1.65	0.41
RX Hya	2.28159	1.5	0.38
BD Vir	2.548439	2.1	0.5
RT Per	0.8494	1.3	0.31
SS Lib	1.437997	1.7	0.4
UW Vir	1.81073	1.75	0.4
RY Aqr	1.966594	1.3	0.3
TW And	4.122773	1.7	0.37
Y Cam	3.305507	1.9	0.4
XX Cep	2.337301	1.7	0.27
XZ Sgr	3.275555	1.8	0.25
R CMa	1.135939	1.5	0.18
S Vel	5.933666	1.6	0.19

SPECTRAL INVESTIGATION OF FIELD BLUE STRAGGLERS

I.V. Chernyshova

Astronomical Observatory, Odessa State University
T.G.Shevchenko Park, Odessa 65014 Ukraine, *chern_irina@yahoo.com*

ABSTRACT. Field blue stragglers are counterparts of cluster blue stragglers. They were selected by Olsen in base of specific Strömgren indices among bright metal-deficient early F dwarfs.

For some stars from this list, the high-resolution and high S/N CCD spectra were obtained. Synthetic spectrum technique was applied for the specification of rotational velocities and chemical composition of program stars. Special attention was payed on FBS with high rotation and broad shallow lines with aim of comparison of their chemical abundances and abundances of λ Bootis type stars calculated with the same methodics. In general, 18 chemical elements were investigated. All metals show moderate deficiency. Most of the stars show normal abundance of sodium. With the exception of HD35863 the "normal" lithium abundance also was found in HD27523, HD45042 and HD88923.

Main question was "What is FBS?" We discussed three hypothesis that could be applied for explanation of their nature:
1) they are really blue stragglers with prolonged evolution;
2) they are normal stars wich were born in metal-deficient medium;
3) they are an extention of λ Boo stars towards lower temperature.

Key words: Stars: abundances; stars: blue stragglers.

1. Introduction

Blue straggler stars (BSs) are found: in open clusters of all ages (Population I, young disk, old disk), in globular clusters (Population II, halo), in the galactic field and in the dwarf galaxies. BSs lie to the left and above the turn-off point in the color-magnitude diagrams. Turnoff the region where normal single stars already have evolved away from the main sequence. BSs which belong to globular clusters are too faint for high-dispersion spectroscopy.

To find comparatively bright counterparts of these BSs Bond and MacConnell (1971) and Carney and Peterson (1981) looked for among the nearby Population II stars, because there is no obvious way to distinguish Population I BSs from the common normal Population I dwarfs on the upper main sequence (O, B, Am, Ap stars) . Since all globular clusters have turn-off points redder than $(B\text{-}V)_0$=0.36, any field halo dwarf redder than this is a straggler suspect.

Olsen (1980) had applied Strömgren photometry to predict spectral classifications of faint stars and finding lists of potentially interesting objects. He has indetified a category of early F type metal-poor dwarfs (so called "week-lined field blue stragglers" (FBSwl)) among stars brighter than $m_v=8^m$. Their δm_1 values indicate abundances in the interval -0.9¡[Fe/H]¡-0.4. A spectroscopic investigation of this group of metal-deficient F dwarfs to clarify their nature was recommended.

FBSwl may be old, metal-poor close binary systems, in wich the former secondaries have gained mass by transfer of material from the former primaries. Alternatively Bond suggested that FBS possibly are cool representatives of the λ Boo class of young stars with weak metallic lines. These λ Boo stars are Pop I hydrogen burning metal poor (except C,N,O and S) A type stars. They fall into two classes with normal (NHL) and peculiar (PHL) hydrogen profiles with weak cores and broad but often shallow wings, have a weak λ4481 lines, often have high $v \sin i$. Relative to a temperature type based on the hydrogen-line cores, the K- and metallic-line types are too early, thus spectrum as a whole appears metal weak. Some of them have IR excesses and strong absorbtion features in IUE spectra. Probably both explanation may be true.

2. Observations and results of spectral analysis

For program stars was obtained high-resolution and high S/N RETICON spectra and two photographic spectra. Preliminary results had been published in Andrievsky et al. (1995, 1996).

RETICON spectra have been obtained with the AURELIE spectrograph on the 1.52m telescope of OHP (Haute Provence Observatory, France). The resolving power was about 11000, signal-to-noise ratio varies from S/N $\approx$ 100. The reduction of the RETICON spectra has been done with an automatic code developed in Paris-Meudon Observatory.

Table 1: Observations and adopted parameters of program stars.

Star	Obs	Region Å	T_{eff},K	*log g*	V_t,km s^{-1}	*v sini*,km s^{-1}
HD11940	OHP	5480-6400	6800	3.6	3.0	60
HD27291	OHP	5480-6800	6750	4.2	2.0	35
HD27523	OHP	5480-6800	6800	3.8	2.2	50
HD35863	OHP	5480-6800	6700	4.0	2.0	23
HD36229	OHP	5480-6400	7100	4.0	2.3	40
HD45042	OHP	5480-6800	6670	3.5	3.0	55
HD54073	OHP	5480-6800	6900	3.2	3.0	120
HD81539	OHP	5480-6800	6500	3.5	1.7	27
HD88923	OHP	5480-6800	6650	3.2	3.0	130
HD119562	OHP	5480-6800	6700	4.0	2.2	40
HD171566	SAO	3900-5000	7100	3.5	4.0	55
HD189652	SAO	3900-5000	6850	3.8	4.0	110

Table 2: Abundances for program stars (SAO spectra)

El	C	Mg	Ca	Sc	Ti	V	Cr	Mn	Fe	Ni	Y	Zr	Ba	Nd
HD171566		-0.3	-0.6	-0.9	-1.0	-0.4	-0.8	-0.4	-1.2	-0.3	-0.3	-0.3	-0.2	-0.3
HD189652	-0.1:	-0.3	-1.3	-1.1	-1.0		-0.7	-0.3	-0.9	-0.7			-0.4	

Table 3: Abundances for program stars (OHP spectra)

El	C	O	Na	Mg	Si	S	Ca	Sc	Ti	Cr	Fe	Ni	Ba
HD11940	-0.2:	-0.2:	-0.2		-0.5	0.0	-0.5	-0.4			-0.5	-0.4	-0.6
HD27291	-0.1:	-0.3:	-0.2	-0.4	-0.2	0.0	-0.4	-0.4	-0.2		-0.2	-0.2	0.0
HD27523	-0.2:	-0.2:	-0.1	-0.4	-0.2	-0.2	-0.3	-0.5		-0.2	-0.3	-0.6	0.0
HD35863	-0.2:	-0.1:	0.0	-0.5	-0.3	-0.1	-0.1	-0.3	-0.3	-0.2	-0.2	-0.4	0.2
HD36229	-0.3:	-0.2:	-0.4	-0.5	-0.3		-0.1	-0.3		-0.3	-0.2	-0.2	-0.1
HD45042	-0.2:		-0.2	-0.8	-0.2	0.0	-0.1	-0.5	-0.2	-0.4	-0.5	-0.6	-0.3
HD54073			-0.3	-1.2	-0.5	0.0	-0.6	-1.1	-0.3	-0.4	-1.0	-0.5	-0.8
HD81539	-0.1:	-0.3:	-0.1	-0.5	-0.5	-0.3	-0.3	-0.8	-0.4	-0.4	-0.3	-0.4	-0.1
HD88923	-0.2:	-0.2:	0.0	-1.0	-0.5	0.0	-0.7	-1.1	-0.3	-0.2	-1.0	-0.4	-0.4
HD119562		-0.2:	0.0	-0.4	-0.2	-0.2	-0.3	-0.6	-0.2	-0.3	-0.3	-0.4	-0.3

Photographic (SAO) spectra have been obtained with 6m telescope Main Stellar Spectrograph (Special Astrophysical Observatory of Russian Academy of Sciences, Russia, Nothern Caucasus (SAO)). The preliminary reduction of the spectrogramss was carried out with an automatical sytem of Crimean Astrophysical Observatory (Academy of Sciences of Ukraine). Dispersion was 9 Å/mm.

Temperatures and gravities of the program stars were estimated using (b-y)-c_1 grid by Kurucz (1991). Strömgren colours were selected from Hauck and Mermilliod (1985). To derive elemental abundances we applied spectral synthesis technique (STARSP code by Tsymbal (1996); atmosphere models come from Kurucz, 1992). Oscillator strengths for investigated lines and blends were corrected performing a procedure of comparison of the solar synthetic spectrum (solar model from Kurucz's grid, V_t=1 km s^{-1} and solar abundances from Grevesse and Noels, 1993) with the solar flux spectrum (Kurucz et al. 1984). Resulting abundances and rotational velocities were found by means of the optimal fitting of the synthetic spectrum to the observed one. Derived abundances for program stars in form [El/H] are given in Tables 2, 3.

3. Discussion

Chemical abundances have changed only for stars with high velocity of rotation, for stars with low velocity of rotation abundances haven't change at all (or a little). *v sin i* values was updated from the preliminary etimates in Andrievsky et al. (1995).

All metals show moderate deficiency on FBS. C and O are in little deficiency on all stars, but lines were very blended and abundance of these elements should be check one more times. But obviously that C and O enhanced with respect to iron. Most of the stars show normal abundance of sulfur (the same for λ Boo type stars). All stars have rather low space velocities and eccentricities (Andrievky et al. 1996). Take into account normal hydrogen profiles of stars we can call them candidates in NHL type stars (of course if all other main features of λ Boo type stars will be found on these stars).

Some of FBSwl and λ Boo type stars have common points on luminosity-temperature diagram that was build by using Hipparcos data and evolutionary isochrones Shaller (1992). As you can see from Tables 2, 3 these stars don't show evident abundance pattern. Possibly FBSwl form an inhomogeneous group wich consist of the stars with different ages (and may be of different types).

The lithium abundance on FBS HD27523, HD45042, HD35863 and HD88923 seem to be equal to its initial abundance expected from the age of the stars. This fact is puzzling, since generally lithium is depleted in BS (Glaspey et al. 1994). Explanation would be that the stars are a young massive stars, formed recently

from abnormally metal-poor material. The coalescence of two low-mass stars and BS formation are excluded, lithium will rapidly destroyed in the deep convective zone of cool low-mass dwarfs in the pre-main sequence and main sequence phases, unless the stars are a short-period binaries. Definitive conclusion can be reached if we will have a statistics of such lithium abundance in higher resolution and signal/noice spectra of FBS.

Acknowledgements. The author is thankful to Dr. T.V. Mishenina for useful discussions and Dr. S.M. Andrievsky for help with obtaining of spectral material and discussions.

References

Andrievsky S.M., Chernyshova I.V., Ivashchenko O.V.: 1995, *As. Ap.*, **297**, 356.

Andrievsky S.M., Chernyshova I.V., Kovtyukh V.V.: 1996, *As. Ap.*, **310**, 277.

Bond H.E., MacConnell, D.J.: 1971, *Ap. J.*, **165**, 51.

Carney B.W., Peterson, R.C.: 1981, *Ap. J.*, **251**, 190.

Grevesse N., Noels A.: 1993, *Origin and evolution of the elements,* Eds. N. Prantzos, E. Vangioni-Flam and M. Cassé, Cambridge Univ. Press, 14.

Hauck B., Mermilliod M.: 1985, *Ap. J. Suppl.*, **60**, 61.

Kurucz, R.L.: 1992, *The stellar populations of galaxies,* Eds. B. Barbuy, A. Renzini, IAU Symp. **149**, 225.

Kurucz R.L.: 1991, *Precision photometry: Astrophysics of the Galaxy,* Eds. A.G.D. Philip, A.R. Upgren and K.A. Janes, L. Davis Press, 1.

Kurucz R.L., Furenlid I., Brault I. and Testerman L.: 1984, *The solar flux atlas from 296 nm to 1300 nm,* National Solar Observatory.

Olsen E.H.: 1980, *As. Ap. Suppl.*, **39**, 205.

Schaller G., Schaerer D., Meynet G., Maeder A.: 1992, *As. Ap. Suppl.*, **96**, 269.

Tsymbal V.: 1996, *Model atmospheres and spectrum synthesis*, Eds. S.J. Adelman, F. Kupka and W.W. Weiss, ASP Conf. Ser., **108**, 198.

STATISTICAL RESEARCH IN EVOLUTIONARY GENETIC RELATIONSHIP OF DMS-, DW-, KW- AND KE-TYPES OF DOUBLE STARS

G.N. Dryomova, M.A. Svechnikov

Ural State University, Lenin prospect, Ekaterinburg 620083 Russia,
Polina.Zakharova@usu.ru

ABSTRACT. Statistical relations as spectrum-period, mass of primary component-semi-major axes of an orbit, excesses of luminosity and radius-mass of component, Karetnikov's diagram, modern and initial distributions of the binaries in the 1 ps^3 of Sun neighbourhood allow to solve the problem of evolutionary relationship for close binary systems and describe conditions at which evolutionary transitions such as DMS $\rightarrow$ DW $\rightarrow$ KW $\leftarrow$ KE take place.

Key words: Stars: close binaries: detached systems: W UMa-stars.

1. Introduction

In this paper we tryed to estimate the degree of evolutionary relation of close binary systems of DMS, DW, KW, KE types located on the Main Sequence MS and are in the "first phase of the mass exchange". These abbriviations are adopted according to classification by (Svechnikov M. A. et.al., 1980). The "Catalogue of approximate photometric and absolute elements of variable stars" is the basis of our research (Svechnikov M. A. et. al., 1990). Content of this catalogue is 437 DMS, 153 DW, 215 KW and 392 KE systems. The summary sample is greate enough to construct statistical diagram.

2. Basic statistical diagrams

Figure 1 plots distributions of given systems on the diagram lgM1-lgA. Two solid lines $A_{min}(q = 1)$ and $A_{min}(q = 0.3)$ restrict fields of distributions of DMS, DW, KW, KE systems. A_{min} is evaluated from $A_{min} = R(M1) \cdot q^{0.2084}/0.378$, $0.1 \leq q \leq 1$ (Plavec M. et. al., 1964), that is interpreted as a least distance between components at which the probability of discovering of double system as eclipsing variable is maximum.

So the large number of DMS stars should be located near line $A_{min}(q = 1)$. But in actual it is true only for systems with primary masses $M1 \geq 10$ Mo. One can see the region poor of DMS systems and known as "forbidden triangle" with coordinates $(lgM = 0, lgA = 0.9), (lgM = 0, lgA = 0.3), (lgM = 0.7, lgA = 1)$. It is not possible to explain this deficiency by effects of observational selection.

In paper by (Tutukov A. V. et.al., 1982) it is shown that for systems with $M1 > 1.5$ Mo the distance between components can not be less than it is allowed by expression $A/Ro = (6 \cdot M1/Mo)^{1/3}$. Whereas nothing prevents systems with $M1 \leq 1.5$ Mo to fall into "forbidden triangle", because such systems have an extensive convective envelopes characterizing by high degree of turbulence and differential rotation. As a result of dynamo action the magnetic field is generated and interacts with stellar wind emanating from the star. Thus in a binary system by magnetic breaking spin angular momentum loss (AML) results in orbital AML.

It is equivalent to components approaching. If velocity of approaching is greater than nuclear evolution rate components not being contact will have small values of A_{min}. But it is namely class of DW-systems. Having continued evolution in a scale of AML DW-systems may turn into KW-systems. The same range of primary masses can be considered as inderect evidence favor such evolutionary transition.

On the basis of analysis of this diagram we would like to propose the following evolutionary chain DMS$\rightarrow$DW$\rightarrow$KW. Such transitions have been investigated by various authors (Svechnikov M. A. 1990, Schatzman E., 1962, Vilhu O., 1982) and here are confirmed on the basis of much more numerous sample (800) from catalogue (Svechnikov M. A. et.al., 1990). Some of KE-systems also fall to "forbidden triangle" and so they may be included into similar scheme DMS$\rightarrow$KE$\rightarrow$KW.

Figure 2 shows distributions of systems on the diagram period-spectrum $lgP - Sp1$. If third Kepler's law is substituted in Tutukov's expression that at $q = 1$ value of $P = \sqrt{2.9/(1+q)}$ is equal $1.^d2$. Visible DMS-distribution shows deficiency of these systems with $M1 > 1.5$ Mo and $P < 1.^d2$. Svechnikov is first who noted deficiency of such DMS stars (Svechnikov M. A.,

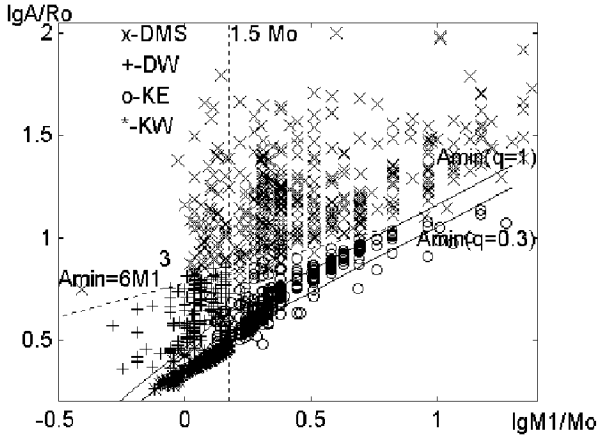

Figure 1: Distributions of DMS,DW,KW and KE stars on the diagram mass of primary component versus semi-major axes

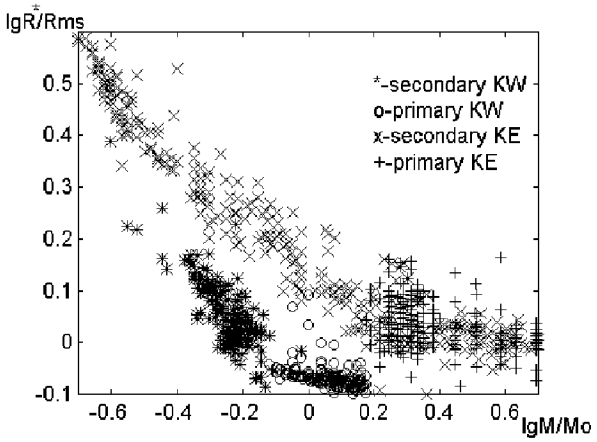

Figure 3: Distributions of KW and KE stars on the diagram radii excess versus mass of component

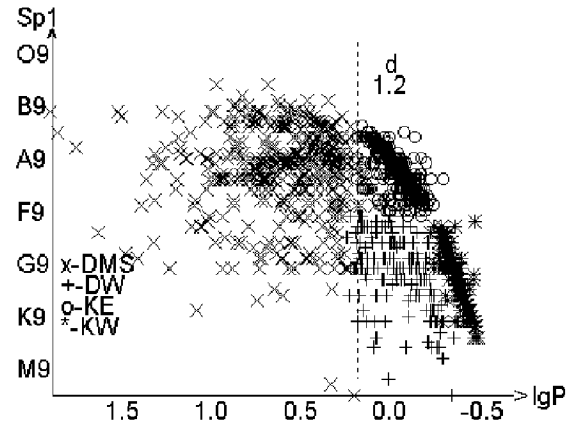

Figure 2: Distributions of DMS, DW, KW and KE stars on the diagram spectrum of primary component versus period

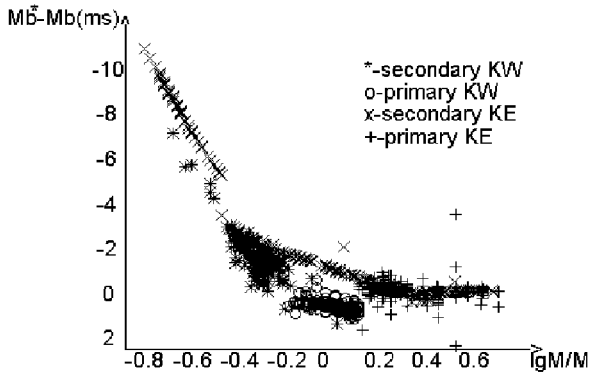

Figure 4: Distributions of KW and KE stars on the diagram luminosity excess versus mass of component

1969). Given diagram serves as one more illustration for this evolutionary transition mechanism. Here one can see the period gap equal 12^h, which is not filled by any systems. This is a bifurcation orbital period that means two possible evolutionary paths with formation converging ultra-close or diverging wide binaries. In our case the class of KW systems describes the first scenery while KE-systems correspond to second variant. The gap origin can be explained by quick choice of evolutionary path by systems of both classes.

Figures 3,4 reflect radii and luminosity excesses versus component mass. Excesses are determined as difference between observed (L) or calculated from observations (R) values and analogous magnitudes but proper to MS stars. DW systems have no radii or luminosity excesses niether for primary no for secondary components. It is expectable because they are close to DMS systems. For KW-satellites appreciable radii and luminosity excesses are exposed while in the case of KE-satellites they are expressed more strongly than for KW systems.

For interpretation of these excesses "role change" for KE class and "mass exchange" for KW class can be proposed. Before "role change" KE-satellites were primary components, which had enough time to evolve from the MS. As for KW-satellites due to orbital decay caused by AML, sizes of Rosha's lobe decrease and thus it is required less time to fill lobe space. In paper by (Istomin L. F., 1986) it is shown that increase of luminosity excesses for KW-satellites takes place due to release of gravitational energy of matter flowing from more massive component.

Karetnikov's diagram (Karetnikov V. G., 1988) (Figure 5) depicts the relative Rosha's lobe fullness versus degree of Rosha's lobe fullness by component. It is well seen that process of "role change" in the KW-systems

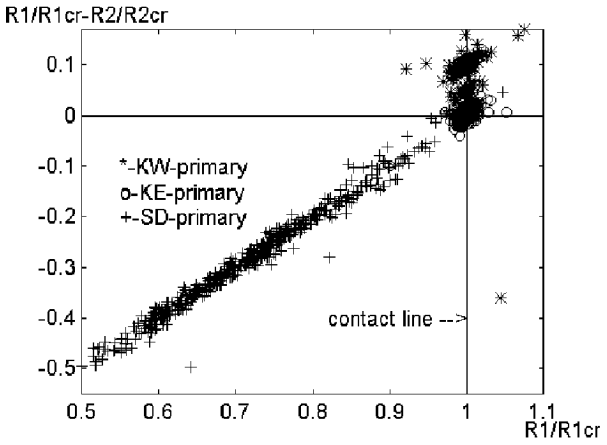

Figure 5: Distributions of SD, KW and KE stars on the diagram by Karetnikov

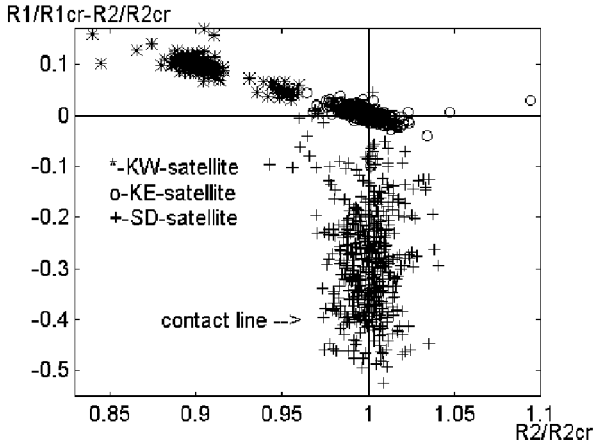

Figure 6: Summary modern spatial distributions of DMS, DW, KW and KE stars

never occured and almost all KW-primaries have overflowed Rosha's lobes while their satellites have no. Primary and secondary components of some KE-systems already intersected contact line.

For SD-systems of R CMa-type with $P < 1.^d2$ one component of which is subgiant while another is MS star it is proved that following relations $R1/R1_{cr} \leq R2/R2_{cr}$, $R2/R2_{cr} \geq 1$, $R1/R1_{cr} \to 1$ are true. It means that the process of "role change" in these systems takes place. Field of SD-distribution partially overlaps field of KE-distribution from this one has probable evolutionary transition SD- into KE-systems.

The next part of our work concerns the modern and initial distributions common presentations of which are $F_m(M1_i, P_i) = f_i/(V_i * W_i)$ and $F_{in}(M1_i, P_i) = f_i/(V_i * W_i * \tau_i)$. These functions are presented as spatial densities of close binary systems containing in the 1 ps^3 of Sun neighbourhood. $W_i(M1, A, q, i)$ and $W_i(M1, q, i)$ are probabilities of discovering for DMS, DW and KW, KE systems, respectively. By linear consequent interpolation between tabular values (Svechnikov M. A. et. al., 1989) we calculated individual W_i^* for each system of every class.

Then we estimate volume V_i for each system independently from it's classification as volume of spherical layer with thickness 180 ps (Istomin L. F., 1978). Radius is taken from equation $Mb_i = mv_i + \Delta mb_i + 5 - 5 \cdot \lg r_i - \overline{A} \cdot r_i$ which is solved with use of average interstellar absorbtion effect. $Mb_i = Mb1_i - \Delta m'$ is absolute bolometrical stellar magnitude of system as a whole in the brightness maximum, mv_i is absolute visible stellar magnitude of system as a whole in a brightness maximum, $\Delta m' = 0.^m48$ (Taidakova T. A., 1981), Δmb_i is bolometrical correction (Allen K. U., 1977), $\overline{A} = 0.0019 ps^{-1}$ is average interstellar absorbtion (Popper D. M., 1980).

τ_i is age of binary system of DMS, DW classes estimated by isochrone method constructed on the basis of evolutionary tracks by Maeder and Meynet with effects of overshooting and mass loss (Dryomova G. N., 1999). f_i is factor of sample incompleteness.

3. Conclusion

All distributions are presented as maps of intensities of given systems in coordinates (lgM1, lgP). So the modern DMS-distribution is quasi negative to one's own initial distribution because positions of local minima and maxima change their places.

The modern DW-distribution continues modern DMS-distribution. Upper boundary of modern KW-distribution is lower boundary of DW-distribution. In actual the initial DW-distribution should be absent and as a support of our proposition we can consider close to zero intensities. We conclude that DW abd KW classes reflect initial and modern distributions respectively of the same evolutionary class of contact double systems.

Figure 6 shows summary modern distribution of all

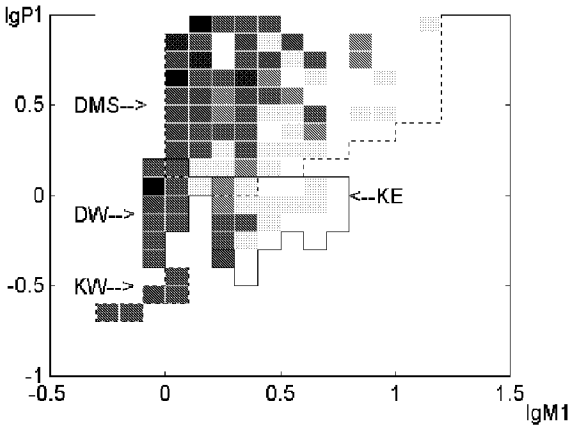

Figure 7:

considered here stellar classes and demonstrate their evolutionary migration. DMS, DW, KW classes intersect each other and the proximity of KW and KE classes permits to assume evolutionary transition KE into KW systems.

References

Allen K. U.: 1977. *Astrophysics magnitudes, Moscow* , 364.

Dryomova G. N. Svechnikov M.A.: 1999, *Catalogue of eclipsing variable stars of DMS-types and some results of its statistical treatment, Ural State University*

Istomin L. F.: 1986, *Thesis of degree of candidate of sciences of Ural University*

Istomin L. F.: 1978, *Stellar clusters and double systems, Ural University*

Karetnikov V. G.: 1988, *Thesis of degree of doctor of sciences, Moscow*

Plavec M., Kratochvil P.: 1964, *Bull. Astron. Inst. Czech* **15**, 165.

Popova E.L., Tutukov A. V., Yungelson L. R.: 1982, *Letter in the Astronomical Journal* **8**, 297.

Popper D. M.: 1980 *Stellar masses, Ann. Rev. Astron. Astrophys.* bf 18, 115.

Schatzman E.: 1962, *Ann. d' Astrophys.* **25**, 18.

Svechnikov M.A.: 1969, *Catalogue of orbital elements, masses and luminosities of close binary systems*

Svechnikov M.A.: 1990, *Investigation of statistical data for close binary stars, Tallin, Valgus* 26.

Svechnikov M.A., Eretnova O. V., Olneva M. N., Taidakova T. A.: 1989, *ISSN, Riga* **67**, 5.

Svechnikov M.A., Istomin L. F., Grehova O. A.: 1980, *Variable Stars* **21**, 399.

Svechnikov M.A., Kuznetzova E. F.: 1990, *Catalogue of approximate photometric and absolute elements of variable stars*

Taidakova T. A.: 1981, *Diploma, Chelyabinsk University*

Vilhu O.: 1982, *Astron. Astrophys.* **109**, 17.

NLTE CALCULATION FOR O II

S.A. Korotin

Astronomical Observatory, Odessa State University
T.G.Shevchenko Park, Odessa 65014 Ukraine, *skyline@eurocom.od.ua*

ABSTRACT. The Kurucz's atmospheric models and a modified version of the MULTI code are applied in a NLTE investigation of the O II spectrum. It is shown that previously performed analyses based on the use of lightly line-blanketed Gold models give results that are in variance with those based on the use of the more heavily blanketed Kurucz's models.

One result of our calculations is a number of useful relationships between the NLTE oxygen abundance, line equivalent width, and stellar atmospheric parameters.

Key words:Stars: abundances – Stars: early type– NLTE -analysis

1. Introduction

Oxygen, one of the most abundant elements, is preferentially formed during explosive nucleosynthesis in Type II supernovae. Despite the participation of the oxygen nuclei in the CNO cycle of hydrogen burning in massive stars, the oxygen abundance is not expected to be significantly altered during the standard evolution of the star from the main sequence to red giant region, much less while the star still resides on the main sequence. Thus, surface oxygen abundances in main sequence B stars should reflect the initial oxygen content in the interstellar medium from which the stars are formed. an investigation of oxygen abundance variations among B stars can accordingly much say about the efficiency of Type II supernovae and possible inhomogeneities within the progenitor material of the B stars.

In the present work we report results from NLTE O II calculations which were performed using a modified version of the MULTI code. The MULTI code has not been used in previously published NLTE determinations of oxygen abundances (e.g. Becker & Butler 1988a). We consider our approach a more realistic one relative to the Becker & Butler analysis as it is based on the use of Kurucz model atmospheres while the Becker & Butler calculations were based upon less line-blanketed models which we feel do not present an adequate description of the atmospheres of early-type stars.

2. NLTE calculations

Simultaneous solution of the radiative transfer and statistical equilibrium equations have been realized using the MULTI-code (Carlsson, 1986) in the approximation of complete frequency redistribution for all lines. The initial version of this code was modified with the aim to apply it in the analysis of early-type stars. In particular,

1) we have included in the code opacity sources from the ATLAS9 program (Kurucz, 1992). This enables a much more accurate calculation of the continuum opacity and intensity distribution in the UV region which is extremely important in the correct determination of the radiative rates of $b-f$ transitions;

2) we have changed the code to calculate the combined profile of blended lines taking into account stellar rotation and instrumental profiles.

In addition to these modifications, we for the first time have applied to the analysis of O II lines in the spectra of hot stars the well-known blanketed atmosphere models of Kurucz (1992).

2.1. Parameters of the oxygen atom

We employed a model oxygen atom consisting of 141 levels: 3 levels in O I, 132 levels in O II with $L \leq 5$ and $n \leq 8$, 5 levels in O III, and the ground state of O IV. The detailed structure of the multiplets was ignored and each LS multiplet was considered as a single term.

Within the described system of oxygen atom levels we considered the radiative transitions between the first 49 levels of O II and the ground level of O III. These energy levels were selected from the compilation of Hirata & Horaguchi (1994). Transitions between the remaining levels were not taken into account and those levels were used only in the equations of population conservation.

Only transitions having $\lambda < 100\,000\,\mathring{A}$ were considered. After numerous test calculations, 86 $b-b$ transitions were included in the linearization procedure. These transitions describe quite well the formation of the lines of interest. Another 170 transitions

were treated as having fixed radiative rates.

Photoionization cross-sections were mainly taken from the Opacity Project (Yan et al., 1987) keeping account within the calculations of the detailed structure of their frequency dependence, including resonances.

Oscillator strengths were selected from the extensive compilation of Hirata & Horaguchi (1994), from the survey of lines which are formed as transitions from the ground level by Verner et al., (1994) and from CDROM 23 of Kurucz (1994). Some information was also obtained through the Opacity Project. As we ignored the multiplet structure of all levels, the oscillator strength for each averaged transition was calculated as $f = \frac{\sum g_i f_i}{\sum g_i}$.

After the combined solution of the radiative transfer and statistical equilibrium equations, the average level populations were redistributed proportional to the statistical weights of the corresponding sublevels to regain the detailed multiplet structure, and finally the lines of the interest were investigated.

Stark parameters are a very important part of the analysis as their influence on the resulting oxygen abundance as derived from O II lines is rather significant. To calculate the Stark parameters for the considered transitions we used the semiempirical formula provided by Dimitrijević (1997) for the full width at the half maximum (FWHM):

$$\begin{aligned} W(\mathring{A}) &= 2.2151 \cdot 10^{-8} \frac{\lambda^2(cm) N(cm^{-3})}{T^{1/2}(K)} * \\ &\left(0.9 - \frac{1.1}{Z}\right) \sum_{k=i,j} \left(\frac{3n_k^*}{2Z}\right)^2 * \\ &\left(2n_k^{*2} - l_k^2 - l_k - 1\right) \end{aligned} \quad (1)$$

Here n^* is an effective principal quantum number and l is an angular momentum quantum number. Calculations using this formula were performed for T=20 000K.

Collisional ionization interactions were described using Seaton's formula (Seaton, 1962):

$$C_{ik} = 1.55 \cdot 10^{13} \frac{\alpha(\nu_0) \overline{g} N_e e^{-u_0}}{\sqrt{T_e} u_0} \quad (2)$$

where $\alpha(\nu_0)$ is the threshold value of the cross-section, $u_0 = \frac{E_0}{kT_e}$, E_0 is the energy of ionization, and N_e and T_e are the electron density and temperature respectively. For the Gaunt factor we adopted a value of 0.3. For all allowed $b-b$ transitions we used the van Regemorter (1962) formula:

$$\begin{aligned} C_{ij} &= 5.465 \cdot 10^{-11} N_e \sqrt{T_e} \cdot 14.5 f_{ij} \left(\frac{I_H}{E_0}\right)^2 * \\ &u_0 e^{-u_0} \max\left[\overline{g}; 0.276 e^{u_0} E_1(u_0)\right] \end{aligned} \quad (3)$$

where I_H is the hydrogen ionization potential and $E_1(u_0)$ is the first-order integral exponential function. Collisional rates for forbidden transitions were calculated with the help of a semiempirical formula (Allen, 1973), with collisional force of 1:

$$C_{ij} = 8.63 \cdot 10^{-6} \frac{N_e e^{-u_0}}{g_i \sqrt{T_e}} \quad (4)$$

3. General results of the calculation

Applying the above prescription we made an attempt to find relationships between the oxygen abundance and oxygen line equivalent width for a range of atmosphere parameters ($T_{\rm eff}$ ranging from 20 000 K to 33 000 K; V_t from 1 $km\ s^{-1}$ to 8 $km\ s^{-1}$ and oxygen abundance (O/H) from 8.37 to 8.87). Approximations were found for three different gravity values: 3.50, 3.75 and 4.00. We found that the NLTE oxygen abundance can be expressed by the following formula:

$$\begin{aligned} (O/H)_{NLTE} &= 10^{\left(a \cdot T_{\rm eff} + b \cdot V_t + c \cdot \log(W) + d \cdot T_{\rm eff}^2\right)} * \\ &10^{\left(e \cdot T_{\rm eff}^4 + f \cdot T_{\rm eff}^5 + g \cdot (\log(W))^2\right)} \end{aligned} \quad (5)$$

Coefficients (for selected O II lines) to be used in this formula are listed in Table **??**- **??** for the different log g values. For this fitting formula $\sigma = 0.02$ with a maximum deviation of 0.1 dex. We hope that this relationship will be of use in the determination of oxygen abundances in hot main sequence stars.

4. Comparison with previous studies

For illustration, in Fig. **??** - **??** we present individual dependencies between a) line equivalent width and effective temperature for a selection of O II lines which were investigated by Becker & Butler 1988b calculated with (O/H)=8.88 and $\log g = 4.0$ and b) equivalent width and relative oxygen abundance (V_t=5 $km\ s^{-1}$, $\log g$ =4.0 and $T_{\rm eff}$=30 000 K).

Note that in the figures we have reproduced only the Becker & Butler (1988b) NLTE results. As one can see from these figures our NLTE equivalent widths are systematically stronger than those derived by Becker & Butler. For the majority of the investigated lines Becker & Butler obtained NLTE equivalent widths which are practically the same as those derived by us in the LTE approximation. The Becker & Butler (1988a, 1988b) calculations were performed using the grid of Gold (1984) models which only take into account the blanketing from the 104 strongest lines present in the spectra of B stars. In our study, the more heavily blanketed Kurucz models were used. We believe that the main source of the disparity between these NLTE results originates in the grids of atmospheric models used

Table 1: Coefficients for $\log g = 4.0$

λ	a	b	c	d	e	f	g
4595.96	1.5124159E-04	-2.0471793E-03	1.1170454E-02	-6.9585345E-09	5.6306715E-18	-8.3406351E-23	2.5195905E-02
4609.43	1.5550496E-04	-1.9760641E-03	3.7945134E-02	-7.2792605E-09	6.0706978E-18	-9.1441341E-23	1.7967415E-02
4610.20	1.5342524E-04	-6.4951778E-04	5.4851509E-02	-7.0222524E-09	5.8144563E-18	-8.7656958E-23	5.2823667E-03
4638.85	1.5098142E-04	-2.9185301E-03	5.3815554E-03	-6.9548807E-09	5.6546257E-18	-8.3610841E-23	3.0510199E-02
4641.81	1.5556961E-04	-4.2725404E-03	-2.0024990E-02	-7.3153636E-09	6.1042202E-18	-9.1532692E-23	4.1677337E-02
4649.14	1.5747199E-04	-5.1880087E-03	-2.8205318E-02	-7.5325189E-09	6.4400702E-18	-9.7818988E-23	4.6517209E-02
4650.84	1.5099143E-04	-2.9357199E-03	4.9863263E-03	-6.9583613E-09	5.6634497E-18	-8.3799094E-23	3.0643451E-02
4661.63	1.5228854E-04	-3.3137111E-03	-3.1963094E-03	-7.0562897E-09	5.7812318E-18	-8.5851170E-23	3.4133706E-02
4673.74	1.4803582E-04	-1.2051937E-03	4.4609172E-02	-6.7489229E-09	5.5337076E-18	-8.2534395E-23	1.1919067E-02
4676.24	1.5139794E-04	-3.0697621E-03	1.7360954E-03	-6.9924989E-09	5.7116551E-18	-8.4694643E-23	3.1920778E-02
4701.18	1.5169998E-04	-8.2484372E-04	5.0335866E-02	-6.9317828E-09	5.7352080E-18	-8.7010008E-23	7.8638346E-03
4701.71	1.5261058E-04	-2.6835721E-04	5.2427504E-02	-6.8918749E-09	5.7108517E-18	-8.7095172E-23	3.1452259E-03
4703.16	1.5283858E-04	-1.1437849E-03	4.8370093E-02	-7.0431963E-09	5.8077093E-18	-8.7432427E-23	1.0043059E-02
4705.35	1.5583200E-04	-2.9512437E-03	1.3518314E-02	-7.3146649E-09	6.0608582E-18	-9.0682382E-23	2.8147661E-02

Table 2: Coefficients for $\log g = 3.75$

λ	a	b	c	d	e	f	g
4595.96	1.5818248E-04	-2.3497411E-03	8.3003630E-03	-7.5308156E-09	6.4044870E-18	-9.6876532E-23	2.8641347E-02
4609.43	1.6206867E-04	-2.1993521E-03	4.0001418E-02	-7.8348275E-09	6.8434770E-18	-1.0496580E-22	1.9773060E-02
4610.20	1.6145329E-04	-7.1977819E-04	5.8161035E-02	-7.6947409E-09	6.8336005E-18	-1.0659798E-22	4.9297307E-03
4638.85	1.5762685E-04	-3.4791378E-03	9.8773155E-03	-7.5576263E-09	6.5305826E-18	-9.9256489E-23	3.3043315E-02
4641.81	1.6260848E-04	-4.8742939E-03	-2.1495756E-02	-7.9535248E-09	7.0787165E-18	-1.0952849E-22	4.5668031E-02
4649.14	1.6528388E-04	-5.7827268E-03	-3.8418733E-02	-8.2057405E-09	7.4888534E-18	-1.1759610E-22	5.2269174E-02
4650.84	1.5768924E-04	-3.4996126E-03	9.3298543E-03	-7.5656412E-09	6.5476069E-18	-9.9616927E-23	3.3237900E-02
4661.63	1.5916635E-04	-3.8998935E-03	-7.5546154E-04	-7.6788990E-09	6.6992830E-18	-1.0243329E-22	3.7288605E-02
4673.74	1.5317344E-04	-1.4847151E-03	5.3207010E-02	-7.2146370E-09	6.2153895E-18	-9.4618969E-23	1.1129314E-02
4676.24	1.5825738E-04	-3.6460966E-03	5.1309199E-03	-7.6127789E-09	6.6202295E-18	-1.0103721E-22	3.4819245E-02
4701.18	1.6217063E-04	-9.9795688E-04	5.5854237E-02	-7.8090002E-09	7.0897737E-18	-1.1299280E-22	7.8873099E-03
4701.71	1.6582553E-04	-3.1353119E-04	5.5320693E-02	-7.9823693E-09	7.4359338E-18	-1.2066954E-22	2.3231178E-03
4703.16	1.5868826E-04	-1.3369163E-03	5.0029739E-02	-7.5227508E-09	6.4489943E-18	-9.8501747E-23	1.1559815E-02
4705.35	1.6194701E-04	-3.2342595E-03	1.0843579E-02	-7.8196774E-09	6.7273954E-18	-1.0192404E-22	3.1383322E-02

Table 3: Coefficients for $\log g = 3.5$

λ	a	b	c	d	e	f	g
4595.96	1.6079796E-04	-2.5305435E-03	1.6841984E-02	-7.8929755E-09	7.1144087E-18	-1.1062902E-22	2.6620385E-02
4609.43	1.6496742E-04	-2.4034305E-03	4.1862426E-02	-8.1890307E-09	7.5067666E-18	-1.1731028E-22	1.9926116E-02
4610.20	1.5921632E-04	-8.2052104E-04	5.8927117E-02	-7.5960925E-09	6.7073715E-18	-1.0275765E-22	5.6171124E-03
4638.85	1.5795731E-04	-3.7836232E-03	1.7160895E-02	-7.7252475E-09	6.8833710E-18	-1.0536840E-22	3.2206704E-02
4641.81	1.6505913E-04	-5.4637484E-03	-2.3209422E-02	-8.2717780E-09	7.6452575E-18	-1.1975818E-22	4.8391266E-02
4649.14	1.6932802E-04	-6.5899926E-03	-4.8219516E-02	-8.6316391E-09	8.2155537E-18	-1.3102738E-22	5.7763210E-02
4650.84	1.5803201E-04	-3.8061369E-03	1.6705296E-02	-7.7353770E-09	6.9057767E-18	-1.0585360E-22	3.2390344E-02
4661.63	1.6001377E-04	-4.2796142E-03	4.9433570E-03	-7.8876596E-09	7.1146639E-18	-1.0977545E-22	3.7236508E-02
4673.74	1.5195166E-04	-1.5761129E-03	5.4466399E-02	-7.2096549E-09	6.2760012E-18	-9.5001266E-23	1.1237115E-02
4676.24	1.5871367E-04	-3.9762727E-03	1.2465191E-02	-7.7945504E-09	7.0006491E-18	-1.0774082E-22	3.4108289E-02
4701.18	1.6058249E-04	-1.0406804E-03	6.3991701E-02	-7.8080825E-09	7.2441869E-18	-1.1638921E-22	4.6312505E-03
4701.71	1.6119949E-04	-3.1750974E-04	5.5109248E-02	-7.6997140E-09	7.1124958E-18	-1.1455931E-22	2.2297030E-03
4703.16	1.6130156E-04	-1.4516562E-03	5.4553511E-02	-7.8557148E-09	7.1009259E-18	-1.1113663E-22	1.0287603E-02
4705.35	1.6823938E-04	-3.5500940E-03	8.2575492E-03	-8.4236977E-09	7.7444909E-18	-1.2102193E-22	3.3036626E-02

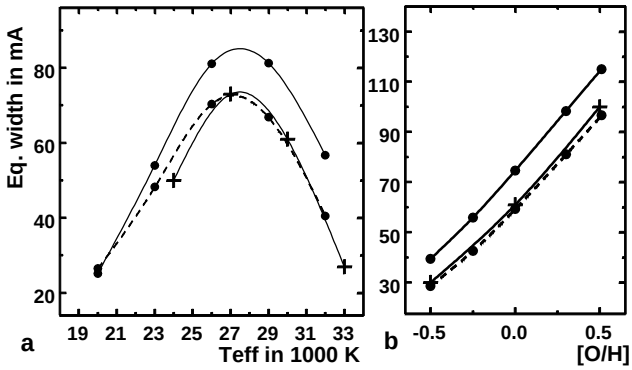

Figure 1: Equivalent width of 4078.84 Å line versus $T_{\rm eff}$ -**a** and[O/H] -**b** for NLTE (solid line) and LTE (dashed line). Our results are indicated by filled circles and those of Becker & Butler (1988b) by crosses.

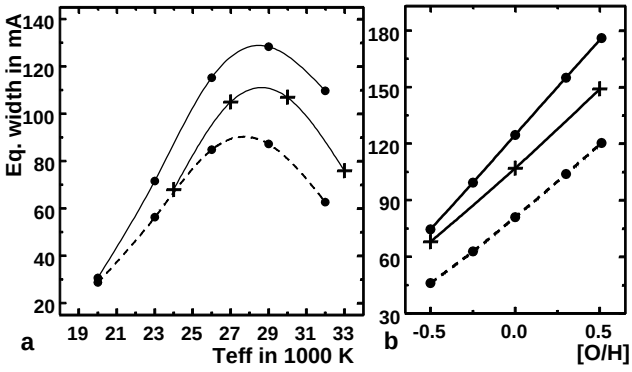

Figure 2: Same as Fig. **??**, but for 4185.45 Å .

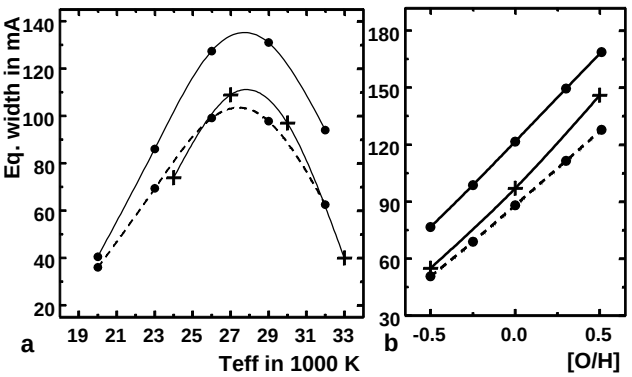

Figure 3: Same as Fig. **??**, but for 4638.86 Å .

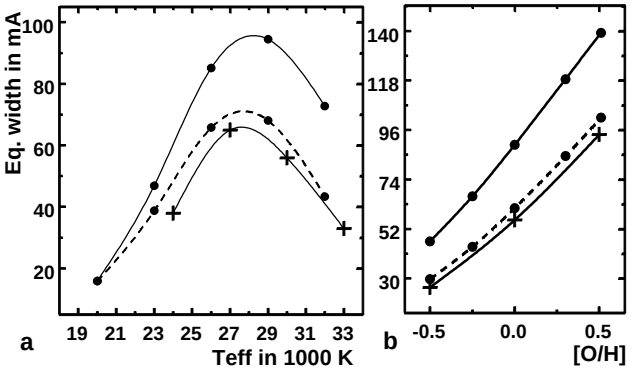

Figure 4: Same as Fig. **??**, but for 4906.83 Å .

in the respective analyses. In fact, it was first noted by Cunha & Lambert (1994) that in NLTE determinations of elemental abundances in hot stars that the more heavily blanketed models should produce a more realistic result. Later, Korotin et al. (1999) discussed this problem having presented direct NLTE calculations of the nitrogen abundance in γ *Peg* based on Kurucz models.

Acknowledgements. The author thanks Dr. M.S. Dimitrijević for providing useful information about Stark parameters.

References

Allen C.W.: 1973, *Astrophysical Quantities*, Athlone Press, London

Becker S.R., Butler K.: 1988a, *As. Ap.* **201**, 232.

Becker S.R., Butler K.: 1988b, *As. Ap. Suppl.*, **74**, 211.

Carlsson M.: 1986, *Uppsala Obs.Rep.* **33**.

Cunha K., Lambert D.L.: 1994, *ApJ*, **426**, 170.

Dimitrijević M.S.: 1997,*ApSS*, **252**, 415.

Gold M.: 1984, Diplomarbeit, Ludwig Maximilian Universität, München

Hirata R., Horaguchi T.: 1994, *Atomic spectral line list.*

Korotin S.A., Andrievsky S.M., Kostynchuk L.Yu.: 1999, *As. Ap.* **342**, 756

Kurucz R.L.: 1992, *The Stellar Populations of Galaxies*, Eds. B. Barbuy, A. Renzini, *IAU Symp.* **149**, 225

Kurucz R.L.: 1994, *CD Roms* N 18, N 23.

Seaton M.J.: 1962, *Proc. Phys. Soc.,* **79**, 1105.

Van Regemorter H.: 1962,*ApJ*, **136**, 906

Verner D.A., Barthel P.D., Tytler D.: 1994, *As. Ap. Suppl.,* **108**, 287

Yan Y., Taylor K.T., Seaton M.J.: 1987, *J. Phys. B: At. Molec. Phys.* **20**, 6409.

ISOTOPIC ABUNDANCES OF MAGNESIUM – ^{24}Mg, ^{25}Mg,^{26}Mg IN THE ATMOSPHERES OF G–K – GIANTS

V.V. Kovtyukh, N.S. Komarov, S.M. Andrievsky, I.F. Dulapchi

Astronomical Observatory, Odessa State University
T.G.Shevchenko Park, Odessa 270014 Ukraine, *val@deneb.odessa.ua*

ABSTRACT. The isotopic abundances of magnesium in the star of thin disk of Galaxy with various chromospheric activity were studied. We use the new data about molecular constants of radiation for isotopes ^{24}Mg, ^{25}Mg, and ^{26}Mg. Values close to solar ratios are generally found.

Key words: Stars: abundances ; stars: late type; stars: individual: BS 165, 168, 2990, 3705, 4301, 4932.

1. Introduction

Isotopic abundance ratios are regarded to be a powerful tool in the application to the stellar evolution studies. Especially it refers to the investigation of late giants, where obtained abundances of isotopes for some elements can much say about physical processes operating inside these stars and their evolutionary stage.

As reviewed by Tomkin & Lambert (1980), in massive stars, ^{25}Mg and ^{26}Mg are produced during He burning that includes thermal pulsing. ^{24}Mg is produced during carbon burning. Explosive carbon burning can produce all three Mg isotopes.

MgH spectra are useful tools for isotopic analysis because the isotopic splitting is frequently larger than the line width. The MgH features analysed here are Q- and R-branch lines of the (0,0) band of the $A^2\prod$ – $X^2\sum^+$ system. These features are those discussed by Tomkin & Lambert (1976) in their analysis of the Mg isotopic abundances in α Boo (Arcturus). This well-known visible region electronic system are detectable in stellar spectra over a large range of temperature and abundances (e.g. McWilliam & Lambert 1988; Barbuy 1985, 1987; Tomkin & Lambert 1976, 1980).

The combination of MgI and MgH lines has been shown to be a spectroscopic probe of surface gravity in six cool giant stars (Bonnel & Bell, 1993).

The solar isotope ratio ^{24}Mg, ^{25}Mg, and ^{26}Mg has been measured as 76:12:12 (Wallace et al., 1999), in agreement with the much better determined terrestrial ratio 79:10:11.

For the present study we selected the following giants having the different level of chromospheric activity: BS 165 (K3 III), BS 168 (K0 IIIa), BS 2990 (K0 IIIb), BS 3705 (K7 IIIab), BS 4301 (K0 IIIa), BS 4932 (G8 II-Iab).

2. The observations and analysis

RETICON spectra have been odtained with AURELIE spectrograph on the 1.52-m telescope of the Haute Provence Observatoire (France) in 1999. The resolving power $\lambda/\delta\lambda \sim 66{,}000$ and signal-to-noise ratio ≈ 500 for all the spectra. The observed wavelength region was 5105 - 5165 ÅÅ. Preliminary reduction of the spectra has been done using IHAP and DECH20 packages. The continuum levels were defined by straight-line fits to the nearest continuum points on either side of the absorption feature being measured.

The aim of the analysis is to estimate the relative abundance of ^{24}Mg, ^{25}Mg, and ^{26}Mg isotopes in each star from the relative strengths of its ^{24}MgH, ^{25}MgH, and ^{26}MgH lines. The spectral region studied is 5134–5138 Å comprising (0,0) and (1,1) vibrational transitions in the system $A^2\prod$ – $X^2\sum^+$ of MgH. The isotopic splitting of the (0,0) band MgH lines is about 0.1 Å.

The synthetic spectra were calculated using STARSP code described by Tsymbal (1994, 1995). Special attention was paid to accurate modelling of the isotopically shifted MgH lines in the vicinity of 5134 Å. For this purpose we specially calculated the oscillator strengths for corresponding transitions in MgH molecule and these oscillator strengths were also tested using observed solar spectrum.

The wavelengths for the MgH lines are given in Barbuy (1987). The line list includes the MgH lines, as well as the atomic and C_2 contaminating lines. We adjusted further our synthetic C_2 lines to the calculated spectrum of Arcturus as calculated by Tomkin & Lambert (1976) using the same stellar parameters as those authors.

The convolution step for the instrumental profile was chosen by fitting thin atomic lines present in the observed region. A value of 0.08 Å for the FWHM was adopted in all cases.

Fig.1 illustrate the computations. The isotopic com-

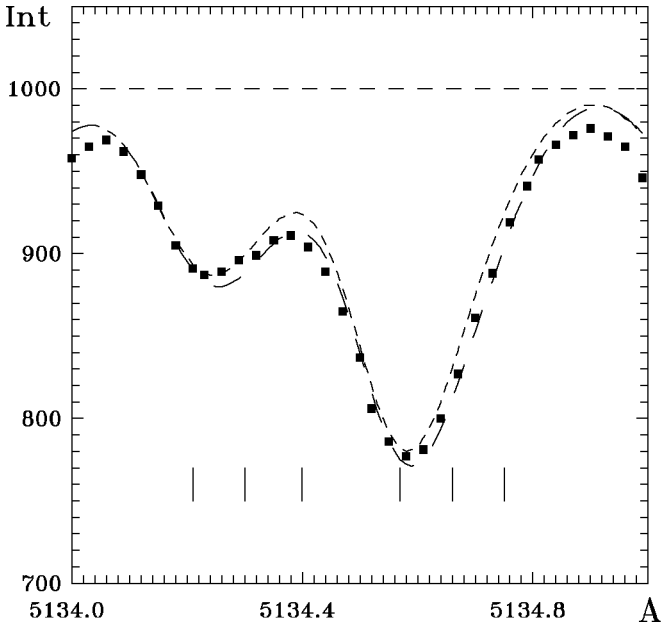

Figure 1: BS 168. Fitting of the observed spectrum (squares) with a synthetic spectrum computed with ^{24}Mg:^{25}Mg:^{26}Mg=79:10:11 (long dashed line) and 70:15:15 (short dashed line)

ponents are seen as red asymmetries on line.

We stress here the importance of the fact that the isotope ratios are rather independent of a precise model atmosphere. Effective temperatures $T_{\rm eff}$, surface gravities logg and metallicities [Fe/H] for the program stars were derived using various methods (in particular, we applied the new method developed by Komarov et al. (1996)).

Table 1: The program stars, atmospheric parameters and isotopic abundances.

Name	BS	Teff	logg	[Fe/H]	Abund.
δ And	165	4640	1.8	0.22	68:11:21
α Cas	168	4950	2.6	0.24	72:14:14
β Gem	2990	4970	2.6	-0.09	84:8:8
α Lyn	3705	3860	1.2	-0.29	74:13:13
α UMa	4301	4940	2.6	-0.05	82:9:9
ϵ Vir	4932	5100	2.8	-0.08	88:6:6

The model atmospheres are obtained by interpolation in the grids by Kurucz (1992). We adopted V_t = 2.0 km/s. The carbon abundances were obtained from a fitting to the unblended 5135.6 $C_2(0,0)$ feature.

For all giants, the profile of the MgH lines are calculated for the different isotopic compositions (the terrestrial composition is presently considered to be 78.99:10.00:11.01 (Lambert & McWilliams, 1986))

The list of stars, together with basic stellar parameters and the isotopic abundances are given in Table 1.

3. Conclusion

The isotopic stellar and terrestrial abundances appear to be very similar in all giants belonging to the thin disk. Perhaps, a two giants (BS 165, 168) of the sample show ^{25,26}Mg isotopes in proportions higher than terrestrial. This might be explained by a mixing with helium shell burning material.

References

Barbuy B.: 1985, *As. Ap.* **151**, 189.
Barbuy B.: 1987, *As. Ap.* **172**, 251.
Bonnell J.T., Bell R.A.: 1993, *MNRAS*, **264**, 334.
Komarov N.S., Korotina L.V., Shevchuk T.V.: 1996, *Kinem. i Fizika Nebesnykh Tel*, **12**, 1.
Kurucz R.L.: 1992, *The Stellar Populations of Galaxies, B. Barbuy, A. Renzini (eds.), IAU Symp.* **149**, 225.
Lambert D.L., McWilliam A.: 1986, *Ap. J.*, **304**, 436.
McWillim A., Lambert D.L: 1988, *MNRAS*, **230**, 573.
Tomkin J., Lambert D.L.: 1976, *Ap. J.*, **208**, 436.
Tomkin J., Lambert D.L.: 1980, *Ap. J.*, **235**, 925.
Tsymbal V.V.: 1994, *Odessa Astron. Publ.*, **7**, 146.
Tsymbal V.V.: 1995, *ASP Conference Ser.*, **108**, 198.
Wallace L., Hinkle K., Li G., Bernath.: 1999, *Ap. J.*, **524**, 454.

OBSERVATIONS OF TYPICAL, RARE AND UNIQUE PHENOMENA IN CLOSE BINARIES WITH EXTREMAL MASS RATIO

Yu.G. Kuznetsova[1], E.P. Pavlenko[2], L.M. Sharipova[2], S.Yu. Shugarov[3]

[1] Kiev National University, Ukraine

[2] Crimean Astrophysical Observatory
p/o Nauchny, Crimea 270014 Ukraine, *pavlenko@crao.crimea.ua*

[3] Sternberg State Astronomical Institute, Moscow, Russia

ABSTRACT. We present the review of different properties of several close binary systems, based on our observations. These binaries are as follow: SU UMa type stars V503 Cyg and V1504 Cyg, X-Ray novae V518 Per and V404 Cyg. They have the extremal mass ratio of the primary component to the secondary $M_1/M_2 > 3$. Some of them show the typical for the SU UMa type stars behaviour, so-called the "positive superhumps" or more rare "negative superhumps". Another display the "forbidden" variability in the ordinary outbursts or the light variation of unknown yet nature.

Key words: Stars: binary: cataclysmic, X-ray novae; stars: individual: V518 Per, V404 Cyg, V503 Cyg, V1504 Cyg.

1. Introduction

25 years ago some phenomenon - the "superhump" phenomenon - was discovered in a long, or superoutburst of the SU UMa dwarf nova VW Hui (Vogt 1974, Warner 1975). Superhumps are periodic light modulations appearing soon after maximum light of the superoutburst, not in the ordinary outburst (the last occure more frequently and have the shorter duration in respect to the superoutburst). Their periods (P_sh) are between 1 and 7 per cent longer then the binary orbital period (P_orb). At the start of superoutburst they have the highest amplitude (sometimes up to $0^m.5$), decaying on a time-scale of a week. The nonsinosoidal puls shape becoming increasingly sinusoidal as the amplitude declines. Accordingly the accepted models (Whitehurst 1998, Hirose and Osaki (1990), Whiterhurst and King (1991), Lubow (1991a,b, 1992), Osaki (1994)), an accretion disk expands to the "instability radius"- 3:1 resonance radius, transforms to an elliptical structure and slowly precess in the binary reference frame. Superhumps are generated by viscous dissipation due to the tidal stressing of the accretion disk by the secondary with a period which is slightly longer than the orbital period due to the precession of the disk.

The model demands the extremal binary mass ratio $q = M_1/M_2$ to be larger than 3 for superhump appearence. So one could believe to see this phenomenon not only in the SU UMa type stars, but in all cataclysmic binaries with such mass ratio.

Besides of common or "positive" superhumps mantioned above (more than 50 targets) there are 11 systems which show more rare "negative" superhumps (Patterson, 1998) with $P_{sh} < P_{orb}$, perhaps, caused by the nodal precession of the accretion disk (Bonnet-Bidaud et al., 1985, Udalski, 1987).

2. Observations

Here we present the behaviour of four binaries - real or potential "superhumpers". They are: the SU UMa type stars V503 Cyg and V1504 Cyg, and X-Ray binaries V518 Per and V404 Cyg. The observations were obtained by authors in Crimean astrophysical observatory (CrAO) and in Crimean laboratory of Sternberg astronomical institute (SAI). The journal of observations is given in the table. There the name of binary, year of observation, telescope and spectral band are given. MTM-500 means the 500-mm meniscus Maksutov telescope of the Crimean observatory (CrAO), equipped with the blue-sensitive TV system (Abramenko et al, 1998), K-380 and B-200 are the CrAO - SAI 380 mm

Table 1: The journal of observations

Binary	Date	Telescope	spectral band
	multicolumn caption		
V503 Cyg	1997	MTM-500	"BV"
V1504 Cyg	1997-99	MTM-500	"BV","RI"
		K-380	
		B-200	
V518 Per	1994	MTM-500	"BV"
V404 Cyg	1998	K-380	"RI"

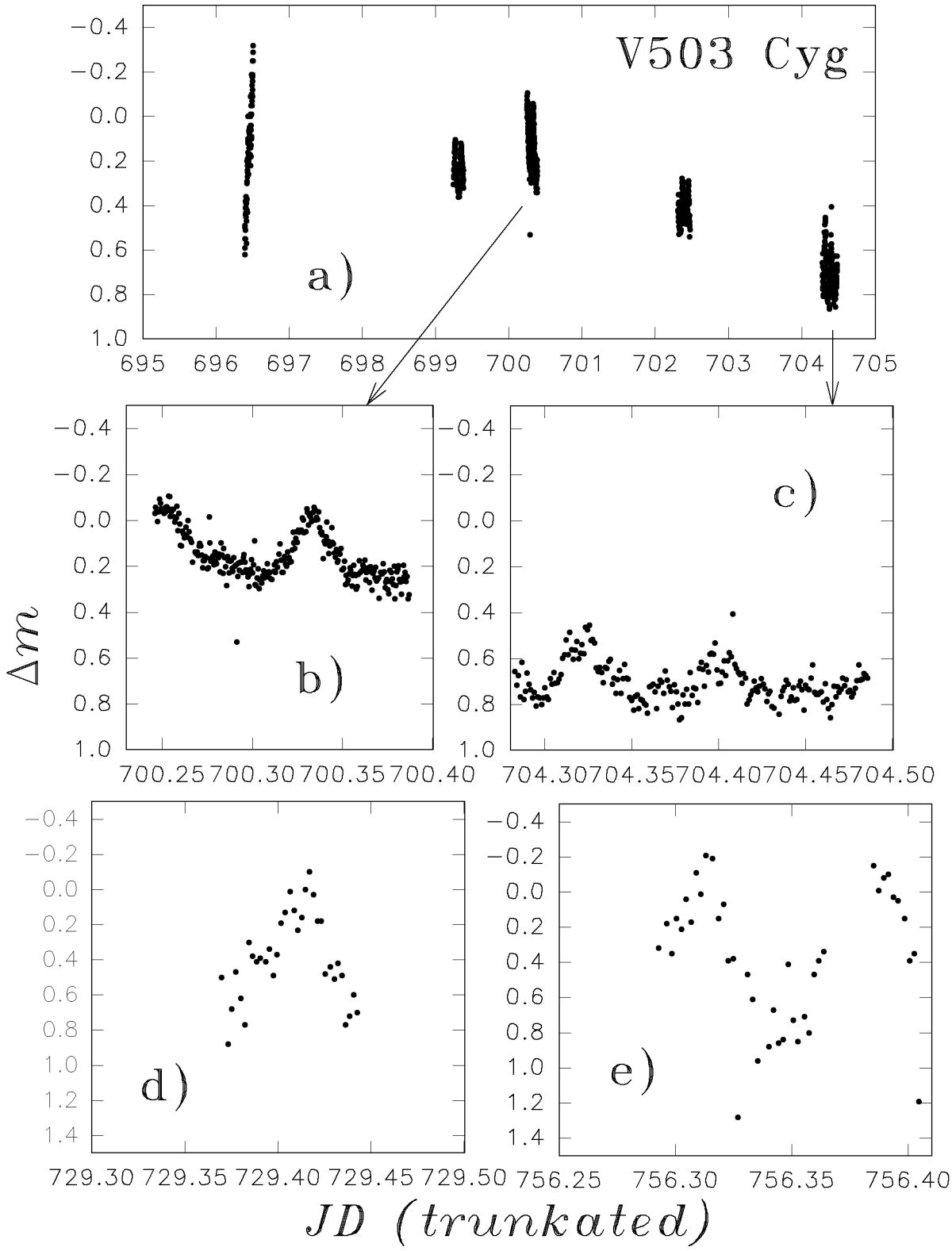

Figure 1: V503 Cyg in the superoutburst and low brightness state: a) the light curve of superoutburst; b) and c) the positive superhumps; d) and e) the nrgative superhumps. The brightness is given in respect to the comparison star. In the superoutburst and in the low state we used two different comparison stars.

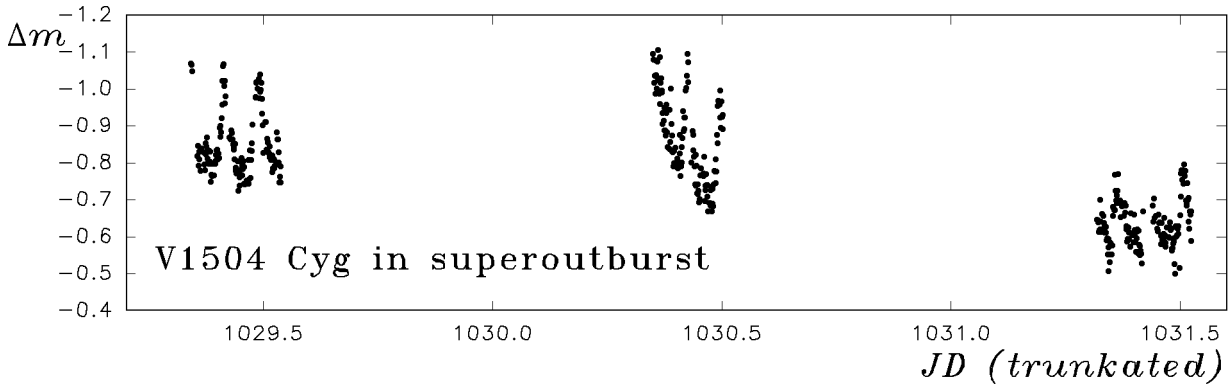

Figure 2: The light curve of V1504 Cyg in the superoutburst in 1998

and 200 mm telescopes respectively, equipped with the red-sensitive CCD ST-7. The TV - observations have been carried out in the broad spectral region including B and V standard band ("BV"), and the CCD - observations were made in the broad "RI" band.

3. SU UMa-type stars

3.1 V503 Cygni

We observed the V503 Cygni during 5 nights in superoutburst and two nights when the system was in the low brightness state. The superoutburst light curve is shown in the Fig.1,a. The star demonstrated the so-called common or positive superhumps (see Fig.1 b,c) with amplitude of $0^m.3$ and period of 117 min. In the minimum we observed another light periodicity - the "negative superhumps" with amplitude of 1^m (Fig.1 d,e). The behavior of V503 Cyg both in the superoutburst and low brightness state in detailes resembles to those studied by Harvey et al. (1995).

3.2 V1504 Cygni

We present the result of observations of V1504 Cygni in low brightness state, during ordinary outburst and during superoutburst. The superoutburst itself is performed in Fig.2. In superoutburst the star displays the light variations with $P_{sh} = 0.07d$ (Nogami, 19997). In ordinary outburst occured in July, 1998, we had observed light variations with $P = 2 * P_{sh}$. One night we made the simultaneous observations in "BV" and "IR" color bands and can't conclude that behaviour in blue and red spectral region is similar. The amplitude of light variation in "RI" band is at least two times less than in "BV" (Fig.3). Another ordinary outburst observed in September, 1998 in "RI" only, did not show any light modulations just as it is observed among the SU UMa stars.

Note that in minimum the star shown the light modulation close to the $1/2 * P_{orb}$ with variable amplitude Pavlenko et al., 2000).

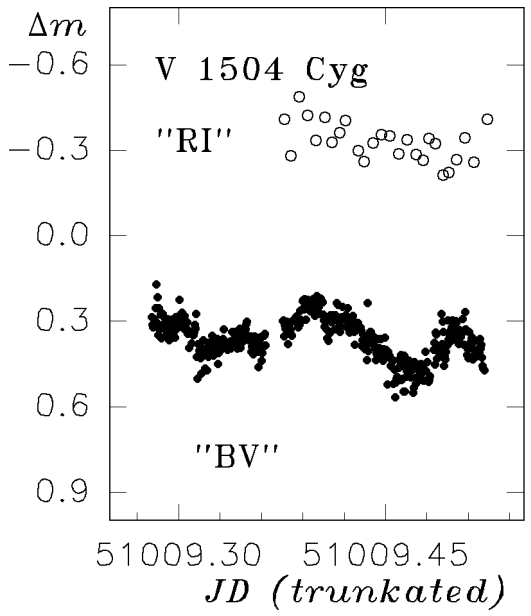

Figure 3: V1504 Cyg in the ordinary outburst.

4. X-Ray Novae

4.1 V518 Per

The long-term behaviour of the X-Ray nova V518 Per during the first two years after the outburst was similar to those of SU UMa type stars: after the long-lasted outburst (over 200 days) the star rapidly faded to the 20^m or less, and the next year erupted twice for a respectively short time (see the overall light curve in Shrader et al., 1995). It was the first X-Ray where the superhumps with $P_{sh} = 5.1h$ were detected by Kato et al.(1995) three months after superoutburst. The orbital period of the system was accurately established by Chevalier and Ilovaisky (1995). However this binary shows unexplained yet photometrical periods. Thus Martin et al. (1995) observed the star in minimum between the two otbursts and did not find any signs of orbital light variations. Instead he detected the $16.2-h$ periodicity.

We also observed this star during the 5 nights in the last mini-outburst occured in January 1994 (see Fig. 4), when the mean brightness of the binary was close to 18^m. The time series analysis yieled the most signigicant period of $5.4h$, but not $5.1h$ (see Pavlenko, Sharipova, 2000 for details)! The data, folded on this period are presented in Fig.4. Note that the $5.4h$ period is three times less of $16.2h$ period, so, probably, it is the harmonic of the unexplained periodicity mentioned above.

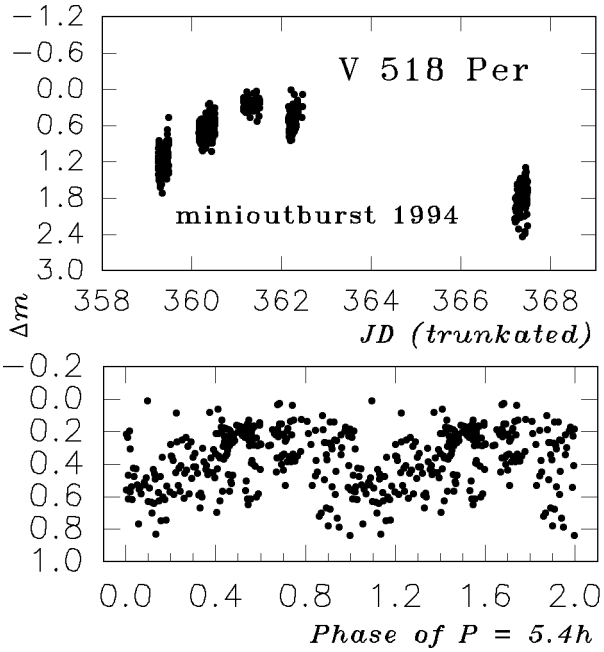

Figure 4: V518 Per during the last (1994 year) minioutburst: The overall light curve (top panel) and the data of one night (JD =...362), folded on the 5.4h period (low panel).

4.2 V404 Cyg

The orbital period of V404 Cyg is rather long among the X-ray novae ($6.47d$), so the superhumps period was not detected during the past outburst. However this binary shown another puzzling quasy-periodic strong light variations with typical time of 6 hours and amplitude up to $0^m.3$ (Pavlenko et al., 1996). The assumption was that the source of the 6-h modulation is localized in the accretion disc and connected with some non-stacionary accretion process. We observed V404 Cyg again in 1998 during subsequent 12 nights and found that the 6-hours variations, which existed for several years after outburst, to the end of decade significantly reduced its amplitude, or disappeared at all.

5. Conclusion

We summarised the different properties of the two dwarf novae and two X-ray novae with the high mass ratio ($M_1/M_2 > 3$) obtained from our observations. We could conclude that V503 Cyg recover its behaviour - the common superhumps in superoutburst and the negative superhumps in quiescent state from year to year. V1504 Cyg SOMETIMES shows "forbidden" light variations over the duration of the ordinary outburst at least in the "BV" spectral region with typical time of twice the superhump period. X-ray novae show the transient light variability of unknown nature.

References

Abramenko et al.: 1998, *Izv. Krim. Astroph. Obs.*, **78**, 182.
Bonnet-Bidaud J.M, et al.: 1985, *A&A*, **142**, 313.
Hirose M., Osaky Y.: 1990, *PASJ,* **42**, 135.
Kato T., Mineshige S., Hirata R.: 1995, *PASJ*, **47**, 31.
Lubow S.H.: 1991a, *Ap. J*, **381**, 259.
Lubow S.H.: 1991b, *Ap. J*, **381**, 268.
Lubow S.H.: 1992, *Ap. J*, **401**, 317.
Nogami D., Masuda S.: 1997, *IBVS*, **4532**
Osaki Y.: 1994, in Duschl W.J. et al., eds, *Theory of Accretion Disks II.* Kluwer, Dordrecht, 93.
Patterson J.: 1998, in press.
Pavlenko E.P., Martin A.C., Casares J. et al.: 1996, *MNRAS*, **281**, 1094.
Pavlenko E.P., Sharipova L.M.: 2000, *AZh*, in press
Pavlenko et al.: 2000, *As. Ap.*, in press
Shrader C.R., Wagner R.M., Hjellming, R.M. et al.:1994, *Ap.J.* **434**, 698.
Udalski A.: 1988, *AcA*, **36**, 369
Vogt N.: 1974, *A.J*, **36**, 368.
Warner B.: 1975, *MNRAS*, **170**, 219.
Whitehurst R.: 1988, *MNRAS*, **233**, 529.
Whitehurst R., King A.R.: 1991, *MNRAS*, **249**, 25.

TIME-DEPENDENT DISK ACCRETION IN BINARY SYSTEMS

G.V. Lipunova[1], N.I. Shakura[1,2]

[1] Sternberg Astronomical Institute, Moscow State University, Universitetskii pr. 13, Moscow, 119899 Russia *galja@sai.msu.su*

[2] Max-Planck-Institut für Astrophysik, Karl-Schwarzschild-Str. 1, 85740 Garching, Germany

ABSTRACT. The analytic investigation of time-dependent accretion in disk is carried out. We consider a disk in a binary system at outburst which has fixed tidally truncated outer radius. The standard model (Shakura–Sunyaev 1973) of the disk is considered. The fully analytic solutions in two different opacity regimes are characterized by power–law variations of accretion rate with time. The solutions supply asymptotic description of the disk evolution after the peak of outburst while the disk is fully ionized. The X-ray flux of multicolor (black-body) α-disk is obtained to vary quasi-exponentially. The application to X-ray novae is briefly discussed concerning observed faster-than-power decays of X-ray light curves. The case of time-dependent advective disk is mentioned.

Key words: Stars: binary: novae, cataclysmic variables; X-rays: bursts; stars: individual: A 0620-00

1. Introduction

The problem of time-dependent accretion is closely related to the phenomena of flares widely observed in binary systems. We consider emission of the flaring source to be generated by the accretion disk and the light curve to be regulated by the accretion rate variations. Such sources are typified by the low massive X-ray binaries and cataclysmic variables.

After Weizsäcker (1948) who considered the evolution of a protoplanetary cloud, the analytic investigations of non-stationary accretion were carried out by Lüst (1952), Lynden-Bell & Pringle (1974), Lyubarskii & Shakura (1987, hereafter LS87) as applied to accretion disks.

LS87 suggested three stages of evolution of a time-dependent accretion disk. Initially a finite torus of the increased density is formed around a gravitational centre. Viscosity causes the torus to spread and develop into the disk (1st stage). After disk approaching the centre the accretion rate reaches the maximum value (2nd stage) and begins to descend (3rd stage). During this stage the total angular momentum of the disk is conserved.

In a binary system variations of accretion rate can be due to the non-stationary exchange of mass between the components of the binary (mass–overflow instability model) or due to the disk instability processes (see Kato et al. 1998 and references therein). At some instant the accretion rate onto the centre begins to augment. We assume that the maximum accretion rate through the inner boundary of the disk corresponds to a peak of outburst and accretion rate decreases afterwards. In a binary system the third stage of LS87 cannot be realized, because the accretion disk around a primary would be confined by the gravitational influence of a secondary. Such disks do not preserve their angular momentum, transferring it to the orbital motion.

In this paper, which is an extension of our previous work (Lipunova & Shakura 1999), we outline the main features of time-dependent accretion in a binary system and make the first step at applying our model to X-ray nova A0620-00 flare of 1975.

2. Basic non–stationary accretion disks equation

In the approximation of Newtonian potential the velocity of a free particle orbiting at r is assumed to be a Kepler one. This is a good approximation to the law of motion for particles in the standard under–Eddington disk, whereas in the advection–dominated accretion flow (ADAF) the particles are substantially subjected to the radial gradient of pressure. The time–independent angular velocity is assumed, although there can possibly be certain variations of ω in the non-Keplerian advective disks, when time–dependent pressure gradient is involved.

Then the basic equation of time–dependent accretion is given by:

$$\frac{\partial \Sigma_{\rm o}}{\partial t} = \frac{1}{2}\,\frac{(GM)^2}{h^3}\,\frac{\partial}{\partial h}\left(\left[\frac{\partial h_*}{\partial h}\right]^{-1}\frac{\partial F}{\partial h}\right)\,, \qquad (1)$$

where Σ_o is the surface density, $F = W_{r\varphi} r^2$, $W_{r\varphi}$ being the height–integrated viscous shear stresses between adjacent layers, h and h_* are the Keplerian and the real specific angular momenta, t is the time, M is the central mass. In the case of the Keplerian disk $\partial h_*/\partial h = 1$.

3. Viscous evolution of Keplerian disk

To solve Eq. (**??**) one needs to know the relation between F and Σ_o. The special case when $F \propto \Sigma_o h^l$ was investigated by Lynden-Bell & Pringle (1974). We use the needed relation in a form

$$\Sigma_o = \frac{(GM)^2 F^{1-m}(h,t)}{2(1-m) D h^{3-n}} \qquad (2)$$

(see also Filipov 1984), suggested by LS87 for α-disks. Then, seeking the solution in the form $F(h,t) = F(t)f(\xi)$, the time–dependent part of the solution is turned to be

$$F(t) = \left(\frac{h_o^{n+2}}{\lambda m D (t+t_0)} \right)^{1/m} \qquad (3)$$

and accretion rate is:

$$\dot{M}(h,t) = 2\pi f'(h/h_o) F(t)/h_o \ , \qquad (4)$$

where D is the constant defined by the vertical structure of the disk, $\xi = h/h_o$, $h_o = (GMr_{out})^{1/2}$, t_0 and λ are to be defined from the initial and boundary conditions, respectively; m and n are the dimensionless constant depending of the specific opacity (see Table 1). We calculated D (Lipunova & Shakura 1999) adopting the results of Ketsaris and Shakura (1998).

In a binary system the accretion picture has particular features. The main feature is the limitation of the outer radius due to tidal interactions. As Ichikawa and Osaki (1994) showed the tidal effects are generally small in the accretion disk, except near to the tidal truncation radius, which is given by the last non-intersecting periodic particle orbit in the disk (Paczyński 1977). We consider the size of the disk to be maximum and invariant over the period of outburst. As the drain of angular momentum occurs in a narrow region near this truncation radius (Ichikawa, Osaki 1994), we treat the region near this radius as the δ-type channel, not considering the details of the process. The derived $f(\xi)$ is shown in Fig. **??**. Let us notice that (**??**) implies a considerably *steeper* time dependence than the solution by LS87 does.

Table 1: Short list of parameters in solutions for two opacity regimes for the Keplerian disk.

		m	n	λ
Thomson scattering:	$_T \gg _{ff}$	2/5	6/5	−3.482
Free-free transitions:	$_{ff} \gg _T$	3/10	4/5	−3.137

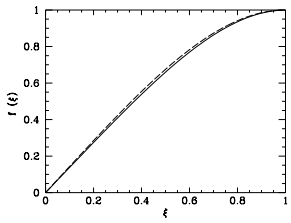

Figure 1: The solution $f(\xi)$ in two cases: when $_T \gg _{ff}$ (solid line) and $_{ff} \gg _T$ (dashed line).

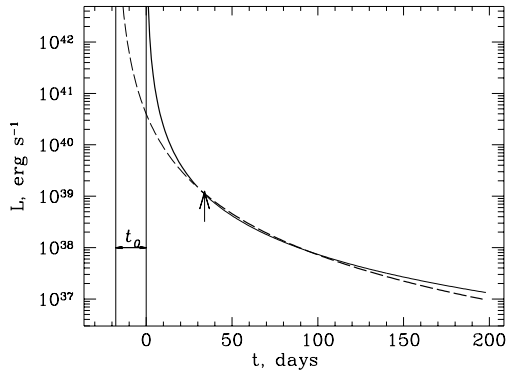

Figure 2: The bolometric luminosity in Thomson opacity regime (solid line) and in the free–free opacity regime (dashed line). Their bold parts represent the resulting light curve of the disk. The arrow marks one of two intersections when $F_1(h,t) = F_2(h, t+t_0)$.

4. Bolometric light curve of time-dependent Keplerian disk

For the most luminous, inner, parts of the disk we take $\dot{M}(t) = \dot{M}(0,t)$ given by (**??**). The overall emission of the disk is defined by the gravitational energy release $L = \eta \dot{M}(t) c^2$, where η is the efficiency of the process. At early t, when the Thomson scattering is dominant, the bolometric luminosity of the disk varies as follows:

$$L_T(t) \propto t^{-5/2} . \qquad (5)$$

As the temperature decreases, the law of decline switches to:

$$L_{ff}(t) \propto (t+t_0)^{-10/3} . \qquad (6)$$

These dependencies give asymptotic laws for *bolometric* luminosity variations of the disk. Transfer between the opacity regimes occurs when the solutions in two regimes sew at the half disk radius. This moment corresponds to:

$$t = t_{tr} \approx 0.52\, t_E \left(m_x (R_\odot/r_{out})^3 (0.1/\eta)^2 (0.5/\mu)\right)^{1/5} ,$$

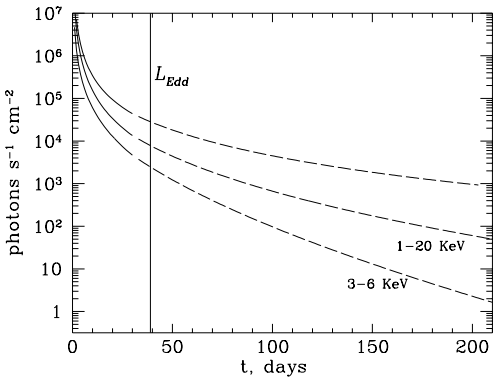

Figure 3: The flux from one side of accretion disk at 1 kpc. The curves show the bolometric flux (upper curve), the 1–20 KeV flux (middle curve) and the 3–6 KeV flux (lower curve) during the Thomson opacity regime (solid parts) and the free–free opacity regime (dashed parts).

where $m_{\rm x} = M/M_\odot$, $t_{\rm E}$ is the time, when $L = L_{\rm Edd} \approx 1.3 \times 10^{38} m_{\rm x}$ erg s^{-1}. Generally speaking, the solution before $t_{\rm E}$ appears to have no application. Yet recall that the Eddington limit is uncertain since a disk has non-spherical geometry.

Fig. **??** represents the bolometric light curve of the disk for $m_{\rm x} = 3$, $\alpha = 0.3$, $\mu = 0.5$, $r_{\rm out} = R_\odot$. For these parameters $t_{\rm tr} \approx 34^{\rm d}$ (the vertical arrow) and $t_0 \approx 17^{\rm d}$. The second intersection of the curves in Fig. **??** at $t \approx 95^{\rm d}$ corresponds to the other intersection of functions $F_1(h,t) = F_2(h, t+t_0)$, meanwhile the physical parameters of the disk are different. Thus the disk is at the same (free-free) opacity regime as before.

When $T_{\rm c}$ decreases to the value $\sim 10^4$ K, the convection (which is presumably appeared in the zones of partial ionization) starts to influence greatly on the disk's structure and the diffusive type of radiation transfer (which we use) is no longer valid. For $m_{\rm x} = 3$ and $\alpha = 0.3$ this happens at $t \approx 190$ days. For investigation of the disk evolution on larger time-scales see e.g. Cannizzo et al. (1995), Cannizzo (1998), Kim et al. (1999).

We remark that the observed X-ray light curves can have *different* (most probably, steeper) law of decay. Indeed, energy band of an X-ray detector usually covers the region harder 1 KeV where the multi–color photon spectrum of the disk (having appropriate temperature) can have specific distribution. The narrower the observed band the more different observed curve could look like in comparison with the expected bolometric flux light curve.

5. Observed light curves

Explaining the observed faster-than-power decay of outbursts in soft X-ray transients one must take into account that the observed slope of the curve depends on width and location of the observing interval. Of course, in each particular case this difference also reflects the spectral distribution of energy coming from the source.

We show here how the slope of the curve changes in the simplest case of multi-color black body disk spectrum according to which spectral range is observed. We calculate I_ν and integrate it over three energy ranges: 3-6 KeV, 1-20 KeV and that one in which practically all energy is emitted. Fig. **??** shows the photon flux variations in two X-ray energy ranges (those of *Ariel 5* and *EXOSAT* or *Ginga* observatories) and the bolometric flux variation, for the face-on disk at an arbitrary distance of 1 kpc. The vertical line marks the time after which bolometric luminosity of the disk's one side is less than $L_{\rm Edd}$.

One can see almost linear trend of the X-ray flux when bolometric luminosity is under the Eddington limit (to the right from the vertical line in Fig. **??**), especially in intervals of ~ 50 days. The decline becomes closer to the exponential one with time. The slope of the curve depends on α, m, $r_{\rm out}$ and other parameters. For the same parameters as in Fig. **??** the e-folding time falls in the range 20 – 30 days for the lower curve (3–6 KeV). For instance, smaller α will result in less steep decline.

The natural explanation of such result is the following: because the spectral shape of the disk emission has Wien-form (exponential fall-off) at the considered X-ray ranges the law of variation of X-ray flux is roughly proportional to $\exp\left(-h_{\rm P}\,\nu/k\,T^{\rm eff}(t)\right)$. In the free-free regime of opacity we have $T^{\rm eff}(t) \propto L_{\rm ff}^{1/4}(t) \propto \dot{M}(t)^{1/4} \propto t^{-10/12}$. Consequently, the observed X-ray flux varies like $\exp\left(-t^{5/6}\right)$ which is quite close to exponential behavior.

6. Discussion and conclusion

In this work, we presented the analytic solutions to time-dependent accretion in binary systems. For two opacity regimes the full analytic time-dependent solutions for Keplerian disk are obtained and *asymptotic* light curve is calculated with smooth transition between opacity regimes. During the decline phase accretion disks around black holes appear to be dominated by the free-free and free-bound opacity in order to comply with the Eddington limit on luminosity. This phase is characterized by the power-law decay of accretion rate $\propto t^{-10/3}$. It is shown that observed decay time scale depends on the real energetic band of detector (Fig. **??**).

The results obtained in this work can be applied to the accreting systems having variable emission of flare type if emission is essentially due to the fully ionized

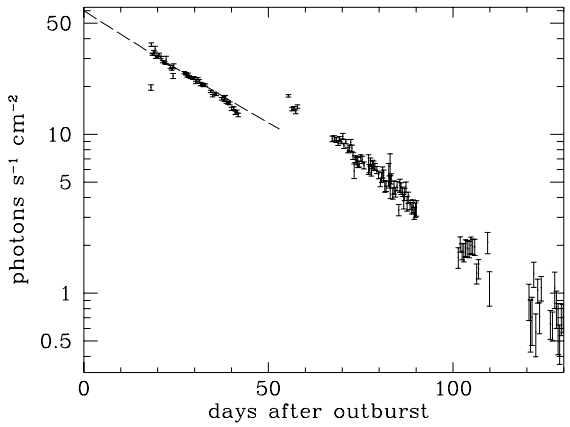

Figure 4: Comparison of the model (dashed line) with the *Ariel-5* A0620-00 (1975) 3–6 KeV light curve.

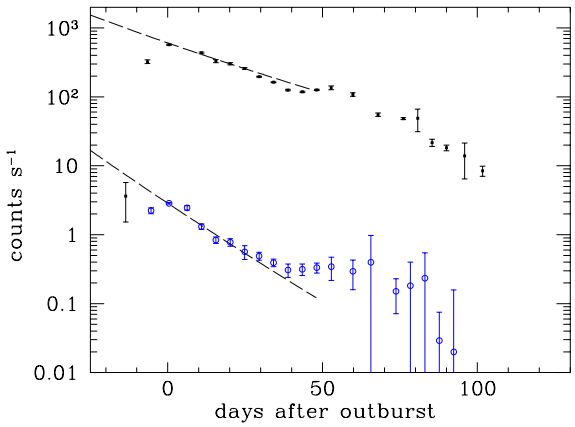

Figure 5: Comparison of the model (dashed lines) with the *Vela 5B* A0620-00 (1975) 3–12 KeV (dots) and 6–12 KeV light curves (open circles).

accretion disk around a black hole, or a neutron star, or a white dwarf.

Typical X-ray novae (XN) outburst light curves (see Tanaka & Shibazaki (1996), Chen at al. (1997) for the review) show quasi-exponential decay. Up to date several approaches have been used to account for XN features (see e.g. Mineshige et al., 1993; Cannizzo et al., 1995; King & Ritter, 1998) Using the results of this work we can explain the general features of XN light curves in the early phase. We show that nearly exponential X-ray decays $\propto \exp(-t^{5/6})$ appear taking into account the fact that the X-ray light curves are observed in the energetic range where the spectrum of the disk has Wien-form.

Figures **??** and **??** represent the comparison of the model for parameters $m_{\rm x} = 10$, $\alpha = 0.5$, $r_{\rm out} = 2.17 R_{\odot}$ with data[1] for XN A0620-00 observed in 1975 by *Ariel-5* and *Vela 5B*. The orbital inclination angle of the disk is taken 66°, the distance is 0.87 kpc (e.g. Tanaka & Shibazaki, 1996). The model parameters were fitted firstly to the *Ariel-5* light curve and then the *Vela 5B* data was applied. The presented model can explain the observations before ~ 50 day, and apparently fails after. This implies that some effects, yet ignored in presented scenario, becomes important. Some possibilities can be suggested: the disk becomes partly ionized (and convection presumably begins), an additional mass supply to the disk occurs, or the irradiation effects of the outer parts of the disk become significant.

If one adopts for the structure of advection-dominated accretion flow (ADAF) the self-similar solution (e.g. Narayan & Yi, 1995), it can be inferred (Lipunova & Shakura 1999) that such disks possibly exhibit the exponential with time behaviour in a binary system and are quickly depleted if α is not small. If this is the case the abrupt steep falls observed in several XN (Tanaka & Shibazaki 1996) in the last phase of the decay, at luminosity levels 10^{36} erg s^{-1}, can be interpreted in terms of quickly depleting ADAF with relevant values of $\alpha \sim 10^{-1}$.

Acknowledgements. This work is partially supported by the RFBR grant 98-02-16801 and the program 'Universitety Rossii' (N 5559) of the Ministry of Teaching and Professional Education.

[1]The data is obtained through the High Energy Astrophysics Science Archive Research Center Online Service, provided by the NASA/Goddard Space Flight Center

References

Cannizzo J.K., Chen W., Livio M.: 1995, *ApJ,* **454**, 880
Cannizzo J.K.: 1998, *ApJ,* **494**, 366
Chen W., Shrader C.R., Livio M.: 1997, *ApJ,* **491**, 312
Filipov L.G.: 1984, *Advances in Space Research,* **3**, 305
Ichikawa S., Osaki Y.: 1994, *PASJ,* **46**, 621
Kato S., Fukue J., Mineshige S.: 1998, *Black–hole Accretion Disks.* Kyoto University Press, Japan
Ketsaris N.A., Shakura N.I.: 1998, *Astronomical and Astrophysical Transactions,* **15**, 193
Kim S.-W., Wheeler J.C., Mineshige S.: 1999, *PASJ,* **51**, 1999
King A.R., Ritter H.: 1998, *MNRAS,* **, 293**, L42
Lipunova G.V., Shakura N.I.: 1999, *in press.*
Lüst R.: 1952, *Naturforsch,* **7a**, 87
Lynden-Bell D., Pringle J.E.: 1974, *MNRAS,* **168**, 603
Lyubarskii Yu.E., Shakura N.I.: 1987, *Soviet Astr. Letters,* **13**, 386
Mineshige S., Yamasaki T., Ishizaka C.: 1993, *PASJ,* **45**, 707
Narayan R., Yi I.: 1995, *ApJ,* **452**, 710
Paczyński B.: 1977, *ApJ,* **216**, 822
Shakura N.I., Sunyaev R.A.: 1973, *A&A,* **24**, 337
Tanaka Y.: Shibazaki N., 1996, *ARA&A,* **34**, 607
Weizsäcker C.F.: 1948, *Z. Naturforsch,* **3a**, 524

STRONG CHANGES OF THE PHOTOMETRIC BEHAVIOUR OF CARBON MIRAS

V.I. Marsakova

Department of Astronomy Odessa State University,
T.G.Shevchenko Park, Odessa 65014 Ukraine
e-mail: astro@paco.odessa.ua

ABSTRACT. Analysis of variations of the light curves parameters of 16 Miras of spectral classes C and S has been made. A number of the peculiarities of these variations has been found. One of the most interesting results is the detection of the mean brightness variations: they are cyclic (with a superperiod of about $10 \cdot P_0$ and not stable cycle length) or secularly decreasing.

Key words: Stars: pulsating variables: Mira stars: carbon stars: light curves; stars: individual: R And, T Cam, V Cnc, S Cas, W Cas, S Cep, V CrB, χ Cyg, R Cyg, U Cyg, T Gem. R Lep, R Lyn, Y Per, S UMa.

1. Introduction

Strong irregularities in the photometric behaviour of carbon Miras were pointed out by many authors (e.g. Alksne et al., 1983)

Changes of the individual cycles characteristics (of carbon long-period variables) are also discussed by Mattei & Foster (1998), correlations between them and the characteristics of mean light curves (of long periodic stars) were studied by Harrington (1965) and Fruchter (1976).

The star S Cep was discussed separately (Marsakova, 1999) and it may be a prototype of the stars with strong quasiperiodic variations of the mean brightness. Isles & Saw (1989) noted the presence of correlation between the magnitudes of different points of cycle and variations of the mean brightness with a cycle length about 6000-9000 days. In the work by Marsakova (1999) was found the cyclicity of 1500-4000 days. But there are gaps in the middle of the observational interval and some cycles are lost. So the value 6000^d given by Isles & Saw (1989) may be an upper limit of the cycle length.

Changes of the mean brightness are probably a typical phenomena for C and S Miras and study of its variations character is an interesting problem.

Other problems related to the cycle-to-cycle changes of light curve parameters and correlations between them (typical for C and S stars) are discussed in this paper.

We have analyzed the variability of 16 Miras intensively observed by amateurs. There are 6 stars belonging to the spectral class C and 10 – to the spectral class S. Some of them belong to transitional types (MS, SC).

2. Methods of analysis

We have used the amateur observations from the AFOEV and VSOLJ databases (Schweitzer, 1998, Nogami, 1998) obtained during a 75-year interval to analyze the period changes and individual cycle characteristics variability of the stars.

The time series analysis was similar to that applied to U Her (Marsakova & Andronov, 1998a).

The mean phase light curves are fitted by using a trigonometrical polynomial fit. The statistically significant degree was determined by using the Fischer's criterion (Andronov, 1994).

Moments of extrema were determined by using a "running parabola" (RP) fit (Andronov, 1997), to avoid affect of humps on the shape of maxima.

Such values as the individual periods, amplitudes, mean brightness were calculated as two values in a cycle: periods are determined by using the moments of maxima and moments of minima, amplitudes of ascending and descending branches, mean brightness as the average between magnitude of maximum and magnitude of both (preceding and successive) minima.

To study long-term cyclicity of the variations of mean brightness, we have used the extension of the Morlet-type wavelet analysis for irregularly spaced data (Andronov, 1998).

To look for possible dependencies between characteristics of the individual cycles we have used the correlation analysis.

We take in consideration the correlations, for which the ratio of correlation coefficient (ρ) to its error estimate (σ_ρ) was more then 3.0. Here $\sigma_r^2 = (1-r^2)/(n-2)$ (e.g. Korn and Korn, 1961).

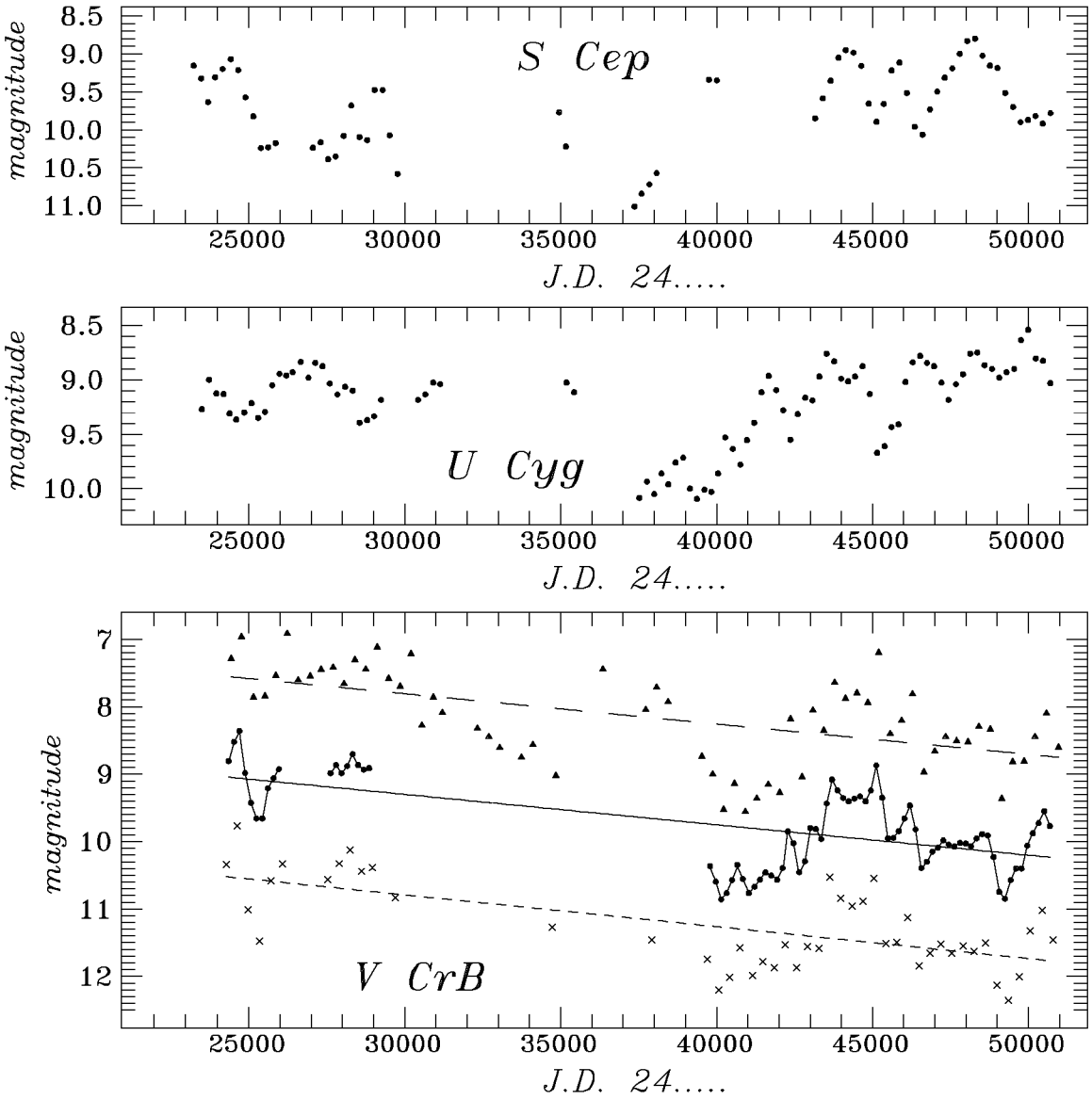

Fig. 1-4. Variations of mean brightness (points) or magnitude of maxima (triangles) and minima (crosses) for the some typical stars

3. Observational results

In the Table 1 the characteristics of 16 C and S Miras are listed. The periods and amplitudes are obtained by trigonometrical polynomial fits, spectral classes are listed according to GCVS (Kholopov et al., 1985). The types of variations of the mean brightness and some correlations obtained from our analysis and the quantities of the observed humps (relatively to the quantities of the observed maxima) are listed in the Table 2. The several periods correspond to the different peaks on the wavelet peiodogram. This swithing multiplicity appear because secondary cycles are unstable.

As the results of our research was found that photometric behaviour of C and S Miras (in the long time scale) show the following properties (in comparison with M-Miras (Marsakova & Andronov, 1997, 1998a):

- Strong chaotic cycle-to cycle changes of all parameters of the light curves;
- Absence of significant systematic changes of period or small abrupt changes of period ($< 0\overset{p}{.}5$) which is typical for other Miras (Marsakova & Andronov, 1997, 1998b);
- Absence of significant amplitude variations and that lead to:
- Correlation between magnitude of different points of the curves (especially typical for C-stars).

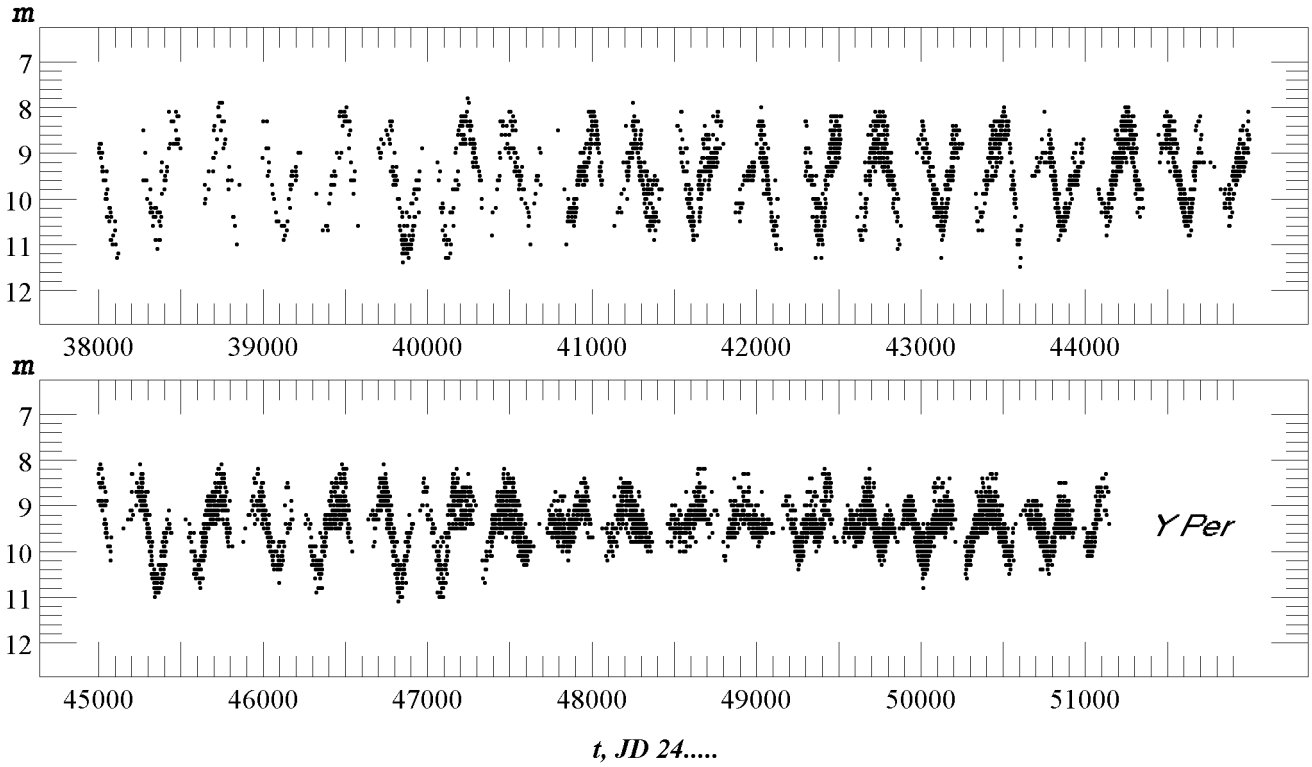

Fig. 5. Strong light curve changes in Y Per.

(*The parallel evolution* of magnitudes of maxima and minima in the Carbon LPVs was also found by (Mattei & Foster (1998));

- Light curves of C-stars are very noisy during one cycle;
- For the some (4) stars a correlation between period and amplitude was obtained ;
- For the some stars a correlation between time between maxima and corresponding magnitude differences was obtained (see discussion below);
- For 5 from 10 S-stars a correlations between period and magnitude in maximum was obtained;
- Strong variations of mean brightness:
  — cyclic: S Cep, U Cyg, V CrB, probably some other stars,
  — decreasing: V CrB, W Cas and probably T Cam, S Cas and V Cnc.

  Cyclic variations are more clear in C-stars. Trends appear in both groups (C and S) of stars.

  (Mattei & Foster (1998) also pointed out that in their sample *about half of the stars are getting fainter, especially in maximum, none shows a brightening*);
- In some stars there are some moments when the photometric behaviour changes abruptly.

  Y Per: at J.D. 2447700 the variability changes from the Mira to the semiregular with double maxima but with keeping the value of the mean period.

  S UMa: abrupt change of O-C behaviour appeared near J.D. 2430000 (change of the mean period and its stability) and simultaneously double maxima in the light curve appeared.
- Low amplitudes of C-Miras and high amplitudes of S-Miras are a well known facts (Alksne et al., 1983);

The shape of light curve and quantities and strength of the humps at the ascending branch do not depend on the spectral type. Similar humps also appear in some M-type stars. Correlation analysis with the hump characteristics have not been applied for all stars: the noised light curves and superimposing of the humps and maxima significantly hindered from this analysis. So it was applied for the 5 stars in this sample only. R Lyn shows a correlation between the magnitudes of minima and hump, χ Cyg – between the magnitudes of minima and hump, and S Cep – both these correlations. In the some M-Miras also appear humps at the ascending branch, but this problem needs a separate discussion.

In the case of faint minima it is impossible to calculate sufficient number of values of the amplitudes and mean brightness. So in R Cyg small correlation bet-

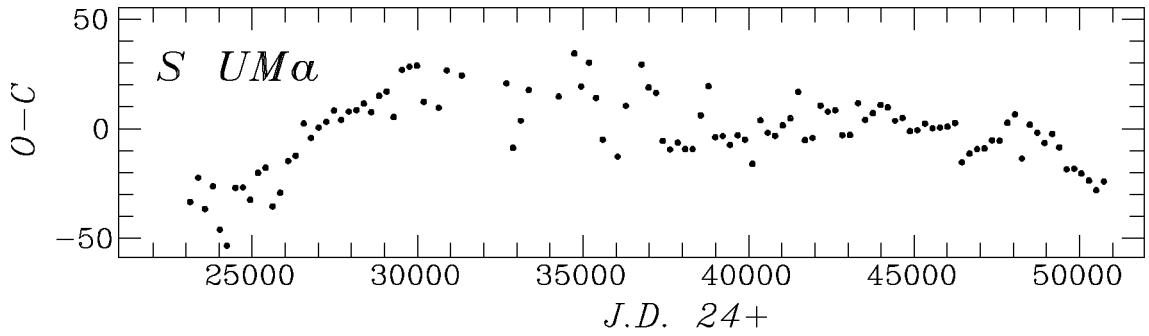

Fig. 6. O-C curve for S UMa.

Table 1. Mean light curve characteristics.

	Period	Amplitude	Asymmetry	Spectral Class	Relative quantity of humps
			C-Miras		
Y Per	248.60 ± 0.09	1.70 ± 0.05	0.40 ± 0.02	C4.3e	0.07
V CrB	358.08 ± 0.02	3.02 ± 0.03	0.39 ± 0.01	C6.2e	0.10
W Cas	405.42 ± 0.04	2.61 ± 0.02	0.490 ±0.006	C7e	0.30
R Lep	427.10 ± 0.09	1.44 ± 0.03	0.43 ± 0.02	C7e	0.19
U Cyg	465.56 ± 0.04	2.57 ± 0.02	0.48 ± 0.01	C7–C9	0.25
S Cep	487.35 ± 0.04	2.28 ± 0.02	0.552 ±0.005	C7.4e	0.57
			S-Miras		
S UMa	226.143±0.004	3.37 ± 0.01	0.506 ±0.005	S0e-S9e	0.70
V Cnc	272.100±0.008	4.85 ± 0.02	0.438 ±0.004	S0e-S7.9e	0.10
T Gem	287.21 ± 0.01	4.93 ± 0.05	0.505 ±0.007	S1.5e-S9.5e	0.36
T Cam	374.05 ± 0.01	4.51 ± 0.03	0.476 ±0.005	S4.7e-S8.5e C3.9E-C6.4E	0.68
R Lyn	378.61 ± 0.01	5.53 ± 0.03	0.441 ±0.004	S2.5e-S6.8e	0.33
W And	395.46 ± 0.01	7.61 ± 0.03	0.42 ± 0.01	S6.1e-S9.2e(M7e) M4-M10	0.25
χ Cyg	408.861± 0.008	7.75 ±0.008	0.447 ±0.004	S6.2e-S10.4e(MSe)	0.29
R And	410.28 ± 0.02	6.49 ± 0.04	0.482 ±0.001	S3.5e-S8.8e	0.06
R Cyg	428.15 ± 0.01	5.80 ± 0.03	0.421 ±0.004	S2.5e-S6.9e	0.07
S Cas	612.74 ± 0.06	4.84 ± 0.09	0.51 ±0.02	S3.4e-S5.8e	0.23

Table 2. Results of the light curves parameters variations and correlation analysis

	Variations of the meam brightness	Wavelet periods	Correlations coefficients between magnitudes of maximum and minimum	amplitude and period	magnitude of maximum and period	magnitude and time differences between successive maxima
			C-Miras			
Y Per	?		–	–	–	–
V CrB	3000-8000, trend	1140, 7180, 9430	0.89	0.58	–	–
W Cas	trend max.		0.60	0.75	–	–
R Lep	?		0.90	–	–	–
U Cyg	2000-7000	1460, 4080, 4860	0.54	–	–	–
S Cep	1500-6000	1600, 4070, 7540	0.70	–	–	–
			S-Miras			
S UMa	–		–	0.50	–	–
V Cnc	trend min?		–	–	–	–
T Gem	?		0.89	–	–	–
T Cam	trend max.		0.64	–	–	–
R Lyn	?		–	–	–	0.57
W And	?		–	0.57	-0.64	–
χ Cyg	?		–	0.54	-0.55	–
R And	?		–	–	-0.47	0.65
R Cyg	–		–	0.69	-0.56	0.69
S Cas	trend		0.89	–	–	0.61

ween period and magnitude of maxima is present but there is not correlation between the period and amplitude. This mechanism may explain also a trend of maximum magnitude without trend of mean brightness.

4. Discussion

Miras and semiregular behaviour of Y Per also was discussed by Kiss & Szatmary (1999). They have pointed out that there is a similar star R Dor which in the GCVS was classified as a semiregular variable. But it has intervals of regular and semiregular pulsations likewise Y Per (Bedding et al., 1998). These authors suggest a mode switching for both these stars.

Harrington (1965) and Fruchter (1967) pointed out a correlation between time between maxima and corresponding magnitude differences $(m_i - m_{i-1})$ that appear in some LPVs. Harrington (1965) wrote that *"such an effect may be explained if we postulate that the light changes of these stars are associated with the outward propagation of disturbances taking more or less time to reach the surface depending upon the energy they carry".*

In the our sample this correlation is present in four stars. Also in some stars an anticorrelation between $(m_i - m_{i-2})$ and time between two preceding maxima is present and in V CrB and V Cnc this correlation appears without the "usual" correlation between $(m_i - m_{i-1})$ and the time between *the same* maxima.

One of the most significant results concerns in the mean brightness variations. It is quite certain that many of carbon stars have dust envelopes (Wallerstein & Knapp G.R., 1998; Alksne et al., 1983 etc). So these cyclic variations of the mean brightness may be connected with irregularity in their density or opacity.

The secondary periods were found also by Fritzova et al. (1954) for Miras and long-periodic semiregular variables (2000-3000^d), by Wood (1999) for semiregular variables in the LMC (8-10 pulsating periods), Houk (1963), Alksnis et al. (1997) (Miras) etc. Rudnitskii et al. (1999) have found a superperiod of 15-16 yr. (13-15 pulsating periods) of H_2O maser emission of semiregular variable W Hya. Stothers & Leung (1971) have interpreted long secondary periods as the *convective turnover time giant convection cells in the stellar envelope.* One may suggest that similar maechanism is present in the majority of LPVs, but there are favourable conditions to see these secondary periods in carbon Miras and semiregular variables.

It is difficult to explain trends. As they are not followed by period trends so they cannot be an evolutionary effect. Probably they also connected with changes of the envelope properties.

Acknowledgements. Author is thankfull to I.L. Andronov and L.S. Kudashkina for helpfull discussions and to the members of AFOEV and VSOLJ for their visual observations.

References:

Alksne Z., Alksnis A., Dzervitis U.: 1983, *Properties of carbon stars of the Galaxy*, Riga, "Zinatne" Publishing House (in Russian).

Alksnis A., Larionov V.M., Larionova L.V.: 1997, *Baltic Astron.,* **6**, 377.

Andronov I.L.: 1994, *Odessa Astron. Publ.*, **7**, 49.

Andronov I.L.: 1997, *As. Ap. Suppl.*, **125**, 207.

Andronov I.L.: 1998, *Kinem. Fiz. Neb. Tel,* **14**, 490.

Bedding T.R., Zijistra A.A., Jones A., Foster G.: 1998, *Mon. Not. R. Astron. Soc.*, **301**, 1073.

Fritzová L., Pěkný L., Švestka Z.: 1954, *Bull. Astr. Inst. Czechosl.,* **5**, N 3, 49.

Fruchter C.A.: 1967, *Astron. J.,* **72**, 702.

Harrington J.P., 1965: *Astron. J.,* **70**, 569.

Isles J.E., Saw D.R.B.: 1989: *J. Brit. Astron. Assoc.,* **99**, 121.

Houk N.: 1963, *Astron J.,* **68**, 253.

Kiss L.L., Szatmary K. : 1999, *Proc. IAU Coll. 176 "The Impact of Large-Scale Surveys on Pulsating Star Research"*, in press.

Khopolov P.N. et al.: 1985, *General Catalogue of Variable Stars 4-th ed.*

Korn G.A., Korn T.M.: 1961, *Mathematical Handbook for Scientists and engneers,* McGraw-Hill Book Comp., New York, Toronto, London.

Marsakova V.I.: 1999, *J. AAVSO*, **27**, 141.

Marsakova V.I., Andronov I.L.: 1997, *Kinem. Phys. Cel. Bodies*, **13**, N 6, 49.

Marsakova V.I., Andronov I.L.: 1998a, *Ap. Space Sci.*, **257**, 49.

Marsakova V.I., Andronov I.L.: 1998, *Proc. 29th Conf. Variable Star Res.*, Brno, 130.

Mattei J.A., Foster G.: 1998, *Proc. of IAU Symp. 177, "Carbon star Phenomena", Kluwer Acad. Publ.*, in press.

Nogami D.: 1998, http://www.kusastro.kyoto-u.ac.jp

Rudnitskii G.M., Lekht E.E., Berulis I.I., 1999: *Astronomy Letters*, **25**, N 6, 398.

Schweitzer E.: 1998, ftp://cdsarc.u-strasbbg.fr/pub/afoev/

Stothers R., Leung K.-C.: 1971, *Astron. Astrophys.,* **10**, 290.

Wallerstein G., Knapp G.R.: 1998, *Annu. Rev. Astron. Astrophys.*, **36**, 369.

Wood P.R.: 1999, *Proc. IAU Coll. 176 "The Impact of Large-Scale Surveys on Pulsating Star Research"*, in press.

RELATIVISTIC STELLAR CLUSTERS

Marco Merafina

Department of Physics, University of Rome "La Sapienza"
P.le Aldo Moro, 5, I-00185 Rome Italy
e-mail: marco.merafina@roma1.infn.it

ABSTRACT. Star clusters with very high densities may play an important role in QSO and nuclei of galaxies. This role is strongly influenced by relativistic instability which can be reached at different critical densities under particular conditions (e.g. the formation of massive black holes in AGN's). On the other hand it exists the possibility to have stable relativistic clusters with arbitrarily large central redshift (and density). The equilibrium and stability of relativistic clusters described by a Maxwellian distribution function with a cutoff in phase space is discussed. The results are compared and contrasted with ones existing in literature.

Key words: Stellar dynamics; general relativity.

1. Introduction

The question of existence of relativistic clusters is open since the discovery of quasars: are the clusters so dense that relativistic corrections to Newtonian theory modify their structure and influence their evolution? Theoretical calculations suggest that clusters might form in the nuclei of some galaxies and quasars, and the formation of massive black holes in quasars and active galactic nuclei (AGNs) could be a result of a collapse of dense stellar clusters. Nevertheless astronomical observations have yielded no definitive evidence about the existence of relativistic clusters, even if, with HST observations, there is the possibility to resolve this issue completely.

The study of models of equilibrium describing relativistic clusters and the investigation of the stability against relativistic collapse of such dense systems were developed in two different papers by Bisnovatyi-Kogan *et al.* (1993, 1998). In these papers were introduced three different stability methods similar to the static criteria for stars. These methods have been applied to sequences of equilibrium models, with different cutoff parameters in the distribution function, which generalize the ones studied by Zel'dovich & Podurets in 1965. Different regions of dynamical stability were discovered at different values of temperature and central redshift extending the range of stable configurations up to very large central densities.

The investigation of the models with different cutoff parameters arises from the necessity to consider all kind of cutoff realized in the stellar clusters. For giant elliptical galaxies, with small rotation and absence of a disk subsystem, we may expect very extended central objects, corresponding to large values of energy cutoff. For AGNs in spiral galaxies, like SyG, the cutoff is probably produced by the tidal action of the spirals and depends on the spiral structure in regions close to the center; here we may expect very small values of energy cutoff.

Dense stellar clusters are essentially represented by massive globular clusters with $M \sim 10^6 M_\odot$, active galactic nuclei and quasars with $M \sim 10^8 - 10^{10} M_\odot$, respectively.

2. History

Starting from the classical paper of Einstein (1939) on relativistic clusters, where a system formed by gravitating masses with circular motion around the center of symmetry was studied, the equilibrium and the dynamical stability of these systems was first analysed by Zel'dovich & Podurets (1965). In this paper was shown that the contraction of an high-density stellar cluster caused by evaporation of star may lead to a loss of stability and cause a relativistic collapse.

In the successive years this problem was developed in several works by Thorne (1966), Fackerell (1968) and Ipser (1969) who introduced virial methods in order to improve the results on stability. In particular the results by Ipser indicated a critical value of central redshift $z_c \sim 0.5$ for which instability occurs. On the other hand, in 1969, Bisnovatyi-Kogan & Zel'dovich had shown the existence of stable configurations with arbitrarily large central redshift for a particular set of solution with density distribution $\rho \sim \beta/r^2$.

The investigation of equilibrium and dynamical stability of relativistic clusters was extended by Suffern & Fackerell in 1976 and systematically studied and generalized in recent papers by Bisnovatyi-Kogan *et al.* (1993, 1998). In these papers the problem was defi-

nitely solved by the analysis of the behaviour of binding energy in the z_c-T diagram of the equilibrium solutions with the extension of the region of dynamically stable configurations even at values of central redshift larger than 0.5; in particular the main result was the existence of stable configurations with arbitrarily large central redshift as indicated by Bisnovatyi-Kogan & Zel'dovich in 1969, for a particular set of solutions, and by Merafina & Ruffini in 1995 with the introduction of an explicit relation between a particular family of stable solutions and the results of the numerical simulations obtained by Rasio *et al.* in 1989 indicating stable models with large values of z_c.

From thermodynamical point of view the results on the stability are incomplete. The methods used for stability analysis give results generally accepted only in Newtonian regime with the well known paper of Lynden-Bell & Wood in 1968 about gravothermal instability and the ones of Katz (1978, 1980), while in relativistic regime the problem is still open.

The problem of gravothermal catastrophe goes back to Antonov theorems (1962) and becomes very popular with the paper of Lynden-Bell & Wood (1968) in which the term "gravothermal catastrophe" was coined. Antonov's discovery was that no state of locally maximal entropy exists for stellar sistems of given energy $E < 0$ and mass M within a spherical box of radius greater than $R = 0.335\ GM^2/(-E)$.

In Lynden-Bell and Wood paper the problem is analysed by studying the behaviour of a gaseous system confined in a spherical box with adiabatic walls. The gravitational equilibrium of the system is granted by the application of the virial theorem. Each particle of the system moves in the field generated by the other particles (mean field approximation). The result is that such a system has a negative total specific heat, with the core of the system with negative value and a *bath* surrounding the core with a positive value. Then, if we start with an isothermal equilibrium state and consider the effect of a perturbation which causes a flow of heat from an inner shell to an outer one, we have that this transfer from central regions will raise the temperature and the central density without limit inducing also the collapse of the core of the system. This phenomenon is the well known process called gravothermal catastrophe.

Clearly, gravothermal catastrophe is possible also in isothermal stellar systems where the equilibrium configurations are similar to gaseous spheres with equivalent velocity distribution. However, while in an isothermal gas gravothermal catastrophe develops by heat conduction with a timescale of the order of diffusion time (by collisions among the particles of the system), in a star cluster, due to stellar encounters, gravothermal catastrophe develops on a timescale of the order of the relaxation time. Globular clusters have a timelife larger than their relaxaton time and therefore gravothermal catastrophe may be realistic in the evolution of these systems.

3. Spherical models

In order to analyze the stability of stellar systems we consider the equilibrium of an isothermal relativistic sphere of particles (stars), of the same mass, with a distribution function fulfilling Boltzmann statistics. The energy of the stars is limited by a cutoff in phase space and the distribution function is given by

$$\begin{cases} f = A\exp(-E/T) & \text{for } E \le E_{cut} \\ f = 0 & \text{for } E > E_{cut}, \end{cases} \tag{1}$$

where $E_{cut} = mc^2 - \alpha T/2$ is the cutoff energy of the stars and T is the temperature "measured by an infinitely remote observer", in energy units, constant on each single equilibrium configuration. The parameter α is a constant for each configuration and can vary from 0 to 2.87. The upper limit on α is a condition on the existence of equilibrium solutions (see Bisnovatyi-Kogan *et al.*, 1998). For $\alpha = 1$ we recover the distribution considered by Zel'dovich & Podurets in 1965.

The equations of gravitational equilibrium for a spherically symmetric system described by the Schwarzschild metric $ds^2 = e^{\nu}c^2dt^2 - e^{\lambda}dr^2 - r^2(d\theta^2 + \sin^2 d\phi^2)$ are given by

$$\begin{cases} e^{-\lambda}\left(\frac{1}{r}\frac{d\nu}{dr} + \frac{1}{r^2}\right) - \frac{1}{r^2} = \frac{8\pi G}{c^4}P \quad \text{with } \nu(0) = \nu_0 \\ e^{-\nu}\left(\frac{1}{r}\frac{d\lambda}{dr} - \frac{1}{r^2}\right) + \frac{1}{r^2} = \frac{8\pi G}{c^4}\varepsilon \quad \text{with } \lambda(0) = 0, \end{cases} \tag{2}$$

where P is the pressure and $\varepsilon = \rho c^2$ is the energy density. The expressions of these thermodynamical quantities are easily obtained from the distribution function given in Eq. 1. We have

$$P = \frac{4\pi A}{3c^3 e^{\nu/2}} \int_{mc^2 e^{\nu/2}}^{mc^2 - \alpha T/2} e^{-E/T}(e^{-\nu}E^2 - m^2c^4)^{3/2} dE \tag{3}$$

and

$$\varepsilon = \frac{4\pi A}{c^3 e^{3\nu/2}} \int_{mc^2 e^{\nu/2}}^{mc^2 - \alpha T/2} e^{-E/T}\sqrt{e^{-\nu}E^2 - m^2c^4}\ E^2 dE. \tag{4}$$

We obtain different families of equilibrium solutions depending on three papameters: α, T and z_c (central gravitational redshift). If we consider the entire range of possible values of α, we can obtain equilibrium configurations characterized by estreme core-halo density profiles as well as more homogeneous configurations. The results of these integrations are summarized in Fig.1. In this diagram we plotted the central redshift z_c as a function of the temperature T. Along each sequence of equilibrium models α is constant and T varies until a maximum value and become constant for large

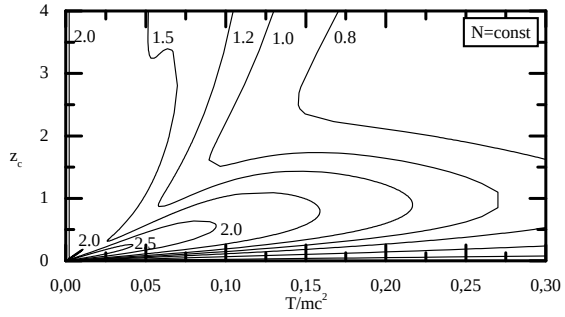

Figure 1: Sequences of equilibrium configurations with different values of α in the plane z_c-T.

z_c. For $\alpha = 1$ we obtain the solution of Zel'dovich & Podurets with the well known limit in the temperature $T/mc^2 = 0.227$.

The calculations have shown that equilibrium solutions exist only for values of $\alpha < 2.87$. It is also evident at small values of the temperature the α–curves deforme so that they become to consist of two separate branches: one looping in the origin ($z_c = 0$, $T = 0$) and one coming from. This fact is due to the behavior of the solutions in Newtonian regime where, for each value of α, more different equilibrium configurations may be.

4. Dynamical stability

Dynamical stability of isothermal configurations is studied since many years. Newtonian solutions are always stable against radial perturbations, being $df/dE < 0$ (Antonov, 1960). In relativistic regime the problem has been analysed by Ipser in 1969 and by Suffern & Fackerell in 1976 for configurations with sufficiently large values of the temperature T. The conclusions were that only configurations with redshift z_c smaller than 0.5 can be stable against radial perturbations. At low temperature regimes, the conclusions were uncertain, even if the possibility to have stable configurations with larger values of z_c was taken into account.

Now, for investigating the dynamical stability of dense stellar clusters with distribution function given by Eq. 1, we use three different approaches (Bisnovatyi-Kogan *et al.*, 1998).

1. Sequences of models with a fixed cutoff parameter, changing in accordance with the adiabatic condition $p_{cut} \sim n^{1/3}$.
2. Sequences of models with constant specific entropy.
3. Sequences of non-Maxwellian models, constructed from the condition of conservation of adiabatic invariant.

4.1. Sequences with a fixed cutoff parameter

The parameters

$$W_0 = \left(\frac{\epsilon_{cut}}{T_r}\right)_{r=0} \qquad \text{and} \qquad \beta = \frac{T_R}{mc^2}\ , \tag{5}$$

where $T_r = Te^{-\nu/2}$ is the local temperature varying along the cluster and $\epsilon_{cut} = (p_{cut}^2c^2 + m^2c^4)^{1/2} - mc^2 = Ee^{-\nu/2} - mc^2$ the kinetic energy cutoff, are connected with T and α by the following relations

$$\beta = \frac{T}{mc^2 - \alpha T/2} \tag{6}$$

and

$$W_0 = \frac{1 - e^{\nu(0)/2}}{T/mc^2} - \frac{\alpha}{2}\ . \tag{7}$$

The first of the sequences used for stability analysis is the sequence with constant W_0 and varying β. The parameter W_0 can be taken as approximately adiabatic. The equivalence of this stability criterion with the one suggested by Ipser in 1980 was definitely shown by Bisnovatyi-Kogan *et al.* in 1993 for models with $\alpha = 1$: this sequence near the critical point corresponds to the one relevant in the application of the Ipser's criterion. This correlation near the critical point keeps also at $\alpha \neq 1$ for models with $T/mc^2 > 1.5$ and leads to results in accordance with the ones given in literature.

4.2. Sequences with a fixed specific entropy

By introducing the expression of the entropy of a system with arbitrary distribution function

$$S = \iint f(1 - \ln f)\ d^3p\ d^3r\ , \tag{8}$$

we investigate the sequences with the fixed specific entropy S/N_0, where N_0 is the total number of stars. The expression of the specific entropy is

$$s \equiv \frac{S}{N_0} = [1 - \ln(A/A_*)] + \frac{\int_0^R e^{(\lambda+\nu)/2}\varepsilon r^2 dr}{T\int_0^R e^{\lambda/2} n r^2 dr}\ , \tag{9}$$

where A_* is an arbitrary constant along the sequence with the dimension of A.

4.3. Sequence with the conservation of the adiabatic invariant

The conservation of the adiabatic invariant $I = pn_c^{-1/3}$ (see Podurets, 1969) along the sequence of models implies the introduction of non-Maxwellian distribution functions

$$f = A\exp\left\{-\frac{e^{\nu/2}}{T_0}\left[p^2c^2\left(\frac{n_{c0}}{n_c}\right)^{2/3} + m^2c^4\right]^{1/2}\right\}\ , \tag{10}$$

with the cutoff parameters

$$p_{cut} = p_{cut0}\left(\frac{n_c}{n_{c0}}\right)^{1/3} = \frac{p_{cut0}}{\kappa}, \quad \kappa = \left(\frac{n_{c0}}{n_c}\right)^{1/3} . \tag{11}$$

The expression for p_{cut0} is determined from the cutoff relation of the initial Maxwellian model with $T = T_0$ and $\nu = \nu_0(r)$. We have

$$(p_{cut0}^2 c^2 + m^2 c^4)^{1/2}\, e^{\nu_0(r)/2} = mc^2 - \alpha T/2 \, . \tag{12}$$

The procedure of construction of approximate equilibrium models with non-Maxwellian distribution function is described in details in the paper of Bisnovatyi-Kogan *et al.* (1993).

By using the three static criteria of dynamical stability mentioned above, we can construct a curve dividing the equilibrium solutions in two separate regions (see Fig.2 below). The results are in accordance for each different criterion. We have stable solutions in the region at small central redshift (close to T–axis) and in the region at small temperature (close to z_c–axis). This line seems to have an asymptotic behavior for large values of T or z_c: in the regime of small central redshifts, investigated by Ipser in 1969, there are no stable solutions with $z_c > 0.4832$ for large T; for small temperature there are no stable solutions with $T/mc^2 > 0.06$ for large z_c. Therefore it exists a new region of stable solutions which extends at even large z_c up to infinite central densities, with temperature T/mc^2 less than 0.06. This stable equilibrium configurations present a regular center without singularities even for very large density. However there is a very sharp separation between core and envelope, the core being up to only 10^{-4} times the radius of the cluster ! The core is in gravitational equilibrium with the external region: there is no possibility of existence for a so dense core without the envelope which permits to the system to be stable as a whole. Moreover the value of the ratio $2GM/Rc^2$ is small and of the order of the ones relevant for Newtonian configurations.

5. Thermodynamical stability

The role of thermodynamical instability in dense stellar clusters is not clear. The results in relativistic regime existing in literature are not yet definitive. Nevertheless it is possible to analyse the thermodynamical stability by applying the *linear series method*, first introduced by Poincaré in 1885, to the sequences which are relevant for this kind of perturbations. In fact, if we consider sequences of equilibrium configurations for which some quantities (invariant during the perturbations) are constant, then the first maximum of binding energy in each sequence indicates the onset of instability. Sequences with N = constant and $f[E_{cut}(r = R)]$ = constant, are relevant for thermodynamical stability.

This criterion was erroneously applied to these particular sequences by Ipser in 1980, in order to obtain the onset of dynamical instability. However, the result was correct anyway because both the onsets of thermodynamical and dynamical instability coincide in the region where the criterion was applied ($z_c \sim 0.5$ and $T/mc^2 > 0.06$). In fact, in that particular region of plane z_c-T, the maximum of binding energy is the same both for sequences with constant W_0, relevant in the analysis of dynamical stability, and for sequences relevant in the analysis of termodynamical instability. The equivalence of these two stability criteria was evidenced by Bisnovatyi-Kogan *et al.* (1993) and is easily deducible from the behaviour of binding energy as function of redshift and temperature (see 3-D diagram of Fig.8 in Bisnovatyi-Kogan *et al.* 1998) and from the sequences at constant $f[E_{cut}(r = R)]$ and W_0. Differences are indeed evident for configurations with sufficiently low temperatures ($T/mc^2 < 0.06$), where the critical curves bifurcate (see below).

In Newtonian regime we recover results in complete accordance with the ones given by Lynden-Bell and by Katz. In relativistic regime the results are shown in Fig.2, where the curve of the onset of thermodynamical instability is compared with the one relevant for dynamical instability in the z_c-T diagram.

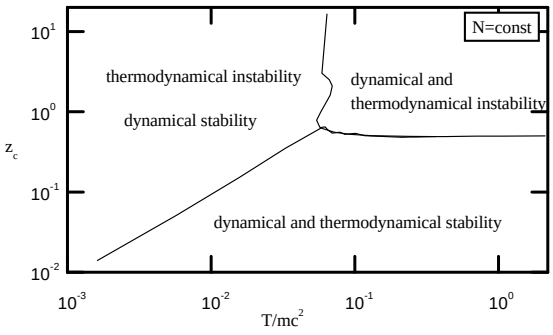

Figure 2: Dynamical and thermodynamical stability diagram in the plane N=const.

As preliminarily indicated, it is interesting to note that for $T/mc^2 > 0.06$ (large stars velocities) both curves coincide in correspondence to the well known critical value of central redshift $z_c \simeq 0.5$ obtained for dynamical instability. The two curves bifurcate for $T/mc^2 < 0.06$ (low stars velocities). The dynamical curve never reaches Newtonian regime and has an asymptotical behaviour towards a critical value of the temperature. All the configurations having a temperature lower than 0.06 mc^2 are dynamically stable for

arbitrarily large values of the central redshift. The thermodynamical curve, indeed, tends to Newtonian region and, for small values of the temperature coincides with the curve corresponding to the family of configurations with $W_0 = 7.6$ (in complete accordance with classical results). The parameter W_0 represents the gravitational potential expressed in terms of the local temperature (in energy units) at the center of the configuration. This parameter is connected with the main quantities by the relation

$$W_0 = \frac{mc^2}{T}\left(e^{\nu_R/2} - e^{\nu_0/2}\right). \qquad (13)$$

It is important to recall here some considerations about the evolution of a system which lost thermodynamical stability in consequence of collisions and evaporation of stars being still dynamically stable. Such a system begins to contract and heat his core, having central regions with negative specific heat (see Lynden-Bell & Wood 1968). This fact implies a motion in the z_c-T diagram towards the region of dynamical instability and the system will fatally cross the critical curve (vertical) at $T/mc^2 \simeq 0.06$, becoming dynamically unstable and leading to a faster collapse.

6. Conclusions

The results of the investigation on the stability against relativistic collapse of families of equilibrium configurations with different cutoff parameters can be summarized as follows (see Fig.2).

The region of the plane z_c-T with $T/mc^2 > 0.06$ corresponds to the traditional families of equilibrium configurations whose dynamical stability was largely investigated in the past. The three different criteria for investigating the stability give results in agreement among them and with the results of previous analysis (see, e.g., Ipser 1969). In this regime there are not stable configurations with z_c larger than 0.5. These results confirm this conclusion and are now obtained with more accuracy.

The region of the plane z_c-T with $T/mc^2 < 0.06$ corresponds to extreme core-halo configurations whose stability analysis carried out by Suffern & Fackerell (1976) did not supply conclusive results. In contrast with that conclusions the results show that these configurations are stable. The dense core is in gravitational equilibrium with a Newtonian envelope, which permits to the system to be stable as a whole. Thus we come to the interesting conclusion that *there exist stable non singular configurations with arbitrarily large central red-shift.*

It must be noted that the results of Ipser (1969) and Fackerell (1970), also reported by Suffern & Fackerell (1976), already indicated that models with small temperatures could be stable even for values of the central red-shift larger than 0.5 but only until a limiting value of z_c. Nevertheless the authors came to a different conclusion by considering the behaviour of the curve of the maxima of the fractional binding energy. Application of these criteria to the particular solution obtained by Bisnovatyi-Kogan & Zel'dovich (1969) has shown that it satisfies the necessary condition for the stability, but is unable to establish the sufficient condition (Bisnovatyi-Kogan & Thorne 1970).

The results on the thermodynamical stability show that the critical curve of onset of thermodynamical instability lies at smaller values of central redshift than ones concerning the dynamical curve. From this follows that *thermodynamic stability always implies dynamical stability.*

Furthermore, while dynamical instability is reachable only in relativistic regime, thermodynamical instability can occur also in Newtonian regime. Consequently, thermodynamical instability always drives the system towards dynamical collapse which occurs only in relativistic regime after a contraction and heating of core. Therefore, even if in principle it is possible to have systems dynamically stable with an arbitrarily large central redshift, the core contraction induced by thermodynamical instability will lead anyway to a dynamical collapse.

References

Antonov V.A.: 1960, *AZh*, **37**, 918.
Antonov V.A.: 1962, *Vest Leningrad Univ*, **7**, 135.
Bisnovatyi-Kogan G.S., Zel'dovich Ya.B.: 1969, *Astrofizika*, **5**, 223.
Bisnovatyi-Kogan G.S., Thorne K.S.: 1970, *ApJ*, **160**, 875.
Bisnovatyi-Kogan G.S., Merafina M., Ruffini R., Vesperini E.: 1993, *ApJ*, **414**, 187.
Bisnovatyi-Kogan G.S., Merafina M., Ruffini R., Vesperini E.: 1998, *ApJ*, **500**, 217.
Einstein A.: 1939, *Ann. Math.*, **40**, 922.
Fackerell E.D.: 1968, *ApJ*, **153**, 643.
Ipser J.R.: 1969, *ApJ*, **158**, 17.
Ipser J.R.: 1980, *ApJ*, **238**, 1101.
Katz J.: 1978, *MNRAS*, **183**, 765.
Katz J.: 1980, *MNRAS*, **190**, 497.
Lynden-Bell D., Wood R.: 1968, *MNRAS*, **138**, 495.
Merafina M., Ruffini R.: 1995, *ApJ Lett*, **454**, L89.
Podurets M.A.: 1969, *AZh*, **46**, 126.
Poincaré H.: 1885, *Acta Math.*, **7**, 259.
Rasio F.A., Shapiro S.L., Teukolsky S.A.: 1989, *ApJ Lett*, **336**, L63.
Suffern K.G., Fackerell E.D.: 1976, *ApJ*, **203**, 477.
Thorne K.S.: 1966, *ApJ*, **144**, 201.
Zel'dovich Ya.B., Podurets M.A.: 1965, *AZh*, **42**, 963.

THE EFFECTIVE TEMPERATURES OF K-GIANTS

T.V. Mishenina, V.V. Korsak

Department of Astronomy, Odessa State University
T.G.Shevchenko Park, Odessa 270014 Ukraine, *astro@paco.odessa.ua*

ABSTRACT. The spectral classification of stars based on the ratios of the line depth, which are sensible to the temperature changes. Such calibrations were used for various stars (Gray, 1994; Kovtyukh et at., 1998). From the high- resolution spectra of K-giants, we selected 15 pairs of atomic lines and we derived 15 analytical relations for the determination of effective temperature T_{eff}. Our calibrations were constructed for 5000 K $< T_{eff} <$ 4000 K and for [Fe/H] from 0 to -1 dex. The abundance dependence is taken from the synthetic spectral calculations by the Kurucz's (1993) models. We determine T_{eff} for Arcturus on the high resolution high dispersion spectra obtained at different times.

Key words: Stars: K-giants: temperature; stars: Arcturus.

1. Introduction

At present the high-dispersion CCD stellar spectra can be obtained with high (100 or more) signal-to-noise (S/N) ratios over a wide wavelength range. Thus, high-accuracy eguivalent widths can be used to analyze the chemical composition and other parameters of the stars. The observed spectra are well described by the methods developed to compute synthetic spectra, suggesting that the theoretical models in use today adequately represent real objects. Recently, fairly reliable sets of oscillator strengths have also appeared. Now, we can reach a qualitatively new level of reliability in analysing the chemical composition of the stars and K-giants, in particular. At the same time there is a problem of the definition of the reliable effective temperatures (T_{eff}). The existing methods of determining T_{eff} are based on the B-V and R-I colour indices of Johnson's system and other photometric systems; on a comparison of observed and synthetic Balmer-line profiles; on the condition of Boltzmann's equilibrium for FeI lines; and on spectrophotometric data. Recently, the method of infrared fluxes, which yields good results for some objects, has been developed. Since all these calibrations give errors up to 200-300 K, and the estimates obtained by different methods are commonly in disagreement with one another. In particular, the colour indices are very sensitive to the surface gravity $\log g$ and to the turbulent velocity V_t. Large errors are due to interstellar reddening; this allowance cannot always be made properly, especially for unique objects. The hydrogen- line profiles are affected by metallicity and by $\log g$ (for [Fe/H] = 0). A spectrophotometric analysis is possible only for sufficiently bright objects, the same is also true for the method of infrared fluxes. As a result, the temperature determination is ambiguous. At that, the knowledge of the precise temperatures is needed for abundance determination, and as well for locating stars in the H-R diagram, for studies of gravity and mass, and so on. Accordingly, determining reliable effective temperatures T_{eff}, in particular, for K-giants, becomes a problem of current importance. Uncertainties in T_{eff} are currently the main source of uncertainties in the chemical composition of K-giants. However, T_{eff} cannot be determined by using the existing methods with an accuracy higher than 150-200 K, which prompts us to search for new approaches to determine the temperatures.

One of them appears to have surfaced in recent years. Sasselov & Lester (1990) showed that the relative temperatures T_{eff} could be determined, in principle, with an accuracy of $\pm$ 30 K from the ratio of CI and SiI lines with widely differing excitation potentials in infrared region of the spectrum. Such calibrations, for the equivalent widths, have long been used for B stars (Kopylov, 1958). Gray (1989) have used the ratio of line depths for two spectral lines to determine stellar temperatures with a high precision for giants. Gray & Johanson (1991), Gray (1994) substantiated the validity of this technique for F-G dwarfs in visible region and noted that the relative temperatures could be determined by this method with high accuracy. Kovtyukh et al. (1998) carried out the determination of T_{eff} for F-G supergiants with an accuracy higher then 50-80 K from spectroscopic criteria. Our aim is to derive analytical relations for determining high-accuracy temperature from spectroscopic criteria in visible spectral range (5000-6700 Å) for K-giants.

2. The observations

To estimate the temperature scale, we used the high-dispersion spectra of K-giants (S/N > 100), obtained with an echelle spectrometer (Musaev, 1993) on the 1-m Special Astrophysical Observatory telescope and

Table 1. Parameters of the spectral lines used to determine T_{eff}

λ, Å	El.	EPL.	λ	El.	EPL.
6495.78	FeI	4.83	6498.95	FeI	0.95
6419.98	FeI	4.73	6349.48	VI	1.85
6378.26	NiI	4.15	6336.1	TiI	1.44
6244.47	SiI	5.61	6233.2	VI	0.27
6175.42	NiI	4.08	6177.26	NiI	1.82
6155.69	SiI	5.61	6224.51	VI	0.28
6106.6	SiI	5.61	6126.22	TiI	1.06
6086.29	NiI	4.26	6092.81	TiI	1.88
5805.23	NiI	4.16	5798.51	CrI	1.03
5772.14	SiI	5.08	5798.51	CrI	1.03
5666.68	SiI	5.61	5668.36	VI	1.08
5655.18	FeI	5.06	5668.36	VI	1.08
5646.61	SiI	4.93	5570.43	MoI	1.33
5398.29	FeI	4.44	5388.35	NiI	1.92
5398.29	FeI	4.44	5392.07	ScI	1.92

Table 2. Polynomial coefficients of the R-T_{eff} calibrations

a_0	a_1	a_2
2382.09	+ 4537.8	- 1770.5
3640.33	+ 359.627	- 23.3282
1575.00	+ 5920.31	- 2705.15
3090.39	+ 3162.83	- 1376.94
1047.75	+ 4233.5	- 798.029
2977.65	+ 12113.5	- 20551.7
3388.56	+ 5244.77	- 3764.43
2946.93	+ 1647.65	- 345.399
3657.57	+ 634.718	- 68.7818
3605.03	+ 748.523	- 105.681
3067.52	+ 3671.43	- 1835.13
2809.85	+ 2316.02	- 541.581
2769.62	+ 2252.7	- 604.371
585.114	+ 5081.71	- 1589.99
3357.59	+ 594.637	- 52.4096

on 1.52-m Haute Provence Observatory telescope (Soubiran et al., 1998). The mean spectral resolution is R=36,000 and 40,000, spectral range 4400-6800 and 4800-6700Å respectively. The spectral reduction was carried out by DECH20 code (Galazutdinov, 1992).

3. The method of temperature determination

To derive analytical relations for determining temperature T_{eff} from spectroscopic criteria we used the visible spectral range 5000-6700 Å . In the range, we studied all unblended Si, Ti, V, Cr, Fe, and Ni lines to check if they are suitable for decision of our task. Sheminova (1993) has shown, that weak metal lines with low excitation potentials are most sensitive to the temperature. We selected pairs of lines that satisfied the following criteria: 1) the excitation potentials of the lines must differ as much as possible; 2) the lines must be close, if possible, to eliminate errors in continuum placement; 3) since ionic lines are quite sensitive to $\log g$, they were excluded from the analysis; 4) we also chose pairs of lines of the same element (occasionally, widely separated) to eliminate a possible dependence of the temperature on abundance (in the case of highly anomalous chemical composition); 5) the lines must be weak enough to eliminate a possible dependence on V_t; 6) a spectral region with a large number of telluric lines was excluded from the analysis.

We chose 15 pairs from all the studied combinations of lines, which were sufficiently sensitive to variations in T_{eff} and have a low scattering of the derived temperatures. Tab. 1 gives the main parameters of our lines: wavelengths (λ), chemical elements, excitation potentials of the lower level (EPL.). The derived calibrations are given in tab. 2.The depth ratios R1 / R2 of the corresponding lines are denoted by R.

To calibrate temperature scale, we used K-giants with well-studied temperatures (Mishenina & Tsymbal, 1997; Haute Provence). Using sufficiently large number of criteria, we can determine T_{eff} by our method with an error no more than ± 50-80 K (depending on the number of used criteria, and the quality of spectra). As soon as high-precision temperatures T_{eff} will be available for giants, we will be able to convert our calibrations to the new scale by applying an additive correction to all relations.

4.The effective temperature of Arcturus

Arcturus (α Boo), Sp K1.5 III (Keenan & McNeil, 1989), is one of the brightest well studied late-type stars. Arcturus has well-determined parallax 0".092 ± 0".005 (Woolley et al.,1970) corresponding to distance of 10.8 ± 0.6 pc. Most of studies of Arcturus have included a determination of stellar effective temperature T_{eff}, a parameter whose accuracy is pivotal in meaningful derivations of chemical abundance and stellar mass. A well-studied star like Arcturus ought by now to be well enough modeled that it can constitute a reliable standard for assessing the quality of the different methods in use (spectral line analysis, classical model atmospheres), and for calculating systematic and random errors, both general to each method and specific to other stars.

Instead, the values of T_{eff} for Arcturus published to date cover a disconcertingly large range (Griffin, 1996), with evident consequences for determinations of the stars mass and the precise pattern of its chemical abundances (Trimble & Bell, 1981). A new value given by Dyck et al. (1996) has increased that range quite dramatically, and was in fact what drove us to examine this issue afresh, with a view to establishing the limits of T_{eff} that are achieved by combining classical models with the best available observational and

Table 3. Effective temperatures of α Boo

source	T_{eff}
this paper (1980)	4467
this paper (1993)	4424
this paper (1998)	4341
Martin(1977)	4300
Johnson et al.(1977)	4250
Blackwell & Shallis(1977)	4400
Blackwell et al.(1975)	4500
Mackle et al.(1975)	4260
Van Paraijs(1974)	4350
Gustafsson et al.(1974)	4030
Griffin & Lynas-Gray(1999)	4290

laboratory data. It has been known for over 30 years (Griffin, 1967) that Arcturus is a mildly metal-poor giants, its weak CN and CH, relative overabundance of light elements, and high space velocity earning it the designation "mild Population II". The atmospheric parameters derived by Peterson et al. (1993) from a thorough classical model-atmosphere analyses appear to represent the consensus of the results from modern spectroscopic analyses, so it was important to discover why the new program of Dyck et al.(1996) to measure the angular diameter of Arcturus and of other cool giants at infrared wavelengths should have produced a value of T_{eff} for Arcturus that was some 300K higher than that consensus.

We determined T_{eff} by our method for Arcturus on the high resolution high dispersion spectra obtained at different times. The R-T_{eff} calibrations were derived for solar metallicity and for Arcturus ([Fe/H] = -0.7) the abundance dependence was taken from the synthetic spectral calculations by the Kurucz's (1993) models. The calculation was made with the code STARSP (Tsymbal, 1994). The photographic spectrum of Arcturus (1980) was obtained on the first camera of 6m Special Astrophysical Observatory telescope by Panchuk V.E. in 1980. The CCD spectrum of Arcturus (1993) was obtained on the 1m Special Astrophysical Observatory telescope and the CCD spectrum of Arcturus (1998) was made on 1.52-m Haute Provence Observatory telescope. The temperatures of Arcturus determined by our method and other researcher are given in tab.3.

5. Conclusion

We selected 15 pairs of atomic lines and we derived 15 analytical relations for the determination of effective temperature T_{eff} on the high-resolution spectra of K-giants. The obtained R - T_{eff} relations make it possible to determine T_{eff} for K-giants with an accuracy higher than 100 K from the spectrum itself.

The derived temperatures of Arcturus on spectra, obtained at different times, are agree within the errors of determination.

Acknowledgements. The authors are thankful to Kovtyuh V.V. for useful discussions.

References

Blackwell D. E., Ellis R. S., Ibbetson P. A., Petford A. D., Willis R. B.: 1975, *Mon. Not. Roy. Astron. Soc.*, **171**, 425.

Blackwell D. E., Shallis M. J.: 1977, *Mon. Not. Roy. Astron. Soc.*, **180**, 177.

Dyck H.M., Benson C.A., van Belle J.T, Ridgway S.T.: 1996, *A. J.*, **111**, 1705.

Galazutdinov G.A.: 1992, *Preprint Spets. Astrof. Obs. Russian Acad. Sci.* N **92**.

Gray D.F.: 1989, *Ap. J.*, **347**, 1021.

Gray D.F., Johanson H.L.: 1991, *P. A. S. P.,* **103**, 439.

Gray D.F.: 1994, *P. A. S. P.,* **107**, 120.

Griffin R., Griffin R.: 1967, *Mon. Not. Roy. Astron. Soc.*, **137**, 253.

Griffin R.E.M.: 1996, *Observatory*, **116**, 404.

Griffin R.E.M., Lynas-Gray A.E.: 1999, *A. J.*, **117**, 2998.

Gustafsson B., Kjaergaard P., Andersen S.: 1974, *As. & Ap.*, **34**, 99.

Johnson H. R., Marenin I., Price S.: 1972, *J. Quant Spectrosc. And Rad. Transf.*, **12**, 189.

Keenan P.C., McNeil R.C.: 1989, *Ap. J. S.*, **71**, 245.

Kopylov I.M.: 1958,*Izv. Krymsk. Astrofiz. Obs.*, **20**, 156.

Kovtyukh V.V., Gorlova N.I., Klochkova V.G.: 1998, *Pis'ma v Astron. Zhurn.*, **24**, 438.

Kurucz R.L.: 1993, *CD ROM,*, **13**.

Martin P.: 1977, *As. & Ap.*, **61**, 591.

Mackle R., Griffin R., Holweger H.: 1975, *As. & Ap.*, **38**, 239.

Mishenina T.V., Tsymbal V.V.: 1997, *Pis'ma v Astron. Zhurn.*, **23**, 693.

Musaev F.A.: 1993, *Pis'ma v Astron. Zhurn.*, **19**, 776.

Peterson R., Dalle K., Kurucz R.: 1993, *Ap.J.*, **404**, 333.

Sasselov D.D., Lester J.B.: 1990, *Ap.J.*, **360**, 227.

Sheminova V.A.: 1993, *Kinemat. Fiz. Nebesnykh Tel.* **9**, 27.

Soubiran C., Katz D., Cayrel R.: 1998, *As. Ap. Suppl.*, **133**, 221.

Trimble V., Bell R.A.: 1981, *Q.J.R.A.S.*, **21**, 361.

Van Paradijis J., Meurs E.J.A.: 1974, *As. Ap.*, **35**, 225.

Wooley R., Epps E.A., Penzton M.J., Pocock S.B.: 1970, *Royal Observatory Annals.*, **5**, 1.

Tsymbal V.V.: 1994, *Odessa Astron. Publ.*, **7**, part 2, 146.

NUMERICAL SIMULATIONS OF BLACK HOLE ACCRETION

D. Molteni, V. Teresi, G. Gerardi, M.A. Valenza

Department of Physical and Astronomical Sciences, Palermo University
Via Archirafi, 36, Palermo, 90123 Italy

ABSTRACT. A resume of fruitful interaction between analytical and numerical approach to the subject of accretion disks around black holes is here presented. We review time dependent simulations of unviscous and moderately viscous accretion flows. Convection or pressure dominated flows admit subkeplerian solutions with or without shocks. The viscous adiabatic solutions, however, don't match smoothly to the keplerian disk solutions. We show also that many different type of mechanisms can trigger quasi periodic oscillations of the flow and consequently of the emitted radiation.

Key words: Accretion disks, shock waves; black holes

1. Introduction

Basic models of accretion disks assume a keplerian rotation of the flow of matter falling onto the compact astrophysical object (Pringle and Rees 1972, Shakura and Sunyaev 1973, Novikov and Thorne 1973). However, the structure of the flow, when the angular momentum is smaller than keplerian or when the advection and pressure term are required, is still far from being clear. Analytical solutions are difficult and often uncertain, due to *ad hoc* simplifications like: vertical equilibrium assuption, self similarity of the flow, neglecting of pressure and viscous terms, unappropriate boundary conditions and so on. Numerical solutions don't have general properties, but can verify the validity of the analytical solutions. Furthermore global stability studies of the analytical solutions are possible only by numerical simulations. They can even point to some new phenomenon as an *experimental* result. We will see some examples of this possibility. We will examine unviscous accretion flows and adiabatic viscous accretion solutions, comparing analytical steady solutions with time dependent numerical solutions obtained with different numerical algorithms. Section 2 describes the physical context and gives the relevant analytical equations to be solved. Section 3 gives the steady state solutions. Section 4 describes briefly the numerical methods. Section 5 resumes the more interesting results.

2. The physical scenario

Let us assume a viscous gas fall onto a black hole with an initial subkeplerian amount of angular momentum. This means that, apart the simple case of bremsstrhalung cooling, we assume there is no cooling in our gas. Despite this limitation, different regimes due to different values of the polytropic gas index $\gamma = c_p/c_v$ will appear. We have considered also the case of bremsstrahlung cooled gas, due to the possibility to make a simple treatment of the derived solutions and their relevant consequences. We assume that the gravitational forces are derived from the Paczyński Wiita potential. This is enough accurate to point out the main physical processes and to produce the relativistic behaviour of the flow, avoiding the complications of an exact general relativistic treatment. Exact relativistic steady state solutions for accretion onto Kerr black holes have been discussed by Chakrabarti (1996). The basic equations to be satisfied are the following ones: Assume axis symmetric case, i.e. $\frac{\partial}{\partial\phi} = 0$.
The mass conservation equation

$$\frac{D\rho}{Dt} = -\rho\nabla\mathbf{v}$$

The angular momentum equation is:

$$\rho\frac{Dv_\phi}{Dt} + \rho\frac{v_\phi v_r}{r} = \left[\frac{1}{r}\frac{\partial}{\partial r}\left(r\tau_{r\phi}\right) + \frac{\tau_{r\phi}}{r}\right] + \frac{\partial\tau_{\phi z}}{\partial z}$$

The energy equation

$$\frac{D\epsilon}{Dt} = -\frac{P}{\rho}\nabla\mathbf{v} + \frac{\Phi}{\rho} + \Lambda$$

where ϵ is the thermal energy per unit mass, Φ is the dissipation function, $\Lambda \sim \rho T^{0.5}$ the cooling function and other symbols have the usual gas dynamic meaning.

The expressions of the stresses will be specified in the subsequent discussion. These are the equations that will be integrated by time dependent codes.

3. Steady state solutions

Let us put the previous general time dependent equations in the typical steady state form:

Mass conservation requires

$$\dot{m} \propto r\rho v_r Z_{disk} = const$$

Radial momentum

$$v_r \frac{dv_r}{dr} = -\frac{1}{\rho}\frac{dP}{dr} - G\frac{M_*}{(r-r_g)^2} + \frac{\lambda^2}{r^3}$$

with λ the angular momentum per unit mass
Tangential momentum

$$\frac{\rho v_r}{r}\frac{d\lambda}{dr} = \frac{1}{r^2}\frac{\partial}{\partial r}\left(r^2\tau_{r\phi}\right)$$

Vertical momentum

$$Z_{disk} \approx \sqrt{\frac{2v_s^2}{\gamma\left(\frac{GM_*}{r}\right)}}\,(r-r_g)$$

Energy equation

$$v_r\frac{d\epsilon}{dr} = -\frac{P}{\rho}\frac{1}{r}\frac{d\left(rv_r\right)}{dr} + \frac{\Phi}{\rho}$$

Viscosity prescription

$$\tau_{r\phi} = -\alpha P$$

or

$$\tau_{\phi r} = \mu r\frac{\partial\Omega}{\partial r}$$

with μ the dynamic viscosity coefficient, $r_g = 2GM_*/c^2$ the Schwartzschild radius of the stellar object and gravitational forces derived by Paczyński Wiita potential $\Psi(r) = -GM_*/(r-r_g)$.

An interesting point, apparently unnoticed in the literature, is the fact that it is possible to have a constant energy property reformulating the energy equation in this way :

$$div\left[\rho\mathbf{v}\left(\frac{1}{2}\mathbf{v}^2 + \Psi(r) + h\right) - \mathbf{v}:\overleftrightarrow{\tau}\right] = 0$$

here h is the enthalpy function $h = \epsilon + \frac{P}{\rho}$. This energy equation, after insertion of the stress definition, even in its differential form, and using the mass conservation equation, in general gives the following relationship :

$$\frac{1}{2}v_r^2 - G\frac{M_*}{(r-r_g)} + \frac{a^2}{(\gamma-1)} - \frac{\lambda^2}{2r^2} + \frac{\lambda\lambda_e}{r^2} = \frac{const}{\dot{m}}$$

Here λ_e is the angular momentum at the inner edge of the disk, where the tangential stress vanishes. Above formulae constitute the typical set of equations to be solved to obtain the steady state solutions.

3.1 Unviscous cases

The unviscous case is simple to be solved, for a full account see Chakrabarti 1990. Essentially it is very similar to Bondi problem (Bondi, 1952). Let us resume the solution for the pure 1D flow.

Mass conservation gives:

$$\dot{m} = \rho r v = \rho r M a$$

M is the mach number, $\dot{m}$ is the accretion rate, ρ is the density, a is the sound speed.

Since the flow is unviscous the total energy is constant, the Bernoulli theorem is valid:

$$\frac{1}{2}v^2 + \frac{a^2}{(\gamma-1)} + \frac{\lambda^2}{2r^2} - G\frac{M_*}{(r-r_g)} = E$$

To solve the system we add the politropic relation valid only for isentropic flow.

$$\frac{\rho}{\rho_0} = \left(\frac{a}{a_0}\right)^{\frac{2}{(\gamma-1)}}$$

If we put together all terms we find:

$$\dot{m} = K\cdot f(M)\cdot A(E,\lambda,r)$$

with

$$f(M) = \frac{M}{\left(\frac{1}{2}M^2 + \frac{1}{(\gamma-1)}\right)^{\frac{\gamma+1}{2(\gamma-1)}}}$$

and

$$A(E,\lambda,r) = r\cdot\left[E - \Phi(\lambda,r)\right]^{\frac{\gamma+1}{2(\gamma-1)}}$$

Φ is function only of λ and r . This solution is valid for any isentropic branch, the constant $K = K(a_0,\rho_0)$ is related to the entropy value.

The f function has a maximum at $M = 1$, the A function has in general two relative minima.To small energy constant E values correspond smaller A values of the minimum at larger distances from the BH. The other relative minimum is related to the λ value: large λ produce smaller A values close to the BH. The $f\cdot A$ product must be constant along a flow. Therefore a minimum of A has to correspond to the maximum of f .

A flow connecting very large distances to the BH horizon has $M \ll 1$ for large r and $M \gg 1$ close to the horizon. As A approaches the outer minimum value $A_{out} = A_{\min}(r_{out})$ the mach number has to increase to $M = 1$,i.e. the solution has one sonic point at r_{out} ; so we may easily find this kind of solutions solving the implicit equation for M(r) with an iteration procedure or with any commercial equations solver :

$$f(1)\cdot A_{out} = f(M)\cdot A(E,\lambda,r)$$

Let us call this solution $M_1(r)$.

We may also say that, if it exists a transonic solution starting subsonically from some region and finishing

supersonically into the BH, it must have the same behavior of the previous solution. However now the sonic point has to correspond to the inner relative minimum of the A function $A_{inn} = A_{\min}(r_{inn})$; so this second solution come from this implicit equation:

$$f(1) \cdot A_{inn} = f(M) \cdot A(E, \lambda, r)$$

Let us call this solution $M_{sub}(r)$.

Now, if a shock on the solution $M_1(r)$ occurs it produces a post shock mach value M_2 given by the Hugoniot relations. If the M2 curve crosses the M_{sub} curve then a shock can , in principle, occur at that position if the M_{sub} solution correspond to an entropy status greater than the M_1 one.

The stable shock position is the outer one and is obtained solving:

$$M_2(r, E, \lambda) = M_{sub}(r, E, \lambda)$$

The solutions so obtained correspond exactly to the ones obtained integrating the differential equations in the way described by Chakrabarti in his book.

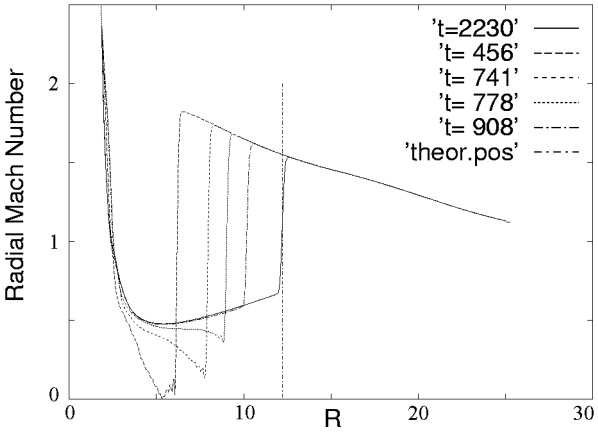

Figure 1: Mach number for steady state 1D solution and time dependent results.

Fig.1 shows the analytical solution with the overplotted numerical solutions obtained at different times. It can be seen the exact agreement between the two solutions for long integration time.

3.2 Viscous isothermal flows

This case mimics flows with very efficient cooling. It is a plain schematic case, but it is useful to learn the topology of the solutions. For the $\tau_{r\phi} = -\alpha P$ prescription it is even possible to have an algebraic solution (i.e. no differential equation). Combining the mass conservation, angular momentum and energy equations we are lead to solve the following algebraic equation:

$$\frac{1}{2}v_r^2 - K^2 \ln|v_r| - G\frac{M_*}{r - r_g} - K^2 \ln(r) - \frac{\lambda^2}{2r^2} + \frac{\lambda\lambda_e}{r^2} = B$$

with $\lambda = \lambda_e + \alpha\frac{K^2 r}{|v_r|}$ This fact allows us to prove a trivial, but interesting, fact: steady keplerian isothermal disks cannot exist, since the substitution of λ with λ_{kepler} leads to contradictory results for v_r, whatever be the initial conditions. However, it is possible to make a numerical simulation, constraining the gas flow to be isothermal, with small constant sound speed, and initial keplerian angular momentum to obtain a plain keplerian disk (cfr. Chakrabarti and Molteni, 1995). We may conclude that the keplerian disks are steady, but in an average way: they are affected by a turbulence (not the S.S. one) producing convection cells. The time dependent S.P.H. simulations agree perfectly with the analytical results obtained taking into account convection, viscosity and pressure terms. For a detailed discussion see Chakrabarti and Molteni (1995).

3.3 Viscous adiabatic cases

We adopt the basic assumptions valid for simple models of ADAFs (Narayan et al. 1998), i.e.: Low cooling efficiency, that is neglect of cooling terms, Shakura Sunyaev viscosity, vertical equilibrium, gradient of pressure and convective terms are retained in the equations. Let us briefly discuss the pure 1D case (i.e. $\frac{\partial}{\partial z} = 0$), whose results can be compared exactly with the time dependent numerical simulations. In the case of $\tau_{r\phi} = -\alpha P$ viscosity prescription we have the following set of equations (to make the formulae clean we are using v instead of v_r).
For mass conservation

$$\dot{m} = r\rho v$$

For the angular momentum

$$\lambda = \lambda_e - \alpha\frac{a^2}{\gamma v}r^2$$

For the radial momentum, retaining first order terms in α, after substitution of ρ P and λ from the above equations and use of the reference quantities r_g, and c (light speed) to adimensionalize the equation, we have

$$\frac{dv}{dr} = \frac{2\lambda_e a^2\alpha + \left[-\left(ra^2 + \frac{\lambda_e^2}{r}\right) + \frac{r^2}{2(r-1)^2}\right]v}{r^2(a^2 - v^2)}$$

Energy equation gives

$$\frac{1}{2}v^2 + \frac{\lambda^2}{2r^2} - \frac{1}{2(r-1)} + \frac{a^2}{(\gamma - 1)} + \alpha\frac{a^2}{\gamma}\frac{\lambda}{r \cdot v} = E$$

where a is the adiabatic sound speed.

Therefore, we have four unknowns variables v, a, ρ, and λ that can be obtained solving the above set of equations, one differential and three algebraic. The radial momentum differential equation shows the presence of a sonic point: The r_s value for which $a(r_s) = -v(r_s)$.

For a regular accretion flow the derivative at r_s must be continuous , this requires that the numerator and the denominator of the equation be simultaneously zero at r_s and consequently the value of the derivative $\left(\frac{dv}{dr}\right)_s$ is well fixed. In this case the value of the derivative at the sonic point depends univocally on the values of α, E and λ_e.

So it is wrong to put its value to zero or whatever other value, as many other authors do (Narayan et al, 1997). Typical solutions of this case are shown in the paper by Chakrabarti 1998.

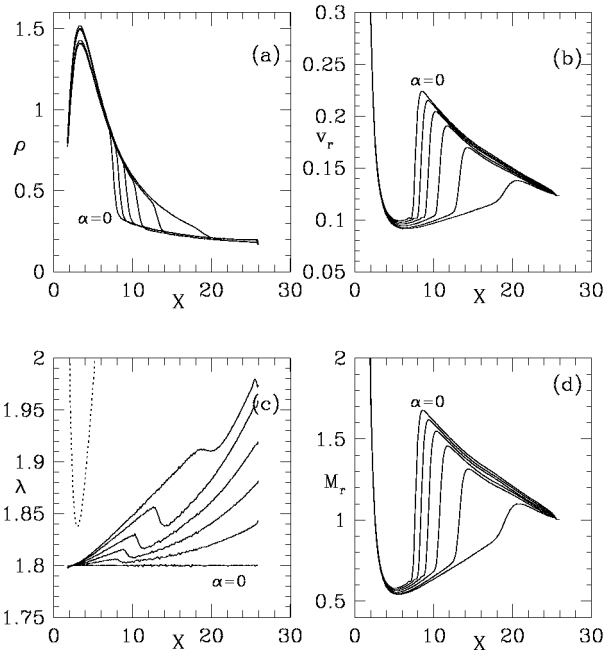

Figure 2: Solutions of 1D adiabatic viscous flows for increasing viscosity α parameter

Fig.2(a-d) show stationary shock locations as functions of Shakura-Sunyaev viscosity parameter α in thin, rotating, accreting flows. In (a), we plot density $\rho(r)$, in (b), we plot radial velocity $v_r(r)$, in (c), we plot $\lambda(r)$ and in (d), we plot Mach number $M_r(r)$. The α values for which the curves are drawn are (left to right in [a, b, d] and bottom to top in [c]): 0, 10^{-4}, 2×10^{-4}, 3×10^{-4}, 4×10^{-4} and 4.6×10^{-4} respectively.

4. The numerical algorithms

We exploited basically two kind of numerical algorithms to integrate the time dependent equations. One is a Smoothed Particles Hydrodynamics code (SPH) formulated in cylindrical coordinates. SPH is a lagrangean method based on interpolation criteria of the fluid variables and of their derivatives. The interpolation points move with the fluid speed. A full discussion of the method is given in Monaghan (1985). For its formulation in cilindric coordinates cfr. Molteni and Sponholz 1994. Another code based on the Total Variation Diminuishing (TVD) procedure have also been used. A comparison of the results of the two code has been performed (Molteni, Ryu and Chakrabarti 1996) confirming the reliability of the simulations results. SPH has been used also for viscous and cooled flows. For the study in the XY plane, using a r ϕ coordinates, another set of two different type of TVD codes has also been used cfr. Molteni, Toth and Kutznezov 1999, in this case SPH had too much shear numerical viscosity.

5. Time variability

Obviously the time dependent approach, by the use of numerical algorithms, allows the time variability study of the solutions. Indeed we found that there are many different ways in which the flow can exhibit time variability.

5.1 Time variability for unviscous cases

For unviscous ideal gas flow we find that axis symmetric 1D solutions are stable. However, if the axis symmetry is broken, then a very interesting phenomenon occurs. We performed simulations on the XY plane (no zeta motion $\frac{\partial}{\partial z} = 0$) of the axis symmetric shock, using a TVD code in r, ϕ coordinates that has a very low numerical viscosity (detailed results are give in Molteni et al. 1999). The shock forms at the predicted position and is stable, but if the flow is perturbed with a small (even 1% is enough) perturbation then the circular shape of the shock changes and the resulting deformation persists for ever, even if the average shock position is close to the original one. Therefore the radiation emitted by the post shock zone changes in time, producing Quasi Periodic Oscillations. The variations are more irregular for shocks produced with large angular momentum, while shocks with small angular momentum may produce quite regular oscillations. Fig.3 shows the isocontours of the radial mach value.

Unviscous solutions for ideal gas may produce oscillations also when the motion along the vertical direction is allowed. In this case, $\frac{\partial}{\partial z} \neq 0$, for low energy constant solutions, the disk thickness is very small and vertical compression and expansion make the solutions more unstable : recurrent shock formation within a finite range of the radial position occurs. Details of these simulations are given in Ryu et al. 1997.

Futher oscillations are possible when a cooling is present. We examined the plain case of an ideal gas with $\gamma = 5/3$ cooled by the bremstrahlung process. We considered therefore optically thin accreting regimes. In this case the oscillations occur when the fall time is close to the cooling time. We observed nearly regular oscillations in the 1D case. The centrifugal barrier

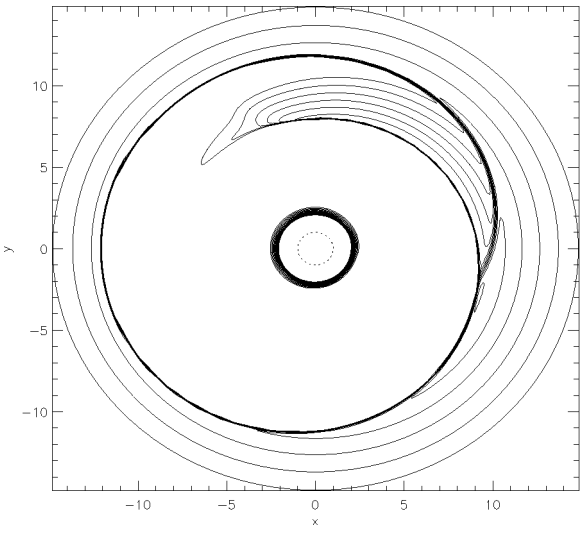

Figure 3: Radial Mach contour levels in the XY plane of a deformed, but permanent shock.

acts like a rigid wall. In the post shock region the gas reaches extremely high temperatures. In the 2D cases the post shock region is also very hot but now it can expand and collapse in the vertical direction producing a large hot corona around the thin accretion flow.

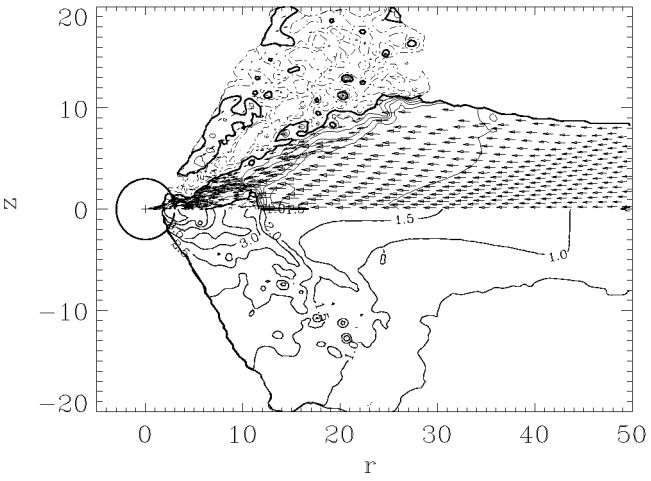

Figure 4: Hot corona of a unviscous accretion flow with shock cooled by bremsstrahlung.

Fig.4 shows the isodensity levels of the hot corona, with the velocity field overplotted, in the maximum expansion phase.

5.2 Time variability for viscous cases

In the case of adiabatic and viscous accretion, the flow in the subsonic region has large viscosity due to the higher post shock temperatures. In these cases the post shock flow forms an almost keplerian disk. The matter piles up in the disk and discharges into the black hole in a recurrent way. Details are given in the work

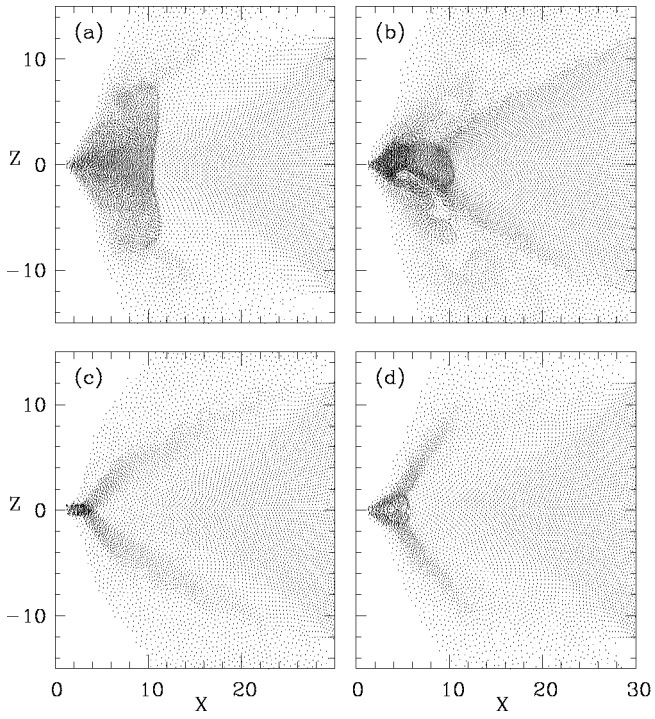

Figure 5: R-Z projection of the particles for viscous adiabatic flow with shock.

by Lanzafame et al. 1998. In Fig.5(a-d), we show the first simulations of shocks in viscous flows where they oscillate periodically. In (a-c), roughly half of the cycle is shown where the shock location decreases monotonically. Total number of particles in this simulation is on an average around 10,000 (see, Fig. 6 below). In (d), the shock drifted again outward. Note that apart from the axisymmetric shock oscillation, a new, corrugated instability, is also apparent in Fig. 4(d). Fig.6 shows the mass of the disk versus the elapsed time.

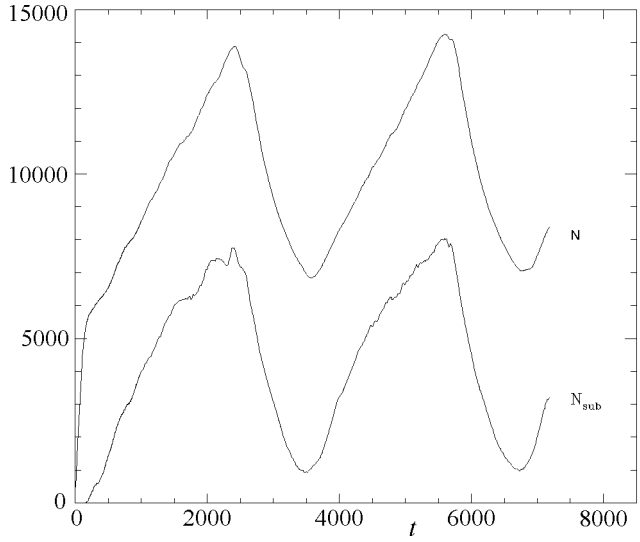

Figure 6. Mass versus time of the adiabatic viscous disk.

6. Conclusions

Numerical time dependent simulations of accretion flows demonstrate that analytical exact solutions can be obtained only if the sonic point conditions are treated appropriately. Furthermore the *numerical experiments* have shown that finite amplitude oscillations of the flow can be produced in many different ways. Consequently the time variability and the Quasi Periodic Oscillation phenomenon of the radiation emitted by accretion disk around black holes may be quite common even with very simple physical ingredients of the models. Unfortunately this make harder to discern the difference between compact stellar object and black holes only on the basis of the time variability.

Acknowledgements. This research has been supported by the CNR contract n.096-477. The authors are grateful to the organizers of the meeting for their generous effort to make so pleasant our staying in Odessa.

References

Bondi H.: 1952, *MNRAS*,**112**,195.

Chakrabarti S.K.: 1990, *Theory of Transonic Astrophysical Flows,* Singapore: World Scientific.

Chakrabarti S.K., Molteni D.: 1995, *MNRAS*, **272**, 80.

Chakrabarti S.K.: 1996, *Ap.J.*, **471**, 237.

Lanzafame G., Molteni D., Chakrabarti S.K.: 1998, *MNRAS*, **299**, 799.

Molteni D., Lanzafame G., Chakrabarti S.K.: 1994, *Ap.J.*, **425**, 161.

Molteni D., Sponholz H., Chakrabarti S. K.: 1996, *Ap.J.*, **457**, 805.

Molteni D., Ryu D., Chakrabarti S.K.: 1996, *Ap.J.*, **470**, 460.

Monaghan J.: 1985, *Computer Physics Reports*, **3** ,71.

Narayan R., Kato S., Honma F.: 1997, *Ap.J.*, **476**, 49.

Narayan R., Mahadevan R., Quataert E.: 1998, *The Theory of Black Hole Accretion Discs*, eds. M.A. Abramowicz, G. Bjornsson & J.E. Pringle (Cambridge).

Novikov I., Thorne K.S.: 1973, *Black Holes, Les Houches 1973*, eds. C.DeWitt and B.S. DeWitt, (New York: Gordon & Breach).

Paczyński B., Wiita P. J.: 1980, *As.Ap.*, **88**, 23.

Pringle J.L., Rees M. J.: 1972, *As.Ap.*, **21**, 1.

Ryu D., Chakrabarti S.K., Molteni D.: 1997, *Ap.J.*, **474**, 378.

Shakura N.I., Sunyaev R.A.: 1973, *MNRAS*, **175**, 613.

KICK ASYMMETRY ALONG A STRONG MAGNETIC FIELD IN THE PROCESS OF NEUTRINO SCATTERING ON NUCLEONS

I.S. Ognev[1], A.A. Gvozdev[2]

[1] Department of Theoretical Physics, Yaroslavl State University
Sovietskaya 14, Yaroslavl 150000, Russia, *ognev@uniyar.ac.ru*

[2] Department of Theoretical Physics, Yaroslavl State University
Sovietskaya 14, Yaroslavl 150000, Russia, *gvozdev@uniyar.ac.ru*

ABSTRACT. The neutrino-nucleon scattering in a collapsing star envelope with a strong magnetic field is investigated. The transferred momentum assymetry along the field direction is obtained. It is shown that neutrino-nucleon scattering gives a contribution to the asymmetry comparable with direct URCA processes. Hence, neutrino-nucleon scattering should be taken into account in estimations of a possible influence of neutrino reemission processes on a collapsing star envelope dynamics.

Key words: neutrino-nucleon scattering: magnetic field: collapsing star remnant.

1. Introduction

The most powerfull star processes (a Supernova II explosion, a coalescense of a closed binary system of neutron stars, an accretion induced collapse) are of a permanent interest in astrophysics. A collapse in such systems can lead to the formation of a millisecond remnant (Bisnovatyi-Kogan, 1970, 1989; Woosley, 1993; MacFadyen et al., 1998; Ruffert et al., 1998; Spruit, 1998). It is assumed usually that the remnant consists of a compact rigid rotating core and a differently rotating envelope. The compact core with the typical size $R_c \sim 10km$, the supranuclear density $\rho \quad 10^{13}g/cm^3$ and the high temperature $T \quad 10MeV$ is opaque to neutrinos. An envelope with the typical size of a few tens of kilometers, the density $\rho \sim 10^{11} - 10^{12}g/cm^3$ and the temperature $T \sim 3 - 6MeV$ is partially transparent to the neutrino flux. Extremely high neutrino flux with the typical luminosity $L_\nu \sim 10^{52}erg/s$ is emitted from the remnant during 2 - 3 seconds after collapse. As result of a high rotating frequency and a medium viscosity of the remnant a turbulent dynamo and a large gradient of angular velosities are inevitably produced during a star contraction. The extremely strong poloidal magnetic field up to $B \sim 10^{15}G$ could be generated by a dynamo process in the remnant (Duncan et al., 1992). On the other hand, a large gradient of angular velosities in the vicinity of a rigid rotating millisecond core can generate a more strong toroidal magnetic field $B \sim 10^{15} - 10^{17}G$ during a second (Bisnovatyi-Kogan et al., 1993). In the present paper we investigate the influence of neutrino-nucleon processes on the dynamics of collapsing star millisecond remnant.

2. Momentum asymmetry in neutrino-nucleon scattering

Due to the parity-violation in neutrino-nucleon processes, the macroscopic momentum can be transfered by neutrinos to the medium in an external magnetic field. A quantitative estimation of the momentum asymmetry is given by the expression for the four-vector of the energy-momentum transfered to the unit volume in per unit time:

$$\frac{dP_\alpha}{dt} = \left(\frac{dQ}{dt}, \vec{\Im}\right) = \\ = \frac{1}{V}\int \prod_i dn_i f_i \prod_f dn_f (1 - f_f) \frac{|S_{if}|^2}{\mathcal{T}} q_\alpha, \quad (1)$$

where dn_i, dn_f are the numbers of initial and final states in an element of the phase space, f_i, f_f are the distribution functions of the initial and final particles, q_α is the momentum transferred to the medium in the single reaction, $|S_{if}|^2/\mathcal{T}$ is the squared S-matrix element of the process per unit time. We calculate the asymmetry of the momentum transfered to the medium along the magnetic field direction in the processes of the neutrino-nucleon scattering:

$$N + \nu_i \Longrightarrow N + \nu_i, \quad (2)$$

$$N + \tilde{\nu}_i \Longrightarrow N + \tilde{\nu}_i, \quad (3)$$

where $N = n, p$; $\nu_i = \nu_e, \nu_\mu, \nu_\tau$. Under the conditions of the remnant envelope, the nucleonic gas is the Boltzmann and the nonrelativistic one. It is known that the

asymmetry of the neutrino momentum is absent in the case of β-equilibrium (Kusenko et al., 1998). Thus, we discribe neutrino by the local nonequilibrium distribution function:

$$f_{(\nu,\tilde{\nu})} = \Phi_{(\nu,\tilde{\nu})}(r,\chi)\cdot\left(\exp\left(\omega/T_{(\nu,\tilde{\nu})} - \eta_{(\nu,\tilde{\nu})}\right)+1\right)^{-1}. \quad (4)$$

Here χ is the cosine of the angle between the neutrino momentum and the radial direction, ω is the energy of the neutrino, $T_{(\nu,\tilde{\nu})}$ is the neutrino spectral temperature, $\eta_{(\nu,\tilde{\nu})}$ is a fitting parameter. Here we are neglected the influence of the magnetic field on the neutrino distribution (see detailes in A.A. Gvozdev, I.S. Ognev, this Proceedings). In calculation of S-matrix element of the processes (**??**), (**??**) we used the vacuum wave functions of the nucleons with polarization $S = \pm 1$ along the magnetic field. We also should take into account the interaction energy of the magnetic moment of nucleon with the magnetic field: $E = m + \vec{P}^2/2m - geBS/2m$ ($g\simeq -1.91$ for neutron, $g\simeq 2.79$ for proton).

Under these assumptions we obtain the following expression for the force density along the field:

$$\Im_{\parallel}^{(\nu)} = -\frac{G_F^2 g}{2\pi}\,\frac{eB}{m_{n,p}T}\,N_{n,p}\,N_\nu\,\times$$
$$\times\Bigg\{\left(c_v c_a\langle\omega_\nu^3\rangle + c_a^2 T\langle\omega_\nu^2\rangle\right)\left(\langle\chi_\nu^2\rangle - 1/3\right) -$$
$$-c_a^2\left(\langle\omega_\nu^3\rangle - 5T\langle\omega_\nu^2\rangle\right)\left(5/3 - \langle\chi_\nu^2\rangle\right) +$$
$$+2c_a^2 J\left(\langle\omega_\nu^3\rangle - 5T_\nu\langle\omega_\nu^2\rangle\right)\left(1-\langle\chi_\nu^2\rangle\right)\Bigg\}. \quad (5)$$

Here G_F is the Fermi constant, c_v, c_a are the vector and axial nucleonic current constants ($c_v = -1/2$, $c_a \simeq -0.91/2$ for neutron; $c_v = 0.07/2$, $c_a \simeq 1.09/2$ for proton); $N_{n,p}, N_\nu$ are local neutron (proton) and neutrinos numbers densities respectively,
$\langle\omega_\nu^n\rangle = N_\nu^{-1}\int \omega^n\, f_\nu\, d^3k$
is the mean energy in the n'th power,
$\langle\chi^2_{(\nu,\tilde{\nu})}\rangle = \int \chi^2\,\omega\, f_{(\nu,\tilde{\nu})}\, d^3k (\int \omega\, f_{(\nu,\tilde{\nu})}\, d^3k)^{-1}$
is the mean square cosine,
$J = (4\pi)^{-1}\int \Phi_\nu(r,\chi) d\Omega$.
In the case of antineutrino we have to change $c_a^2 \to -c_a^2$:

$$\Im_{\parallel}^{(\tilde{\nu})} = \Im_{\parallel}^{(\nu)}(c_a^2 \to -c_a^2). \quad (6)$$

We note, that the process of the neutrino scattering on protons is supressed by the smallness of the proton number density (for the conditions under consideration $N_p/N_n \simeq 0.07$). As one can see from exp. (**??**), the momentum asymmetry exist if the spectral neutrino temperature differs from the medium temperature ($T_\nu \neq T$) or the neutrino distribution is anisotropic ($\langle\chi_\nu^2\rangle \neq 1/3$).

In the case of the Boltzmann neutrino distribution function: $f_{(\nu,\tilde{\nu})} = \Phi_{(\nu,\tilde{\nu})}(r,\chi)\exp(-\omega/T_{(\nu,\tilde{\nu})})$, the expression for the force density is simplified:

$$\Im_{\parallel}^{(\nu_i)} = -\frac{6G_F^2 g}{\pi}\,\frac{eB}{m_{n,p}}\,N_{n,p}\,N_\nu\,T_\nu^2\,\times$$
$$\Bigg\{4c_a^2\left(2-\langle\chi_\nu^2\rangle\right) + 5T_\nu/T\Bigg[c_v c_a\left(\langle\chi_\nu^2\rangle - 1/3\right) -$$
$$-c_a^2\left(5/3 - \langle\chi_\nu^2\rangle\right)\Bigg]\Bigg\}. \quad (7)$$

Under an envelope conditions neutrino and antineutrino parameters for μ and τ species are equal approximately (Yamada et al., 1998): $T_\nu = T_{\tilde{\nu}}$, $\langle\chi_\nu^2\rangle = \langle\chi_{\tilde{\nu}}^2\rangle$. Thus, the expression for summary (neutrino and antineutrino) force density for each of these species is simplified and can be presented in the form:

$$\Im_{\parallel}^{(\nu_i)} + \Im_{\parallel}^{(\tilde{\nu}_i)} = -\frac{G_F^2 c_v c_a g}{\pi}\,\frac{eB}{m_{n,p}T}\,\times$$
$$\times N_{n,p}\,N_\nu\,\langle\omega_\nu^3\rangle\left(\langle\chi_\nu^2\rangle - 1/3\right), \quad (8)$$

and this force density not equal to zero when the neutrino distribution is anisotropic only.

3. Numerical estimations

We estimate the momentum asymmetry in collapsing star envelope in the presence of the strong toroidal magnetic field on the stage of the basic neutrino emission. For numerical estimations we used the typical value of the envelope density $\rho = 5\cdot 10^{11} g/cm^{-3}$ and the magnetic field strength $B = 4.4\cdot 10^{16} G$.

The neutrino parameters are taken from the paper by Yamada et al. (1998):

$$T_{\nu_e}\simeq 4MeV,\ \ T_{\tilde{\nu}_e}\simeq 5MeV,\ \ T_{\nu_{\mu,\tau}}\simeq T_{\tilde{\nu}_{\mu,\tau}}\simeq 8MeV,$$
$$N_{\nu_e}\simeq 5\cdot 10^{32} cm^{-3},\ \ N_{\tilde{\nu}_e}\simeq 2.1\cdot 10^{32} cm^{-3},$$
$$N_{\nu_{\mu,\tau}}\simeq N_{\tilde{\nu}_{\mu,\tau}}\simeq 1.8\cdot 10^{32} cm^{-3},$$
$$\langle\chi^2_{\nu_i}\rangle \simeq \langle\chi^2_{\tilde{\nu}_i}\rangle \simeq 0.4,\ \ \eta_{\nu_i}\simeq\eta_{\tilde{\nu}_i}\simeq 0.$$

With these parameters we obtained the following numerical estimation on the total (summarised over all neutrino species) force density in the neutrino-nucleon scattering:

$$\Im_{\parallel}^{(scat)} \simeq 3.4\cdot 10^{20} dynes/cm^3\,\times$$
$$\times\left(\frac{B}{4.4\cdot 10^{16} G}\right)\left(\frac{\rho}{5\cdot 10^{11} g/cm^3}\right). \quad (9)$$

Let us compare this result with the estimation of the force density in URCA processes (see A.A. Gvozdev,

I.S. Ognev, this Proceedings):

$$\Im_{\parallel}^{(urca)} \simeq 2 \cdot 10^{20} dynes/cm^3 \times \\ \times \left(\frac{B}{4.4 \cdot 10^{16} G}\right)\left(\frac{\rho}{5 \cdot 10^{11} g/cm^3}\right). \quad (10)$$

We stress that these quantities are of the same sign and sufficiently large numerically. The total force spins up quickly the envelope along the magnetic field direction. The estimation of the angular acceleration:

$$\dot{\Omega} \sim 10^3 s^{-2} \left(\frac{B}{4.4 \cdot 10^{16} G}\right)\left(\frac{R_c}{10 km}\right) \quad (11)$$

shows that the "neutrino spin up" effect can influence substantially on the envelope dynamics.

4. Conclusions

In the processes of neutrino-nucleon scattering the macroscopic momentum is transfered to the envelope along the magnetic field direction. This momentum is large enough in the case of the strong magnetic field and coincides in the sign with the similar momentum in the direct URCA processes. The force which appears in the neutrino-nucleon processes in the toroidal magnetic field generates the torque. This torque can spin up quickly the part of the envelope filled by the strong magnetic field. Therefore the "neutrino spin up" effect could essentially influence on the dynamics of the remnant envelope.

Acknowledgements. The authors express there deep gratitude to the Organizing Committee of the GMIC 99 Conference for the possibility to participate in this conference and worm hospitality. This work was supported in part by the INTAS Grant No. 96-0659 and by the Russian Foundation for Basic Research Grant No. 98-02-16694.

References

Bisnovatyi-Kogan G.S.: 1970, *Astron. Zh. Akad. Nauk. SSSR,* **47**, 813.

Bisnovatyi-Kogan G.S.: 1989, *Physical Problems of the Theory of Stellar Evolution* [in Russian], Nauka, Moscow.

Bisnovatyi-Kogan G.S., Moiseenko S.G.: 1993, *Astron. Astrophys. Transactions,* **3**, 287.

Duncan R.C., Thompson C.: 1992, *Astrophys. J.,* **392**, L9.

Kusenko A., Segre G., Vilenkin A.: 1998, *Phys. Lett.,* **B437**, 359.

MacFadyen A., Woosley S.E.: 1998, *http://xxx.lanl.gov/abs/astro-ph/9810274.*

Ruffert M., Janka H.-T.: 1998, *Astron. Astrophys,* **338**, 535.

Spruit H.C.: 1998, *http://xxx.lanl.gov/abs/astro-ph/9811007.*

Woosley S.E.: 1993, *Astrophys. J.,* **405**, 473.

Yamada S., Janka H.-T. and Suzuki H.: 1998, *http://xxx.lanl.gov/abs/astro-ph/9809009.*

VARIATIONS OF THE β CEPHEI Hα LINE PARAMETERS IN 1993 - 1998.

E.A. Panko[1], A.E. Tarasov[2]

[1] Kalinenkov astronomical observatory, Nikolaev State Pedagogical University, Nikolskaja, 24, Nikolaev, 327030, Ukraine, *pea@aok.mk.ua*

[2] Crimean Astrophysical Observatory, Nauchny, Crimea, 334413, Ukraine *tarasov@crao.crimea.ua*

ABSTRACT. We use high-dispersion CCD spectrograms obtained in 1993 - 1998 to study parameter variations of the absorption and emission components Hα line of the star β Cephei. We show that radial velocity of the emission component does not depend on star pulsation and systematically differs from the star radial velocity. The star radial velocity measured on doublet CII lines and corrected for pulsation decreases quickly than ensues from orbital moving ephemeris. We suppose the envelope appears around the closer β Cep companion, and the changes of the radial velocity of the emission components Hα partially reflects the orbital moving of the closer companion. It is possible, the system periastron passage will come earlier than ensues from the present significance of the orbital period.

Key words: Line: profiles - stars: emission line; Be-stars: individual: β Cephei

1. Introduction

β Cep stars are the group of early-type pulsating variables, in which both radial and non-radial, mono- and multiperiodic pulsations occur. These stars show the rapid changes of radial velocity, magnitude and profiles of spectral lines related to nonradial pulsations. β Cephei (HD 205021, HR 8238, HC 106032, B0.5-B2 IV) is the prototype of this class variables.

The periodic radial-velocity variations of β Cep were discovered by Frost (1906) and then the light variations with the same period were found by Guthnic & Prager (1914). Now β Cep is considered to be a nonradial pulsating object with five modes: the fundamental radial mode with $P = 0^d.1904852$ and 4 low-amplitude nonradial modes, possibly, with $l = 2$ (Telting et al., 1997). The radial-velocity curve has quasi-sinusoidal form and the amplitude of this curve exhibits considerable cycle-to-cycle variations: from 19 to 46 km s^{-1} (Struve et al., 1953), and from 29 to 35 km s^{-1} (Aerts et al., 1993).

β Cep is a bright member of the visual pair ADS 15032; the separation between the components is 13".4 and $\Delta m = 4^m.6$ (Heintz, 1978). Speckle observations (Gezari et al., 1972) revealed a faint, closer (0".25) companion with the presumed orbital period of about 100 years and a magnitude difference of $3 - 4^m$. Pigulski & Boratyn (1992) found for this pair a period of 91.6 ± 3.7 yrs, $K_1 = 8.0 \pm 0.5$ km s^{-1}; $e = 0.65$ and $T_0 = 1914.6 \pm 0.4$. So, the next periastron passage is predicted for the 2006. Fitch (1969) suspected the presence of yet another, closer companion with an orbital period of $\approx 11^d$, but Pigulski & Boratyn (1992) failed to confirm this period.

β Cep has a low rotational velocity, $v\,sini = 25$ km s^{-1} (Telting et al., 1997), but the development of an emission feature in the Hα line (Karpov, 1934; Greaves et al., 1955; Wilson & Seddon, 1956; Mathias et al., 1991; Panko & Tarasov, 1997) allow to define β Cep as a Be star. Last emission episode began in 1990 (Mathias et al., 1991). Kaper & Mathias (1995) expect that the Hα emission phase will end around 1998.

β Cep is a magnetic Bp star too. It's magnetic field strength of $810 \pm 170\,G$ was measured by Rudy & Kemp (1978). Henrichs at al. (1993) reported variations of the ultraviolet line profiles and of the intensity of the magnetic field with a period of 12^d. They interpreted this as the rotational period of the star.

So, β Cep is a complicated object with different kinds and typical times of variability.

2. Observations

All our observations were carried out at the Crimean Astrophysical Observatory with coude spectrograph of 2.6-m telescope. The detector was a GEC CCD array P8600 (576 x 380 pixels) in 1993 - 1994 and an Electronix CCD array (1024 x 260 pixels) in 1995 - 1998. We performed the Hα observations in the first and second

Table 1: The parameters of Hα line in 1993 - 1998.

$JDh\,2400000+$	φ	W	W_{emi}	V/R	V_{emi}	V_{abs}	V_{CII}	V_γ
49195.36141	0.19497	0.78	-1.65	0.96	8.00	-28.63	-29.40	-11.00
49654.18449	0.90221	1.25	-1.15	0.98	11.23	-13.86	-11.28	-8.43
49897.49354	0.21430	1.24	-1.26	0.96	16.00	-28.62	-32.30	-14.99
49933.47067	0.08530	1.36	-1.06	0.95	18.16	-29.47	-33.81	-14.52
49937.25447	0.94931	1.09	-1.12	0.98	15.05	-17.85	-22.66	-14.26
49938.40798	0.00495	1.30	-0.94	0.97	13.56	-23.76	-26.60	-12.42
49939.28509	0.60956	1.19	-1.08	1.00	21.50	4.20	6.68	-13.24
49944.24774	0.66224	1.18	-1.10	1.00	22.10	3.66	2.50	-17.20
49945.39570	0.68875	1.29	-0.99	1.01	15.86	3.10	3.44	-15.27
49946.39642	0.94228	1.36	-0.95	0.98	11.49	-16.62	-21.48	-13.79
49970.41200	0.01811	1.05	-1.22	0.97	8.89	-28.07	-34.66	-19.33
49975.44510	0.44063	0.89	-1.27	0.99	16.54	-11.22	-11.92	-19.36
49999.36945	0.03753	0.96	-1.25	0.96	17.08	-27.78	-34.90	-18.08
50006.40632	0.97935	1.01	-1.20	0.96	16.17	-24.63	-31.82	-20.05
50015.37442	0.05965	0.90	-1.17	0.96	15.19	-31.90	-37.86	-19.62
50296.53181	0.06613	1.79	-0.26	0.96	13.76	-31.51	-36.63	-21.15
50401.27434	0.93840	1.69	-0.66	0.98	20.02	-21.84	-28.36	-21.00
50475.19944	0.02682	1.35	-0.76	0.96	18.20	-33.80	-40.26	-24.26
50755.16191	0.76027	1.63	-0.36	0.97	26.71	-19.94	-25.14	-38.90
51015.53413	0.64976	1.80	-0.20	0.97	26.93	-21.67	-23.41	-43.35

Note: φ is the pulsation phase, W, W_{emi} are, respectively, the equivalent widths of the entire line profile and emission component in Å; V/R is the ratio of intensities blue V and red R peaks for entire line profile. $V_{emi}, V_{abs}, V_{CII}$ and V_γ are, respectively, the radial velocities of the emission and absorption components of Hα line, the average velocity of the CII doublet and the calculated pulsation V_γ of the star in km s^{-1}.

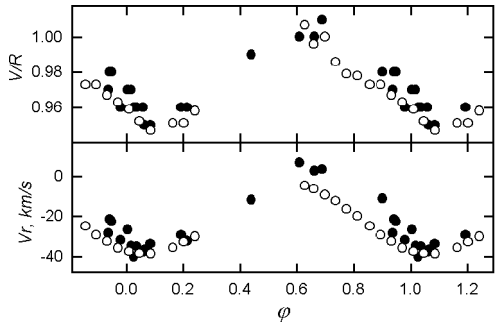

Figure 1: Variations of CII radial velocity and V/R ratio versus fundamental mode pulsation phase. Observations in 1993 – 1998 we mark as solid circles, data for 13.11.1996 are shown as open circles.

orders of a diffraction grating with a reciprocal dispersion of 6 and 3 Å mm^{-1} and with spectral resolution of 25 000 and 35 000, respectively. Since we took a 60-Å long spectrum during each observations, the CII 6578, 6583 doublet fell within the range under consideration, in addition to the Hα line. The duration of a single exposure was from 10 to 15 *min*, and the signal-to-noise ratio was 100-200. In total, we obtained 20 Hα spectra between 1993 and 1998. Moreover 16 spectra covered 2/3 of pulsating period were obtained 13.11.1996.

We reduced the spectrograms by standard techniques, which included sky-background and dark-current subtraction, flat-field division, and normalization to the local continuum. For the wavelength calibration, we used the comparison spectrum of a thorium-argon lamp; we reduced the wavelength scale to the barycenter of the Solar System. The mean calibration error was no greater than 0.5 km s^{-1}.

3. Parameter variations

Over the entire observing period, the line was in emission with a pronounced two-component structure and a small intensity above the continuum level. This profiles essentially identical to those observed by Wilson & Seddon (1956). The intensity of the Hα emission feature gradually decreased, while the profile shape remained essentially unchanged.

We determined the equivalent width W and radial velocity V_r for entire profile and emission components of the line, radial velocity for doublet CII (6578.03 and 6582.85 Å), ratio of intensities blue V and red R peaks for entire line profile (V/R). For subsequent identification of the emission component, we used a pho-

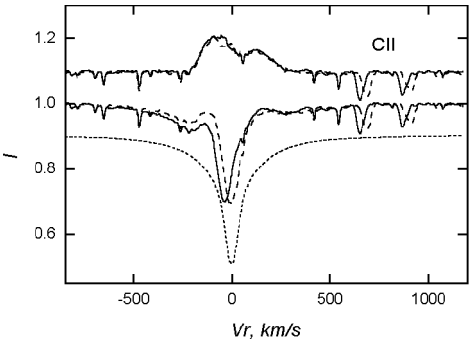

Figure 2: Change of form of the emission component (above) and entire Hα profile, with pulsation phase (observations in 13.11.1996.). The solid line conforms to phase 0.63, dash line - to phase 0.05. The "normal" photocpherical profile is shown as short dash line. Except of line Hα, the CII and telluric water lines are present.

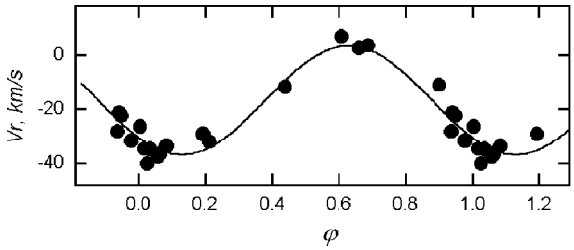

Figure 3: The radial velocity of star (circles) and the middle phase radial-velocity curve (line) with the fundamental mode period. Observations 1993 - 1998.

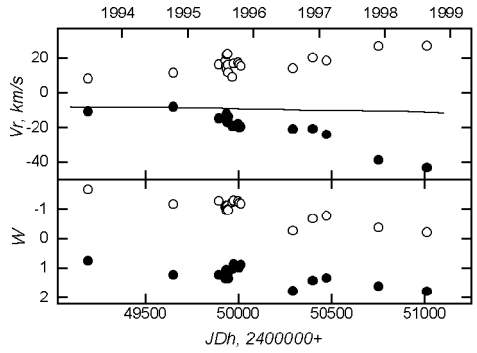

Figure 4: At the upper panel we show the variations of the radial velocity of emission component Hα line (open circles) and pulsation γ-velocity (solid circles) in 1993 - 1998. The solid line shows the radial velocity of an orbital movement agrees with ephemeris. At the bottom panel we show the variations of the equivalent width of emission component (open circles) and entire profile (solid circles) of Hα line.

tospherical profile obtained by Rachkovskaya (1990). We subtracted it from our spectra after correction by pulsation radial velocity. The mean measurement errors are $V_{emi} = 5\,\mathrm{km\,s^{-1}}$, $V_{abs} = 3\,\mathrm{km\,s^{-1}}$, and $V_{CII} = 1\,\mathrm{km\,s^{-1}}$. The results are present in Tab. 1.

V/R ratio shows a strong correlation with the pulsation radial velocity. The correlation coefficient of V/R ratio and CII radial velocity is equal to 0.95 for all observations and to 0.97 for observations made on 13.11.1996. On Fig. 1 we represented the phase radial-velocity CII doublet curve of the star's fundamental radial pulsation mode and variations of V/R ratio of the entire Hα line profile with phase (above). Both curves are similar for all observations as well as for one cycle data. Displacement of elementary pulsation epoch related to orbital star moving with 92 yrs period (Pigulski & Boratyn, 1992)

On Fig. 2 we represented two entire profiles and emission components Hα line for pulsation phases 0.05 and 0.63. One can see that the emission component of Hα profiles and telluric water lines remain at the same place but CII lines and absorption core displace in accordance with changes of pulsation radial velocity. Thus, periodicity of V/R changes with pulsation phase related to superposition of emission envelope line and absorption photospherical profile, and the radial velocity of emission component does not depend on star pulsation.

For further research we constructed the middle phase radial-velocity curve with the fundamental mode period. For all data the pulsation $V_\gamma = 16.8\,\mathrm{km\,s^{-1}}$ and amplitude $2K = 40.2\,\mathrm{km\,s^{-1}}$ (see Fig. 3.) and for data of 13.11.1996 observations the pulsation $V_\gamma = 21.4\,\mathrm{km\,s^{-1}}$ and amplitude $2K = 35.0\,\mathrm{km\,s^{-1}}$. The amplitude $2K = 40.2\,\mathrm{km\,s^{-1}}$ is considerably greater than the value obtained by Aerts et al. (1994) but does not exceed the value obtained by Struve et al. (1953). Then for each observation we calculated pulsation V_γ as the difference between observation and calculated radial velocity. These values are represented in Tab. 1 as $V\gamma$. The mean error of the pulsation $V\gamma$ is no greater than $4\,\mathrm{km\,s^{-1}}$.

Fig. 4. shows our results foretold the radial velocity of the orbital motion from the Pigulski & Boratyn, (1992) ephemeris. The emission decrease is shown on the bottom panel.

3. Discussion

Duration of the last emission episode is more, than it was observed previously. The emission intensity

decreased[1] and the equivalent width of the emission components changed from -1.65 Å in 1993 to -0.2 Å in 1998.

The pulsation V_γ of β Cep changed from $-8\,\mathrm{km\,s^{-1}}$ in 1994 to $-24\,\mathrm{km\,s^{-1}}$ in 1996 and $-43\,\mathrm{km\,s^{-1}}$ in 1998. Hadrava & Harmanec (1996) in their research of β Cep in 1994 – 1996 got the closer value of β Cep radial velocity ($-13\,\mathrm{km\,s^{-1}}$ in 1994 and $-18\,\mathrm{km\,s^{-1}}$ in 1996). Value of radial velocity of emission component, which was obtained by Hadrava & Harmanec (1996) in comparison with our result is too large. We don't confirm the displaying of the emission component with pulsation phase as given in their research too. Probably, the distinctions are related to procedure of reconstruction of the emission component, which has low intensity.

The range of β Cep of variations of the pulsation γ-velocity in 1993 - 1998 is equal to $35\,\mathrm{km\,s^{-1}}$, but Pigulski & Boratyn (1992) determined full amplitude of the radial velocity variations for orbital moving only $16\,\mathrm{km\,s^{-1}}$. The radial velocity changes are more quicker than ensues from Pigulski & Boratyn (1992) ephemeris (see Fig. 4). The value of β Cep radial velocity in 1997 - 1998 is close to value corresponding to periastron passage. The accuracy of determination of the elements of the β Cep binary system allow to suppose system periastron passage already in 2002.

Lack of dependence between pulsations β Cep and changes of radial velocity of Hα emission line component and the difference of radial velocity of the primary and emission envelope testifies the assumption that an envelope appears around less massive and less bright companion (probably, late B star), but not around the primary. Slow rotation of the primary with 12^d significance of rotational period (Henrichs et al., 1993) supports this too.

Augmentation of radial velocity of emission component attached to essential diminution of radial velocity β Cep, probably, partially reflects the orbital moving of closer companion around which emission envelope appears.

3. Conclusion

We show that radial velocity of the β Cep, emission component does not depend on star pulsation and systematically differs from the star radial velocity. The V/R ratio of the entire profile shows strong correlation with the pulsation radial velocity. The emission envelope appears around the closer β Cep companion and we observe the superposition of the emission from the companion envelope and absorption profile of the primary.

The star radial velocity measured on doublet CII lines and corrected for pulsation decreases quicker than ensues from orbital moving ephemeris. It is possible, the system periastron passage will come earlier than ensues from the present significance of the orbital period.

Acknowledgements. E. Panko is grateful to staff of Crimean Astrophysical Observatory for help in work during her visits.

References

Aerts C., Mathias P., Gillet D., Waelkens C: 1993, *As.Ap.,* **286**, 109.
Fitch W.S: 1969, *ApJ.,* **158**, 269.
Frost E.B.: 1906, *ApJ.,* **24**, 24, 259.
Gezari D.Y, Labeyrie A., Stachnik R.V.: 1972, *Ap.J.,* **173**, L1.
Greaves W.M.H., Baker E.A., Wilson R.: 1955, *Publ. R. Obs. Edinburgh,* **1**, 115.
Guthnick P., Prager R.: 1914, *Veröff. Königlichen Sternwarte zu Berlin-Babelsberg,* **1**, 23.
Hadrava P., Harmanec P.: 1996, *As.Ap.,* **315**, L401.
Heintz W.D.: 1978, *Double Stars,* Dordrecht.
Henrichs H.F., Bauer F., Hill G.M., at al.: 1993, in: *New Perspectives on Stellar Pulsation and Pulsating Variable Stars,* Ed. by J.M. Nemec and J.M. Matthews, Proc. of IAU Col. **139**. Cambridge, 186.
Kaper L., Mathias P.: 1995, in *Astrophysical Applications of Stellar Pulsations,* Ed. by R.S. Stobie & P.A. Whitelock, *ASP Conf. Ser.,* **83**, 295.
Karpov B.C.: 1934, *Lick Obs. Bull.,* **457**, 159.
Mathias P., Gillet, D., Kaper, L.: 1991, in *Rapid Variability of OB Stars: Nature and Diagnostic Value,* Ed. by D. Baade, ESO Conference and Workshop Proc. **36**, 193.
Panko E.A., Tarasov A.E.: 1997, *PAZh.,* **23**, 620.
Pigulski A., Boratyn, D.A.: 1992, *As.Ap.,* **253**, 178.
Rachkovskaya T.M.: 1990, *Izv. Krym. Astrofiz. Obs.,* **82**, 3.
Rudy R.J., Kemp J.C.: 1978. *MNRAS,* **183**, 595.
Struve 0., McNamara D.H., Kung S.M., Beumer C., 1953, *ApJ.,* **118**, 39.
Telting J.H., Aerts C., Marhias P.: 1997, *As.Ap.,* **322**, 493.
Wilson R., Seddon H.: 1956, *Observatory,* **76**, 145.

[1] 21.07.1999 - 7.08.1999 we observed the β Cep Hα line without emission sign, so, the emission episode of β Cep finished.

OPTICAL SPECTRA OF L-DWARFS

Ya. Pavlenko

Main Astronomical Observatory of NASU
Golosiiv wood, Kyiv-127 03680 Ukraine, *yp@mao.kiev.ua*

ABSTRACT. Theorertical spectra of L-dwarfs (T_{eff} < 2200 K) were computed for a grid of the "dusty" C-model atmospheres of Tsuji (1998). To fit the observed spectra of L-dwarfs we used two additional (evristic) suggections:

- molecular densities of TiO and VO governed the visible spectra of M-dwarfs are reduced due to the *extra* depletion of V and Ti atoms into grains in atmospheres of T_{eff} < 2200 K;
- There are (a few) additional opacity κ sources in L-dwarf atmospheres;

A few kinds of κ=f(λ) dependences were used to get "the better fit" of observed spectra of L-dwarfs. We show:

- We may fit the observed sequence of L-dwarf spectra using in the frame of our simple model.
- Observad sequence of the L-dwarf spectra is *the temperature* sequence.
- At firt time, the region of 860 nm contained CrH bands is well fitted.
- There are a few possibilities to get the reliable fits to the observed spectra.
- In the frame of our approah we have found the solution even for the case of Gl229B.

Key words: late brown dwarfs, stellar spectra, lithum abundances.

In this paper we intend to provide an interpretation of the optical (6400–9100 Å) spectra of the very cool dwarfs recently discovered. Using Tsuji's (1998) "dusty" model atmospheres in LTE (C-models, i.e. computed for the "dust-gas" segregation phase). Chemical equilibrium is computed for more than 100 molecular species. Opacity sources included in our computations are described in Pavlenko et al. (1995, 1999), Pavlenko (1998). Note: at first time, CrH band feature at 860 nm has been well fitted in all L-dwarf spectra. Furthemore, we show, that additional opacity sources have to be incorporated in the spectral synthesis procedure in order to fit the overall shape of our data for objects cooler than M8. This extra opacity can be described as a potential law of the form $a_o\,(\nu/\nu_o)^N$. Note, it may be caused by dust scattering and/or absorption. In contrary to Pavlenko et al. (1998) paper (in which B-models of Tsuji (1996) models were used) we found that the better fit for the C-models may be found for N = 1 - 4, i.e. scattering by aerosol. For same cases (for example, BRI0021-024, see Fig. 1) we got "the better fits" for N=1. Still to be here in the frame of selfconsistentcy we show results obtained mainly for the N=4. (see Fig. 2 for Kelu1).

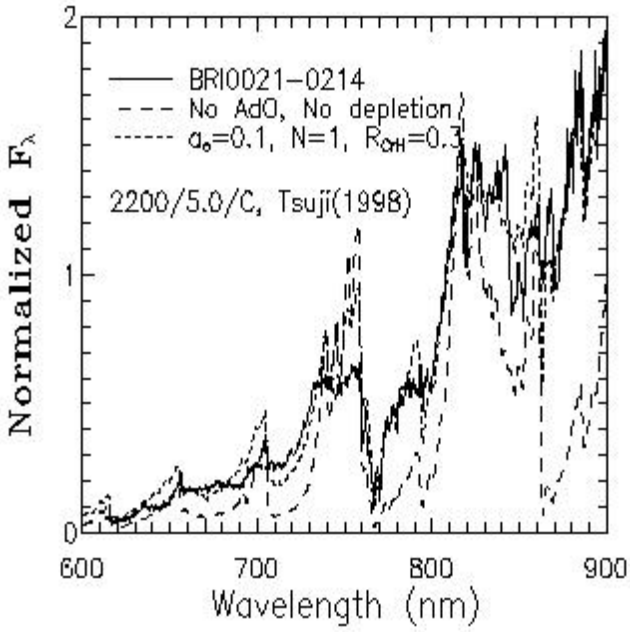

Figure 1: Comparison of the observed spectrum of BRI 0021–0214 with computations adopting Tsuji's model atmospheres of Teff = 2200 K and log g = 5. We notice that the discrepancy between the observed and the computed spectra is minimized by implementing additional opacity with a_o = 0.1.

Additionally, we find that the depletion factors for with TiO and VO molecular densities exceed that provided by their own gas-dust transition phase (Pavlenko 1998). Only assuming a strong Ti and V (EXTRA) de-

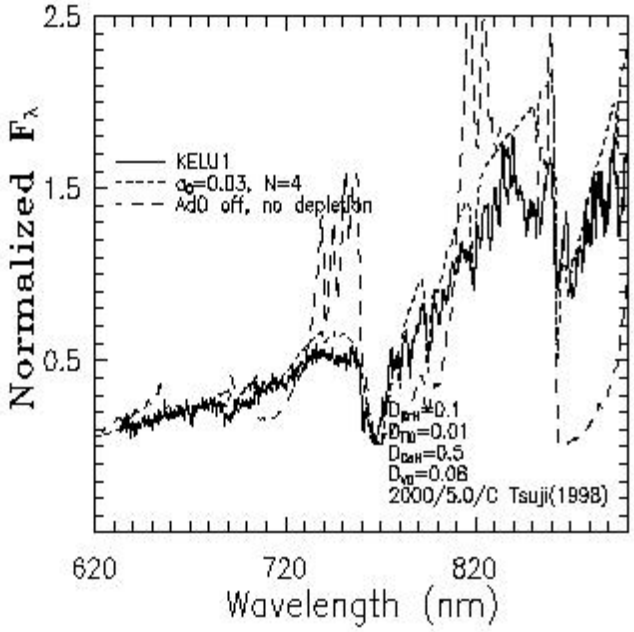

Figure 2: Comparison of the observed spectrum of Kelu 1 with synthetic spectra adopting Tsuji's C-model atmospheres of Teff = 2000 K, log g = 5. Dotted line stands for a computation with complete depletion of Ti and V into grains. Note the poor fit on the spectra. Solid line denotes a computation incorporating an opacity source (a_o = 0.03) and different depletion factors R for molecules with respect to chemical molecular equilibrium.

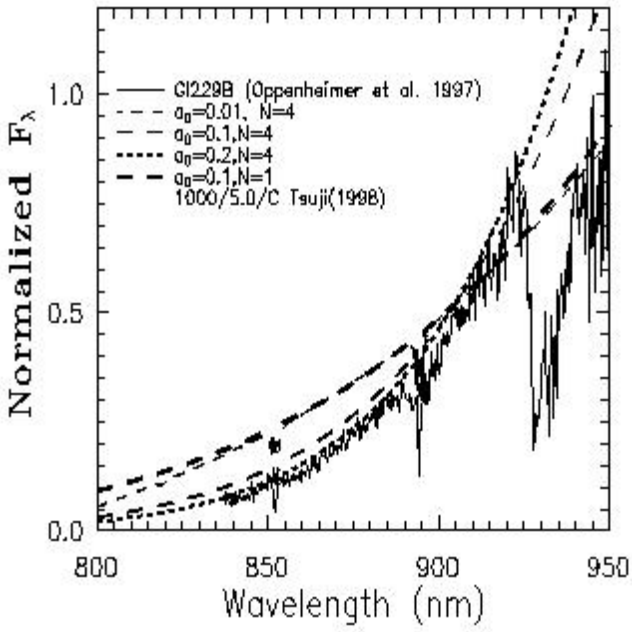

Figure 4: Comparison of the observed spectrum of Gl229B (Oppenhaimer et al. 1997) with synthetic spectra adopting Tsuji's model atmospheres of Teff = 1000 K, log g = 5. Dotted line stands for a computation with didderent AdO parameters. We remark that the slope of the overall shape of the observed data is well reproduced. Only Cs I lines are visible at wavelengths bluer than 900 nm.

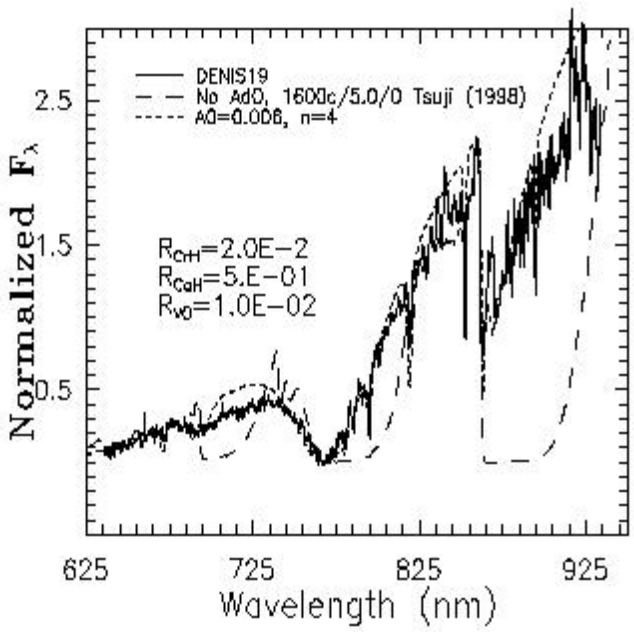

Figure 3: Comparison of the observed spectrum of DBD J1228–1547 with synthetic spectra adopting Tsuji's C-model atmospheres of Teff = 1600 K, log g = 5. Dotted line stands for a computation with complete depletion of Ti and V into grains. Note the poor fit on the spectra. Solid line denotes a computation incorporating an opacity source (a_o = 0.03) and different depletion factors R for molecules with respect to chemical molecular equilibrium.

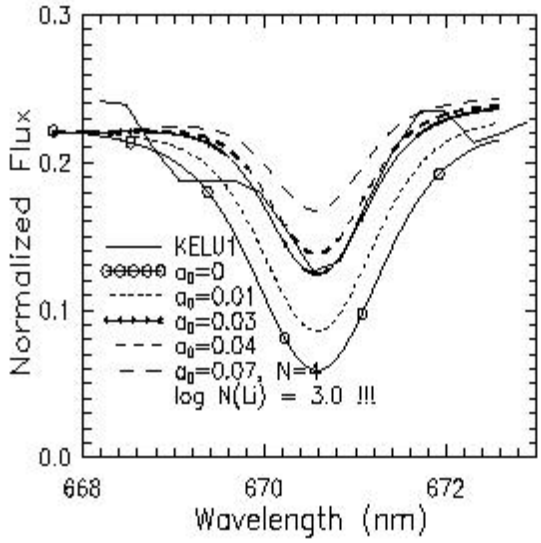

Figure 5: Fit computed for different a_o Li I resonance doublet profiles (λ 670.8 nm) to Kelu 1 spectrum. We got the better fit for log N(Li)=3.0.

pletion into grains we can reasonably fit the shape of the observed spectra.

The most striking features in the spectra (pseudo-equivalent widths of roughly several hundreths to more than 1000 Å) are well fitted in our computations (Figs 2 and 3) and it can be undoubtly attributed to the KI + Na I resonance doublets. Furthemore, both blue and red wings of the KI lines can only be modeled when the extra opacity is considered in the computations.

Our approach allows to find the solution even for the extreme case of H-dwarf[1] Gl229B (Fig. 4).

Other alkaline absorptions (from Li, Rb and Cs) are also present. We have investigated the impact of the additional opacity on the formation of the absorption lines of alkalies. In particular, lithium is severely affected by any extra source of opacity. The larger the opacity, the more veiled the lithium line becomes (Fig. 5). Therefore, weak lithium lines in the coolest brown dwarfs do not necessarily imply a depletion of this light element.

Finally, we claim that the observed sequence of the L-dwarf spectra is *the temperature sequence*:

Object	Teff	log g
BRI0021-024	2200	5.0
Kelu1	2000	5.0
DBD J1228–1547	1600	5.0
DBD J0205–1159	1400	>5.0
Gl229B	1000?	>5.0???

Acknowledgements. Author is thankful to R. Rebolo, M.R.Zapatero Osorio (IAC, Spain), and B. Oppenheimer (Calteck, USA) for the providing of observed spectra and T.Tsuji (Tokyo University, Japan) for providing a grid of "dusty" model atmospheres in digital form, respectively. author thanks LOC and SOC of GMIC99 for the financial support of his participation in the Meeting.

References

Pavlenko, Ya.V., Rebolo R., Martín E.L., García López R.J.: 1995, *Astron. AStrophys*, **308**, 807

Pavlenko, Ya.V. 1998.: *Astron. Reports*, **42**, 787

Pavlenko, Ya.V. 1999.: *Astron. Reports*, **43**, accepted

Pavlenko Ya.V., Rebolo, R., Zapatero Osorio, M.R. 1998.: *in Euroconference on "Low mass stars and brown dwarfs is dtellar clusters and associations", Los-Cancajos, La Palma*, Spain, May 11-15, in press.

Pavlenko Ya.V., Rebolo, R., Zapatero Osorio, M.R.: 1999, *Astron. Astrophys.*, submitted.

Tsuji, T. 1998.: *in Euroconference on "Low mass stars and brown dwarfs is dtellar clusters and associations", Los-Cancajos, La Palma*, Spain, May 11-15, in press.

Tsuji, T., Ohnaka, K., Aoki, W.: 1996a, *Astron. Astrophys.*, **305**, L1

[1] H-dwarfs occupy the intermediate mass region between L-dwarfs and gint planets

MODELS OF ENERGY DISTRIBUTION IN SPECTRUM OF SAKURAI'S OBJECT

Ya. Pavlenko, L. Yakovina, H. W. Duerbeck

[1]Main Astronomical Observatory of NASU Golosiiv wood, Kyiv -127, 03680 Ukraine
yp@mao.kiev.ua, yakovina@mao.kiev.ua
[2]Free University Brussels – VUB, Pleinlaan 2, B-1050 Brussels, Belgium
hilmar@uni-muenster.de

ABSTRACT. Theoretical energy distributions in a spectrum of Sakurai's object (SO) are calculated for a grid of hydrogen-deficient and carbon-rich model atmospheres of $T_{\rm eff}$ = 5000-6200 K and log g= 0.0-1.0. Model atmospheres of SO are computed by the technique of opacity sampling with account of atomic and molecular absorption. Theoretical energy distributions are compared with the spectrum of SO in April 1997 at $\lambda\lambda$ 300 − 1000 nm. We show, that (1) theoretical energy distributions agree well at least qualitavely with the observed ones and depend strongly on $T_{\rm eff}$; (2) an absorption by the C_2 and CN bands is dominated in visible and near IR region of the SO spectrum, an atomic absorption becomes important in UV and blue region. We estimate for SO $T_{\rm eff} \approx$ 5500K and its interstellar reddening $E_{\rm B-V}$ = 0.70 for April, 1997.

Key words: Sakurai's object, AGB and post-AGB evolution, model atmospheres, synthetic spectra.

1. Introduction

Sakurai's object (SO, V4334 Sagittarii) was discovered on February 20, 1996 (Nakano et al., 1996) as "nova-like object in Sagittarius" at $\sim 11^{\rm m}$, but no emission lines were found in its spectrum. Its progenitor was a faint blue star ($\sim 21^{\rm m}$) in the centre of a low surface brightness planetary nebula.

It is supposed that the beginning of the flash was in the end of 1994. Then the effective temperature of SO decreased, but its optical luminosity increased in 1995-1997. In early and in late 1998 abrupt declines of brightness at all colours occurred. This is interpreted as onsets of dust formation, very similar to those observed in R CrB variables (see Duerbeck et al. 1999). The nature of observed processes testifies that SO is an AGB star at a final stage of helium source flare (Duerbeck & Benetti 1996), that was predicted by theory (Iben 1984). The exact spectral classification of SO is essentially hindered due to the unusual abundances: there is a hydrogen deficit in the atmosphere, and C/O > 1 (Asplund et al. 1997, Kipper & Klochkova, 1997). From the spring of 1997 SO is classificated as C-star (Arhipova et al. 1998).

We compute and compare with observations theoretical energy distributions in the SO spectrum and determined the effective temperature of SO in April 1997. This requires calculations of model atmospheres with peculiar chemical abundances and synthetic spectra taking into account the numerous atomic lines and molecular bands in the wide spectral region.

2. Observations

In our work we use an observed spectrum of SO in the range of $\lambda\lambda$ 300-1000 nm, taken April 29, 1997 (see Duerbeck et al. 1999 for more details). No obvious dust obscuration is seen in the light curve of SO at this data. However, Kamath & Ashok (1999) claim that some dust had formed in April-May 1997.

The extinction is still an unclear point. We use the correction for the interstellar reddening $E_{\rm B-V}$=0.54 as well 0.70 (see Pavlenko et al. 2000).

3. Procedure.

Our computations of model atmospheres and synthetic spectra are carried out for classical approaches: LTE, plane-parallel model atmosphere, no energy divergence. The chemical composition of SO of Asplund et al. (1997) is used (see Table 1). It agrees well enough with the data of Kipper & Klochkova (1997). Ionization-dissociation equilibrium is calculated for a set of 70 atoms, ions and molecules. For computing of absorption by atoms and ions we use VALD line lists (Piskunov et al. 1995). Molecular absorption in frequencies of 20 band systems of diatomic molecules (see Table 2) is calculated in the "just overlapping approximation" (JOLA) approach. The input information for

Table 1: Abundances of chemical elements in the atmosphere of SO (Asplund et al. 1997), $\sum N_i = 1$

Z	Element	log N (SO)	log N (Sun)
1	H	-1.73	-0.04
2	He	-0.03	-1.05
3	Li	-7.83	-10.88
6	C	-1.73	-3.48
7	N	-2.53	-3.99
8	O	-1.93	-3.11
10	Ne	-2.13	-3.95
11	Na	-4.73	-5.71
12	Mg	-4.83	-4.46
13	Al	-4.83	-5.57
14	Si	-4.33	-4.49
16	S	-4.83	-4.83
19	K	-6.63	-6.92
20	Ca	-5.83	-5.68
21	Sc	-8.33	-8.94
22	Ti	-7.33	-7.05
24	Cr	-6.93	-6.37
26	Fe	-5.13	-4.37
28	Ni	-5.33	-5.79
29	Cu	-6.53	-7.83
30	Zn	-6.73	-7.44
37	Rb	-7.73	-9.44
38	Sr	-6.53	-9.14
39	Y	-8.13	-9.80
40	Zr	-8.43	-9.44
56	Ba	-9.93	-9.91
57	La	-9.83	-10.82

this calculations is described in Pavlenko & Yakovina (1999). Note, that we suppose that all carbon exists in the form of ^{13}C.

Opacity sampling model atmospheres of SO and its synthetical spectra are computed by SAM941 (Pavlenko 1999) and WITA6 programs, respectively. The last is the version of the program WITA31 (Pavlenko 1997). In WITA6 some additional opacity sources, i.e. bound-free absorption of C I, O I, C^- are included (see Pavlenko et al. 2000 for more details).

We put microturbulent velocity in SO atmosphere 5 km/s, as a typical value for atmospheres of post AGB stars. Theoretical spectra are convolved by a gaussian with half-width 0.5nm.

4. Results

In Fig. 1 we show an identification of the main features in the SO spectrum of April 1997. Its overall shape is governed by the bands of C_2 Swan system and by violet and red systems of CN. In the near UV

Table 2: Band systems of diatomic molecules that were taken into account in this paper

Molecule	System	
C_2	$e^3\Pi_g$-$a^3\Pi_u$	Fox-Herzberg
C_2	$d^3\Pi_g$-$a^3\Pi_u$	Swan
C_2	$A^1\Pi_u$-$X^1\Sigma_g^+$	Phillips
C_2	$b^3\Sigma_g^-$-$a^3\Pi_u$	Ballik-Ramsay
CN	$B^3\Sigma^+$-$X^3\Sigma^+$	violet
CN	$A^3\Pi$-$X^3\Sigma^+$	red
CS	$A^1\Pi$-$X^1\Sigma^+$	
CO	$A^1\Pi$-$X^1\Sigma^+$	
CO	$C^1\Sigma^+$-$A^1\Pi$	Herzberg
CO	$B^1\Sigma^+$-$A^1\Pi$	Angström
NO	$A^3\Sigma^+$-$X^3\Pi_r$	γ
NO	$B^3\Pi_r$-$X^3\Pi_r$	
NO	$C^3\Pi_r$-$X^3\Pi_r$	δ
MgO	$B^1\Sigma^+$-$X^1\Sigma^+$	
AlO	$C^3\Pi_r$ -$X^3\Sigma^+$	
AlO	$B^3\Sigma^+$-$X^3\Sigma^+$	
SiO	$E^1\Sigma^+$-$X^1\Sigma^+$	
SiO	$A^1\Pi$-$X^1\Sigma^+$	
SO	$A^3\Pi$-$X^3\Sigma^-$	
CaO	$C^1\Sigma$-$X^1\Sigma$	

($\lambda < 400$ nm) the atomic absorption becomes important. In our low-resolution spectrum only the strongest atomic lines can be identified: Ca^+ H and K (λ 393.48, λ 396.96 nm), Na D (λ 589.16, λ 689.75 nm), IR triplet of Ca^+ (λ 850.03, λ 854.44, λ 866.45 nm).

A comparison of observed and computed energy distributions shows their reasonably good *qualitative* agreement. Thus, the main opacity sources in the atmosphere of SO can be considered as well defined. At the same time, the comparison of observed and computed flux intensities of C_2 and CN bands in the near UV part of the spectrum of SO shows that the theo-

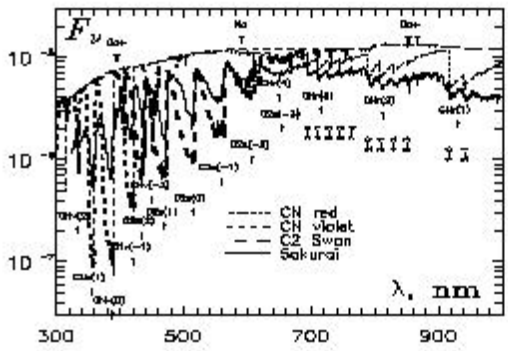

Figure 1: Identification of the strongest features in the SO spectrum of April 1997.

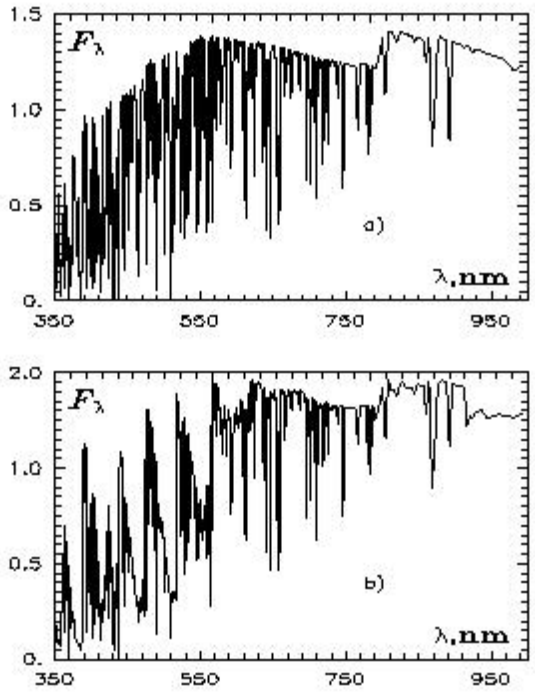

Figure 2: Theoretical energy distributions computed for SO model atmosphere 6250/1.0 without (a) and with (b) molecular (JOLA) absorption.

retical bands appear essentially deeper.

Our calculations show, that strong enough molecular bands appeares in the spectum computed for $T_{eff} \sim 6000$ K (Fig. 2). They become stronger, when T_{eff} drops, because molecular densities of C_2 and CN should increase with the lowering of effective temperature. Comparison of observed and computed fluxes F_λ for model atmospheres with $T_{eff} = 5000$ and 6000 K is shown in Fig. 3. This picture shows that the energy distribution in the spectrum of SO depends critically on T_{eff} . The best fit we obtained for an intermediate $T_{eff} \sim 5500$ K. It can be seen on Fig. 4.

To study an inpact of log g on the SO spectrum we computed two model atmospheres 5500/1.0 and 5500/0.0 and theoretical energy distributions for these models. We conclude that the dependence of the SO spectrum on log g is of "second order importance" and it also can be affected by the sphericity effects in the SO atmosphere.

In Fig. 4 we show the fits to the observed SO spectrum, corrected for $E_{B-V} = 0.70$ and 0.54. The fit with $E_{B-V} = 0.70$ looks better, especially in the red part of the spectrum.

There are several hints that the chemical abundances in the SO atmosphere are changed in short time scales (1995-1997, see Asplund et al. 1997 for details). Therefore, a study of a dependence of the output fluxes on the H, C, N, O abundances is of interest. First of all, the abundance changes affect the chemical balance, and, hence, the emitted spectra of SO. Furthe-

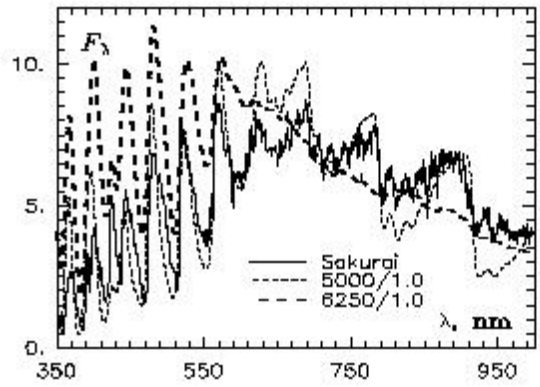

Figure 3: Comparison of the observed and computed radiative fluxes for model atmospheres with T_{eff} = 5000 and 6000 K

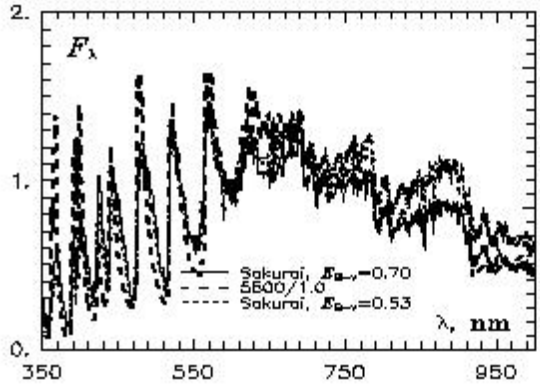

Figure 4: Comparison of computed radiative fluxes for atmosphere models with T_{eff} = 5500 and observed SO spectrum corrected for E_{B-V}= 0.54 and 0.70.

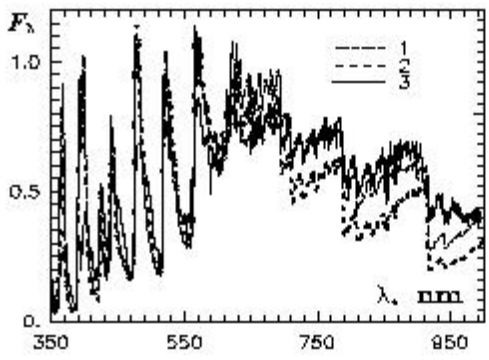

Figure 5: Comparison of the observed spectrum of SO and theoretical ones on different input hydrogen abundances

more, a structure of model atmospheres is changed also. As a result, we have a complicate dependence of the SO spectra on abundances. We computed several model atmospheres for different abundances and found that variations of the hydrogen abundance, for example from the $logN(H) = -4.0$ (hydrogen abundance in R CrB atmosphere, see Asplund at al. 1997) up to $\log N(H) = -1.73$ (a case of SO, see Table 1), show a rather weak impact on the model atmospheres or output spectra of SO (fig. 5). In general, a dependence of the theoretical spectra of SO from the H, C, N, O abundances is rather complicate.

5. Discussion

There are several essensial subjects for discussion in this work: adopted approaches for computations, the enormous intensities of the theoretical spectra of carbon-containing molecules in blue and UV region, the estimations of T_{eff} for SO in April, 1997 and interstellar reddening E_{B-V}.

Our computations were carried out in the framework of plane-parallel approach. We simplify the real situation (see Asplund et al. 1997) by ingoring of the sphericity effects. Note, however, that there are a few other problems to be studied even in the framework of this simple approach. Furthemore, shpericity effects should affect mainly the outermost layers, whose structure depends also on many processes: dust particles formation, depletion of molecular species, chromospheric-like effects, interaction with the dusty envelope, nonhomogenuity, etc. Unfortunately, for the time being, physics of the processes is poorly known yet.

Also the accuracy of JOLA approach can be unsufficient for faint molecular bands. But we note, that only due to using JOLA we could to make such a wide work, while the contribution of faint bands in total molecular absorption is usually small.

We note some enhancening of the theoretical C_2 and CN bands in blue and UV region. One may interpret these results within the frame of the phenomenon of "too strong carbon lines" (see Asplund et al. 1997) for type R CrB stars or as an impact of the dust (Duerbeck et al. 1999). It can be also a consequence of the lack of the continuum or line opacities in the blue part of the spectrum (Pavlenko & Yakovina 1999). The last is caused by incompletness of lists of the used atomic lines and molecular bands.

Obtained in this work T_{eff} SO in April 1997 $T_{eff} \sim 5500$ K is lower than the value of Kipper and Klochkova (1997) $T_{eff} = 7250$ K for July, 1996. In general, effective temperatures of SO were reduced by time in 1995 - 1997. Arhipova et al. (1998), using the photometric calibration of "normal" C-giants, determined for SO T_{eff} =5100 K in March, 1997 and 4600 K in June, 1997. Their T_{eff} are lower than our estimation for April, 1997, but one should remember about uncertainties of spectral classification of SO due to its unusual evolutionary status.

We found that the observed spectrum of Sakurai's object in April, 1997 corrected by interstellar reddening E_{B-V}= 0.70 is well fitted by theoretical spectra computed for model atmosphere 5500/1.0. In that way, in the frame of our self-consistent approach, we *independently* obtained also the interstellar reddening parameter which was poorly known for SO (see discussion in Pavlenko et al. 2000).

Acknowledgements. We thank Prof. T.Kipper and Dr.M.Asplund for the helpful discussions. Ya.Pavlenko thanks of LOC and SOC of the GMIC99 for the financial support of his participation in the Meeting. Authors thank VALD database team for the helpful service.

References

Arhipova V.P., Esipov V.F., Noskova R.I., Sokol G.V., Tatarnikov A.M., Shenavrin V.I., Yudin B.F., Munari U., Rechkuba M.: 1998, *Pis'ma v Astron. Zhurn.*, **24**, 297.

Asplund M., Gustafsson B., Lambert D.L., Rao N.K.: 1997, *Astron. Astroph.*, **321**, L17.

Duerbeck H.W., Benetti S.: 1996, *Astrophys.J.*, **468**, L111.

Duerbeck H.W., van Genderen A., Jones A., Liller W.: 1999, *Southern Stars*, **38**, 80.

Iben I.: 1984, *Astrophys.J.*, **277**, 333.

Kamath U.S., Ashok N.M.: 1999, *Mon. Not. R. Astron. Soc.*, **302**, 512.

Kipper T., Klochkova V.: 1997, *Astron. Astroph.*, **324**, L65.

Nakano S., Sakurai Y., et al.: 1996, *IAU Circ.*, 6322.

Pavlenko Ya.V.: 1997, *Astroph. Space Sci.*, **253**, 43.

Pavlenko Ya.V.: 1999, *Astron. Reports*, **43**, 94.

Pavlenko Ya.V., Yakovina L.A.: 1999, *Astron. Reports*, accepted.

Pavlenko Ya.V., Yakovina L.A., Duerbeck H.W.: 2000, *Astron. Astrophys*, submitted.

Piskunov N.E., Kupka F., Ryabchikova T.A., Weiss V.V., Jeffery C.S.: 1995, *Astron. Astroph., Suppl.*, **112**, 525.

Pollacco D.: 1999, *Mon.Not.R.Astron.Soc.*, **304**, 127.

EVIDENCE ON HOT SPOT IN CONTACT BINARY VW CEPHEI

I.B. Pustylnik[1], P.G. Niarchos[2]

[1] Department of Astrophysics, Tartu observatory
Tartu region, Toravere 61602, Estonia, *izold@aai.ee*
[2] Department of Astrophysics, Astronomy and Mechanics
Faculty of Physics,University of Athens,GR-157 84
Athens, Greece, *pniarcho@atlas.cc.uoa.gr*

ABSTRACT. We study the nature of asymmetry and the intrinsic variability in the light curves of VW Cep. We analyze our own B,V light curves as well as the other data from literary sources. In view of the presence of significant intrinsic brightness variations at a level of $0^{\rm m}.01 - 0^{\rm m}.03$ on time scales comparable to the orbital period we deal only with *individual* light curves sampled possibly in one-two consecutive orbital cycles. The evidence for the presence of the small hot spot region close to the neck connecting both components will be summarized: a) displacements of the brightness maxima from the predicted epochs of elongations suggestive of an additional energy input supposedly of the hot chromospheric origin, b) the overall pattern of asymmetry in brightness maxima and minima, c) systematic colour changes with the orbital phase, d) the presence of significant cosine odd harmonics in truncated series of the observed light curves. We find that the hot spot with a characteristic size of $R \sim 0.7 - 1.2 \cdot 10^{10} cm$ and the temperature contrast $\Delta T/T = 1.3 - 1.4$ located on the surface of a more massive star can explain the afore-mentioned peculiarities whereas model light curves based on our model give rather good fit to the observed data studied so far. The possible physical nature of the hot spot in the light of our results confronted with the spectroscopic data (specifically Mg II resonance doublet) and flare activity signatures are briefly discussed.

Key words:stars:binary: contact; stars: individual: VW Cep.

1. Introduction

The contact binary VW Cephei (*HD 197433 = BD* $+75^{\rm o}752, 20^{\rm h}38^{\rm m}03^{\rm s} + 75^{\rm o}25'.0(1950), G5, P = 6^{\rm h}41^{\rm m}$) from the moment of its discovery in 1924 till now remains the target of intensive astrophysical research. In recent period the wave-like distortions of the light curves superimposed upon the regular brightness variations caused by mutual eclipses and tidal distortions of both components nearly filling in their respective Roche lobes received considerable attention. New observational data have been accumulating suggestive of a variable chromospheric and coronal activity ,both regular and of a flaring nature (see, for instance, Bradstreet and Guinan 1990, Pustylnik 1995, Choi and Dotani 1998).

There is now consensus among the investigators of close binary systems that AB component of VW Cephei consists of two low mass main sequence stars ($m_1 \simeq 0.9 m_\odot, m_2 \simeq 0.25 m_\odot, R_1 = 0.93 R_\odot, R_2 = 0.5 R_\odot, T_{1\rm eff} \simeq 5000^{\rm o} K, T_{2\rm eff} \simeq 5200^{\rm o} K$) (see Hill 1989). By all evidence VW Cep system "oscillates" between the contact and semi-detached configuration. In its present state mass transfer caused by magnetic wind from the low mass component should result in a gradual merging of the components (for details of evolutionary scenarios, see Robertson and Eggleton 1977, Lucy and Wilson 1979).

And yet despite the variety of the observational data the nature of the wave-like distortions of the light curves and their possible connection with the short term orbital period variations remain obscure. To interpret the different brightness maxima heights (O'Connell effect) the idea of dark spots or of circumstellar (circumbinary) matter have been exploited (for more details see Karimie 1983, Hendry *et al* 1992, Pustylnik and Sorgsepp 1975). The purpose of our contribution is to draw attention to a supplementary source of information which in our view may throw an additional light on the nature of asymmetry of the light curves in VW Cephei system: the phase behaviour of the light maxima.

2. Epochs of maxima, displacement in respect to elongation

In an earlier paper (Pustylnik and Kreiner 1997) we reported for the first time about the discovery of small but significant phase displacements of light maxima in VW Cep from the predicted epochs of elongation. Recently we have extended the data base including ob-

servations by Linnell (1980) and Niarchos *et al* (1998) in our analysis. We used polynomial approximation for normalized brightness $l(T) = \sum_{j=0}^{n} a_j T_i^j$ (T_i being the Julian date for the observation considered) and normally $n = 6$ was adopted.The observed moments of brightness maxima have been determined iteratively with the aid of Newton's method solving equation $dl/dt = 0$ (for more details see Pustylnik and Kreiner 1997). We used the data only of high quality with the observational points covering the total light curve and never used average light curves. In this way a number of epochs for the primary and of the secondary maxima have been determined and summarized in Table 1. In all these cases we see small but significant

Table 1: Epochs of the primary $E_{\rm pr}$ and secondary $E_{\rm sec}$ maxima and $(O-C)$

$E_{\rm pr}$	$O-C$	$E_{\rm sec}$	$O-C$
2439467.3288	0.006	2439467.4622	-0.003
2439467.6074	0.004	2439521.4620	0.005
2439521.3184	0.001	2439918.3260	-0.007
2439748.4222	0.004	2439918.6089	-0.004
2439935.4510	0.002	2439935.5836	-0.004
2439964.3967	0.003	2439964.5304	-0.003
2444477.8083	0.002	2444477.6674	-0.001
2448531.4173	0.005	2448152.2112	0.002
2449278.3863	0.005	2449276.4298	-0.004

displacements of the brightness maxima in respect to the predicted moments of elongation. The displacement amounts to $0.^{\rm d}005 - 0.^{\rm d}008$, i.e $0.03P_{\rm orb}$, whereas the formal accuracy of the position of the brightness maximum from the smooth curve is no less than $0.^{\rm d}0002 - 0.^{\rm d}0003$. We regard thus determined displacements of the brightness maxima as real, since in no cases studied so far we have found displacements of the moments of brightness minima from predicted epochs exceeding $0.^{\rm d}001$.

As we see from the data of Table 1, a higher maximum (following the primary minimum) is observed at a later epoch than it follows from the value of the orbital period whereas the lower maximum (preceding the primary minimum) preferentially comes at an earlier epoch. This can be interpreted as an evidence for the asymmetric (in respect to the line of centres) brightness distribution over the hemisphere of a primary component facing its low mass companion. It is obvious that this subtle effect will be smoothed out if one deals with the average light curves in view of the intrinsic light variations. To analyse in more detail brightness changes during maxima we have approximated full light curves with the aid of truncated series

$$L(\phi) = \sum_{j=0}^{n} (A_j \cos j\phi + B_j \sin j\phi), \qquad (1)$$

and determined the coefficients A_j, B_j for 6 nights for which observational points covered the whole light curve. The results are indicated for 2 nights in Table 2. In addition in the last lines of the Table we are attaching the coefficients of even harmonics of the cosine truncated series tabulated by Rucinski (1995) which approximate the light curves of W UMa type binaries for different angles of orbit inclination i, mass ratios q and fill-out parameter f. Figure 1 illustrates typical

Table 2: Coefficients of the truncated series JD2439000+...

JD467	$-A_1$	$-A_2$	$-A_3$	$-A_4$	$-A_5$	$-A_6$
B	0.022	0.133	0.006	0.024	0.009	0.012
V	0.022	0.124	0.007	0.021	0.009	0.011
JD748	$-A_1$	$-A_2$	$-A_3$	$-A_4$	$-A_5$	$-A_6$
B	0.022	0.132	0.011	0.026	0.010	0.011
V	0.020	0.123	0.012	0.025	0.008	0.011
$f = 0.0$	–	-0.103	–	-0.021	–	-0.008
$f = 0.5$	–	-0.128	–	-0.013	–	-0.005

results for JD2444477 in V colour. Similar results are obtained for other 4 nights.

As one can see from the plot there is in general a good agreement between the observations and approximation by truncated series except for the phase interval $\phi = 0.95 - 1.05P$, i.e. the bottom of the primary minimum. The coefficients of even harmonics A_2, A_4, A_6 are in good agreement with the values found from Rucinski's paper. But in addition to even harmonics considerable odd harmonics are present. Their sums are $C_1 = A_1 + A_3 + A_5$. For JD2439748 we have respectively $C1 = -0.043, -0.040$ (in B and V), JD2439467 -0.037, -0.038(B and V), JD2439918 - 0.030, -0.052(B and V), JD2444472 -0.020,-0.034,-0.063, -0.008 (B,V,R,I respectively), JD2444477 -0.034,-0.033 (B and V). We interpret it as the contribution from the "hot spot" which would have been best visible at the phase angle value $\phi = 0.5P$ but it is hidden (at least partially) because of the transit eclipse of a more massive component. The value of C_1 is very close to the amplitude of the colour curves and the differences in brightness minima depths.

3. Estimate of the parameters of the hot spot

Displacement of the maxima positions from elongations along with the pronounced overall asymmetry of the light curves can be interpreted as an evidence of an additional energy input (apparently of non-thermal origin) which affects the regular light variations caused by the tidal distortions of both components nearly filling in their Roche lobes. Whatever is the nature of mechanism responsible for the observed asymmetry, to cause the displacement in phase of maximum by $\Delta\phi$ an additional energy input is needed $L \geq C \frac{dl}{d\phi} \Delta\phi$ where the value $dl/d\phi$ can be estimated with the aid of the

theoretical light curve and the constant C should be of order $C \simeq 1-10$. Taking use of the data for the effective temperatures and the radii of the components from Hill(1989) we have found $L = 2 \cdot 10^{29} ergs/s$ and $L = 2 \cdot 10^{30} ergs/s$ for $C = 1$ and $C = 10$ respectively. An average value of the difference between the heights of the adjacent maxima for the Julian dates given in Table 1 yields the estimate $L = 3.5 \cdot 10^{30} ergs/s$. Next assuming that mutual eclipses and tidal distortions fully determine the shape of the light curve for a standard limb darkening law we shall attempt now to estimate the size and the temperature of the putative spot. In doing that we neglect small differences in temperature between the component stars (according to various authors $\Delta T \sim 150^{\circ} K$) and the gravity darkening effect. Since in U, B, V colours and even in R and I we can safely use Wien's approximation a simple expression holds for the total luminosity of the binary in wave-length λ_j for the phase angle ϕ in orbit

$$L_{\lambda j}(\phi) = \frac{c_1}{\lambda_j^5} \exp(-\frac{c_2}{\lambda_j T_{\rm st}}) [S_{1\rm st}(\phi) + S_{2\rm st}(\phi)] + \frac{c_1}{\lambda_j^5} \exp(-\frac{c_2}{\lambda_j T_{\rm sp}}) S_{\rm sp}(\phi), \quad (2)$$

where $T_{\rm st}$ and $T_{\rm sp}$ are respectively the effective temperatures of the components and the spot whereas $S_{1\rm st}, S_{2\rm st}, S_{\rm sp}$ are projected areas upon the plane of the sky of the components and the spot. Now introducing the temperature contrast $\delta T_{\rm sp} = (T_{\rm st} - T_{\rm sp}/T_{\rm st})$ and relative area $\delta_{\rm sp}(\phi)$ in units of the total area of a binary visible at a given phase angle ϕ in orbit we can easily find that

$$\delta_{\rm sp}(\phi) = 0.921034 [\Delta m_{\lambda j(\phi,0)} - 2.5 \lg(L_{\lambda j}(0)/L_{\lambda j}(\phi))] \exp(-\frac{c_2 \delta T_{\rm sp}}{\lambda j T_{\rm sp}}) \quad (3)$$

where $\Delta m_{\lambda j} = m_{\lambda j}(\phi) - m_{\lambda j}(0)$ is the observed difference in stellar magnitudes of VW Cep for phase angles 0 and ϕ. Taking the data for the full amplitude of the light curves in U,B,V,R,I from the paper of Linnell (1980) the orbital elements from the paper of Hill(1989) and calculating from the model light curves $L_{\lambda j}(0)/L_{\lambda j}(\phi)$ we arrive at the below-given values for $\delta_{\rm sp}(\phi = \pi/2)$,(see data in Table 3) for different assumed values of the temperature of the hot spot. Applying (3)

Table 3: Relative size of the hot spot

$T_{sp}(K)$	U	B	V	R	I
6000	0.063	0.053	0.041	0.038	0.020
7000	0.021	0.024	0.023	0.023	0.016
8000	0.012	0.014	0.014	0.017	0.012

to the luminosity of VW Cep, for instance, in B and V colors we have the following relation between the relative size of the hot spot $\delta_{\rm sp}(\phi)$ and the colour change $\Delta(B-V)$ between maximum and primary minimum

$$\Delta(B-V) = 1.086 \delta_{\rm sp} [\exp(-\frac{c_2 \delta T_{\rm sp}}{\lambda_b T_{\rm sp}}) - \exp(-\frac{c_2 \delta T_{\rm sp}}{\lambda_v T_{\rm sp}})]. \quad (4)$$

Because of a crude nature of the estimate we have neglected possible differences in the size of the spot in different colors when deriving relation (4). Applying it to different colors we find the amplitudes of color changes for different values of $T_{\rm sp}$. The results are summarized below in Table 4. In the last line the average observed values are indicated for VW Cep. As we see there is a good agreement between the observed and model color indices, if one assumes that $T_{\rm sp} = 7000^{\circ} K$. The deri-

Table 4: Full amplitudes of colour changes

$T_{sp}(K)$	$\Delta(B-V)$	$\Delta(U-B)$	$\Delta(V-R)$	$\Delta(V-I)$
6000	0.020	0.031	0.016	0.10
7000	0.038	0.070	0.029	0.049
8000	0.057	0.117	0.040	0.064
Δ_{obs}	0.040	0.072	0.030	0.044

ved parameters of the hot spot depend on the adopted orbital elements, notably on the value of fill-out parameter f. The above-given values of δ were obtained assuming $f = 0.05$. However, the results are not specially sensitive to the assumed value of f. For instance if one takes $f = 0.4$, one finds δ smaller by about 20 per cent than those given-above.

To verify how the hot spot with the above-given parameters can be helpful in interpreting the observed light curves of VW Cep we used commercially available computer package *BINARY MAKER* and modelled with its aid the light curves of VW Cep assuming the orbital and physical parameters from Hill (1989) and changing only the inclination angle $i \simeq 65^{\circ} - 67^{\circ}$.

We have found the best fit for the following values of the hot spot parameters:$R_{\rm sp} = 7^{\circ} \pm 1^{\circ}, \delta T/T \simeq 1.35 - 1.4, L_3 = 0.02 - 0.03$ (the third light),$f = 0.05, l = 80^{\circ} \pm 2^{\circ}, \chi = 357^{\circ} \pm 2^{\circ}$ (l being the latitude and χ the longitude of the centre of the hot spot upon the surface of more massive component). Figure 2 illustrates results for light curve in V for Julian date 2439467. Although the agreement between the observed and model light curves is not fully satisfactory, we see that the model light curves reproduce the observed phase displacements of maxima and produce the overall observed pattern of asymmetry.

We find especially encouraging that the derived value of the temperature of the hot spot is practically coincident with the temperature needed to generate $MgII\lambda 2795, 2802 \dot{A}$ strong resonance doublet feature, whereas both the flux in this feature and the phase of its maximum are in good accord with the above given estimate of the luminosity of the hot spot and

its location(for details see Pustylnik 1995 and the graphical data in Bradstreet and Guinan 1990 for $MgII\lambda 2795, 2802\dot{A}$ and H_α line composite profile). To summarize, we find the proposed hot spot is an essential cohesive element of the model for VW Cep because it solves an old enigma of the color changes on one hand and gives natural explanation to small differences in depths of minima for practically equal effective temperatures of the components on the other. With its application the discrepances between the photometric and spectroscopic data find natural explanation.

Acknowledgements. We acknowledge with gratitude support of the current investigation by the Grant D00 974 in the framework of the NATO Science Fellowship and by the Grant 2629 of Estonian Science Foundation.

References

Bradstreet D.H., Guinan E.F.: 1990, *In: Active Close Binaries,* ed. C.Ibanoglu (Dordrecht: Kluwer), 467.
Choi C.S., Dotani T.: 1998, *Ap.J.*, **492**, 761.
Hendry P.D., Mochnacki S.W., Collier Cameron A.: 1992 *Ap.J.*, **399**, 246.
Hill G.: 1989, *Astron. Astrophys.*, **218**, 141.
Karimie M.T.: 1983, *Astrophys. Space Sci.*, **92**, 53.
Linnell A.P.: 1982, *Astrophys.J. Suppl.Ser.*, **50**, 85.
Lucy L.B., Wilson R.E.:1979, *Astrophys.J.*, **231**, 502.
Niarchos P.G., Hric L., Manimanis V., Theodossiou E.: 1998, in: *Proc. of the 20th Stellar Conference of the Czech and Slovak Astr. Inst.*, 89.
Pustylnik I., Sorgsepp L.: 1975, *Publ. Tartu obs.*, **43**, 130 (in Russian).
Pustylnik I.: 1995, in: *Stellar Surface Structure, IAU Symp.* **176**, Wien, Poster Proceedings, ed. K.G.Strassmeier, 215.
Pustylnik I., Kreiner J.: 1997, in: *"Astronomical Time Series",* ed. D.Maoz, A.Sternberg, E.Leibowitz, Kluwer Publishers, 207.
Robertson J.A., Eggleton P.P.: 1977, *Monthly Not. Roy. Astr. Soc.*, **179**, 359.
Rucinski S.M.: 1995, *Astron. J.*, **109**, 2690.

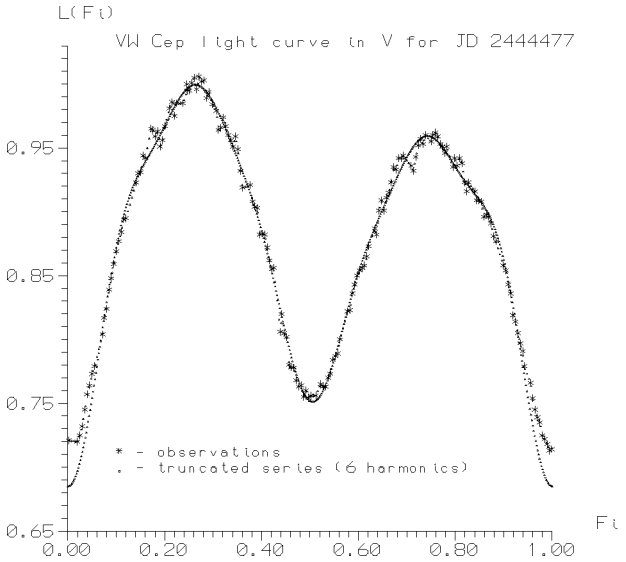

Fig. 1. Observed V light curve of VW Cephei for *J.D.*2444477 and approximation by truncated series(see formula (1) in text).

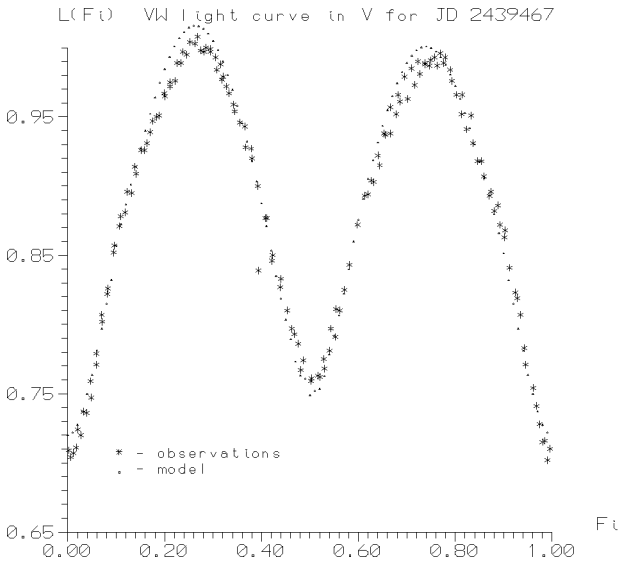

Fig. 2. Observed V light curve of VW Cephei for *J.D.*2439467 and the model light curve assuming presence of a small hot spot upon the surface of the primary component close to the neck region.The physical parameters and location of the spot are given in the text.

BLOB PARAMETERS OF ACCRETION STREAMS IN MAGNETIC CATACLYSMIC VARIABLES

N.M. Shakhovskoy[1], I.L. Andronov[2], S.V. Kolesnikov[3], A.V. Halevin[2]

[1] Crimean Astrophysical Observatory
Crimea, Ukraine, *shakh@crao.crimea.ua*
[2] Department of Astronomy, Odessa State University
T.G.Shevchenko Park, Odessa 270014 Ukraine, *astro@paco.odessa.ua*
[3] Astronomical observatory, Odessa State University
T.G.Shevchenko Park, Odessa 270014 Ukraine, *astro@paco.odessa.ua*

ABSTRACT. Results of investigations of the autocorrelation functions for two magnetic cataclysmic variables BY Cam and QQ Vul are presented. Significant variations of this characteristic are detected. They are interpreted as caused by variations of the blob length or by changes of the accretion column height. For the first time, the dependence "shot noise decay time - circular polarization" was discovered.

Key words: stars: close binaries: magnetic field; accretion: accretion discs; stars: cataclysmic, X-ray sources; individual: BY Cam, QQ Vul.

Here we describe some results of study of the fast optical and polarization variability of the magnetic cataclysmic variables with a synchronizing (BY Cam) and synchronous (QQ Vul) magnetic white dwarf.

Except quasi-periodic oscillations at a time scale of seconds (Langer, Chanmugam & Shaviv, 1982), the fast variability up to minutes is often described by a shot noise characterized by an exponential decay of the autocorrelation function (Andronov, 1998). This shot noise is interpreted as the product of inhomogeneous blob accretion (Aslanov, Kornilov & Cherepashchuk, 1978; Panek, 1980; Kuijpers & Pringle 1982; Beardmore & Osborne 1997). Asymmetry of the nonstationary 3-D accretion column may produce few types of the structure variations (Andronov, 1987).

In order to investigate these effects, the orbital and other hour-scale variability was removed from the light curve (Fig. 1a) by using a 3-rd order polynomial fit. The parameters which describe the emission, are the shot rate and the shot decay time τ. It can be determined from the $1/e$ time-scale of the autocorrelation function (ACF) of the detrended data.

At the Fig. 1a, one can see the light curve of BY Cam, obtained at 2.6m Shain telescope by N.M.Shakhovskoy and S.V.Kolesnikov with a time resolution $\delta = 4.12$ sec. The solid line represents a 3-rd order polynomial fit. The detrended light curve (Fig. 1b) was subdivided into sections of uninterrupted sequences of data, which were used for calculation of autocorrelation functions. In the Fig. 2, the mean ACF from individual runs of length $n = 256$ is shown. The thick line is the AR2 model fit obtained taking into account the finite length of data run n and trend removal according to Andronov (1994). The ratio "signal/(signal+noise)" is r_0=0.888. Corresponding root mean squared deviation of the observed ACF from the theoretical expectation is 0.055.

Such investigations were applied to BY Cam and QQ Vul, which were observed at 1.25m telescope AZT-11 (UBVRI and circular polarization) and at the 2.6m Shain telescope (WR - 0.5-0.75 micron filter + circular polarization). These observations cover a wide energy range and allow to investigate different sources and mechanisms of variability caused by accretion in magnetic cataclysmic variables.

If the shot time-scale τ represents the characteristic emitting time of a blob of length L, then τ is just the fall time needed for blob to pass through the emitting region. Thus one can estimate L from

$$L \sim v_{\rm ff}\tau/4 \qquad (1)$$

where $v_{\rm ff}$ is the free-fall velocity at the shock front, and the factor of $1/4$ arises from the strong shock conditions.

The shot decay time covers a wide range from 20 to 120 seconds. There are hour-to-hour variations which are observed at some nights of observations of BY Cam. However, in different colors, the differences of the shot decay times are not significant. Most interesting results were obtained from the investigations of the "polarization - shot noise decay time" dependencies. In the Fig. 3,4, the graphs for 2.6m Shain telescope observations

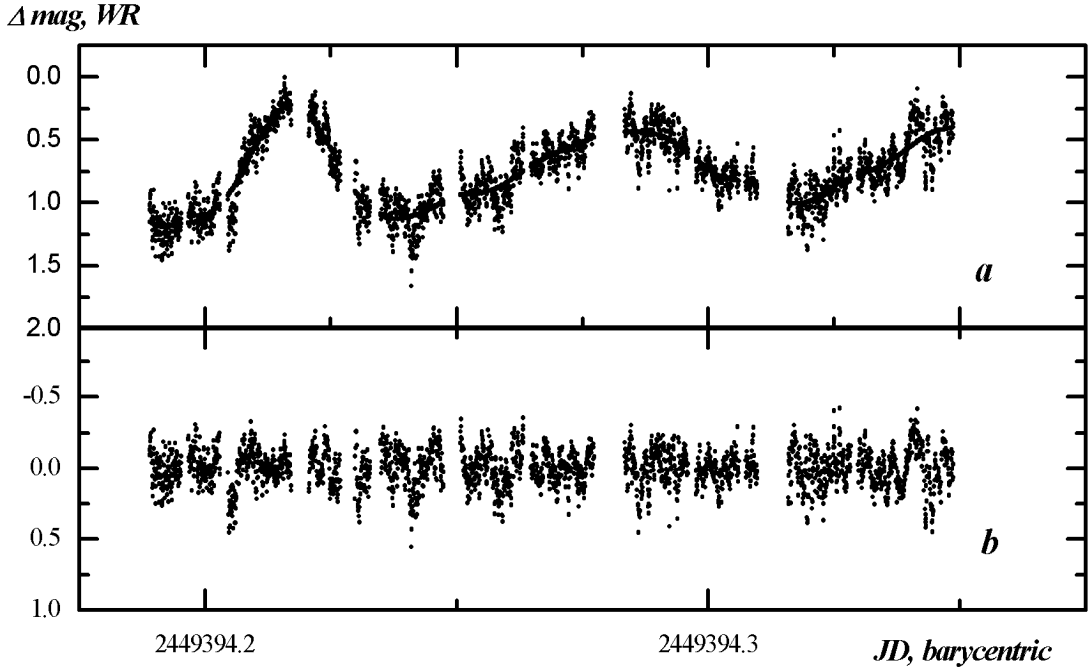

Figure 1: Original *(1a)* and detrended *(1b)* photometric data for BY Cam, obtained at the 2.6-meter Shain telescope.

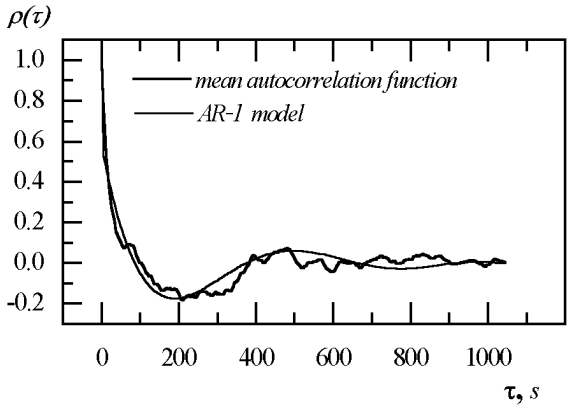

Figure 2: Mean autocorrelation function for current (fig 1b) run and its AR-1 model (Andronov, 1994).

of BY Cam and QQ Vul are shown.

It seems that in BY Cam (Fig. 3a) one may suggest two superimposed dependencies - the first is more smoothly decreasing from 60 to 10 seconds with an increase from negative to positive values of the polarization curve, and the second one is a sharp increase from 20 to 80 seconds with increasing positive polarization.

Similar properties were pointed out by Shakhovskoy, Andronov and Kolesnikov (1992) in a case of AM Her.

We associate two dependencies with two switching poles in this asynchronously rotating magnetic cataclysmic variable (Mason et al., 1998). To explain this phenomenon, we supposed next qualitative model for BY Cam. Two switching poles are not diametrically opposite, they have unequal magnetic field strength (Silber et al., 1992; Piirola et al., 1994), and, therefore, different character of accretion matter motion.

Above the more strong magnetic pole, the plasma freezes earlier to magnetic field. Dense blobs thread into magnetic field lines before the gas accelerates and the stream is shattered into small fragments. For a weak pole, on another hand, the gas arriving at r_μ is therefore suggested to consist predominantly of a spray of small blobs (typically with radii $< 10^8$ cm), with a small probability of some threaded larger blobs that survived intact.

In another figure (Fig. 3b) for QQ Vul, there is no any "decay time - polarization" dependence. This effect can be explained by a presence of weak magnetic pole with a higher Rayleigh-Taylor instability rate of stream, then for BY Cam.

In QQ Vul one may suggest only decade-scale variations of the orientation of the white dwarf in respect to the secondary filling its Roche lobe (Andronov and Fuhrmann, 1987), whereas in BY Cam the stream periodically switches from one pole to another (Mason et al., 1998) causing much larger changes of the structure of the accretion.

The second possibility of the shot decay time variations is the effect of accretion column height changes. When $(r + h)$ increases by 10 times, v_{ff} decreases by about 3.16 times, as a square root of $(r + h)$:

$$v_{ff} = \sqrt{2GM/(r + h)}. \qquad (2)$$

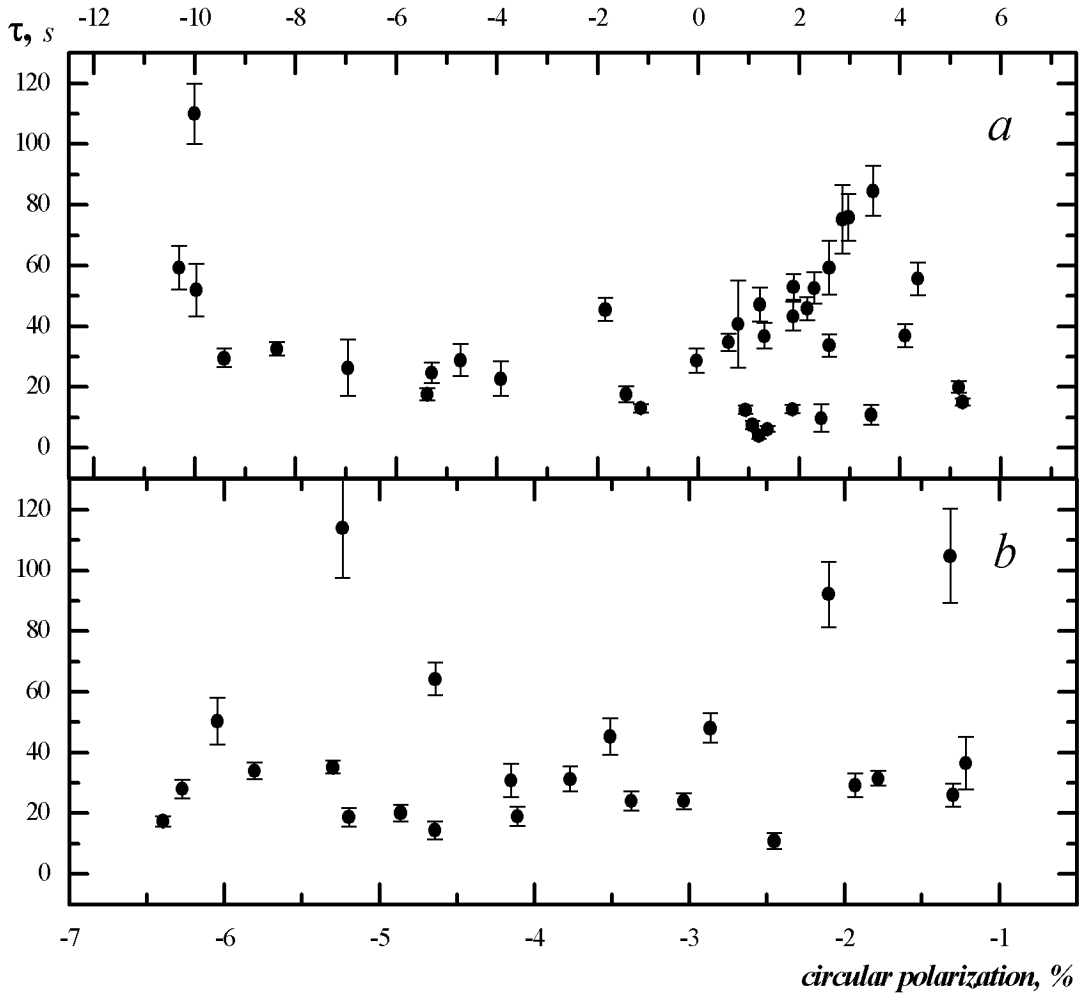

Figure 3: "Polarization - exponential decay time" dependence for BY Cam *(a)* and QQ Vul *(b)*.

Here r is the white dwarf radius and h is the radiative shock height which may be estimated in the case of bremsstrahlung cooling (Yi, 1994) as

$$h \approx (3 \times 10^7 \mathrm{cm}) s_0 m^{23/14} r^{3/2} \mu_{33}^{-4/7} \dot{m}^{-5/7} \qquad (3)$$

In this equation s_0 is some effective column area, $m \equiv M_{wd}/M_\odot$ - white dwarf mass in solar masses, $\dot{m} = \dot{M}/10^{18}$ g s^{-1} is scaled accretion rate and $\mu_{33} = \mu/10^{33}$ G cm^3 is scaled white dwarf magnetic moment.

One more mechanism, which can provide shot decay time variations within one orbital cycle is the changes of orientation of the accretion column (cf. Andronov, 1987). In this case we can see different parts of accretion structure in different orbital phases. It means that different parts of accretion column correspond to different effective blob lengths or shock height.

References

Andronov I.L.: 1987, *Astron. Nachr.,* **308**, 229.
Andronov I.L.: 1994, *Astron. Nachr.,* **315**, 353.
Andronov I.L.: 1998, *As. Soc. Pacif. C. S.,* **169**, 326.
Andronov I.L., Fuhrmann B.: 1987, *I.B.V.S.* **2976**, 1.
Aslanov A.A., Kornilov V.G., Cherepashchuk A.M.: 1978, *Pis'ma AZh,* **4**, 183.
Beardmore A.P., Osborne J.P.: 1997, *M.N.R.A.S.,* **290**, 145.
Langer S.H., Chanmugam G., Shaviv G.: 1982, *ApJ,* **252**, 289.
Kuijpers J., Pringle J.R.: 1982, *As.Ap.*, **114**, L4.
Mason P.A., Ramsay G., Andronov I.L., Kolesnikov S.V., Shakhovskoy N.M., Pavlenko E.P.: 1998, *M.N.R.A.S.,* **295**, 511.
Panek R.J.: 1980, *Ap.J.,* **241**, 1077.
Piirola V., Goyne G.V., Takalo L., Larsson S., Vilhu O.: 1994, *As.Ap.*, **283**, 163.
Shakhovskoy N.M., Kolesnikov S.V., Andronov I.L.: 1992, -in *"Stellar Magnetism",* St.Petersburg, Nauka, 148.
Silber A., Bradt H.V., Ishida M., Ohashi T, Remillard R.A.: 1992, *Ap.J.*, **389**, 704.
Yi I.: 1994, *Ap.J.*, **422**, 289.

ACCRETION ONTO A MAGNETIC DIPOLE: RESULTS OF 2D NUMERICAL SIMULATIONS

Yu.M. Toropin[1], O.D. Toropina[2]

[1] Keldysh Institute of Applied Mathematics, Russian Academy of Sciences, Moscow, Russia; *toropin@spp.keldysh.ru*

[2] Space Research Institute, Russian Academy of Sciences, Moscow, Russia; *toropina@mx.iki.rssi.ru*

ABSTRACT. Different regimes of accretion to a star with a dipole magnetic field were investigated using 2D numerical axisymmetric resistive MHD simulations. Numerical technique was improved over our recently published results (Toropin et al., 1999, refered as T99 below).

A new model for the gravitating star with a dipole magnetic field was adopted for presented simulation set. Spherical accretion to a non–rotating star with a dipole field was modeled. Existence of the stationary accretion flow with polar columns inside the Alfvén surface was confirmed. The accretion rate to the dipole in the axially symmetric flow is always smaller than in the Bondi accretion to corresponding non–magnetized star. Relations, obtained in previous paper (T99), between the accretion rate to the non–rotating dipole $\dot{M}_{dip}$ and the magnetic momentum μ, the density of surrounding medium ρ_∞, the magnetic diffusivity η_m are qualitatively confirmed in simulations with new model of dipole. Specifically, $\dot{M}_{dip} \propto \left(\varrho_\infty / \mu^2\right)^{0.5} \cdot \eta_m^{0.38}$ and the Alfvén radius is $R_A \propto \left(\varrho_\infty / \mu^2\right)^{-0.3} \cdot \eta_m^{0.07}$.

Investigations of the cylindrical accretion (parrallel to the star's magnetic momentum) were started. If the value of the star's gravitational capture radius is close to its Alfvén radius then the magnetic field surves as an effective obstacle for the incoming flow deflecting it from the star. Simulated flow structure is discussed.

Key words: accretion; dipole; MHD; OINS

1. Introduction

A general analytic solution for spherical accretion to a non–magnetized star was obtained by Bondi (1952). His results were confirmed recently with the help of numerical three–dimensional (3D) hydrodynamic simulations by Ruffert (1994). Accretion of matter with low angular momentum to non–magnetized center was investigated by Bisnovatyi–Kogan & Pogorelov (1997).

Less attention has been given to quasi–spherical accretion to a *magnetized star*. Although in many cases accretion occurs through a disk, in other cases, where accreting matter has small angular momentum the accretion flow is quasi–spherical. Examples include some types of wind fed pulsars (see review by Nagase 1989). Also, quasi–spherical accretion may occur to an isolated star (especially, to an Old Isolated Neutron Star, OINS) if its velocity through the interstellar medium is small compared with the sound speed.

Due too intristic multidimensional nature of accretion flow to the dipole and nonlinearity of MHD equations only numerical calculations could unveil darkness from the real flow structure. Questions of interest are:

- the position & the shape of the Alfvén surface;
- the departures of the flow from spherical inflow to highly anisotropic polar column accretion inside the dipole's magnetosphere;
- dependence of the accretion rate to the dipole on the star's magnetic momentum and rotation rate, the sorrounding matter's density and the magnetic diffusivity (considered by Lovelace et al. 1995 for the case of disk accretion).

In our recent work (T99) a spherical accretion to a rotating star with an aligned dipole magnetic field was investigated by 2D MHD numerical simulations. In this paper development of that investigations with an improved dipole model is presented.

2. Model

Axisymmetric MHD simulations of spherical and cylindrical accretion to a (rotating) star with an aligned dipole magnetic field were performed under following approach. We consider the equation system for resistive MHD,

$$\frac{\partial \rho}{\partial t} + \nabla \cdot (\rho\ \mathbf{v}) = 0\ , \qquad (1)$$

$$\rho \left(\frac{\partial \mathbf{v}}{\partial t} + (\mathbf{v} \cdot \nabla) \cdot \mathbf{v} \right) = -\nabla p + \frac{(\mathbf{J} \times \mathbf{H})}{c} + \mathbf{F}^g, \qquad (2)$$

$$\frac{\partial \mathbf{H}}{\partial t} = \nabla\times(\mathbf{v}\times\mathbf{H}) + \frac{c^2}{4\pi\sigma}\nabla^2\mathbf{H}\ , \qquad (3)$$

$$\frac{\partial(\rho\varepsilon)}{\partial t} + \nabla\cdot(\rho\varepsilon\mathbf{v}) = -p\,(\nabla\cdot\mathbf{v}) + \frac{\mathbf{J}^2}{\sigma}\ . \qquad (4)$$

All variables had their usual meanings. The equation of state was considered to be that for an ideal gas, $p = (\gamma-1)\,\rho\varepsilon$, with $\gamma = 7/5$ the usual specific heat ratio. The equations incorporated Ohm's law $\mathbf{J} = \sigma(\mathbf{E} + \mathbf{v}\times\mathbf{H}/c)$, where σ was the electrical conductivity. The corresponding magnetic diffusivity $\eta_m \equiv c^2/(4\pi\sigma)$ was constant in whole calculation region.

We used an inertial cylindrical coordinate system (r, ϕ, z), its origin coincided with the star's and dipole's centers, the z–axis was parallel to the star's rotation axis and dipole magnetic momentum μ. Axisymmetry was assumed, $\partial/\partial\phi = 0$, and the z–axis was threated as a symmetry axis.

In order to guarantee that $\nabla\cdot\mathbf{H} = 0$ holds for all time in the numerical simulations, we used the vector potential $\mathbf{A}$ for the magnetic field, $\mathbf{H} = \nabla\times\mathbf{A}$, instead of magnetic field $\mathbf{H}$ itself. The magnetic field of the central gravitating object was chosen as an exact dipole one, $\mathbf{A} = \mu\times\mathbf{R}/R^3$. The corresponding magnetic field was $\mathbf{H} = [3\mathbf{R}\,(\mu\cdot\mathbf{R}) - R^2\mu]/R^5$, which was a **"pure" dipole** field.

This was the main methodological advantage over the dipole's model in (T99) where the magnetic potential was builded up as a potential of a "current" disk with a small but finite size placed in the equatorial plane. With the "point" dipole, used in describing simulations, we usually observed more narrow polar columns in comparison with previously published results with dipole, created by the distributed electric current system (T99). This could be explained by better convergence of the field lines to the axis in the star's vicinity in the case of the point dipole.

In eq. (2) the gravity force $\mathbf{F}^g(\mathbf{R}) = -GM\rho\mathbf{R}/R^3$, is due to the central star, where $\mathbf{R}$ is the radius vector, and M is the star's mass. The gravity force and the magnetic potential without softering were used because a totally absorbing object, an "accretor" was placed close around the origin. Its surface could be treated as a star's surface that absorbs all accreted matter. The size of the accretor was chosen to be small, $r_{accr} << R_{max}$. We were experimenting with "accretors" of two sorts (see Fig. 1 and compare to Fig. 1 from T99). The first one is a coarse approximation of the sphere on rectangular grid, the second one is the simplest case with square shape accretor. Test simulations showed very small differences in flow around these two accretors, in fothcoming text only simulations with the square accretor will be described.

The magnetic potential was fixed on the surface of the accretor during whole simulation. This followed from the electromagnetic conditions on the surface of the perfectly conductingh star and protected the star's magnetic field against destruction (T99). Full descriptions of set method for the boundary conditions on the star's surface could be found in T99.

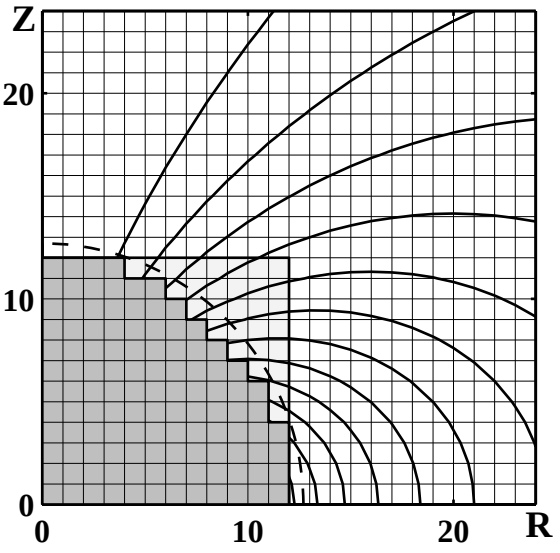

Figure 1: A scheme of the "accretor" for two cases, a coarse approximation to the circle and a square shaped "accretor" together with the dipole magnetic field lines are presented. Only 25×25 cells around the origin of the whole 257×257 calculation grid are shown.

Two dimensionless plasma parameters define the solution of the equations (1)–(4) after reduction to the dimensionless form. The first parameter is

$$\beta \equiv \frac{8\pi P_\infty}{H_0^2} \propto \dot{M}_B/\mu^2\ . \qquad (5)$$

The important quantity $\dot{M}_B/\mu^2$ is referred to as the "gravimagnetic" parameter by Davies & Pringle (1981). The second parameter is

$$\tilde{\eta}_m \equiv \frac{\eta_m}{R_A V_A} = \frac{1}{Re_m}\ . \qquad (6)$$

– dimensionless magnetic diffusivity. The third parameter connected to gravity is "hidden" by choosing Bondi radius $R_B = GM_\star/\,c_\infty^2$ as a scale unit.

3. Results

3.1. Spherical accretion onto a magnetic dipole

Symmetry about the $z = 0$ plane was assumed for spherical accretion onto a dipole and so it was possible to perform they in one quater of the (r, z) plane. Typically an equidistant orthogonal grid with 257×257 resolution was used.

Following boundary conditions were adopted. The region of the equatorial plane $(0 < r \le R_{max}, z = 0)$

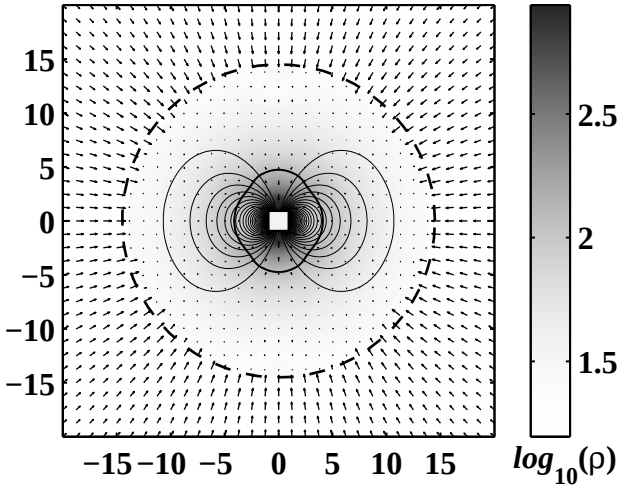

Figure 2: Simulation of the spherical accretion onto a non–rotating dipole. Position of the shock wave is marked by the dashed line and the Alfvén surface is marked by solid line, its equatorial radius is $R_A^{eq} \approx 4.1R_\star \approx \frac{1}{35}R_B$. Calculation grid is 257×257, vectors are drawn at every 32nd knot at every directions.

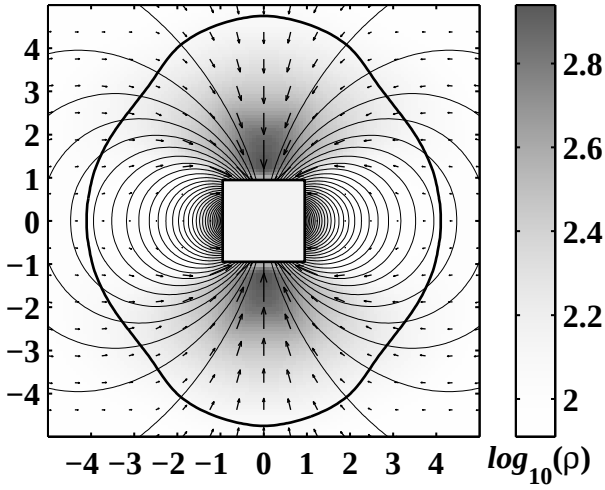

Figure 3: Vicinity of the magnetized accreting object. The Alfvén surface is marked with the solid line and inside it matter flows along the magnetic field lines. Polar columns accretion could be seen on this picture. Vectors are drawn at every 8th point along both directions, $\beta = 10^{-5}$, $\eta_m = 10^{-4}$.

was treated as a symmetry plane. The z–axis was treated as a symmetry axis. For outer boundaries we assume spherically symmetrical inflow with physical values given by the classical Bondi (1952) solution with maximum possible accretion rate

$$\dot{M}_B = 4\pi\lambda \left(\frac{GM}{c_\infty^2}\right)^2 \rho_\infty c_\infty \ , \qquad (7)$$

defined by the density ρ_∞ and the sound speed c_∞ at infinity and by the mass of the central object M. Bondi solution gave physical parameters for the inflow boundaries ($r = R_{max}$, $0 \le z \le Z_{max}$) and ($0 \le r \le R_{max}$, $z = Z_{max}$). Computational region lies inside the sonic surface $R_{max} = Z_{max} = 20R_\star = R_S/\sqrt{2}$, where the sonic radius is $R_S = (5-3\gamma)/4R_B$, and $R_B = GM/c_\infty^2$ is the Bondi radius. The accretion is supersonic, all gas dynamical variables could be fixed at the outer boundaries.

Simulations for different values of $\beta \propto \dot{M}_B/\mu^2$ and magnetic diffusivity η_m were performed. We can make following conclusions based on simulations.

Spherical accretion to a magnetic dipole is very different from that to a non–magnetized star. Instead of supersonic steady inflow, which is observed in standard Bondi accretion, a shock wave forms around the dipole just after begin of simulation. The supersonic inflow outside the shock becomes subsonic inside it. In all cases we observe that the shock wave gradually expands outwards. Figure 2 shows the main features of the flow at time when the shock has moved to the distance $R_{sh} = 14R_\star$.

We observe that for $R > R_{sh}$ the flow is unperturbed Bondi flow, used as initial and boundary conditions, whereas inside the shock for $R < R_{sh}$ it is subsonic. Initially, the subsonic accretion to dipole is spherically symmetric, but closer to the dipole it becomes strongly anisotropic. Near the dipole matter moves along the magnetic field lines and accretes to the poles in two polar columns. Figure 3 shows the inner subsonic region of the flow in greater detail. The dashed line shows the Alfvén surface, which we determine as the region where the matter energy–density $W = \rho(\varepsilon + \mathbf{v}^2/2)$ is equal to the magnetic energy–density $E_m = \mathbf{H}^2/(8\pi)$.

New method of central star setup (see section 2) allowed **to define the shape and sizes of the Alfvén surface more**. It is ellipsoidal, but in contrast with our previous simulations (see T99), it's more elongated along the poles. For simulations, presented on figures 2 and 3, the equatorial radius of the Alfvén surface is $R_A^{equ} \approx 4.1R_\star$, while its polar size along the symmetry axis z iz $R_A^z \approx 4.8R_\star$. This could be explained by the fact that electromagnetic energy density near the axis is higher in the field of the "point" dipole, used in this simulations set, in comparison to the energy of the field, created by the distributed current system, used in T99. But this correction is not too high, the Alfvén surface polar radius differs only by ≈ 30 % in two simulations, while the equatorial radius is around the same.

A significant deviation from spherically symmetric flow is observed for $R \le 2R_A$, because magnetic field starts to influence the flow before it reaches the Alfvén surface. The initial vacuum dipole magnetic field is

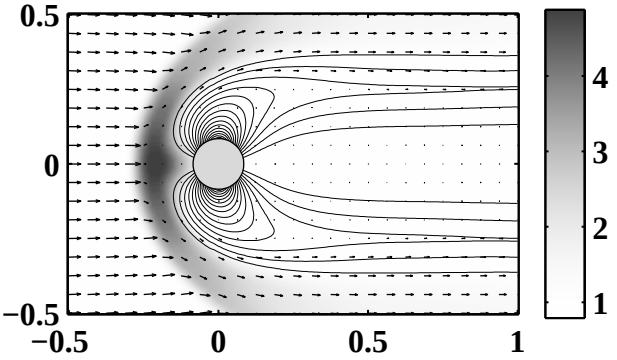

Figure 4: Cylindrical supersonic accretion to the non–rotating dipole (weak gravity case, $R_A \approx 0.25 R_B$). Density distribution in greyscale, magnetic field lines and velocity vectors at every 16th knots are shown. Mach's number is 3.

compressed inside by the accreting matter. A new stationary subsonic solution is formed around the dipole (the complete description of its pattern could be found in T99). The stationary accretion rate to the dipole $\dot{M}_{dip}$ could be measured from the simulation results.

As was pointed out first in T99, the accretion rate to the dipole is always smaller than to corresponding non–magnetized star, even if the dipole is not fast rotating. For the system, discussed here and shown on illustration, the accretion rate is $\dot{M}_{dip} \approx 0.17 \dot{M}_B$ when $R_A^{equ} \approx 4.1 R_\star$. The accretion rate to the dipole was found to be depended on the magnetic momentum of the star, the surrounding density and the magnetic diffusivity as

$$\dot{M}_{dip} \propto \left(\varrho_\infty / \mu^2\right)^{0.5} \cdot \eta_m^{0.38} \ . \qquad (8)$$

The equatorial Alfvén radius varries as

$$R_A^{equ} \propto \left(\varrho_\infty / \mu^2\right)^{-0.3} \cdot \eta_m^{0.07} \ . \qquad (9)$$

Combining equations (**??**) and (**??**) with the fact that when the Alfvén radius equals to $\sim 4 R_\star$ the dipole accretion rate $\dot{M}_{dip}$ is equal to $\sim 0.17 \dot{M}_B$, we can immediatly estimate the accretion rate for systems with stronger magnetic field. For example, if the Alfvén radius will be $R_A \approx 100 \cdot R_\star$ for isolated neutron star accreting quasi–spherically from surrounding medium the accretion rate (and accretion luminosity, in advance) will be less than 1% of the Bondi's accretion rate. So, corrections needed when studing possibility of finding old isolated neutfon stars (OINS) (see, for ex., Treves & Colpi, 1991, Blaes & Madau, 1993) and they will lead to decreasing of the number of principally observable OINS by $2 \ldots 3$ order of magnitude.

3.2. Cylindrical accretion to the dipole

Simulations of the cylindrical accretion in 2D axially symmetric formulation are limited only by the flows where velocity of the matter according to the star (or vice verse) is parrallel (or antiparrallel) to the magnetic momentum of the aligned dipole.

Simulations were performed in a rectangular box ($Z_{min} \le z \le Z_{max}, 0 \le r \le R_{max}$) of the ($r$–$z$) plane, covered with a 129×385 equidistant grid with equal steps along r and z axes. The gravitating accretor with dipole magnetic field frozen ib its surface was anchored at the origin of cylindrical coordinate system. Next set of boundary conditions was used. Supersonic inflow with Mach number $M = 3$ with temporary constant accretion rate was set up on the upstream (left on the fig. 4) boundary ($z = Z_{max}, 0 \le r \le R_{max}$). On the outer cylindrical boundary ($Z_{min} \le z \le Z_{max}, r = R_{max}$ and on the downstream boundary ($z = Z_{min}, 0 \le r \le R_{max}$) so called "free boundary conditions" (i.e., $\partial / \partial \mathbf{n} = 0$) were implied.

First, the case of relatively strong magnetic field and weak gravity was investigated (see results at fig. 4). This simulation is characterezed by foolowing relations: $R_\star = R_{accr} \approx 0.1 \cdot R_B$, $R_A \approx 0.25 \cdot R_B$, where $R_B = GM/c_\infty^2$ is the Bondi radius. In corresponding hydrodynamical simulation of cylindrical accretion to non–magnetized star (see Ruffert 1994, 1995) the head conical bow shock is attached to the accretor surface. In the dipole case the strong magnetic field serves as an obstacle, a shield for accreting matter, deflecting it from the star and preventing accretion.

What will be the accretion flow pattern if the Alfvén radius will be much smaller in comparison to the Bondi radius? For typical space condition it is estimated to be $R_A \sim 0.01 \cdot R_B$ or even less. One can proposes that there will be a conical bow shock in accretion flow far from the dipole but in the immediate vicinity of the Alfvén surface and inside it the flow will be quasi–spherical.

For investigating of such interesting system we plan to incorporate so called "nested grids" method to our code. It allows to increase resolution around the dipole but at the same time allows to use coarse grids far from it. This will allow us to model system which will be cloaser to reality, with $R_A \sim 10^2 \ldots 10^3 R_\star$ and $R_A \sim 0.01 \cdot R_B$ at the same time.

Acknowledgements. The authors are thankfull to their co–authors, Dr. Romanova, Dr. Savelyev, Dr. Chechetkin and Prof. Lovelace for long fruitfull, stimulated and productive work.

References

Bisnovatyi–Kogan G.S., Pogorelov N.V. 1997, *Astron. and Astrophys. Transactions*, **12**, 263

Blaes O., Madau P.: 1993, *ApJ*, **403**, 690
Bondi H.: 1952, *MNRAS*, **112**, 195
Davies R.E., Pringle J.E.: 1981, *MNRAS*, **196**, 209
Lovelace R.V.E., Romanova M.M., Bisnovatyi-Kogan G.S.: 1995, *MNRAS*, **275**, 244
Nagase F.: 1989, *PASJ*, **41**, 1
Ruffert M.: 1994, *ApJ*, **427**, 342
Ruffert M.: 1995, *As.Ap.Suppl.*, **113**, 133
Ruffert M.: 1996, *As.Ap.*, **311**, 817
Toropin Yu.M., Toropina O.D., Savelyev V.V., Romanova M.M., Chechetkin V.M., Lovelace R.V.E.: 1999 *ApJ*, **517**, 906 (**T99**)
Treves A., Colpi M.: 1991, *As.Ap.*, **241**, 107.

ON MASS LOSS FROM EVOLVED MASSIVE STARS

A.V. Dorodnitsyn, G.S. Bisnovatyi - Kogan

Space Research Institute
Profsoyuznaya st. 84/32, Moscow, Russia,
dora@mx.iki.rssi.ru,
gkogan@mx.iki.rssi.ru

ABSTRACT. We consider stationary outflowing stellar envelopes accelerated by a radiation flux pressure. A method is developed describing a spherically symmetric flow in radiational hydrodynamics in regions with arbitrary optical depth (τ). The solution of the derived system of differential equations is obtained numerically. It proceeds through the singular point, where a velocity is eqial to the isothermal sound speed, and satisfies zero temperature and pressure boundary conditions at the infinity. Method is discussed of self- consistent evolutionary calculations for massive stars on the stage of yellow and red supergiants, with a mass loss determined unambiguously.

Key words: Evolution of starswith mass loss: outflowing envelopes.

1. Introduction

Evolution of massive stars ($M >\sim 20M_\odot$) is accompanied by a mass loss, initiated by a high luminosity and high radiation pressure. In blue supergiants, situated near the main sequence, mass loss rate is moderate $M \sim 10^{-6}M_\odot$/yr, and is connected with the outflow of layers having small optical depth. This mass loss rate is determined by radiation pressure in lines, where spectral absorption coefficient may be very high. Evolved massive stars may lose mass with much higher rate than the blue supergiants. Formation of single Wolf-Rayet stars probably took place as a result of such intense mass loss. The main goal of the theory of mass loss from stars is to determine the mass loss rate as an eigenfunction of the problem, together with its luminosity and radius. The evolutionary scenario of the WR star formation as a result of the intensive mass loss on the stage after finishing of a hydrogen burning in the core, was first suggested in the paper of Bisnovatyi-Kogan and Nadyozhin (1972) on the base of a crude calculations of self-consistent evolutionary models of mass-losing massive stars. The main shortcoming of this paper was connected with ignoring of the transition to a small optical depth in the outer regions of the flow, and with using everywhere of the equations with the equilibrium radiation pressure and energy density. In subsequent papers of Zytkow (1972,1973), Kato (1985), Kato and Iben (1992) different types of simplifications were used, which do not take into account the difference of the outflowing envelopes from the static ones.

The goal of the present paper is to derive equations, which are approximately valid at all optical depths, giving exact limiting equations for the case of very large and very small τ. Solution of these equations is obtained at correct boundary conditions at large r (infinity), where gas density ρ and gas temperature T tend to zero. Such procedure after fitting the solution to the stellar core will give self-consistent values of $\dot{M}$, as well as the parameters in the critical point and τ_{ph}.

We derive relations for pressure, energy density, and energy flux of radiation, which describe smoothly the transition of the flow between optically thick and optically thin regions. In the limiting cases they reduce to corresponding solutions of the radiative transfer equations in Eddington approximation. These relations are used in the equations of the radiative hydrodynamics with a constant total energy flow. Singular points of the equations are analyzed, and expansion in the isothermal sonic point is obtained, necessary for obtaining a numerical solution. Then the numerical solution which satisfies the boundary conditions at infinity is obtained. The parameters characterizing the properties of the underlying star have been prescribed.

2. Basic equations

A system of equations of radiation hydrodynamics describing continuous transition between optically thick and optically thin regions for the stationary outflow is written as:

$$u\frac{du}{dr} = -\frac{1}{\rho}\frac{dP_g}{dr} - \frac{GM(1-\tilde{L}_{th})}{r^2}, \quad (1)$$

$$\tilde{L}_{th} = \frac{L_{th}(r)}{L_{ed}}, \qquad L_{ed} = \frac{4\pi cGM}{\kappa},$$

$$L = 4\pi\mu\left(E + \frac{P}{\rho} - \frac{GM}{r} + \frac{u^2}{2}\right) + L_{th}(r) \quad (2)$$

$$L_{th} = -\frac{4\pi r^2 c}{\kappa\rho}\left(\frac{dP_r}{dr} - \frac{E_r\rho - 3P_r}{r}\right), \quad (3)$$

$$\frac{\dot{M}}{4\pi} \equiv \mu = \rho u r^2, \quad (4)$$

$$P = \frac{aT^4}{3}\left(1 - e^{-\tau}\right) + \frac{L_{th}^{\infty}}{4\pi r^2 c} + P_g, \quad (5)$$

$$E\rho = aT^4\left(1 - e^{-\tau}\right) + \frac{L_{th}^{\infty}}{4\pi r^2 c} + E_g\rho, \quad (6)$$

$$P_g = \rho\mathcal{R}T, \qquad E_g = \frac{3}{2}\mathcal{R}T, \quad (7)$$

$$\tau = \int_r^{\infty} \kappa\rho dr, \quad (8)$$

where L - is a constant total energy flux consisting of the radiative energy flux together with the energy flux of the matter flow, u is a rate of the outflow, κ is an opacity, assumed to be constant, a is the constant of a radiative energy density, $\mathcal{R}$ is a gas constant. E_r - part of energy density, that is due to radiation.P_r - pressure due to radiation. We consider here the flow in the gravitational field of a constant mass M, neglecting self-gravity of the outflowing envelope . This system of equations provides a description of a stationary outflowing envelope accelerated by a radiative force at arbitrary optical depth, where continuum opacity prevails. In the optically thick limit $\tau \to \infty$, when terms with L_{th}^{∞} are negligible, and $E_r\rho = 3P_r$, a solution of this system was obtained by Bisnovatyi-Kogan (1967). In the case of a small τ for the anisotropic radiation flux we find: $E_r\rho \simeq P_r$, what follows from the solution of the transfer equation in Eddington approximation (Sobolev, 1967).

When optical depth is becoming small, separation of radiation and matter should be taken into consideration. It means that only a part of radiation is determined by the outflowing gas. For this part of quanta we assume LTE to be valid, what means that the mean energy of such quanta is characterized by the temperature of the outflowing gas For the rest part of radiation, another "temperature"- mean energy of quanta should be introduced. This part of radiation transfers momentum to the outflowing matter (pushes it) and thus produces only the anisotropic part of the pressure, determined by the term L_{th}. The separation of radiation into two different parts occurs near the photosphere and the mean energy of the free propagating quanta are characterized by the effective temperature of the photosphere.

The solution passing continuously this critical point, which is of a saddle type (Parker, 1963). This point corresponds to the "isothermal sonic" point where

$$u^2 = u_s^2 \equiv \left(\frac{\partial P}{\partial\rho}\right)_T$$

.

The second singular point of the system of equations is situated at infinity $r \to \infty$, where

$$T = 0, \quad \rho \sim \frac{1}{r^2} \to 0, \quad u \to \text{const} = u_{\infty}. \quad (9)$$

This condition is related to the fact that far from the star the density in the stellar wind is very small.

Let us introduce nondimensional variables

$$\tilde{T}(r) = \frac{T(r)}{T_{cr}}, \quad \tilde{\rho}(r) = \frac{\rho(r)}{\rho_{cr}}, \quad \tilde{x} = \frac{r_{cr}}{r}. \quad (10)$$

After transformations we obtain a dimensionless system of equations

$$\frac{d\rho}{dx} = \left(\frac{x^4}{\rho^3} - \frac{T}{\rho}\right)^{-1}\left\{\frac{dT}{dx}\left(1 + A_1(1-e^{-\tau})\frac{T^3}{\rho}\right)\right. \quad (11)$$

$$\left. -A_3 + \frac{1}{4}\frac{A_1 e^{-\tau}}{A_5}\frac{T^4}{x^2} + 2\frac{x^3}{\rho^2}\right\} \quad ,$$

$$\frac{dT}{dx} = -\left(\frac{5}{2}T - A_3 x + \frac{1}{2}\frac{x^4}{\rho^2} + (1-e^{-\tau})A_1\frac{T^4}{\rho}\right. \quad (12)$$

$$\left. + \frac{e^{-\tau}}{4A_2A_5}\frac{T^4}{x^2} + 2L^{\infty}A_3A_5\frac{x^2}{\rho} - \frac{A_4}{A_2}\right)\frac{A_2\rho}{T^3(1-e^{-\tau})} \quad ,$$

$$\frac{d\tau}{dx} = \frac{\rho}{A_5x^2} \quad . \quad (13)$$

Where $L^{\infty} \equiv \tilde{L}_{th}^{\infty}$. To simplify writing here and further we omit tilde. Dimensionless coefficients A_i are the same as in (Bisnovatyi-Kogan and Dorodnitsyn, 1999)

Additional fifth parameter A_5 is not independent,

$$A_5 = \left(\frac{3}{4}\right)^{1/5}\frac{A_3^{1/5}\mathcal{R}^{4/5}}{A_1^{3/5}A_2^{4/5}\kappa^{1/5}a^{1/5}c^{4/5}(GM)^{1/5}}. \quad (14)$$

It is of the order of the reciprocal optical depth in the critical point. Condition of a continuous transition of the solution through the critical point reduces the number of independent dimensionless parameters.

In addition to coefficients A_i, we have independent nondimensional papameters L^{∞}, and the optical depth

in the critical point τ_{cr}, so before satisfying the boundary conditions at infinity, we have 5 "independent" nondimensional parameters of the problem.

Sample numerical solution

In order to satisfy boundary conditions far from the star we need to integrate (11)-(13) from the critical point outward to the infinity. We exit the critical point by means of expansion formulae. Expanding the solution in the vicinity of the critical point $x = T = \rho = 1$ in powers of $(1 - x)$ we have

$$T = 1 + a(1 - x), \quad \rho = 1 + b(1 - x), \qquad (15)$$

$$e^{-\tau} \simeq e^{-\tau_{cr}}(1 + \frac{y}{A_5}), \qquad (16)$$

where $y = 1 - x$. a and b coefficients are given in (Bisnovatyi-Kogan and Dorodnitsyn, 1999)

A numerical integration is started from the critical point making the first step by means of the expansion formulas. Integrating outward to the infinity we satisfy the boundary conditions. To satisfy condition of zero T at infinity we find a unique dependence $A_3(A_1, A_2, L^{\infty}_{th}, \tau_{cr})$. After that the value of τ_{cr} is found uniquely for the given values of A_1, A_2 and L^{∞}_{th} by matching the condition v^{∞} =const. When $r \to \infty$ velocity tends to a constant and thus $\rho \sim 1/r^2$. Only a unique value of τ_{cr} allows to obtain the proper behavior of u (and ρ) at the infinity.

The obtained solution corresponds to the following dimensionless parameters: $A_1 = 50$, $A_2 = 10^{-4}$, $A_3 = 43.88$, $\tau_{cr} = 125$, $L^{\infty}_{th} = 0.6$. This set of parameters corresponds to the following values in the critical point: $T_{cr} = 1.4 \cdot 10^4 K$, $r_{cr} = 2.6 \cdot 10^{13}$cm, $\rho_{cr} = 6.6 \cdot 10^{-12}$ g/cm^3. We accepted here $M = 2 \cdot 10^{34}$ g. The velocity of the flow in the critical point is $v_{cr} \approx 11$ km/s, and the mass loss rate $\dot{M} \approx 9 \cdot 10^{-3} M_{\odot}$/yr.

A behavior of the solution with a Mach number rapidly decreasing inside at $r < r_{cr}$, gives a possibility to match it to a static solution in the core. In reality the opacity peak is situated near the critical point, the opacity inside is decreasing and the velocity drops inside more rapidly, then in the case of κ=const (Bisnovatyi-Kogan and Nadyozhin, 1972). Deep inside the star, all hydrodynamical solutions converge to a static one. In the static atmosphere, at L =const, and M =const, we have $\rho \sim T^3$ and $T \sim 1/r$ (Bisnovatyi-Kogan, 1973). Since $u \sim 1/(\rho r^2)$, the velocity in the subsonic region tends to zero $\sim r$. In reality, deeper in the star $\dot{M}$ decreses, tending to zero. That means, that the velocity goes to zero faster, than $\sim r$. The Mach number M_a, is defined by the relation $M_a = u/\sqrt{\gamma P/\rho}$, where P is taken without the anisotropic term.

The effective temperature of the photosphere is obtained from the relation: $L^{\infty}_{th}/4\pi r^2 = \sigma T^4$. For the given set of parameters we get $x_{ph} = 0.03$, $\tau_{ph} = 4$, $T_{eff.} = 0.06$, and $\tilde{\tau}_{ph} = 3.75$. That corresponds to $r_{ph} = 8.6 \cdot 10^{14}$ cm, $T = 840$ K, what corresponds to a very luminous infrared star with an extended outflowing atmosphere. It is possible that on the stage of a very intensive mass loss the massive star is transformed into an infrared object. We should have in mind, that for realistic functions $\kappa(\rho, T)$, $P(\rho, T)$, the observed quantities should be different. Below the temperature of several thousands Kelvin the opacity drops (Iglesias and Rogers, 1996; Seaton, 1996), the photosphere approaches the star, and the effective temperature is greater.

The condition of matching of the solution of the outflowing envelope to the static core determine uniquely the values of r_{cr} and L, leading to the unique solution of the mass-losing star with a self-consistent mass loss rate.

References

Bisnovatyi–Kogan G.S.: 1967, *Prikl. Mat. Mech.*, **31**, 762.

Bisnovatyi–Kogan G.S., Nadyozhin D.K.: 1972, *Ap. Space Sci.*, **15**, 353.

Bisnovatyi-Kogan G.S., Dorodnitsyn A.V.: 1999, *As.Ap.*, **344**, 647.

Chandrasekhar S.: 1939, *Stellar structure*, Chicago.

Kato M.: 1985, *PASJ*, **37**, 19.

Kato M., Iben I.: 1992, *ApJ*, **394**, 879.

Parker E.N.: 1963, *Interplanetary dynamical processes.* Interscience Publishers, New York - London.

Sobolev, V.V.: 1967, *Course of theoretical astrophysics.* Moscow, Nauka Publ..

Żytkow A., 1972.: *Acta Astron.*, **22**, 103.

Żytkow A., 1973.: *Acta Astron.*, **23**, 121.

PERIOD CHANGES IN THE GROUP OF ALGOL-TYPE BINARY SYSTEMS WITH ASYNCHRONOUS ROTATION OF THE MAIN COMPONENT

L.V. Glazunova

Astronomical Observatory, Odessa State University
T.G.Shevchenko Park, Odessa 65014 Ukraine,
astro@paco.odessa.ua

ABSTRACT. The period change for the group Algol-type binaries with an asynchronous rotation of a main component is studied. Under the observational data, available in the literature, a general tendency in change of periods of these systems was obtained. As against to the majority of Algols, for 6 of 8 systems of this group the period decrease is observed for last decades.

Key words: binary systems, period changes; individual: U Cep, S Cnc, SW Cyg, RX Gem, RY Gem, RW Per, U Sge, RW Tau

Variations of the period P appear to be connected with the configuration of the binary; they occur predominantly in systems containing at least one the Roche limit. Algols are product of the mass transfer process and they display various kinds of activity including the period changes. Some of these period variations are implied by the evolutionary processes during the mass exchange, but the observatios suggest that additional mechanisms are needed in most cases. Evolution period changes caused by mass transfer from one star onto its companion often determinent for the case conservative mass transfer. Matter just flows from the loser to the gainer - both total mass ratio and angular momentum of the binary are constant. In this case for Algols, matter is flowing from the less massive loser onto the more massive gainer, dominant increase of the length of P should be therefore observed. Such a monotonous period change would be most easily distiguishable. However, large mass transfer rate ($\dot{m} = 10^{-6} M_{\odot} yr^{-1}$) is needed for producing an O-C change detectable on the time scale of decades. This value of $\dot{m}$ would have to be even larger for the non-conservative transfer which could, in principle, lead to more complicated course of O-C. Large $\dot{m}$ occurs only in the initial phase of the mass transfer before the mass ratio reversal. It means that the number of Algols with $\dot{m}$ still high enough for producihg observable period changes is expected to be small. Several kinds of period changer for binary systems described in the article by Šimon (Šimon, 1998).

The group of Algols with asynchronous rotation main star's (19 systems, Glazunova 1999) differ from other Algols bigest mass transfer rate and them what main star systems rotatio rapidest, them necessary at synchronous rotation stars in system. The understanding nature this asinchonous can help investigation of the period changes this systems and his distinction from them Algols. In detail study the period changes for four system this group: RW Tau (Šimon, 1998), SW Cyg and U Sge (Šimon, 1997a, b), U Cep (Olson et al. , 1981). The O-C diagrams of these Algols have diferend kinds, but general tendencies on a background of monotone change of period short-term jumps, identical. The possible reasons of such behaviour of the diagram O-C (the third body, the Applegate theory, modification of an internal structure of the cool loser) do not allow to explain to its feature.

The study of period changes at other systems of this group with large meaning of the factor asynchronous F would continue: RX Gem, S Cnc, RW Per.

In Fig. 1–3 the O-C variability for these systems is presented. In Table 1 is given the parameters of this group of systems with previously investigated period changes. The O-C calculations are carried out using all published during 100 years data (Hall 1973, Schaefer 1991, Crawford 1980) data using different methods. We can not investigate in detail the short-period variability for systems having periods several times longer than in RW Tau and U Cep (for which there are obtained good quality observations). We can study only the general tendency of period variability on that timescales. As we see, in RW Per the period was increased and later on decreased. The accuracy of moments of minima determination of this system is low, due to variability of the amplitude of the primary minima and presence of total eclipse. In RX Gem, during the ob-

served time interval, period was increased. The shortest time interval of observations we have for S Cnc, but due to high accuracy of minima determination , we can mark decreasing of periods during the last decades. We can conclude, that six from eight systems show the period decrease for the last decades.

In the Table 1 there are given the period variability estimations. for the last decades $\Delta P/P$.

Star	P d	F	Sp	$\Delta P/P$
RW Tau	2.76	4.5	B9 V+K3 IV	$-2{\cdot}10^{-5}$
SW Cyg	4.57	6.1	A2 V+K0	$-6{\cdot}10^{-5}$
U Sge	3.38	1.7	B8 IV +G2	$-1{\cdot}10^{-5}$
U Cep	2.49	4.0	B7 V+G8 III	$+1{\cdot}10^{-5}$
RY Gem	6.86	7.4	A2 V+K2 IV	$-4{\cdot}10^{-5}$
RW Per	13.2	10	B9 III+K2 III	$-2{\cdot}10^{-7}$
RX Gem	12.21	8.7	A2 III+K2	$+3{\cdot}10^{-5}$
S Cnc	9.48	9.6	B9 V+K0	-410^{-7}

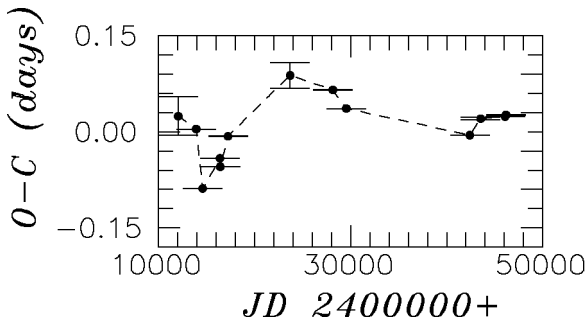

Figure 1: RW Per

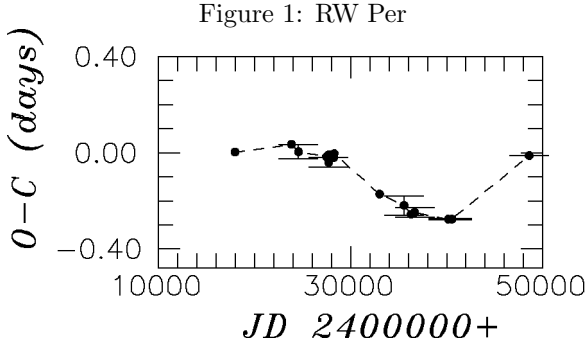

Figure 2: RX Gem

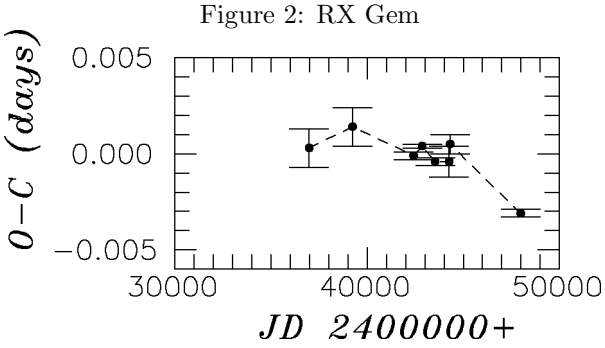

Figure 3: S Cnc

References

Crawford R.C., Olson E.C.: 1980, *Publ. Astron. Soc. Pac.*, **92**, 833.

Glazunova L.V.: 1999, *Pis'ma A.Zh.,* **6**, 1.

Hall D.S., Woolley K.S.: 1973, *Publ. Astron. Soc. Pac.*, **85**, 618

Olson E.C., Crawford R.C., Louth H., Markworth N.L., Piirola V.: 1981, *Publ.Astron.Soc.Pacif.,* **93**, 464.

Schaefer B.A., Fried R.E.: 1991, *AJ*, **101**, 208

Šimon V.: 1998, *Proceedings of the 29th Conference on Variable Star Refsearch, 7-9 November 1997, Brno, 193.*

Šimon V.: 1997a, *Astron. Astrophys.,* **319**, 886.

Šimon V.: 1997b, *Astron. Astrophys.,* **327**, 1087.

POINT EXPLOSION WITHIN A CAVITY WITH A POWER-LAW DENSITY DISTRIBUTION

V.V. Martiushov[1], S.A. Silich[2]

[1] Department of Astronomy, Kyiv Shevchenko University
Glushkov ave., 6 , Kyiv 03022, Ukraine, *mart@alfven.ups.kiev.ua*
[2] Main Astronomical Observatory NAS of Ukraine,
03680, Kyiv-127, Golosiiv, Ukraine, *silich@mao.kiev.ua*

ABSTRACT. An exact analytic solution based on the Kompaneets approximation is found for a shock wave expansion from a point explosion within a pre-existing interstellar gas cavity with a power-law gas density distribution. An obvious shock deviation from the spherical symmetry is revealed for the off-center explosion. It is assumed this may give a reason for the complex morphology that is observed in some supernova remnants.

Key words: Shock waves: supernova remnants: interstellar medium.

1. Introduction

Massive stars, precursors of types II and Ib supernovae (SN), intensively lose mass during their evolution. The ejecta velocities reach 2000 km s^{-1}, and the mass loss rate is 10^{-5} - 10^{-7} $M_\odot$ yr^{-1}. Energetic stellar winds push powerful shock waves through an ambient interstellar medium (ISM), and produce large cavities, which are surrounded by the dense shells, and are filled with a hot, low density gas. The characteristic scale of the cavities around massive star clusters may be compatible or even exceed the characteristic thickness of the galaxy gas layer and reach several hundred parsecs (Heiles, 1982). Thus, one could expect that many SN explosions occur within a pre-existing interstellar gas cavities. This rises the problem of a point explosion inside a cavity with a *radially-increasing* density distribution (Cox D.P. & Franco J., 1981). A general problem is not a spherically-symmetric because a precursor star proper motion with respect to the ISM. A propagating star formation (Palouš et al., 1994) with the young HII regions at the large-scale cavity edge is an another reason for the off-center energy deposition.

In the current consideration we use Kompaneets (1960) approximation. The shape of the shock front then follows from the equation (Korycansky, 1992):

$$\left(\frac{\partial\theta}{\partial y}\right)^2 = \frac{\rho_0}{\rho}\left[\left(\frac{\partial\theta}{\partial r}\right)^2 + \frac{1}{r^2}\right], \qquad (1)$$

where r and θ are spherical coordinates, y is the dimensionless time, and ρ is the ambient gas density distribution.

2. The input model and it's limitation

For simplicity, here we assume a power-law density distribution within a cavity and ambient medium. For expanding, rather young cavity the initial gas density distribution is assumed to be

$$\rho(r) = \begin{cases} \rho_0 \left(\frac{r}{R_0}\right)^n, & r < R_0, \\ \rho_0 \left(\frac{r}{R_0}\right)^m, & R_0 < r < R_1, \\ \rho_{ism}, & r > R_1, \end{cases} \qquad (2)$$

where R_0 and R_1 are the shell inner and outer radii, ρ_0 and ρ_{ism} are the shell maximum and the interstellar gas densities, $n > 0$ and $m < 0$.

For an old, stall cavity, shell gets thicker, and disperses within an ambient medium. In this case we assume the initial density profile to be flat out of cavity, and reads as

$$\rho(r) = \begin{cases} \rho_0 \left(\frac{r}{R_0}\right)^n, & r < R_0, \\ \rho_0, & r > R_0, \end{cases} \qquad (3)$$

where index $n > 0$, R_0 is a cavity radius, and $\rho_0 = \rho_{ism}$ is the ISM gas density.

Four characteristic times (or length scales) are relevant to the problem discussed (Brighenti & D'Ercole, 1994). The main sequence lifetime (McKee et al. 1984):

$$t_{ms} = 4.4 \times 10^6 L_{36}^{-1/6}\, yr, \qquad (4)$$

where L_{36} is the mechanical input rate in the 10^{36}erg s^{-1} units.

The wind-blown cavity cooling time (Mac Low & McCray, 1988)

$$t_{cool} = 4.6 \times 10^6 \xi^{-35/22} n_{ism}^{-8/11} L_{36}^{3/11} yr, \qquad (5)$$

where ξ is the hot gas metallicity with respect to the solar one, and n_{ism} is the ambient ISM gas density. Later on it is assumed through out the paper that $t \leq t_{cool}$, e.g. that hot inner gas cooling rate is negligible, and density drops from the contact discontinuity to the bubble center. This puts a limit to the external gas density n_{ism}:

$$n_{ism} \leq 1.06 \xi^{-36/16} L_{36}^{1/2} cm^{-3}. \qquad (6)$$

When the inner bubble pressure equals with the external gas thermal pressure, the bubble stalls at a characteristic time t_{stop}

$$t_{stop} = 2.2 \times 10^6 (L_{36}/n_{ism})^{1/2} a_{10}^{-5/2} yr, \qquad (7)$$

where a_{10} is the external gas sound speed in the 10 km s^{-1} units. This characteristic time defines the transition to a subsonic motion, and the onset of the shell dispersion: The comparison of equations (7) and (4) shows, that SN explosion occurs before shell dispersion if $n_{ism} < 0.25 L_{36}^{4.2}/a_{10}^{-5}$.

Once the hot bubble interior was formed, a subsequent blast wave may to become subsonic at the fractional radius $x_{sound} = r_{sound}/R_0$ (Mac Low & McCray, 1988). For the main sequence lifetime t_{ms} this value reads as

$$x_{sound}(t_{ms}) \approx 1.2 L_{36}^{-5/36}. \qquad (8)$$

Thus, if the bubble is formed by a single star, the gas motion at the edge of the cavity remains supersonic only for low-energetic winds. Note that for O6 stars $L_{36} \approx 1.27$ (Brighenti & D'Ercole, 1994).

The mass of the hot bubble interior may be expressed at the different characteristic times as follows:

$$M(R_{ms}) = 263 n_{ism}^{2/15} L_{36}^{101/210} \mathrm{M}_\odot, \qquad (9)$$

$$M(R_{stop}) = 119 \left(\frac{L_{36}^{19}}{n_{ism}^{9} a_{10}^{41}} \right)^{1/14} \mathrm{M}_\odot. \qquad (10)$$

Equations (9)-(10) show that $10^2 - 10^3$ $\mathrm{M}_\odot$ may be evaporated into a cavity before the explosion. Thus remnant may get the Sedov stage, especially if explosion occurs at the edge of the cavity which is created by a massive star cluster.

3. The results of the calculations

Equation (1) may be solved analytically for some particular density distributions with the complete integral method (Silich & Fomin, 1982; Kontorovich & Pimenov, 1998). Figures 1a and 1b show the resulting shock wave morphologies for a shell-like density profile (2). In the both cases explosion position is indicated by a cross. It occurs nearby a density ridge (dashed line circles), at the distance $a = 0.7R_0$ (figure 1a) or $a = 0.9R_0$ (figure 1b) from the cavity center. The inner pre-existing bubble structures are identical, and assume a power-law density profiles (2) with the power-law index $n = 2$. However, the ISM gas densities are assumed to be quite different. The first model corresponds to the bubble expansion within a homogeneous ISM. The ratio of the pick to the interstellar gas density equals to $\rho_0/\rho_{ism} \approx 4$, and density gets the ISM value immediately after the density pick, at $R_1 = 1.2R_0$. The second solution may be applied for a bubble expansion within a medium with a fast density drop. In this case $\rho_0/\rho_{ism} \gg 1$, and density gets the ISM value much later, at $R_1 = 4R_0$. This corresponds approximately to the expected sharp density drop in the gaseous halo of the starburst galaxy VII Zw403, which exhibits the elongated kpc-scale X-ray emitting extensions (Papaderos et al. 1994). The deviation from the spherical symmetry is obvious for both of the models. Obviously, it is more prominent for the ISM with a sharp density gradient. However, to produce a very elongated shock structure, which is similar to the X-ray morphology of the VII Zw403, one needs a very

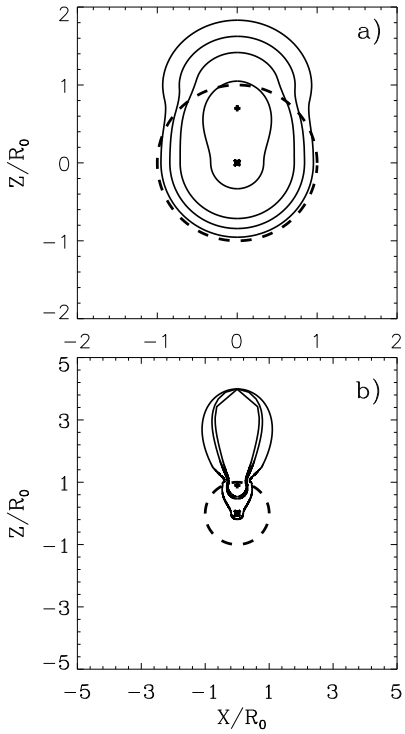

Figure 1: Shock morphology for a shell-like density distribution. a) Shock shape time evolution: $a = 0.7R_0$, $n = 2$, $R_1 = 1.2R_0$, and $m = -8$; b) Shock shape for different external gas density gradients: $a = 0.9R_0$, $n = 2$, $R_1 = 4R_0$, and $m = -8, -12, -14$.

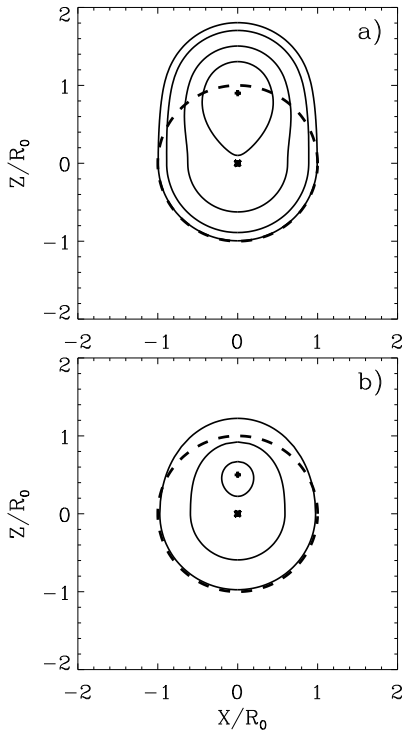

Figure 2: Shock morphology for old cavity density distribution. a) $a = 0.9R_0$, $n = 2$; b) $a = 0.5R_0$, $n = 2$.

sharp density gradient with an unacceptably low halo gas density (the halo to the ridge gas density ratio equals to $\rho_{ism}/\rho_0 = 1.4 \times 10^{-5}$, 5×10^{-8} and 3×10^{-9} for $m = -8$, -12 and $m = -14$).

The results of the calculations for the point explosion within the old cavity are shown in the figures 2a and 2b. Figure 2a represents shock morphology for the edge on explosion ($a = 0.9R_0$). Shock shape for the modest displacement of the explosion point ($a = 0.5R_0$) is shown in the figure 2b. The gas density distribution within the cavities are the same as in the previous cases, with a power-law density profile (2), and $n = 2$.

In the case 2a shock blows out of the nearest cavity wall soon after explosion, and forms a well defined cylindrical shape, whereas in the case 2b the remnant morphology remains almost spherically throughout the calculations.

4. Conclusions

- The off-center point explosion within a cavity with a radially-stratified density distribution can produce a variety of non-spherical remnants, even if the external gas density is homogeneous.
- The ultimate shock morphology depends strongly on the explosion position within a cavity and the external gas distribution. Energy deposition at the edge of the pre-existing cavity can produce an elongated remnant. However it is difficult to believe that this mechanism is responsible for the large scale extensions in the VII Zw403 because it predicts too high density gradients, and unreasonably low galaxy halo gas density.

Acknowledgements. VVM thanks support from All Ukrainian Council of Young Scientists and Specialists. SAS acknowledges support from a Royal Society grant for joint projects with the former Soviet Union states.

References

Brighenti F., D'Ercole A.D.: 1994, *MNRAS*, **270**, 65.
Cox D.P., Franco J.: 1981, *ApJ*, **251**, 687.
Heiles C.: 1982, *ApJ*, **262**, 135.
Kompaneets A.S.: 1960, *Doklady Akad. Nauk SSSR,* **130**, 1001.
Kontorovich V.M., Pimenov S.F.: 1998, *Izv. Vuzov. Radiofizika*, **XLI**, N6, 698.
Korycansky D.G. 1992, *ApJ,* **398**, 184.
Mac Low M.-M., McCray R., 1988, *ApJ.,* **324**, 776.
McKee C.F., Van Buren D., Lazareff B.: 1984, *ApJ,* **278**, L115.
Palouš J., Tenorio-Tagle G., Franco J.: 1994, *MNRAS,* **270**, 75.
Papaderos P., Fricke K.J., Thuan T.X., Loose H.-H. 1994, *Astron. Astrophys.,* **291**, L13-L16.
Silich S.A., Fomin P.I. 1983, *Dok. Acad. Nauk SSSR,* **268**, 861.

DETECTION AND STUDY OF LUMINESCENCE COMETARY CONTINUUM IN SPECTRA OF COMETS SCHAUMASSE (24P), SCORITCHENKO-GEORGE (C/1989 Y1) AND HALE-BOPP (C/1995 O1)

K.I. Churyumov, V.V. Kleshchonok

Astronomical Observatory of Kyiv National University
Observatorna 3, Kyiv 254053 Ukraine, *E-mail: klim@aoku.freenet.kiev.ua*

ABSTRACT. The authors investigated spectra of four comets with the aim to determine the real level of the non-solar origin continuum in the spectral region 350-500 nm. Spectra of three comets Schaumasse (24P), Scoritchenko-George (C/1989 Y1) and Hale-Bopp (C/1995 O1) were observed with the help of the 6-m BTA telescope and the spectrograph with the long slit at the Special Astrophysical Observatory of the Russian Academy of Sciences. Spectra of two comets Hyakutake (C/1996 B2) and Hale-Bopp (C/1995 O1) were obtained with the 1-meter Zeiss telescope and echelle-spectrometer of the SAO RAS. As a result of processing the cometary spectra we obtained: 1) For comet Schaumasse (24P) March 14-15, 1993 the level of the non-solar-origin continuum equal to 44 per cent of the sum continuum level at 430 nm; 2) For comet Scoritchenko-George (C/1989 Y1) February 27 , 1990 the level of the non-solar-origin continuum equal to 40 per cent of the sum continuum level at 387 nm, 68 per cent - at 430 nm (max) and 23 per cent - at 480 nm; 3) 2) For comet Hale-Bopp (C/1995 O1) April 17 , 1997 the level of the non-solar-origin continuum equal to 32 per cent of the sum continuum level at 397 nm and 77 per cent - at 438 nm; 4) For comet Hyakutake (C/1996 B2) March 25, 1996 the continuum of the non-solar origin was not detected. We suppose that in spectra of comets Schaumasse (24P), Scoritchenko-George (C/1989 Y1) and Hale-Bopp (C/1995 O1) we detected the real cometary continuum tied with the luminescence of the comet organic spices which are in comet dust particles.

Key words: comet, spectrum, continuum, luminescence.

1. Introduction

For the first time the luminescence continuum of the cometary dust was discovered in a spectrum of comet Halley by G. Nazarchuk (1987a;1987b). However, up to this day the existence of this effect has been discussed. The authors investigated of spectra of several comets and showed independently that this effect took place really at observations of comets with big telescopes having high space and spectral resolution. Below results of search of luminescence cometary continuum for 4 comets are given.

2. Comet Schaumasse (24P)

Spectra of comet Schaumasse (24P) were obtained March 14/15, 1993 with the CCD-scanner installed on 6-m BTA reflector of the Special astrophysical observatory of the RAS (Churyumov and Kleshchonok, 1994).Observations were held using the slit with the sizes 2"x1'. Altogether three spectra of the comet in the spectral range 370-600 nm with the quantity 0.2 nm were obtained . The spectral resolution was 0.4 nm. Peculiarity of the comet is anomaly big relation $Q(C_3)/Q(CN)$ equal to 0.94. This is approximately four times bigger than for the "normal" comet. Authors studied a range of the solar spectra near the intensive Fraunhofer line G. This line is almost unseen in the cometary spectrum though only a cometary continuum and the weak lines of the CH radical are present in this range of the cometary spectrum. Then the solar spectrum was compared with the cometary spectrum divided on the solar spectrum. This procedure is made in order to receive the parameters of the particles scattered light in the cometary atmosphere. The obtained curve has a very strong anticorrelation with the solar spectrum. This indicates the presence of luminescence of the cometary dust. It is this effect that must lead to decrease in the depths of the Fraunhofer lines in the cometary spectra. Luminescence of dust is clearly seen in the violet range of the spectrum and not substantial

in more longwave range (470-570 nm) of one.

3. Comet Scoritchenko-George (C/1989 Y1

The spectra of comet Scoritchenko-George (C/1989 Y1) were obtained Feb. 27.6 UT, 1990 with the 6-m BTA reflector of the Special Astrophysical Observatory of the RAS using the TV-scanner, installed in the focus of Nasmith. Record of the spectra were made in three spectral ranges: 335-445 nm, 429-539 nm and 529-639 nm. The spectral resolution of the obtained spectra is 0.2-0.4 nm. From the observations of the standard star in the same spectral ranges a relative intensity of radiation in the cometary spectrum was determined. All the spectra were reduced to the standard step 0.1 nm. Further record from the central region of the coma were combined in one spectrum.

In this cometary spectrum as well as in the spectrum of comet Schaumasse, the effect of luminescence of the cometary dust was also detected. In order to determine its contribution the following technique was used. The solar spectrum for the particular spectrograph was calculated by convolution of the initial spectrum of the Sun with the high resolution and function of the response of the spectrograph which was approximated by the function of the type

$$0.5 \cdot \exp(- \mid \lambda - \lambda_c \mid \backslash \delta\lambda)$$

where $\delta\lambda$ - the spectral resolution of the spectrograph.

For strong absorption lines in the solar spectrum (in the absence of strong emissions in the cometary spectrum in this spectral range) the additional value i_f which was selected so to equalize the values of the contrast of the selected Fraunhofer line in the solar and cometary spectra:

$$\frac{i_o^c - i_f^c}{i_l^c - i_f^c} = \frac{i_o^s}{i_l^s}$$

where i_o is the intensity level of the solar continuum spectrum close to the line, i_l - the intensity level of the spectrum in the center of the Fraunhofer line, indices c and s are related to the spectra of the comet and the Sun respectively. The value i_f thus determined was taken as the intensity level of the luminescence continuum of the cometary dust.

Because strong Fraunhofer lines were selected, the result is almost weak dependence from the inaccuracy in selecting the function of the spectrograph's response. Fig.1 shows the range of the spectrum where substantial contribution of the luminescence continuum was observed. The filled circles mark the values i_f, obtained by the formula and the dashed curve marks approximation of the luminescence continuum, determined using these circles.

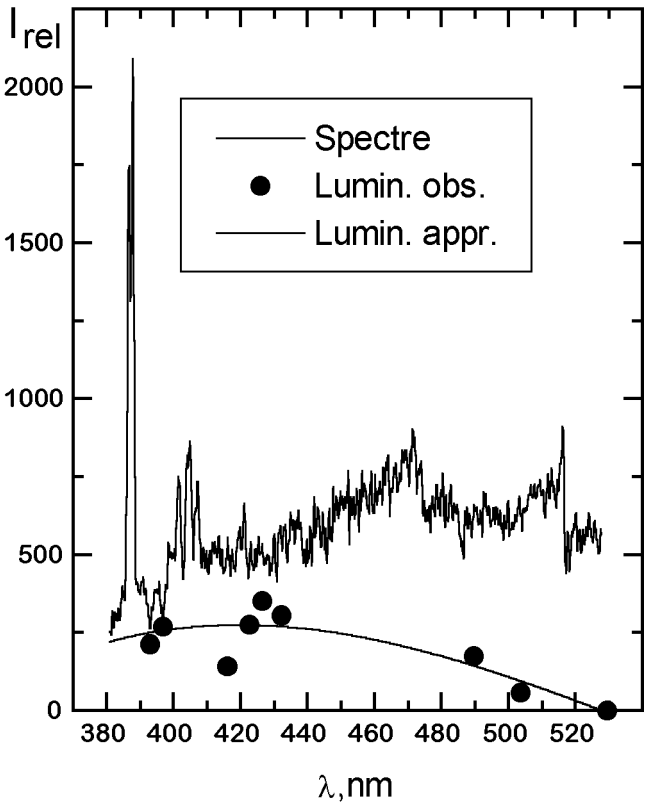

Figure 1: The range of the spectrum of comet Scoritchenko-George in which the luminescence continuum was detected.

4. Comet Hale-Bopp (C/1995 O1)

Spectra of the bright comet Hale-Bopp were obtained on 6-m telescope (SAO of RAS) with the UAGS spectrograph and CCD-camera in the prime focus of the telescope (Churyumov et al., 1997). In observations the diffraction grate which gives dispersion nearby 0.3 nm per pixel and spectral resolution 0.5-0.6 nm was used. The scale of images along the slit (perpendicular to dispersion) is 0.41" per pixel. For determination of intensity of the emission lines subtraction of the solar spectrum was made. In places of the strong lines of the absorption of H and K of Ca^+ of the Fraunhofer spectrum inversion is observed - absorption lines are converted in emission lines analogous to observations of Nazarchuk (1987a; 1987b) in comet Halley (1P) and authors in comets Schaumasse and Scoritchenko-George (see above). Comet Hale-Bopp was also observed with the high spectral resolution on the 1-m Zeiss reflector of the SAO of the RAS (Churyumov et al., 1999). In observations the echelle-spectrometer installed in the Coude-focus was used, and during Apr. 17-19, 1997, five spectra of the comet (the comet's heliocentric distances $\Delta = 0.96 - 0.97$ A.U.) were obtained. As the results of processing of the spectra contributions of the solar and luminescence continuum in

common cometary spectrum in different spectral ranges were determined: a) 77 and 23 per cent respectively for the spectral range 4370 - 4390 ÅÅ ; b) 68 and 32 per cent for 3960-3980 ÅÅ ; c) 100 and 0 per cent for 4920-4940 ÅÅ ; d) 100 and 0 per cent for 5490-5510 ÅÅ . We think that the cometary continuum of the nonsolar origin for the spectral ranges 4370 - 4390 ÅÅ and 3960-3980 ÅÅ was detected.

4. Comet Hyakutake (C/1996 B2)

Comet Hyakutake (C/1996 B2) was observed March 23, 1996 with the high spectral resolution on the 1-m Zeiss reflector of the SAO of the RAS. In observations the echelle-spectrometer installed in the Coude-focus with the spectral resolution $\lambda\backslash\delta\lambda \approx 50000$ was used. Record of the spectrum were made with the CCD-camera. After preliminary processing a search of the luminescence continuum according to the above mentioned technique was undertaken. However in this case for all spectral ranges the continuum intensity level was less 8 per cent that is less than the values of the errors of its determination. Thus in comet Hyakutake the luminescence radiation of the cometary dust was not detected or it is on the level of errors of observation.

4. Conclusion

1) For comet Schaumasse (24P) March 14-15, 1993 the level of the non-solar-origin continuum equal to 44 per cent of the sum continuum level at 430 nm;

2) For comet Scoritchenko-George (C/1989 Y1) February 27 , 1990 the level of the non-solar-origin continuum equal to 40 per cent of the sum continuum level at 387 nm, 68 per cent - at 430 nm (max) and 23 per cent - at 480 nm;

3) For comet Hale-Bopp (C/1995 O1) on April 17 , 1997 the level of the non-solar-origin continuum equal to 32 per cent of the sum continuum level at 397 nm and 77 per cent - at 438 nm;

4) For comet Hyakutake (C/1996 B2) March 25, 1996 the continuum of the non-solar origin was not detected.

We suppose that in spectra of comets Schaumasse (24P), Scoritchenko-George (C/1989 Y1) and Hale-Bopp (C/1995 O1) we detected the real cometary continuum tied with the luminescence of the comet organic spices which are in comet dust particles.

Acknowledgements. This research was support in part by grant 96-0328 from INTAS.

References

Churyumov K.I., Kleshchonok V.V.: 1994, *Planetary and Space Sciences*, **42**, 9, 70.

Churyumov K.I., Kleshchonok V.V., Mussaev F.A., Bikmaev I.F., Galazutdinov G.H.: 1999, *Earth, Moon and Planets*, **78**, N 1, 105.

Churyumov K.I., Kleshchonok V.V., Vlassyuk V.V.: 1999, *Earth, Moon and Planets*, **78**, N 2, 111.

Nazarchuk H.K.: 1987a, *Kometnyj Tsirkulyar*, **372**, 2.

Nazarchuk H.K.: 1987b, *Kometnyj Tsirkulyar*, **377**, 2.

ANALYTICAL ESTIMATE OF INFLUENCE OF THE LIMITED ANGULAR SIZE OF THE SUN IN A PROBLEM OF TWILIGHT SOUNDING OF THE ATMOSPHERE

L.S. Shakun

The Odessa Astronomical Observatory
T.G. Shevchenko Park, Odessa 65014 Ukraine,
spirits@tm.odessa.ua

ABSTRACT. The Sun has finite angular size. Therefor sunrays from different points of the solar disk have different trajectories in the atmosphere. General illumination produced by different parts of the solar disk differs even if the brightness of these parts is identical. Thus the illumination of some point in the atmosphere produced by the solar disk and the illumination of the same point produced by the Sun taken as a point source are different. It is shown that into a consideration angular size of the Sun doesn't influence the brightness of twilight sky. However, the brightness of some parts of twilight ray significantly increases. A new method of computing illumination of some point in the atmosphere is propound that takes into account angular size of the Sun.

Keywords: Earth atmosphere; aerosols; Solar radiation

1. Introduction

Except large bodies fly in the Earth's atmosphere, there are a number of small particles constantly hit it — a space dust. As dust does not radiate itself it can't be seen at night, and in daytime the scattering of Solar light caused by dust is insignificant in comparison with a scattering of solar light in the lower atmospheric layers. However, during morning and evening twilight the high atmospheric layers are irradiated much better, than lower ones. It allows defining a composition of the upper atmospheric layers by means of measuring brightness of the twilight sky.

The method of twilight sounding on measured luminosity of the twilight sky calculates a content of an aerosol in the upper atmosphere. Its procedure supposes there is a certain mode permitting to calculate a part of the twilight sky brightness that is caused by a single scattering of light on particles of an atmosphere. Theoretically, it may be found under the formula

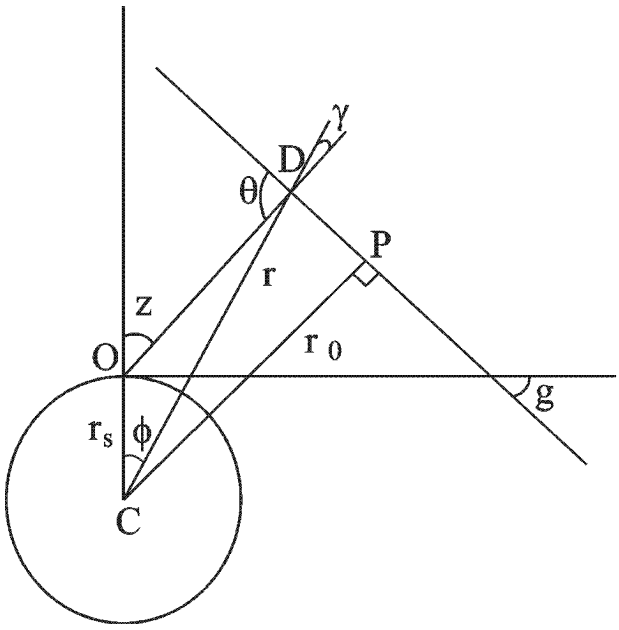

Figure 1: The plan of distribution of a not refractive ray of the Sun in Solar meridian.

$$B_1 = E_0 p^m \int_0^m \sigma(\theta, h) F(h, q) \sec\gamma dh \qquad (1)$$

Where B_1 — the brightness of primary twilight (brightness of an observable segment of the sky stipulated by single scattering);
E_0 — illumination of a site on the border of the Earth's atmosphere;
p^m — transparence of an atmosphere in a direction of a sighting;
$\sigma(\theta, h)$ — directional dissipation factor at the altitude h above a surface of the Earth;
$F(h, q)$ — transparence of an atmosphere up to a point of scattering along a trajectory of a light ray.

θ — the angle, under which scattering happens;
q — the set of parameters, from which also depends a transparence of an atmosphere up to a point of scattering.

Brightness of single scattering and transparence of an atmosphere in a direction of a sighting are being measured from observations. Illumination intensity on the border of an atmosphere is been supposed a constant. The directional dissipation factor depends on a distribution of atmospheric components, and therefore it is used for determination of a structure of an atmosphere and, hence, it is obtained from equation. The magnitude of a transparency depends on the various factors and, as a rule, calculates theoretically. For its calculation usually suppose, that the solar rays are spread rectilinearly, and the angular sizes of the Sun are neglected. Sometimes those who wish to receive results that are more precise take into account effects of a refraction and limited size of the Sun. But if effects of refraction essentially change the theoretical magnitude of brightness of single scattering, the influence of limited angular size of the Sun on magnitude of brightness of the twilight sky is estimated by authors differently. Some suppose this magnitude not essential, and others offer to take it into account. We shall try to estimate the magnitude of the correction that takes into account limited angular size of the Sun. In this time about the structure of the atmosphere, we make only common suppositions.

One of the reference suppositions of a method of twilight sounding is the supposition about a spherical symmetry of an atmosphere. It allows considering light scattering in the chosen plane. Usually it is a solar meridian. In the case, when the Sun has defined size, its part will be outside of a solar meridian, and, hence, rays will be spread outside of this meridian. Each point in the solar meridian on the disk of the Sun will correspond with a line on the disk of the Sun. However angular size of the Sun is small and radius of the Earth is large enough. Let's assume that the transparence of an atmosphere along a line on the disk of the Sun relevant to one point in a solar meridian does not vary (Link, 1962). Then the Sun can be considered as a segment in a solar meridian which length is equal to an angular size of the Sun.

The evaluation of the correction to a transparency of an atmosphere in such suppositions can be divided into two components. First, one consists in definition of a modification of illumination intensity created by a partial segment of the Sun in a solar meridian outside of an atmosphere. The second one — in the definition of a transparency of an atmosphere for each partial segment of the solar disk and evaluation of convolution of a transparency of an atmosphere and illumination intensity from each partial segment.

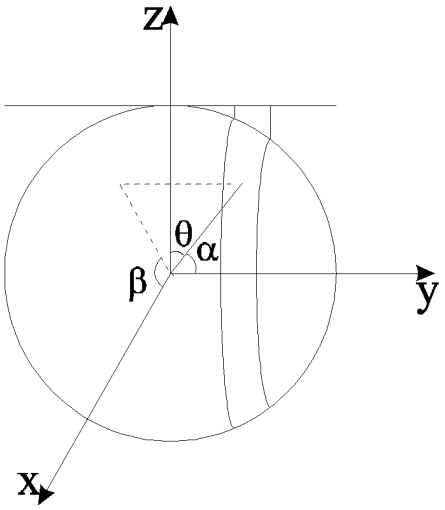

Figure 2: Coordinates on a surface of the Sun

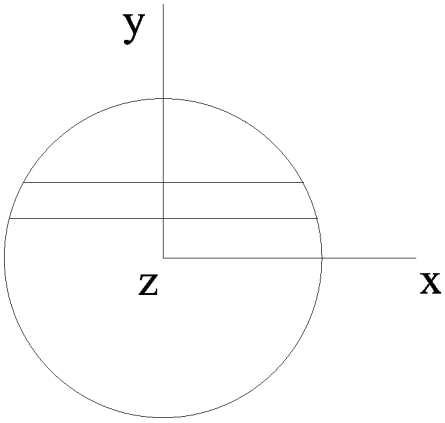

Figure 3: Aspect of a Cartesian coordinates (x, y, z) on the disk of the Sun from a place of a position of the observer.

2. Brightness of a partial segment of the Sun

The brightness of the Sun we shall name Illumination from a narrow horizontal band of the disk of the Sun referred to an angular length of a segment in a Solar meridian that is relevant to a horizontal band of the disk. Let's use spherical coordinates on a surface of the Sun. A polar angle α we'll calculate from a direction to zenith (fig. 2, 3). The z-axis is perpendicular to a picture plane. In such coordinates a band on the disk the Sun is determined by α angle. Then illumination that is created by a band of the disk of the Sun between angles α_1 and α_2 is

$$E = \left(\frac{R}{l}\right)^2 \int_{\alpha_1}^{\alpha_2} \int_0^{\pi} B(\theta) \sin^2 \alpha \sin \beta d\beta d\alpha \qquad (2)$$

Where R — radius of the Sun;
l — distance from the Sun to the Earth;

$B(\theta)$ — brightness of a site on the disk of the Sun.

$$B(\theta) = B(0)(1 - u - v + u\cos(\theta) + v\cos^2(\theta)). \quad (3)$$

Where u, v - some coefficients depending on a wave length. The angle θ is linked to a polar coordinates (α, β) by following relation $z = \cos(\theta) = \sin(\alpha)\sin(\beta)$. Then

$$\frac{dE}{d\alpha} = 2\left(\frac{R}{l}\right)^2 B(0)((1 - u - v)\sin^2\alpha + \frac{\pi}{4}u\sin^3\alpha + \frac{2}{3}v\sin^4\alpha) \quad (4)$$

Let angle δ is a visual angular distance from the center of the solar disk. Then the angles α and δ are also interlinked by following relations $l\sin\delta = R\cos\alpha$, $l\cos\delta d\delta = -R\sin\alpha d\alpha$

They allow to proceed from an angle α to an angle δ if necessary.

3. Transparence of an atmosphere for various parts of the solar disk

Illumination of some partial volume in an atmosphere assigned by coordinates (r, r_0) is

$$E = \int_{-\delta'}^{\delta'} F(r, r_0(\delta))\frac{dE}{d\delta}d\delta. \quad (5)$$

Here $F(r, r_0(\delta))$ — transparence of an atmosphere up to partial volume along trajectories of distribution of solar rays;
δ' — angular sizes of the Sun;
$\frac{dE}{d\delta}$ — illumination of a site outside of an atmosphere from a segment of the Sun in a solar meridian with visual angular distance δ.

Let's suppose, that the transparence can be submitted by association

$$F(r, r_0(\delta)) = exp\left(-e^{f(r, r_0(\delta))}\right). \quad (6)$$

Transparence of an atmosphere may be decomposed in a Taylor series on degrees of a smallness $\Delta r_0 = r_0(\delta) - r_0(0)$.
The zero term of expansion is $F_0(r, r_0(\delta)) = exp(-\tau_0)$, where $\tau_0 = e^{f(r, r_0(0))}$.
The first term of expansion

$$F_1(r, r_0(\delta)) = -\tau_0 f'(r, r_0(0))exp(-\tau_0)\Delta r_0.$$

The second term of expansion

$$F_2(r, r_0(\delta)) = \frac{1}{2}e^{-\tau_0}(\tau_0 f'(r, r_0(0)))^2 - \tau_0 f''(r, r_0(0)) - \tau_0(f'(r, r_0(0)))^2)\Delta r_0^2.$$

In all terms of expansion only Δr_0 depends from δ. Therefore, it is possible to bear all remaining factors of each term of expansion for a sign of integration.

In the supposition of rectilinear distribution of solar rays

$$\Delta r_0 = -r(2\cos\phi\sin^2\frac{\delta}{2} - \sin\phi\sin\delta). \quad (7)$$

Here ϕ — angle between radius by vector indicating on dispersing volume, and radius by vector indicating on minimum distance of a ray above a ground surface.
$\frac{dE}{d\delta}$ — an even function from an angle δ. Therefore convolution δ with an odd function from an angle δ (For example, $\sin\delta$) in symmetric limits is equal to zero. Hence, the terms containing only even degrees from a sine of an angle will remain. Let's note the formula for an evaluation of illumination intensity of partial volume of an atmosphere, in which we shall be restricted to the second degrees from $\sin\delta$.

$$E = e^{-\tau_0}\int_{-\delta'}^{\delta'} dE + 2\tau_0 e^{-\tau_0} f'(r, r_0(0))r\cos\phi\int_{-\delta'}^{\delta'}\sin^2\frac{\delta}{2}\frac{dE}{d\delta}d\delta + \frac{1}{2}e^{-\tau_0}\tau_0(\tau_0(f'(r, r_0(0)))^2 - f''(r, r_0(0)) - (f'(r, r_0(0)))^2)(r\sin\phi)^2\int_{-\delta'}^{\delta'}\sin^2\delta\frac{dE}{d\delta}d\delta \quad (8)$$

In all integrals it is possible to pass from an integration on an angle δ to an integration on an angle α. It allows easily calculating integrals analytically. We shall not do it, and we shall conduct a numerical estimation of integrals to reveal the basic regularity of a modification of illumination intensity at limited angular sizes of the Sun from optical depth. Let optical depth varies under the exponential law. Then a second derivation from function $f(r, r_0) = 0$. For the Earth's atmosphere, the first derivative from function f is approximately equal to $0,125$. Let's assume radius the Earth, $r = 6370km$. Radius of the Sun $R = 696000km$. Medium distance from the Sun to the Earth $l = 150mln.km$. Let the atmosphere thickness is $100km$. Then $r\cos\phi = 6370km$, $r\sin\phi = 1133km$

Then an angular sizes of the Sun is $\delta' = 15,95'$
For a wavelength 371 nm.

$$E = E_0(1 + 0.0015\tau_0 + 0.038\tau_0(\tau_0 - 1)). \quad (9)$$

Based on the obtained estimation it is possible to make a following deduction. That for optical depths about one the modification of illumination intensity taking into account limited angular size of the Sun does not exceed 20 of percent. Large optical depths, as a rule, correspond to feebly irradiated stratums and that

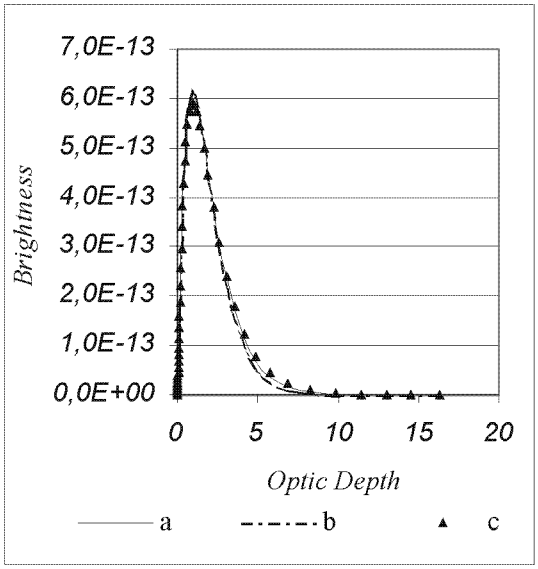

Figure 4: Dependence of various atmospheric slices luminosity on optical length of a trajectory up to a scattering point. a — illumination intensity of scattering volume calculated as a series; b — the illumination intensity calculated neglecting the angular size of the Sun; c — illumination intensity calculated by replacement of the Sun by 7 equidistant radiant points.

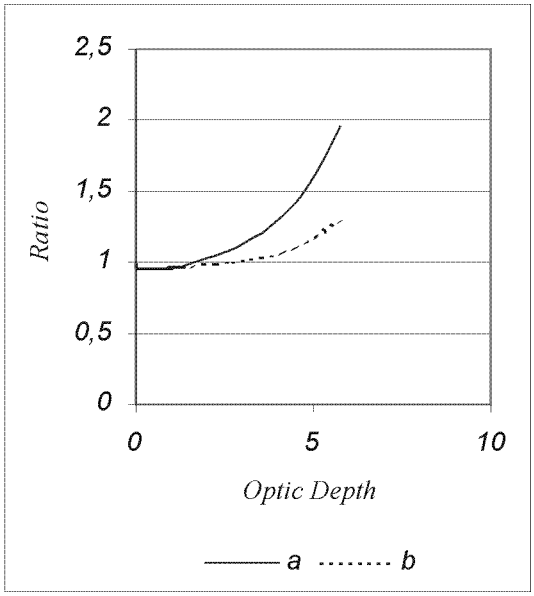

Figure 5: Dependence of the luminosity's ratio on the optical depth for various atmospheric slices. a — the ratio of luminosity's of the scattering volume calculated according to the 7 points model and neglecting angular size of the Sun; b — the ration of luminosity's of scattering volume calculated according to the 7 points model and as the series.

is why their influence on the twilight sky character is small

As an example we shall make calculation of the dependence of twilight atmosphere stratum brightness on the height for a wave length 371 nm and zenith distance in the direction of a sighting 0°, the Sun depth 7°. This wavelength was chosen to position the twilight ray high enough above the surface. It excludes a possible situation, when the Sun is partially closed by a surface of the Earth. Let's conduct calculations for three cases. First case does not take into account angular solar size. Second case takes them into account according to the above mentioned theory and the third one uses Solar model where the Sun is substituted by 7 equally distant points of various intensity placed in the solar meridian (fig. 4). Observing this figure, We are possible to make the next conclusions.

Takings into account angular size of the Sun feebly influence the total brightness of the twilight sky. However, the brightness of some layers of the atmosphere changes significantly. When optic depth is large enough the brightness of the twilight sky significantly increases due to angular size of the Sun (fig. 5).

Methodic given in the paper permits effective calculation of corrections in the field of optical depth about one. These optical depths correspond with the atmospheric layers that contribute main part of the twilight sky brightness. For lager optical depth, the correction may be calculated by taking into account a greater number of terms of the series. However, this way may appear not effective.

The undoubted advantage of this procedure in comparison with the 7-point model is an acceleration of correction computing. Multipoint model increases computing time proportionally (and even more) to the number of points. Our model increases computing time less then twice comparing with the case that neglects angular size of the Sun.

References

Link F.: 1962, *Bull. Astron. Inst. Chechosl.*, **13**, 1, 1.

Наукове видання

Вісті Одеської астрономічної обсерваторії

том 12 (1999)

Англійською мовою

Технічний редактор М. І. Кошкін

Підписано до друку 12.12.99. Формат 60x84/8.
Ум. друк. арк. 29,76. Друк офсетний. Папір офсетний. Тираж 300 прим. Зам. 588.

Видавництво «АстроПринт»
65026, м. Одеса, вул. Преображенська, 24.
Тел.: +38 (0482) 26-96-82, 26-98-82, 37-14-25.